



Adhesion Mechanisms of Silicone Adhesives on Aluminum

Dissertation

zur Erlangung des Grades des Doktors der Ingenieurwissenschaften
der Naturwissenschaftlich-Technischen Fakultät
der Universität des Saarlandes

In Kooperation mit Robert Bosch GmbH

Von

Ana Lucia Palencia Penagos

Saarbrücken
2017

Tag des Kolloquiums:	11. Juli 2017
Dekan:	Prof. Dr. Guido Kickelbick
Berichterstatter:	Prof. Dr. Wulff Possart
	Prof. Dr. Guido Kickelbick
Vorsitz:	Prof. Dr. Hans-Georg Hermann
Akad. Mitarbeiter:	Dr.-Ing. Frank Aubertin

Declaration of original authorship:

I hereby declare that this dissertation is my own original work except where otherwise indicated. All data or concepts drawn directly or indirectly from other sources have been correctly acknowledged. This dissertation has not been submitted in its present or similar form to any other academic institution either in Germany or abroad for the award of any other degree.

Saarbrücken, 20.03.2017

Ana Lucia Palencia Penagos

Dedicated to my Abba Kadosh, my parents Olmedo & Tine, my siblings Karol, Paola & Juan David, and to the memory of my grandmother Margarita.

> *…"For the Lord gives wisdom, from him comes knowledge and understanding"…*
>
> *Prov. 2:6*

Kurzzusammenfassung

Silikonklebstoffe und Aluminium zählen zu den meistverwendeten Materialien in der Transportindustrie wegen des erhöhten Bedarfs an Leichtbaustrukturen. Klebverbindungen können hinsichtlich Qualität und Leistungsfähigkeit prinzipiell optimiert werden durch Kenntnis und Verständnis der Wechselwirkungen an der Grenzfläche. Das Hauptziel dieser Arbeit ist die Aufklärung der Wechselwirkungen an der Grenzfläche zwischen einzelnen Silikon-Modellkomponenten (SSMC) und Aluminium sowie das Aufstellen plausibler Adhäsionsmechanismen. Zur Untersuchung von Chemie und Molekülorientierung an der Grenzfläche wurden Adsorptions- und Co-Adsorptionsexperimente der SSMCs, gelöst in Tetrahydrofuran (THF), auf nativem Aluminium durchgeführt und in-situ mittels Externer Infrarot-Reflexions-Absorptions-Spektroskopie verfolgt. Die Adsorbatstabilität wurde mithilfe konsekutiver THF-Spülungen überprüft und somit zwischen stark und schwach adsorbierten Molekülen differenziert. Die Ergebnisse zeigen die vorherrschende Rolle von Siloxanbindungen (Si-O-Si) bei der Adhäsion von Silikon auf Aluminium. Neue spektrale Merkmale und eine Desorptionsresistenz gegen THF belegen die feste Anbindung der SSMCs an die Oberfläche. Mehrere simultane Adhäsionsmechanismen wurden postuliert. Außerdem wurde eine Vorzugsorientierung von Polydimethylsiloxan mit Si-O-Si-Segmenten parallel zur Aluminiumoberfläche abgeleitet. Bei der Co-Adsorption wirkt sich die Vernetzung in der Interphase deutlich auf die molekulare Orientierung aus. Kein katalytischer Einfluss der Aluminiumoberfläche auf die Vernetzung wurde gefunden.

Abstract

Silicone adhesives and aluminum are among the most widely used materials in the transportation industry due to the increased need for lightweight structures. The quality and final performance of the adhesive joints can potentially be improved if the nature of the interactions at the interface are known and understood. Thus, this thesis is devoted to elucidating possible interactions between single silicone model components (SSMC) and native aluminum which allows the proposal of plausible adhesion mechanisms. The chemical state and orientation of the molecules at the interface have been evaluated via infrared external reflection absorption spectroscopy (IR-ERAS) from in-situ adsorption and co-adsorption experiments of the SSMC from dilute solution in tetrahydrofuran (THF). The stability of the adsorbate has also been examined by sequential THF rinsing steps which help to distinguish between strongly and weakly adsorbed molecules. The results show the dominant role of siloxane bonds (Si-O-Si) in the adhesion of silicones. New spectral features and resistance against solvent desorption have been consistently observed, indicating that the adsorbed SSMC firmly adheres to aluminum. Different possible concurrent mechanisms of adhesion have been proposed and preferential orientation of polydimethylsiloxane (PDMS) with Si-O-Si segments aligned parallel to the surface is also inferred. A significant impact of crosslinking in the interphase on the molecular orientation is exhibited during co-adsorption. No catalytic effect of the aluminum surface on crosslinking has been found.

Acknowledgments

During this enriching PhD path, besides learning about silicones and adhesion phenomena, I have had the opportunity to meet many wonderful people along the way. It is a great pleasure to thank everyone, who helped me to complete this dissertation, it would have been impossible without their support, guidance, friendship and encouragement.

First and foremost, I would like to express my profound thankfulness to my academic supervisor, Prof. Dr. Wulff Possart, for his great patience, support, kindness, encouragement, valuable contributions, and especially for being my guide through this work. Thanks for seeing in me not only a present but also a future and for helping me to develop into an independent researcher. I felt much honor to have had the opportunity of working with him.

I would like to thank Robert Bosch GmbH for opening the doors to this PhD opportunity, this research would have not been possible without its financial support. My most sincere gratitude to Mr. Kai von Garnier, for allowing me to be part of such an interesting project, for his patience, guidance, motivation, advices and for sharing his knowledge about adhesives. My special thanks to Dr. Martin Giersbeck for his support to this research.

I also acknowledge Prof. Dr. Guido Kickelbick for his support, his interest in this work, important contributions and for his kind acceptance as second reviewer.

Thank you infinitely to everyone in the research group of Prof. Possart for all the help, motivation and such a nice work atmosphere. Your company during my years in Saarbrücken made my work much more enjoyable. Special thanks to Alice Goldschmidt, to Werner Rauber for his help in setting up the Glovebox, to Christophe Nies for the spectra discussion, to Leo Depollier for the running sessions in the mornings, to Ludovic Krogh for his motivational words, to Frank Fug for his help with software problems, special thanks to Ernesto Sanchez for his valuable friendship during all these years in Germany and to Bettina Zimmer for her friendship and help in translation.

I appreciate all the kindness and help I received from the people at Robert Bosch GmbH for carrying out measurements and laboratory work. Particularly, I would like to thank Harrald Wilharm, Christian Hoffmann, Sonja Koppe and Christoph Üffig.

I express my deep thanks to my friends Adrian Benitez, Camilo Cruz and Veronica Torres for their willingness to help and appropriate suggestions to my thesis. Thank you for your precious friendship and for being by my side when I have needed.

I am heartily grateful to my dear and closest friends Loriana Galindez, Isabel Perez and Vicky Dellaia for their support, encouragement, trips, wise advices, unending conversations and interminable laughs.

I feel very grateful with my friends in Berlin, Saarbrücken, Stuttgart and Colombia.

My most special and greatest thankfulness goes to my family in Colombia for their unconditional love, support, patience, encouragement and motivation during these years far away from them. You are my rock and my everything, I could not have achieved anything if not for you. Thank you for loving me as I am and for making my life precious and happy.

Finally, thanks to God, I am done!

Abbreviations and symbols

1-C	One-component
2-C	Two-component
2-D	Two-Dimensional
3-D	Three-Dimensional
Al	Aluminum
ARXPS	Angle Resolved X-Ray Photoelectron Spectroscopy
ATMS	Allyltrimethoxysilane
ATR	Attenuated Total Reflection
CAS-Nr.	Chemical Abstract Service Registry Number
CSA	Commercial Silicone Adhesive
D	Dimethylsiloxane unit
DEPT	Distorsionless Enhancement by Polarization Transfer
DSC	Differential Scanning Calorimetry
EDX	Energy Dispersive X-Ray
ERAS	External Reflection Absorption Spectroscopy
FEICA	Association of the European Adhesive and Sealant Industry
FMSA	Formulated Model Silicone Adhesive
FTIR	Fourier Transform Infrared
GPC	Gel Permeation Chromatography
GPS	Glycidoxypropyltrimethoxysilane
H-bonding	Hydrogen bonding
HSQC	Heteronuclear Single Quantum Coherence
IR	Infrared radiation
IRE	Internal Reflection Element
M	Monofunctional siloxane unit
MMD	Molar Mass Distribution
NMR	Nuclear Magnetic Resonance
p-polarization	parallel polarization
PDI	Polydispersity Index
PDMS	Polydimethylsiloxane
PDPS	Polydiphenylsiloxane
PMPS	Polymethylphenylsiloxane
PS	Polystyrene
Pt cat.	Platinum catalyst

PVD	Physical Vapor Deposition
Q	Quatrifunctional siloxane unit
s-polarization	perpendicular polarization
SEM	Scanning Electron Microscopy
SFM	Scanning Force Microscopy (known as AFM)
SLSJ	Single-Lap Shear Joints
SSMC	Single Silicone Model Components
S/N	Sinal-to-Noise ratio
T	Trifunctional siloxane unit
TDMS	Tetrakis(dimethylsiloxysilane)
TGA	Thermogravimetric Analysis
THF	Tetrahydrofuran
TIR	Total Internal Reflection
TMS	Tetramethylsilane
ToF-SIMS	Time of Flight Secondary Ion Mass Spectroscopy
UV	Ultraviolet radiation
XPS	X-Ray Photoelectron Spectroscopy
ZnSe	Zinc Selenide Crystal

C_p	Heat capacity[J g^{-1} K^{-1}]
HF	Heat Flow [J s^{-1} g^{-1}]
n	refractive index [-]
M_n	Number-average molar mass [g mol^{-1}]
M_w	Weight-average molar mass [g mol^{-1}]
RT	Temperature [°C]
T_c	Crystallization temperature [°C]
T_{dp}	Dew Point [°C]
T_g	Glass transition temperature [°C]
T_m	Melting temperature [°C]
$T_{5\%}$	Onset degradation temperature at 5 % mass loss [°C]
$T_{10\%}$	Onset degradation temperature at 10 % mass loss [°C]
ν_s	Symmetric stretching
ν_{as}	Asymmetric stretching
δ_s	Symmetric bending
δ_{as}	Asymmetric bending
ρ	Rocking
ω	Wagging
γ	Scissoring
τ	Twisting

Contents

Kurzzusammenfassung **7**

Abstract **9**

Acknowledgments **11**

Abbreviations and symbols **13**

1. Introduction **21**

2. Motivation and Strategy **25**

2.1. Problem statement and motivation 25
2.2. Aim of the work 27
2.3. Strategical approach 28
2.4. Thesis structure 29

3. Silicone Adhesives – an Overview **33**

3.1. Silicones - generalities, properties and applications 33
3.2. Silicone crosslinking - Hydrosilylation 38
3.3. Adhesion mechanisms of silicones – State of the art 42
3.3.1. Adhesion of PDMS 43
3.3.2. Adhesion of Silanes 47

4. Characterization of Silicone in Bulk **51**

4.1. Goal and methodology 51
4.2. Chemical characterization - Experimental 54
4.2.1. ATR-FTIR Spectroscopy 54
4.2.1.1. Theoretical considerations 54
4.2.1.2. Experimental procedure 57
4.2.2. NMR Spectroscopy 58
4.2.2.1. Fundamentals 58
4.2.2.2. Experimental procedure 62

4.3. Results of the characterization in bulk of the CSA 63
4.3.1. Chemical characterization 64
4.3.1.1. ATR-FTIR Spectroscopy 65
4.3.1.2. NMR Spectroscopy 79
4.3.2. Additional characterization 88
4.3.2.1. Molar mass determination by GPC 88
4.3.2.2. Thermal analysis 91
4.3.3. Synopsis - Characterization of the CSA 106
4.4. Results of the characterization in bulk of the SSMC 108
4.4.1. Bifunctional hydride terminated PDMS - Prepolymer 1 108
4.4.1.1. ATR-FTIR Spectroscopy 108
4.4.1.2. NMR Spectroscopy 111
4.4.1.3. Molar mass determination by GPC 114
4.4.2. Bifunctional vinyl terminated PDMS - Prepolymer 2 115
4.4.2.1. ATR-FTIR Spectroscopy 115
4.4.2.2. NMR Spectroscopy 117
4.4.2.3. Molar mass determination by GPC 120
4.4.3. Tetrakis(dimethylsiloxysilane) (TDMS) - Crosslinker 121
4.4.3.1. ATR-FTIR Spectroscopy 121
4.4.3.2. NMR Spectroscopy 122
4.4.4. Platinum-divinyltetramethyl-disiloxane complex in vinyl PDMS - Karstedt catalyst. 124
4.4.4.1. ATR-FTIR Spectroscopy 124
4.4.4.2. NMR Spectroscopy 126
4.4.5. Allyltrimethoxysilane (ATMS) – Adhesion promoter 128
4.4.5.1. ATR-FTIR Spectroscopy 128
4.4.5.2. NMR Spectroscopy 129
4.4.6. Synopsis – Characterization in bulk of the SSMC 132
4.5. Results of the characterization in bulk of the FMSA 134
4.5.1. Formulation of the FMSA 135
4.5.2. In-situ ATR-FTIR studies - Crosslinking of the FMSA 137
4.5.2.1. Crosslinking in the absence of the Karstedt catalyst 138
4.5.2.2. Crosslinking in the presence of the Karstedt catalyst 141
4.5.3. Characterization of the crosslinked FMSA 149
4.5.3.1. Chemical characterization 149
4.5.3.2. Thermal Characterization 153
4.5.4. Summary – Characterization in bulk of the FMSA 158

5. Adsorption of the SSMC on Aluminum 161

5.1. Purpose of the in-situ adsorption experiments....161
5.2. Introductory remarks....162
5.3. Experimental approach....164
5.3.1. Aluminum substrate....165
5.3.1.1. Preparation of the Al substrate by PVD....165
5.3.1.2. Chemical composition of the Al surface studied by XPS....167
5.3.2. In-situ adsorption experiments - FTIR-ERAS study....176
5.3.2.1. Fundamentals of FTIR-ERAS....176
5.3.2.2. Description of the adsorption experiments....183
5.4. Spectra evaluation-Methodology....189
5.5. Results and interpretation....192
5.5.1. Prepolymer 1 - bifunctional hydride terminated PDMS....193
5.5.1.1. Case 1: short storage time (1 h)....193
5.5.1.2. Case 2: long storage time (24 h). 206
5.5.2. Prepolymer 2 - bifunctional vinyl terminated PDMS....216
5.5.2.1. Case 1: short storage time (1 h)....216
5.5.2.2. Case 2: long storage time (24 h). 224
5.5.3. Crosslinker – Tetrakis(dimethylsiloxy)silane (TDMS)....236
5.5.4. Karstedt catalyst: Pt(0)-divinyltetramethyldisiloxane complex in monovinyl terminated PDMS. 247
5.5.5. Adsorption of Allyltrimethoxysilane (ATMS) 257
5.6. Conclusive Discussion....262
5.6.1. Effect of end-group on the adsorption of PDMS....262
5.6.2. Influence of storage time on the adsorption of PDMS....267
5.6.3. Effect of molecular size in the adsorption of siloxanes on Al....272
5.6.4. Adsorption of alkoxysilanes vs. siloxanes 274
5.6.5. Role of -Si-OH traces in the adsorption of PDMS....276
5.6.6. Influence of the Pt complex (Karstedt catalyst)....277
5.6.7. Adsorption/desorption of organic contaminants....277
5.6.8. Effect of the solvent (THF)....278
5.6.9. Chemical state of the aluminum surface....279
5.6.10. Molecular orientation of adsorbed PDMS on Al....280
5.6.11. Adhesion mechanisms of silicones on Al....285

6. Co-Adsorption of the SSMC on Aluminum 291

6.1. Aim of coadsorption experiments....291
6.2. Experimental methodology....292
6.2.1. Materials....292
6.2.2. Viability of co-adsorption experiments....293

6.2.3. In-situ co-adsorption experiments 295
6.3. Results and interpretation 296
6.3.1. Co-Adsorption – without the Karstedt catalyst 296
6.3.2. Co-Adsorption – with Karstedt catalyst 308
6.4. Conclusive discussion 320
6.4.1. Crosslinking of silicones at the interface 320
6.4.2. Preferential adsorption 321
6.4.3. Effect of time 322

7. Outlook: CSA on Technical Aluminum 325

7.1. Introduction and aim of the study 325
7.2. Preparation of the aluminum surface 326
7.2.1. Technical aluminum substrate 326
7.2.2. Surface pretreatments 327
7.2.2.1. Acetone degreasing 327
7.2.2.2. P2 Etching 328
7.2.2.3. Atmospheric pressure air plasma 329
7.3. Characterization of the pretreated surfaces 331
7.3.1. Topography 332
7.3.1.1. Scanning Electron Microscopy (SEM) 332
7.3.1.2. Scanning Force Microscopy (SFM) 336
7.3.2. Chemical composition 341
7.3.2.1. X-Ray Photoelectron Spectroscopy (XPS) 341
7.3.2.2. Energy-Dispersive X-ray Spectroscopy (EDX) - mapping 348
7.4. Bonding analysis 350
7.4.1. Fabrication of the single lap adhesive joints 350
7.4.2. Single-lap shear testing 352
7.4.3. Classification of interfacial failure 353
7.5. Summary 355

8. Conclusions and Perspectives 357

9. Bibliography 363

10. Appendix 387

10.1. Appendix A 387
10.2. Appendix B 388
10.3. Appendix C 390
10.4. Appendix D 391

10.5. Appendix E 393
10.6. Appendix F 394

1 Introduction

According to the ASTM definition, adhesives are materials used for joining and holding two surfaces together [1]. Naturally, they must wet the surface, adhere to the surface, and after being applied, they must develop strength and remain stable over a certain period of time [2,3]. The product formed by adhering two materials creates an area which has neither the properties of the substrate nor the properties of the adhesive; this area is called the interface, and plays the central role in adhesion science [3–8]. The dimensions of the interface depend on the system used, but it usually lies within the molecular range [nm] [8]. Correspondingly, an adhesion phenomenon is defined as the intermolecular interactions existing at the interface that are responsible for attaching two surfaces together, and it is exclusively referred to as an interfacial event [4–6].

Understanding the adhesion phenomenon of a desired system is crucial, since the formation, development, and quality of the interface, is determinant for the appropriate final performance of an adhesively bonded product [4–6]. The performance, stability and success of adhesive joints are determined by numerous factors including theoretical knowledge, adequate surface preparation before applying the adhesive, as well as experience in fabrication of the joints [3,5,9,10]. In other words, adhesion is a complex phenomenon which involves interdisciplinary areas such as material science, chemistry, physics, surface science, and engineering [4,5]. Each adhesive-substrate system is unique and specific analysis is required.

Adhesive bonding has become a key technology in everyday life and in manufacturing production [2,5]. According to the Association of European Adhesives and Sealants Manufacturers (FEICA) more than two million tons of adhesives and sealants are produced and consumed each year only in Europe, and that number is

continuously growing. [11]. The increasing utilization of adhesives in the industrial world is mainly due to their versatility, their many application potentials and their decrease in production operations. In fact, the new challenges faced by the automotive, railway and aerospace sectors towards the improvement of the strength/weight ratio, corrosion resistance and thermal stability of joined products; has converted adhesive bonding as the best alternative for replacing traditional joining techniques such as welding, riveting or bolting [5,12–14].

For industrial applications, the term structural adhesive is rather employed in adhesive technology. According to Adams and Wake [15], "a structural adhesive is one used when the load required to cause separation of the joints is substantial such that the adhesive provides for the major strength and stiffness of the structure". Therefore, structural adhesives are expected to reduce the mechanical tension at loading and overloading, decrease damping of vibrations and increment absorption of deformation and impact energy [6,15,16].

Among the commercial structural adhesives available, silicones represent an appropriate alternative for numerous applications [13,17]. Silicones (polysiloxanes) are hybrid polymers composed of an inorganic backbone with organic side groups attached to the silicon atom [13,18–20]. Unique features and properties of silicones are due to the chemical nature of the siloxane bond (-Si-O-Si-) [21]. Concerning the mechanical properties of silicones, they are usually poor at room temperature when compared with other common structural adhesives. For instance, the tensile stress at fracture of polydimethylsiloxane (PDMS) at room temperature (RT) is approximately 0.35 MPa [22], unless it is crosslinked and reinforced with a filler. Albeit, even for chemically crosslinked and reinforced silicones, tensile strengths at RT of 2 to 10 MPa [23–25] are still relatively low compared to epoxy (35-55 MPa) [25] and polyurethane adhesives (15-30 MPa) [25]. However, what makes silicones very attractive for industrial applications is their high flexibility, thermal stability over a wide range of temperatures (from -50°C to over 250°C) [19,23,25], capacity of absorbing energy, biological compatibility and resistance to thermal shock, pressure, salt spray, engine fluids, moisture and UV light [19,20,22]. Particularly in the automotive sector, silicones are used on a large scale in car exteriors and interiors as well as in the electronics and electrical systems. They must not only have a good adhesion performance over a wide range of temperatures (from -40 up to 150 °C), but they must also act as good sealants to prevent permeation of any aggressive substance. Additionally, silicones help preventing and eliminating squeaks, rattles, noise, vibration and harshness (NVH) in automobiles [26].

Despite the wide use of silicones, investigations at the interface for elucidating the mechanisms of adhesion on aluminum metal, are still limited. Reported research works have studied the adsorption behavior of PDMS on glass, alumina, silica and various metal surfaces [27–35]. Adhesion mechanisms of silanes (organosilicon monomers) as adhesion promoters or primers on metal surfaces, including aluminum, have been extensively published [36–39]. Additional available studies have been focused on how the durability and bond strength of adhesively bonded joints using silicones could be improved by applying surface pretreatments to the substrates [29,40,41]. In summary, the fundamentals of adhesion of silicones, have been examined but not fully verified; consequently, studying the chemical behavior of silicones on aluminum is still an undefined subject.

Moreover, characterization of the interface has been restricted by the limitation of available experimental methods that can lead to reliable and reproducible results. Amongst suitable methods employed for interface examination, Fourier Transformed Infrared (FTIR) spectroscopy, more strictly, External Reflection Absorption Spectroscopy (FTIR-ERAS) technique (also known as Infrared Reflection Absorption Spectroscopy -IRRAS) has been successfully applied for this purpose [8,42–46]. Through FTIR-ERAS a spectrum based on the vibrations and rotation of atoms of thin adsorbed layers on a substrate is obtained, offering valuable and extensive information about the state of the adsorbed molecules and their direct vicinity [46]. Interactions and orientation changes of the molecules on the substrate can be deduced with this technique [42,43]. Thus, the application of the FTIR-ERAS method permits the determination of interactions responsible for the adhesion of molecules on a specific substrate.

This work is concerned with the study of the chemical structure at the interface of thin layers of siloxanes on aluminum by FTIR-ERAS measurements. The experimental approaches are in-situ adsorption experiments of silicone single model components and co-adsorption experiments of a formulated model silicone, on a model aluminum surface. The adherence of the adsorbate and its behavior on aluminum is evaluated after sequential rinses with tetrahydrofuran directing the analysis to the monolayer scale. The analysis and interpretation of the FTIR-ERA spectra of the adsorbate will allow the elucidation of possible interactions existing at the silicone-aluminum interface; hence, adhesion mechanisms can be proposed. A more detail explanation of the methodology, aim of the work and the structure developed in this thesis is given in the next chapter.

2 Motivation and Strategy

2.1. Problem statement and motivation

As mentioned in the introduction, silicones as structural adhesives are widely used for the automotive, construction, aerospace, medical and packaging industry. The quality and performance of silicone adhesively bonded joints can be improved if the structure-property relationships, established at the interface, are known and understood. However, research studies at the interface concerning the specific system: silicone (PDMS)-aluminum metal are of reduced availability.

Published works concerning the adhesion of silicones are principally focused on the adsorption of PDMS in multiple types of substrates or on the adhesion of silanes as primers or adhesion promoters. Such investigations have found that silanes, under precise experimental conditions, bond covalently to the aluminum surface by sequential steps including hydrolysis, hydrogen bonding, and condensation which results in the formation of a siloxane polymer covalently attached to the metal surface [47,48]. On the other hand, research studies associated with adhesion of silicones (PDMS), have suggested that PDMS is able to adhere on numerous substrates through physical interactions including hydrogen bonding between siloxane bonds and hydroxyl groups present on the surface [32,49]. However, the applicability and validity of such mechanisms to an oxidized aluminum metal substrate is still unverified. Moreover, the individual contributions provided by the different single components of a silicone adhesive (except adhesion promoters) has not yet been fully studied. Examination of the adsorption behavior of different end-functionalized PDMS molecules have been

carried out by other authors [34,50,51], but not strictly on the substrate of interest: oxidized aluminum metal.

This subject is of special concern in automotive industries where silicones are routinely used for joining aluminum pieces of automobile parts. Consequently, this research work has emerged from the practical importance and real necessity of understanding the fundamentals of adhesion of silicone-aluminum systems, *i.e.* to study the physicochemical interactions in the interphase (Figure 2.1). As a result, common issues involving silicone adhesives in the manufacturing process of car parts could be better understood and controlled, leading to improved final performance of the fabricated product.

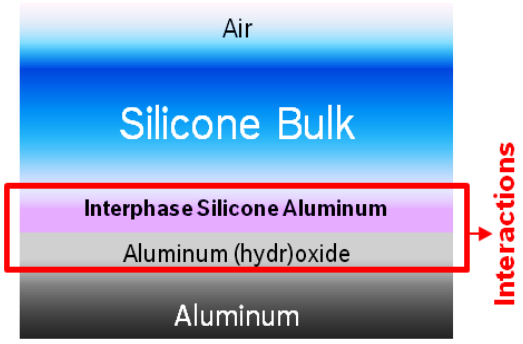


Figure 2.1. Illustration of the interphase in a silicone-aluminum system [52,53]

Considering that a commercial silicone product is typically a complex system containing various functionalized PDMS polymers, different organosilanes, additives and fillers, understanding the adhesion phenomenon throughout studies at the interface with a real silicone system would be inappropriate. In order to discriminate the effect of each component in the adhesion of a commercial silicone system on aluminum, it was necessary to identify and select single model components for carrying out adsorption and co-adsorption experiments that allow the elucidation and proposal of adhesion mechanisms of silicones on aluminum.

Aluminum was selected as the substrate in this work due to its wide applicability in diverse industrial sectors. Principally, efforts directed towards the production of lightweight vehicles to improve fuel economy, have increased its use in the automotive industry [54,55]. The utilization of aluminum for manufacturing automotive body structures and car parts is a well-known practice.

In this work, five different single silicone model components (SSMC) referenced to an addition-curing commercial silicone adhesive, were employed. The analysis consisted of performing individual in-situ adsorption experiments from a diluted solution of each SSMC on aluminum, and first attempts of co-adsorption experiments from a diluted solution of a formulated model silicone adhesive (FMSA) on aluminum. The examination of the interface and its interactions was achieved by characterizing the ultra-thin adsorbed layers on aluminum by in-situ FTIR-ERAS. This methodology has been successfully applied for studying the interactions at the interface polyurethane- and epoxy-aluminum systems and permitted to establish the adhesion mechanisms within the two materials [8,52,53]. In-situ techniques have the advantage that the formation of the interface can be studied during the respective process in the environment of interest [56].

2.2. Aim of the work

The aim of this research work and scope of this thesis was to gain a better understanding of the adhesion mechanisms of silicone adhesives on aluminum substrates. It was the main purpose to elucidate the type of interactions existing at the interface between single model components and aluminum, which allow the proposal of possible adhesion mechanisms between silicones and aluminum. To achieve this main goal, secondary objectives were established and are detailed in the paragraphs below.

1. Identify and select the appropriate single silicone model components (SSMC) based on a reference system: an addition-curing commercial silicone adhesive (CSA) commonly employed in the automotive industry. Characterization of the CSA in bulk is essential for this purpose, as well as the verification of the chemical structure and quality of the acquired SSMC.
2. Implement in-situ adsorption experiments from diluted solution of the SSMC on aluminum. The measured spectra of the SSMC in their adsorbate state are compared with bulk-like calculated ones. Discrepancies are attributed to intermolecular interactions existing at the interface between the SSMC and aluminum. Thus, possible adhesion mechanisms can be suggested.
3. Execute in-situ co-adsorption experiments of a formulated model silicone system from diluted solution on aluminum that provides hints on how adhesion occurs in real silicone-aluminum systems. The spectra of the adsorbates permit to evaluate concurrent events influencing adhesion as competitive adsorption

between different single components and feasibility of crosslinking reaction at the interface.

4. Evaluate the performance of a commercial silicone adhesive product on a technical aluminum substrate. Different surface pretreatments were applied to the substrates and the effectiveness was assessed via single lap-shear tests of the adhesively bonded joints according to DIN EN 2564 standard.

2.3. Strategical approach

As previously mentioned, selecting the adequate SSMC was fundamental for achieving the principal aim of this work. Commercial silicone adhesives are usually formulated as multicomponent systems for practical applications. Each of these components can create intermolecular interactions at the interface with themselves and with the substrate, making the analysis of commercial systems highly complex. Thus, single model components were analyzed instead.

The selection of the SSMC was based on the characterization in bulk of a reference commercial silicone, CSA. Different methods, such as Attenuated Total Reflectance-Fourier Transform Infrared Spectroscopy (ATR-FTIR), Nuclear Magnetic Resonance (NMR), Gel Permeation Chromatography (GPC), Differential Scanning Calorimetry (DSC) and Thermogravimetric Analysis (TGA), were used for the characterization in bulk of the CSA and the SSMC. With the two first techniques, the principal chemical functionalities were identified. The CSA was characterized before and after curing to observe inherent changes associated with crosslinking and to validate a single set of curing conditions (temperature and time) suggested by the manufacturer and commonly applied in the industry.

Subsequently, in-situ adsorption experiments of each SSMC were carried out on aluminum and evaluated via FTIR-ERAS. Foremost, for the FTIR-ERA measurements a flat and smooth aluminum surface (roughness < 1 nm) was required; hence, the substrates were prepared by physical vapor deposition (PVD) of pure aluminum on silicon wafers. This method was the same employed in the previous research works of Wehlack [8], Nies [52] and Fug [53]. It is well-known that when exposed to ambient conditions, aluminum creates a layer of aluminum oxide that also consists of chemisorbed and physisorbed water, hydroxyl groups and carbonaceous contaminants. Possible reactions or interactions occur between the single components and water or hydroxyl groups present on the aluminum surface. Therefore, the characterization of

the initial aluminum surface was essential in order to correlate the interactions at the interface with the chemical structure of the substrate.

Additionally, in-situ co-adsorption experiments were carried out for studying the simultaneous processes of competitive adsorption and crosslinking at the interface. These studies were of particular interest due to their applicability in real bonding processes. The methodology applied here was the same used for the individual adsorption experiments.

Ultimately, the compilation of the measured FTIR-ERA spectra provided sufficient information for drawing significant conclusions concerning the adhesion of silicones on aluminum surfaces.

2.4. Thesis structure

This thesis is divided into eight chapters. Each of them is briefly described below.

Chapter 1. Introduction
This chapter presents a short background of the interdisciplinary areas involved in adhesion science, as well as a summarized description of adhesion mechanisms of silicones. The reader is introduced to the main topic of this work.

Chapter 2. Motivation and strategy
This section describes the problems that motivated the execution of this research together with the main objectives, methodology approach and thesis structure.

Chapter 3. Silicone adhesives – an overview
This part provides a general overview of silicones, their main properties, characteristics and applications in different fields. A review of the types of silicone adhesives existing in the market and the specific crosslinking reaction for addition-curing silicones are given, as well as a state of the art relating the adsorption and adhesion of silicones or PDMS polymers on different substrates. The chapter also presents a literature survey of adhesion mechanisms suggested at the interface between silicones and different substrates.

Chapter 4. Characterization of silicone in bulk
This chapter deals with the chemical and physical characterization in bulk of the commercial silicone adhesive (before and after curing) employed as a reference for

selecting the adequate single components. Furthermore, each of the selected single components was chemically characterized in bulk and the formulation of a model silicone is presented together with in-situ characterization of its crosslinking reaction. The bulk crosslinked model silicone material was also characterized. The principles of operation of the methods used for the characterization in bulk of the commercial silicone, the single components, and the formulated silicone are also described here.

Chapter 5. Adsorption experiments of the SSMC

This section includes the description of the procedure of the in-situ adsorption experiments implemented for the SSMC. Also, the procedure of the substrate preparation and its surface characterization is supplied. It discusses the spectra obtained for each single component and highlights the principal spectral features observed. Finally, types of adhesion mechanisms existing between the components and aluminum are proposed.

Chapter 6. Co-adsorption experiments of the SSMC

In this part, the events of competitive adsorption and crosslinking in silicones were investigated throughout in-situ co-adsorption experiments, in the presence and absence of a catalyst. The SSMC used for this purpose were those employed for the formulation of the FMSA. Discussion of the spectral features displayed by the adsorbate are rendered.

Chapter 7. Outlook: CSA on technical aluminum

This chapter outlines the importance of surface pretreatments on the analysis of adhesively bonded joints. A short review on conventional types of surface pretreatments is given. The three types of pretreatments applied to the technical aluminum substrate are described. An important section is devoted to the characterization of the modified surfaces. The final part deals with the effectiveness of the pretreatments on the adhesion strength of the CSA on technical aluminum assessed by comparative single lap-shear tests.

Chapter 8. Conclusions and perspectives

This final chapter is concerned with drawing the most significant conclusions from this research and highlighting the most important observations and results, while commenting on some areas for improvement. Lastly, this chapter suggests future work and perspectives that could be performed to provide further insight into the adhesion of silicones on aluminum substrates.

The literature sources are listed in the section named Bibliography. Appendices A to F briefly present complete tests results, experimental conditions of certain experiments and methodologies implemented in the experimental work.

3 Silicone Adhesives - an Overview

This literature review is focused on the unique properties of polysiloxanes and how these materials are applicable to industrial and commercial areas. The nomenclature and crosslinking of silicone compounds via hydrosilylation and adhesion mechanisms of silicones on different substrates are also discussed. More detailed information on these subjects can be found in a number of exceptional books [19,26,57–63] and published articles [13,22,64–67].

3.1. Silicones - generalities, properties and applications

Silicones are compounds derived from the element silicon which is the second most abundant element on the Earth's surface after oxygen [66]. They are a unique class of polymers, denominated as semi-organic materials due to the stronger metallic character of silicon compared to carbon [68]. The term "silicone" was coined in 1901 by Kipping for describing compounds with the general formula R_2SiO [13,19]. The name was then redefined for polymeric materials based on siloxane bonds (-Si-O-Si-), especially for polydialkylsiloxanes with the general formula presented in Figure 3.1a.

The development of silicones has gone through different periods dating back to 1824, with the discovery of silicon by Berzelius, followed by the first production of an organosilicon compound in 1863 by Friedel and Craft [19]. In 1871 Ladenburg observed the formation of an oil which decomposed only at very high temperatures and obtained the first siloxane polymer. In 1901 Kipping founded organosilicon chemistry, and finally, by 1940 Müller and Rochow independently produced liquid methylchlorosilanes,

which are currently the starting materials for industrial manufacturing of silicones [19,26].

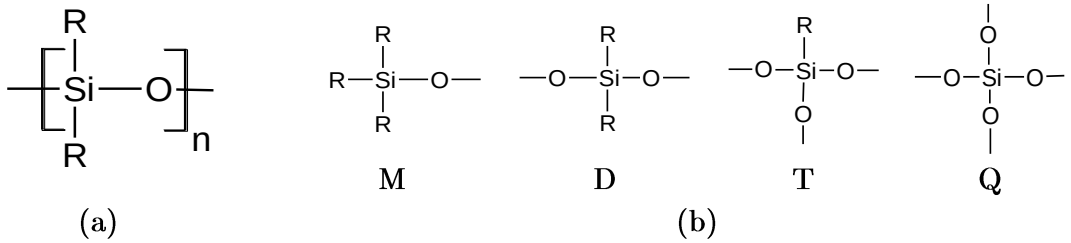


Figure 3.1. (a) General formula of a linear silicone polymer [19,26], (b) Nomenclature of polysiloxanes [13].

A system of abbreviation is used in silicones according to the number of oxygen atoms attached to the silicon element (Figure 3.1b). This nomenclature is widely used for simplification of different silicone structures [13]. The letter "M" (monofunctional) is used when only one oxygen atom is bonded to silicon, The difunctional unit is designated as "D", trifunctional unit as "T" and "Q" for quadrifunctional or tetrafunctional units, when four oxygen atoms are attached to silicon.

Properties and applications

The most widely employed silicone in the industry is polydimethylsiloxane (PDMS) in which R = CH_3 (Figure 3.1). Commercial silicones are usually synthesized from chlorosilanes by either direct hydrolysis and condensation reactions or by ring opening polymerizations [19,26]. The properties of the final product can be readily tailored by varying the type of substituents in the polymer backbone, the molecular structure of the skeleton, the end-groups, the molar mass distributions (MMD), and the degree of crosslinking [19,22]. Depending on the desired properties, methyl groups along the backbone can be replaced by other functionalities, for instance by phenyl, vinyl, hydrogen, hydroxyl and trifluoropropyl groups [13,19]. The presence of such organic groups bonded to the backbone gives silicones an outstanding versatility and permits their use in different fields such as automotive, aerospace, building industries, electronics, cosmetics, health care and coatings, among others. [19,22].

The special features, unique properties and wide range of applications of all technical silicon compounds have been attributed to the chemical structure of silicones, especially to the nature of the siloxane bond (Si-O). The outstanding flexibility and inertness properties that contrast with the corresponding organic ethers and alcohols

imply that the electronic features that distinguish Si from other members of its family in the periodic table are a key factor [69]. Numerous theoretical and experimental studies have been directed to explain the anomalous character of the Si-O vs. C-O binding. The most distinctive differences between Si-O and Si-C bonds are summarized in Table 3.1.

Table 3.1. Properties of Si-O vs. C-O bonds [13,19,23].

Element	Bond length [Å]		Ionic bond character [%]		Bond energy [kJ mol^{-1}]	
X	Si-X	C-X	Si-X	C-X	Si-X	C-X
Si	2.34	1.88	-	12	222	318
C	1.88	1.54	12	-	318	346
H	1.47	1.07	2	4	318	411
O	1.63	1.42	50	22	452	358

Bond angle [Degree °]			
Si-O-Si	O-Si-O	C-Si-C	C-O-C
140 ± 10	109-112	106	110

The position of the silicon element in the periodic table, led to a belief of the existence of analogue compounds to the carbon atom, although, most of these analogue compounds do not exist, or behave very differently [21,69]. In contrast to carbon, silicon fails to form multiple bonds that are stable at room temperature due to the larger size of silicon atoms in comparison with carbon [70]. However, silicon can expand its valence shell to accommodate 10 electrons due to the empty 3d orbitals (sp^3d hybridized – 5 substituents) and even 12 electrons (sp^3d^2 hybridized – 6 substituents) [19,21]. Due to the 3d free orbitals, silicon can act as an electron acceptor in the formation of a donor-acceptor interaction $(p\text{-}d)_\pi$ bond with the unshared p electrons of oxygen [21,71], resembling a double pi bond. The relatively high freedom of rotation around the siloxane bond is not affected by this type of $(d\text{-}p)_\pi$ bonding and thus, the Si-O-Si angle presents a great flexibility [21]. On the other hand, the conceptual Si=O double bond is unstable, unlike the C=O double bond in ketones [72].

The concept of the $(p\text{-}d)_\pi$ bonding has been used to justify most of the unique structural key features dominating the properties of silicones [19,23,73,74]. However, as mentioned by Jones et al. [26], theoretical calculations have shown that the contribution of the d orbitals at Si to the total electron distribution of Si-O is small, and different researches have attributed these features to the strongly ionic character of the Si-O bond and hyperconjugation $(p(O)\rightarrow\sigma^*(Si\text{-}X))$ where X is any atom bound to silicon.

However, other authors have suggested that the $(p\text{-}d)_\pi$ concept should not be totally abandoned, as the theoretical calculations did not provide unequivocal information about the character of the Si-O bond. The controversy is still unresolved, new research work of West et al. [69,75] has confirmed the dominant role of hyperconjugation, for instance in the low basicity of the Si-O bond, which paradoxically, is due to the inherently large Si-O-Si bond angle that results from the semi-ionic character of the Si-O linkage. However, Passmore et al. [76] have highlighted the importance of hyperconjugation but assigned the inherent semi-ionic character of the Si-O bond as the dominant effect in the low basicity of Si-O.

The configuration of PDMS is described as a helix with the methyl groups shielding the polar Si-O-Si backbone and poorly interacting with each other (Figure 3.2) [13]. Such PDMS helical configuration has a preferential trans-configuration instead of a gauche-configuration [73]. The coiling of the siloxane molecule into a helix has been explained by the tendency of the weak Si-O dipoles to undergo intramolecular compensation, confirmed by the insignificant change of the dipole moment with an increase of the molecular mass of PDMS [73].

Due to the structure conformation and weak intermolecular interactions existing in PDMS, the surface tension, the boiling point, heat of evaporation and the viscosity are much lower than for common carbon compounds with similar molar mass. The high flexibility of polysiloxanes, which results from the long Si-O and Si-C bonds, high polarity of the Si-O bond, the lack of substituents at every second atom of the chain, and the low barrier of rotation around the chemical bonds, is responsible for the very low glass transition temperature of silicones, T_g~153 K [26,67]. Additionally, PDMS is considered hydrophobic and therefore useful as water repellent. Hydrolysis under Si-O-Si cleavage in neutral conditions is slow, requiring acid or base catalysis, whereas Si-C cleavage is not observed [67]. The main properties of silicones are shown in the diagram of Figure 3.3.

Due to the aforementioned unique and versatile properties, silicones have found a wide number of applications in most branches of industry involving synthetic materials such as sealants, lubricants, oils, surfactants, rubbers, coatings, adhesives with numerous substrates, as fire retardants and insulators in housing, as high temperature electrical insulators and as heat-resistant tubing and anti-foams, and as stationary phases in chromatography [19,22,26].

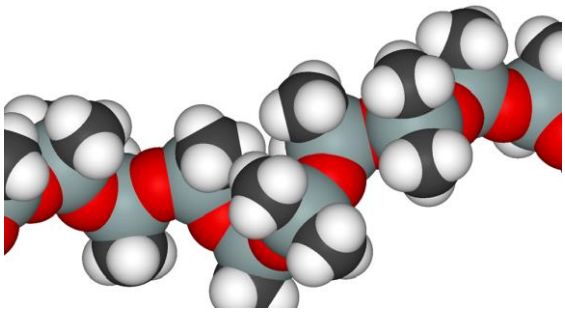


Figure 3.2. Three-dimensional representation of a PDMS molecule [25]. (O: red, Si: light gray, C: dark gray, H: white).

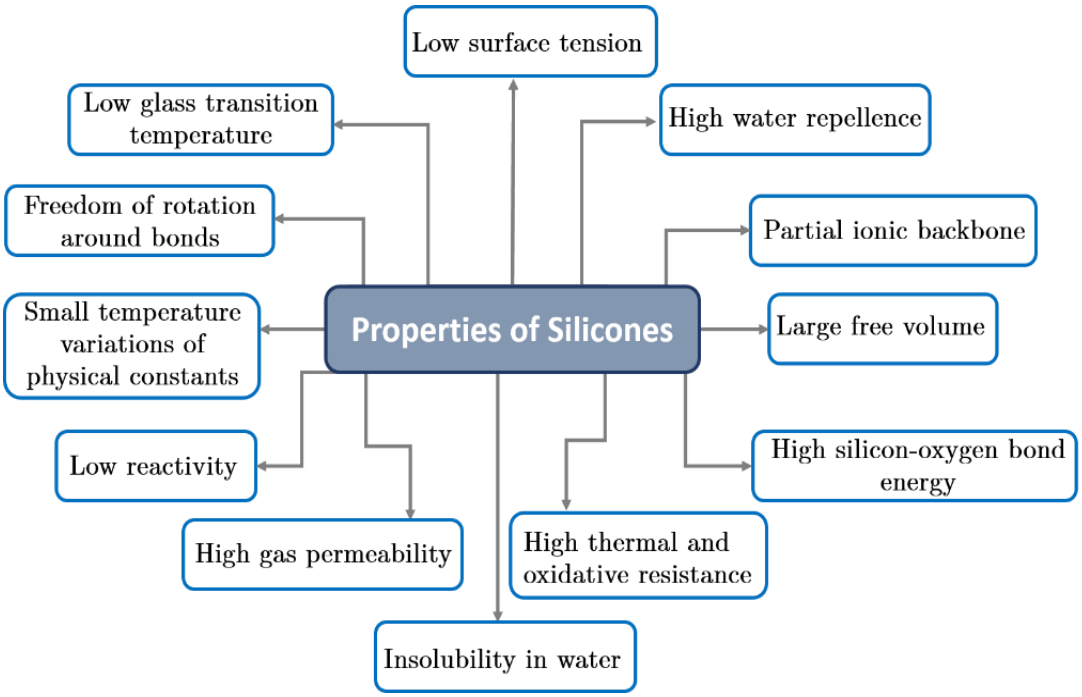


Figure 3.3. Principal properties of silicone materials [17]

The principal application fields of silicones are summarized in Figure 3.4. In the case of silicone adhesives and rubbers, the poor mechanical properties are compensated by reinforcing the silicone polymers with particulate material. Fumed silica is the most commonly used reinforcing fillers for these materials. Strong polymer-filler interactions are responsible for the improvement of the mechanical properties. In general silicone adhesives and sealants typically contain polymer, fillers, cross-linker, catalyst, and

other additives. Other fillers and pigments, such as carbon black and titanium dioxide, are also widely employed.

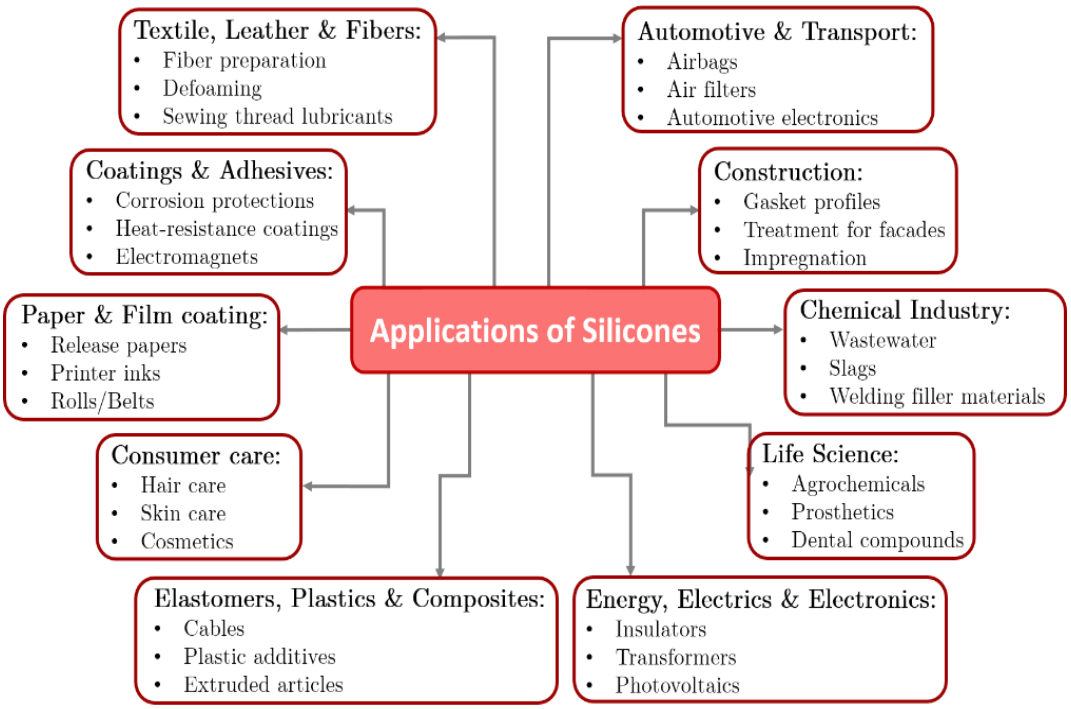


Figure 3.4. Principal applications of silicone materials [68].

3.2. Silicone crosslinking - Hydrosilylation

Silicone adhesives are commercially available as one- and multicomponent forms, although the one- and two-component types are the most widely used industrially [17]. These are silicones that cure at room temperature or higher, and are transformed into a three-dimensional (3-D) network by a curing or crosslinking reaction. The curing of silicones can be largely classified as radiation curing (free radical polymerization), thermal curing (polyaddition), or moisture curing (polycondensation) [13,17,19]. The free radical curing includes peroxide crosslinking, induced by decomposition of organic peroxides, and radiation crosslinking, activated by the action of an electron beam (EB) or UV radiation, either on the polymer itself or on a photoinitiator added to the system [13,19]. Alternatively, in polycondensation processes (moisture curing) groups present in the polymer such as hydroxyl, alkoxyl and acetoxyl are used to crosslink polysiloxanes [13,17]. The addition curing refers to the crosslinking of polysiloxanes

based on the catalytic addition of Si-H bonds to double bonds, normally known as hydrosilylation reaction [13,17,22]. The silicone system of interest in this work is an addition-curing silicone, therefore, crosslinking via hydrosilylation is the focus of this section.

Hydrosilylation is one of the most versatile, fundamental and widely employed reaction process available for the synthesis of silanes, siloxane compounds and organic silyl derivatives [77,78]. It is considered second in importance in silicon organic chemistry after the Rochow reaction. One of the advantages of this addition chemistry is that it does not produce cure byproducts, unlike the moisture curing process [13].

As with the Si-O bond, the nature of the Si atom affects the reactivity of the Si-H bond in silicone hydrides when added to multiple bonds.[79] The electronegativity of silicon is not only lower than carbon and oxygen but also lower than that of hydrogen, leading to a reversal in the polarity of the covalent $Si^{\delta+}$-$H^{\delta-}$ bond in comparison to the $C^{\delta-}$-$H^{\delta+}$ bond [63,79]. This allows silicon hydrides to undergo a nucleophilic attack on the silicon atom or an electrophilic attack on the hydride hydrogen. In addition, since the energy of this bond is lower in comparison to that of the C-H bond, homolytic cleavage of the Si-H bond leads to a radical mechanism for the substitution and addition reactions [79]. Therefore, the addition of the Si-H bond to unsaturated compounds proceeds either in the presence of free radical initiators (homolytic addition) or with catalysts through a heterolytic mechanism [79]. These catalysts may be nucleophilic, such as tertiary amines, Lewis acids, metal salts and Group VIII metal complexes.

Catalyst

In the early 1970's, Karstedt developed a platinum complex containing siloxane ligands which exhibited highly improved activity and selectivity as well as higher solubility in vinylpolysiloxanes and products of hydrosilylation in comparison to the Speier's catalyst (Figure 3.5a) [77]. The catalyst is well known as the Karstedt catalyst (Figure 3.5b). The development of this catalyst resulted in the wider application of hydrosilylation in silicon chemistry. Since then it remains as the standard system for the development of new hydrosilylation catalysts.

In general, Pt complexes are extremely active catalysts for hydrosilylation; the catalyst is often used at such low levels that it is not separated from the product. Due to economical reasons, recent efforts have been directed toward the development of new commercially viable nonprecious metal catalysts [80]. However, owing to their unparalleled catalytic activity, industry still relies largely on Platinum-based catalyst systems, especially on the Karstedt catalyst [77,80]. The development of a well-designed

catalytic system with higher selectivity and activity is still an intense research topic for obtaining more economical silicone products with superior quality properties.

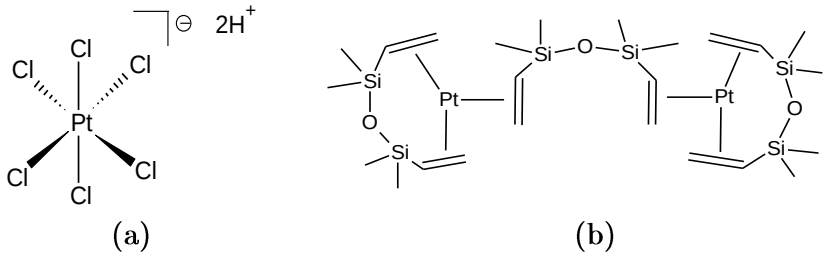


Figure 3.5. Principal Pt complex catalysts for hydrosilylation (a) Spier's catalyst (Hexachloroplatinic acid) and (b) Karstedt catalyst [81].

At ambient conditions, the Karstedt-catalyzed hydrosilylation reaction is typically fast, hence, inhibitors are commonly included in the silicone's formulation to allow easy handling and storage of the reaction mixture, to prevent premature crosslinking of PDMS, but to permit rapid platinum-catalyzed crosslinking reactions at higher temperatures [82].

Reaction mechanism

In spite of the high applicability in the industry, the exact mechanism of the Karstedt-catalyzed hydrosilylation is still not fully understood. In this regard, the hydrosilylation reaction has been widely investigated at the molecular level for many years and many efforts have been directed to clarify the reaction pathway [77,80,83–85]. The Chalk-Harrod mechanism, developed during the 1960s is the most often cited mechanism for hydrosilylation [77,79]. It is based on fundamental steps of organometallic chemistry. The understanding of the catalytic cycle has been difficult and slow, mainly due to the undefined nature of intermediates formed [80,86], and to some unexplained phenomena, such as the presence of an induction period (the time between the start of a chemical reaction and its observable occurrence), formation of colored bodies and co-catalysis by oxygen (kinetic data have suggested competing equilibria and requirement of oxygen) [80]. The model proposed by Chalk and Harrod is based on work using the Speier's catalyst and for the addition of Si-H to organic olefins, but is still widely accepted as the mechanism of hydrosilylation using most platinum catalysts. The Chalk-Harrod catalytic cycle for Karstedt-catalyzed hydrosilylation of silicones is presented in the reaction in Figure 3.6.

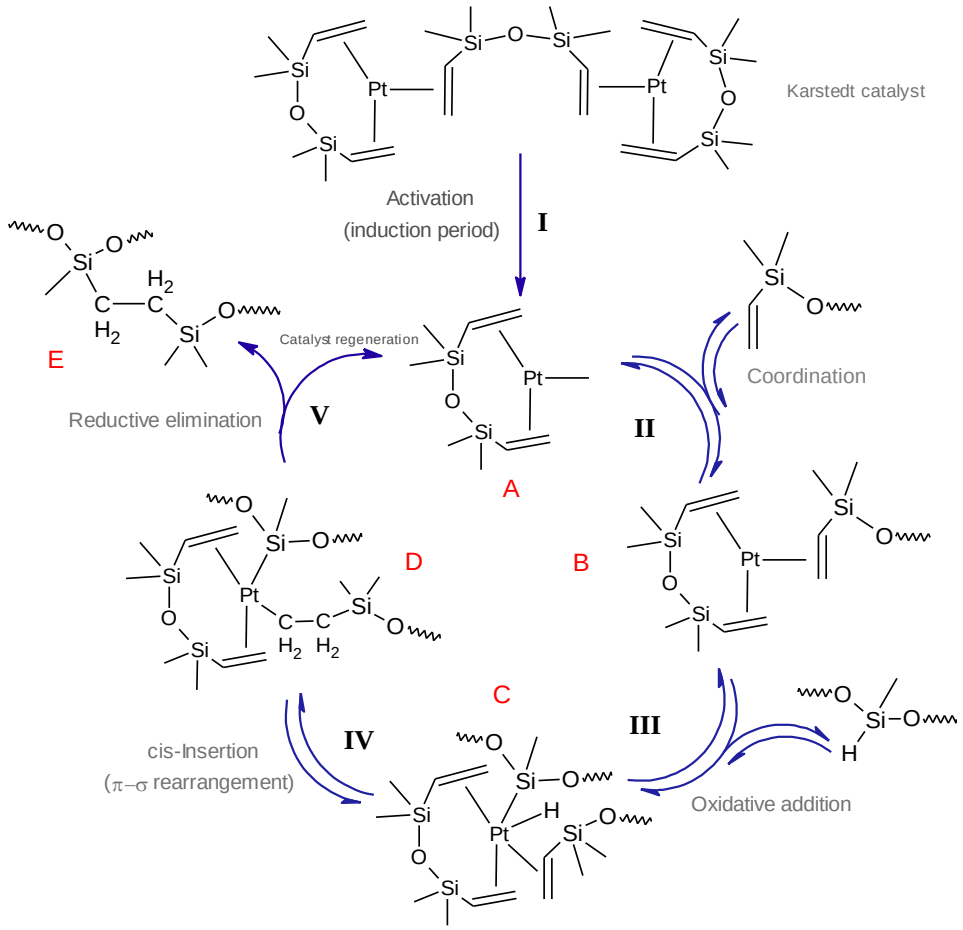


Figure 3.6. Chalk-Harrold mechanism for the Karstedt-catalyzed hydrosilylation reaction [22,80,86,87].

In the general scheme for the addition of silicon hydrides to the C=C bond in the Chalk-Harrod mechanism, five principal stages are involved and are described as follows [79,87]: **I.** Activation of the initial complex during the induction period obtaining complex A. **II.** Coordination of the unsaturated silicon-compound to the Pt center, forming complex B. Such coordination occurs as result of bonding involved a α-type electron donation from the double bond to the dsp^2 hybridized orbitals of the Pt, and a back-donation of electron density from the Pt orbitals to the antibonding π-orbitals of the double bond compound. **III.** Oxidative addition of the Si-H bond to the Pt center, producing complex C. The stability of complex C depends on the nature of the Pt ligands. **IV.** Reversible cis-Insertion of the double bond into the Pt—H bond (π-σ rearrangement), forming complex D. **V.** Reductive elimination of the hydrosilylation

product (Product E). Complex D reacts with more unsaturated silicon-compound regenerating the real catalyst (Complex B) and forming the organosilicon compound E. Steps II-IV are believed to be reversible, whereas step V is considered to be the rate-determining, irreversible step.

Hydrosilylation reactions are usually performed with excess of Si-H groups in order to drive the reaction to completion. The addition of silicon-compounds containing methyl substituents at Si atoms to the double bond in most Karstedt-catalyzed hydrosilylation reactions means that the product is almost exclusively β-addition or anti-Markovnikov, creating ethylene (-CH_2-CH_2-) bridges [79,86,88]. However, traces of α-addition (Si-(CH-CH_3)-Si) have been occasionally observed. The formation of the anti-Markovnikov product indicates insertion of the olefin into the Pt–H, rather than into the Pt–Si bond. The intermediates on the Chalk-Harrod cycle are reactive and short-lived and their isolation is difficult [86]. Thus, complexes of type A in the Chalk-Harrod cycle are still not well-defined.

General aspects concerning the Chalk-Harrod mechanism have been determined by Meister [80], from the works of Lewis and Stein [83,84], Roy and Taylor [89], and others [77], they are: **(i)** the reaction proceeds homogeneously, **(ii)** the active species contains Pt−Si and Pt−C bonds, **(iii)** vinyl insertion into the Pt−Si bond is not facile **(iv)** oxygen exerts a beneficial effect on hydrosilylation of poorly coordinating olefins through prevention and/or destruction of multinuclear platinum species associated with catalyst deactivation.

3.3. Adhesion mechanisms of silicones – State of the art

The various types of intrinsic forces existing across the interface of two materials are commonly referred to as the mechanisms of adhesion [90]. Unfortunately, investigation of the molecular structures at the interface is very challenging due to limitations of appropriate analytical techniques [91,92], therefore, mechanisms of adhesion are still not fully understood. Four main mechanisms of adhesion have been widely discussed, in the literature they are: a) mechanical interlocking, b) diffusion theory, c) electronic theory and d) adsorption theory [90,91]. The adsorption theory is the most generally accepted [91], since it involves intermolecular forces between adhesive and substrate such as dipole-dipole interactions, van der Waals forces, coordinating interactions and chemical interactions (ionic, covalent and metallic binding) [4,90,91]. Nowadays, a thermodynamic mechanism has also been included and adsorption theory has been

better denoted as molecular bonding [4]. The emphasis of this review is to give a compact state of the art regarding the adsorption or adhesion of PDMS on different substrates, and to describe some of the proposed mechanisms of adhesion based on adsorption theory or molecular bonding.

3.3.1. Adhesion of PDMS

Pioneering investigations of PDMS at interfaces date back several decades to the work of Hunter and coworkers in 1947 [93], who studied PDMS films deposited onto hydrochloric acid solution, water and glass. They found that on hydrochloric acid solution, the polymer molecules were oriented with respect to the aqueous surface. They suggested an ion-dipole interaction between HCl and the Si-O bonds, enhanced by a strong dipole-dipole interaction between the water centers and terminal OH groups of PDMS. They also found that on water, polar centers (siloxane segments) were concentrated on the film-water interface. On the glass surface, they observed that PDMS layers were firmly adhered. The authors suggested dipole association or hydrogen bonding of the Si-OH in PDMS to the Si-O-Si or SiOH groups of the glass and viceversa. They also proposed a possible condensation reaction between OH groups present on both PDMS and the glass surface. In addition, they have suggested a possible conformation of the polysiloxane on the water surface with methyl groups oriented outwards. In the same year, Fox et al. [94] also evaluated the behavior of PDMS onto water and glass. The authors concluded that the energy of adhesion was maximized when silicone molecules were completely uncoiled and the Si-O bonds were in contact with the surface. They suggested electrical attraction due to the polarity and semi-ionic nature of the Si-O bonds.

Significant contribution to this subject was given more than a decade later by Perkel and Ullman in 1961 [32], who proposed two main possible adhesion mechanisms based on the adsorption of PDMS from solution on oxidized iron spheres and Pyrex glass. The study included PDMS of different molar mass, and various solvents differing in chemical nature and affinity to PDMS. The authors found that the amount of adsorbed PDMS was sensitive to the presence of moisture and the presence of Si-OH terminal groups. They also observed that the adsorption increased with molar mass and strongly depended on the nature of the solvent used. They proposed three main mechanisms: **1)** Si-O-Si linkages of PDMS oriented parallel to the surface, which adsorbed strongly due to dipole-dipole interactions with the Si-O-Si bonds of glass, and **2)** adsorption occurred between the oxygen of OH groups on the polymer and a hydroxyl linkage on the silica. They claimed mechanism 1 to be more efficient than 2,

and **3)** stress relaxation mechanism due to bond or chain interchange over time between Si-O-Si linkages of PDMS and Si-O-Si bonds in silica.

Later in 1967 Sato et al. [95] examined the adsorption of PDMS on polar (titanium dioxide, chrome yellow and red iron oxide) and nonpolar (carbon black and phthalocyanine blue) pigment particles. Although they did not propose mechanisms of adhesion, they suggested that PDMS oriented at the interface with adsorbing Si-O groups on the polar surface and extending CH_3 groups into the nonpolar (or weakly polar) liquid. In contrast, they found that PDMS adsorbed more on the nonpolar substrates.

Shortly after, in 1968, Jemmet [30,31] evaluated the chemical behavior of siloxanes at metal interfaces by FTIR spectroscopy. In a first study [30], six different siloxanes were examined on steel. The author concluded that siloxanes in prolonged contact with steel at high temperatures (150 °C) formed a strong adherent coating, which resulted from the interaction of the metal surface and the oxygen in the siloxane molecule. His deductions were based on remarkable changes of the IR absorption bands related to Si-O-Si linkages. The author claimed that the formation of a coating might be assisted by the presence of electron donor substituent groups in the siloxane, since dimethyl siloxane formed such a coating more rapidly than, for instance, methyl chlorophenylsiloxane. In a second study, the author used different polysiloxanes on aluminum, cadmium, mild steel, stainless steel, copper alloy and copper. He found that the ease of formation of a bonded coating was connected to the oxidation state of the metal, while the strength of the metal-siloxane bond was related to the chemical structure of the siloxane and the thickness of the bonded coating. He suggested that the hyperconjugation effect associated with the methyl groups in PDMS increases the electron density at the oxygen on metal bond and thereby strengthens it, whereas aryl/methyl substituents at the silicon atom lower the electron density at the oxygen to metal bond and hence, the bond is weakened.

In 1971, Ashmead and Owen [49] examined the adsorption of PDMS from solution on Pyrex glass powder. They used different solvents, eight trimethyl terminated PDMS samples of diverse molar mass (five self-synthesized and three commercial), and one hydroxyl terminated PDMS polymer. The findings of the authors were consistent with those found by Perkel and Ullman [32]. They supported the hypothesis that adsorption is greatly affected by the type of solvent and by the molar mass of the PDMS samples. The authors finally proposed three different mechanisms: **1)** dipole-dipole interactions between Si-O-Si bonds in PDMS and those in the glass, **2)** adsorption of the silanol containing materials through a hydrogen-bonding mechanism between hydroxyls on the

surface, and **3)** interaction with the surface through the surface hydroxyl groups and the oxygen of the Si-O-Si bond in PDMS.

In 1967 and 1977, Eltekov [96,97] investigated the adsorption of polymers from dilute solutions on porous and nonporous adsorbents of different chemical nature. The author attributed the positive adsorption of PDMS onto porous hydroxylate silica to interactions of the siloxane units of the chains with hydroxyl groups of the silica surface, and from non-specific interactions (caused mainly by dispersion attraction forces).

Later in 1981, Berrod et al. [98], studied the interactions between cyclic and linear oligosiloxanes on fumed silica at 150 °C via FTIR spectroscopy. Their observations were indicative of a chemical reaction between the free silanol groups of the filler (silica) and the siloxane. No hydrogen bonding interaction was found. They proposed a series of mechanisms involving opening the siloxane ring of the cyclic compounds and further condensation of the newly formed OH terminal groups in siloxanes with OH bonds on the silica surface. They also speculated that siloxane bond cleavage of the linear siloxanes by OH groups of the silica leads to the formation of shorter OH terminated siloxanes that can undergo further condensation with silanols of the silica. They also suggested a reaction of water (hydrolysis) not only with cycle siloxanes but also with linear chains, yielding in both cases to hydroxylated compounds which could also be involved in condensation either with the surface or other hydroxylated siloxane molecules.

In the 1990s, the investigation of the adhesion of PDMS was intensified due to the growing importance in understanding the mechanisms of adhesion of silicones. Significant contribution to the subject was given by Cosgrove and coworkers [33,34,50,99,100] who have intensively studied the adsorption behavior of cyclic and linear PDMS on silica and alumina from solution and melt at room temperature. They have proposed a mechanism of adhesion for poly(hydrogen-methylsiloxane) in which Si-H moieties undergo condensation with OH groups on the surface, eliminating molecular hydrogen and becoming chemically bound to the surface after one week of contact. For cyclic siloxanes, they have proposed physisorption, while for block PDMS copolymers they have found both chemisorbed and physisorbed segments, depending on the number of segments in the molecule. They have also suggested that interaction between PDMS and silica is strong due to hydrogen-bonding, which under certain conditions can lead to chemisorption. Very important input was given by the study of different end-functionalized PDMS samples on fumed silica and alumina from solution. The results showed the following order of adsorption for the different terminal groups on both silica and alumina substrates: -OH>H>CH_3>CH=CH_2. They have suggested that interactions between PDMS and silica from non-aqueous solution occur through

weak hydrogen bonds between surface hydroxyl groups and the oxygen of the Si-O-Si bonds in PDMS. Two main mechanisms were proposed: **1)** adsorption of trimethyl terminated PDMS due to physisorption through Si-O bonds of PDMS and Si-O linkages on silica, and **2)** interaction of OH terminated PDMS via hydrogen bonding with hydroxyl groups on a silica surface. They suggested that chemical bonding due to condensation of OH groups of the polymer and the surface can occur extensively at higher temperatures and in the presence of a catalyst.

Later in the 2000s, Barthel and coworkers [101–105] focused on investigating the role of different interactions at the interface of PDMS and silica via IR spectroscopy and inelastic neutron scattering (INS). In terms of interaction energies, classical hydrogen bonding was described by the authors as exhibiting a minor contribution, while van der Waals forces were claimed to govern the system. In particular, Si-O dipole interactions were reported as playing the dominant role.

More current work includes the study of adhesion mechanisms of PDMS on substrates different to those commonly used before. The study was directed to the investigation of possible interactions between liquid crystal polymer (LCP) and silicone adhesive. It was carried out in 2012 by Lie et al. [106]. They found that covalent bonding did not occur, and the system was instead governed by hydrogen bonding interactions.

Further studies have been carried out since then. They strongly support the mechanisms that have been proposed throughout the last 70 years. A compilation of relevant literature regarding the adsorption of PDMS is given in Table 3.2, organized for different substrates. In addition, an illustration of the proposed and sketched mechanisms of adhesion of silicones given by Perkel and Ullman [32], Patel et al.[34], and Ashmead and Owen [49], is presented in Figure 3.7.

Table 3.2. Literature sources of relevant studies regarding the adhesion of PDMS.

Substrate	References	Substrate	Reference
Silica	[34,35,97,107–113]	Carbon black	[95,97]
Aluminum	[34,99,114,115]	Aluminum	[27,31,116]
Glass	[32,49,50,117–123]	Gold	[124–126]
PDMS	[127,128]	Zinc	[129]
Other Polymers	[106,122,130]	Cooper	[31,131]
Water	[51,132]	Iron	[32,95,120]
Silicon	[126,133–135]	Silver	[136,137]
Steel	[30,31]	Other	[31,50,138]
Titanium dioxide	[95–97,108,139]		

As concurrence of different mechanisms of adhesion is most likely to be observed in the adhesion of silicones, determination of which mechanism prevails is not straightforward. Attempts have been made to better understand the role of such interactions, although opposing arguments have also been given. In some studies, irreversible or strong adsorption was observed and was attributed to a dominant hydrogen bonding mechanism [30,31,34,35,98,117,126]. However, quantum chemistry calculations have yielded results contradicting H-bonding (except for hydroxyl terminated siloxanes) [122,140]. Infrared spectroscopy and inelastic neutron scattering experiments support this statement. They suggest that dominant interactions between PDMS and silica surface include permanent-induced Si-O-Si dipoles and non-specific Van der Waals interactions, rather than strong H-bonding [102,105]. The controversy is still open and unresolved.

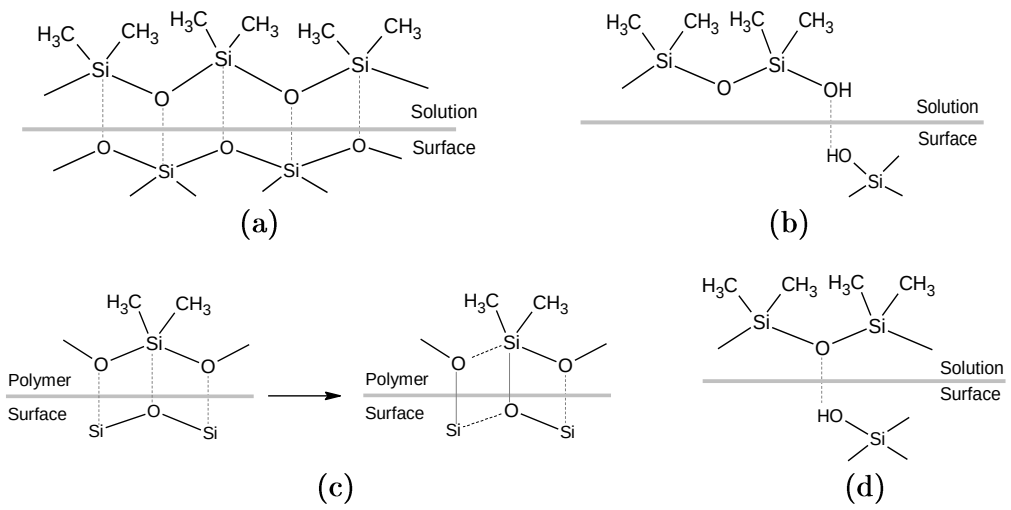


Figure 3.7. Illustration of the mechanisms of adhesion of PDMS onto glass and silica as proposed and sketched by Perkel and Ullman (a.b,c) [32], Ashmead and Owen (a,b,d) [49] and Patel et al. (a,b) [34].(a) dipole interactions, (b) hydrogen bonding for OH terminated PDMS, (c) stress relaxation mechanism due to chain interchange, and (d) interaction between Si-O-Si bond of PDMS and OH groups of the surface.

3.3.2. Adhesion of Silanes

Organosilanes have been widely employed in adhesive technology as adhesion promoters or primers for many decades [141], principally because they have the ability to migrate to the substrate interface and improve bonding [47]. Organosilanes are defined as hybrid

molecules with at least one hydrolysable alkoxysilane group [48]. The hydrolyzed silane should be able to react with both the polymer and the substrate, thus forming durable covalent bonds across the interface. It has been proposed that these bonds are hydrolyzable, but can reform. This fact provides a means of stress relaxation at the organic/inorganic interface [47], which improves the adhesion and durability at the interface. Typical silanes include the alkoxysilane groups at one end and an organic functionality at the other [48]. The general formula is R'-Si$(OR)_3$, where R' corresponds to the main chain (or organic functionality) and OR is the hydrolysable alkoxy group. A general well-accepted mechanism of adhesion of alkoxysilanes (Figure 3.8) on hydroxylated surfaces (such as metals) has been widely discussed in the literature. The mechanism of adhesion between alkoxysilanes and a hydroxylated surfaces involves four main steps [47,48,142–146], described as follows:

- **I. Hydrolysis:** the alkoxy groups present on the silane molecule are converted into silanols (-Si-OH) with the production of alcohol. This is a vital step in the adsorption of silanes. Hydrolysis is usually preferable, although it is not obligatory that the molecule should be hydrolyzed prior to bonding [48]. The kinetics of hydrolysis depend on the ease of hydrolyzing the alkoxy, which is affected by steric hindrance of the alkoxy groups.
- **II. Condensation:** two types of condensation are possible. One is self-condensation, while the other is condensation with a hydroxylated surface (step IV) [48]. The condensation step leads to the formation of a siloxane polymer network with Si-O-Si bonds and with the loss of water. The self-condensation reaction can be controlled by using fresh solutions, alcoholic solvents, dilution, and by careful selection of pH ranges [47].
- **III. Hydrogen bonding:** Compared to the hydrogen of a carbinol moiety, the silanol hydrogen is more electrophilic and much more reactive due to the larger, more electropositive atomic structure of silicon. This results in a high dipole moment for the silanol group, which favors the formation of hydrogen bonding [47]. Thus, formation of hydrogen bonds between the silanol groups of the formed polysiloxane and the hydroxyl groups of the substrate hydroxides usually occur [142].
- **IV. Bond formation:** the last step is the formation of covalent bonds between the OH groups on the surface and the siloxane bonds of the polymer network. This is a critical step, which in many cases requires thermal or catalytic activation [142].

Important variables of the hydrolysis and condensation steps, such as reaction conditions, kinetic considerations and the reaction mechanism, have been well documented [147–153]. The adhesion and adsorption of silanes on numerous substrates has also been widely investigated by numerous authors [143,153–163]. Moreover, silanes can also be employed under anhydrous conditions, i.e. no hydrolysis and condensation steps are involved. In this case, the silanes are bonded directly to the desired substrate. However, long reaction times (4-12 hours) and elevated temperatures (50°-120°C) are typically required. Among the alkoxysilanes available, only methoxysilanes are effective without catalysis [164].

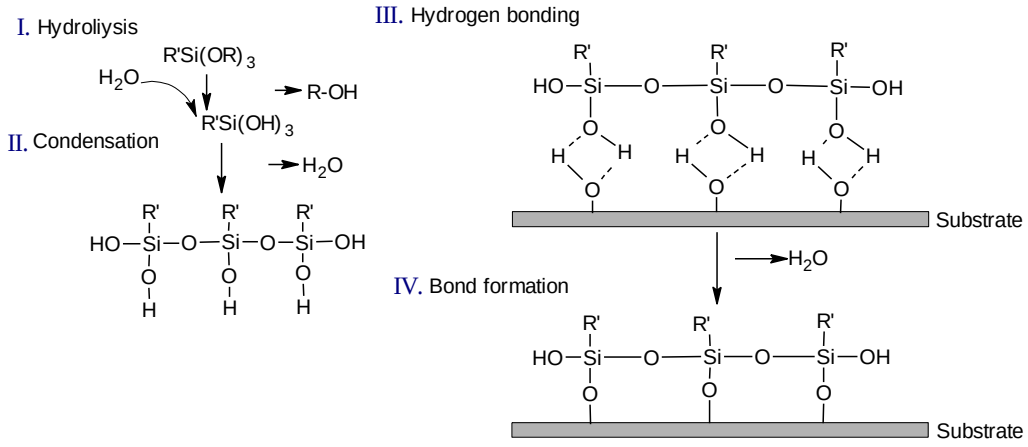


Figure 3.8. Mechanisms of adhesion of organosilanes on hydroxylated surfaces [47,48,142–146].

4 Characterization of Silicone in Bulk

4.1. Goal and methodology

Typical commercial silicone adhesives are formulated as complex mixtures containing a variety of components such as PDMS polymers, fillers, additives, catalysts, and adhesion promoters, among others. When silicones are cured (Figure 4.1), multimodal networks with different crosslink sites, physical entanglements, free chains, and filler phases influence and control the overall network properties and final performance of the product [165]. Therefore, elucidating adhesion mechanisms from interfacial analysis using a commercial silicone would be, apart from challenging, inaccurate. Thus, individual analyses employing single silicone model components (SSMC) were implemented as an alternative. The characterization in bulk of the commercial silicon was, therefore, indispensable for selecting appropriate single components. In addition, the characterization in bulk of the SSMC was crucial for interfacial analysis.

This chapter presents the characterization of the bulk properties of the commercial silicone adhesive (CSA), the single model components (SSMC) and the formulated model silicone adhesive (FMSA). First, the uncured CSA was characterized and the components exclusively involved in crosslinking, i.e. crosslinker, PDMS polymer, catalyst, and adhesion promoter, were selected. Exact recognition of the total components of the CSA was beyond the scope of this study. In addition, the cured CSA material was examined for evaluating network properties that could be related to bonding analysis of adhesive joints. Subsequently, the chemical quality of the selected SSMC was evaluated with the aim to correlate the bulk- and adsorbate-states. Finally,

a basic model silicone (FMSA) was formulated and the obtained polymer network was characterized to observe the influence of additional components on the thermal properties of a silicone. The course of the crosslinking reaction of the FMSA, with and without a catalyst, was also monitored in-situ.

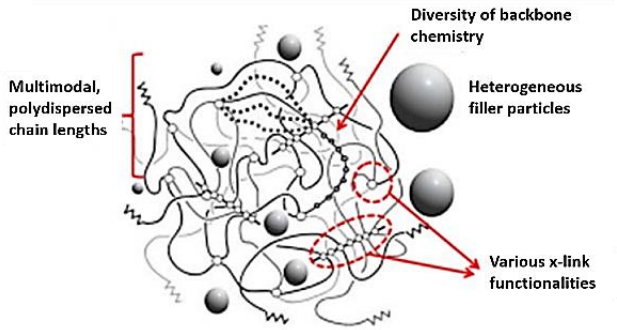


Figure 4.1. Illustration of a typical silicone network configuration with highlighted complexities associated with this type of system [165].

Methodology

The main part of this chapter is devoted to the chemical characterization, the principal method employed for this purpose was ATR-FTIR spectroscopy since it allows the determination of the molecular structure in a relatively simple and rapid way. Specifically, in the case of silicone products, IR absorption bands with intensities five to ten times greater than those of organic compounds converts ATR in a very effective technique for their analysis [166]. NMR spectroscopy was also implemented for supporting and complementing the results obtained via ATR-FTIR. NMR methods offer valuable and detailed information regarding the chemical structure of a compound through the identification of functional groups, their molecular environment and position. The principal advantage of the two aforementioned techniques was their implementation without the strict requirement of physical separation.

Additional techniques were applied for further characterization of the materials in bulk. Gel permeation chromatography (GPC) was employed for obtaining the molecular weight distribution curves and for determining the molar masses. The thermoanalytical technique TGA (thermogravimetric analysis) was implemented for evaluating the thermal stability of the CSA and FMSA in a determined temperature range and in two different atmospheres. Differential scanning calorimetry (DSC) was included for

exploring the phase transitions of the material and for monitoring the crosslinking reaction of the CSA. Table 4.1 and 4.2 compile the techniques employed for the characterization of the different silicone materials.

Table 4.1. Purpose of the chemical characterization of the CSA, SSMC, and FMSA.

Product		Chemical characterization	
		ATR-FTIR	NMR
CSA	Uncured	• Identification of functional groups	• Corroboration of functionalities and their molecular position. Recognition of traces • Estimation of Si-vinyl/Si-H molar ratio for the formulation of FMSA
	Cured	• Acquisition of the chemical state of the polymer network formed after curing • Evaluation of the crosslinking path by comparing uncured and cured spectra. (In-situ measurement, unfeasible at T>RT)	
SSMC		• Verification of the chemical structure of the purchased products • Purity control • Bulk spectrum of each SSMC necessary for calculating a bulk-like spectrum in the FTIR-ERAS configuration	• Verification of chemical structure • Purity control • Estimation of the number average molar mass, M_n (if applicable)
FMSA		• Monitoring the crosslinking reaction at RT by in-situ measurements with and without catalyst • Analysis of the crosslinked product	• Examination of chemical properties of the polymer network (Solid state NMR)

Table 4.2. Additional methods employed for the characterization in bulk.

Sample		Additional characterization		
		GPC	TGA	DSC
CSA	Uncured	• Acquirement of molar mass distribution curve • Estimation of M_w, M_n, and PDI	• Evaluation of thermal and thermo-oxidative stability • Possible recognition of filler	• Study of crosslinking reaction. • Validation of curing conditions
	Cured		• Analysis of thermal and thermo-oxidative stability	• Evaluating post-curing reaction • Determination of phase transitions (T_g, T_m, T_c)
SSMC		• Acquisition of the molecular weight distribution curve • Estimation of M_w, M_n, and PDI		
FMSA			• Analysis of thermal and thermo-oxidative stability • Observe effect of filler on thermal stability of silicones	• Inspecting completion of crosslinking reaction • Identification of phase transitions (T_g, T_m, T_c)

4.2. Chemical characterization - Experimental

In this section, a brief description of the principles of operation of each technique is given first, followed by the experimental procedure implemented.

4.2.1. ATR-FTIR Spectroscopy

4.2.1.1. Theoretical considerations

As defined by Smith [166],"infrared spectroscopy is the study of the interaction of infrared light with matter". ATR-FTIR is an essential and versatile technique used to elucidate the structure of matter at the molecular scale. It has found innumerable applications for the analysis of an extensive variety of samples since the only requirement is that the sample surface is in good contact with the internal reflection element (IRE). Therefore, almost all types of materials including polymers, powders, films, solutions, and gels can be easily characterized with the advantage of simple or no sample preparation [166–168]. The IRE object is usually a polished face of diamond, germanium (Ge) or zinc selenide (ZnSe) crystals. For polymers, ATR-FTIR is routinely applied to obtain both chemical composition and bonding arrangements [167,168].

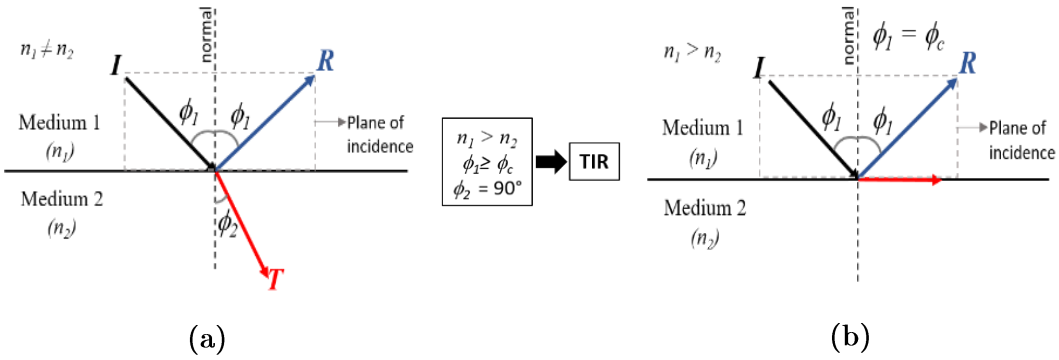
Radiation in the mid-IR spectroscopic range (400-4000 cm^{-1}) is characterized by its wavenumber ν [cm^{-1}] that is related to the wavelength λ [μm], angular frequency ω [s^{-1}] and to the velocity of electromagnetic radiation in vacuum, c_o, by:

$$\nu = \frac{1}{\lambda} = \frac{\omega}{2\pi c_o} \tag{4-1}$$

When a sample, represented as a system of oscillators with resonance frequencies $\nu_{o,i}$, is irradiated with IR light, photons with frequencies $\nu = \nu_{o,i}$ will be absorbed and eliminated from the initial composition of the radiation; thus, the measurements of the disappearing intensity as a function of ν (absorption spectrum) enable to extract microscopic information about the material as molecular structure, conformation, intra- and intermolecular interactions, or crystal-field effects [45].

ATR-FTIR method is based on a phenomenon known as total internal reflection (TIR). In general, if an electromagnetic wave is irradiated at the interface of two different optical media, one portion of the radiation is reflected and the other is refracted (Figure 4.2a). However, when the radiation passes through a medium with a

higher refractive index into another with lower refractive index, total internal reflection occurs if the incident angle is larger than the "critical angle" ϕ_c, [169,170]. In this case, the radiation is "trapped" and no refraction takes place (Figure 4.2b).



(a) (b)

Figure 4.2. (a) internal reflection and (b) total internal reflection (TIR). I: incident, R: reflected- and T: transmitted- radiation [169].

The angle of incidence, ϕ_1, and the angle of refraction, ϕ_2, are measured with respect to the surface normal and are related to n_1 and n_2 refractive indexes of medium 1 and 2, respectively, according to the Snell's law given below [169,170]:

$$n_1 sin\phi_1 = n_2 sin\phi_2 \tag{4-2}$$

When TIR occurs, it implies that $\phi_2 = 90°$ and thus, radiation is not refracted (Figure 4.2b). The critical angle of incidence ϕ_c can be therefore calculated exclusively from the refractive indexes of the media involved as observed in Equation 4-3.

$$\phi_c = sin^{-1}\left(\frac{n_2}{n_1}\right) \tag{4-3}$$

Consequently, for assuring TIR, the angle of incidence must be set at higher values than the critical angle ϕ_c. This condition is also favorable for obtaining more intense spectra since the noise level is decreased, *i.e.* the signal-to-noise ratio S/N is increased [171,172].

Since ATR-FTIR operates under the principle of TIR, the electromagnetic field *E*, outside the IRE, must be non-propagating and no energy loss must occur. Hence, *E* extends beyond the reflecting interface in a so-called "evanescent wave" (Figure 4.3) [43,172]. The evanescent wave interacts with the sample absorbing energy and in that way, a spectrum of the sample is obtained. The non-propagating evanescent wave decays in amplitude from the reflecting interface towards the sample and even though no energy is withdrawn from this evanescent field, energy is extracted. This event constitutes the basis of the ATR-FTIR technique [43,172]. The decay of the field amplitude inside the less dense medium is exponential, as defined in Equation 4-4 [43,169,170,172].

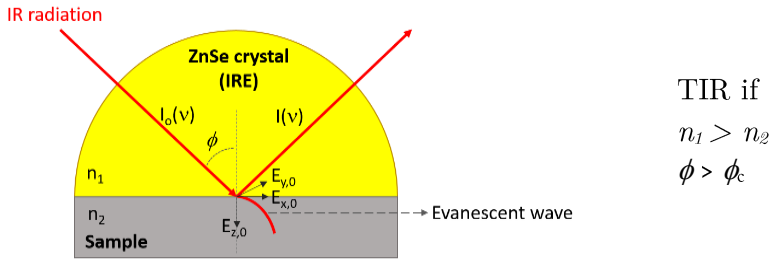


Figure 4.3. ATR-FTIR configuration. The radiation propagates through the IRE as a reflected wave and penetrates the sample as a non-transverse, exponentially decaying field (evanescent wave) [43,52].

$$E = E_0 \cdot exp\left[-\frac{2\pi}{\lambda}\left(sin^2\phi - \left(\frac{n_2}{n_1}\right)^2\right)^{1/2} Z\right] \qquad \textbf{(4-4)}$$

Where *E* is the amplitude of the field in the sample at depth Z and E_0 is the field amplitude at the sample surface (z = 0) [172]. It would be expected that the evanescent wave decays to zero intensity at infinite depth according to Equation 4-4; however, in reality, it does not occur, and the evanescent wave decreases to relatively negligible intensity at fairly small depths [172]. This means that in ATR-FTIR, the radiation only interacts with the sample at a superficial layer of few micrometers deep, avoiding propagation through the entire sample [166,171,172]. The penetration depth d_p defined in Equation 4-5, represents the distance from the surface of the sample that the radiation penetrates [43,170,172]. The resulting spectrum is extracted from this penetration depth, d_p.

$$d_p = \frac{1}{2\pi n_1 \nu \sqrt{sin^2\phi - \left(\frac{n_2}{n_1}\right)^2}} \quad (4\text{-}5)$$

d_p is independent on the polarization type of the incident radiation. It should be noted that the spectral information is the average obtained for the exponentially decaying evanescent wave. In effect, the evanescent wave can "bridge" an air gap of up to several micrometers, thus, good but not perfect physical contact of the sample with the IRE must be ensured [172]. The fact that the incident radiation does not pass through the sample gives ATR-FTIR a great advantage in analyzing thick, opaque, colored or filled samples. Due to its sensitivity at few micrometers from the surface, the ATR technique is ideal for studies in which the components of interest are mainly concentrated near the sample surface. On the other hand, ATR-FTIR has limitations in detecting additives or substituents present in small concentrations as they may be overlooked [173]. Also, the technique is not very sensitive to differences in molecular weight or molecular weight distributions of polymers, factors which may have a significant effect in their characterization [173].

4.2.1.2. Experimental procedure

The ATR-FTIR measurements were carried out in a Bruker IFS 66v/s FTIR spectrometer (Bruker AG, Germany). Total internal reflection (TIR) was ensured with a ZnSe crystal (hemisphere) as IRE (refractive index, n=2.4) and by adjusting the angle of incidence to 60 ° ($\phi > \phi_c$). Moreover, the signal-to-noise ratio (S/N) was increased by setting the number of scans to 500. The resolution of the obtained spectra was 4 cm^{-1}, and *p*-polarized IR light was applied for irradiating the samples. Additional experimental parameters can be found in detail in Appendix A. The software tool OPUS® (Bruker AG, Germany) was utilized for setting up the variables in the apparatus and for collecting the spectra. OriginPro® 8.6 was employed for further processing of the data. The standard experimental procedure for ATR-FTIR measurements consisted of three main steps summarized in Figure 4.4. In total, 9 spectra for a single substance or product were measured. The montage of the samples for ATR-FTIR analysis varied according to the type of material being characterized, as described in Figure 4.5a-c.

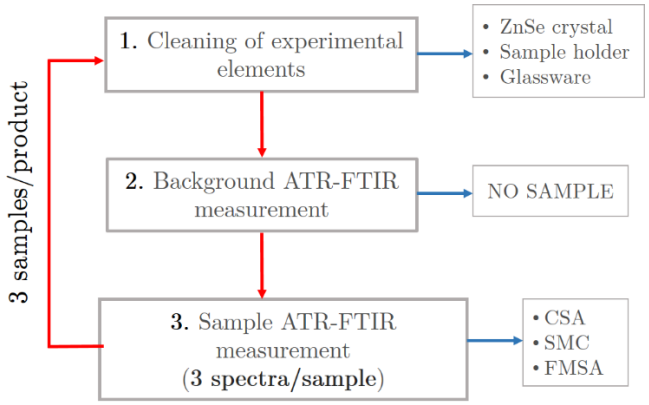
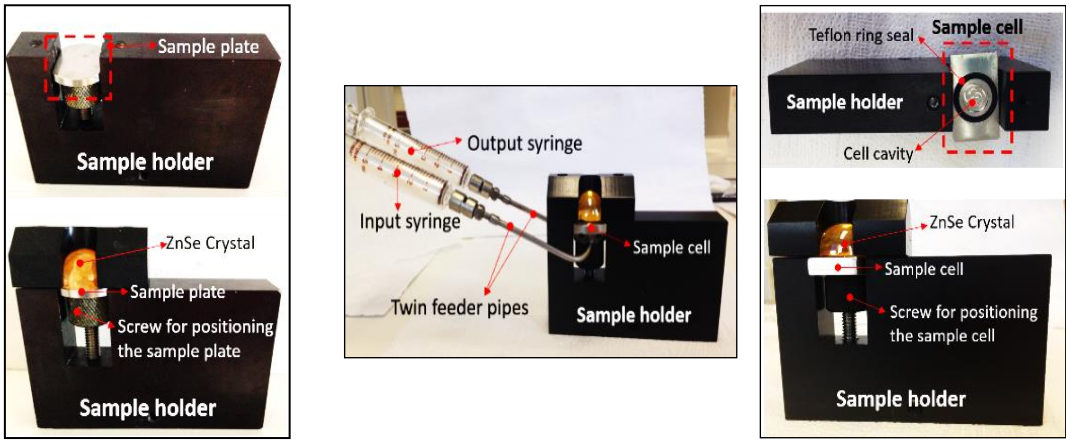


Figure 4.4. Standard procedure applied for the ATR-FTIR measurements



(a) (b) (c)

Figure 4.5. ATR-FTIR experimental setup for different type of samples (a) plate for analysis of solid samples as the cured CSA and crosslinked FMSA, (b) sample cell equipped with syringes for the analysis of liquid samples such as the SSMC, and (c) sample cell for monitoring crosslinking of the FMSA. The uncured CSA was directly spread on the base of the ZnSe crystal.

4.2.2. NMR Spectroscopy

4.2.2.1. Fundamentals

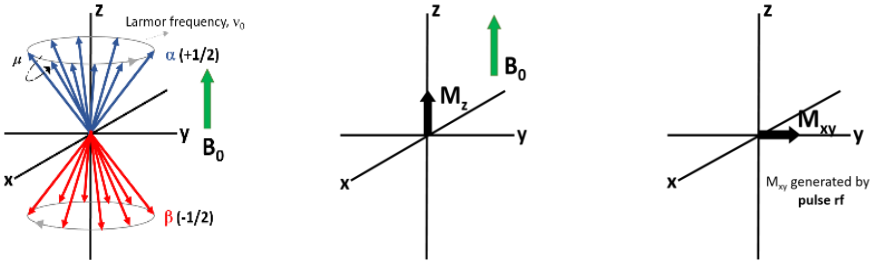
For silicone materials, NMR is a versatile tool for evaluating complex formulated products, and for analyzing elastomeric networks formed after crosslinking [2,165,174–176]. The main reasons include: **(i)** individual chemical groups usually give signals that

can be resolved, **(ii)** the NMR signals are sensitive to environment, and **(iii)** the relationship between spectral parameters and the information of interest (such as concentration or structure) is relatively straightforward [2]. Advanced multi-dimensional methodologies combined with isotopic enrichment allow the elucidation of the structure in multicomponent silicones since the elemental constituents are NMR-active nuclei (^{1}H, ^{13}C, and ^{29}Si) [165,174,175]. Additionally, standard 2-D (two-dimensional) NMR methods such as COSY (Correlation Spectroscopy), HSQC (Heteronuclear Single Quantum Coherence) and HMBC (Heteronuclear Multiple-Bond Correlation Spectroscopy) are also applied to characterize complex multicomponent mixtures and soluble siloxane polymers from low to moderate molecular weight [165,177].

NMR technique is based on the capability of certain atomic nuclei, that when charged positively, can spin on an axis with spin I (spin angular momentum) creating a small magnetic field with magnetic moment μ [178,179]. There are $2I+1$ stationary spin states for a nucleus, corresponding to the direction of the angular momentum relative to an arbitrary axis z. Nuclei with spin I=½, have two spin states identified by the eigenfunctions, $\alpha \geq (m_I = ½)$ and $\beta \geq (m_I = -½)$. The two states are energetically equal; thus, the nuclei are just as likely to have a spin state of α as of β [174,179,180]. However, in order for a magnetic nucleus to absorb and emit electromagnetic radiation, an energy difference ΔE between the two spin states must exist. The required energy difference (ΔE) between α and β is created when the spins are exposed to an external magnetic field, B_0. In that way, the spins acquire two types of orientation respect to B_0: parallel (lower energy) or antiparallel (higher energy) (Figure 4.6a) [174,176]. As soon as ΔE is created, the nuclei are capable of absorbing energy. This absorption occurs when a nucleus is excited from state α to β by an energy quantum of ΔE (Equation 4-6), in the case of NMR, by radio frequency (radio waves) pulses [174,176].

$$\Delta E = \frac{h\gamma B_0}{2\pi} \quad with \ \ v_0 = \frac{2\mu B_0}{h} = \frac{\gamma B_0}{2\pi} \tag{4-6}$$

Where h: Planck's constant, v_0 is the frequency in Hz of the radiation which results in resonance of the nuclei (also called Larmor frequency) and γ is the magnetogyric ratio of the nucleus under study.



(a) (b) (c)

Figure 4.6. (a) Representation of the two spin orientations with respect to B_0. (b) The sum of all vectors denoted as M_z, due to α spins in excess than β spins. (c) Effect of rf pulse at 90° respect to Bo generates M_{xy} [176].

When the sample is introduced within the magnet in an NMR equipment, there is a net magnetization of the group of spins denoted as a single vector, M_z [176]. This vector is aligned with B_0, along z, if spins in the α state are more numerous than those in the β state (Figure 4.6b). If a secondary magnetic field B_1 is applied perpendicular to B_0 via radio-frequency (rf) pulse radiation, a vector with components in the xy plane, M_{xy} is generated (Figure 4.6c). The new vector is called transverse magnetization, and it induces a current in the coil wound around the sample, which is converted into the signal of the NMR spectrum [176].

The electrons involved in covalent bonds cause the NMR active-nuclei to feel the net field less intensely than the applied one, this is known as electronic shielding [91]. The more shielded an atom is, the greater the strength of the applied field must be in order to achieve resonance and to produce a signal [174,182]. Consequently, one atom with different shielded levels in a molecule gives signals at different frequencies, relative to a reference peak (usually tetramethylsilane, TMS). Such dependence of the resonance frequency of a nucleus with its molecular environment is called chemical shift (δ). δ is expressed in parts per million [ppm], referred to the difference in frequency between the reference compound and the sample [174,182,183].

Among the active nuclei for NMR, proton NMR (^{1}H-NMR) is the most widely used NMR method due to the vast natural abundance of the ^{1}H isotope (~ 99.98%). It provides information about the number of different hydrogens present in a sample and their chemical environment. Moreover, the area under the peaks is proportional to the number of hydrogens responsible for that signal; hence, information regarding the relative number of chemically distinct protons can be found by integrating the ^{1}H-NMR signals [180,182]. In the case of ^{13}C-NMR, despite the low natural abundance of ^{13}C (~1 %), it is a very useful technique for characterizing silicone-base products since carbon

is notably present in these materials [182]. Unlike ^{1}H-NMR, ^{13}C-NMR spectral peaks are not integrated and appear in a wide range of resonance: 0-200 ppm, while the range for protons is 1-10 ppm. Basically, ^{13}C-NMR spectra offer information concerning the number of non-equivalent carbons present in a sample and their chemical environment. In addition, ^{29}Si-NMR is essential in the chemical characterization of silicon-containing products. ^{29}Si isotopes possess a natural abundance of 4.7% and a nucleus with a small negative gyromagnetic ratio γ [184]. These two aspects cause a decrease in the intensity of the ^{29}Si-NMR spectrum since the signal-to-noise (S/N) relationship in NMR depends on both the natural abundance and the magnetogyric ratio, as described in Equation 4-7 [101]. Therefore, polarization transfer techniques such as DEPT (Distorsionless Enhancement Polarization Transfer) are preferentially used as the intensity of the received signal can be increased up to 5 times more than the basic ^{29}Si-NMR method [185]. In addition, the silicon signals associated with the glass tubes can be suppressed by DEPT technique since no signal of silicon atoms bonded to protons is received. The chemical shift range for ^{29}Si-NMR spectra is found between +50 and -200 ppm.

$$\frac{S}{N} \propto \frac{A}{T} \cdot B_0^{\frac{3}{2}} \cdot \gamma^{\frac{5}{2}} \cdot \tau^* \cdot (ns)^{1/2} \tag{4-7}$$

Where, A: number of NMR sensitive nuclei in the samples, T: temperature, τ^*: transverse relaxation time and, ns: number of scans. Furthermore, 2-D NMR techniques help to identify, quantify, and correlate molecules in solution. Especially, HSQC allows the resolution of complicated spectral regions due to the additional dimension [186,187]. This method effectively overcomes problems such as poor S/N ratio and overlapping of signals, facilitating spectral interpretation [186]. The HSQC technique involves pairing ^{1}H nuclei with other spin-nuclei, as ^{13}C and ^{29}Si. Thus, the resultant signals correspond exclusively to protons attached to those spin-nuclei. The magnetization is transferred from the ^{13}C or ^{29}Si to ^{1}H before detection, immensely improving sensitivity to ^{13}C and ^{29}Si. The main advantage of using HSQC is that the spectra are much better resolved, allowing a more accurate assignment of the chemical shifts [186]. HSQC was, for instance, efficient for supporting the identification of the unknown components in the commercial silicone, CSA.

4.2.2.2. Experimental procedure

All NMR measurements applied for characterization in bulk of the CSA, the SSMC, and the FMSA were performed externally on behalf of Robert Bosch GmbH. The description of the NMR measurements for the different samples is provided below.

Commercial silicone adhesive (uncured CSA)

The solution state NMR measurements of the uncured CSA were carried out at the research group of Prof. Dr. Dietrich Gudat at the Institute of Organic Chemistry, University of Stuttgart (Stuttgart, Germany). The measurements were performed at 303 K on a Bruker AVANCE 400 MHz spectrometer (Bruker AG, Germany) with a 9.4 T widebore superconducting cryomagnet, cooled by liquid Helium/Nitrogen. Probehead of 5 mm BBOBB-1H was used for all measurements. Operating resonance frequencies of 400.1 MHz (^{1}H), 100.6 MHz (^{13}C) and 79.5 MHz (^{29}Si) were applied.
The sample was dissolved in $CDCl_3$ at a concentration of 200 g/ml and the mixture was agitated for several minutes. Insoluble material was then allowed to settle, and the soluble fraction was transferred to an NMR tube and characterized by ^{1}H-, ^{13}C-, ^{29}Si- and HSQC-NMR measurements. Commercially available glass NMR tubes of 5 mm were employed for analysis of the samples. Pulse frequency (pf) NMR technique was applied. The chemical shifts were referenced to tetramethylsilane (TMS). TopSpin® 2.0 software (Bruker AG, Germany) was utilized for setting up the measurement parameters, collecting and processing the data. All spectra were obtained using standard pulse sequences from the Bruker pulse program library. Spectral widths were +9 – (-2.5) ppm for ^{1}H, 225 – (-25) ppm for ^{13}C and 125 – (-175) ppm.

Single silicone model components (SSMC)

The solution state ^{1}H-NMR measurements of the SSMC were performed at the research group of Prof. Dr. Michael R. Buchmeiser at the Institute of Polymer Chemistry, University of Stuttgart (Stuttgart, Germany) by Mrs. Mengjia Zhang. The spectrometer used was a Bruker AVANCE 400 MHz (Bruker AG, Germany) with a widebore superconducting cryomagnet (9.4 T) cooled by liquid Helium/Nitrogen with a 5 mm PABBO BB probehead. The temperature of operation was 303 K, and the resonance frequencies were 400.1 MHz for ^{1}H and 100.6 MHz for ^{13}C. The solvent for dissolving each SSMC was $CDCl_3$ and 5 mm NMR tubes were used for preparing the samples. The samples were prepared at a concentration of 80 g/ml. TopSpin® 3.0 software (Bruker AG, Germany) was utilized for setting up the measurement parameters and collecting the spectra. ACD/NMR® Version 12.0 (Advanced Chemistry

Development Inc., Canada) was utilized for managing the spectra and OriginPro® 8.6 was used for processing the data. Chemical shifts were referred to tetramethylsilane (TMS). All spectra were obtained using standard (rf) pulse sequences from the software program library. Additional ^{29}Si-NMR measurements for the two PDMS prepolymers were performed at the Group of Prof. Gudat using the equipment and setup parameters already described for the uncured CSA. Also ^{29}Si-NMR measurements of the catalyst, the crosslinker and the adhesion promoter were carried out at the INM-Leibniz-Institute for New Materials at the University of Saarland (Saarbrücken, Germany) by Mr. Stefan Brück in a Bruker AVANCE 400 MHz spectrometer (Bruker AG, Germany). TopSpin® 3.2 (Bruker AG, Germany) software was employed for recording the spectra. ACD/NMR® Version 12.0 (Advanced Chemistry Development Inc., Canada) was utilized for managing the spectra and OriginPro® 8.6 was used for processing the data. Chemical shifts were referred to tetramethylsilane (TMS). All spectra were obtained using standard (rf) pulse sequences from the software program library.

Formulated model silicone adhesive (FMSA)

The examination of the crosslinked structure by solid-state ^{1}H-, ^{29}Si- and ^{13}C-NMR measurements was performed at the group of inorganic chemistry of Prof. Dr. Werner R. Thiel at the University of Kaiserslautern (Kaiserslautern, Germany) by Dr. Dirk Schaffner. The NMR spectra were recorded on BRUKER DSX300 spectrometer at 7.05 T. The frequencies of resonance were set at 300 MHz for ^{1}H, 75.43 MHz for ^{13}C, and 59.595 MHz for ^{29}Si. Samples were placed in a rotor speed at 10000 Hz for spinning at the magic angle (MAS). The spectra were referenced to tetramethylsilane (TMS). TopSpin® 3.1 software (Bruker AG, Germany) was used for acquiring the spectra, ACD/NMR® Version 12.0 (Advanced Chemistry Development Inc., Canada) was implemented for spectra processing and OriginPro® 8.6 was employed for further data analysis.

4.3. Results of the characterization in bulk of the CSA

The commercial silicon adhesive, CSA, was selected based on its applicability and frequent use in the fabrication of automobile parts. The adhesive was a thermally curable, addition-curing one component (1-C) silicone adhesive produced by Wacker Chemie AG (Burghausen, Germany). According to the material safety data sheet (MSDS) [24], CSA does not contain any toxic or corrosive substance which required

special handling precautions. The standard curing condition recommended by the manufacturer was used: isothermal curing at 130 °C for 1 h. The curing conditions applied satisfy manufacturing criteria for producing automobile electronic parts. The curing reaction of the CSA is usually accelerated by platinum-based catalysts and it is better known as hydrosilylation (Figure 4.7) [88].

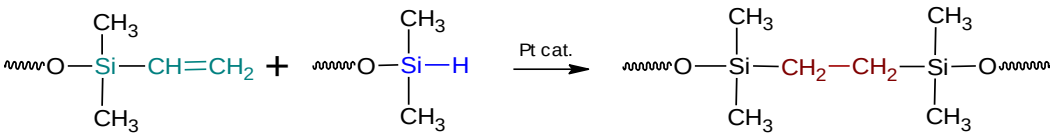


Figure 4.7. Addition-curing reaction (hydrosilylation) of the CSA.

4.3.1. Chemical characterization

From the reaction above, through the chemical characterization of CSA, it was expected to identify vinyl and hydride groups for the uncured system, and ethylene "bridges" for the cured one. Moreover, silanol (-Si-OH) traces were presumed to be present since, in the synthesis of commercial silicone products, the respective subunits are built from chlorosilanes via hydrolysis. Hence, residues of unreacted -Si-OH groups usually remain due to incomplete condensation [49,64,188]. Furthermore, alkoxy groups in organosilanes, added as adhesion promoters, should also be present. Table 4.3 lists the main functionalities and other components expected to be recognized in the CSA.

Table 4.3. Functionalities and components expected to be identified in CSA.

Uncured CSA		Cured CSA	
-Si-CH=CH_2	Vinyl	-CH_2-CH_2	Ethylene "bridges"
-Si-H	Hydride or silyl	-$Si(CH_3)_2$-O-	Dimethylsiloxane (D unit)
-$Si(CH_3)_2$-O-	Dimethylsiloxane (D unit)		
Additional functionalities and components			
-Si-OH	Silanols		
R_1-Si-(O-R_2)$_3$	Alkoxysilanes (adhesion promoter)		
Fillers			

4.3.1.1. ATR-FTIR Spectroscopy

The assignment of the IR absorption bands is based on various literature sources [88,160,173,189–194]. Additional sources used, are indicated in the text. For the ease of spectral interpretation, the measured ATR-FTIR spectra were sectioned into four sequential regions, labeled A, B, C and D, as follows:

A. Region 1: 3800-3150 cm^{-1}
B. Region 2: 3200-2600 cm^{-1}
C. Region 3: 2300-1800 cm^{-1}
D. Region 4: 1700-450 cm^{-1}

A. Region 1: 3800-3150 cm^{-1}

This region is characteristic of the O-H stretch vibration mode, the spectra obtained for the uncured and cured product is illustrated in Figure 4.8. The spectrum of the uncured CSA does not point out to tangible presence of -OH groups; thus, it cannot be confirmed via ATR-FTIR if -OH groups were present in the pristine product. The attained signal is almost unresolved from noise, exposing limitations of the technique in detecting functionalities at very low concentrations. Most probably, -OH moieties were present in trace amounts which were masked by other more abundant functionalities. As described by Lipp [195], identification of silanol traces by FTIR spectroscopy is a very challenging task when concentrations are lower than 1000 ppm due to the involvement of -OH groups in H-bonding between silanol molecules or other polar species. Also due to peak overlapping with alcohols or water molecules [196]. Effective methods have been implemented by Lipp [195], Aragão et al. [197] and Vučković et al. [198] for identifying silanol fragments in polysiloxanes by FTIR measurements even at concentrations of 10 ppm. The implementation of these alternatives was beyond the scope of this thesis. In practical applications, quantification of silanol groups (even at trace levels) is in many cases necessary and important for predicting the suitability of a silicone product for a particular application [195]. Silanol groups are key moieties in organosilicon chemistry due to their ease of reactivity and most likely, the final properties of a material can be influenced by condensation reactions undergone through silanol linkages (both desirable and undesirable).

On the other hand, for the cured silicone, a weak but broad band between 3660 and 3200 cm^{-1} is perceived. This band evidences an increase of -OH groups after curing.

The hydroxyl groups detected could result from the curing process or from moisture adsorbed on the surface of the solid sample. Despite the well-known hydrophobicity of silicone surfaces, water could have been adsorbed and possibly absorbed, due to the existence of hydroxyl traces that can induce a hydrophilic behavior of the polymer [199]. In fact, three possible scenarios can be considered to have favored the formation of OH groups by side reactions during the curing process of the CSA (Figure 4.9).

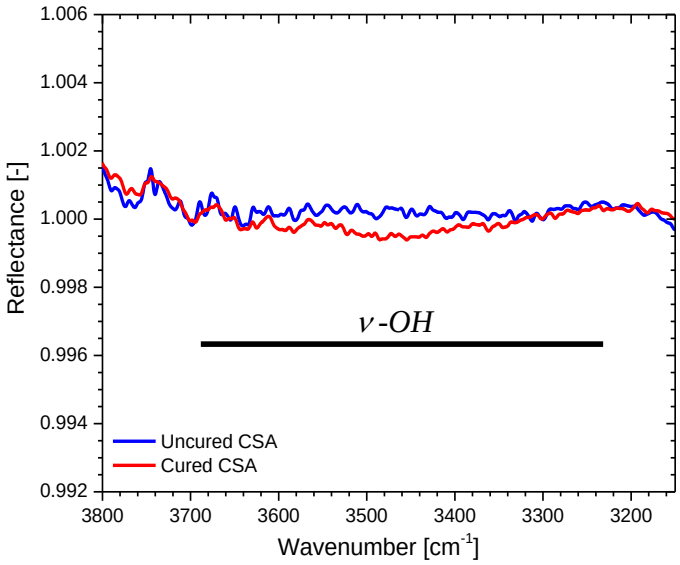


Figure 4.8. Stretching of -OH groups for the uncured and cured CSA

(1) **Hydrolysis of alkoxy groups.** If hydrolysis of trialkoxysilanes occurred during the curing process, one to three silanol groups could have been formed per molecule [200]; thus, the concentration of -Si-OH functionalities could have been considerably incremented. Additionally, production of alcohol may have also contributed to an increase of OH groups (Figure 4.9-(1)).

(2) **Cleavage of siloxane bonds.** -Si-O-Si- bonds in PDMS molecules could have been hydrolyzed leading the formation of two -Si-OH groups per siloxane bond [201] (Figure 4.9-(2)).

(3) **Conversion of Si-H end groups.** Si-H terminal groups could undergo hydrolysis forming terminal Si-OH groups. Silanols could also condensate creating siloxane bonds (Figure 4.9-(3)) [202].

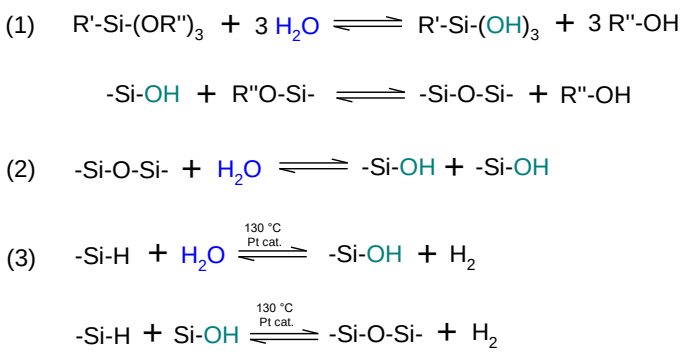


Figure 4.9. Secondary reactions that could occur during curing of CSA at 130 °C for 1 h. (1) Hydrolysis and condensation of alkoxy groups in silanes, (2) cleavage of siloxane bonds and (3) conversion of Si-H into SiOH and further condensation towards Si-O-Si formation [200–202]

If simultaneous condensation of Si-OH towards -Si-O-Si- formation took place, the amount of OH groups was reduced. Consequently, competitive reactions may have affected the final concentration of hydroxyl groups in the sample, but an overall increase of OH concentration after curing is observed.

B. Region 2: 3200-2600 cm^{-1}

Vibrations associated with -C-H bonds are distinctive in this region. Herein, identification of bands ascribed to methyl groups (characteristic of PDMS polymers), vinyl groups (involved in crosslinking) and additional alkyl or aryl substituents (ethyl, allyl, phenyl, and alkoxy) that could have been included in the CSA, is feasible. The measured spectra are shown in Figure 4.10 for the uncured and cured CSA.

For the cured and uncured material, a prominent and sharp absorption band is perceived at 2963 cm^{-1} corresponding to asymmetric stretching of CH_3 (ν_{as}-CH_3). A less intense band at 2905 cm^{-1} related to symmetric stretching of CH_3 (ν_s-CH_3) is also identified. These two bands undoubtedly confirm the presence of methyl substituents in the CSA before and after hydrosilylation. Although at first glance the spectra of the uncured and cured samples in this region appear to be similar, closer inspection of sections I and II (indicated in Figure 4.10), reveals interesting spectral differences that are shown in Figure 4.11a-b and discussed in the next.

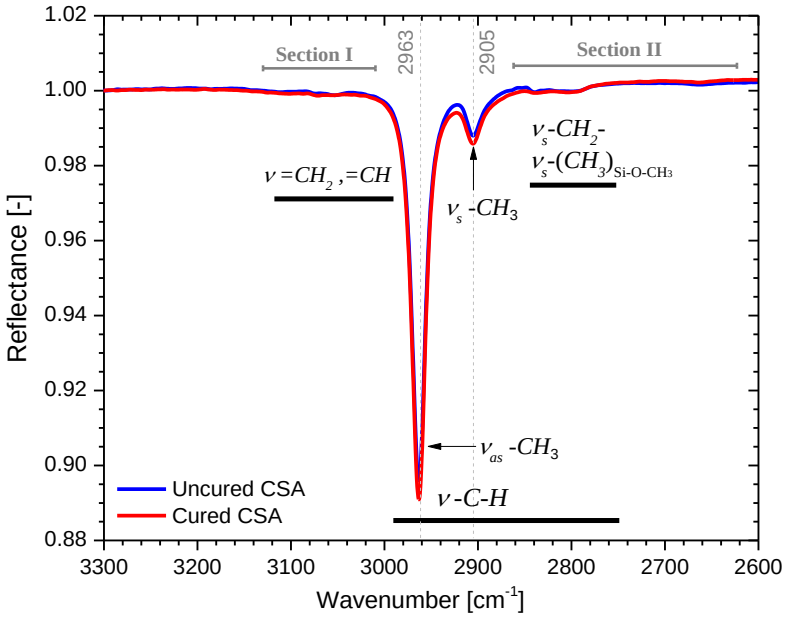


Figure 4.10. ATR-FTIR spectra from 3300-2600 cm^{-1} of the CSA before and after curing. Typical bands associated with symmetric and asymmetric stretch of C-H bonds are disclosed.

- **Section I (3140-3000 cm^{-1})**

The spectra in this region (Figure 4.11a) display three weak bands. The first one is detected at 3074 cm^{-1} assigned to asymmetric stretching of double bonds in phenyl or allyl substituents [160,189,190,203]. For the cured material, slight shifting towards lower wavenumbers (~3071 cm^{-1}) is observed due to effects caused by the contiguous band at 3053 cm^{-1}. Unremarkable changes in peak intensity and peak shape suggest that groups related to this band did not participate in crosslinking reaction; thus, the band may be ascribed to phenyl rather than to allyl groups, since the latter can be involved in hydrosilylation. The incorporation of phenyl substituents in the CSA is not surprising since the inclusion of such groups is a well-known practice for improving thermal stability and mechanical properties of silicone products and organosilanes [204–208]. Five possibilities regarding the inclusion of phenyl groups in the commercial system are proposed:

1. Siloxane homopolymer: Poly(diphenylsiloxane) (PDPS)
2. Siloxane homopolymer: Poly(methylphenylsiloxane) (PMPS)
3. Siloxane copolymer with dimethyl and diphenyl segments (PDMS-co-PDPS)
4. Siloxane copolymer with dimethyl segments and methyl-phenyl segments (PDMS-co-PMPS)
5. Organosilane: Phenyltrialkoxysilane

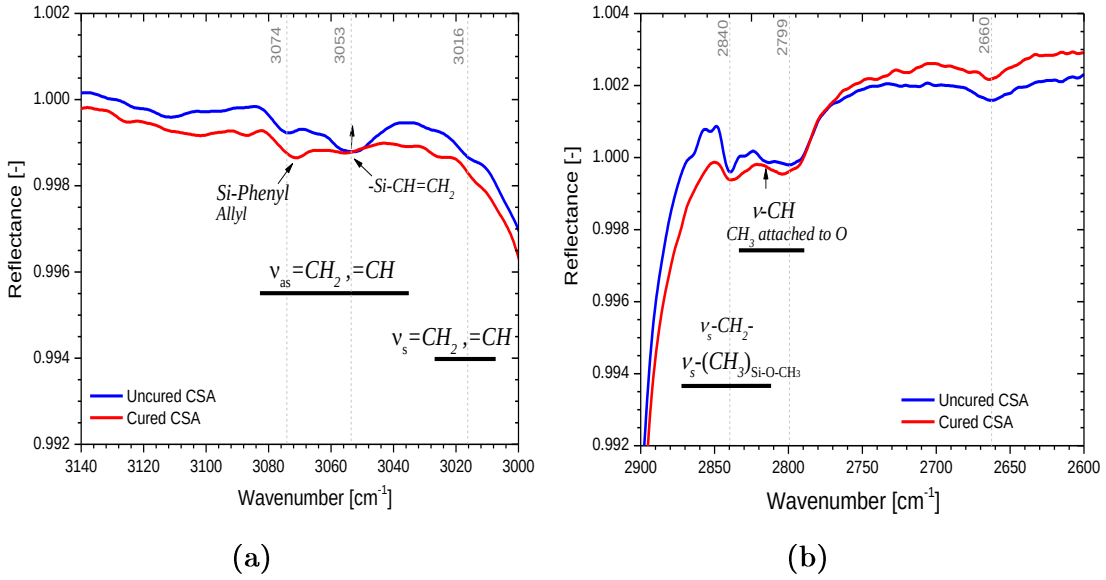


Figure 4.11. ATR-FTIR spectra of the uncured and cured CSA in: (a) section I: from 3150 to 3000 cm^{-1} distinctive of stretch vibrations of double bonds. (b) Section II: from 2900 to 2600 cm^{-1}, representative of stretch vibrations of methylene and methoxy groups.

The incorporation of PDMS-co-PMPS or PDMS-co-PDPS in silicones usually increases the onset degradation temperature up to 400 °C [204]; therefore, silicone adhesives including phenyl groups are preferentially employed for high-temperature service applications [208]. On the other hand, allyl groups are normally incorporated as adhesion promoters (allyltrimethoxysilane) [144,164,209,210].

The second band found in this spectral section is observed only for the uncured CSA and corresponds to asymmetric stretching of vinyl groups (ν_{as}-Si-CH=CH_2) at 3053 cm^{-1} [88,189,190]. Hence, the presence of vinyl groups for hydrosilylation is confirmed. The spectrum of the crosslinked product does not exhibit this band, verifying the consumption of vinyl groups during crosslinking. Total consumption is however, not evident as the signal is unresolved from noise.

The third band observed in Figure 4.11a is a weak shoulder at 3016 cm^{-1} characteristic of symmetric stretching of double bonds. The reduction in peak intensity observed for the cured material corroborates once more the involvement of vinyl groups in crosslinking. Quantitative analysis of the crosslinking reaction is presented later.

- **Section II (2900-2600 cm^{-1})**

The spectra represented in Figure 4.11b disclose a bunch of weak bands ranging from 2900 to 2780 cm^{-1} associated with stretch vibrations of methylene (-CH_2) and methoxy (-OCH_3) functionalities. Specific and precise assignment of the bands is uncertain due

to the influence of the adjacent band ν_s-CH_3 at 2905 cm^{-1} and to peak overlapping effects. A significant aspect to consider is that recognition of the bands ascribed to those functionalities (-OCH_3 and -CH_2-) corroborates the presence of methylene moieties and methoxysilanes in the pristine CSA, but also the formation of ethylene bridges (-CH_2-CH_2-) after curing. Yet, the contribution of newly formed ethylene bonds could be masked by fillers, additives or other more abundant components. Fluctuations in band intensity before and after curing may be caused by two concurrent events; first, partial consumption of -OCH_3 groups in the reaction described in Figure 4.9-(1) and second, formation of new -CH_2- bonds during hydrosilylation (Figure 4.7).

An additional band is perceived at 2660 cm^{-1} in the two spectra, although its exact attribution is undefined, it can be tentatively assigned to an overtone band of C-H deformation vibrations at ~ 1400-1200 cm^{-1} as overtone bands are usually observed at approximately twice the frequency of strong fundamental absorption bands [189].

C. Region 3: 2300-1800 cm^{-1}

This spectral region evidences the presence of -Si-H groups in the CSA by the characteristic peak associated with stretch vibrations at 2165 cm^{-1} (Figure 4.12)[189,191,192]. This band is not overlapped by any other vibrational mode; hence, its assignment and analysis is direct and very precise. The notable reduction in peak intensity for the cured material verifies that hydrosilylation was accomplished in the expected way. The Si-H concentration decreased as the hydride-vinyl addition took place. However, in opposition to the peak at 3053 cm^{-1} of Si-vinyl, the -Si-H peak is still noticeable after crosslinking advocating an excess of silyl species in the CSA product. In addition, the relatively high intensity perceived for the uncured sample leads to tentatively assign the hydride-PDMS as the crosslinker for hydrosilylation. As mentioned in Section 3.2, excess of crosslinker is typically added in the formulation of addition-curing silicones to ensure complete crosslinking of the vinyl groups.

Furthermore, two additional bands are observed at 2053 cm^{-1} and 1946 cm^{-1}. Karlsson [211], and Pop [212] have attributed the last peak to vibrations of the PDMS backbone. Interestingly, the intensity of this peak remains unchangeable after curing, pointing out that siloxane bonds in the polymer skeleton were almost unaffected by the curing process. Hence, hydrolysis of -Si-O-Si- bonds (Figure 4.9-(2)) can be neglected. Assignment of the peak at 2053 cm^{-1} is still undefined; nonetheless, it can be also related to the siloxane backbone as its intensity after crosslinking remains also unaffected.

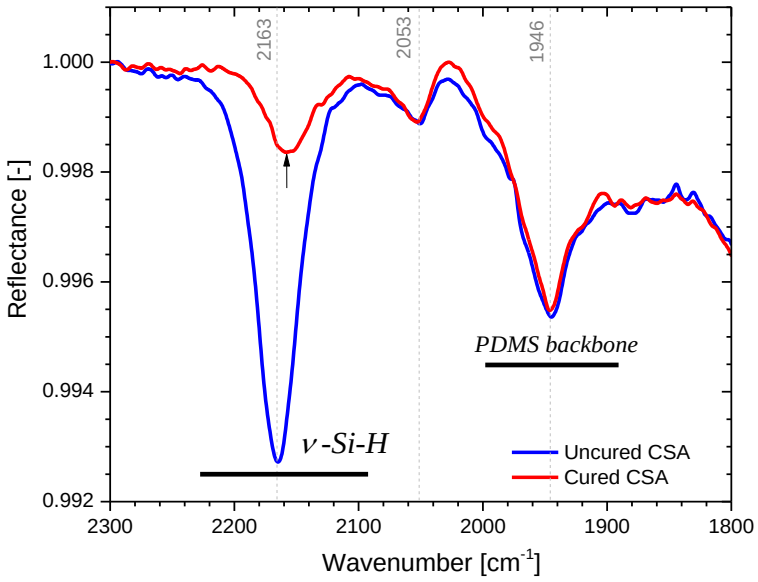


Figure 4.12. Bulk ATR-FTIR spectra from 2300 to 1800 cm^{-1} of the uncured and cured CSA. This region displays the distinctive stretch vibration of Si-H and a peak related to vibration of the PDMS backbone at 1946 cm^{-1} [189,211].

The degree of conversion and the initial molar ratio of Si-H/Si-Vinyl groups in CSA can be estimated from the peak areas of the Si-H and Si-vinyl bands at 2163 cm^{-1} and 3053 cm^{-1}, respectively. This quantitative analysis requires normalization based on an internal reference which should not participate in any physical process or chemical reaction, and its spectral range should not be obscured by other vibration modes. The peak detected at 1946 cm^{-1} fulfills such requirements; thus, it was chosen as the internal reference for spectra normalization of CSA. This band has been used as a reference for normalization in quantitative FTIR analysis of silicones [211–213]. The calculated peak areas for the uncured and cured CSA, of the Si-H band at 2163 cm^{-1}, Si-vinyl at 3053 cm^{-1}, and the internal reference at 1946 cm^{-1} are tabulated in Table 4.4.

Table 4.4. Calculated areas of the silyl and vinyl stretch vibration peaks and the reference band.

Sample	Area (2163 cm^{-1})	Area (3053 cm^{-1})	Area Internal reference (1946 cm^{-1})
Uncured CSA	0.3159	0.0092	0.1764
Cured CSA	0.0702	0.0004	0.1755

The intensity of an IR absorption band is directly proportional to the concentration of the oscillator in the vibrating mode [170]. Therefore, the initial and final concentrations of the silyl and vinyl groups can be estimated from the normalized areas of the uncured and cured respective peaks based on Equation 4-8

$$c_i|_{initial} \propto A_{n,i}\big|_{uncured}$$
$$c_i|_{final} \propto A_{n,i}\big|_{cured} \quad \textbf{(4-8)}$$

Where c_i: concentration of group i, and $A_{n,i}$: normalized peak area of group i. The normalized peak areas were calculated following Equation 4-9, with A_i: peak area of group i, and $A_{internal\ reference}$ peak area of the internal reference taken for normalization.

$$A_{n,i} = \frac{A_i}{A_{internal\ reference}} \quad \textbf{(4-9)}$$

Then, the degree of conversion [%] of Si-H and Si-vinyl groups to ethylene bonds, can be evaluated from:

$$degree\ of\ conversion_i[\%] \approx\ 100 \times \left(\frac{A_{n,i}|_{uncured} - A_{n,i}|_{cured}}{A_{n,i}|_{uncured}}\right) \quad \textbf{(4-10)}$$

Therefore, the results obtained for the conversion of Si-H and Si-vinyl functionalities are:

$$conversion_{Si-H} \approx 77.7\ \%$$

$$coversion_{Si-Vinyl} \approx 95.9\ \%$$

These results suggest that the crosslinking yield under isothermal curing of the CSA at 130 °C for 1 h, was ~ 96 %. The excess of Si-H groups can be estimated from the difference between conversion of vinyl and hydride groups (Equation 4-11):

$$\%\ excess_{Si-H} = conversion_{Si-vinyl} - conversion_{Si-H} \quad \textbf{(4-11)}$$
$$\%\ excess_{Si-H} \sim 18\ \%$$

From the stoichiometric ratio of silyl to vinyl groups in hydrosilylation (1:1) (Figure 4.7), the molar ratio of Si-H/Si-vinyl in the CSA can be approximated to 1.2. In practical cases, the excess amount of crosslinker is an important factor to be considered in the formulation of silicones. Too little crosslinker can decrease the crosslinking density, whereas too much crosslinker may cause post-curing problems with unreacted hydrides [211].

D. Region 4: 1700-450 cm^{-1}

The fingerprint region (Figure 4.13) is sectioned in three parts for facilitating the analysis and the interpretation. The most prominent peaks are perceived in section IV, therefore, this fragment is the first one being analyzed.

- **Section IV (1300-800 cm^{-1})**

Strong IR absorption bands:

Three main peaks are observed in this region. The first is the IR band at 1260 cm^{-1} allocated to symmetric "umbrella" deformation (bending) of methyl groups (δ_s-CH_3). This peak is intense, sharp, and not easily misidentified. Its detection reaffirms the presence of methyl substituents in the silicone backbone. In addition, vibrations of -CH_3 bonds from methoxy groups in organosilanes may contribute to its total intensity.

The second prominent IR band is perceived as a doublet at 1100-1010 cm^{-1}. The peak is ascribed to stretch vibration of the Si-O linkage with peak maxima located at 1073 and 1015 cm^{-1}. Usually, the doublet displays maximum absorption at approximately 1086 and 1020 cm^{-1} when dimethyl groups are attached to silicon [189,191]. Experimentally, the peak maxima are seen located at lower frequencies than those suggested for pure PDMS; this advocates that not only methyl groups were contained in the backbone. The presence of phenyl groups as substituents in the polymer chains may support this observation. Additional contribution to this band may arise from strong absorption of Si-O bonds related to methoxy groups in silanes (-Si-O-C-), from silica (SiO_2), possibly included as a filler [189,214], and from plausible presence of ether linkages (-C-O-C-).

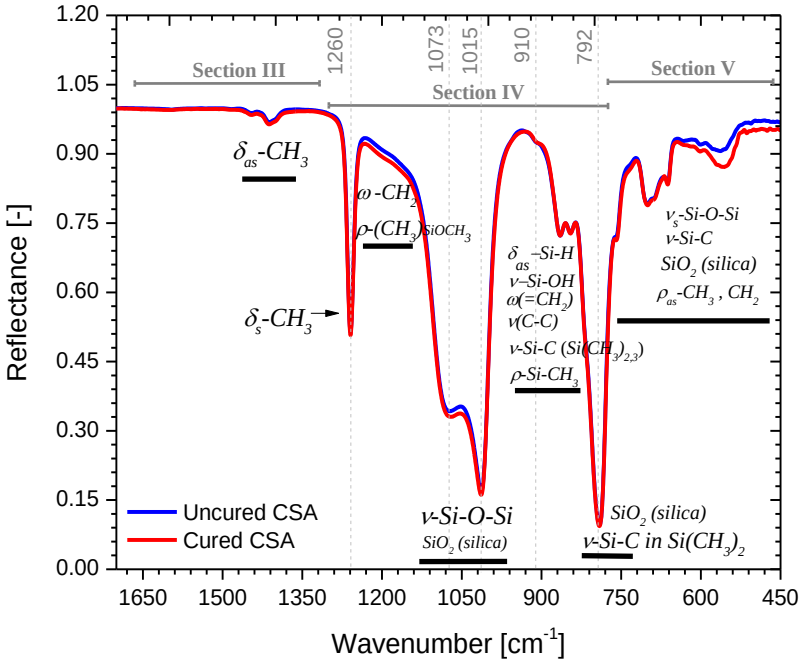


Figure 4.13. Fingerprint region from 1700 to 450 cm^{-1} of the bulk ATR-FTIR spectra of the non-crosslinked and crosslinked CSA. The spectra are subdivided into three sections III, IV and V for ease of analysis. The most outstanding bands are associated to symmetric bending of methyl groups at 1265 cm^{-1}, stretching of siloxane bonds at 1073 and 1015 cm^{-1}, and stretch of Si-C bonds at 792 cm^{-1}[173,189–191].

The third striking feature observed in this region is a sharp intense band near 792 cm^{-1} ascribed to asymmetric stretch vibrations of Si-C bonds in -$Si(CH_3)_2$- units[88,189–191,193,194]. It seems to be one of the most promising bands for confirming that methyl groups are the predominant substituents at silicon atoms. Additionally, vibration involving silica fillers also gives rise to bands at 790-810 cm^{-1} [102,189].

Weak IR absorption bands:

The band at 910 cm^{-1} is tentatively assigned to deformation of the Si-H bond (δ-Si-H). However, unchangeable intensity after curing suggests contributions from other vibrating modes such as ν-SiOH (955-830 cm^{-1}) [147,189,190,193] and ω=CH_2 (980-900 cm^{-1}) [38,88,189]. The two bands of similar intensity near 865 and 845 cm^{-1} are attributable to ν_s-Si-CH_3 and ρ-CH_3 vibrations of middle -$Si(CH_3)_2$-O- units but also to terminal -Si-$(CH_3)_3$ groups [189,190,193,194]. Methyl terminated PDMS are commonly added as softeners and plasticizers in silicone products [19]. Additionally, as reported by Launer [190], the band at 845 cm^{-1} can also suggest the presence of copolymer containing blocks of D units (-$Si(CH_3)_2$-O-), which could be a plausible indication of

the presence of PDMS-co-PMPS or PDMS-co-PDPS in the CSA, or to the existence of PDMS copolymers with middle hydride (-Si(CH_3)(H)-O-) and vinyl (-Si(CH_3)($CH=CH_2$)-O-) groups. The intensity of these two peaks is perceived to be invariable after curing.

Interestingly, a closer examination of the region representative of the vibration of -Si-CH_2-CH_2-Si- groups between 1200 and 1100 cm^{-1} reveals the lack of band or shoulder for either uncured or cured silicone. Again, poor spectral evidence regarding the newly formed ethylene bridges is exposed. The speculation that ethylene segments were masked by other, more abundant, groups in the polymer network, is reinforced.

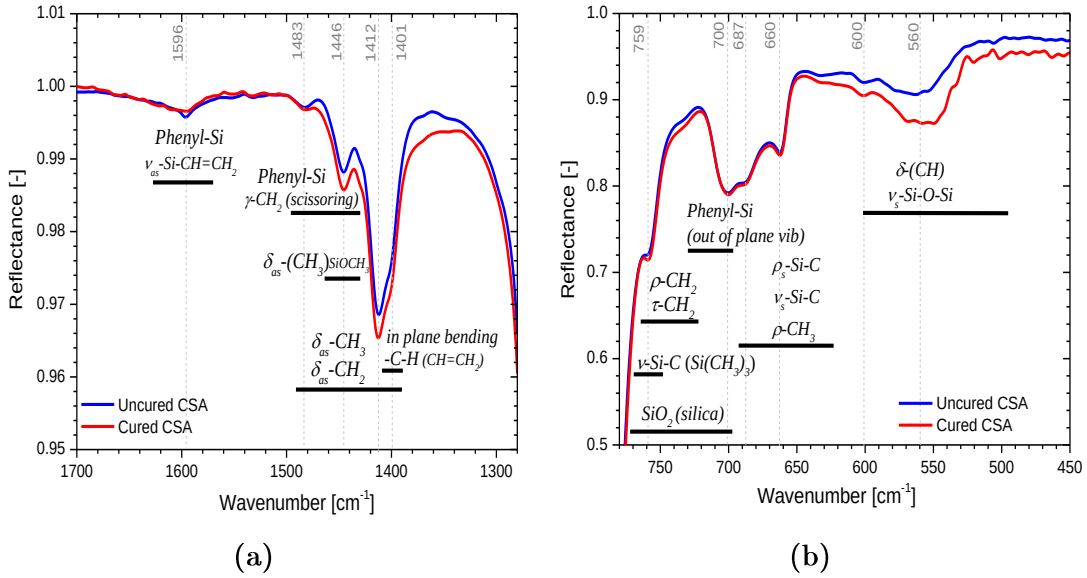
- **Section III (1700-1300 cm^{-1})**

Vibrations involving stretch of double bonds from vinyl and phenyl groups gives rise to bands in this region (Figure 4.14a). The peak at 1596 cm^{-1} features a reduction in peak area of ~16 %. When compared with the 96 % estimated for vinyl groups at 3053 cm^{-1}, suggests overlapping of vibrations of phenyl and vinyl groups. The contribution of vibrations of the aromatic ring might be masking the effect of vinyl consumption during hydrosilylation. Therefore, unambiguous assignment is unfeasible.

The band near 1483 cm^{-1} is related to bending in-plane of aromatic C-H in phenyl groups and to -CH_2 scissoring of vinyl linkages. As reported by Smith [191], phenyl substituents at the silicon atom present three simultaneous bands at 1595, 1480 and 1431 cm^{-1}. Correspondingly, the bands perceived in the spectra at 1595, 1483 and 1446 cm^{-1} can confirm the presence of aromatic rings in the silicone skeleton.

The band lying between 1434 and 1374 cm^{-1} can be ascribed to asymmetric deformation (bending) of both CH_2 and CH_3 groups attached to silicon with a maximum located at 1412 cm^{-1} and a shoulder at 1401 cm^{-1}.

Adsorption of water on the solid surface of the cured CSA is not verified by the characteristic H-O-H bending band at 1650-1630 cm^{-1} since it is difficult to be distinguished from noise. Most likely, the major contribution to the increment of hydroxyl groups after curing was the conversion of methoxy groups -Si-OCH_3 into -Si-OH groups.



(a) (b)

Figure 4.14. Enhanced ATR-FTIR spectra of the CSA before and after crosslinking, (a) Section III: from 1700 to 1300 cm^{-1} related to deformation and stretch vibrations of double bonds in vinyl and phenyl substituents. (b) Section V: between 800 and 450 cm^{-1} ascribed to stretch and rocking vibrations of C-H and Si-C, and to symmetric stretch of Si-O-Si bond.

- **Section V (800-450 cm^{-1})**

The specific and exact ascription of bands in this last spectral region (Figure 4.14b) is uncertain and challenging due to numerous overlapping vibration modes. However, different ranges have been proposed connected with functional groups present in the CSA. The bands from 740-690 cm^{-1} can be due to out of plane vibration of phenyl substituents and to aromatic ring bending, as well as to vibrations of possible fillers as silica or magnesium carbonate [102,189,214]. The weak shoulder at 759 cm^{-1} can be attributed to methyl-terminated PDMS [23,189,190,194,215,216] reaffirming the presence of M units (monosubstituted silicon, -Si(CH$_3$)$_3$) in the CSA. However, ρ-CH$_2$ and out of plane deformation of -CH$_2$-CH$_2$- linkages are also displayed in this range. The bands from 680-620 cm^{-1} can be assigned to symmetric stretching vibrations of Si-C bond, symmetric rocking vibration of Si-CH$_3$ and rocking of CH$_3$ groups. Importantly, the characteristic symmetric stretching vibration of the siloxane bonds Si-O-Si, usually displayed at 500-410 cm^{-1} is indiscernible due to its proximity to the measurement frequency limit and strong noise signals in that spectral range.

In an attempt to identify the type of filler in CSA, bands displayed by the measured spectra are compared with characteristic IR absorption bands of common fillers that are listed in Table 4.5. In summary, lack of solid spectral evidence of peaks related to

ZnO, TiO_2, Sb_2O_3, $CaCO_3$, $MgCO_3$, $NaCO_3$, $ZnCO_3$ and SO_4, strongly suggests that silica is the filler of the CSA. This is reasonable due to the ability of silica in establishing strong interactions with polysiloxanes that allows to obtain a homogeneous material. Further identification of other type of particulate material such as additives or pigments was not within the scope of this study.

Table 4.5. Characteristic IR absorption bands of common fillers [189,214]

Filler	IR absorption bands [cm^{-1}]
Zinc oxide (ZnO)	1050 (m), 1000 (w), 980 (s), 810 (v.s)
Titanium dioxide (TiO_2)	800 (br, s), 470 (br, s)
Silica (SiO_2)	1225-1200 (br shd), 1175-1150, 1100 (br, v.s), 800-785 (sh m) ,725-700 (sh), 670-500 (m-w)
Magnesium oxide (MgO)	700 (s, br), 1476-1413 (w)
Antimony trioxide (Sb_2O_3)	738 (br), 580, 537 and 500 (unresolved)
Calcium carbonate ($CaCO_3$)	1430 (s, br), 1795 (sh), 876 (sh), 712 (sh)
Magnesium carbonate ($MgCO_3$)	1482 and 1420 (strong), 1120, 886, 853, 803, 719, 593 (m-w)
Sodium carbonate ($NaCO_3$)	1431 (br, s), 875 (sh, m) and 713 (sh, m)
Zinc carbonate ($ZnCO_3$)	1046, 951, 834, 738 and 708 (all sh), 1384 (C=O) and 1507
Sulfates ($CaSO_4$ and $BaSO_4$)	1150 (br, s), 1180, 1120 and 1080 (unresolved, m)

v.s: very strong intensity; s: strong intensity; m: medium intensity; w: weak intensity; br: broad; sh: sharp; shd: shoulder

Compilation of all functionalities identified in the experimental ATR-FTIR spectra of CSA, with their respective characteristic peak positions and their tentative corresponding single component, is presented in Table 4.6.

Table 4.6. Compiled ATR-FTIR results of the uncured and cured CSA.

Group	Associated IR bands [cm^{-1}]	Tentative corresponding single component
$Si\text{-}CH{=}CH_2$	3053 (ν_{as}=CH2, =CH)	Vinyl-PDMS prepolymer
	3015 (ν_s=CH_2, =CH)	Vinyltrimethoxysilane
Si-H	2164 (ν-Si-H)	Hydride PDMS prepolymer (Crosslinker)
	910 (δ_{as}-Si-H)	
Si-O-Si	1070, 1011 (ν_{as}-Si-O)	PDMS prepolymers
	600-480 (ν_s-Si-O)	
$-CH_3-$	2964 (ν_{as}-CH_3)	Dimethyl groups in PDMS prepolymers
	2904 (ν_s-CH_3)	
	1412, 1400 (δ_{as}-CH_3)	
	1259 (δ_s-CH_3)	
	792 (ν)	
$-CH_2-$	1230-1100 (ω-CH_2)	Cured CSA (ethylene "bridges" formed)
	2880-2820 (ν_s-CH_2)	
	1490-1390 (δ_{as}-CH_2)	Organic substituent in organosilanes (Adhesion promoter)
	765-722 (ρ-CH_2, τ-CH_2)	
-Si-OH	3700-3200 (ν-OH)	Traces of Hydroxyl terminated polysiloxane
	955-830 (ν-Si-O)	Newly formed hydroxyl groups (Scheme 4.2)
$-O(CH_3)_3$	2840 (ν_s-OCH_3)	Trimethoxysilane (Adhesion promoter)
	1462-1430 (δ_{as}-CH_3)	
	1100-1000 (ν_{as}-Si-O-C)	
$-Si\text{-}CH_2\text{-}CH{=}CH_2$	3074 (ν_{as}=CH_2, =CH)	Allylsilane (Adhesion promoter)
	2900-2864 (ν_s-CH_2)	
	1480-1400 (δ_{as}-CH_2)	
	980-900 (ω-CH_2)	
-Si-Phenyl	3074 (ν_{as}=CH)	Homopolymer: PDPS or PMPS
	3025-3000 (ν_s=CH)	Copolymer (PDMS-PDPS or PDMS-PMPS)
	1596, 1483, 1445, 1431	Phenylsilane
$-Si(CH_3)_3-$	865, 845 (ν-Si-C)	Methyl terminated PDMS
	759 (ν-Si-C)	
SiO_2 (silica)	1100-1000 (ν_{as}-Si-O)	Filler
	800-790	
	700-500	

4.3.1.2. NMR Spectroscopy

The signals identified in all NMR spectra were assigned based on available NMR studies of PDMS and silanes [73,211,217–237]. Other additional sources used, are cited in the text.

The ^{1}H-NMR spectrum of the uncured CSA is shown in Figure 4.15. At first glance, the spectrum on the left reveals only a prominent signal at δ from -0.5 to 0.5 ppm representative of methyl groups attached to silicon [238,239]. The high-intensity of the signal evidences the abundancy of D units (-O-Si(CH_3)$_2$) in the sample. However, terminal methyl groups (-O-Si(CH_3)$_3$) or M units might be contributing to the total intensity. Besides the dominant signal, a number of relatively weak signals covering the whole spectral range between 0.5 and 8.0 ppm are also perceived in the magnified spectrum on the right of Figure 4.15. The appearance of multiplets reveals indirect spin-spin coupling existing between vicinal protons and overlapping signals. In addition, coupling with other spins such as ^{13}C and ^{29}Si leads to smaller satellite lines on the left and right of the main peaks in the ^{1}H-NMR spectrum.

The Si-H group displays a singlet at about 4.7 ppm distinctive of Si-H in -O--Si(CH_3)(H)- units; however, terminal Si-H groups (-O-Si(CH_3)$_2$(H)) might contribute to the total intensity of the peak and to the appearance of additional weaker signals around the peak. The plausible presence of both terminal and middle Si-H groups suggests the incorporation of a hydride siloxane polymer as the crosslinker. The protons of vinyl groups can be found downfield at δ ~ 5.5-6.5 ppm displaying a set of multiplets characteristic of Si-vinyl moieties. The complex signal may also have contribution from vinyl protons in allyl groups (-Si-CH_2-CH=CH_2) [224]. The presence of phenyl substituents is confirmed by the group of peaks perceived at δ 7.0-7.7 ppm [204,221,222,239]. As described by Plett [239] and Birkfeld [222] diphenylsiloxane units display a typical double set of peaks with the center at approximately 7.2 and 7.5 ppm which coincide with those recognized in the spectrum. However, whether they belong to a homopolymer or to a copolymer is still unresolved.

The signal between 4.8 and 5.5 ppm, assigned to protons in -OH groups, could arise either from water, silanol or alcohol traces [217,227,240]. Also, according to Brus et al. [241], and Hampton et al. [229], signals of -OH involved in H-bonding with water or silanol molecules can display peaks in this range. Peaks attributed to protons in methoxy groups (-OCH_3) are recognized by a prominent signal between 3.3 and 3.7 ppm [220,238,242]. The intensity of this signal is comparable to that related to phenyl groups, and it is larger than the one related to Si-H and Si-vinyl groups; indicating that methoxy groups are present in pristine CSA in a fairly high concentration. Other peaks

observed from δ 3.2 to 4.0 ppm are presumably due to silanol (-SiOH), alcohol (-COH) and additional -OCH_n (n=1-3) groups [202,229,241].

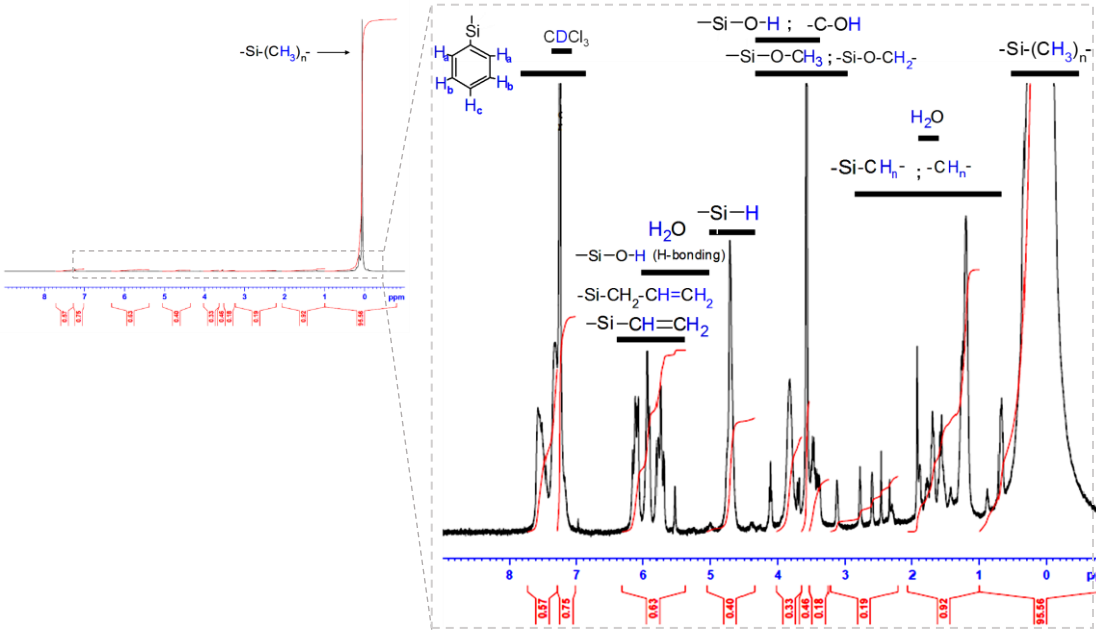


Figure 4.15. Complete solution state ^{1}H-NMR spectrum of the soluble part of the uncured CSA in $CDCl_3$ (left). Magnified spectrum (right). The strong signal detected at 0 ppm confirms PDMS as the major constituent of the CSA [237].

The set of peaks perceived from δ=1.2 to 2.8 ppm is representative of -CH_n- groups in alkyl substituents, most likely in organosilanes included as adhesion promoters [220,238,242]. Also, protons arising from water traces [217,227], solvent traces, organic impurities [217] and organosilanol [229,241] can be possibly displayed in this range. Accordingly, protons associated with the α carbon of allylsilane (-Si-C$\underline{H_2}$-CH=CH_2-) can also be distinguished at 1.48-1.61 ppm [224]. Finally, the small peak at about 7.0 ppm is attributed to the solvent $CDCl_3$ (deuterated chloroform) [217].

In ^{1}H-NMR, the functional groups can be identified qualitatively by the chemical shifts of the signals, and quantitatively by the integrated peak intensities [243]. Thus, the direct relationship between the integral of the signal peak and the molar amount of the nucleus allows the estimation of the Si-Vinyl/Si-H molar ratio without the strict requirement of a reference compound [211]. The quantitative analysis of the signals in the ^{1}H-NMR spectrum was based on relative integrals of the signals as relative molar percentages (%), i.e. the sum of all integrated ranges was set to 100%. This relative

method was sufficient for determining molar ratios of importance without the strict use of an internal standard. The relative integrals of the ^{1}H NMR signals of -Si-CH=CH_2 and Si-H functions (integral ratio 0.6:0.4) that were obtained suggest that in the CSA, the -Si-H groups were approximately 1.5 times more abundant than the Si-vinyl moieties. This result is in good agreement with the previous estimated value (1.2) from the ATR-FTIR spectra. Accordingly, hydride groups were added in excess to the formulation for ensuring a total conversion of the vinyl groups in ethylene bonds. This value of Si-H/Si-Vinyl=1.5, is used in this study for the formulation of the model silicone adhesive, FMSA.

A more precise assignment of the individual signals found in ^{1}H-NMR was possible by the evaluation of ^{1}H and ^{13}C chemical shifts (assigned via ^{1}H,^{13}C-HSQC correlation signals). Due to the low natural abundance of ^{13}C isotope (~1.1%), ^{13}C-NMR can generate uncertainties in the recognition of signals that can be overcome by the more sensitive HSQC-NMR technique which correlates chemical shifts of hetero bound nuclei [186,244,245]. In HSQC-NMR, every crosspeak represents single coupling ($^{1}J_{^{13}C^{1}H}$) between unique sets of bonds of ^{1}H and ^{13}C nuclei. Generally, signals detected in ^{1}H,^{13}C-HSQC can correspond to CH, CH_2 or CH_3 groups; quaternary carbons are, for obvious reasons, not perceived in the 2-D map. A special feature of this technique is that magnetically non-equivalent methylene (CH_2) protons attached to the same ^{13}C atom, retain the geminal coupling and are shown as a doublet in the 2-D spectrum [246]. In contrast, magnetically equivalent protons are displayed in one signal or singlets.

Figure 4.16 shows the magnified ^{1}H,^{13}C-HSQC spectrum from -0.5 to 1.5 ppm (^{1}H) of the soluble part of the uncured CSA dissolved in $CDCl_3$. The dominant correlation at $\delta_{^{13}C}/\delta_{^{1}H}$ [ppm/ppm] = (-2)-(2)/(-0.4)-(0.4) ppm is attributed to methyl groups in the PDMS backbone and in end-groups. The strong signal is seen surrounded by satellites due to spin-spin coupling [247,248].

The complete ^{1}H,^{13}C-HSQC spectrum of uncured CSA (Figure 4.17) yielded to characteristic crosspeaks associated with protons and carbons of all different functional groups present. For the CSA, 22 crosspeaks corresponding to protons (^{1}H) directly bonded to carbon (^{13}C) with different chemical environments, are identified. The crosspeaks arrowed and numbered in purple (peaks 7, 9, 14 and 18) correspond to non-equivalent methylene protons with residual $^{2}J_{HH}$ splitting. On the other hand, the singlet signals in red correspond to methyl -CH_3 and -CH- bonds.

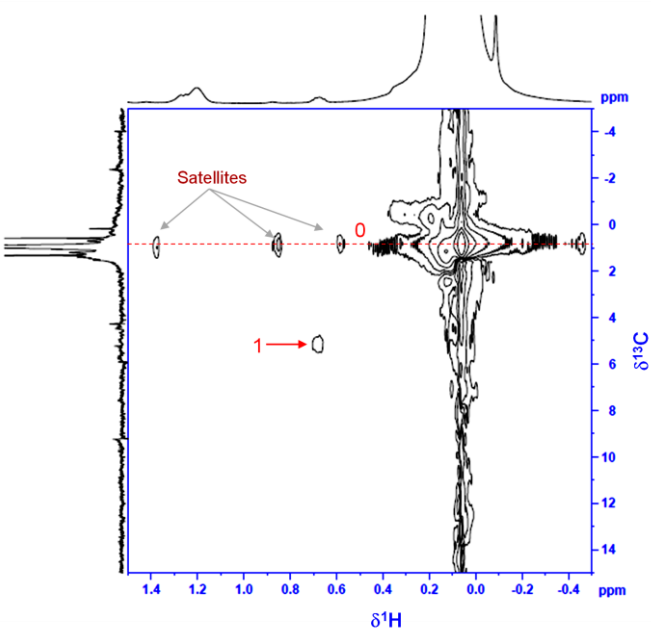


Figure 4.16. Solution state $^{1}H,^{13}C$-HSQC NMR spectrum of the uncured CSA in $CDCl_3$ [237]. The cross signal centered at ~ 0.05 ppm (^{1}H) and ~ –1 ppm (^{13}C) is associated with D units. The signal is flanked by satellites.

The signal at $\delta_{^{13}C}/\delta_{^{1}H}$ ~77 ppm/7.2 ppm is attributed to the solvent $CDCl_3$ [217]. The absence of a correlation signal for the resonance at 4.6-5.2 ppm in the ^{1}H-NMR spectrum validates its previous ascription to Si-H groups.

Although specific and exact assignment of each detected crosspeak (Figure 4.17) was challenging; tentative assignments are provided in Table 4.7. In general, $^{1}H,^{13}C$ correlations for -O-Si-$(CH_3)_n$ (n=1-3) can be found at ($\delta^{13}C$) from -2 to 2 ppm and at ($\delta^{1}H$) from -0.4 to 0.4 ppm. -$\underline{CH_n}$- groups (n=1,2) attached directly to silicon atom are represented by crosspeaks 1 to 3. Further -CH_n-, not directly attached to silicon but in alkyl substituent groups, are distinctive at (20-70)/(0.5-4.0) ppm/ppm ($\delta^{13}C/\delta^{1}H$) corresponding to crosspeaks 4 to 15.

Interestingly, through exhaustive literature review, the crosspeaks 9 and 14 are associated with two non-equivalent hydrogens in methylene groups, and the singlets 11 and 15 are assigned to an epoxy silane, most likely to glycidoxypropyltrimethoxysilane (GPS). As reported by Duplock et al. [219], de Buyl et al. [242], Torry et al. [249] and Hoebbel et al. [250], GPS (Figure 4.18) display distinctive ^{13}C and ^{1}H signals of the CH_2 group usually at ~ 44 ppm ($\delta^{13}C$) and at 2.45 and 2.62 ppm ($\delta^{1}H$), and the signal of CH bond normally exhibited at 51 ppm ($\delta^{13}C$) and 3.0 ppm ($\delta^{1}H$). These reported chemical shifts related to carbons 1 and 2 of GPS in Figure 4.18 coincide with those observed for crosspeaks 9 and 11, respectively (Table 4.7).

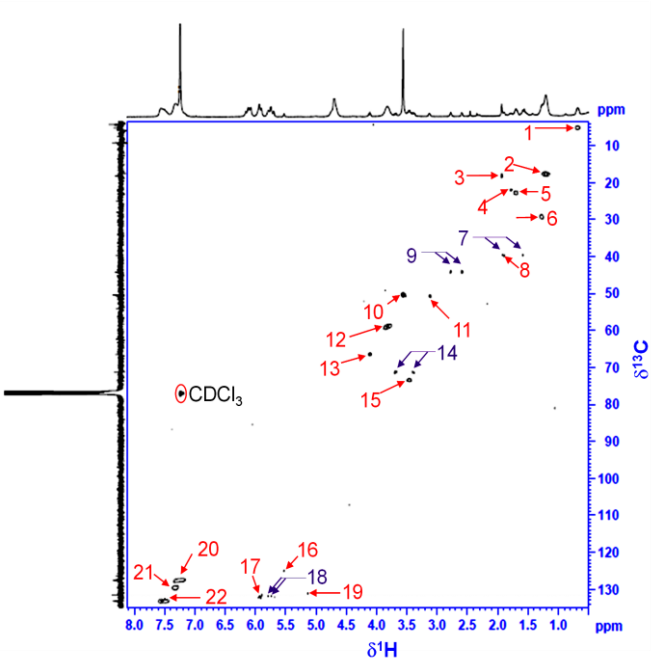


Figure 4.17. Solution state $^{1}H,^{13}C$-HSQC NMR map of the uncured CSA in $CDCl_3$ [237]. 22 crosspeaks are identified. Red signals are related to equivalent protons attached to a single carbon (-CH- or -CH_3 groups). Purple signals correspond to two non-equivalent protons bonded to the same carbon (-CH_2- groups).

Furthermore, the crosspeak 14 at ($\delta^{13}C/\delta^{1}H$) 71.3 ppm/(3.5 and 3.4) ppm can be related to carbon 3 in GPS and the crosspeak 15 at ($\delta^{13}C/\delta^{1}H$) 73.5 ppm/3.46 ppm can be correlated to carbon 4 (Figure 4.18), according to the aforementioned authors. Additionally, the signals corresponding to -OCH_n-(n=1-3) are exhibited at 50-75 ppm/3.0-4.2 ppm ($\delta^{13}C/\delta^{1}H$) corroborating the presence of alkoxy groups. Hence, GPS silane a well-known adhesion promoter [144,164,209], is included in the CSA, as suggested in a patent of the same manufacturer of the CSA [210]. Surprisingly, from the ATR-FTIR measurements, the exact recognition of this component was not inferred. A plausible reason could be overlapping of the C-O-C band with the strong -Si-O-Si- peak at 1100-1000 cm^{-1}.

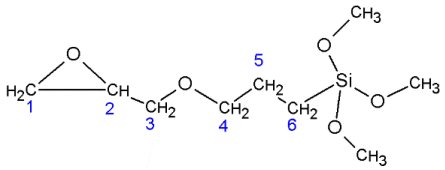
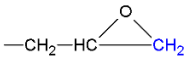
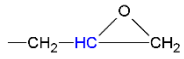
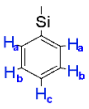


Figure 4.18. Glycidoxypropyltrimethoxysilane (GPS).

The strong ^{1}H-NMR signal at 3.5 ppm, which shows a correlation to a ^{13}C NMR signal at ~51 ppm, is assigned to methanol [217,237,251], which may have either been present in the original sample or originated from hydrolysis of Si-OCH$_3$ functions.

Furthermore, double bonds corresponding to vinyl and/or allyl terminal groups are represented by crosspeaks 16 to 19 at ($\delta_{^{13}C}/\delta_{^{1}H}$) 125-133 ppm/5.5-6.0 ppm with crosspeak 18 featuring splitting of the ^{1}H signal related to =CH$_2$. Lastly, the correlation signals of phenyl substituents are observed at 122-126 ppm/7-8 ppm ($\delta_{^{13}C}/\delta_{^{1}H}$) by crosspeaks 20 to 22.

Table 4.7. Tentative assignments of signals in the ^{1}H,^{13}C-HSQC spectrum

Crosspeaks	Correlation $\delta^{13}C/\delta^{1}H$ [ppm/ppm]	Suggested assignment
0	(-2)-2/(-0.4)-0.3	Si-**(CH$_3$)$_x$** x=1-3
1	5.1/0.67	Si-**CH**- ; Si-**CH$_2$**-
2	17.9/1.2	Si-**CH$_2$**-
3	18/1.93	
4	22/1.78	Si-CH$_2$-**(CH$_2$)$_x$**-CH$_n$
5	22.8/1.7	
6	29.3/1.27	x≥1 and n=0-3
7	39.4/1.59 39.4/1.92	C-**CH$_n$**-C-O
8	39.7/1.93	CH$_n$-**CH$_n$**- (n=0-2)
9	44/2.59 44/2.78	
10	50.3/3.56	**CH$_3$**-OH
11	50.8/3.12	
12	58.9/3.82	Si-O-**CH$_3$**
13	66.5/4.1	Si-O-**CH$_2$**-CH$_n$ (n=0-3)
14	71.3/3.7 71.3/3.4	CH$_n$-**CH$_2$**-O-**CH$_2$**-CH(O)(CH$_2$)
15	73.5/3.46	CH$_n$-**CH$_2$**-O-CH$_2$-CH(O)(CH$_2$) (n=0-3)
16	125/5.53	Si-**CH**=CH$_2$
17	132.37/5.93	
18	133/5.74 133/5.79	Si-CH=**CH$_2$**
19	132.2/5.68	
20	126/7.25	
21	126/7.31	
22	122.8/7.51	

Further characterization of the CSA was feasible by ^{29}Si-DEPT NMR. For the sake of clarity, the well-established nomenclature for siloxanes is employed and the conventional symbols of the building units are shown in Figure 4.19. A general assignment of the individual signals to different building blocks is based on available ^{29}Si-NMR literature [175,222,225,237,243,252–258]. Additional sources used are referenced in the text.

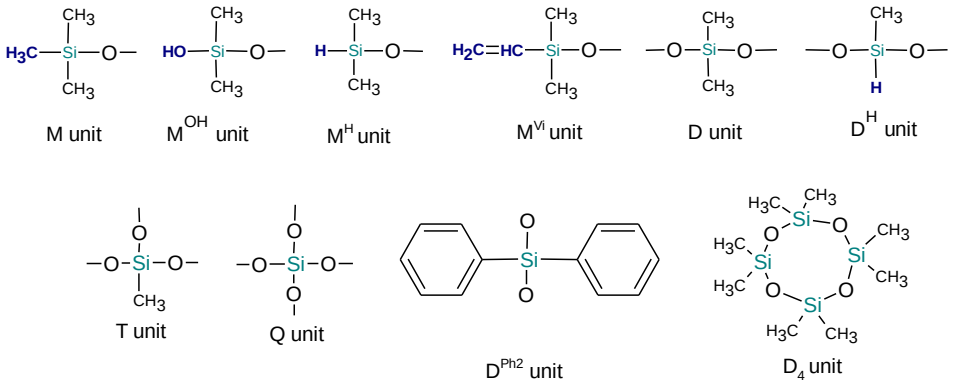


Figure 4.19. Abbreviation of siloxane building blocks [175,222,243].

As it occurred for the ^{1}H-NMR spectrum, in the ^{29}Si DEPT spectrum (Figure 4.20) a dominant signal attributed to D units is perceived at -22 ppm. In addition, a broad and weak signal is recognized at δ ~ 8-14 ppm which is attributed to terminal methyl groups or M units (-OSiMe$_3$). The large linewidth of this signal suggests either the presence of a substantial variation in the chemical environment [237]. Explanation for the broad feature can be given by contribution of Me$_3$SiOH groups that display a ^{29}Si signal at ~ 13-14 ppm [258,259].

Due to the low intensity of additional signals arising from other functionalities, further elucidation of the chemical nature of the silicone substituents in the CSA was achieved by the ^{1}H,^{29}Si-HSQC method. The principal correlations of ^{1}H to ^{29}Si nuclei are recognized and marked in the spectrum of Figure 4.21. The first crosspeak is seen at $\delta_{^{29}Si}/\delta_{^{1}H}$ ~ -43 ppm/3.5 ppm, exact assignment is uncertain but it can be related to silanes containing -OCH$_3$/-OH groups or to hydroxyl groups attached to a silicon atom with pendant phenyl groups (M^{Ph_2OH}) [256,260]. The crosspeak 2 with (^{29}Si) signal at ~ -35 ppm shows a correlation via $^{n}J_{SiH}$ to a ^{1}H-NMR signal at 0.13-0.2 ppm. The crosspeak can be ascribed to methyl groups in D^{H} and D^{Vi} units, which implies that both hydride and vinyl groups were not only present as end-groups but also as middle functionalities. The crosspeak 3 at (δ^{29}Si) -22.07 ppm is the most predominant signal

and it is ascribed to the repeating D units of a linear siloxane polymer. This peak is flanked by satellites due to spin-spin coupling and by weak crosspeaks that could result from cyclic siloxane traces as D_4 at $\delta^{29}Si/\delta^{1}H$ ~ -20 ppm/0.8 ppm [261], and fragments of D units near to M^{OH} groups.

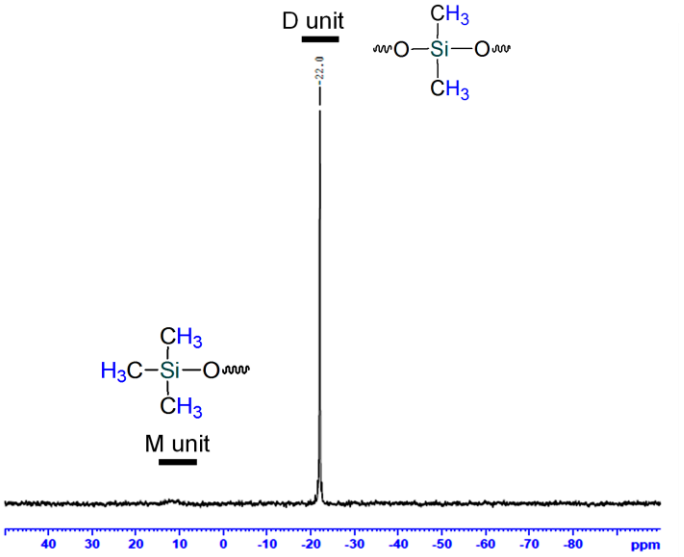


Figure 4.20. Solution state ^{29}Si-DEPT NMR spectrum of the soluble part of the uncured CSA in $CDCl_3$ [237].

The crosspeak 4 at $\delta^{29}Si/\delta^{1}H$ ~ -4 ppm/0.15 ppm is assigned to D units close to M^{Vi} units confirming the presence of terminal vinyl groups [228]. Surprisingly, the expected direct correlation between terminal vinyl protons and ^{29}Si atoms at -4.0 ppm/5.2-6.0 ppm ($\delta^{29}Si/\delta^{1}H$) [211,228,236,262], and between terminal Si-H at -35 ppm/4.7 ppm ($\delta^{29}Si/\delta^{1}H$) [234,236,258,263], are not observed. Also, the expected signal associated with D units near M^{H} units at -7/0.08-0.12 ($\delta^{29}Si/\delta^{1}H$) [236,258], is not perceived. Possible low concentration of terminal Si-H and Si-vinyl moieties prevented the appearance of correlated atoms in the 2-D spectrum. In addition, connection between methylene protons and ^{29}Si atoms possibly from organosilanes is evidenced by the crosspeak 5 with chemical shift from -2.5 to 0.5 ppm (^{29}Si) and (^{1}H) at 0.18-0.21 ppm.

Ultimately, the crosspeak 6 at ~ 8-13 ppm/0.08-0.18 ppm ($\delta^{29}Si/\delta^{1}H$) is related to M units and to Me_3SiOH units as mentioned earlier. Finally, Q units were neither detected in ^{29}Si-DEPT nor in ^{1}H, ^{29}Si-HSQC spectra indicating that at room temperature crosslinking of the CSA did not occur.

Table 4.8 summarizes all the information extracted from all NMR spectra obtained for the uncured CSA. The relative integrals estimated from the proton NMR spectrum (Figure 4.15) are included.

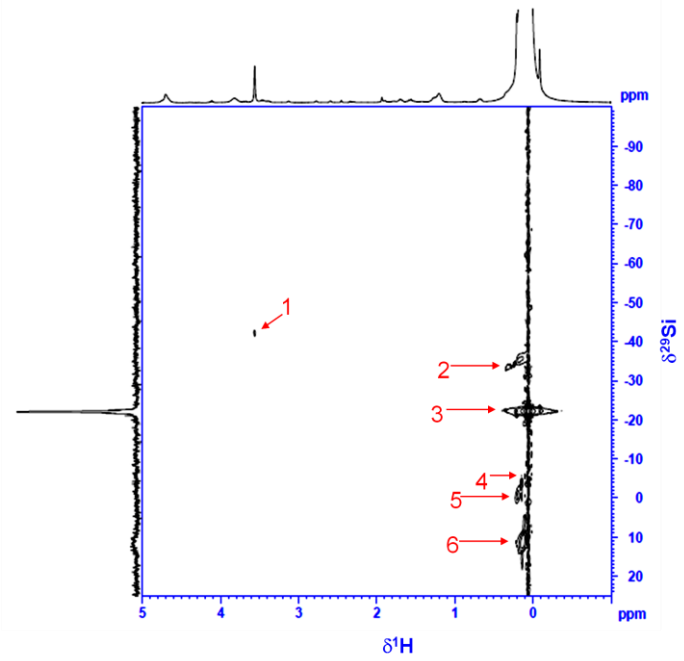


Figure 4.21. Solution state ^{1}H, ^{29}Si-HSQC spectrum of the soluble uncured CSA in $CDCl_3$ [237]. Six principal correlations or crosspeaks from different structural units are perceived.

Table 4.8. ^{1}H-, ^{13}C- and ^{29}Si-NMR signals associated with functional groups found in the CSA.

δ ^{1}H [ppm]	δ ^{13}C [ppm]	δ ^{29}Si [ppm]	Relative integral (%) from ^{1}H-NMR	Associated functional groups
0.5-0.5	2.0-2.0	-22	95.6	-Si-$(CH_3)_x$ x=1-3
0.5-3.0	6.0-45	-2-2	1.1	-CH_n- n=1-3
3.0-4.2	45-75	-42; -2	1	-O-CH_n n=1-3
4.5-5.0	-	-35; -7	0.4	-Si-H
5.5-6.5	125-133	-36; -4	0.6	-Si-CH=CH_2
7.0-8.0	122-126	-45	0.6	-Si-C_6H_5 (Phenyl)

4.3.2. Additional characterization

4.3.2.1. Molar mass determination by GPC

The molar mass distribution (MMD) or molecular weight distribution influences the performance properties of a polymeric material [264,265]. Among the various characterization techniques for determining the molar mass of polymers, gel permeation chromatography (GPC), also known as size exclusion chromatography (SEC), is probably the most popular since the complete MMD curve is attained [264]. The principle of GPC is based on separation of molecules according to their hydrodynamic volumes in solution which are directly related to their molar masses [264–266]. From proper calibration of the GPC system; average mass values including weight-average molar mass (M_w), number-average molar mass (M_n), and polydispersity index (PDI=M_w/M_n), of known and unknown polymers, can be determined [264–266].

The GPC method consists of eluting a dilute polymer solution in a mobile phase through a column set (stationary phase) of swollen, macroporous polymer gels of different porosities [264,267]. As the solution passes through the column system, the smaller molecules diffuse in and out of the pores; whereas the larger ones pass by, being eluted first. The eluate fractions are analyzed by a detector (UV, viscometer or refractive index) giving elution profiles which approximate to Gaussian curves. The conversion from elution volume to molar mass is achieved by applying an adequate calibration method. A more detailed description of the GPC principles can be found elsewhere [264–266,268].

As calibration is crucial in GPC, polymer standards of known molar masses and narrow molar mass distributions (low PDI) are required in order to obtain quantitatively correct data [268]. Accordingly, the calibration method is valid only if the standard and the sample have similar polymer-solvent interactions since the true size of the polymer molecule in solution is affected not only by the structure of the polymer chain but also by their interactions. Commonly, polystyrene (PS) is used as a standard for calibration because PS with low PDI can be attained via anionic polymerization. However, PS is not the most appropriate GPC standard for silicones due to significant differences in their hydrodynamic volumes and to dissimilar interactions with typical GPC solvents [269,270]. Therefore, calibration based on PDMS standards are rather employed and suggested for the analysis of siloxane based polymers [270]. Toluene is a preferred solvent for the analysis of silicones by GPC

because it has a significantly high refractive index, resulting in a good response when using a refractive index detector (RID) [271,272].

Experimental

The analysis of the uncured CSA by GPC was carried out externally on behalf of Robert Bosch Ltd at Polymer Standard Services (PSS) Ltd (Mainz, Germany) by Ms. Verena Mützel. The equipment employed was a PSS SECcurity GPC modular system (PSS Ltd, Mainz, Germany) equipped with a 1260 RID. The separation was performed on a set of PSS SDV columns (PSS Ltd, Mainz, Germany) consisting of one pre-column and three columns. The pre-column had a pore size diameter of 100 Å and dimensions of 8.0 mm internal diameter (i.d.) x 50 mm. The three columns had pore sizes of 100, 1000, and 100000 Å with dimensions of 8.0 mm i.d. x 30 cm each. The average particle size of the packing materials in the pre-column and columns was 5 µm diameter. The temperatures of the column system and detector were set at 23 °C ensuring efficiency and consistent results. HPLC-grade toluene was used as the mobile phase at a flow rate of 1.0 ml/min. Fifty microliters (50 µl) of the sample solution, in toluene (HPLC-grade), at a concentration of 5 g/l were injected into the GPC system. The uncured CSA was used as received and the sample solution was prepared at RT (~23 °C). No filtration of the samples was applied prior to GPC measurement. The GPC column system was calibrated with a PSS-pdmskit (PSS Ltd, Mainz, Germany) consisting of eight different certified standards (ISO/EN 13885) of PDMS polymers with narrow molar masses ranging from 230000 to 311 Da (which covered the molar mass range of interest). The absolute methods applied for determining the molar mass of the standards were NMR and light scattering. PSS-WinGPC UniChrom®, Version 8.0 software (PSS Ltd, Mainz, Germany) was used for data acquisition and calculations.

Results

The elution volumes obtained in the calibration for each standard are given in Table 4.9, and the calibration curve is presented in Figure 4.22. The experimental GPC chromatogram obtained for the uncured CSA (Figure 4.23) indicates a notable wide molar mass distribution ranging from 300 to $6x10^5$ Da, corroborated by the high discrepancy between M_n and M_w (PDI=6.6) (Table 4.10). It is known that M_w is sensitive to high molar masses while M_n to lower molecular weight, hence the greater value obtained for M_w than for M_n for the uncured CSA [273].

Table 4.9. Elution volume of the eight PDMS standards used for calibration [274].

Elution volume (V_e) [ml]	Molar mass (M) [Da]
18.99	$2.30x10^5$
19.75	132000
20.87	59500
22.02	28500
24.01	10800
26.32	3450
29.35	1110
32.15	311

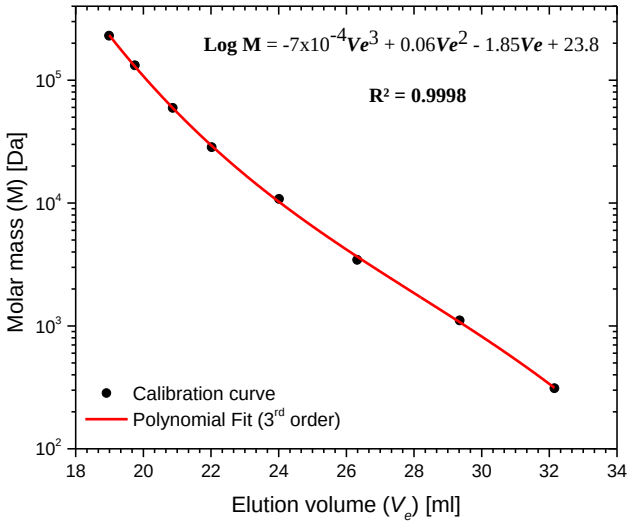


Figure 4.22. GPC calibration curve obtained from eight PDMS standards

The chromatogram of the uncured CSA (Figure 4.23) exhibits one representative peak corresponding to high molecular weight PDMS ranging from $1x10^4$to $2x10^5$ Da and a low molecular weight shoulder between 300 and 3000 Da. The first can be connected to vinyl, hydride, phenyl and methyl functionalized PDMS polymers, and the latter can be associated with oligomeric species of different chemical nature and to molecules of remarkable smaller size, such as monomers, cyclic siloxanes, silanes, inhibitors, catalyst and other components.

Additionally, the disparity between M_w and M_n could also arise from possible existing branched polymers, since they have lower hydrodynamic volumes, thus having lower apparent molecular weight by GPC [275].

The broad molar mass distribution curve obtained for uncured CSA by GPC, evidences the complex nature inherent to the commercial silicone system analyzed.

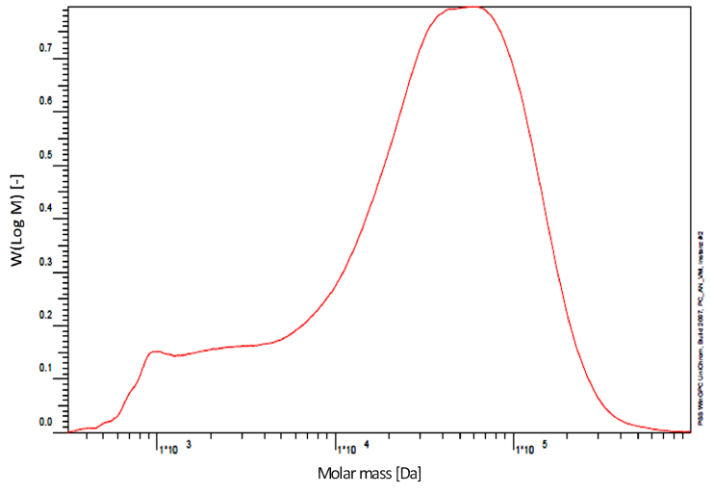


Figure 4.23. GPC chromatogram of uncured CSA [274].

Table 4.10. Average molar masses calculated for the uncured commercial silicone CSA [274].

M_n [Da]	M_w [Da]	PDI	M_p [Da]
8520	56300	6.6	69400

4.3.2.2. Thermal analysis

Despite the well-known superior thermal stability of silicone elastomers [17,19,26,208], the CSA may face hostile environments where heat, oxidizing atmospheres or ultraviolet radiation may accelerate its degradative processes [14,276–278]. Through degradation, silicones can lose part of their original properties and may in time become inappropriate for their intended use; therefore, degradation of the silicone product should be understood to ensure a successful application. The degradation process depends on both the external conditions at which the silicones are exposed, and on inherent physicochemical properties of the material such as its MMD, the chemical nature of the components, and the type and amount of filler or additives included.
Techniques such as TGA and DSC allow the determination of important temperatures at which state changes in silicones occur, thus, improvement of processing efficiencies

and development of products with longer shelf-life can be achieved [279]. Subsequently, in this work, TGA and DSC measurements were implemented with the aim of providing a general impression of the thermal behavior and stability of the unaged CSA.

A. TGA Analysis

TGA (thermogravimetric analysis) is a method in which changes in the mass (m) of a material are measured in a controlled atmosphere as a function of temperature (T) and time (t). Dynamic or non-isothermal measurements ($\Delta m=f(T)$) and isothermal measurements ($\Delta m=f(t)$) can be applied [264,279]. In a routine TGA measurement, the weight of the sample is recorded continuously as temperature rises from room temperature (RT) to T>500 °C. Weight loss of material can be attributed to processes of volatilization, dehydration, decomposition, crosslinking, oxidation/reduction, and other chemical reactions [264,279]. Consequently, the processes associated with thermal and thermo-oxidative stability of a polymer can be inferred, predicted or modeled. Additionally, determination of filler or additive content in silicones is also feasible [280]. Thermal events such as melting, glass transition and other phase transitions, are not detected by TGA as no alteration in sample mass occurs.

Experimental

The characteristic non-isothermal weight loss was performed on a TA Instruments Q5000 (TA Instruments, Hüllhorst, Germany) containing a balance of sensitivity < 1 µg. Approximately 7-10 mg of sample were loaded onto a platinum sample pan (previously cleaned and weighed). The pan containing the sample was placed on the TGA balance automatically by the autosampler. The samples were heated from 308 K (35 °C) to 1173 K (900 °C) at a heating rate of 10 K/min in a flowing air atmosphere and in a nitrogen atmosphere. Both the nitrogen and air flow rate were set to 25 ml/min. The mass loss data were recorded by the software Universal Analysis 2000 V4.5A (TA Instruments) and the thermograms were further analyzed and processed in OriginPro 8.6®. Two types of samples were analyzed: (a) initially uncured CSA (used as received) and, (b) initially cured CSA (cured in an air circulating oven at 130 °C for 1 h).

Results

The weight loss vs. temperature curves together with their derivatives (DTG curves) in nitrogen and air atmospheres are illustrated in Figure 4.24a-b for initially uncured

and initially cured CSA samples. DTG curves represent the rate of weight loss as a function of temperature (dm/dT) and their peaks indicate the temperature of maximum weight loss rate. It can be observed that the CSA samples underwent different mechanisms during degradation in air and nitrogen. A higher thermal stability of the CSA in nitrogen than in air atmosphere can be evoked. As reported by Jovanovic et al. [281], the thermal stability of polysiloxanes is considerably decreased by the presence of oxygen, even at trace levels.

The less smooth DTG curves observed for the initially uncured CSA, expose a more complex degradation behavior of this sample in both atmospheres. Table 4.12 includes the most important features of mass loss events undergone by the CSA. These values include the temperatures for 5% weight loss ($T_{5\%}$) which is often claimed as the onset degradation temperature of silicones [282–285], and provides a first indication of thermal stability. The results obtained reveal a tendency of the $T_{5\%}$ to be delayed when the measurements are carried out in a nitrogen atmosphere. The TGA curves display insignificant weight loss up to ~ 300 ° and accelerated decomposition above 400 °C. These results are consistent with those commonly obtained for PDMS and silicone rubbers [204,282,286,287]. Differences in thermal stability for the two types of samples analyzed could be due to differences in the 3D polymer network structure formed during curing process.

The values of onset degradation in air and in nitrogen (Table 4.11) are in good agreement with those found by Ghanbari-Siahkali et al. [288] and Deshpande et al. [204,205] for polysiloxanes containing phenyl groups. Normally, silicones lacking phenyl substituents exhibit degradation at lower onset temperatures ~ 300-350 °C [289,290]; therefore, the presence of phenyl groups in the CSA is also confirmed by TGA. Besides phenyl substituents, contribution to thermal stabilization of CSA could result from unreacted residual vinyl groups. It has been proposed by Camino et al. [286], that in air, unreacted vinyl can crosslink further at higher temperatures with radicals formed during depolymerization.

The decomposition of CSA evolved through multiple consecutive events, each of them identified as a peak or hump on the DTG curves. The overlapping of peaks observed, suggests concurrency of different mechanisms. Three principal weight loss steps can be tentatively assigned for degradation of CSA in air and N_2; however, further work is proposed for confirmation. The multifaceted degradation path verifies the complexity of the CSA since, for pure PDMS, it has been reported that degradation proceeds in a single step in nitrogen or in two steps in air [283,286,290].

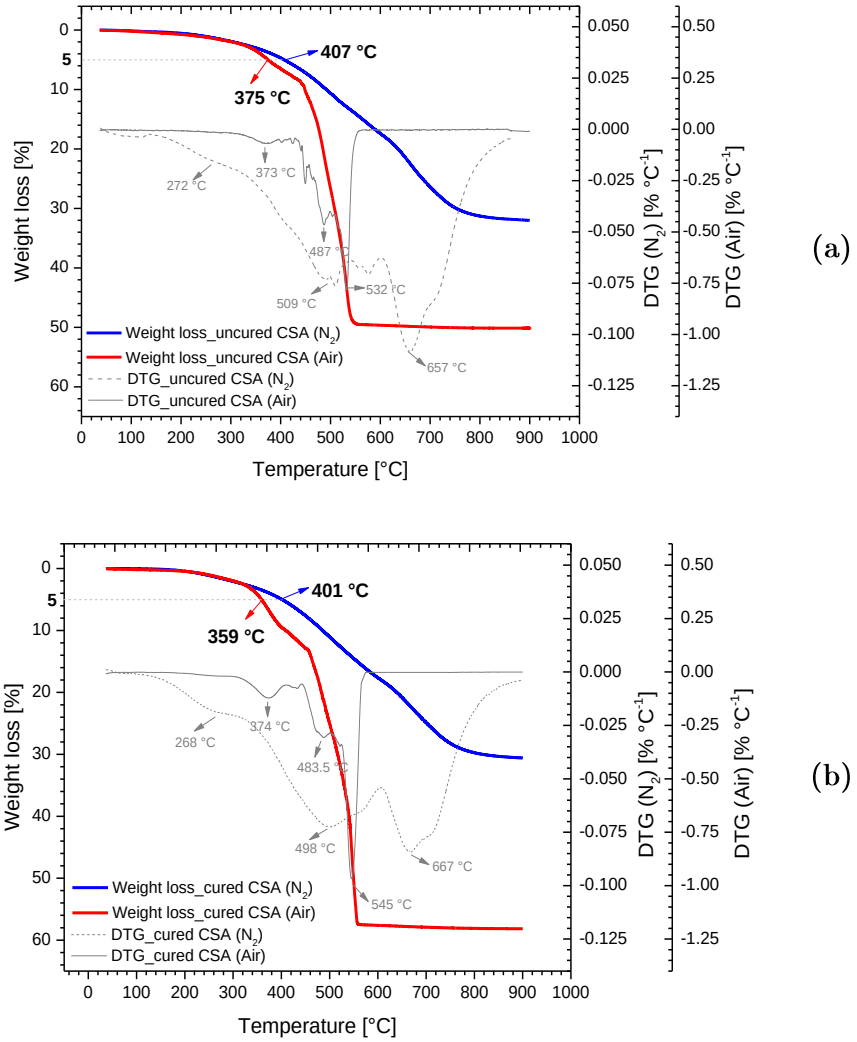


Figure 4.24. TGA and DTG curves in nitrogen and air at a heating rate of 10 K/min for (a) initially uncured CSA and (b) initially cured CSA.

Table 4.11. Important temperatures and total mass loss of the CSA obtained from TGA measurements in nitrogen and air atmospheres

Sample (CSA)	Purging gas	Temperature of 5% weight loss, $T_{5\%}$ [°C]	Temperature of 10% weight loss, $T_{10\%}$ [°C]	Temperature end mass loss T_e. [°C]	Total mass loss at 900 °C [%]
Initially uncured	N_2	407	490	820	32
	Air	375	450	560	52
Initially cured	N_2	401	484	850	30
	Air	359	410	580	58

The weight loss step observed at T< 340 °C in both atmospheres can be connected to the release of adsorbed water (despite the hydrophobic character of silicones), elimination of impurities or to partial volatilization of low molar mass species contained in the silicone [282,291]. Importantly, the insignificant weight loss of the CSA perceived at this temperature range in both atmospheres, advocates that there is no pertinent degradation process or mass loss during curing at 130 °C. In contrast, above 340 °C, decomposition of CSA proceeds abruptly both in nitrogen (up to ~ 850 °C) and in air (up to ~ 580 °C), indicating that oxygen catalyzes degradation as claimed by Thomas and Kendrick [292].

The exact degradation mechanisms of the CSA, in air and nitrogen, were not deducible from the TGA measurements applied in this work since the method did not give information about the nature of the volatilized species. Possibly, PDMS in the CSA followed the degradation mechanism in air described by Jovanovic et al. [281], consisting in heterolytic cleavage of the Si-O bonds yielding a mixture of volatile and low molecular weight products (predominantly cyclic siloxanes) that have the same chemical composition as the original polymer, but being more thermodynamically stable at those degradation temperatures. The decomposition producing cyclic siloxanes is described to proceed indefinitely until the residual linear structure is too short to cyclize or elimination of the shortened chain fragments favorably competes with cyclization [286]. It has been explained that the driving force during degradation of PDMS towards formation of cyclic siloxanes, is the use of the empty 3d-orbitals in silicon atoms in creating more energetically favorable states through bond rearrangement [286,292], leading to the expulsion of cyclic molecules and to the shortening of the residual chain length (volatile oligomers) [286,290]. Therefore, degradation process of silicones has been claimed to be governed by molecular structure and kinetic considerations rather than bond energies. The cyclization process occurring during depolymerization of PDMS is presented in Figure 4.25.

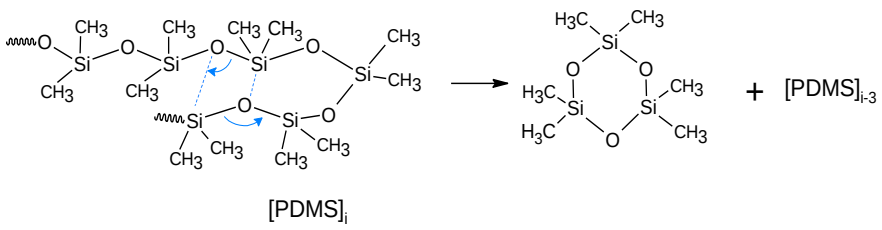


Figure 4.25. Depolymerization mechanism of PDMS towards formation of cyclic siloxanes described by Camino et al. [286].

On the hand, degradation mechanisms proposed for PDMS in air [290,292,293], state that oxygen and free radicals lead to oxidation and cleavage of organic substituents at the silicon atom instead of attacking the backbone directly; consequently, pure silica (SiO_2) is obtained as the only degradation product above 500 °C. In fact, the white/gray color observed in the TGA measurement residue of the CSA (in air) proves the yield of silica, suggesting that the residue and the filler had the same nature. Therefore, silica can be confirmed as the filler in the CSA. The inclusion of silica as the filler may have positively contributed to the thermal and thermos-oxidative stability of the CSA.

Lastly, based on the TGA results it can be stated that the CSA can be cured at 130 °C and can be used in applications up to 300 °C without serious concerns of thermal degradation and weight loss. The differences in the thermal behavior of the CSA compared to pure PDMS or other silicone systems reported in other works, results from complexity of the commercial system in discrepancies such as molecular weight, end group chemistry, presence of phenyl groups, fillers and additives, as well as the presence of impurities.

B. DSC Analysis

Differential scanning calorimetry (DSC) is a useful technique for phase transition analysis. It yields peaks relating to endothermic (heat absorption) and exothermic (heat release) processes of materials during transitions caused by phase changes, melting, oxidation and environmental degradation [264,279]. DSC is a method in which the heat flow rate difference between a sample and a reference is measured as a function of temperature or time, while the sample is subjected to a defined temperature program [279,294]. The obtained transition temperatures, heats, and heat capacities and all DSC results depend strongly on the application of an adequate calibration method prior to sample measurements [264,294]. In general, two types of transitions can be inferred from a DSC measurement: first order transitions as melting (T_m), crystallization (T_c), and crystal-to-crystal transitions, and second order transitions as glass transition temperature (T_g). Additionally, processing conditions of polymers can be monitored via DSC and heat of fusion, heat of reactions, heat capacity, and liquid-crystal transitions can be estimated [264].

Experimental

Curing behavior

The measurements for the CSA, as received, were all conducted on a heat-flux DSC Q2000 equipment (TA Instruments, Hüllhorst, Germany) under nitrogen atmosphere with a purging flow of 50 ml/min. Universal Analysis 2000 V4.5A (TA Instruments, Germany) was used as the software for operation and data recorder of the DSC measurements. The temperature was calibrated with zinc and indium using a baseline obtained with sapphire. The hydrosilylation reaction was monitored by non-isothermal and isothermal DSC scans with the heat flow being measured as a function of temperature and time, respectively. Firstly, the non-isothermal measurement was conducted from 293 K (20 °C) to 523 K (250 °C) at constant heating/cooling rate of 10 K/min. Two consecutive heating/cooling cycles were applied in the temperature range mentioned. Cooling was applied to verify the existence of possible reversible reactions. Secondly, isothermal curing at 130 °C was accomplished by heating up the samples at a ramp of 100 K/ min from 303 K (30 °C) to 403 K (130 °C) and thereafter, the temperature was held at 130 °C for 60 min emulating the CSA standard curing conditions. Immediately after the 60 min of curing were finished, the sample was heated from 303 K (30 °C) to 513 K (240 °C) at a heating rate of 10 K/min, in order to corroborate if the sample was fully cured at the isothermal conditions applied.

Additionally, the CSA cured in an air circulating oven at 130 °C for 1 h was inspected throughout a non-isothermal DSC scan from 298 K (25 °C) to 473 K (200 °C) at a heating/cooling rate of 10 K/min. The aim was to determine if possible post-curing reactions of CSA took place.

For all measurements, a sample ranging in weight from 5 to 10 mg was placed in hermetically sealed aluminum pans of 50 µl, previously weighed. The encapsulated sample was incorporated in the DSC sample holder and an empty aluminum pan with lid was used as a reference. The DSC curves were normalized with respect to the mass of the sample for further processing. TA Universal Analysis and OriginPro8.6® software were used for analysis and further data processing. The weight losses after the tests were found to be negligible. Table 4.12 lists the temperature program applied for the non-isothermal and isothermal measurements for evaluating the curing of CSA.

Table 4.12. DSC temperature program applied for analyzing the thermal curing of the CSA.

Uncured CSA		Cured CSA
Non-isothermal DSC	Isothermal DSC	Non-isothermal
1. Equilibrate at 298 K (isothermal for 5.0 min)	1. Equilibrate at 303 K (isothermal for 5.0 min)	1. Equilibrate at 298 K (isothermal for 5.0 min)
2. Heating at 10 K/min to 523 K	2. Heating at 100 K/min to 403 K	2. Heating at 10 K/min to 473 K
3. Cooling at 10 K/min to 298 K	3. Isothermal at 403 K for 60.0 min	3. Cooling at 10 K/min to 298 K
4. Heating at 10 K/min to 523 K	4. Heating at 10 K/min from 303K to 523 K	4. Heating at 10 K/min to 473 K
5. Cooling at 10 K/min to 298 K	5. Cooling at 10 K/min to 303 K	5. Cooling at 10 K/min to 298 K

Cured CSA

The transition temperatures of the cured product were determined by non-isothermal DSC scans. They were conducted externally on behalf of Robert Bosch Ltd at the Institute of Technology of Plastics, at the University of Stuttgart (Stuttgart, Germany) by Ms. Steffi Müller. The apparatus used was a heat-flux device Mettler DSC821e/700 (Mettler Toledo, Switzerland) hooked up to a liquid N_2 cooling device. The measurements were carried out under nitrogen atmosphere (50 ml/min). Calibration of temperature was carried out using indium, water, n-heptane, and zinc. Samples of about 14 ± 2 mg were placed and sealed hermetically in a standard aluminum pan of 40 µl. The non-isothermal DSC scans were performed in a temperature range from 133 K (-140 °C) to 293 K (20 °C) since important phase transitions of silicones as T_g, T_m and T_c, occur below -30 °C [23]. The heating and cooling rate applied was 5 K/min. This rate was selected based on preliminary DSC runs from -80 °C to 20 °C at different heating/cooling rates of 10, 5 and 3 K/min. From those trials, it was found that crystallization peak appeared only when cooled at 5 K/min or at lower rates, as suggested by Dollase and coworkers [295]. The temperature program applied for the analysis of the cured CSA by non-isothermal DSC scan is presented in Table 4.13.

The transition temperatures of CSA were estimated from the inflection points of the 2nd heating/cooling DSC curves. The glass transition temperature (T_g) was estimated from the first derivative of the heat flow (HF) with respect to temperature (d(HF)/dT). T_g was set as the temperature at peak maximum in the first derivative curve, and the T_g range was defined by $T_{g,o}$ (onset of T_g) and $T_{g,e}$ (endset of T_g). Furthermore, first order phase transition temperatures were obtained from peak maxima, the crystallization point (T_c) from the exothermic peak, and the melting point (T_m) from the endothermic peak. The variation of heat capacity at the glass transition defined by ΔC_p was also calculated from the heat flow curve.

Table 4.13. DSC temperature program applied for determining phase transitions of cured CSA.

Non-isothermal DSC
1. Equilibrate at 133 K (-140 °C) (isothermal for 8.0 min)
2. Heating at 5 K/min to 293 K (20 °C)
3. Cooling at 5 K/min to 133 K (isothermal at 133 K for 8 min)
4. Heating at 10 K/min to 293 K
5. Cooling at 10 K/min to 133 K (isothermal at 133 K for 8 min)
6. Heating at 10 K/min to 293 K

Results

Curing behavior

Upon heating the initially uncured CSA from 25 to 200 °C a prominent exothermic peak is observed in the DSC curve (Figure 4.26a) related to the addition curing reaction (Figure 4.7). The singlet suggests that despite the presence of many different components that could undergo chemical reactions, hydrosilylation mechanism dominated in the curing process of the CSA. By defining the 2nd heating scan curve as a pseudo-baseline, it is established that the curing reaction took place between 115 °C (T_{onset}) and 187 °C (T_{end}), with 130 °C (T_{peak}) as the peak temperature (temperature in which the reaction rate was the maximum). The value of T_{peak} verifies that 130 °C is a suitable and appropriate condition for curing the CSA. The discrepancy between the two heating curves from 25 °C to T_{end}, is due to a different C_p as the initial material was uncured. The occurrence of secondary simultaneous reactions as those described in Figure 4.9, is not inferred from the DSC curve. Such side reactions could have been masked by the prominent single peak. Also, possible secondary Si-Si self-coupling reaction is discarded as no peak from 70 to 100 °C is perceived [296,297].

The absence of peaks in the 2nd heating scan indicates that the reaction yielded a maximum crosslinking density during the 1st heating run and post-curing process did not occurred. The curing time (Δt_{curing}) was approximately 7.2 min at the heating rate applied, advocating a considerably fast reaction. Normally, hydrosilylation of silicones has been reported to occur in relatively short times, even at lower temperatures and in the presence of triorganophosphites inhibitors [298–301]. The two cooling curves (Figure 4.26b) coincide perfectly and do not display any peaks, evidencing the irreversibility of the curing process. Finally, the heat released during curing or heat of reaction (Δh), at the applied DSC conditions, was -16.7 J/g. This value is consistent with those registered in other studies related to the curing of silicones via hydrosilylation [295,300,302].

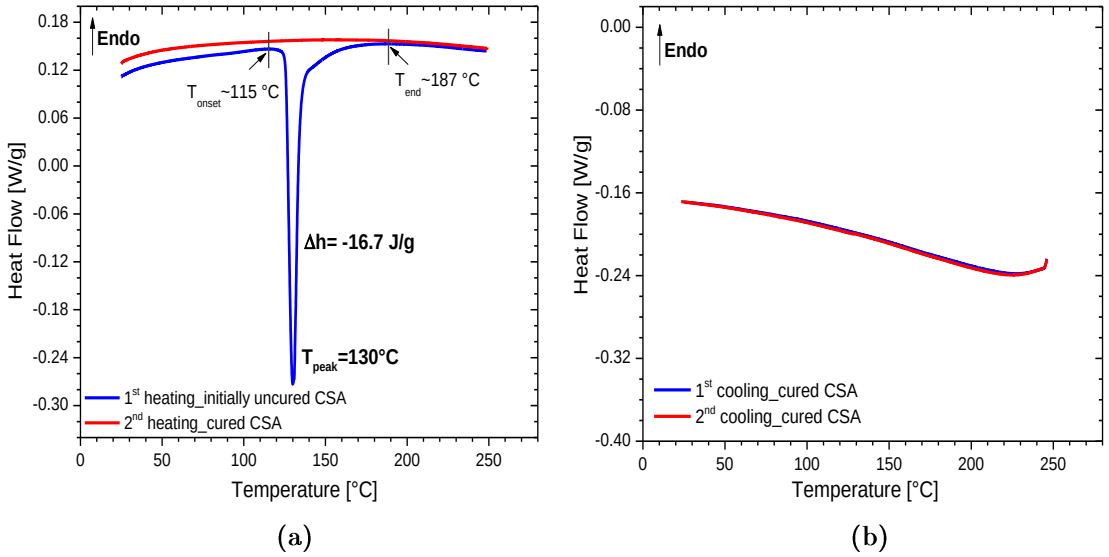


Figure 4.26. Non-isothermal DSC curves, for the initially uncured CSA, from 298 K (25 °C) to 523 K (250 °C) at 10 K/min in nitrogen (50 ml/min). (a) 1st and 2nd heating scans and (b) 1st, and 2nd cooling scans

The isothermal curing DSC profile of the CSA at 130 °C (Figure 4.27-left) shows initially an endotherm signal followed by an exotherm one. The first is due to a thermal lag of the sample when it is heated up rapidly to the desired temperature [303]. This endotherm occurs because there is certain induction time (temperature dependent) before a reaction, leading to the release of any detectable heat, takes place. Correspondingly, the exotherm observed results from heat production by the curing reaction.

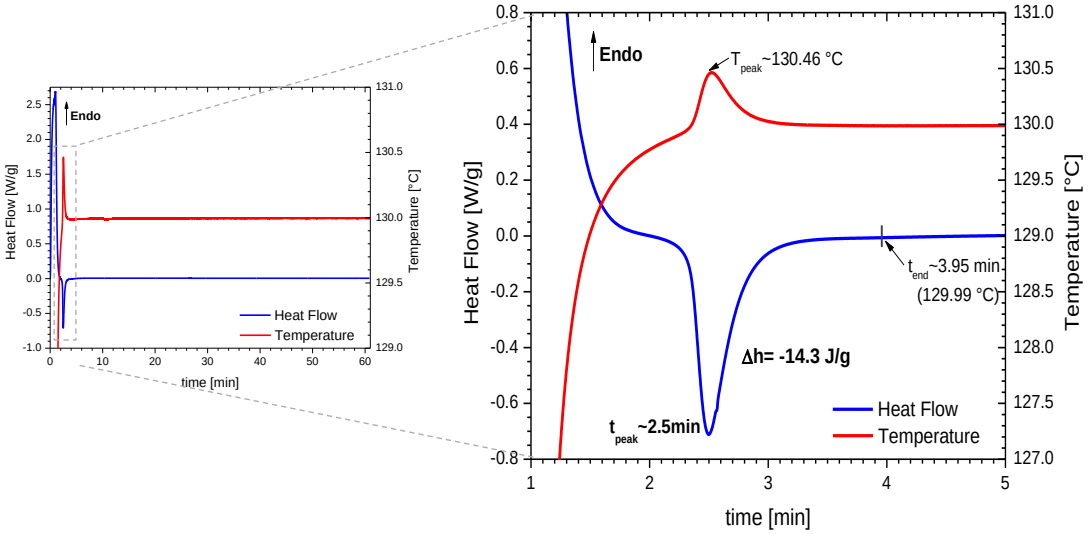


Figure 4.27. Isothermal curing of the pristine CSA at 130 °C for 60 minutes in DSC. Left: complete isothermal DSC profile. Right: magnification of the exothermal signal associated with curing.

From the expanded DSC curve (Figure 4.27-right) the exact starting point of the curing reaction is undefined since it is found before the set temperature is reached. This suggests that when the CSA is cured at 130 °C, the reaction is instantaneously initiated. Instantaneous isothermal crosslinking of PDMS has also been observed by Andersson et al. at 120 °C [302]. An approximate calculation of the heat of reaction (Δh) from the area under the peak is possible by assuming the starting point of the reaction at 1.7 min (~129.5 °C) and the end-point at 3.95 min (t_{end}). It could be state that the isothermal curing of the CSA at 130 °C was completed in approximately 2.3 min (Δt_{curing}) with a maximum reaction rate at 2.5 min (t_{peak}). This result evidences again, that curing of the CSA is a notable rapid process. The heat of reaction (Δh), estimated for $\Delta t_{curing} = 2.3$ min, was -14.3 J/g. Comparison between the heat of reaction calculated from isothermal and non-isothermal DSC measurements would be inappropriate.

The incidence of post-curing reactions was evaluated by a non-isothermal measurement immediately after the isothermal run analyzed above. The absence of peaks in the DSC curve of Figure 4.28a suggests that a maximum crosslinking density of the CSA was attained under the applied isothermal curing conditions. Nonetheless, it is believed that some uncrosslinked PDMS remains in the final network. As stated by Andersson et al. [302], approximately 5 to 20 % of PDMS can remain uncrosslinked in the polymer network after curing.

Finally, Figure 4.28b presents the DSC thermogram of the CSA sample cured isothermally inside an air circulating oven. As expected, no exotherm signals are

displayed, confirming total curing and irreversibility of the reaction when the CSA is cured isothermally at 130 °C for 1 h. Consequently, the standard isothermal conditions employed for curing the CSA, are validated. Although, the total curing time can potentially be reduced, lessening operational costs in industrial applications where the CSA is employed.

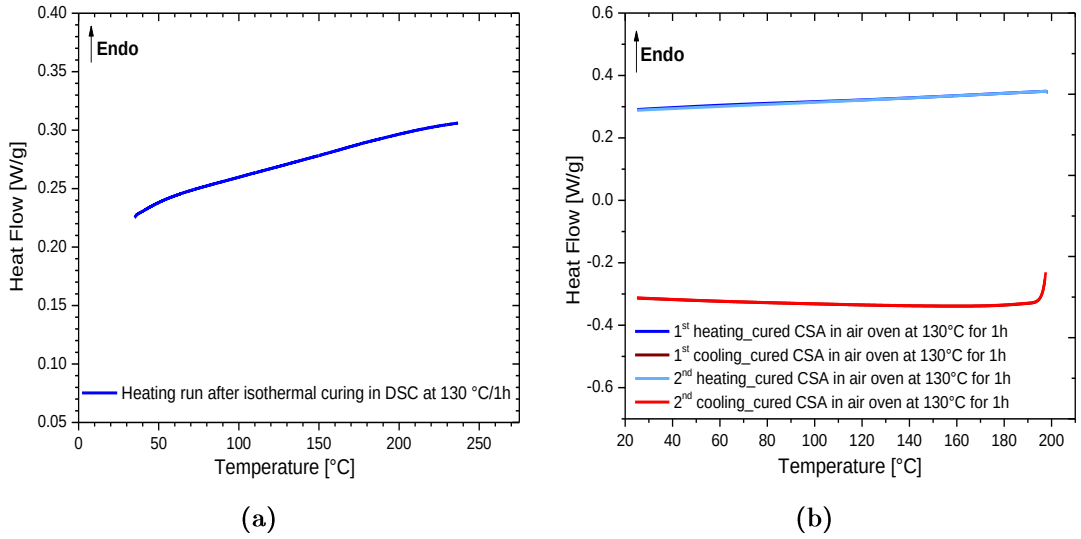


Figure 4.28. Heating scan (10 K/min) of cured CSA (a) when cured isothermally at 130 °C for 1 h in DSC and (b) when cured isothermally at 130 °C for 1 h in an air circulating oven

Cured CSA

From the DSC curves (Figure 4.29a,b) four different thermal transitions are detected for the 1st heating scan: **(1)** glass transition temperature (T_g), **(2)** cold-crystallization ($T_{c,1^{st}H}$), **(3)** melting (T_m) and **(4)** crystallization (T_c). The appearance of these transitions, allows to define the cured CSA as a semicrystalline silicone network. The differences seen between the 1st and the other two heating scan curves at $T<T_m$, can be attributed to a change in the degree of crystallinity after the first heating scan, as confirmed by the appearance of a cold-crystallization peak ($T_{c,1^{st}H}$). The four transitions observed for the cured CSA are described below in more detail. The onset, endset and peak temperatures for each transition are tabulated in Table 4.14 accompanied with their estimated enthalpies.

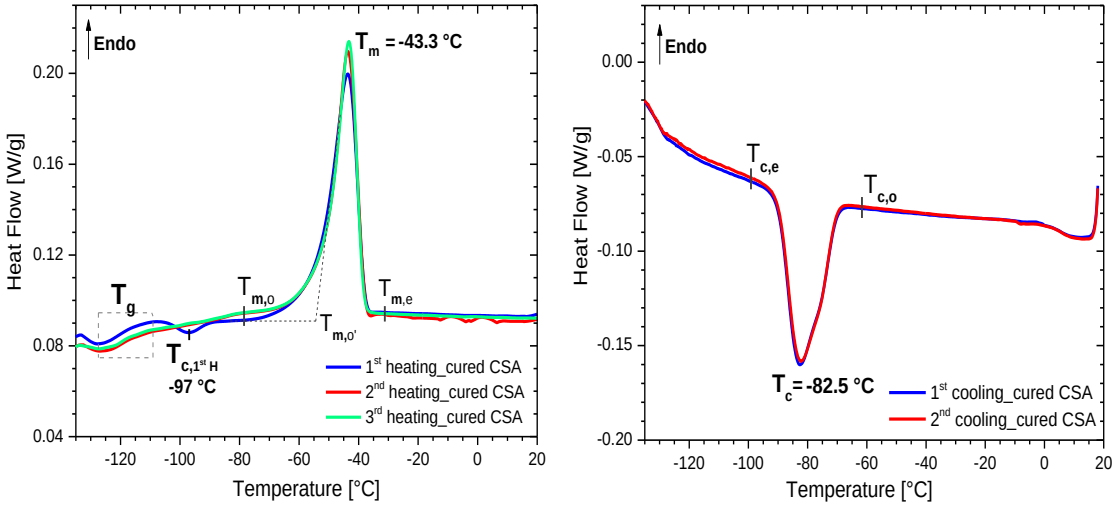


Figure 4.29. DSC curves from 133 K (-140 °C) to 293 K (20 °C) for the cured CSA. (a) heating scans at 5 K/min and (b) cooling scans at 5 K/min.

Table 4.14. Thermal transitions of the cured CSA obtained from the 2nd heating and cooling scans by DSC.

1. Glass transition	$T_{g,o}$ [°C]	$T_{g,e}$ [°C]	T_{g1}[°C]	T_{g2} [°C]	
	-127.8	-107.2	-119.6	-112.3	
2. Cold-crystallization	$T_{c1,o}$ [°C]	$T_{c1,e}$ [°C]	T_{c1} [°C]	Δh_{c1} [J/g]	
	-108	-83.2	-97	-0.54	
3. Melting	$T_{m,o}$ [°C]	$T_{m,o'}$ [°C]	$T_{m,e}$ [°C]	T_m [°C]	Δh_m [J/g]
	-78.4	-54.1	-31.2	-43.3	13.4
4. Crystallization	$T_{c,o}$ [°C]	$T_{c,o}$ [°C]	$T_{c,o}$ [°C]	Δh_c [J/g]	
	-61.6	-99.1	-82.5	-14.5	

(1) Glass transition temperature (T_g)

The increase of the heat flow due to the increment of C_p upon heating above T_g is illustrated in Figure 4.30 (2nd heating run). The curve of the first derivative of heat flow (HF) with respect to temperature (T) is included for the estimation of T_g.

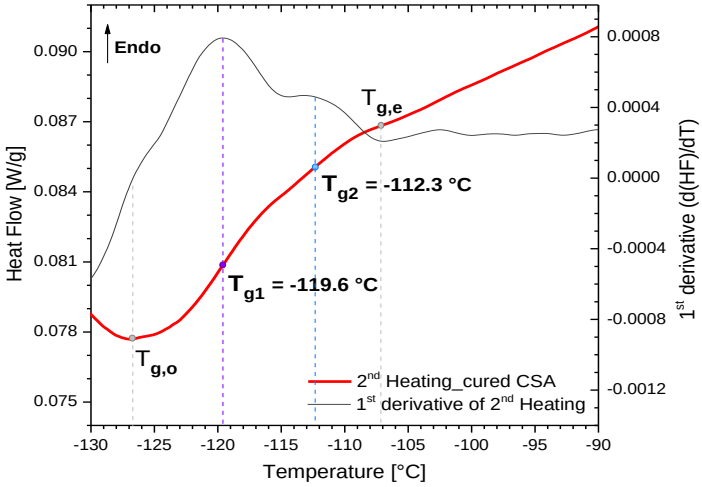


Figure 4.30. 2nd heating run of the cured CSA from 133 K (-140 °C) to 183 K (-90 °C). T_g is estimated from the first derivative curve of the 2nd heating DSC curve.

The first derivative curve discloses a main peak with a shoulder, suggesting an apparent double glass transition for the cured CSA. The maximum temperature of the peak, assigned as T_{g1}, was detected at ~ -120 °C; whereas the one for the shoulder (T_{g2}) was perceived at ~ -112 °C. The onset glass transition temperature ($T_{g,o}$) was set at -127 °C and the endset temperature ($T_{g,e}$) at -107 °C. The apparent double T_g suggests that the bulk material possessed two domains differing in chain mobility. The higher the mobility, the lower the glass transition temperature. As explained by Boyer [304], a double T_g arises from the morphology of a crystallized polymers consisting of chain-folded crystals, tight and loose loops, tie molecules, amorphous material rejected by the crystallites and interlamellar material (Figure 4.31) [304]. Subsequently, the T_g found for the CSA at a lower temperature (T_{g1}) most likely corresponds to a higher movable polymer fraction consisting of: free end chains (cilia), rejected molecules by crystallites, unreacted low molar mass oligomers and other short free molecules included in the CSA. The second T_g perceived at a higher temperature could be attributed to less movable polymer segments associated with loose loops in the crosslinked network, tie molecules and crosslinked PDMS fragments that are interacting strongly with silica filler. Values of T_g for linear PDMS polymers are typically found from -126 to -124 °C [305], whereas for crosslinked or filled PDMS, the T_g has been reported to increase to -111 °C [306] and even to -105 and -104 °C [288]. So far, silicone systems displaying a double T_g have not been reported. However, this distinctive feature of the CSA, seems to be reasonable.

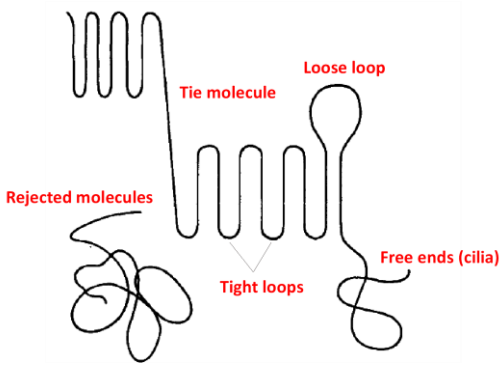


Figure 4.31. Morphological features proposed and depicted by Boyer [304] of crystallized chain folded crystals that might give rise to the double glass transition.

Ultimately, the change in heat capacity, ΔC_p, of the CSA can be estimated following Equations 4-12 and 4-13 [294]. Where φ is the heat flow (HF) [J $s^{-1}g^{-1}$] and β is the heating rate applied (5 K min^{-1}).

$$\varphi = \frac{dq}{dT} \qquad \beta = \frac{dT}{dt} \qquad C_p = \frac{\varphi}{\beta} \tag{4-12}$$

$$\Delta C_p = C_p\big|_{T_{g,e}} - C_p\big|_{T_{g,o}} = \frac{\varphi|_{T_{g,e}} - \varphi|_{T_{g,o}}}{\beta} \tag{4-13}$$

$$\Delta C_p = 0.11 \frac{J}{g \cdot K}$$

(2) Cold crystallization peak ($T_{c,1^{st}H}$)

This transition is perceived as a weak exothermic peak in the 1st heating scan with maximum at ~ -97 °C ($T_{c,1^{st}H}$). This peak is an indicative of previous undercooling; i.e., rapid cooling of the CSA sample from room temperature to -140 °C for applying the first heating run. This peak is observed due to the additional formation of crystals since the polymer did not crystallize to its maximum capacity when cooled at a fast cooling rate. The value is consistent with that found by Dollase et al. [307] at ~-93 °C for PDMS. The heat of cold crystallization was found to be ($\Delta h_{c,1^{st}H}$) = -0.54 J/g.

(3) Melting peak (T_m)

This transition is related to the melting process of the PDMS crystallites. The temperature of melting (T_m) of the cured CSA is identified by a single endothermic

peak upon heating with maximum at -93 °C. The melting peak of crosslinked PDMS is associated with shorter chains, loose loops, unreacted polymer since they have higher mobility and are more capable of forming crystals. By contrast, crosslinked segments are less capable to crystallize. The T_m of cured CSA at -43 °C is consistent with reported values for crosslinked PDMS [295,308]. The enthalpy of crystallites melting estimated was $(\Delta h_{m\ (2^{nd}H)}) = 13.4$ J/g.

(4) Crystallization (T_c)

Crystallization was evidenced by an exothermic peak at -80 °C (T_c) in the two cooling curves. It has been claimed that crystallization of PDMS is enhanced by constraints as entanglements, crosslinks, and presence of silica particles as they favor nucleation [295]. This value is in agreement with reported data of T_c for PDMS polymers [306,308]. The crystallization enthalpy estimated for the CSA was $(\Delta h_c) = -14.5$ J/g.

4.3.3. Synopsis - Characterization of the CSA

Based on the results presented in this screening assessment, it is determined that the methods applied for characterizing the CSA, met the expectations of attaining specific and detail information regarding the structure of the silicone product. It is concluded that the CSA is a multicomponent complex system with PDMS as its principal component and with a wide molar mass distribution.

The measured ATR-FTIR spectra of the commercial silicone system disclosed distinctive peaks that allowed its characterization in bulk. Indeed, this method proved to be an assertive approach for characterizing an unknown commercial silicone system without the strict necessity of physicochemical separation of the product. The principal chemical groups included in its formulation and listed in Table 4.6 were certainly identified. Valuable information was extracted from the measured spectra and reproducibility was achieved in a relative simple manner. Hence, it can be stated that ATR-FTIR is a potential tool for characterizing silicones with known or unknown composition. The feasibility of identifying the principal functionalities of silicones in bulk validates the use of FTIR spectroscopy for elucidating the adhesion mechanisms from adsorption experiments of single model components.

The characterization by diverse NMR methods complemented the information obtained by ATR-FTIR spectroscopy and permitted to confirm the functionalities detected. Additionally, NMR results suggested that vinyl and hydride groups were both present at different positions within the polysiloxane chains. Hence, explicit recognition

of the crosslinker in the system is ambiguous. However, since Si-H groups were added in excess with respect to vinyl PDMS (molar ratio Si-H:Si-vinyl = 1.5:1), a hydride siloxane is selected as crosslinker in this group.

Moreover, evaluation of the NMR spectra evidenced the existence of traces of silanol groups in the CSA product and suggested that different organosilanes as glycidoxypropyltrimethoxysilane, allyltrimethoxysilane or vinyltrimethoxysilane were included in the silicone system for promoting adhesion of the CSA with numerous type of substrates.

From the DSC analysis, it was established that isothermal curing of the CSA, via hydrosilylation reaction, was completed within few minutes (2.3 min) when catalyzed with a Pt complex catalyst. Most likely, inhibitors were included in order to prevent premature crosslinking at ambient temperature, but they permitted rapid platinum-mediated crosslinking reaction at higher temperature.

Reduction of the curing time for the CSA at 130 °C is proposed. This lessening can represent an industrial benefit since shorting production times can result in production costs savings. The optimal time for curing the CSA at 130 °C can be determined by deeper DSC isothermal studies. From DSC measurements of the cured CSA, it was determined that the crosslinked material is a semicrystalline polymer featuring double T_g (at ~ -120 °C and at ~ -112 °C), T_m at -43 °C and T_c at -82 °C. Therefore, in typical service temperatures (-40 up to 200 °C) of the cured CSA, the material possesses high mobility, flexibility and extensibility.

From TGA analysis, it was proven that in those typical service temperatures, the CSA is thermally and thermo-oxidative stable as the onset temperature of degradation in air and nitrogen was above 300 °C and insignificant mass loss events occur below that value.

The characterization of the silicone permitted to establish that the filler included in the commercial product was silica. Effects of silica on the thermal stability and on the transition temperatures of CSA were possible to be ascertained based on the TGA and DSC analysis when compared with reported results of pure crosslinked PDMS without filler.

Finally, based on the results attained from the chemical characterization of the CSA (Table 4.6 and 4.8), the following single silicone model components have been selected for the formulation of a model silicone adhesive and for executing in-situ adsorption and co-adsorption experiments on aluminum:

- Bifunctional hydride terminated PDMS: Prepolymer 1
- Bifunctional vinyl terminated PDMS: Prepolymer 2

- Tetrakis(dimethylsiloxysilane) (TDMS): Crosslinker
- Platinum-based catalyst: Karstedt catalyst (Platinum-divinyltetramethyl-disiloxane complex)
- Allyltrimethoxysilane (ATMS): Adhesion promoter

4.4. Results of the characterization in bulk of the SSMC

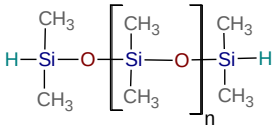
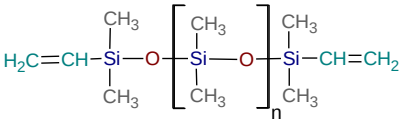
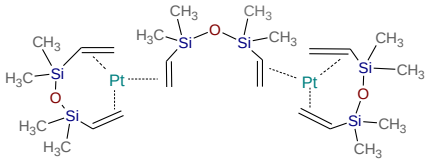
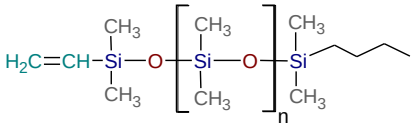
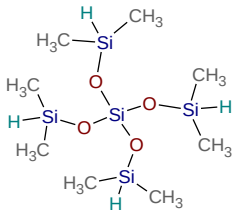
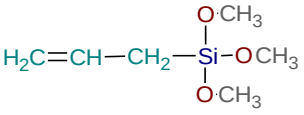
The single silicone model components (SSMC) were selected based on the results obtained in the previous characterization of the CSA. Table 4.15 includes the principal properties of the acquired SSMC provided by the supplier. All compounds were purchased from Gelest, Inc. (Gelest, Inc., Frankfurt, Germany) and stored at 5 ± 1 °C. Handling of the single components prior to every experimental measurement was performed inside a Glovebox purged with dry air (T_{dp}=-65 °C). All components were used as received and characterized by ATR-FTIR spectroscopy following the method described in Section 4.2.1.2. Supplementary ^{1}H-, ^{13}C- and ^{29}Si-NMR measurements were also implemented. In the specific case of the prepolymer 1 and prepolymer 2 additional ^{1}H,^{29}Si-HSQC NMR measurements and GPC analysis were carried out following the experimental conditions given in Section 4.2.2.2 and 4.3.2.1, respectively. The assignments of the ATR-FTIR peaks and NMR signals found in the spectra of the SSMC are based on the results found in the characterization of the CSA in bulk (Section 4.3).

4.4.1. Bifunctional hydride terminated PDMS - Prepolymer 1

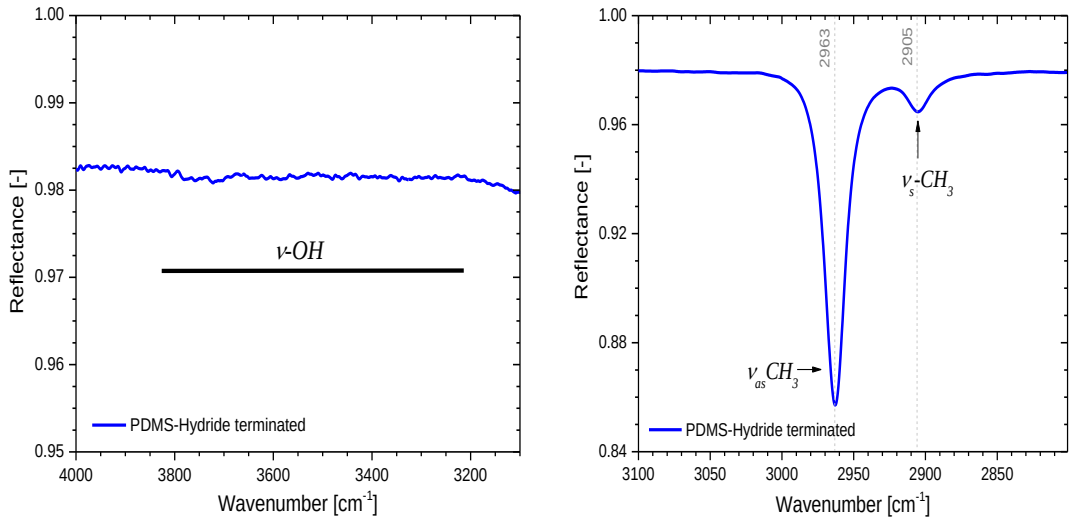
4.4.1.1. ATR-FTIR Spectroscopy

The ATR-FTIR spectra (Figure 4.32) show the characteristic peaks of CH_3, Si-H and Si-O-Si groups which confirm the chemical structure of a hydride terminated PDMS. The possible presence of silanol fragments was not detectable by ATR-FTIR as no absorption band is observed between 3700 and 3200 cm^{-1} (Figure 4.32a). However, their presence might not be discarded, as hydroxyl terminated oligosiloxanes are believed to be present in most commercial samples of functionalized PDMS [32,195,196].

Table 4.15. List of the SSMC acquired including the properties given by the supplier.

Component	Chemical structure	Properties
Prepolymer 1 Bifunctional hydride terminated PDMS		**CAS No.:** 70900-21-9 **Viscosity [cSt]:** 7-10 **M_n [g/mol]:** 900-1200 **Purity [%]:** >95 **Relative density at 23 °C:** 0.93 **Eq/g:** 0.0018
Prepolymer 2 Bifunctional vinyl terminated PDMS		**CAS No.:** 68083-19-2 **Viscosity [cSt]:** 4-8 **M_n [g/mol]:** 700-850 **Purity [%]:** >95 **Relative density at 23 °C:** 0.93 **Eq/g:** 0.00265
Karstedt catalyst Platinum-divinyltetramethyl-disiloxane complex **dissolved in:** Mono vinyl terminated PDMS, n-butyl terminated Catalyst solution with traces of divinyltetramethyl-disiloxane Catalyst employed in room temperature curing silicones	 	**CAS No.:** 68478-92-2 **M_w [g/mol]:** 474.68 **Concentration Pt [% wt.]**: 3.2 **CAS No.:** 68951-99-5 **Viscosity [cSt]:** 200 **M_n [g/mol]:** - **Relative density of the catalyst solution at 23 °C:** 0.98
Crosslinker Tetrakis(dimethylsiloxy) silane		**CAS No.:** 17082-47-2 **M_w [g/mol]:** 328.73 **Purity [%]:** >95% **Relative density at 23 °C:** 0.88
Adhesion promoter Allyltrimethoxysilane		**CAS No.:**2551-83-9 **M_w [g/mol]:** 162.26 **Purity [%]:** >95% (traces of methanol) **Relative density at 23 °C:** 0.96

The vibrations involving methyl groups were identified by two bands at 2963 and 2905 cm^{-1} (Figure 4.32b) corresponding to asymmetric and symmetric stretching of C-H bonds, respectively. The two peaks observed at 1411 and 1260 cm^{-1} (Figure 4.32d) are due to asymmetric and symmetric bending of CH_3. As expected, the bands at 2127 cm^{-1} (Figure 4.32c) and at 910 cm^{-1} (Figure 4.32d) corroborates the presence of Si-H end-groups. The Si-C bonds were evidenced by the band at 864 cm^{-1} and the strong peak at 791 cm^{-1} ascribed to rocking and stretching vibration modes, respectively (Figure 4.32d). The siloxane bond was evidenced by two strong bands at 1100-950 cm^{-1} corresponding to stretch vibration of the Si-O linkage with specific maxima of absorption at 1082 and 1015 cm^{-1}. The splitting into two components is a distinctive feature of large siloxane chains. Thus, the doublet band proved the polymeric nature of the hydride terminated PDMS sample. Moreover, the weak band at 1947 cm^{-1} (Figure 4.32c) is related to the vibration of the complete PDMS backbone, which also proves the macromolecular character of the sample. Finally, for the additional peaks observed below 700 cm^{-1}, exact and specific assignment was challenging as different types of vibrations overlap; although, the general vibration modes contributing in that spectral region are indicated in the spectrum. In summary, through the ATR-FTIR technique the chemical units that constitute the bifunctional hydride terminated PDMS such as Si-H, CH_3, and Si-O-Si were successfully recognized, validating its use for the adsorption experiments.



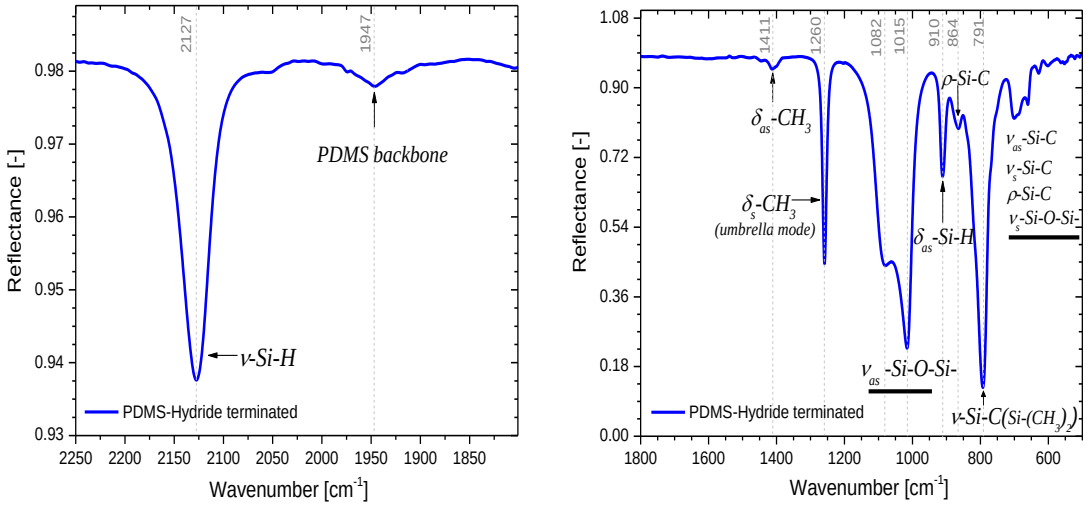


Figure 4.32. ATR-FTIR spectra of bifunctional hydride terminated PDMS in the spectral region (a) from 4000 to 3100 cm^{-1} distinctive of stretching of -OH groups, (b) between 3100-2800 cm^{-1} corresponding to stretch of C-H bonds, (c) from 2250 to 1800 cm^{-1} representative of Si-H stretching and (d) fingerprint region between 1800-500 cm^{-1}.

4.4.1.2. NMR Spectroscopy

The ^{1}H-NMR spectrum of the hydride terminated PDMS (Figure 4.33) shows three principal peaks indicating the existence of three protons with different chemical environments. Those hydrogens are defined based on their molecular position and are labeled as H_a, H_b and H_c in the structural formula. The respective NMR signals of the three protons are indicated in the spectrum. The ^{1}H-NMR spectrum discloses the typical signals of a H-terminated linear silicone. The strong singlet at 0 ppm is related to protons H_c in D units (–$OSi(CH_3)_2O$-) of linear polydimethylsiloxanes and the additional doublet at ~ 0.1 ppm is associated with CH_3 protons of terminal M^H units (-$OSi(CH_3)_2(H)$). This signal appears as a doublet due to $^{3}J_{HH}$ coupling with the hydrogen of the vicinal Si-H bond. The signal associated with protons H_a appears at 4.6 ppm. The peak is displayed as a septet due to $^{3}J_{HH}$ coupling with the six vicinal protons of the dimethyl groups. This feature ensures that only terminated hydride segments were present in the prepolymer 1. The small peaks observed around the strong signals can be attributed to satellites due to $^{1}J_{^{29}Si\text{-}^{1}H}$ and $^{1}J_{^{13}C\text{-}^{1}H}$ coupling. The signal at 7.2 ppm is due to $CDCl_3$.

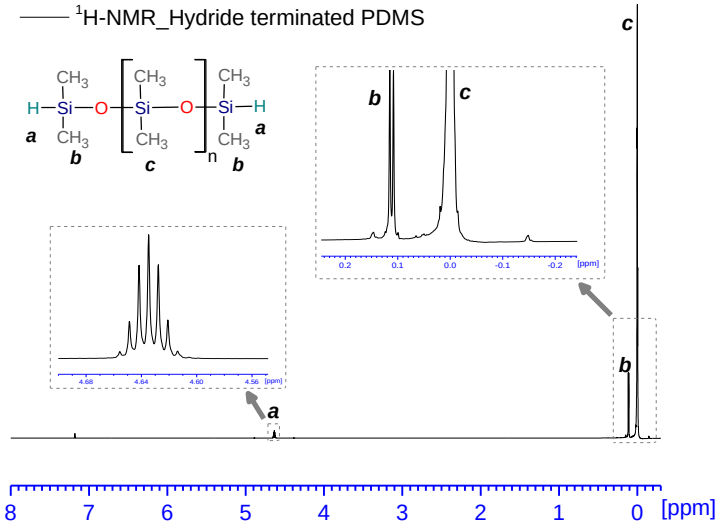


Figure 4.33. Solution state ^{1}H-NMR spectrum of prepolymer 1 in $CDCl_3$.

The relative integral areas of the proton signals permitted the estimation of the number average molar mass of the prepolymer 1 (Appendix B). The integrals are referred to as relative since the sum of all areas was assigned as the unity [211]. For prepolymer 1, the integral ratio of methyl protons from D and M^H units was approximately 14.2:2. Thus, in average, the chain consisted of 16 units in total (14 D units and 2 M^H end units) with n~14. Consequently, the number average molar mass estimated for the prepolymer 1 was approximately M_n=1170 g/mol.

In addition, the ^{29}Si-DEPT NMR spectrum of hydride terminated PDMS is shown in Figure 4.34. The spectrum shows the signals of two non-equivalent Si atoms labelled Si_a and Si_b, as indicated in the spectrum. The strong peak at δ -22 ppm is related to D units. This signal is accompanied by several weaker lines of similar intensity which can be attributed to repetition units (D) adjacent to end Si-H groups or to chains with terminal -OH groups. Two signals tentatively assigned to cyclic siloxanes D_4 and D_5 are perceived at -19.4 and -20.2 ppm, respectively [222,258]. The silicon atoms associated with terminal units M^H is represented by a peak at -7 ppm.

The prepolymer 1 was also characterized by ^{1}H,^{29}Si HSQC-NMR. The spectrum (Figure 4.35a,b) displays the expected signal related to M^H units, together with the characteristic strong signal for D units. Satellites due to $^{1}J_{^{29}Si\text{-}^{1}H}$, $^{1}J_{^{29}Si\text{-}^{13}C}$ and $^{1}J_{^{13}C\text{-}^{1}H}$ coupling are evidenced by the very small peaks and signals in the chemical shift range from -18 to -22 ppm.

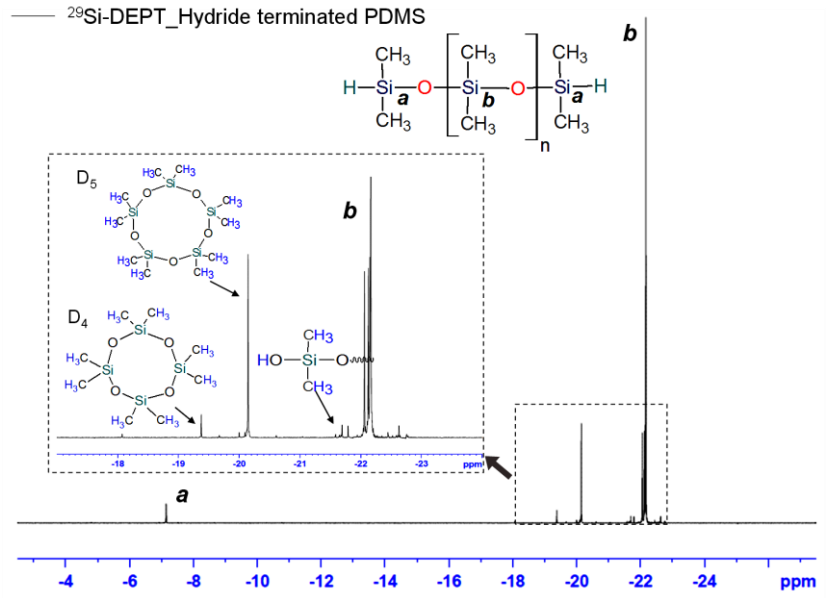


Figure 4.34. Solution state ^{29}Si DEPT spectrum of prepolymer 1 in $CDCl_3$ [237].

The 2-D NMR results also indicate the presence of cyclic oligosiloxanes by crosspeaks at $\delta_{^1H}/\delta_{^{29}Si}$ ~ 0-0.1 ppm/-19.4 ppm attributed to D_4 and at $\delta_{^1H}/\delta_{^{29}Si}$ ~ 0-0.1 ppm/-20.4 related to D_5 [222,225,258]. The signal of D_5 is relatively intense which indicates that a considerable amount of this cyclic siloxane remained as unreacted monomer. It can be inferred that the prepolymer 1 was synthetized via ring opening polymerization of cyclic siloxanes. The additional existence of traces of D_4 can support this supposition.

The existence of silanol traces was exposed by a signal at $\delta_{^1H}/\delta_{^{29}Si}$ ~ 0-0.1 ppm/-21.4 ppm due to D units near terminal M^{OH} units [258]. The signals of these traces in the ^{1}H-NMR spectrum (Figure 4.33) were not recognized straight away as they may have been masked by the stronger signal of H_b protons. The presence of M^{OH} units advocates two possible situations; first, that they remained as unreacted species from the synthesis process, and second, Si-H or Si-O-Si bonds of prepolymer 1 could have hydrolyzed, creating OH groups.

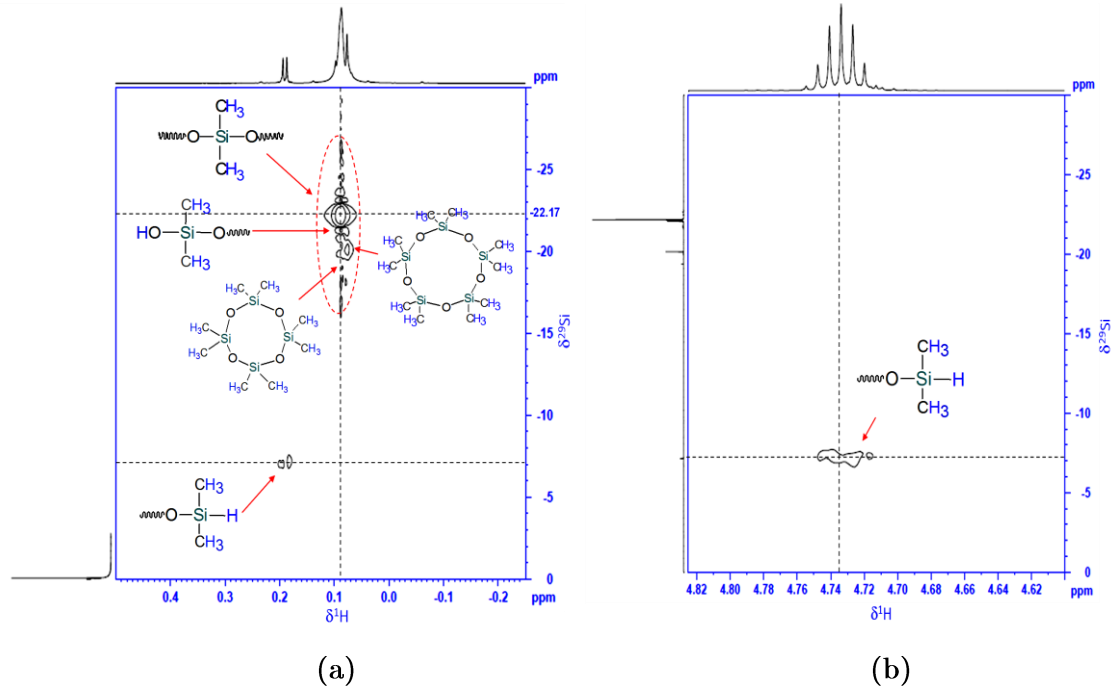


Figure 4.35. Solution state $^{1}H,^{29}Si$ HSQC-NMR spectrum of bifunctional hydride terminated PDMS dissolved in $CDCl_3$ (a) signals associated with D units (b) signal of M^H units [237]..

4.4.1.3. Molar mass determination by GPC

The number average molar mass of the bifunctional hydride terminate PDMS was also obtained by GPC measurements. The GPC chromatogram of hydride terminated PDMS (Figure 4.36) shows a very broad molar mass distribution (MMD) ranging from $2x10^2$ to $1x10^4$ Da. The MMD can be classified as a principal unimodal distribution from ~$3.5x10^2$ to $1x10^4$ Da with a small shoulder from $2x10^2$ to $5x10^4$ Da. The small shoulder on the GPC chromatogram can be related to cyclic units since the R_g (radio of gyration) of cyclic compounds differs from lineal molecules of the same chemical nature. The shoulder also suggests a distribution within cyclic oligomers, probably ranging from D_3 (222 g/mol) molecules up to D_6 (444 g/mol), with D_4 and D_5 (312 and 370 g/mol, respectively) as the most abundant cyclic compounds. The average molar masses and PDI of prepolymer 1 are given in Table 4.16. The number average molar mass (M_n) obtained was 1290 g/mol (n~16), which is consistent with the value estimated by ^{1}H-NMR (1170 g/mol). The two values are also within the M_n range given by the supplier of 900-1200 g/mol (Table 4.15).

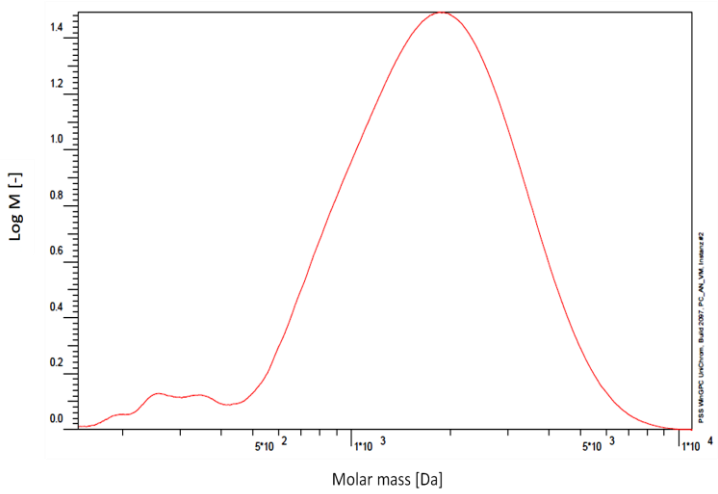


Figure 4.36. GPC chromatogram of bifunctional hydride terminated PDMS (prepolymer 1) [274].

The PDI value of 1.54 also suggests that the prepolymer 1 was synthesized via ring opening polymerization since this method is commonly implemented for obtaining lineal PDMS products with low PDI [255,275,309]. Accordingly, the shoulder of the GPC chromatogram representing a distribution of cyclic compounds can justify the small signals observed from -18 to -24 ppm in the ^{29}Si-DEPT spectrum of prepolymer 1 (Figure 4.34).

Table 4.16. Average molar masses of prepolymer 1 obtained by GPC [274]

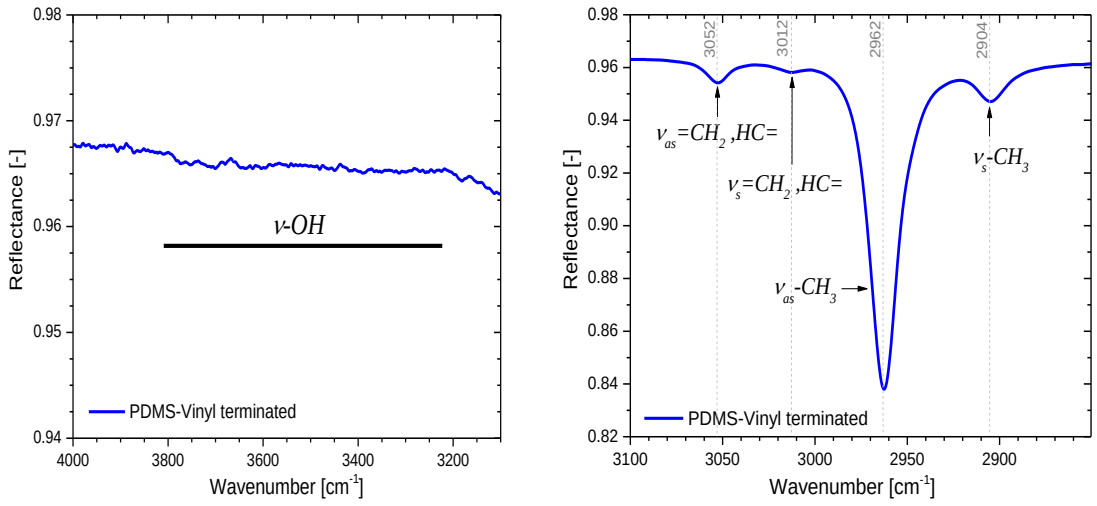
M_n (g/mol)	M_w (g/mol)	M_z (g/mol)	PDI (M_w/M_n)
1290	1980	2700	1,54

4.4.2. Bifunctional vinyl terminated PDMS - Prepolymer 2

4.4.2.1. ATR-FTIR Spectroscopy

The ATR-FTIR spectrum of the prepolymer 2 (Figure 4.37a-d) provides the characteristic absorption peaks that corroborates the chemical structure of a bifunctional vinyl terminated PDMS. As it occurred with hydride terminated PDMS, the presence of silanol fragments is not confirmed by ATR-FTIR as no band is observed in the spectral range between 3700 and 3200 cm^{-1} (Figure 4.37a). The C-H stretch

vibration modes of vinyl and methyl groups are recognized from 3100 to 2850 cm^{-1} (Figure 4.37b); specifically, the vinyl groups are identified by two weak bands at 3052 and 3012 cm^{-1}, corresponding to asymmetric and symmetric stretching modes, respectively. The methyl groups are associated with a mediat peak at 2962 cm^{-1} corresponding to asymmetric stretch, and with a weaker band at 2904 cm^{-1} due to symmetric stretch. Deformation vibrations of methyl groups are, as regular, observed at 1408 cm^{-1} and at 1260 cm^{-1} with the last being a prominent sharp peak. In the fingerprint region (Figure 4.37d) the bands at 1595 cm^{-1} and 957 cm^{-1} are related to -$CH{=}CH_2$ groups, the last is accompanied with an overtone at ~ 1913 cm^{-1} (Figure 4.37c) [189]. Additionally, the two weak bands at 837 cm^{-1} and at ~636 cm^{-1} (Figure 4.37d), can be related exclusively to vinyl moieties since they are not perceived in the ATR spectrum of hydride terminated PDMS (Figure 4.32d). The noticeable doublet with maxima at 1082 and 1015 cm^{-1} indicates the presence of siloxane bonds (asymmetric stretching). The symmetric Si-O-Si stretching vibration lies at lower wavenumbers (~ 490 cm^{-1}) and it is difficult to be recognized. The typical vibration mode ascribed to the whole polymer backbone is perceived at 1943 cm^{-1} (Figure 4.37c). Vibrations involving stretch and rocking of the Si-C bonds give rise to numerous overlapping bands below 700 cm^{-1} which are indistinctly ascribed. Categorically, the experimental ATR-FTIR spectra confirmed the expected chemical nature of the prepolymer 2, agreeing with a vinyl terminated PDMS.



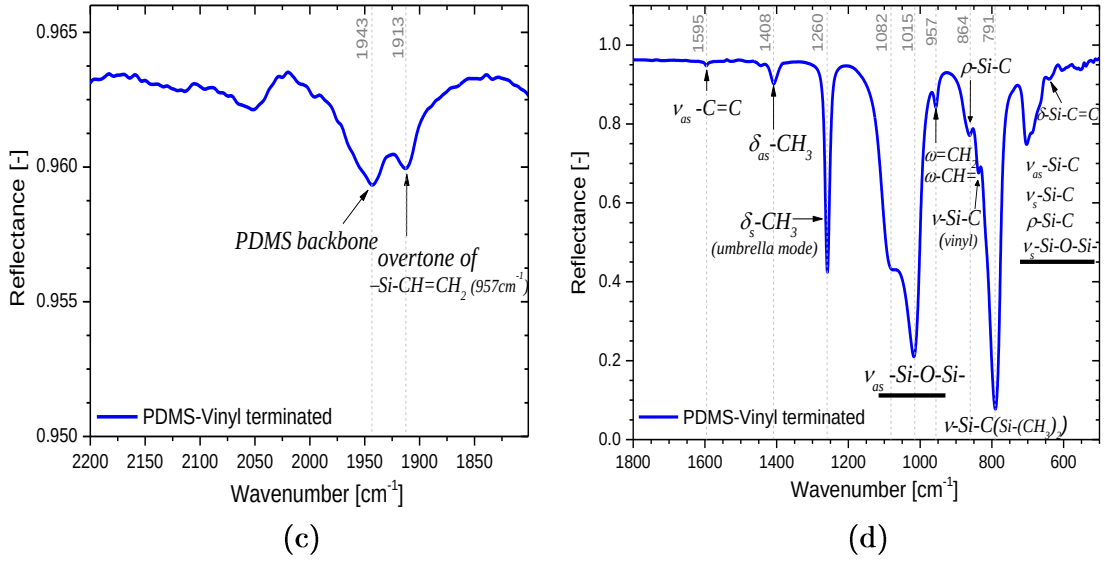


Figure 4.37. ATR-FTIR spectra of bifunctional vinyl terminated PDMS at different spectral regions (a) from 4000-3100 cm^{-1} corresponding to stretch of OH, (b) 3100-2850 cm^{-1} associated with stretching of C-H bonds in vinyl and methyl groups, (c) 2250 to 1800 cm^{-1} vibration of the PDMS backbone and (d) fingerprint region between 1800-500 cm^{-1}.

4.4.2.2. NMR Spectroscopy

The proton NMR spectrum of the bifunctional vinyl terminated PDMS is presented in Figure 4.38. Five non-equivalent protons (H_a, H_b, H_c, H_d and H_e), indicated in the structural formula inside the spectrum, give the expected signals at different chemical shifts. Vinyl substituents on silicon have distinctive proton resonances around 6.0 ppm, represented as a set of multiplets due to ${}^{2}J_{HH}$ and ${}^{3}J_{HH}$ coupling of the protons. The protons H_e of the repeating units in PDMS feature the characteristic peak at $\delta \sim 0$ ppm, and the H_d protons associated with methyl groups in M^{Vi} segments display a singlet at slightly higher chemical shift than protons of D units. The appearance of several low intensity signals around the principal peak, suggests the presence of a mixture of several oligomers with different chain lengths and cyclic compounds, as it occurred with the prepolymer 1. The signal related to the solvent ($CDCl_3$) is observed at $\delta \sim 7$ ppm.

Integration of the peaks provides the overall content of functional groups and allows the calculation of the number average molar mass of the prepolymer. Details of the integration (integrated spectrum) and molar mass estimation are included in Appendix B. The ratio of the relative integral (relative to a total unity) of D units (protons H_e) over the integral of the signals ascribed to M^{Vi} (protons H_a, H_b, H_c and H_d) was approximately 8:2. This ratio allows to estimate an average chain length of

approximately 10 units (8 D and 2 M^{Vi} units) which represents a vinyl terminated PDMS with number average molar mass of M_n 778 g/mol.

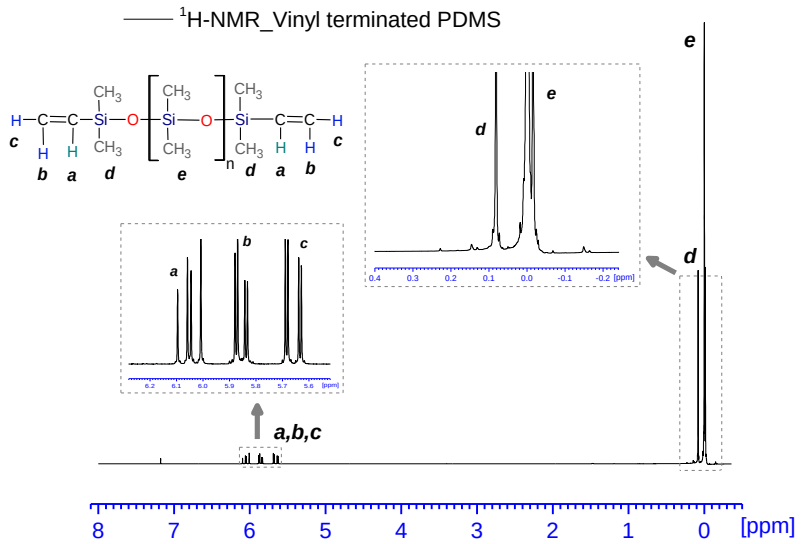


Figure 4.38. Solution state ^{1}H-NMR spectrum of bifunctional vinyl terminated PDMS (prepolymer 2) in $CDCl_3$.

The ^{29}Si-DEPT NMR spectrum of the vinyl terminated PDMS is illustrated in Figure 4.39. The signals corroborate the chemical formula of the prepolymer 2. The peak perceived at -4 ppm is assigned to silicon attached to vinyl groups, whereas the signals between -21 to -23 ppm are due to D units in PDMS. The presence of traces of cyclic siloxane D_4 is evident by the small peak at $\delta \sim$ -19.4 ppm [237,258]. The intensity of the peak associated with D_4 in vinyl PDMS, compared with the peak in hydride terminated PDMS, evokes a lower amount of D_4 traces present in this prepolymer 2. Additionally, traces of silanol groups were also detected for vinyl PDMS from the weak signal at $\delta \sim$ -21.8 ppm [237,258,262].

The previous ascriptions were supported by means of ^{1}H,^{29}Si-HSQC NMR (Figure 4.40) The strong ^{29}Si signal at $\delta \sim$ -22 ppm shows a correlation to a ^{1}H signal at ~ 0.1 ppm which is associated with D units. The crosspeak at $\delta_{^{29}Si}/\delta_{^1H} \sim$ -21.2 ppm/0.08 ppm is related to D units closer to end M^{Vi} segments, as marked in Figure 4.40a [236,237,258,310], and the crosspeak at $\delta_{^{29}Si}/\delta_{^1H} \sim$ -4 ppm/0.17 ppm is associated with the terminal units M^{Vi}. Finally, the three cross peaks in Figure 4.40b at chemical shifts $\delta_{^{29}Si}/\delta_{^1H}$ -4 ppm/5-6 ppm are categorically connected to terminated vinyl groups. Each crosspeak corresponds to a single non-equivalent proton H_a, H_b and H_c. Consequently,

The NMR results validate the chemical structure of the prepolymer 2, where traces of cyclic compounds and hydroxyl end groups were identified.

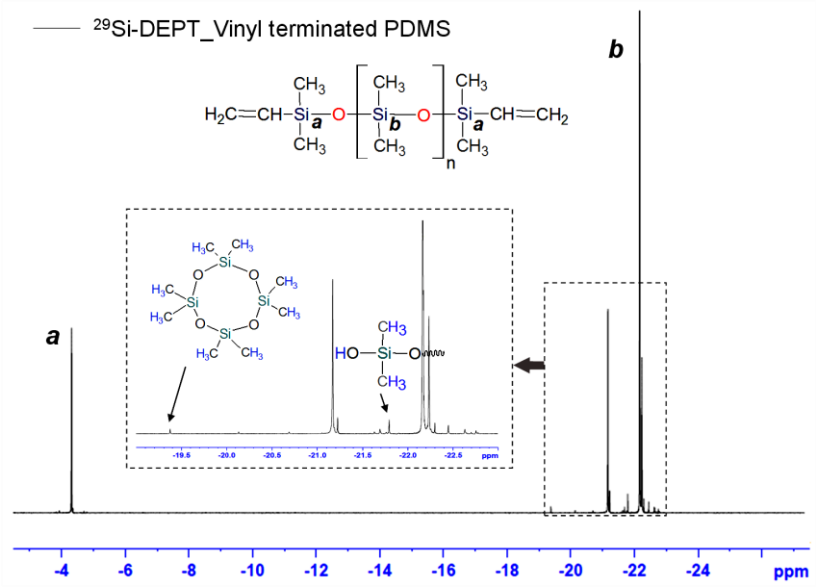


Figure 4.39. Solution state ^{29}Si-DEPT NMR spectrum of bifunctional vinyl terminated PDMS in $CDCl_3$ [237].

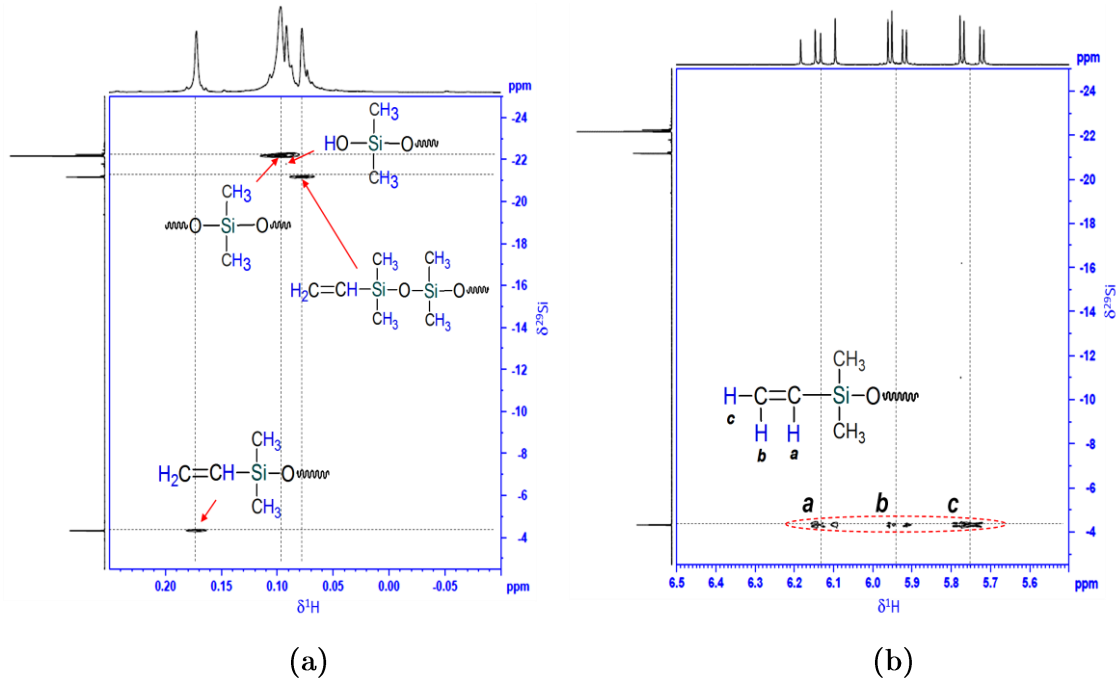


Figure 4.40. Solution state ^{1}H,^{29}Si-HSQC NMR spectra of prepolymer 2 in $CDCl_3$ (a) ^{1}H-NMR spectrum from 0.3 to -0.1 ppm and (b) ^{1}H-NMR spectrum from 6.5 to 5.5 ppm [237].

4.4.2.3. Molar mass determination by GPC

The chromatogram of prepolymer 2 (Figure 4.41) presents a unimodal MMD of the prepolymer 2 ranging from $2x10^2$ to $7x10^3$ Da. The MMD is narrower than the one obtained for hydride terminated PDMS and no shoulder was identified. This is likely due to a lower concentration of cyclic siloxanes present in this prepolymer when compared to prepolymer 1, as inferred by NMR. Sequential small, unresolved peaks in the lower molar mass range of the curve are observed, indicating a complex distribution of low molar mass oligomers content in the PDMS sample [311]. The average molar mass M_n and M_w, and the PDI of prepolymer 2 are listed in Table 4.17. The number average molar mass (M_n) obtained (853 g/mol) suggests that the degree of polymerization (n) of prepolymer 2 is ~9. This is in close agreement with the result obtained by ^{1}H-NMR, where the M_n estimated was 778 g/mol (n~8). These two values are within the range given by the supplier: 700-850 g/mol. Moreover, the lower PDI of prepolymer 2 compared to the PDI of prepolymer 1 can be attributed to a relatively higher content of cyclic siloxanes for the latter.

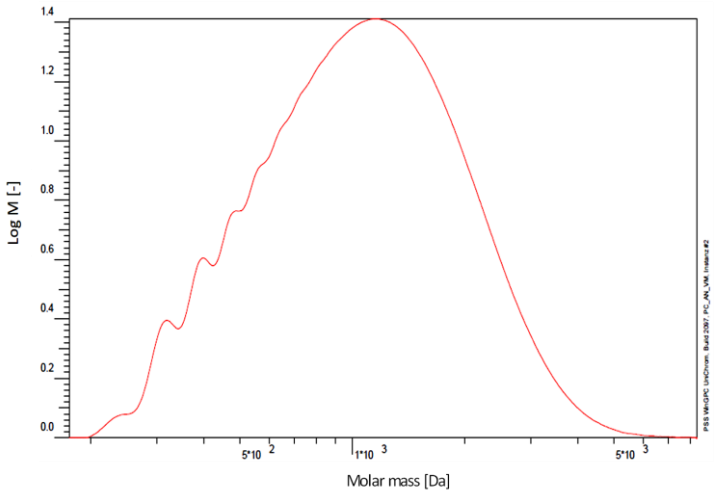


Figure 4.41. GPC chromatogram of bifunctional vinyl terminated PDMS (prepolymer 2) [274].

Table 4.17. Average molar masses of prepolymer 2 obtained by GPC [274]

M_n (g/mol)	M_w (g/mol)	M_z (g/mol)	PDI (M_w/M_n)
853	1230	1720	1,44

The characterization of the di-vinyl terminated PDMS, prepolymer 2, via ATR-FTIR, NMR and GPC corroborated its chemical structure and evidenced the presence of silanol groups and cyclic siloxanes in trace amounts. Moreover, it was proved that the prepolymer contains a considerable amount of short linear chains or oligomers.

4.4.3. Tetrakis(dimethylsiloxysilane) (TDMS) - Crosslinker

4.4.3.1. ATR-FTIR Spectroscopy

The characteristic IR bands of TDMS are exhibited in four spectral regions in Figure 4.42a-d. As expected, the spectra contain four distinguishable bands confirming the presence of methyl substituents in TDMS (Figure 4.42b,c). They appear as two sharp prominent peaks at 2963 cm^{-1} (asymmetric stretch) and at 1254 cm^{-1} (symmetric bending), and as two weak bands at 2905 cm^{-1} (symmetric stretch) and 1421 cm^{-1} (asymmetric bending). The characteristic Si-H vibrations are identified by two intense bands, one ascribed to asymmetric stretch at 2133 cm^{-1} (Figure 4.42c) and the other to bending vibration positioned at 893 cm^{-1} (Figure 4.42d). Contrary to the two prepolymers previously analyzed, TMDS displays a singlet for the Si-O-Si asymmetric stretching mode with maximum at 1065 cm^{-1}. This fact confirms that the splitting of the band of Si-O-Si groups into two components is due to the increase in the number of siloxane units in polysiloxanes [189,190]. In addition, lack of the band at ~1945 cm^{-1} confirms its previous assignment to the vibration of the PDMS skeleton. The bands below 850 cm^{-1} usually associated with methyl groups attached to Si atoms are also perceived. The most significant ones are recognized at 834 and 767 cm^{-1} ascribed to stretch and rocking vibrations of the Si-C bond, respectively. Below 750 cm^{-1}, precise assignments are difficult due to the mixing of vibrational modes in this region. Lastly, the absence of an absorption band between 3700-3200 cm^{-1} (Figure4.42a) does not allow to identify the possible presence of Si-OH groups in the sample by ATR-FTIR.

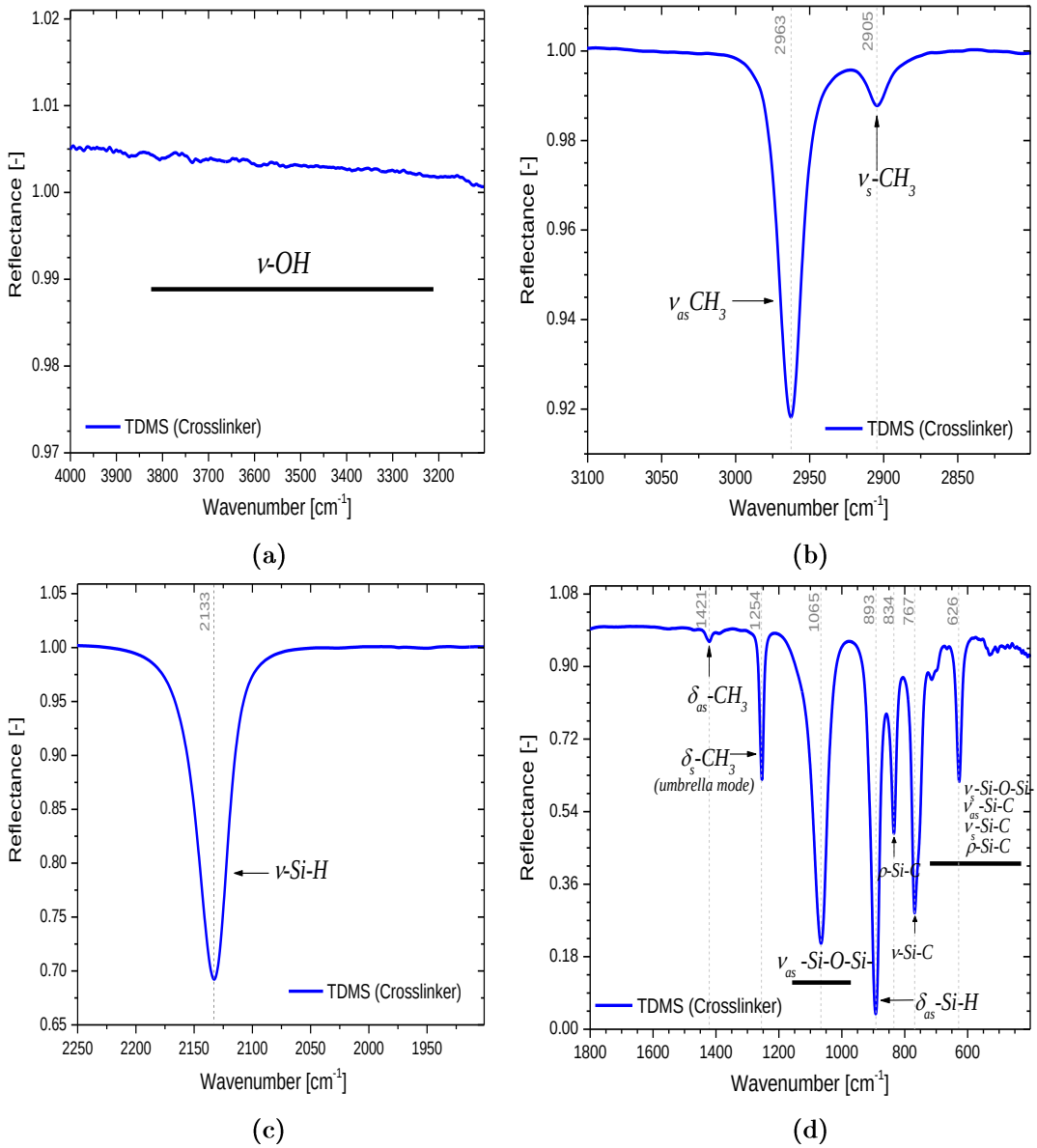


Figure 4.42. ATR-FTIR spectra of TDMS (a) from 4000-3100 cm^{-1} characteristic of OH stretching, (b) 3100-2850 cm^{-1} ascribed to stretch of CH bonds, (c) 2250 to 1800 cm^{-1} distinctive for stretching of Si-H bonds and (d) fingerprint region between 1800-500 cm^{-1} displaying vibration modes of CH_3, Si-O-Si and Si-C bonds.

4.4.3.2. NMR Spectroscopy

The crosslinker, TDMS, possesses two non-equivalent protons named H_a and H_b and indicated in the chemical structure inside the ^{1}H-NMR spectrum (Figure 4.43). The spectrum exhibits the distinct strong signal at 0 ppm associated with protons H_a in D units. Due to $^3J_{HH}$ coupling with the single vicinal proton H_b (Si-H) the signal of the

dimethyl protons is displayed as a strong doublet. The multiplet perceived at 4.7-4.5 ppm is ascribed to terminal Si-H protons. As already explained for the hydride terminated PDMS, the signal is displayed as a septet due to $^{3}J_{HH}$ coupling of Si-H protons to the six protons of the dimethyl groups. The solvent ($CDCl_3$) signal is observed at ~ 7 ppm.

The ^{29}Si-NMR spectrum (Figure 4.44) discloses the signals of the two silicon atoms in TDMS named Si_a and Si_b. The peak at ~ -6-7 ppm is ascribed to silicon, Si_b, in terminal M^H units. The peak at ~ -104 ppm is due to silicon Si_a in Q units. One additional weak signal at -96 ppm is shown, suggesting the existence of Q units in different chemical environment. Conceivably, Q units with -OH groups could be present since chemical shifts at δ ~ -100 ppm have been reported for this situation [254]. This finding advocates two possible cases; first, that Si-H were hydrolyzed, and second, that OH groups were originally present as traces. The signal corresponding to TMS is observed in the spectrum as it was initially added to the sample's solution for the measurement.

It is concluded that the chemical structure of the purchased TDMS product was qualitatively approved by the two spectroscopic methods applied and its use for adsorption experiments is validated.

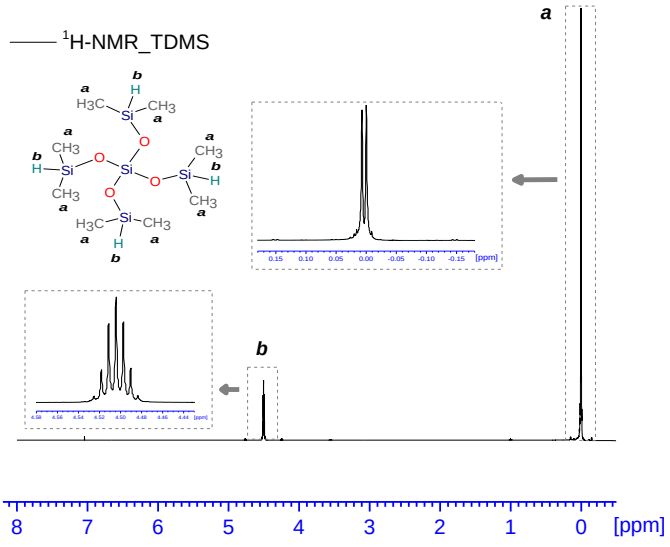


Figure 4.43. Solution state ^{1}H-NMR spectrum of the crosslinker (TDMS) in $CDCl_3$.

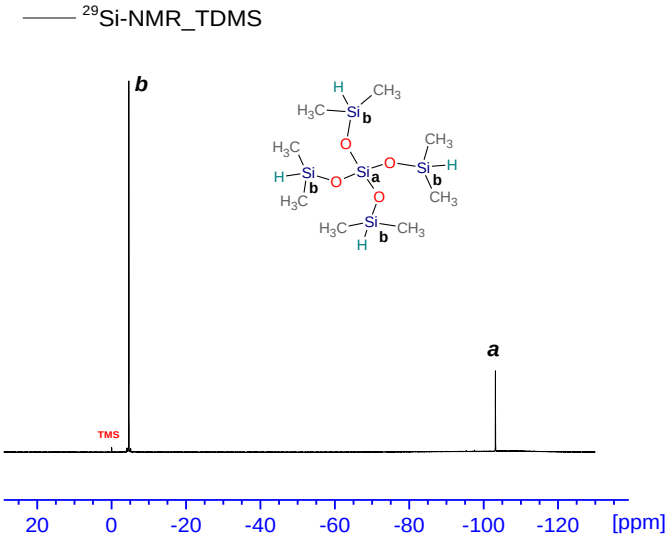


Figure 4.44. Solution state ^{29}Si-NMR of TDMS (crosslinker) in $CDCl_3$

4.4.4. Platinum-divinyltetramethyl-disiloxane complex in vinyl PDMS - Karstedt catalyst.

4.4.4.1. ATR-FTIR Spectroscopy

Figure 4.45a-d exhibits the characteristic IR absorption bands of the Karstedt catalyst. As expected the catalyst displays typical spectral features of a vinyl PDMS polymer since it is dissolved in mono vinyl, n-butyl terminated PDMS (Table 4.15). However, the bands ascribed to vinyl groups at 3052, 1595 and 954 cm^{-1} were faintly recognized and closer inspection was necessary. Even more, the other bands related to vinyl groups at 3012, 837 and 637 cm^{-1} were imperceptible (Figure 4.45b,d). This fact suggests that the catalyst is dissolved in a PDMS polymer of high molar mass. Additionally, bands associated with the n-butyl end-groups at 2808-2792 cm^{-1} are also very weak (Figure 4.45b). The doublet of the ν_{as}-Si-O-Si peak at 1100-1000 cm^{-1} (Figure 4.45d) and the band at 1945 cm^{-1} related to PDMS backbone (Figure 4.45c), confirms that the Pt-complex catalyst is dissolved in PDMS of high molar mass.

The expected absorption bands corresponding to different vibration modes of the C-H bonds in methyl groups are distinguished at 2963, 2905, 1408 and 1260 cm^{-1} and for CH_2 groups at ~1400-1200 cm^{-1} (Figures 4.45b and 4.45d). However, the last feature were difficult to recognize due to the possible low concentration of n-butyl terminal groups and overlapping with other stronger absorption bands. The prominent peak at

788 cm^{-1} together with the band at 863 cm^{-1} are associated with stretching and rocking vibration modes of the Si-C bonds, respectively. Fragments of Si-OH were not detected by ATR-FTIR as no band appeared in Figure 4.45a.

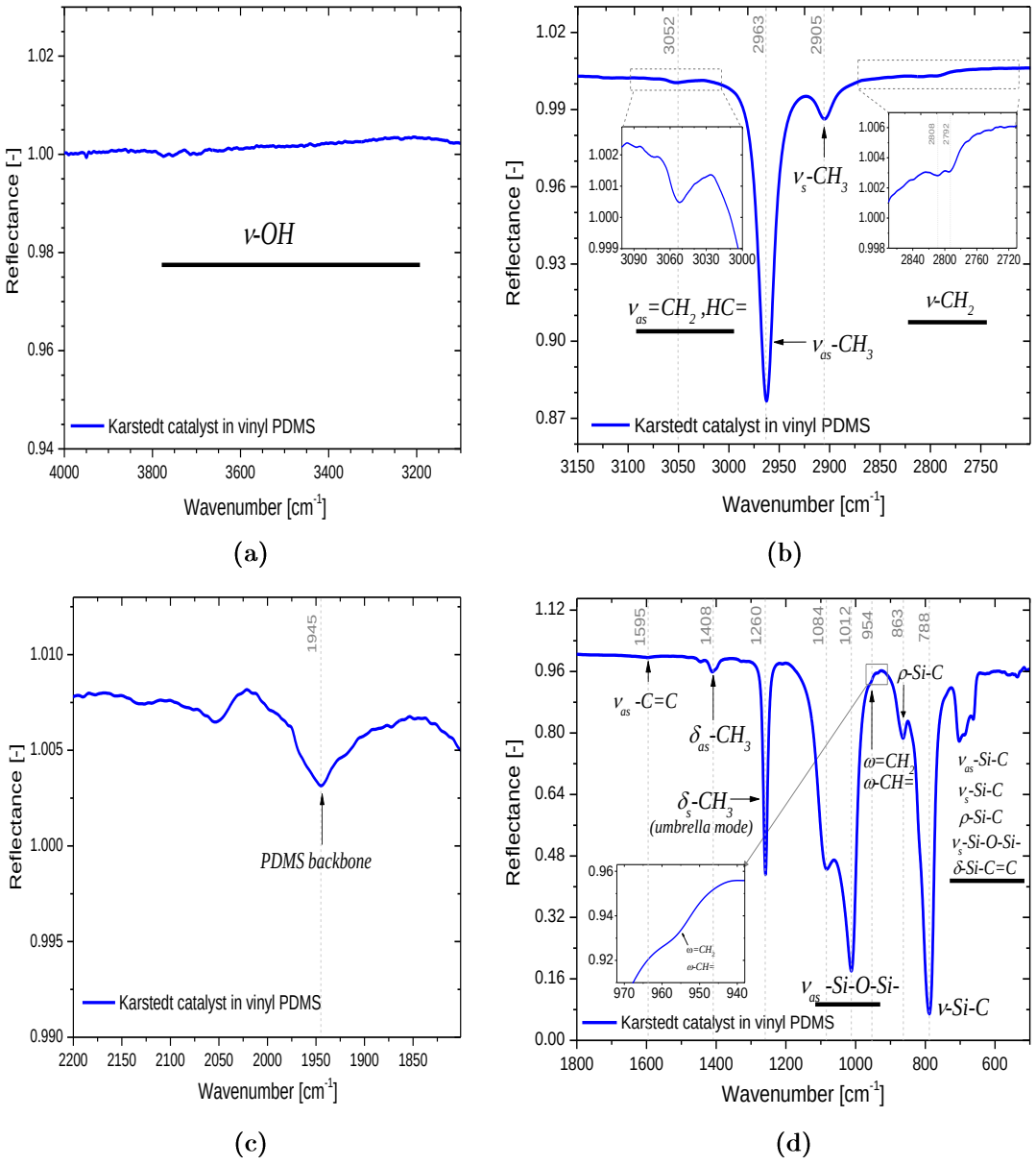


Figure 4.45. ATR-FTIR spectra of Karstedt catalyst in vinyl PDMS at different spectral regions (a) from 4000-3100 cm^{-1}, (b) 3100-2850 cm^{-1} with expanded regions at 3100-3000 cm^{-1} (left) and 2800-2700 cm^{-1} (right), (c) 2250 to 1800 cm^{-1} and (d) fingerprint region between 1800-500 cm^{-1} including a magnified spectrum from 970-940 cm^{-1}.

4.4.4.2. NMR Spectroscopy

At first sight, the ^{1}H-NMR spectrum (Figure 4.46) of the catalyst reveals only the strong signal at 0 ppm associated with hydrogens in D units (H_d, H_e, H_f). This notable feature also proves that the Pt-complex is dissolved in a PDMS of high molar mass. Although, a closer look at the spectrum evidences numerous signals of non-equivalent protons. These signals are tentatively assigned based on tabulated chemical shifts and are associated with those protons labelled in the structural formula of the Pt-complex and the mono vinyl, n-butyl terminated PDMS, included in the spectrum.

Several undefined signals are observed at δ 3-4ppm and at 5 ppm, most likely due to trace impurities in $CDCl_3$ such as dichloromethane, dichloroethane and water [217]. Integration of the spectral signals associated with protons of n-butyl and D units, leads to an estimated number average molar mass of ~ 7112 g/mol (Appendix B). This result corroborates the supposition stated that the PDMS, in which the Pt-complex is dissolved, is a polymer with higher molar mass than prepolymer 2.

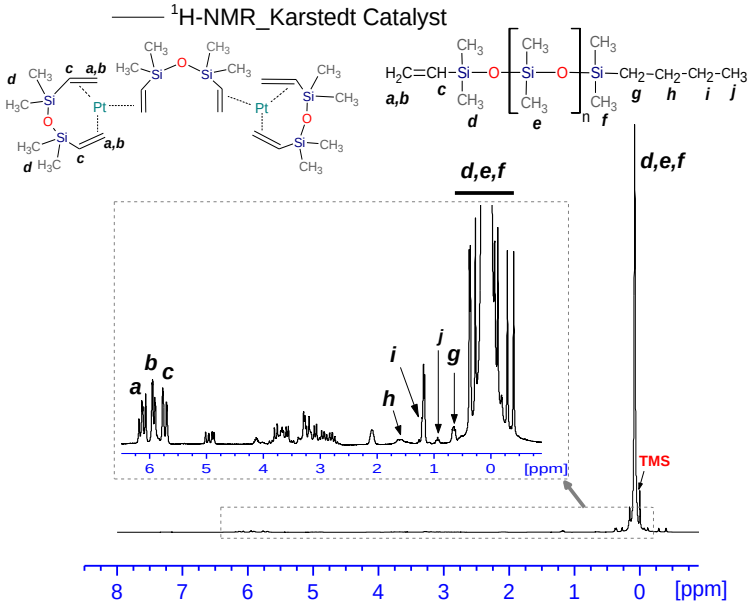


Figure 4.46. Solution state ^{1}H-NMR spectrum of catalyst solution (Karstedt catalyst in mono-vinyl terminated PDMS) in $CDCl_3$.

Adjacent peaks to the dominant signal are observed at 0.5-(-0.5) ppm. They may arise from protons in D units with a different chemical environment, such as those in the Pt-complex, mono vinyl PDMS and traces of divinyltetramethyl-disiloxane.

Ultimately, the ^{29}Si-NMR spectrum (Figure 4.47) exhibits the signals of different silicon atoms of the Pt-complex and the PDMS. The most prominent signal is perceived at -22 pm, which is distinctive of silicon atoms (Si_b) in D units. The peak associated with silicon in M^{Vi} units (Si_a) is recognizable at -4 ppm, and the silicon attached to CH_2 of n-butyl (Si_c) is represented by one of the two signals observed at 7-9 ppm. The two peaks between 7 and 9 ppm suggest that M units (methyl end-groups) were also present in the catalyst sample. Additionally, several weak signals reveal the possible presence of M^{OH} units (δ^{29}Si ~ -15 ppm) [258,262], and cyclic siloxanes D_4 and D_5 (δ^{29}Si ~ -19-(-20) ppm) [222,225,258]. The signal of TMS is shown at 0 ppm. Assignment of all weak signals is unfeasible and some may correspond to satellites due to $^1J_{^{29}Si^1H}$, $^1J_{^{29}Si^{13}C}$ coupling.

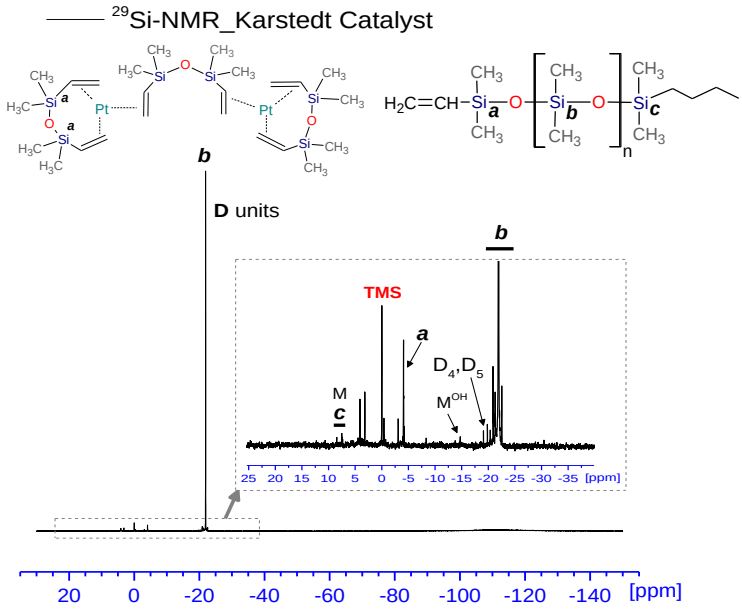


Figure 4.47. Solution state ^{29}Si-NMR spectrum of catalyst solution (Karstedt catalyst in mono-vinyl terminated PDMS) in $CDCl_3$.

In summary, it was proven that the Pt-complex is dissolved in PDMS of relatively high molar mass with vinyl and n-butyl end groups. Potential presence of traces of cyclic siloxanes and hydroxyl terminal groups was inferred from the ^{29}Si NMR spectrum.

4.4.5. Allyltrimethoxysilane (ATMS) – Adhesion promoter

4.4.5.1. ATR-FTIR Spectroscopy

The ATR-FTIR spectra of ATMS (Figure 4.48a-d) differ from the spectra of the other four components previously analyzed, due to the absence of Si-O-Si bond and presence of methoxy groups (-OCH_3).

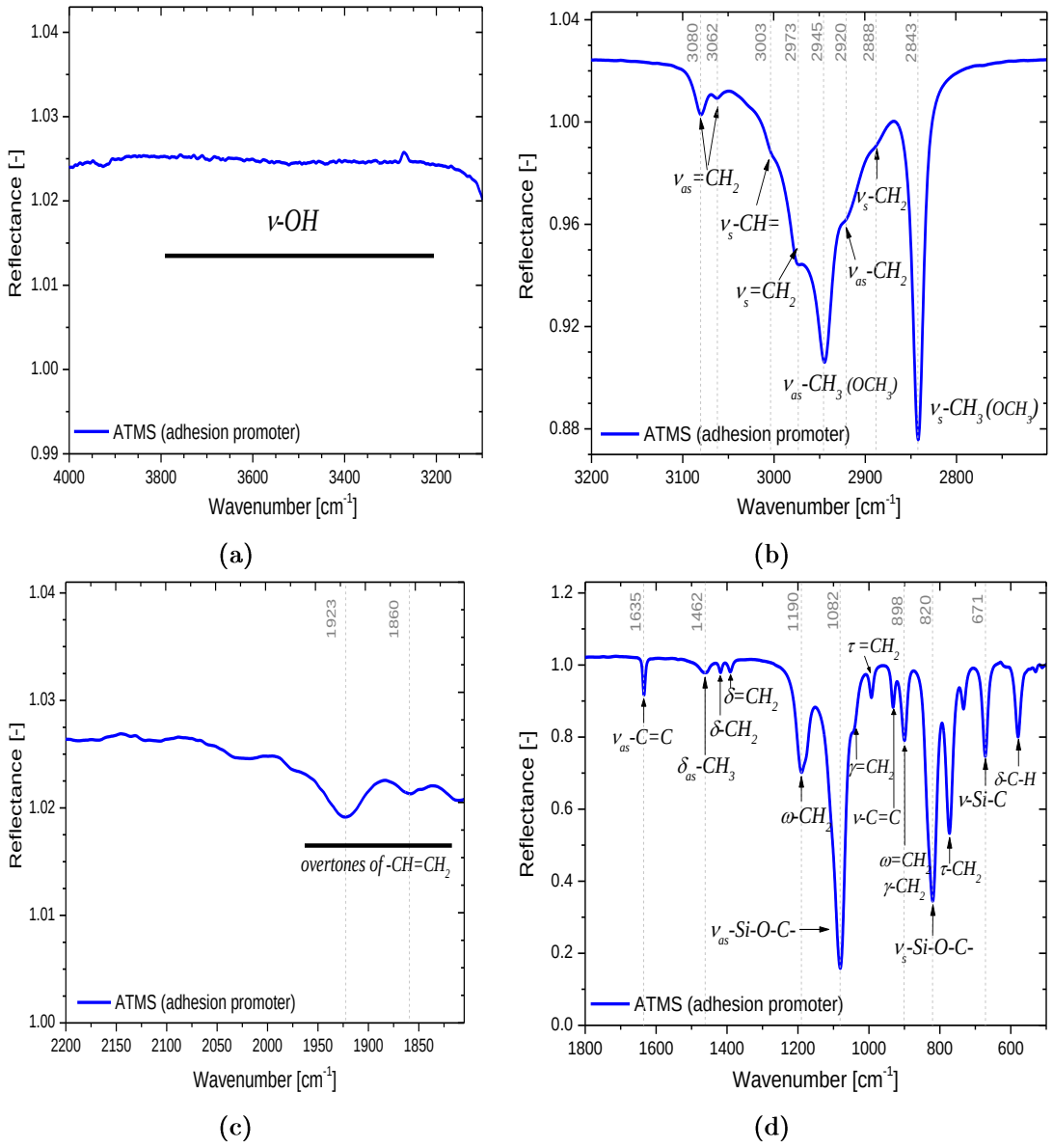


Figure 4.48. ATR-FTIR spectra of ATMS (a) from 4000-3100 cm^{-1}, (b) 3100-2850 cm^{-1}, (c) 2250 to 1800 cm^{-1} and (d) fingerprint region between 1800-500 cm^{-1}.

Vibrations related to -OCH_3 groups are identified at 2945, 2843, 1462, 820 and 590 cm^{-1} and the presence of allyl terminal groups was confirmed by the IR bands at 3080, 3062, 3003, 2973, 1635, 1391, 1040, 932, 898 and 578 cm^{-1} with overtones between 1930 and 1830 cm^{-1}. The methylene group (-CH_2-) is recognized by the peaks at 2920, 2886, 1418, 1190, 991, 898 and 773 cm^{-1}. The two prominent and sharp peaks observed at 1082 and 820 cm^{-1} are due to stretching of Si-O-C bonds. The peaks below 700 cm^{-1} are associated with Si-C and C-H bond vibrations, but exact assignment is unfeasible.

Importantly, no direct spectral indication of hydrolyzed silane was perceived due to the lack of band in the range of 3700 to 3200 cm^{-1} (Figure 4.48a). Thus, significant spontaneous hydrolysis did not occur at room temperature for the ATMS sample employed. This fact is crucial for the analysis of adsorbed ATMS on Al. As mentioned in Section 3.3.3, hydrolysis is known for being essential in the adhesion of alkoxysilanes on hydroxylated surfaces.

4.4.5.2. NMR Spectroscopy

The chemical characterization of ATMS was complemented via ^{1}H NMR spectroscopy. The molecular formula of ATMS, included in the ^{1}H-NMR spectrum (Figure 4.49) shows five non-equivalent protons named H_a, H_b, H_c, H_d and H_e. A signal observed downfield at 5.8-5.5 ppm is associated with protons H_a of the allyl group [224,228]. The multiple character is due to coupling with the 4 vicinal protons (2 from vinyl and 2 from methylene). The signals of protons H_b and H_c are detected between 4.9 and 4.7 ppm; correct assignment is based on the work of Delmulle et al. [224], who established that protons H_b are displayed at a slightly higher chemical shift (δ_{H_b} ~4.81 ppm) than protons H_c (δ_{H_c} ~4.79 ppm). The strong singlet at 3.4 ppm is corresponding to protons H_e related to trimethoxy groups [242,312]. This prominent peak may obscure the possible presence of SiOH groups. Furthermore, the signal at 1.54-1.46 ppm is attributed to protons H_d of -CH_2- based on reported data of methylene substituents on silicon atom [219,221]. This signal is mainly displayed as a doublet due to coupling ($^3J_{HH}$) with the vicinal proton H_a. Comparing the signals of vinyl groups in ATMS with those of vinyl terminated PDMS, the vinyl protons of allyltrimethoxysilane were displayed at different chemical shifts. It has been stated that the presence of the methylene group in ATMS may be influencing the $(p\text{-}d)_\pi$ interaction between vinyl and silicon and thereafter, affecting the chemical shifts of the protons.

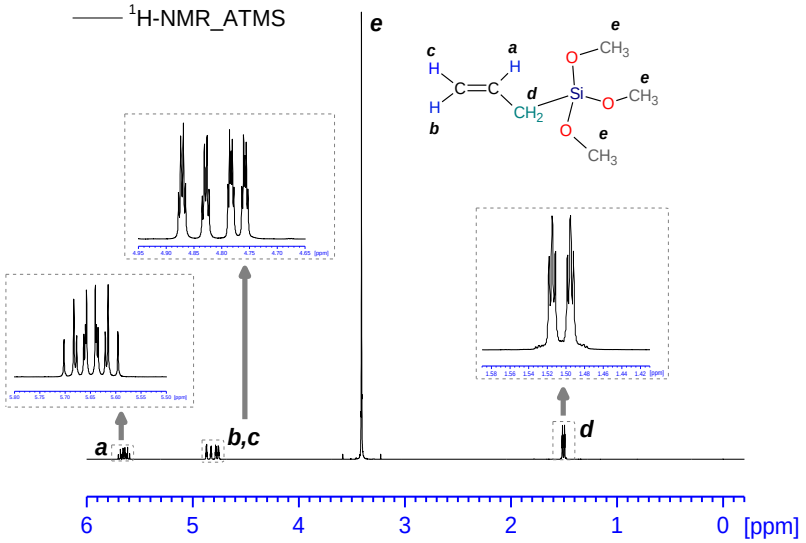


Figure 4.49. Solution state ^{1}H-NMR spectrum of ATMS in $CDCl_3$.

From the ^{1}H-NMR spectrum, evidence of hydrolyzed species was not directly inferred. It has been reported that ^{13}C-NMR is more effective for determining if methoxygroups of silanes have been hydrolyzed [218]. Specifically, carbon signals, related to methylene groups adjacent to silicon, usually display additional small signals at a higher chemical shift if OH groups are present in the silane. Consequently, the ^{13}C-NMR spectrum of ATMS is also included. The spectrum (Figure 4.50) displays the expected signals of the four different carbons in ATMS (C_a,C_b,C_c and C_d). Closer examination of the signal associated to C_c reveals a small peak at ~ 18.22 ppm. This signal possibly corresponds to methylene carbon of a hydrolyzed silane M_2 as indicated in the ^{13}C spectrum. However, the low intensity suggests that M_2 was only present at trace levels; thus, ATMS only underwent spontaneous hydrolysis to a very short extent. It should be reiterated that the SSMC were at all times stored at 4-5 °C, which could have hindered spontaneous hydrolysis of ATMS. Moreover, hydrolysis of alkoxysilanes, even in aqueous solutions, has been described to be a very slow process [48,313]. This plausible presence of hydrolyzed silanes is an important aspect to consider in the adsorption behavior of ATMS on Al.

In addition, the ^{29}Si-NMR spectrum (Figure 4.51) exhibits the single prominent signal of the single Si atom at -47 ppm; nonetheless a small silicon peak is identified at -55 ppm which could correspond to silicon in M_2 (hydrolyzed ATMS), as depicted in the spectrum. The signal of TMS is also detected at 0 ppm.

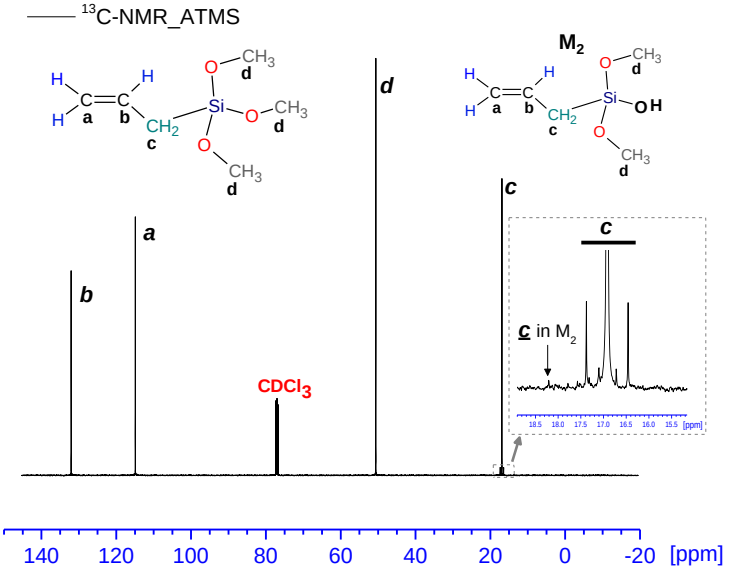


Figure 4.50. Solution state ^{13}C-NMR of ATMS in $CDCl_3$

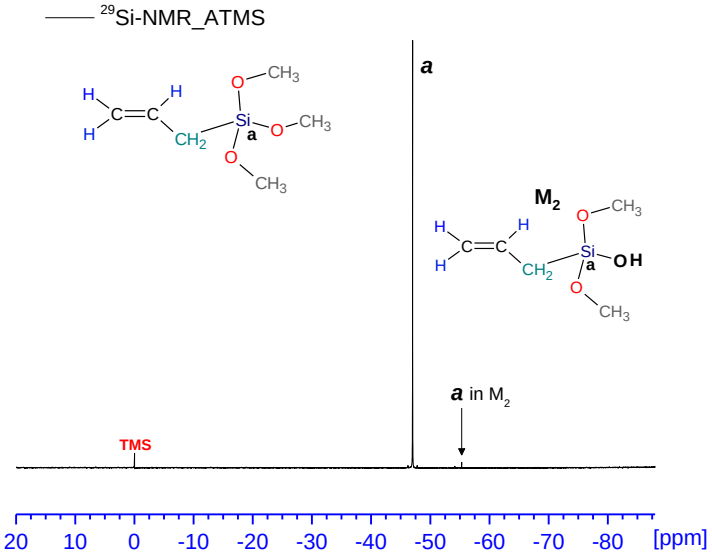


Figure 4.51. Solution state ^{29}Si-NMR of ATMS in $CDCl_3$ with 1% of TMS

The quality of the acquired ATMS was confirmed via ATR-FTIR and NMR spectroscopy. In particular, the NMR spectra advocates the presence of hydroxyl groups in ATMS only at very low trace levels.

4.4.6. Synopsis – Characterization in bulk of the SSMC

Conventional ATR-FTIR and NMR spectroscopic methods (^{1}H-, ^{13}C-, ^{29}Si-NMR) successfully validated the chemical structure of the five single silicone model components selected in this work. Additional ^{1}H,^{29}Si-HSQC NMR method, implemented in the analysis of the two prepolymers, was effective for a more detailed analysis of their composition. It was confirmed that the two prepolymers and the catalyst contained traces of hydroxyl groups, as they are often present in commercial PDMS samples. The presence of cyclic siloxanes was also inferred from NMR spectra, suggesting that the two prepolymers, and most probably the PDMS polymer in which the catalyst is dissolved, were synthesized via ring opening polymerization. The molar masses of the bifunctional vinyl and hydride terminated PDMS were estimated from NMR and GPC measurements which showed good correlation in the results. The values of number average molar mass (M_n) obtained by GPC will be used for further analysis. The results obtained by the chemical characterization of the SSMC through ATR-FTIR and NMR, allowed their use for adsorption and co-adsorption experiments as well as for the formulation of a model silicone product. Finally, the ATR-FTIR results for each SSMC are compiled in Table 4.18a-e. This information is useful for the analysis of the SSMC in their adsorbate state.

Table 4.18. Principal IR absorption bands of the SSMC. (a) prepolymer 1, (b) prepolymer 2, (c) TDMS, (d) Karstedt catalyst and (e) ATMS.

(a) Hydride PDMS – Prepolymer 1

	IR band [cm^{-1}]		Assignment
1	2963	m, shp	ν_{as}-CH_3
2	2905	w	ν_{s}-CH_3
3	2127	m,shp	ν-Si-H
4	1947	w	PDMS backbone
5	1411	w, br	δ_{as}-CH_3
6	1260	s, vshp	δ_{s}-CH_3
7	1082	vs, shd	ν_{as}-Si-O-Si
8	1015	vs	ν_{as}-Si-O-Si
9	910	m, shp	δ_{as}-Si-H
10	864	m	ρ-Si-C
11	791	vs, shp	ν-Si-C

(b) Vinyl PDMS – Prepolymer 2

	IR band [cm^{-1}]		Assignment
1	3052	W	ν_{as}=CH_2 ; ν_{as}-CH=
2	3012	Vw	ν_{s}=CH_2 ; ν_{s}-HC=
3	2962	m, shp	ν_{as}-CH_3
4	2904	W	ν_{s}-CH_3
5	1943	W	PDMS backbone
6	1595	Vw	ν_{as}-C=C-
7	1408	W	δ_{as}-CH3
8	1260	s, vshp	δ_{s}-CH3
9	1082	vs, shd	ν_{as}-Si-O-Si
10	1015	Vs	ν_{as}-Si-O-Si
11	957	m, shp	ω=CH_2 ; ω-CH=
12	864	m, shd	ρ-Si-C
13	851	vw, shd	ν-Si-C (vinyl)
14	791	vs, shp	ν-Si-C (methyl)

(c) TDMS – Crosslinker

	IR band [cm^{-1}]		Assignment
1	2963	m, shp	ν_{as}-CH_3
2	2905	w	ν_{s}-CH_3
3	2133	m,shp	ν-Si-H
4	1421	w	δ_{as}-CH_3
5	1254	s, vshp	δ_{s}-CH_3
6	1065	vs, shp	ν_{as}-Si-O-Si
7	893	m, shp	δ_{as}-Si-H
8	834	m	ρ-Si-C
9	767	vs, shp	ν-Si-C
10	626	s, shp	ν_{as}-Si-C ; ν_{s}-Si-O-Si

(d) Karstedt Catalyst

	IR band [cm^{-1}]		Assignment
1	3052	w	ν_{as}=CH_2 ; ν_{as}-CH=
2	2962	m, shp	ν_{as}-CH_3
3	2905	w	ν_{s}-CH_3
4	2808	vw, br	ν-CH_2
5	2792	vw, br	ν-CH_2
6	1945	w	PDMS backbone
7	1595	vw	ν_{as}-C=C-
8	1408	w	δ_{as}-CH3
9	1260	s, vshp	δ_{s}-CH3
10	1084	vs, shd	ν_{as}-Si-O-Si
11	1012	vs	ν_{as}-Si-O-Si
12	954	vw, shd	ω=CH_2 ; ω-CH=
13	863	w, shd	ρ-Si-C
14	788	vs,vshp	ν-Si-C

(e) ATMS – Adhesion promoter

	IR band [cm^{-1}]		Assignment
1	3080	w	ν_{as}=CH_2
2	3062	vw	ν_{as}=CH_2
3	3003	vw, shd	ν=CH
4	2973	w, shd	ν_s=CH_2
5	2945	m, shp	ν_{as}-CH_3 (OCH_3)
6	2920	w, shd	ν_{as}-CH_2
7	2888	w, shd	ν_s-CH_2
8	2843	ms, shp	ν_s-CH_3 (OCH_3)
9	1635	m, shp	ν_{as}-C=C-
10	1462	m	δ_{as}-CH_3
11	1418	w, br	δ-CH_2
12	1390	w	δ=CH_2
13	1190	ms	ω-CH_2
14	1082	s, shp	ν_{as}-SiOC
15	1041	vw, shd	γ=CH_2
16	993	w	τ=CH_2
17	932	w	ν-C-C
18	898	m, shp	ω=CH_2 ; γ-CH_2
19	820	s, shp	ν_s-SiOC
20	772	m	τ-CH_2
22	671	m	ν-Si-C
23	580	m	δ-C-H

4.5. Results of the characterization in bulk of the FMSA

A model silicone was formulated based on the commercial addition-curing silicone CSA, implying that the model silicone must crosslink via hydrosilylation between Si-vinyl and Si-H groups (Figure 4.7). However, unlike the CSA, crosslinking of the formulated silicone must be viable at room temperature for the sake of executing co-adsorption experiments which are only suitable at room temperature (RT). This formulated model silicone adhesive (FMSA) excluded any filler or any other components that were not involved exclusively in crosslinking and whose inclusion could have effects on the adhesion behavior and also on the physical, chemical and structural bulk properties of the polymer network formed.

Usually, a silicone network attained via hydrosilylation is sensitive to alterations in parameters such as: concentration and nature of the reactants (e.g. vinyl PDMS, crosslinker and catalyst), variations on external factors such as presence of oxygen or moisture, and processing temperature [298]. Consequently, for the formulation of the FMSA, only one type of vinyl PDMS, one type of crosslinker, one type of catalyst (Pt-complex), a single concentration of the catalyst, and a constant molar ratio of Si-

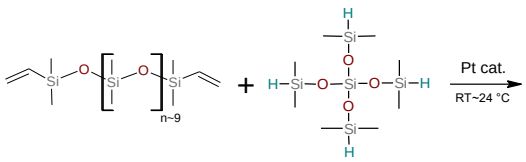
Vinyl/Si-H groups (the same estimated for the CSA via ^{1}H-NMR measurements) were employed. Moreover, the reaction was performed at only one temperature (RT) in dry air atmosphere (T_{dp} ~ -65 °C) inside a Glovebox.

It was convenient to monitor the course of crosslinking in order to know if the reactions proceeded in the expected way, and to acquire information regarding the composition of the networks formed. For that reason, a description concerning the experimental formulation of the FMSA is given first, followed by the supervision of the crosslinking reaction at RT, with and without the Karstedt catalyst, via in-situ ATR-FTIR measurements. Additionally, the crosslinked product was characterized in bulk by ATR-FTIR, solid NMR spectroscopy, TGA and DSC methods. It was of special interest to observe how the absence of certain components, commonly included in a commercial system, could affect the physico-chemical properties of a silicone.

4.5.1. Formulation of the FMSA

The formulated model silicone, FMSA, was prepared through a hydrosilylation reaction between prepolymer 2 (linear di-vinyl-terminated PDMS) (M_n=853 g/mol (n~9), Eq/g= 0.00265) and the crosslinker TDMS (tetrakis(dimethylsiloxysilane), Mw= 328.73 g/mol, δ= 0.886 g/ml) in the presence of the Karstedt catalyst (Platinum-divinyltetramethyl-disiloxane complex in mono-vinyl PDMS, active at RT (Concentration Pt(0) [%wt.] = 3.2). The reader is referred to the prior section 4.4. for the detailed description and characterization of the selected components.

The components for the formulation were used as received and handled in all cases inside a Glovebox at RT, purged with dry air (T_{dp}~-65 °C). The crosslinking was also carried out under the mentioned conditions. No hydride PDMS (prepolymer 1) was added in the formulation, despite containing Si-H groups, because it does not lead to a crosslinked material; for that reason, TDMS was employed instead. The crosslinking reaction of the model system FMSA is depicted in Figure 4.52.



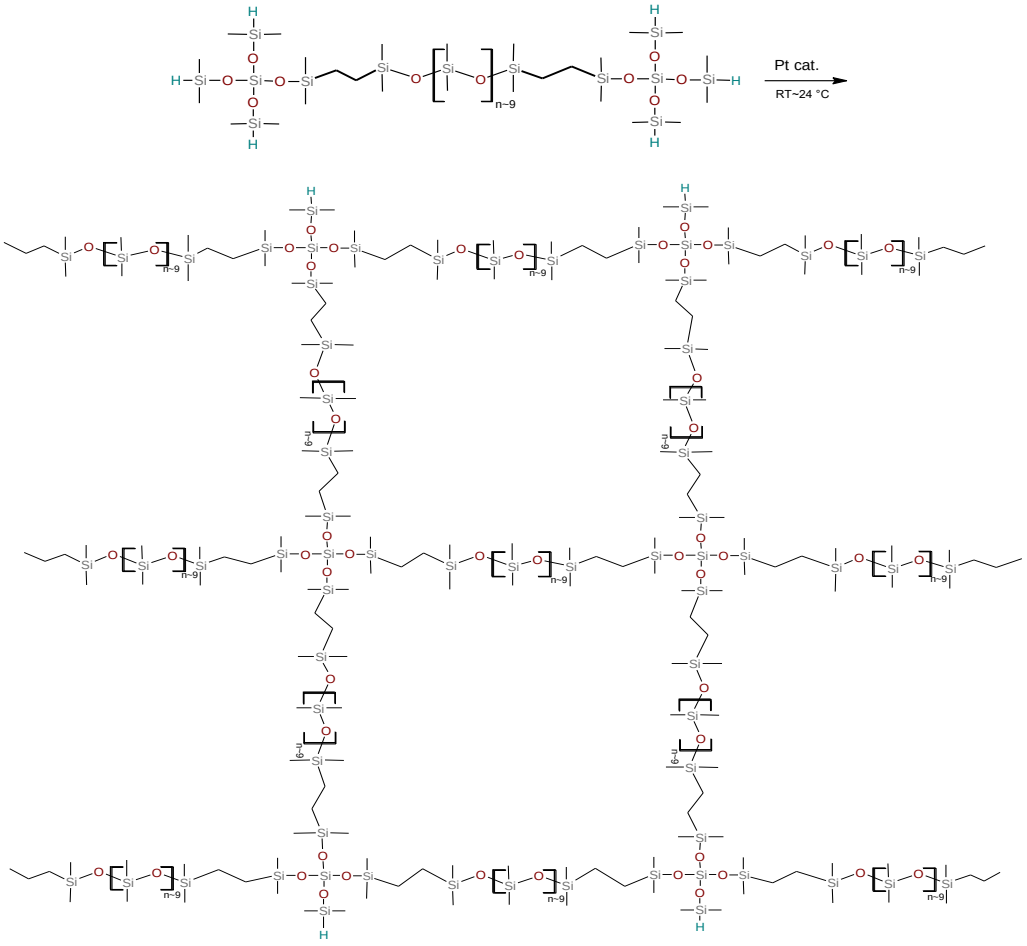


Figure 4.52. Scheme of the FMSA network formation through hydrosilylation reaction at RT in the presence of a Pt(0) catalyst by prepolymer 2 and the crosslinker TDMS.

As previously mentioned, the molar ratio of Si-H/Si-Vinyl groups = 1.5/1.0, estimated for the reference CSA system by ^{1}H-NMR measurements, was used here for the formulation of the FMSA. The catalyst concentration used for the experimental formulation of FMSA was selected based on published literature related to hydrosilylation of silicone systems employing a platinum catalyst. The literature survey included patents [210,314] research studies [88,202,212,298] and the Gelest catalogue in which different formulations are suggested [315]. It was found that a typical platinum catalyst is usually added at concentrations ranging from 10 to 50 ppm of Pt relative to vinyl PDMS. In this work 20 ppm of Pt(0) was selected based on the literature mentioned above.

A typical formulation and crosslinking procedure implemented in this work, was performed in a Glovebox where 1.474 g of prepolymer 2 was weighed into a cleaned 20

ml glass flask. Subsequently, 0.576 g (0.650 ml) of crosslinker TDMS were added to the flask. The amount of TDMS was added volumetrically in order to avoid mass ambiguities by weighing the crosslinker in the same flask already containing the prepolymer 2. The amounts of crosslinker and prepolymer 2 kept the Si-H/Si-Vi molar ratio of 1.5/1.0 invariable for every formulation carried out. Subsequently, the flask containing the mixture was agitated by a magnetic stirrer for 2 min and afterwards, 0.95 µl of the Karstedt catalyst solution, equivalent to 20 ppm of Pt(0) in relation to prepolymer 2, was added to the flask and the mixture was stirred further for approximately 30 s in a magnetic stirrer.

4.5.2. In-situ ATR-FTIR studies - Crosslinking of the FMSA

The crosslinking of the FMSA, with and without the Karstedt catalyst, was studied via in-situ ATR-FTIR spectroscopy during a defined time interval for each case. Basically, the effect of the catalyst on crosslinking was examined by the change in intensity over time, of IR bands associated with Si-vinyl groups and with Si-H functionalities. The reaction was also monitored by the appearance of a new band at 1130-1140 cm^{-1} corresponding to newly formed ethylene bonds ($-CH_2-CH_2-$). On the other hand, bands ascribed to methyl groups were expected to remain unaltered during the course of hydrosilylation, since they do not participate in crosslinking. However, if Markovnikov's product was formed, the bands associated with methyl groups may increase in intensity due to creation of $-CH-CH_3$ groups instead of $-CH_2-CH_2-$.
The assignments of the ATR-FTIR bands obtained were based on Table 4.18a-e and on the results of the previous Sections 4.3 and 4.4, including the references used there.

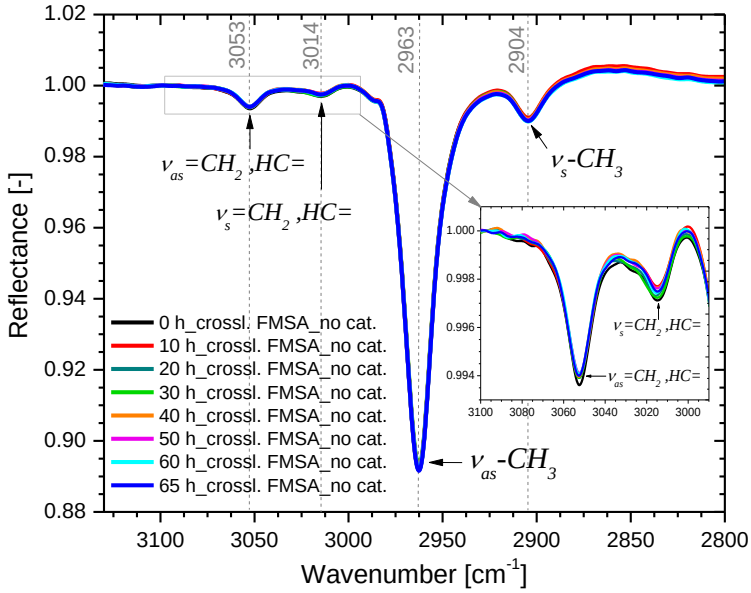
ATR-FTIR Spectroscopy - Experimental

For in-situ ATR-FTIR measurements of the crosslinking without the Karstedt catalyst, the reactive mixture (prepared as described above) was poured into the ATR sample cell (Figure 4.5a) and subsequently, after 10 min of atmospheric stabilization inside the IR compartment, the spectra were recorded every hour for a period of 65 h. On the other hand, for in-situ ATR-FTIR measurements including the Karstedt catalyst, the appropriate amount of the catalyst solution (0.95 µl) was added rapidly to the reaction partners and the reactive mixture was agitated for approximately 30 s. Subsequently, the ATR sample cell (Figure 4.5a) was filled and immediately after, the spectra started to be collected and no time was given for atmospheric stabilization inside the IR measurement compartment. The purpose was to begin the measurements as soon as

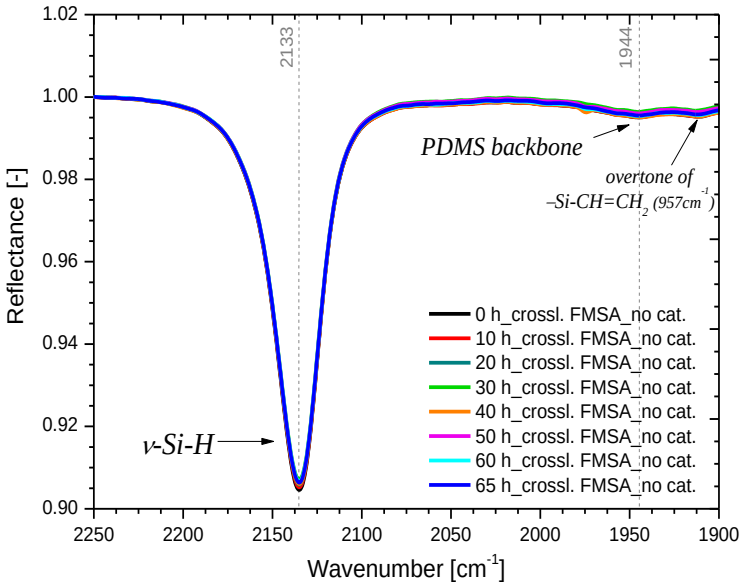
possible after the addition of the Karstedt catalyst since the reaction was seen to proceed very rapidly. The monitoring of the crosslinking reaction started at the shortest experimental time conceivable between the addition of catalyst and the collection of ATR-FTIR spectra, approximately 1 min. The in-situ spectra were collected every minute during 30 min.

4.5.2.1. Crosslinking in the absence of the Karstedt catalyst

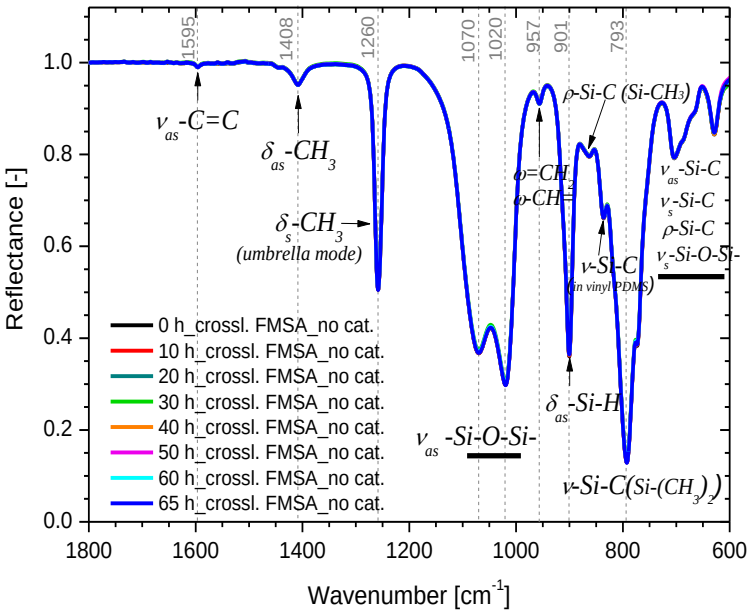
The measured ATR-FTIR spectra over time of the formulated silicone without the catalyst (FMSA-no cat.) are presented in Figure 4.53a-c. Comparing the IR absorption bands of FMSA-no cat. with those related to vinyl PDMS (prepolymer 2) and TDMS (Table 4.18b,c), significant differences can be perceived. Firstly, the stretching and deformation vibration modes of Si-H in TDMS were observed at 2133 and 912 cm^{-1}; whereas in the mixed state they appear at 2133 and 901 cm^{-1} (Figure 4.53b,d). The last band seems to be affected by other vibration modes occurring in that range, as wagging of vinyl groups and stretching of silanol. Secondly, the double band characteristic of ν_{as}-Si-O-Si bonds in FMSA-not cat is also disclosed at lower wavenumbers than for prepolymer 2. The peak maxima for the mixture are located at 1070 and 1020 cm^{-1} (Figure 4.53c), whereas for prepolymer 2 they were found at 1082 and 1015 cm^{-1}. The peak at the higher frequency is also more pronounced in the FMSA-no cat. spectrum as it is in the spectrum of prepolymer 2. The lower peak is probably more affected by the stretching mode of siloxane bonds in TDMS (strong singlet at 1065 cm^{-1}) than the upper peak. Thirdly, the representative peaks of bending of methyl groups appear in the mixture at 1408 and 1260 cm^{-1} respectively (Figure 4.53c). These values coincide with the peaks of prepolymer 2, whereas for TDMS, those peaks were identified at 1421 and 1254 cm^{-1}. The higher concentration of methyl groups in di-vinyl PDMS than in TDMS, might have a greater contribution to those peaks of methyl groups in the mixture. This is validated by the two bands corresponding to Si-C rocking and stretching at 863 and 793 cm^{-1}, which were found for vinyl PDMS at 864 and 791 cm^{-1} while for TDMS they were perceived at considerably lower frequencies: 834 and 767 cm^{-1}. The principal IR bands recognized for the FMSA-no cat are listed in Table 4.19.


3053
3014
2963
2904
ν_{as}=CH_2,HC=
ν_s=CH_2,HC=
ν_s-CH_3
ν_{as}-CH_3
0 h_crossl. FMSA_no cat.
10 h_crossl. FMSA_no cat.
20 h_crossl. FMSA_no cat.
30 h_crossl. FMSA_no cat.
40 h_crossl. FMSA_no cat.
50 h_crossl. FMSA_no cat.
60 h_crossl. FMSA_no cat.
65 h_crossl. FMSA_no cat.
Reflectance [-]
Wavenumber [cm^{-1}]

(a)


2133
1944
PDMS backbone
overtone of
–Si-CH=CH_2 (957cm^{-1})
ν-Si-H
0 h_crossl. FMSA_no cat.
10 h_crossl. FMSA_no cat.
20 h_crossl. FMSA_no cat.
30 h_crossl. FMSA_no cat.
40 h_crossl. FMSA_no cat.
50 h_crossl. FMSA_no cat.
60 h_crossl. FMSA_no cat.
65 h_crossl. FMSA_no cat.
Reflectance [-]
Wavenumber [cm^{-1}]

(b)



(c
)

Figure 4.53. In-situ ATR-FTIR spectra of the evolution of the crosslinking reaction of the FMSA with time when no Karstedt catalyst was added. (a) from 3100 to 2800 cm^{-1}, (b) from 2250 to 1900 cm^{-1} and (c) fingerprint region from 1800 to 600 cm^{-1}.

Table 4.19. Principal IR bands observed for the FMSA without the Karstedt catalyst

Peak	Wavenumber [cm^{-1}]	Assignment
1	3053	ν_{as}=CH_2, CH=
2	3014	ν_{s}=CH_2, CH=
3	2963	ν_{as}-CH_3
4	2904	ν_{s}-CH_3
5	2133	ν-Si-H
6	1596	ν_{s}=CH_2, CH=
7	1408	δ_{as}-CH_3
8	1260	δ_{s}-CH_3
9	1070	ν_{as}-Si-O-Si
10	1020	ν_{s}-Si-O-Si
11	957	ω=CH_2
12	901	δ-Si-H
13	858	ρ-Si-C
14	793	ν-Si-C

The evolution of the spectra over time reveal insignificant variations in peak intensities suggesting that hydrosilylation reaction did not take place in 65 h of observation. This is proven in Figure 4.54 where the peak areas of the vinyl and silyl bands at 3053 and at 2133 cm^{-1}, respectively, are plotted against time. The peak area of the two bands remains unaltered over time. The minor changes observed follow the same trend in both cases; therefore, disparities may result from baseline effects.

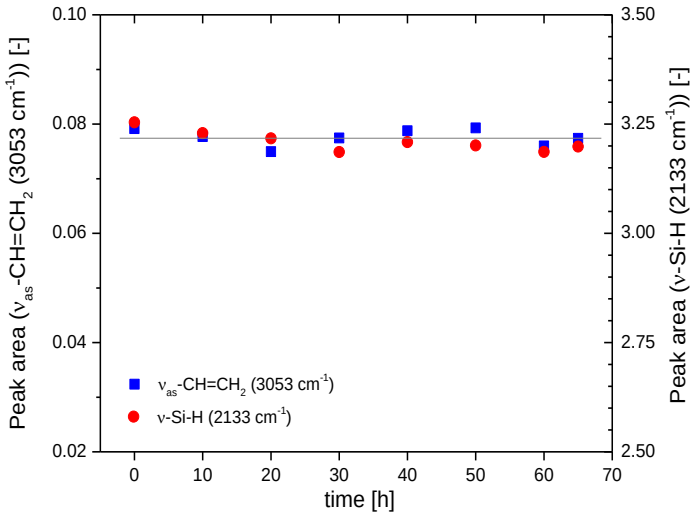


Figure 4.54. Change in peak area over time of vinyl and silyl bands at 3053 and 2133 cm^{-1}, respectively. The peak areas remained unaltered; thus, hydrosilylation did not occur in the absence of the Karstedt catalyst.

In conclusion, crosslinking of FMSA without the Karstedt catalyst did not occur under the conditions applied in this work. This is in accordance with the work of Fustin et al. [316], who explained that when a catalyst is not present, hydrosilylation is unlikely to occur since hydrosilane species or Si-H groups are conceivably only able to dimerize. This situation, eloquently, opened the possibility of analyzing any catalytic effect of the aluminum substrate on crosslinking of the FMSA (without the Karstedt catalyst) at the interface between the two materials. The analysis is included in Chapter 6.

4.5.2.2. Crosslinking in the presence of the Karstedt catalyst

The crosslinking reaction of the FMSA in the presence of the Karstedt catalyst was monitored during 30 min. However, since the reaction was completed in a shorter time, only the ATR-FTIR spectra obtained for the first 17 min are shown. The first spectrum

refers to a reaction time t=1 min and not to zero time (t=0), as usual, due to the lapse existing between the sample preparation and the spectra collection of roughly one minute. The spectral region from 3100 to 2800 cm^{-1} (Figure 4.55a) exhibits the common bands associated with stretch vibrations of C-H bonds in vinyl, methyl and ethylene groups. The bands, due to asymmetric and symmetric stretching of methyl groups, are observed at 2962 and 2906 cm^{-1}, respectively. A slight increase in intensity of these peaks is noticed; especially for the methyl band at 2906 cm^{-1} (ν_s-CH_3). The spectral behavior of this band is believed to be considerably affected by the new appearance of the adjacent shoulder at 2873 cm^{-1}. Accordingly, the appearance of this new band at 2873 cm^{-1}, as well as the band at 2792 cm^{-1}, is accompanied by a gradual increase in intensity during the first 8 minutes, as seen in the expanded image of Figure 4.55b. These two bands at 2873 and 2792 cm^{-1} correspond to stretching vibrations of C-H bonds in methylene groups (CH_2). Therefore, the creation of ethylene bridges (-CH_2-CH_2-) between vinyl PDMS and the crosslinker is confirmed. No further increment in peak intensity of such bands after 8 min is seen, which ratifies that the crosslinking reaction was culminated at that time. Additionally, the progressive decrease in intensity during the first 8 min for the bands associated with vinyl groups at 3053 cm^{-1} (ν_{as}-$CH{=}CH_2$) and 3012 cm^{-1} (ν_s-$CH{=}CH_2$) (Figure 4.55a), also confirms the occurrence of the crosslinking reaction. These bands are no longer appreciated after t=8 min, indicating that the maximum possible amount of vinyl groups was consumed at that time. Unreacted vinyl groups could have remained in the system but their signal is unresolved from noise. In addition, bands related to vinyl groups are usually weakly displayed in FTIR [189].

The characteristic and sharp band corresponding to the asymmetric stretch vibration of hydride groups (ν_{as}-Si-H) is shown in Figure 4.56. For this peak the prior trend was also observed; the intensity of the peak decreased continuously up to 8 min and then remained constant. However, contrary to the pattern perceived for vinyl groups, the spectra show that a considerable amount of crosslinker remained unreacted in the silicone after the double bonds were consumed. This was expected since the crosslinker was added in excess (H/Vi:1.5/1). Thus, after 8 min of hydrosilylation the double bonds were almost consumed, but unreacted Si-H groups remained. The unchanged intensity of the peak after t=8 min also indicates that Si-H groups were not further consumed by secondary reactions, of the type illustrated in Figure 4.9(3), under the conditions applied here. According to Esteves et al. [298][316], side reactions in the presence of a platinum catalyst usually occur slower than the hydrosilylation reaction and are relevant only when the Si-H groups are present in significant excess and the temperatures are higher than 60 °C.

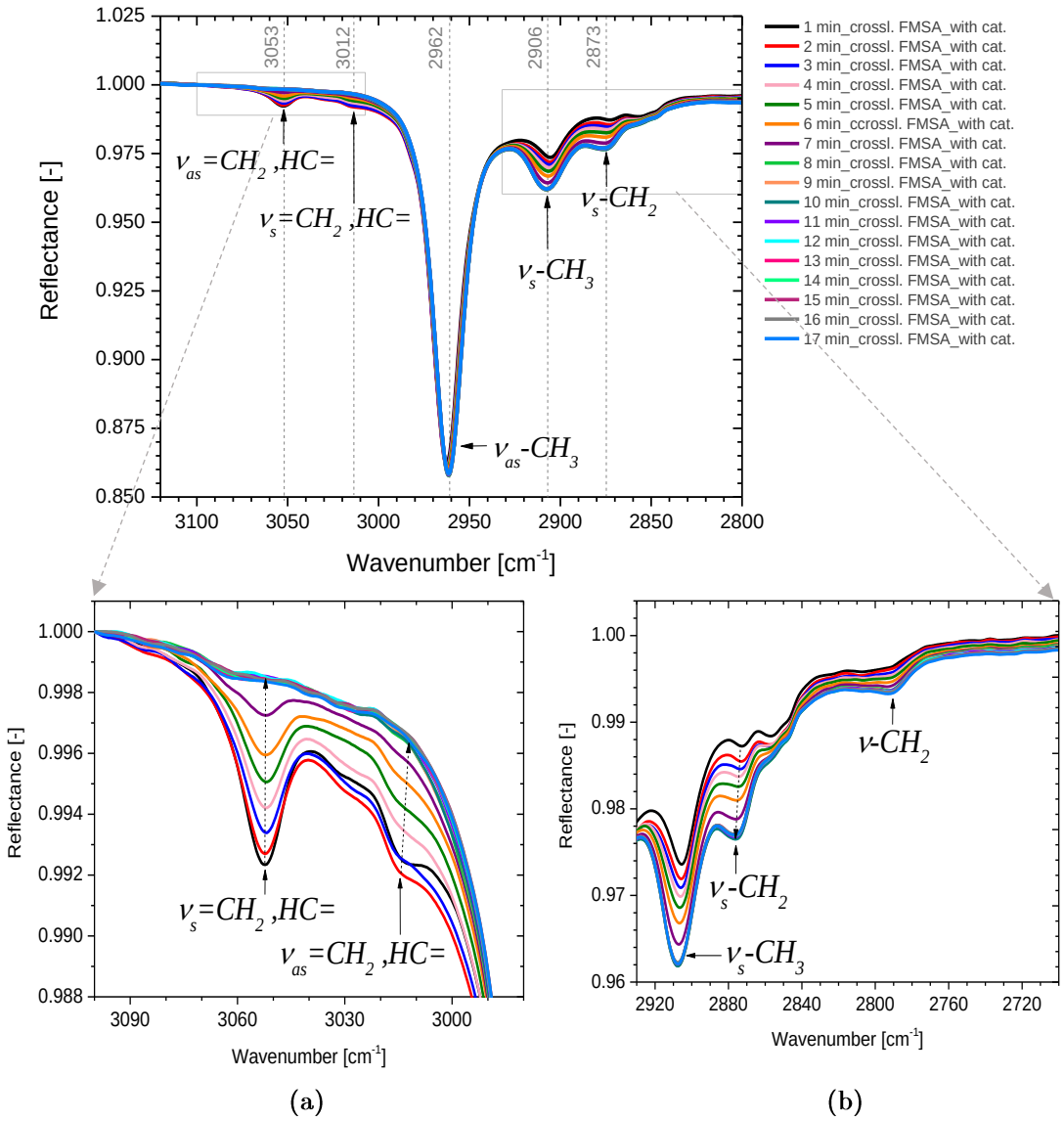


Figure 4.55. Karstedt-catalyzed hydrosilylation (in bulk) monitored by in-situ ATR-FTIR measurements during 17 min. The ATR-FTIR spectra from 3100 to 2800 cm^{-1} is magnified at (a) 3100 to 2900 cm^{-1} and (b) at 2920-2720 cm^{-1}.

Although, it might be considered that suppression of side reactions may not hold true for all hydrosilylation systems, particularly, in some real applications where crosslinking is carried out under air atmosphere, with temperatures above 24 °C and a considerable excess of crosslinker. From the analyzed commercial system, CSA, it was also observed that side reactions associated exclusively with hydrosilylation were not significant. Furthermore, the appearance of bands related to CH_2 groups and their continuous increase in peak intensity exposes the selectivity of the Karstedt catalyst towards the

formation of crosslinked β product (against Markovnikov's rule) at room temperature (Figure 4.57).

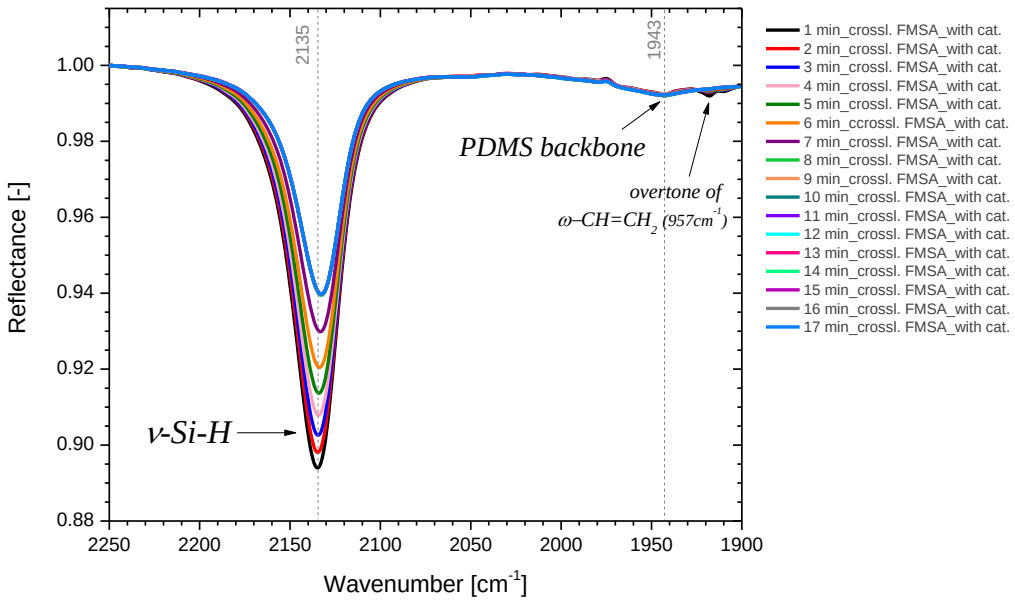


Figure 4.56. Evolution of the crosslinking of FMSA in bulk. ATR-FITR spectra from 2250 to 1900 cm^{-1} characteristic of stretching of Si-H and vibration of the PDMS backbone in PDMS.

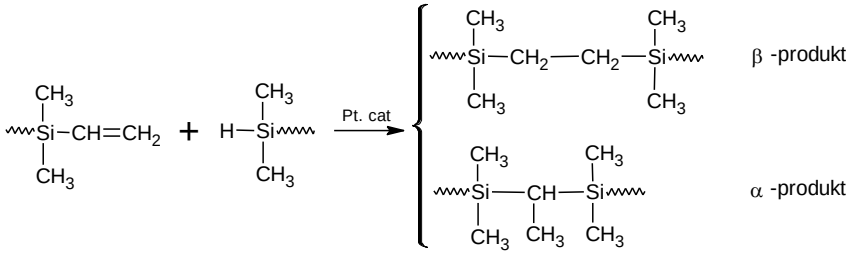


Figure 4.57. Hydrosilylation reaction according to or against Markovnikov's rule resulting in α– or β–product, respectively [88].

The analysis of the fingerprint region depicted in Figure 4.58 indicates that bands associated with vinyl and Si-H follow the same trend previously described, indicating that crosslinking of the FMSA by hydrosilylation was completed in approximately 8 min. After that time further modifications of the spectra are undetected. A series of small peaks are noticed in the fingerprint region at 1700-1500 cm^{-1}. These peaks are

ascribed to moisture since waiting for atmospheric stabilization was not feasible for the analysis of the crosslinking reaction in the presence of catalyst.

For the sake of interpretation, regions involving vinyl and methylene groups in the fingerprint region are enhanced in Figure 4.59a-c.

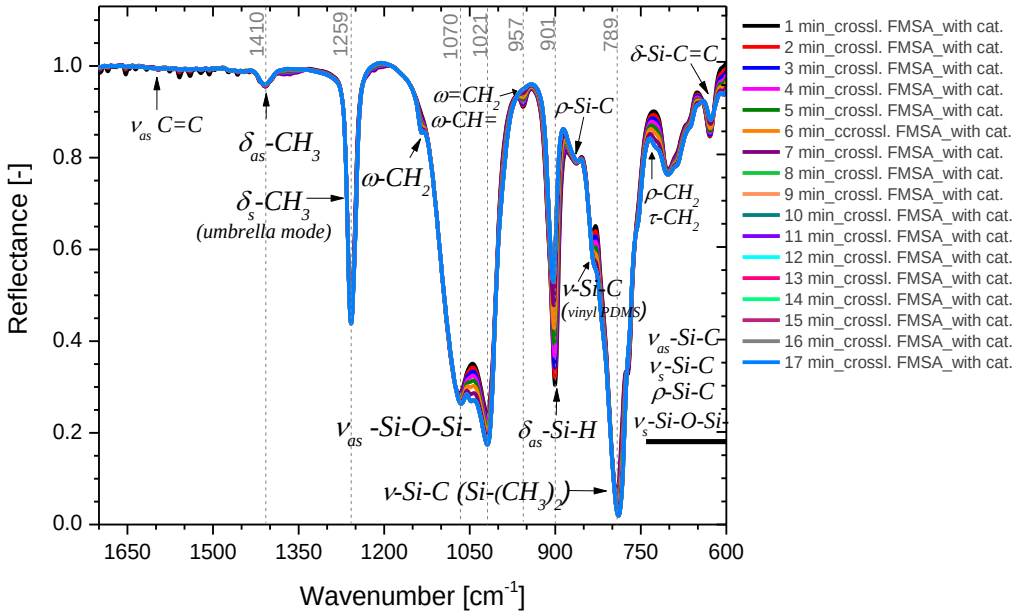
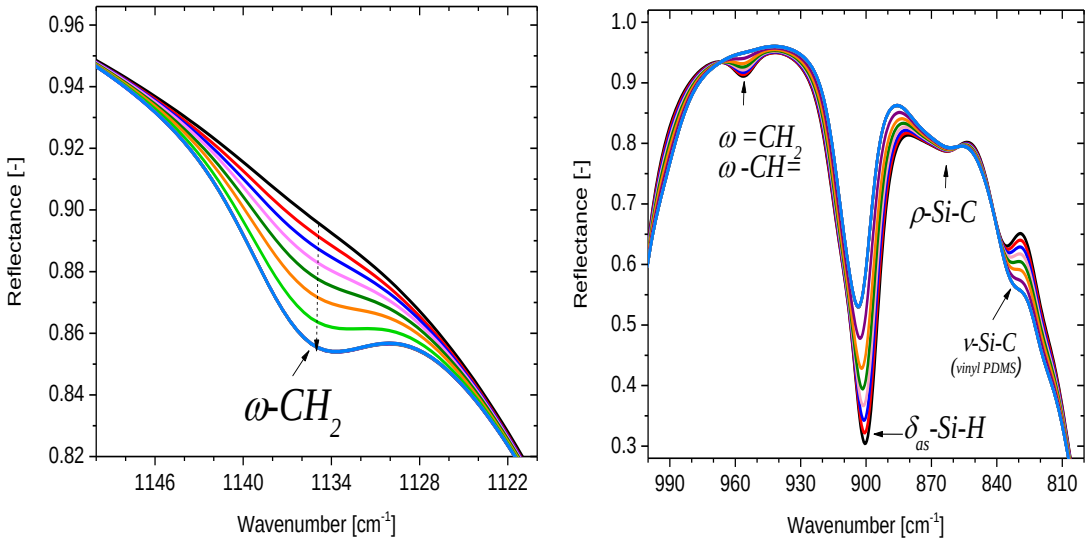


Figure 4.58. In-situ ATR-FTIR spectra of the crosslinking reaction in bulk of FMSA over time (from 1 to 17 min) (a) spectral region from 2250 to 1900 cm^{-1} and (b) fingerprint region from 1650-600 cm



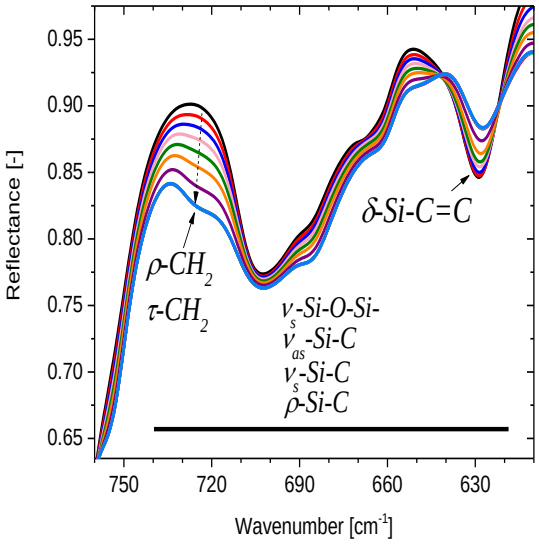


Figure 4.59. Expanded regions of the ATR-FTIR spectra of the fingerprint region at (a) 1160-1120 cm^{-1} (b) 1000-800 cm^{-1} and (c) 760-600 cm^{-1}.

The principal spectral features exhibited in the fingerprint region are summarized below.

- New emerging band at 1135 cm^{-1} associated with wagging of ethylene linkages (-CH_2) progressively increases in intensity for the first 8 min and remains unchangeable afterwards (Figure 4.59a).
- The bands associated with methyl groups at 1410, 1259, 864 and 789 cm^{-1} present a slight increment in intensity during the first 8 min of the measurement and remained constant after that time.
- Band of asymmetric stretching of siloxane bonds (ν_{as}-Si-O-) (Figure 4.59b) is displayed as a strong doublet with maxima at 1068 and 1021 cm^{-1}. The peak exhibits an increase in intensity during the first 8 min and, curiously, it develops a third maximum at ~1050 cm^{-1}. These observations suggest an increase in the concentration of Si-O-Si groups during crosslinking, despite the fact that they are not directly involved in the hydrosilylation reaction. There are different explanations for this behavior. First, secondary reactions between Si-H and traces of Si-OH groups eventually occurred, forming new Si-O-Si linkages. However, this contradicts previous statements which suggest that side reactions were suppressed during hydrosilylation of the FMSA. Second, Si-H bonds underwent hydrolysis creating Si-OH groups that further condensate towards Si-O-Si formation. However, no IR absorption bands at 3700-3200 cm^{-1} associated with stretching of O-H bonds resulting from hydrolysis are observed as the reaction evolves (Figure

4.60). Third, ring opening polymerization of cyclic siloxane traces producing linear oligosiloxanes may have occurred, which increased the concentration of Si-O-SI bonds. Fourth, changes of the double peak are an exclusive consequence of the crosslinking process. As mentioned by Launer [190], if the siloxane chains become more branched or crosslinked, the Si-O-Si absorption band becomes broader and more complex, showing two or more overlapping bands. Consequently, alterations related to the absorption band of siloxane bonds were most likely due to changes in the polymer structure ensuing from crosslinking of the FMSA.

- Bands related to vinyl end-groups at 956 cm^{-1} and at 836 cm^{-1} (Figure 4.59b) progressively diminished, to finally vanish after 8 min, since they were involved in crosslinking.
- The strong sharp peak at 901 cm^{-1} corresponding to bending of Si-H (Figure 4.59b) features the same behavior as the Si-H band at 2135 cm^{-1}; its intensity gradually decreases up to 8 min, afterwards no further changes are detected.
- Bands in the region of 760-600 cm^{-1} (Figure 4.59c) are difficult to assign exactly, however particular spectral modifications, for instance, the a new band appearing at ~762 cm^{-1} can be associated with the newly formed ethylene groups. The band at 629 cm^{-1} can be connected to Si-H and Si-Vinyl groups since its intensity is reduced over time.

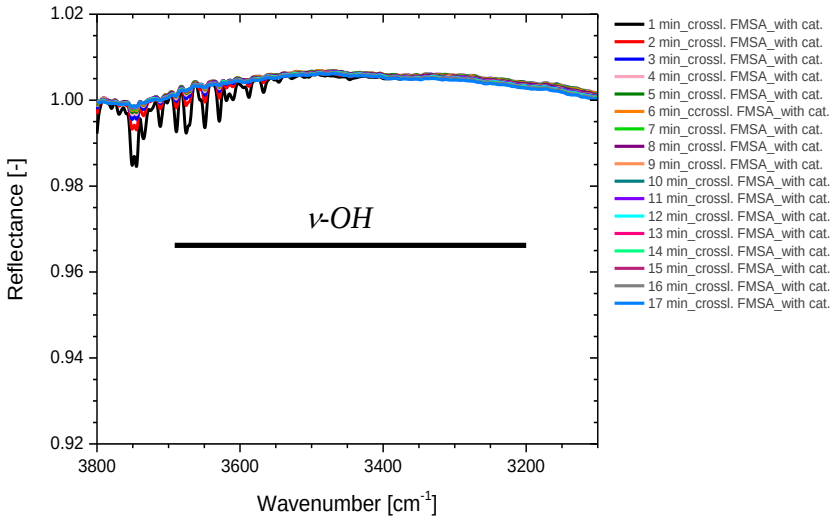


Figure 4.60. O-H stretching mode. The lack of peak suggests that OH formation did not occur. Series of peaks are due to humidity in the IR chamber at the beginning but vanished over time due to continuous purging with dry air.

The conversion of the Si-vinyl and Si-H groups over time was calculated based on Equation 4-10 for the representative peak at 3053 and 956 cm^{-1} ascribed to vinyl and at 2135 and 901 cm^{-1} related to Si-H. The peak areas were normalized in respect to the band at 1943 cm^{-1} corresponding to the vibration of the siloxane backbone, since it remained unaltered during the reaction time. The rate of conversion is plotted in Figure 4.61. It is inferred from the graph that hydrosilylation was the only mechanism occurring, since the behavior of vinyl and silyl groups coincide by following the same consumption path. This supports the assumption that no secondary reactions took place during the crosslinking of the FMSA. Although the crosslinker was added in 50% excess, the ATR-FTIR results revealed that 54 % remained unreacted. Hence, the reaction yield can be assumed to be of approximately 96 %.

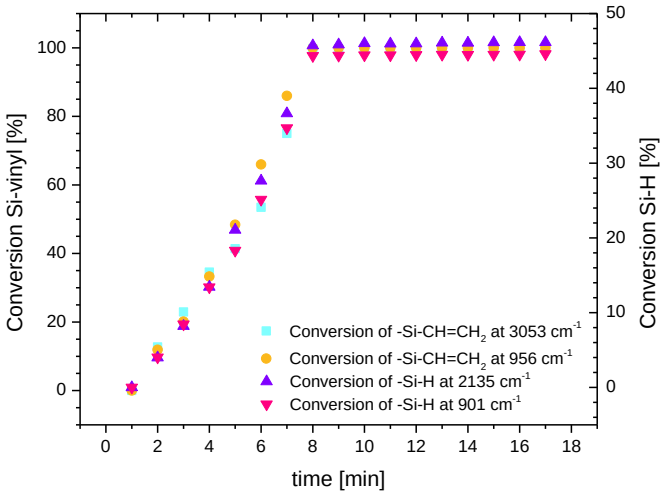


Figure 4.61. Consumption of Si-vinyl and Si-H groups during crosslinking of the FMSA at RT. The reaction is completed after 8 min.

Slight increase in peak intensity within the 8 minutes of the reaction observed for the bands ascribed to methyl groups, suggests possible formation of α product (Figure 4.57). The plausible percentage of α product created is estimated from the peak area of the symmetric bending mode of methyl groups located at 1259 cm^{-1} (normalized respect to the peak at 1943 cm^{-1}) at the beginning (t=1 min) and end of the reaction (t=8 min), according to Equations 4-14 and 4-15

$$\alpha\ product\ formed\ (\%) \propto increment\ in\ [CH_3](\%) \propto increment\ of A_{(\delta_s - CH_3)} \quad \textbf{(4-14)}$$

$$\alpha\ product\ formed\ (\%) = \frac{A_{(\delta_s - CH_3)}\big|_{8\ min} - A_{(\delta_s - CH_3)}\big|_{1\ min}}{A_{(\delta_s - CH_3)}\big|_{1\ min}} \times 100\% \quad \textbf{(4-15)}$$

$$\alpha\ product\ formed\ (\%) \sim 4.5$$

Where $[CH_3]$ is the concentration of CH_3 groups in the system and $A_{(\delta_s - CH_3)}$ is the normalized area of the symmetric bending peak of methyl groups at 1259 cm^{-1}. The estimated percentage of α product formed is low, exhibiting high selectivity of the Karstedt catalyst towards β product. It can be claimed that hydrosilylation of the formulated system, FMSA, yielded 95.5 % of crosslinked product with ethylene bridges at room temperature in the presence of the Karstedt catalyst.

4.5.3. Characterization of the crosslinked FMSA

The crosslinked FMSA (crosslinked in bulk inside the Glovebox) was characterized by ATR-FTIR spectroscopy, solid NMR spectroscopy, TGA and DSC methods.

4.5.3.1. Chemical characterization

A. ATR-FTIR Spectroscopy

The ATR-FTIR spectra (Figure 4.62) of the crosslinked FMSA is consistent with the previous spectrum obtained by the in-situ inspection of the crosslinking reaction when the Karstedt catalyst was present. As expected, bands connected to vinyl groups are not perceived, indicating their consumption in crosslinking, whereas peaks associated with Si-H were still noticed at 2133 and 904 cm^{-1} due to excess. Bands corresponding to newly formed ethylene bonds were detected at 2875 and 1134 cm^{-1}. Additionally, the band related to Si-O-Si bond displays the three maxima feature also detected at the end of the hydrosilylation reaction during in-situ measurements. Consequently, the spectra show that the sample was crosslinked following the reaction path illustrated in Figure 4.7. Table 4.20 listed the principal IR bands distinctive of the crosslinked FMSA.

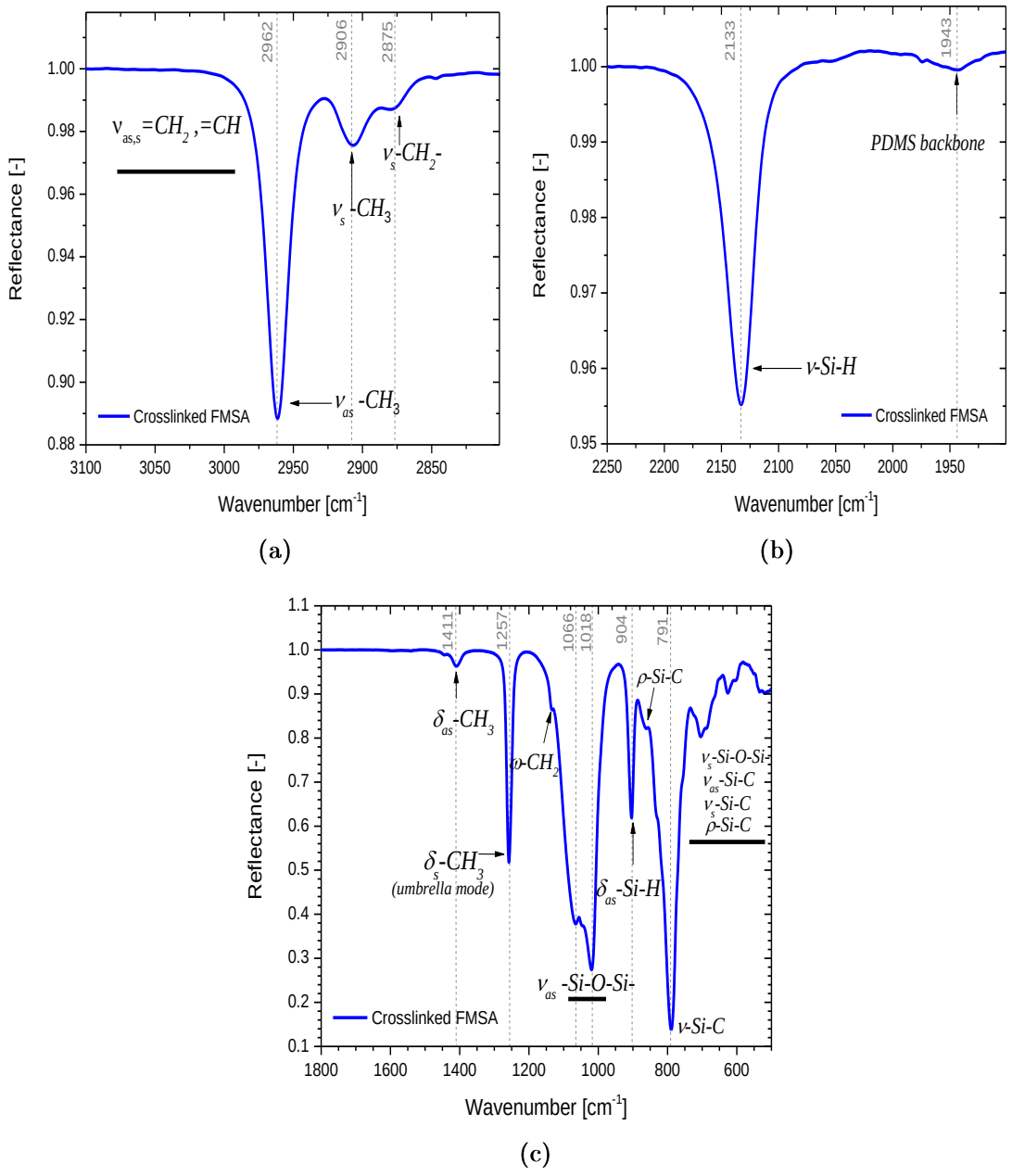


Figure 4.62. ATR-FTIR spectra of crosslinked FMSA at room temperature in dry air (T_{dp}~-65°C), (a) from 3100-2800 cm^{-1}, (b) from 2250 to1900 cm^{-1} and (c) from 1800 to 500 cm^{-1}.

Table 4.20. Principal IR bands of crosslinked FMSA

Peak	Wavenumber [cm^{-1}]	Assignment
1	2962	ν_{as}-CH_3
2	2906	ν_{s}-CH_3
3	2875	ν-CH_2
4	2133	ν-Si-H
5	1411	δ_{as}-CH_3
6	1257	δ_{s}-CH_3
7	1137	ω-CH_2
8	1066	ν_{as}-Si-O-Si
9	1018	ν_{s}-Si-O-Si
10	905	δ-Si-H
11	851	ρ-Si-C
12	791	ν-Si-C

B. Solid state NMR spectroscopy

The obtained ^{1}H-NMR spectrum is depicted in Figure 4.63. The strong, prominent signal at chemical shift $\delta \sim 0.0$ ppm evidences the protons in the repeating D units of the PDMS network. The peak at ~4.7 ppm indicates that unreacted Si-H groups remained in the system, as expected. Moreover, no peaks are recognized at 6-7 ppm where signals of vinyl groups are usually displayed, suggesting that vinyl groups were consumed during hydrosilylation. The shoulder signal perceived at ~ 0.1 ppm corresponds to protons in D units near to unreacted Si-H groups, to newly formed ethylene bonds and to -Si-CH of α product (Figure 4.57). The ethylene groups are a characteristic of the formation of β-product displays a signal at ~ 0.5 ppm, whereas production of α-product is suggested by the signal at ~1 ppm associated with hydrogens of methyl groups. This last signal supports the prior observation by FTIR-ATR that α-product was also formed during hydrosilylation.

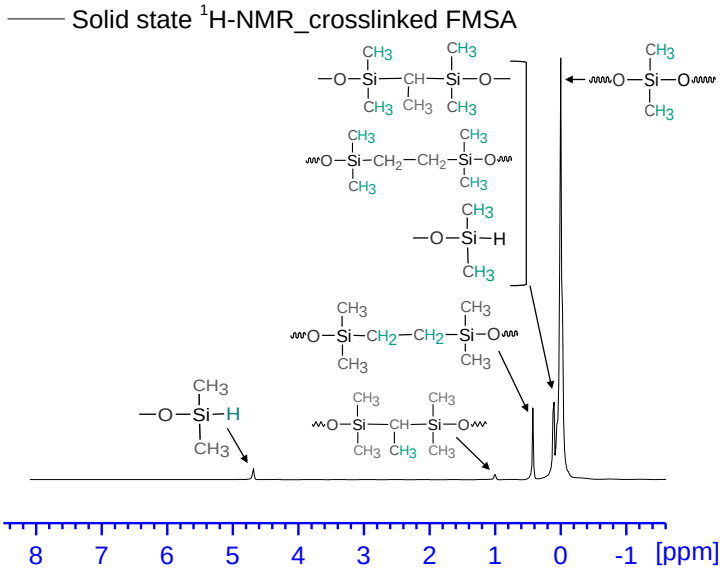


Figure 4.63. Solid state ^{1}H-NMR of the crosslinked FMSA

Additionally, in the ^{13}C-NMR spectrum (Figure 4.64) three principal signals can be seen. The prominent peak at ~ 0 ppm is assigned to carbons of dimethyl groups in D units present on the model silicone. Signals associated with vinyl carbons at ~ 120-135 ppm are not perceived, indicating that they were consumed for crosslinking. The carbons of the newly formed ethylene bonds (Si-CH_2-CH_2-Si) display a signal at ~ 8.0 ppm. Carbons of D units near ethylene and silyl groups are disclosed at 0-(-2) ppm.

Ultimately, the ^{29}Si-NMR spectrum (Figure 4.65) features four principal signals resolved in multiple peaks. The first, at ~ -22.5 ppm attributed to silicon in D units, the second at ~ -6.2 ppm distinctive of silicon in M^H units, the third at ~ 7.72 ppm can be ascribed to silicon in β-product (with methylene groups attached), and a fourth signal at ~ 9 ppm can be related to silicon in α-product. Interestingly, no signal is perceived at ~ -100-(-110) ppm associated with Q units (-SiO_4-), low signal-to-noise ratio is likely the reason.

In summary, the NMR results support the previous findings by ATR-FTIR revealing the high selectivity of the catalyst producing β product. As expected, unreacted Si-H groups remained on the polymer network.

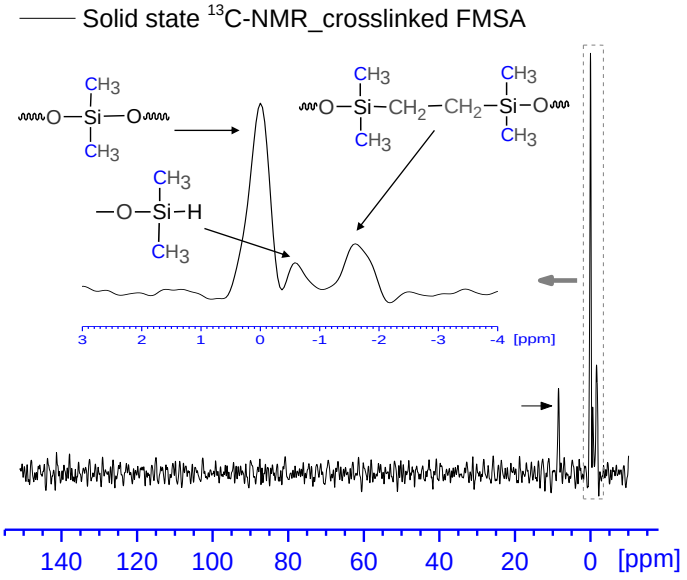


Figure 4.64. Solid state ^{13}C-NMR of the crosslinked FMSA

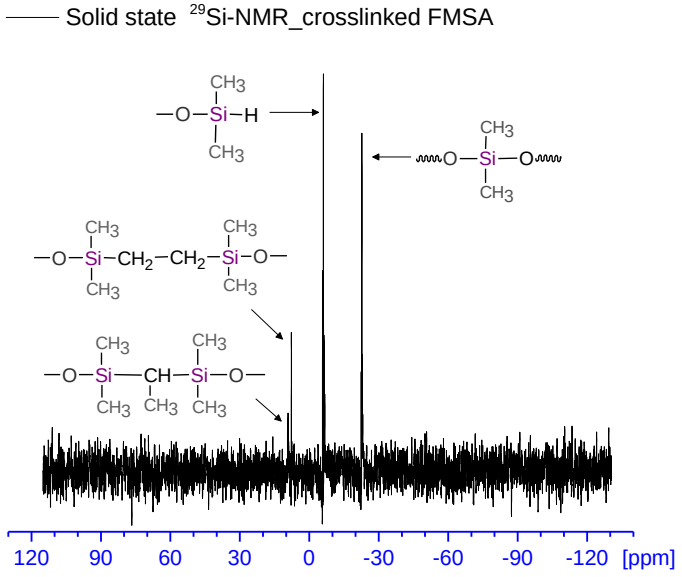


Figure 4.65. Solid state ^{29}Si-NMR of the crosslinked FMSA

4.5.3.2. Thermal Characterization

The thermal behavior of the crosslinked FMSA was analyzed by TGA and DSC measurements following the same experimental procedure described for the cured CSA in Section 4.3.2.2.

A. TGA Analysis

The weight loss curves of FMSA are presented in Figure 4.66 in air and nitrogen atmospheres. The thermograms in both atmospheres display the common degradation behavior described for crosslinked PDMS exposing thermal stability of the model system up to ~388 °C in N_2, and thermo-oxidative stability up to 278 °C in air. In analogy with the cured CSA, weight loss of the crosslinked FMSA over temperature in air, also followed a more complex path than in nitrogen as implied by the DTG curves (1st derivative curve). Thus, for silicone systems, degradation in air involves a more complex path than in nitrogen. The degradation of the FMSA compared to the decomposition of the CSA (Figure 4.24) involved fewer steps in both atmospheres; thus, the presence of additional components affect the degradation path of silicones in a specific atmosphere.

Thermal degradation of the crosslinked FMSA occurred in a single step, with the maximum at approximately 498 °C; whereas thermos-oxidative decomposition took place in two main steps with maxima at 288 and 472-505 °C. These results are in good agreement with those described for pure PDMS networks [283,290,317]. Loss of material below $T_{5\%}$ in both atmospheres can be attributed to evaporation of low molar mass molecules such as water, linear oligomers and traces of cyclic siloxane. As described for the CSA, the driving force for thermal degradation of silicones is the formation of cyclic compounds by shortening of the polymer chains (Figure 4.25) [286]. The most important features of mass loss events experienced by the FMSA in air and in N_2 are listed in Table 4.21.

Comparing the tabulated TGA values of the FMSA (Table 4.21) with those of the CSA (Table 4.11), the influence of different factors such as the structure of the silicone network and presence of additional components such as silica filler, phenyl substituents, inhibitors and additives, is observed. For instance, the $T_{5\%}$ for the CSA is reduced by 20 K in N_2 and reduced by almost 100 K in air compared to the $T_{5\%}$ values of the FMSA. Moreover, the final weight loss difference between the CSA and FMSA is approximately 70 % in N_2, whereas in air it does not change, due to the similar nature of the residue and the filler added in the CSA (silica). Interestingly, opposite to the CSA, FMSA does not undergo degradation above 600 °C; hence, decomposition of silicones occurring at T>600 °C is not attributed to crosslinked PDMS.

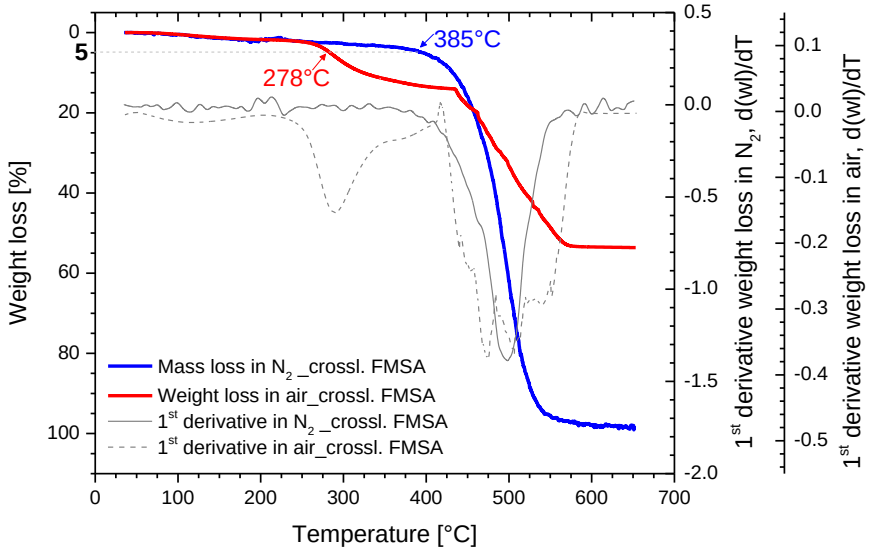


Figure 4.66. TGA and DTG curves from 35 to 650 °C for cured FMSA in air and nitrogen atmospheres.

In summary, for typical service temperature ranges of silicones (-40 to ~200 °C) [13], the formulated model system, FMSA, is stable and it does not exhibit degradation or significant weight loss of material.

Table 4.21. Relevant temperatures and total weight loss of FMSA obtained from TGA measurements from 35 to 700 °C in nitrogen and air atmospheres.

Atmosphere	5% weight loss, $T_{5\%}$ [°C]	10% weight loss, $T_{10\%}$ [°C]	End of degradation, T_e. [°C]	Total mass loss [%]
N_2	388	432	600	100
Air	278	320	582	54

B. DSC Analysis

The crosslinked FMSA was additionally studied via DSC with two different purposes; first, to determine if post-curing occurs from 20 to 200 °C, and second, to detect phase transitions from -140 to 20 °C.

The DSC scan of the crosslinked FMSA at a heating rate of 10 K/min from 20 to 200 °C (Figure 4.67), indicates that the material was fully crosslinked at room temperature and post-curing does not occur at higher temperatures for the formulated system examined. As suggested by Esteves et al. [202,298], post-curing involving

secondary reactions of residual Si-H groups usually takes place at temperatures above 60 °C. However, this was not the case.

The DSC scans from -140 to 20 °C (Figure 4.68) of the crosslinked FMSA, reveal that the material is an amorphous polymer network since only glass transition, and neither melting nor crystallization peaks, were observed in the three heating and two cooling runs, respectively. In contrast, for the CSA four phase transitions were identified (glass transition, melting, cold-crystallization and crystallization). Thus, in the evaluated system, the crosslinking process of the FMSA reduced its ability to crystallize. As reported in various works [295,307,318], different crosslinked PDMS systems display crystallization peaks. Therefore, differences in molar mass of PDMS, type of prepolymer, crosslinker, a catalyst and the presence of other components such as fillers all play a role in the formation of crystallites during curing.

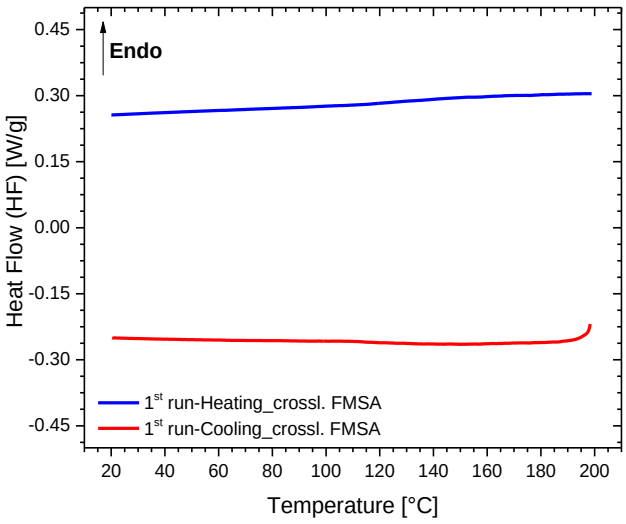


Figure 4.67. DSC curve of the crosslinked FMSA from 20 to 200 °C in nitrogen at a heating/cooling ramp of 10 K/min.

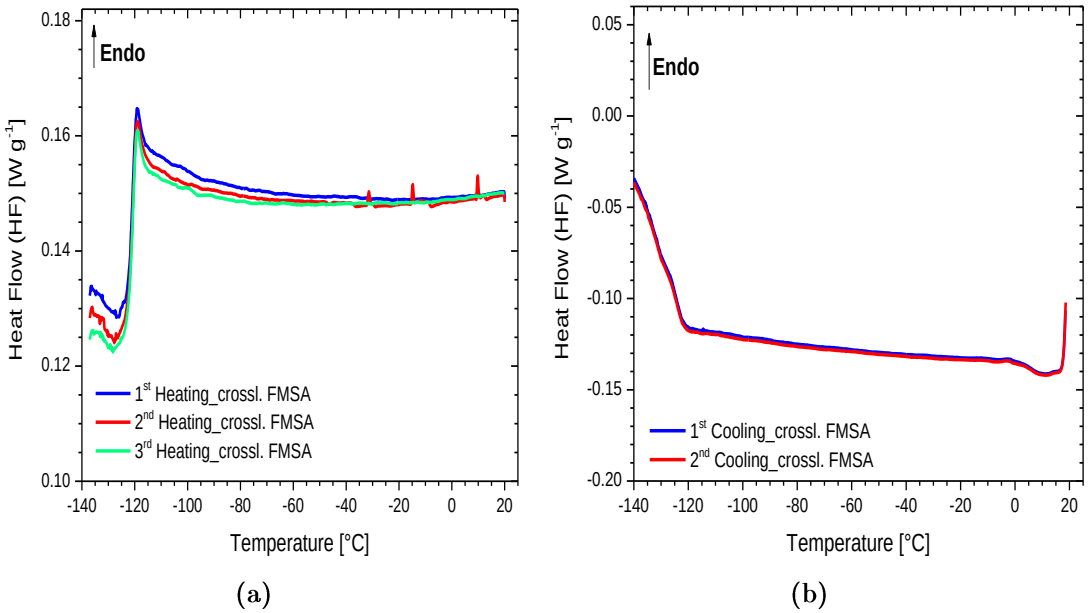


Figure 4.68. DSC curves of the crosslinked FMSA sample from -140 °C to 20 °C at 5 K/min in nitrogen (a) heating scans and (b) cooling scans

The glass transition temperature of the crosslinked FMSA was determined from the 1st derivative of the 2nd heating scan (Figure 4.69). The glass transition occurs in a temperature range from ~ -128 to -111 °C and T_g was found to be -120.7 °C. This temperature is consistent with the value found for T_{g1} for the cured CSA at ~ -119.7 °C. The assumption made for the CSA (displaying two T_g) in which the lower T_g value was associated with crosslinked PDMS and the higher $T_{g'}$ at ~ -112 °C with PDMS bounded to silica particles, is reasonable based on the results obtained for the crosslinked FMSA where no silica is included. The T_g obtained for the crosslinked FMSA is also in good agreement with reported values of pure crosslinked PDMS[305]. The consistency in T_g values for a commercial silicone system and the model system also shows that additional components slightly affects the T_g associated exclusively with PDMS. Curiously, the glass transition exhibits a small endothermic peak immediately after T_g (~ -117 °C) referred to as enthalpy of relaxation, which is associated with volume expansion due to physical aging [319,320].

This physical aging is characterized by the reduction of the free volume of the material when it is maintained in the glass state ($T<T_g$) for a finite time. When cooling a polymer to the glass state at temperature T_a, where $T_a<T_g$, the material is no longer able to remain in a state of structural equilibrium within a finite time scale and thus, falls into a metastable state [320,321]. During the time in which the material is held at T_a, there is a driving force towards its thermodynamic equilibrium; consequently, the

glass polymer undergoes relaxation with a reduction of excess volume and enthalpy Such loss in enthalpy experienced by the polymer is then recovered as an endothermic peak on the DSC scans when the polymer is again heated above its T_g [320–322]. In the case of crosslinked FMSA, the polymer underwent reversible physical aging during the DSC measurement when it was cooled to its glass state from 20 °C to -140 °C and held isothermal for 8 min at -140 °C. Crystallization and orientation are believed to reduce the rate and extent of physical aging. Therefore, the amorphous cured FMSA was more susceptible to physical aging throughout the DSC analysis applied in this work. In the case of the semicrystalline cured CSA, a physical aging event was not perceived.

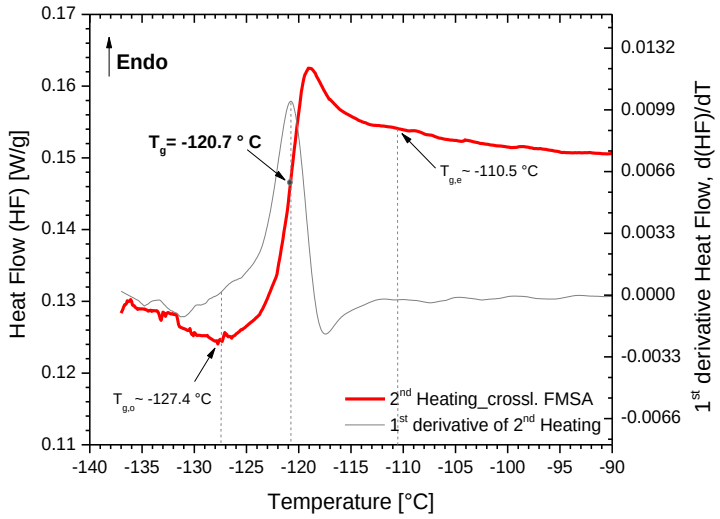


Figure 4.69. Glass transition of the crosslinked FMSA.

4.5.4. Summary – Characterization in bulk of the FMSA

The characterization of the crosslinking reaction in bulk evidences the key role of the Pt catalyst (Karstedt catalyst) in the hydrosilylation reaction. As claimed in the literature, the Karstedt-catalyzed hydrosilylation reaction occurred rapidly at room temperature, it was completed after 8 min. By contrast, in the absence of catalyst it did not occur during 65 h of observation.

The values of onset degradation temperatures of the crosslinked silicone in both nitrogen and oxygen are in good agreement with those values documented in literature, and evidenced the good thermal and thermo-oxidative properties of silicones. even for unfilled products and in the absence of phenyl pendant groups. Although the influence of these two variants

The glass transition temperature at -120 °C is consistent with reported values for crosslinked PDMS and supports the hypothesis that in the commercial product the lower T_g found correspond to PDMS molecules non-bound to the silica filler.

It can be stated that the FMSA exhibits the distinctive properties of a silicone material at room temperature, such as good thermal and thermo-oxidative stability, high flexibility and mobility (T_g=-120 °C). However, unlike commercial silicones, FMSA is not a crystalline material.

5 Adsorption of the SSMC on Aluminum

5.1. Purpose of the in-situ adsorption experiments

An interest in understanding the mechanisms of adhesion has significantly increased in recent years, as many industries have been oriented towards the development and implementation of lighter materials. Yet, describing adhesion mechanisms in a simple manner is a challenging task, due to the complexity and continuously growing comprehension of the subject [4]. As outlined in Section 3.3, adhesion phenomenon is principally defined by the nature of the attractive forces existing at the interface, which lead to the formation of adsorbed layers [96]. Therefore, the nature of such attractive forces can be investigated through adsorption experiments. In effect, adsorption studies are some of the most apposite approaches for understanding the fundamentals of adhesion [323], supported by the continuous development of highly sensitive methods for characterizing molecules in their adsorbate state, such as FTIR-ERAS. However, more in-situ work is needed in order to monitor and understand the formation, behavior and stability of the interface.

In the case of silicones, researchers have extensively studied the adsorption of organosilanes and PDMS from the solution and melt on diverse types of substrates such as silica and alumina, as documented in Section 3.3. These works have demonstrated that under certain conditions, silane compounds having hydrolyzable bonds proceed by the formation of silanols as intermediates which are then covalently bonded to a hydroxylated surface, first through hydrogen bonding, and subsequently through a condensation reaction [324]. For PDMS polymers, it has been suggested that PDMS molecules adsorb via van der Waals forces and hydrogen bonding, featuring chain

flattening [32,124,125,325]. Despite the intensive research, many major questions about the adsorption behavior of silicones on aluminum, such as the conformation state of the molecules, adsorption dynamics, stability of the adsorption (reversibility), and nature of the interactions remain unresolved and require clarification.

The principal aim of executing adsorption experiments is to consistently investigate the individual behavior of the single silicone model components (SSMC) on Al, at room temperature and dry air, in an attempt to obtain information regarding: the interacting forces at the interface, the orientation, conformation and stability of the adsorbate over time and its resistance to solvent desorption. It was intended that the study was sufficiently complete so that a fairly clear picture of the adhesion of silicone adhesives on aluminum could be obtained that can lead to the proposal of the adhesion mechanisms between silicones and aluminum.

In this study, a series of systematic adsorption studies from dilute solution of the single silicone model components (SSMC) onto a well-defined aluminum oxide surface have been conducted. The adsorption behavior of the SSMC onto Al was analyzed by in-situ FTIR-ERAS measurements. This chapter is set out as follows: firstly, introductory remarks regarding adsorption phenomenon followed by the description of the preparation and characterization of the aluminum surface via XPS are provided. Subsequently, a brief explanation of the fundamentals of the FTIR-ERAS technique is given, together with the strategy employed for analyzing and interpreting the measured spectra and the procedure of the adsorption experiments is described. Finally, the spectra are presented and a detailed evaluation of the spectra is given with a conclusive discussion regarding the adsorption of silicones that includes the proposal of plausible adhesion mechanisms.

5.2. Introductory remarks

Adsorption phenomenon deals with the process in which molecules accumulate on the interfacial layer (Figure 5.1) [326,327]. It can be referred as the change in concentration of a given substance at the interface as compared with the neighboring phases [326]. The adsorbed molecules interact with the individual atoms, molecules or ions present on the substrate surface, and also with other adsorbed molecules. This collective effect is defined as energy of adsorption [328]. Thus, when an adsorbed molecule receives energy equal or greater than the energy of adsorption, it will leave the surface in a reverse process called desorption.

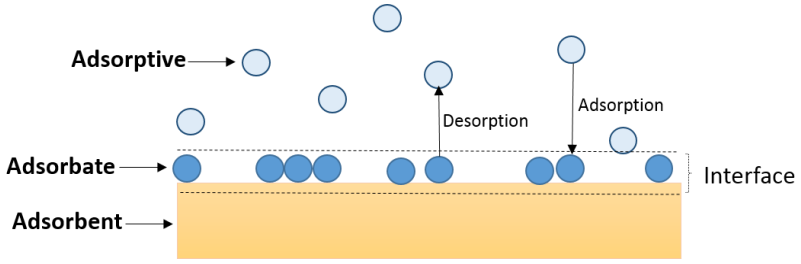


Figure 5.1. Representation of the adsorption process and its terminology [329].

When chemical (short-range) interactions are involved at the interface, the adsorption process is called chemisorption [326,328], and denotes those cases wherein the electronic structure of the atoms is significantly perturbed and hybridized orbitals are formed due to charge transfer [328,330]. Accordingly, some electrons of the two participants are shared, with the consequent formation of a chemical bond [328]. Chemisorption is characterized by relatively high bonding energies (200-600 kJ/mol) [91], and of being irreversible [326,328]. It is also highly selective and occurs only as a monolayer. On the other hand, when physical (long-range) interactions govern, the process is defined as physisorption [326,328]. In this case, the electronic structure of the atoms is almost unperturbed, although some distortion or rearrangement is still possible. Principally, in physisorption, no sharing or transfer of electrons occurs. Therefore, the physisorbed molecules are highly mobile since they are not bound to specific locations [326] and due to low binding energies (0.5-40 kJ/mol) [91]. Contrary to chemisorption, physisorbed molecules can be more easily desorbed. The forces or interactions responsible for physisorption are predominantly van der Waals forces. Hydrogen bonding is considered a special case since in terms of bond energy, it lies between physical and chemical interactions [91]. Under favorable conditions, both chemisorption and physisorption processes can occur simultaneously or alternately [52]. For instance, a layer of molecules may be physically adsorbed on top of an underlying chemisorbed layer. In some cases, a same adsorbent-adsorbate system can feature both physisorption and chemisorption depending on the temperature.

The adsorption of polymers differs from the adsorption small molecules in various aspects [331]. Firstly, the repeating units of a polymer have the possibility to be bound to numerous sites of the adsorbent surface, whereas smaller molecules normally adsorb at a single site. Secondly, polymer molecules diffuse slowly due to a greater mass. Thirdly, when adsorption takes place, some of the internal degrees of freedom of the polymer chains are restricted or even lost. Typically, the interfacial polymer layers contain both two-dimensional adsorbed train segments and three-dimensional large loops and tails extending into the bulk. In the adsorption of polymers, adsorbate layer

formation is unavoidable even when weakly attractive surfaces come into contact with a diluted polymer solution [332]. This occurs because by giving up their bulk translational entropy, which costs a free energy of only k_BT (k_B: Boltzmann constant, T: temperature), polymer chains achieve an energy advantage proportional to the number of monomers per chain, N [332].

Important aspects must be considered in the analysis of the adsorption behavior of macromolecules, which are as follows:

1. Chemical structure of the molecule: presence and nature of chemical groups which could interact strongly with the adsorbent.
2. Molar mass or molecular size: macromolecules or small molecules.
3. Molar mass distribution of the polymer
4. Solvent from which adsorption takes place: good, bad or θ solvent.
5. Temperature
6. Adsorbent: chemical nature and roughness of the surface
7. Presence of other chemical species in the solvent, in the solute or on the adsorbent surface: traces of impurities or contaminants.
8. The degree of reversibility of the adsorption process: depending on different parameters such as solvent used and temperature.

5.3. Experimental approach

The experimental approach implemented in the current investigation was first developed and employed in the previous works of Nies and coworkers [43,333], and Fug et al. [42], for the adsorption of polyurethanes on different metals. The approach involves four main sections or steps outlined in Figure 5.2 and which constitute the subsequent subdivisions of this chapter. The first stage deals with the preparation of the model aluminum substrate and its chemical characterization via X-ray Photoelectron Spectroscopy (XPS). The second step involves the execution of the in-situ adsorption experiments. The third step refers to the spectral analysis in which bulk-like spectra were simulated in the ERAS configuration and compared with the measured ERA spectra. The fourth step deals with the discussion of the results in which the main aspects concerning adsorption are analyzed for the proposal of adhesion mechanisms.

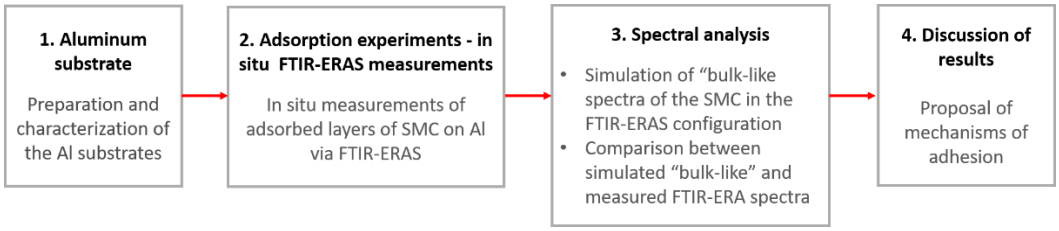


Figure 5.2. Methodological approach implemented for elucidating the adhesion mechanisms.

5.3.1. Aluminum substrate

Principally, the substrate must be planar, smooth and uniform in order to allow reflection for the FTIR-ERAS measurements. In general, typical technical aluminum substrates do not meet these requirements and therefore a more suitable aluminum substrate was necessary. The substrates used in this research were prepared following the procedure previously employed in analogous studies [8,42,43,333]. The method allowed to obtain a "mirror-like" aluminum surface with reproducible surface properties (roughness and chemical composition) suitable for adsorption studies via FTIR-ERAS.

5.3.1.1. Preparation of the Al substrate by PVD

The model aluminum substrates were prepared by physical vapor deposition (PVD) of pure aluminum on polished silicon wafers (Si-wafer) in high vacuum. PVD is a well-known technique for transferring atoms from a specific source to a substrate. The film formation and growth proceed atomistically under high vacuum [334]. The material to be deposited (solid or liquid source) is physically converted to a vapor phase either by addition of heat (evaporation) or through the physical dislodgment of surface atoms by momentum transfer (sputtering) [334]. In evaporation (the method applied in this study) the vapor atoms propagate almost instantaneously and condense on the substrate, forming a thin deposited film [334]. The characteristic structure of the deposited film (e.g., film thickness) is essentially determined by the process operating conditions applied [334]. The chemical purity of the films usually depends on the nature and level of contamination initially present in the source (metal), in the heater or from residual gases present in the vacuum system. The heaters are elements that reach the evaporation temperature of the source (aluminum) while having a negligible vapor pressure. Ideally, they should not contaminate, react or alloy with the evaporant or

release gases such as oxygen, nitrogen or hydrogen at the evaporation temperature [334].

Materials

Si-wafers (p-type, 1-30 Ω cm) were acquired from Si-Mat (Silicone Materials, Kaufering, Germany) as monocrystalline discs (orientation <100>) of 100 mm diameter, 525 ± 25 µm thickness and with a single side polished. The aluminum source used was an aluminum wire of hire purity (99.999 %) supplied by GoodFellow Ltd (Bad Nauheim, Germany) with a 0.5 ± 0.05 mm diameter.

Experimental procedure

First, the Si-wafers were carefully cut in rectangular shapes of 20 x 25 mm^2 in size and then blasted with dried air for removing dust or solid particles incrusted on the surface. For every adsorption experiment, three substrates were prepared. Subsequently, the three slices were transferred in a sample box to the PVD system and were placed on the sample carrier of the equipment, which was located 15 cm below the electrical resistance heater. The heater was a conical basket of Tungsten-filament (9 mm H x 7 mm ϕ) inclined 40°-45° in respect to the substrate surface for improving deposition. Next, approximately 6.2 cm (~2.5 g) of Al wire was cut, rolled, and inserted inside the heater. The equipment was then closed and vacuum was applied. Before reaching high vacuum (5 x 10^{-4} mbar), the PVD chamber was flushed with argon gas for 30 s in order to eliminate atmospheric impurities. Subsequently, the tungsten wire was heated by electrical energy at a current of 10 A during 3-5 s. The current was then increased to 16 A for melting and subsequent evaporation of the aluminum. As soon as no more aluminum was observed inside the heater, the current was dropped to 0 A and the deposition process was finalized. The chamber was then flushed with argon until it reached atmospheric pressure. Finally, the freshly prepared Al-PVD substrates were taken out from the PVD equipment and transported to the FTIR-ERAS laboratory for their storage in dried air for 18 h prior to adsorption experiments. Importantly, during the transportation of the substrates from the PVD equipment to the storage compartment, they were exposed to ambient conditions for a lapse of 5-7 min in which a native aluminum oxide film was formed on top of the surface.

The Al-PVD substrates obtained were visually smooth such as a “mirror-like” surface (Figure 5.3a). The characterization of the surface topography by scanning force microscopy (SFM) in tapping mode conducted by Summa [335], established that the substrates possessed a very fine-grained, smooth, polycrystalline layer structure (Figure 5.3b) with average roughness in the sub-nanometer region, $R_a \leq 1$ nm which does not

interfere with the reflection of IR light (λ: 2.5-25 μm). The low roughness was transferred from the Si-wafer to the aluminum layer due to a uniform deposition of the metal on the silicon wafer [8,42,43,333]. Moreover, crystallites from the surface of the Al-PVD substrates are seen projecting out of the plane (Figure 5.3c) with a distance between the highest and the lowest crystallite of about 10 nm estimated from the texture profile (Figure 5.3d). The surface topography of the Al-PVD substrates was proven to be appropriate for the adsorption experiments. As reported by Wehlack [8], the thickness of the aluminum layer formed on the Si-wafer following this exact procedure was of ~70-100 nm.

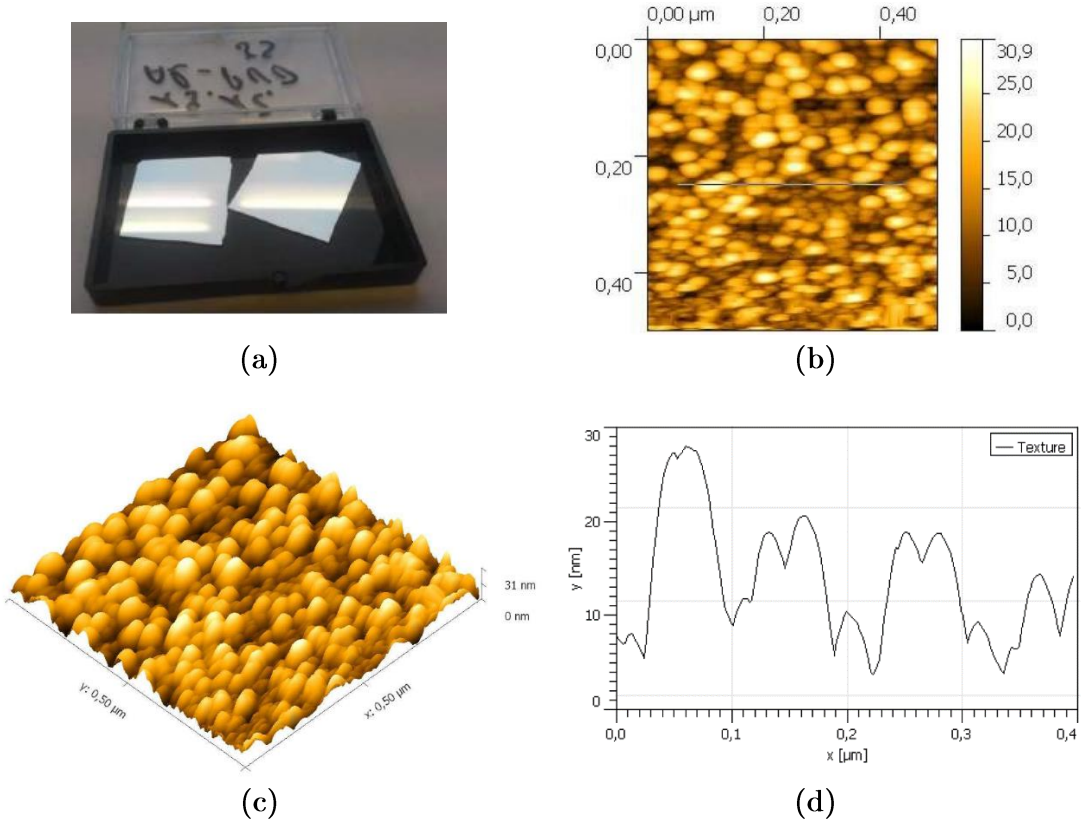


Figure 5.3. (a) "Mirror-like" aluminum substrates obtained by PVD, (b) SFM image top view of the Al-PVD surface, (c) and (d) represent the corresponding 3D image and line profile or texture. (Photos courtesy of Jannik Summa [335]).

5.3.1.2. Chemical composition of the Al surface studied by XPS

The chemical constitution of the aluminum surface (prior to adsorption experiments, i.e. after 18 h of preparation) was evaluated by X-ray photoelectron spectroscopy

(XPS). A rigorous and extensive investigation of the chemical state of the aluminum surface was out of the scope of this work. Instead, a basic insight is provided.

XPS - Background

XPS is considered a very powerful technique, utilized to investigate the chemistry at the surface of a sample (information depth ≤ 10 nm) by determining its electronic state [336,337]. The method measures the kinetic energy and intensity of electrons emitted when the sample's surface is exposed to X-ray photons (100-2500 eV) under ultra-high vacuum [4,337]. Through irradiation, penetration and subsequent absorption of X-ray photons, photoelectrons from the inner shells or valence bands of the near surface region are excited and emitted, due to the photoelectric effect, at kinetic energy E_{kin} defined by Equation 5-1 [337]. Experimentally, the kinetic energy of the ejected photoelectrons is measured by a typical hemispherical sector analyzer, and the corresponding electron binding energy relative to the Fermi level is calculated from Equation 5-1. A typical XPS spectrum shows photoelectron intensity as a function of binding energy, characteristic of the elemental composition and binding state of the atoms present at the sample's surface [4,337].

$$E_{kin} = h\upsilon - E_b - \Phi_s \tag{5-1}$$

Where $h\upsilon$ is the energy of the photon, E_b is the binding energy of the atomic orbital from which the electron originates (known), and Φ_s is the sample work function, which refers to the energy needed to remove the electron from the solid, and is a constant value for a given analyzer. The binding energy of a core electron is affected by the atom's electron density and, thereby, the oxidation state and the chemical environment of the atom [338]. As the oxidation state becomes more positive, the electron density decreases and the effective nuclear charge experienced by the core electrons increases. Therefore, the core-electron binding energies increase with decreasing electron density about the emitting atom [338].

In this work, angle resolved XPS (ARXPS) was applied for a surface enhanced study by varying the take-off angle (angle of the emitted photoelectrons with respect to the sample surface normal). The take-off angle of the ejected electron affects the sampling depth since only electrons near the surface escape at larger take-off angles [339]. Thus, the analysis is most sensitive to the surface at higher photoemission angles or take-off angles.

For the correct analysis of an aluminum XPS spectrum, the metal surface structure must be first understood. The surface of aluminum has been ideally described as a multilayer system as the one illustrated in Figure 5.4 by McCafferty and Wightman [340]. Normally, pure aluminum forms a native oxide layer (Al_2O_3) of thickness d, when the surface is exposed to air. This oxide layer acts as a barrier, protecting the aluminum from many types of corrosion and offering high hardness properties [341,342]. The aluminum oxide/hydroxide film chemisorbs, at least, a monolayer of water when exposed to moisture at room temperature [342]. Hence, the outermost sublayer of the oxide film consists of chemisorbed water with thickness t_{H2O}. The middle sublayer is associated with a hydroxylated region of depth t_{hxyd}, and the innermost portion corresponding to the oxide film of depth t_{ox} [340]. On top of the entire oxide film an overlayer of adsorbed organic contamination of thickness t_c exists [340]. Consequently, by means of XPS measurements, the described multilayer surface was expected to be characterized for the Al-PVD substrate. In addition, the thickness of the complete oxide layer, d, was presumed to be estimated.

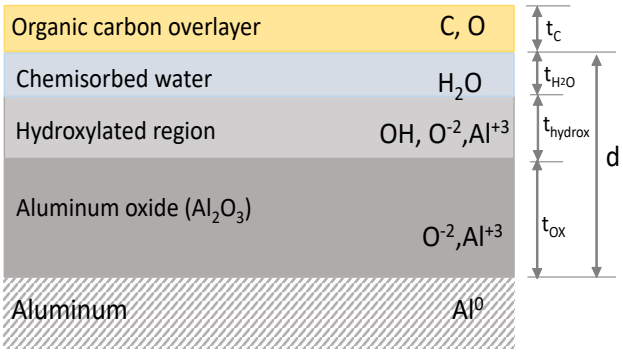


Figure 5.4. Scheme of an aluminum surface with an oxide layer of thickness d [340].

Experimental

The surface analysis of the Al-PVD substrates by ARXPS was carried out externally in behalf of Robert Bosch Ltd at OFG-Analytik GmbH (Münster, Germany) by Dr. Markus Deimel. The substrates were evaluated "as received" after 18 h of their preparation using a Thermo VG Scientific Sigma Probe system which employs a monochromatic Al-Kα X-ray source (1476.68 eV, 75 W). The spectrometer was equipped with a hemispherical analyzer working at a pressure of 10-7 mbar. The general survey spectra were recorded at pass energy of 80 eV with spectral resolution of 1 eV.

Instead, the high-resolution spectra for C 1s, O 1s, and Al 2p were acquired with an analyzer pass energy scan of 30 eV with spectral resolution of 0.1 eV. Angle variation was done automatically and the principal photoelectron peaks were measured at take-off angles of 0°, 40° and 80° (measured with respect to the surface normal of the sample). Assignment, fitting and deconvolution of the signals were executed by the software QUASES-IMFP-TPP2M Version 2.2, with the peaks adjusted to a Gaussian-Lorentz function.

For a detection angle θ, the information depth or penetration depth λ, is given by the projection of photoelectrons pass λ_m (the maximum escape depth) at the detection direction, as described in Equation 5-2.

$$\lambda = \lambda_m \, Cos\theta \qquad (5\text{-}2)$$

From the measurements performed, the emitted electrons came from a depth of approximately 5 nm [343]. Therefore, for the respective evaluated take-off angles, the information depth achieved was:

- 0° ~ 5nm
- 40° ~ 3.8 nm
- 80° ~0.9 nm

Results

The XPS survey spectra of the Al-PVD substrates at different take-off angles reveal the presence of oxygen (O 1s), carbon (C 1s) and aluminum (Al 2s, Al 2p) on the surface (Figure 5.5a-c). This suggests the existence of an aluminum oxide film (including layers associated with Al-hydroxide and chemisorbed water) covered by a thin layer of organic impurities being consistent with the surface model depicted in Figure 5.4. The assignment of the detected photopeaks in the spectra was based on XPS literature of aluminum substrates [336,338,340,344,345]. The weak signals perceived at ~100 eV are related to silicon and silicon oxide (Si 2p) of the Si-wafer. As expected, the spectra show dependency of the Al, O and C signals with the take-off angle, i.e. with the penetration depth. The atomic ratios of the peaks are tabulated in Table 5.1. From the table, it is noted that C 1s and Al 2p lines behave oppositely, with the first increasing when the information depth decreases. This trend is reasonable due to a more superficial XPS analysis at higher take-off angles where detection of the outermost carbon layer is enhanced. In contrast, only slight changes in function of the take-off angle are observed for the O 1s signal.

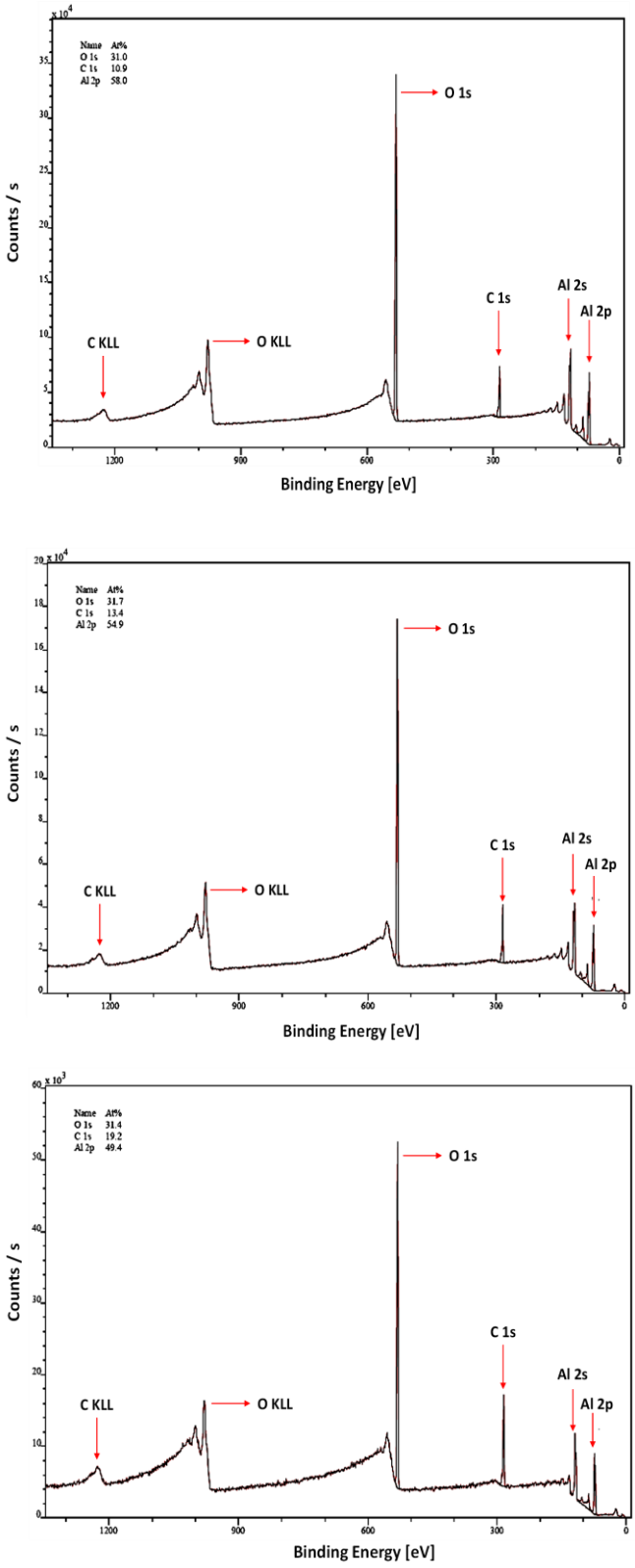


Figure 5.5. XPS survey spectra of the Al-PVD substrates after 18 h of preparation [343]. Presence of photopeaks for Al, O and C elements are perceived at different take-off angles (a) 0°, (b) 40° and (c) 80°.

Table 5.1. Elemental analysis resulted from XPS measurements at different information depths (different take-off angles) [343].

take-off angle	Information depth [nm]	Atomic ratio [%]		
		Al 2p	O 1s	C 1s
0°	5.0	58	31.1	10.9
40°	3.8	55	31.7	13.4
80°	0.9	50	31.4	19.2

The high-resolution Al 2p spectra (Figure 5.6a-c) were resolved into two individual photopeaks at 71.7 and 74.4 eV corresponding to metallic aluminum and to aluminum oxide, respectively. The second peak contains contributions from aluminum atoms in Al_2O_3 and from those bound to OH-groups. The binding energy separation of the oxide and metallic components was estimated to be 2.7 eV, which is a characteristic value for air-passivated amorphous aluminum oxide [346]. A decrease of the aluminum metal peak and increase of the aluminum oxide peak was observed when the angle went from 0° to 80°. This indicates that the surface was predominantly aluminum oxide when the XPS sampling depth was ~0.9 nm (80°). The peak areas calculated for the two resolved Al 2p peaks in dependence of the take-off angles are quoted in Table 5.2.

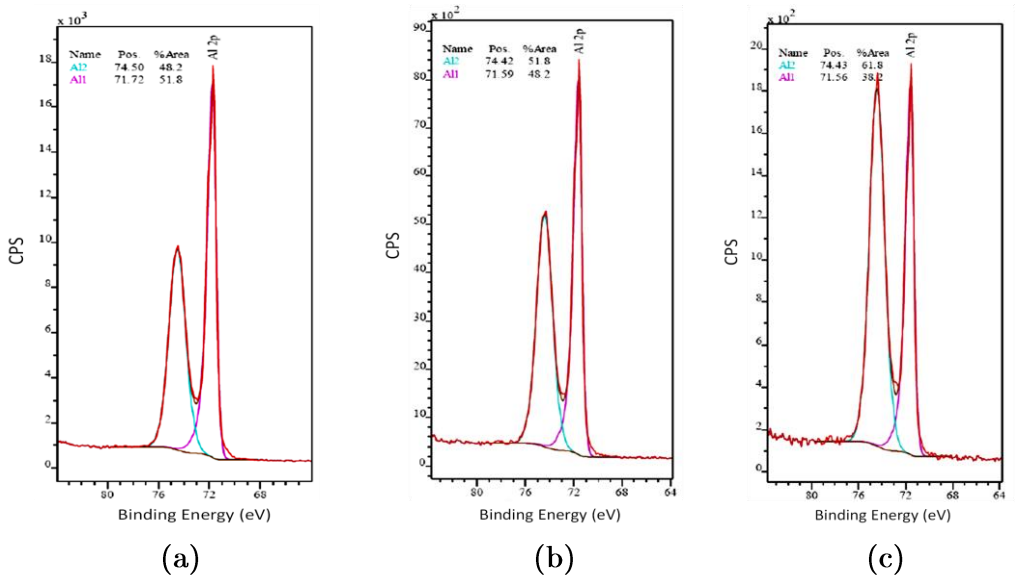


Figure 5.6. Aluminum XPS Al 2p photopeaks at different take-off angles (a) 0°, (b) 40° and (c) 80° [343].

Additionally, from the resolved Al 2p peaks, the thickness d [nm] of the oxide film can be calculated by the relative intensity of photoelectrons from the oxide to those from the underlying metal, assuming a uniform overlayer, shown as follows in Equation 5-3 [340,347].

$$d\ [nm] = \lambda_o[nm]\ Sin\theta\ ln\left[\frac{N_m\lambda_m}{N_o\lambda_o}\left(\frac{I_o}{I_m}\right) + 1\right] \quad \textbf{(5-3)}$$

Where I_o and I_m are the intensities (i.e. peak areas) of the metal and oxide photoelectron peaks [340,347]. N_o and N_m are the atomic densities of metal atoms in the oxide film and in the underlying metal substrate, respectively, and λ_o and λ_m are the corresponding inelastic mean free paths (IMFP) of electrons [340,347], θ is the electron take-off angle with respect to the sample surface. The IMFP in the aluminum oxide (λ_o) is 2.8 nm and in the aluminum metal (λ_m) is 2.6 nm for Al-Kα-generated Al 2p photoelectrons emitted normal to the surface of a γ-Al_2O_3 overlayer on aluminum [344,347]. In this study, a N_m/N_o ratio of 1.5 was used [348]; hence, Equation 5-3 can be simplified in Equation 5-4, as shown below:

$$d\ [nm] = 2.8[nm]\ ln\left[1.39\left(\frac{I_o}{I_m}\right) + 1\right] \quad \textbf{(5-4)}$$

The thickness d [nm] of the oxide layer formed on the Al-PVD substrate calculated was 2.3 nm. This value is consistent with previous estimations of d for Al-PVD substrates employed by Wehlack [8].

Figure 5.7(a)-(c) presents the high-resolution O 1s spectra for the three measured take-off angles. The O 1s signal shows different states of binding of the atom resulted from the presence of a hydroxylated region (Al-OH), the innermost portion of the oxide film (Al_2O_3) and a chemisorbed water layer. Consequently, the O 1s peak was resolved into three individual peaks corresponding to oxygen species O^{2-}, OH and oxygen of chemisorbed water. The corresponding resolved peaks are positioned from the lowest to highest binding energy, respectively as indicated in Figure 5.7. The peak positions are 1.25 to 1.37 eV apart, which is consistent with published values related to deconvoluted signals of the O 1s photopeak [340]. The peak area related to aluminum hydroxide increases proportionally with the take-off angles, as expected. This confirms that hydroxyl species are mainly present on the outer regions of the oxide layer. In contrast, the peak related to Al_2O_3 decreases when the take-off angle increases. The

presence of hydroxyl groups in the outer layers of the oxide film is of great importance, since the nature and properties of such groups play an important role in adhesion phenomenon of polymers. For instance, acid-based properties are of considerable importance in the interaction between polar organic molecules and oxide surfaces [340]. Consequently, the presence of surface hydroxyl groups on the Al-PVD surface is significant for elucidating possible adhesion mechanisms.

Interestingly, the peak ascribed to oxygen in water is considerably small. This indicates that water was adsorbed on the oxide layer in trace amounts, which is understandable as the substrates were stored in dry air.

Finally, for quantitative analysis purposes, it may be considered that oxygen-containing functional groups are also present in the outermost layer of organic carbon contamination; hence, the total intensity of the O 1s line also contains contribution from those groups [336,340,346].

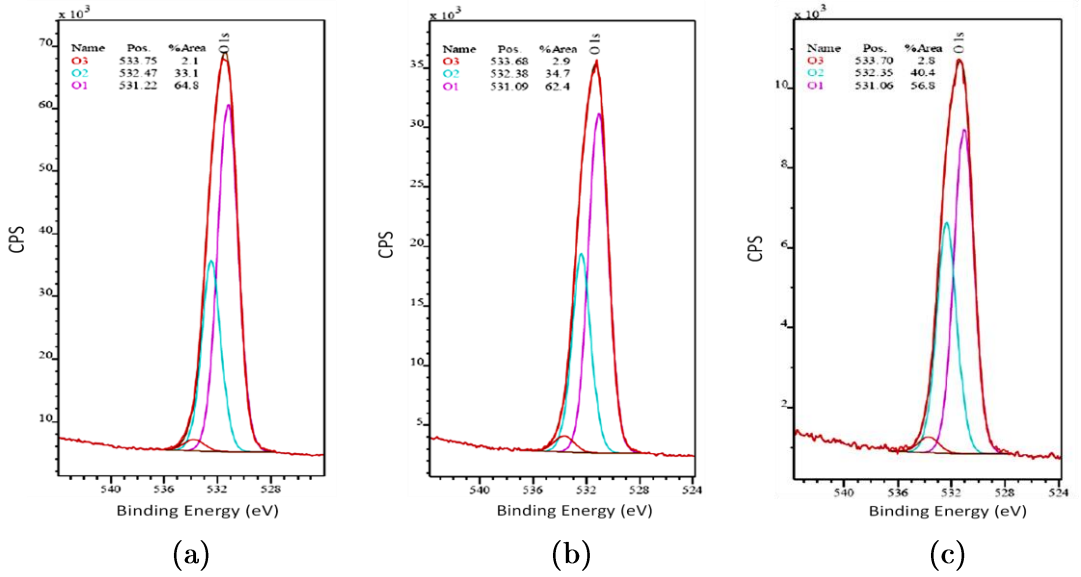


Figure 5.7. Oxygen O 1s resolved peaks of the Al-PVD surface exposed to different take-off angles (a) 0°, (b) 40° and (c) 80° [343].

Ultimately, the C 1s peaks of the spectra at different take-off angles (Figure 5.8a-c) consistently reveal the presence of an adventitious carbon contamination layer on top of the oxide layer. It is believed that this contamination attenuates the photoelectron signals of the oxide and the metal to some extent depending on the thickness of the carbon layer; however, the thin carbon layer is believed to have an insignificant effect on the estimated oxide thickness d in the nm range.

Due to the high surface energy of aluminum, contaminants from the atmosphere accumulated easily on the substrate surface. The XPS C 1s signal was resolved into four components characteristic of C–C/C-H, C-O, C=O and COOR species located from lower to higher binding energies, respectively. The reported data in Table 5.2 of the deconvoluted peaks indicate that the principal contamination arises from aliphatic groups. This is in agreement with XPS studies of the Al-PVD substrates which showed that these carbonaceous contaminations contained principally aliphatic chains near the interface with the atmosphere [8].

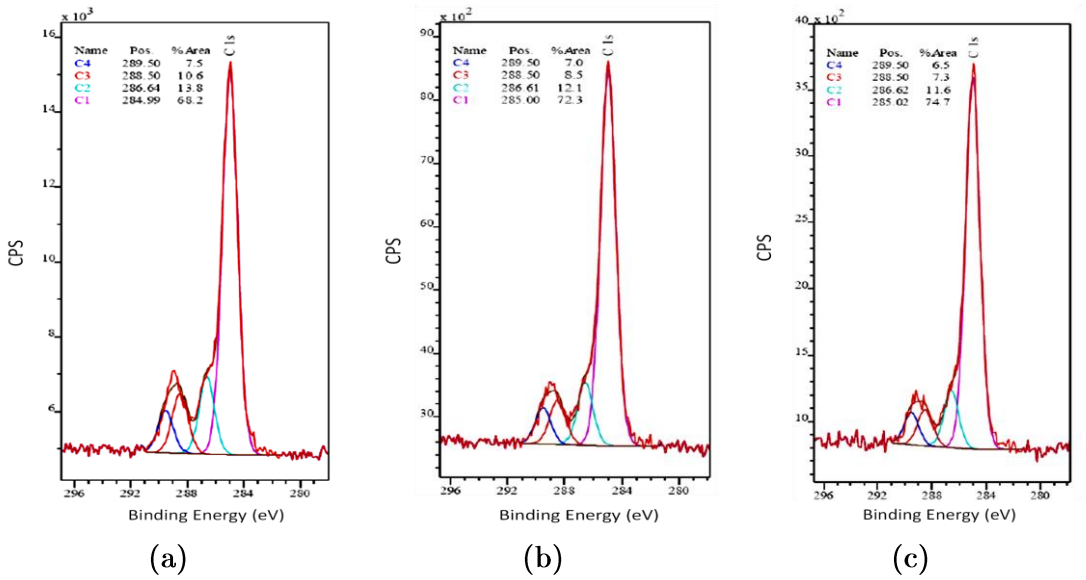


Figure 5.8. High resolution C 1s spectra of the Al-PVD substrate obtained at different take-off angles (a) 0°, (b) 40° and (c) 80° [343].

Table 5.2. Peak areas of the photopeaks of Al 2p, O 1s and C1s and their resolved components at different take-off angles [343].

take-off angle	Peak area [%]								
	Al 2p		O 1s			C 1s			
	metal	oxide	O^{2-}	Al-OH	H_2O	C-C/C-H	C-O / COOR*	C=O	C*OOR
0°	52	48	65	33	2	68	14	11	8
40°	48	52	62	35	3	72	12	9	7
80°	38	62	57	40	3	75	12	7	6

In summary, it was found that the chemical composition of the model aluminum substrate prepared for adsorption experiments is comparable to a typical technical aluminum substrate used in real applications. The surface properties established for the Al-PVD substrate include the presence of an adventitious carbon contamination layer covering the oxide layer, the multilayer character of the oxide film (adsorbed water, -OH and oxide layers) and the thickness (d[nm]) estimated to be ~ 2.3 nm. Consequently, the employment of the model Al-PVD substrates for analyzing the adsorption behavior of the SSMC is valid for understanding real silicone-aluminum systems.

5.3.2. In-situ adsorption experiments - FTIR-ERAS study

5.3.2.1. Fundamentals of FTIR-ERAS

Fourier transform infrared-external reflection absorption spectroscopy (FTIR-ERAS) emerged as a very useful tool for examining molecular structure of thin films deposited on metals and other types of substrates such as semiconductors, glassy carbon, coal, water and other liquid surfaces [349–351]. The formation and structure of thin layers can be investigated by this method because the thickness of the layer is very small in comparison with the wavelength of radiation [350]. The ratio d/λ (d: thickness of the layer and λ: wavelength of radiation) usually lies between 10^{-3} to 10^{-4} for the mid-infrared region [350]. Typically, FTIR-ERAS experiments consist of irradiating p-polarized infrared light at a grazing angle to a thin film with the reflected intensity being collected at the same angle [351]. The recorded p-polarized reflectivity $R_p(d)$ of the film is normalized with respect to that of the bare substrate $R_p(0)$ [352]. The particularity of the FTIR-ERAS method is the dependence of reflection on the optical functions of the adsorbate and the metal substrate, the angle of incidence, and polarization of the incident light [351]. To obtain analytical information from ERA spectra, the physical phenomena behind the nature of such spectra must be understood. Thus, a general insight of the theoretical background involved in FTIR-ERAS is provided.

Through a homogeneous, isotropic and semi-infinite medium, the propagation of light in direction k as a plane wave $\vec{E}$ can be described as:

$$\vec{E} = \vec{E}_o e^{i(\vec{k}\cdot\vec{s}-\omega t)} \tag{5-5}$$

Here, $\vec{s}$ is the vector that denotes the spatial location of the wave at time t, ω is the angular frequency and $\vec{\mathrm{k}}$ is the wave vector of the propagation of light in a medium. Additionally, the wave travels in a medium with velocity v, called the phase velocity of the electromagnetic wave in this medium, and it is defined by [45]:

$$\mathrm{v} = \frac{\omega}{\vec{\mathrm{k}}} \tag{5-6}$$

This phase velocity v, is related to the absolute refractive index n of a medium and the velocity of radiation in vacuum c_0 by the following expression:

$$n = \frac{c_0}{\mathrm{v}} \tag{5-7}$$

The refractive index describes the attenuation of the electromagnetic wave when passing through a medium; thus, it determines the part of the light which has been refracted when entering a material. From Equation 5-6 and 5-7 for an isotropic non-magnetic medium, k and ω are related by:

$$\mathrm{k}^2 = \frac{\omega^2}{{c_o}^2}\hat{n}\ ;\ \mathrm{k}^2 = \hat{n}\mathrm{k}_o^2 \tag{5-8}$$

For an absorbing medium, the wave vector, $\vec{\mathrm{k}}$ and $\hat{n}$ are complex quantities that depend on the frequency of the incident radiation. They are defined by Equation 5-9 and 5-10, respectively. The optical function or complex refractive index is composed by the refractive index n (real part) and the extinction coefficient or absorption index k (imaginary part) [45].

$$\vec{\mathrm{k}} = \vec{\mathrm{k}}' - i\vec{\mathrm{k}}'' = \hat{k}\vec{e} = (k' - ik'')\vec{e} \tag{5-9}$$

$$\hat{n} = n - ik \tag{5-10}$$

Where $\vec{e}$ corresponds to the unit vector along the direction of the propagating wave, $\hat{k}$ is confusingly named the wavenumber, like the parameter ν [cm^{-1}] used in an IR spectrum (Equation 4-1) [45]. Because the symbol k is used to designate both the wavenumber and extinct coefficient; the wavenumber here has been labelled as $\hat{k}$ to distinguish it [45]. From Equations 4-1, 5-8 and 5-9 the following expressions are given:

$$\vec{\mathrm{k}} = \frac{2\pi}{\lambda}\hat{n}\vec{e} \tag{5-11}$$

$$\vec{\mathrm{k}} = \frac{2\pi}{\lambda}n\vec{e} - \frac{2\pi}{\lambda}k\vec{e} \tag{5-12}$$

$$k' = \frac{2\pi}{\lambda}n \;; k'' = \frac{2\pi}{\lambda}k \tag{5-13}$$

Consequently, based on the above relations, Equation 5-5 can be rewritten as:

$$\vec{E} = \vec{E}_o e^{\left(\frac{2\pi}{\lambda}n\vec{e}\cdot\vec{s}-\omega t\right)i} e^{\left(\frac{2\pi}{\lambda}k\vec{e}\cdot\vec{s}\right)} \tag{5-14}$$

From this equation, it is shown that the real part of the refractive index (n) determines the phase velocity of the wave in the medium, whereas the imaginary part (k) defines the attenuation of the electromagnetic field along the direction of propagation of the wave [45]. Therefore, Equation 5-14 evidences that the principal macroscopic parameters which characterize the interaction of an electromagnetic wave with an absorbing optical medium are n and k (optical parameters). For this reason, the optical function is the most appropriate parameter for comparing optical properties between bulk and thin adsorbed layers of the same material [45,170]

The intensity $I(\nu)$ of an electromagnetic wave is proportional to the average of the magnitude of the squared electric field strength. Hence, for a homogeneous wave of the type described in Equation 5-14 and propagating in z-direction, the intensity is expressed as:

$$I(z) = I_o e^{\frac{-4\pi}{\lambda}kz} \tag{5-15}$$

Where, I is the intensity of the electromagnetic radiation, I(0) is the intensity for z = 0 inside the medium, and z is the distance that the wave has passed through the absorbing medium. Equation 5-15 represents the relationship existing in an absorbing homogeneous medium where the intensity decreases exponentially with its path. From Equation 5-15, the absorption coefficient α or decay constant can be defined as:

$$\alpha(\nu) = \frac{4\pi}{\lambda}k = 4\pi\nu k = \frac{2\omega}{c_0}k \tag{5-16}$$

To conclude, the absorption of a medium, characterized by the absorption coefficient α, is essentially described by the extinction coefficient k and the wavenumber ν. Finally, from the intensities I and I_0, any absorption spectrum with absorbance A(ν) can be estimated by:

$$A(\nu) = ln\left(\frac{I(\nu)}{I_0(\nu)}\right) \tag{5-17}$$

In FTIR-ERAS measurements the samples are always spatially restricted by boundaries; therefore, the behavior of electromagnetic waves at interfaces is analyzed.

External reflection for a multilayer system

In this work, thin layers of SSMC are adsorbed on aluminum metal. The substrate surface acts as the "sample holder" and as the inner reflective unit. However, an oxide/hydroxide layer is formed on aluminum, therefore, the IR absorption must be considered for a multilayer system, represented in Figure 5.9. In this case, air is the medium 1 ($\hat{n}_1$), the thin layer the medium 2 ($\hat{n}_2$), and the oxide/hydroxide layer is the medium 3 ($\hat{n}_3$).

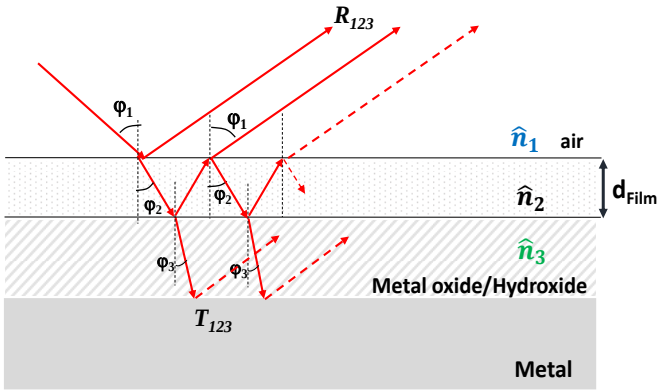


Figure 5.9. Representation of external reflection for a multilayer system. Air is the medium 1 ($\hat{n}_1$), the adsorbed thin layer is the medium 2 ($\hat{n}_3$), and the oxide/hydroxide film is the medium 3 ($\hat{n}_3$) [170,353].

When light enters onto a film between two planar interfaces, a partial reflection and refraction of the incident light takes place at each interface. This procedure is repeated several times and thus, the intensity collected at the detector is a result of the

interference of the individual beams that have experienced multiple reflection and transmission events.

The reflection and refraction of the incident and transmitted light at each interface are defined by the Fresnel equations (Equations 5-18 and 5-19) for the two polarization types p (parallel to the plane of incidence) and s (perpendicular to the plane of incidence) [170,354]. Fresnel equations describe the dependency of the reflection and transmission coefficients on the geometry (φ_i), on the optical functions of the media involved ($\hat{n}$) and on the type of polarization (p- and s-polarized light).

$$\hat{r}_p^{12} = \frac{\hat{E}_p^{(r)}}{\hat{E}_p^{(i)}} = \frac{\hat{n}_2 cos\varphi_i - \hat{n}_1 cos\varphi_t}{\hat{n}_2 cos\varphi_i + \hat{n}_1 cos\varphi_t}, \qquad \hat{r}_s^{12} = \frac{\hat{E}_s^{(r)}}{\hat{E}_s^{(i)}} = \frac{\hat{n}_1 cos\varphi_i - \hat{n}_2 cos\varphi_t}{\hat{n}_1 cos\varphi_i + \hat{n}_2 cos\varphi_t} \tag{5-18}$$

$$\hat{t}_p^{12} = \frac{\hat{E}_p^{(t)}}{\hat{E}_p^{(i)}} = \frac{2\hat{n}_1 cos\varphi_i}{\hat{n}_2 cos\varphi_i + \hat{n}_1 cos\varphi_t}, \qquad \hat{t}_s^{12} = \frac{\hat{E}_p^{(t)}}{\hat{E}_p^{(i)}} = \frac{2\hat{n}_1 cos\varphi_i}{\hat{n}_1 cos\varphi_i + \hat{n}_2 cos\varphi_t} \tag{5-19}$$

Where $\hat{r}$ and $\hat{t}$ are complex numbers, denoting the reflectance and transmittance amplitude coefficients, respectively. Since in infrared spectroscopy, intensities (I), instead of amplitudes ($\hat{A}$), are measured, the following relation is provided [170] :

$$I \sim \left|\hat{E}\right|^2 = \left|\hat{A}\right|^2 = \hat{A} \cdot \hat{A}^* \tag{5-20}$$

$\hat{E}$ represents the amplitude of the defined electromagnetic waves according to its polarization. Thus, the reflectance R and transmittance T of the reflected and transmitted intensities, for p- and s- polarization in a single interface, are obtained from the squares of the coefficients defined in Equations 5-18 and 5-19:

$$R_{p,s} = \left|\hat{r}_{p.s}\right|^2 = \hat{r}_{p.s} \cdot \hat{r}_{p.s}{}^* \ , \quad T_{p,s} = \frac{n_2}{n_1} \cdot \frac{cos\varphi_t}{cos\varphi_i} \left|\hat{t}_{p,s}\right|^2 \tag{5-21}$$

In the multilayer system, the reflection and transmission coefficients $\hat{r}_{p,s}^{123}$ and $\hat{t}_{p,s}^{123}$ for p- and s-polarized light are defined by:

$$\hat{r}_{p,s}^{123} = \frac{\hat{r}_{p,s}^{12} + \hat{r}_{p,s}^{23} \cdot e^{-2i\hat{\beta}}}{1 + \hat{r}_{p,s}^{12} + \hat{r}_{p,s}^{23} \cdot e^{-2i\hat{\beta}}} \ , \ \hat{t}_{p,s}^{123} = \frac{\hat{t}_{p,s}^{12} + \hat{t}_{p,s}^{23} \cdot e^{-2i\hat{\beta}}}{1 + \hat{r}_{p,s}^{12} + \hat{r}_{p,s}^{23} \cdot e^{-2i\hat{\beta}}} \tag{5-22}$$

Where β is named the optical phase thickness $\beta = 2\pi \frac{d}{\lambda_0}\sqrt{\hat{n}_2^2 - \hat{n}_1^2 sin^2\varphi_1}$. For films or layers with a thickness smaller than the wavelength of the irradiated light, the so-called thin-film approximation can be applied [45], thereafter:

$$e^{-2i\beta} \approx 1 - 2i\beta \tag{5-23}$$

Consequently, for film thicknesses up to 100 nm [45], the reflection coefficient $\hat{r}_{p,s}^{123}$ in Equation 5-22 can be simplified to:

$$\hat{r}_{p,s}^{123} = \frac{\hat{r}_{p,s}^{12} + \hat{r}_{p,s}^{23} \cdot (1 - 2i\beta)}{1 + \hat{r}_{p,s}^{12} + \hat{r}_{p,s}^{23} \cdot (1 - 2i\beta)} \tag{5-24}$$

Finally, the reflectance (R) and transmittance (T) intensities of the multilayer system are defined as follows:

$$R_{p,s}^{123} = \left|\hat{r}_{p,s}^{123}\right|^2 , \quad T_{p,s}^{123} = \frac{n_2}{n_1} \cdot \frac{cos\varphi_2}{cos\varphi_1} \left|\hat{t}_{p,s}^{123}\right|^2 \tag{5-25}$$

These two relations in Equation 5.25 are those responsible for describing external reflection of three media separated by two plane parallel interfaces. The FTIR-ERA spectrum depends on the optical functions of the media involved (air, adsorbate and metal substrate), on the angle of incidence (φ_i), on the polarization of the incident light (p- or s-) and on the thickness (d) of the thin layer. All of them are quoted as "optical effects" [45]. These factors strongly influence the position, intensity and shape of the IR absorption bands in the spectrum [45]. Experimentally, the reflectances (R) of the FTIR-ERA spectra of the thin adsorbed layers of SSMC on aluminum were always defined as the quotient of the single channel spectrum intensity (I_{SC}) of the adsorbed thin-layer ($d>0$) on the substrate, over the single channel spectrum intensity of the bare substrate ($d=0$), referred to as the reference measurement. Hence, reflectance spectra were obtained as the quotient:

$$R(\nu, d) = \frac{I_{SC,thin-layer}\,(\nu, d)}{I_{SC,Reference}\,(\nu, 0)} \tag{5-26}$$

Effect of polarization type on the FTIR-ERA spectra

Polarization of the incident light plays an important role in FTIR spectroscopy, especially if metal substrates are used. A brief explanation is provided in order to understand the effect of IR light polarization on the spectral features of FTIR-ERA spectra. By definition, the intensity (I_i^{abs}) of an infrared absorption band *i,* is proportional to the intensity of the electric field, the magnitude of the net change of the dipole moment and the concentration of the vibrating group [170], which is described as follows:

$$I_i^{abs} \propto \left|\vec{E} \cdot \Delta\vec{\mu_i}\right| \cdot \left|\vec{E}\right| \cdot c_{oscillator,i} \qquad \textbf{(5-27)}$$

Where $\vec{E}$ is the electric field vector of the incident wave (mathematically described by Equation 5-5), $\Delta\vec{\mu_i}$ is the net change of the dipole moment of the group *i* and $c_{oscillator,i}$ is the concentration of the vibrating group *i* in the sample. Equation 5-27 indicates that in order for IR absorption to occur, $\vec{E}$ must not be perpendicular ($\perp$) to $\Delta\vec{\mu_i}$, and $\Delta\vec{\mu_i}$ must be positive, i.e., $\Delta\vec{\mu_i} > 0$ [170,333]. This implies that if $\vec{E}$ is parallel ($\parallel$) to $\Delta\vec{\mu_i}$, the intensity becomes maximum.

As explained by Handke [353], in the absence of adsorbate, a surface wave (with electric field E_s) is created on the irradiated area of the metal surface as a result of the combination of the incident and reflected waves[353]. Such resulting electromagnetic field E_s is the one interacting with the adsorbed molecules on the surface. When parallel polarized light (*p*-polarized) enters a dielectric medium at an incidence angle φ_1, the incident electric field $\hat{E}_p^{(i)}$ is perpendicular to the direction of propagation. In this case, the electrical field of the surface E_s, is in the plane of incidence inclined to the normal surface at an angle ϕ, with $\tan\phi = cot\ \varphi_1 \frac{1+|r_p^{12}|}{1-|r_p^{12}|}$ (φ_1: angle of incidence) [353]. For strongly reflecting substrates (like metals), the surface field E_s becomes perpendicular to the interface and its parallel component disappears at any angle of incidence [353] . Thus, the component of dipoles perpendicular to a strong reflecting surface can be excited with *p*-polarized radiation in a wide range of angles of incidence. On the other hand, for *s*-polarization (perpendicular), both the incident and reflected waves have electric fields parallel to the reflecting surface. Consequently, for *s*-polarized light, molecular dipole moments parallel to the strongly reflecting surface cannot be excited at any angle of incidence and are not perceived on the spectrum [353].

Additionally, the highly mobile free electrons of the metal generate an image dipole ($\overrightarrow{\Delta\mu_{ima}}$) which is oriented opposite to the dipole of the absorbed molecule ($\overrightarrow{\Delta\mu_{molec}}$). Hence, the parallel components to the metal surface of both the $\overrightarrow{\Delta\mu_{ima}}$ and

$\overrightarrow{\Delta\mu_{molec}}$ cancel out, whereas the vertical components of $\overrightarrow{\Delta\mu_{ima}}$ and $\overrightarrow{\Delta\mu_{molec}}$ are added up (Figure 5.10). Therefore, the IR-ERA spectra of metals contain only those vibrations of adsorbed molecules in which their transition dipole moments have perpendicular components to the metal surface. Consequently, the intensity of these bands is enhanced [170]. This dependence on polarization is commonly referred to as the "surface selection rule" [351].

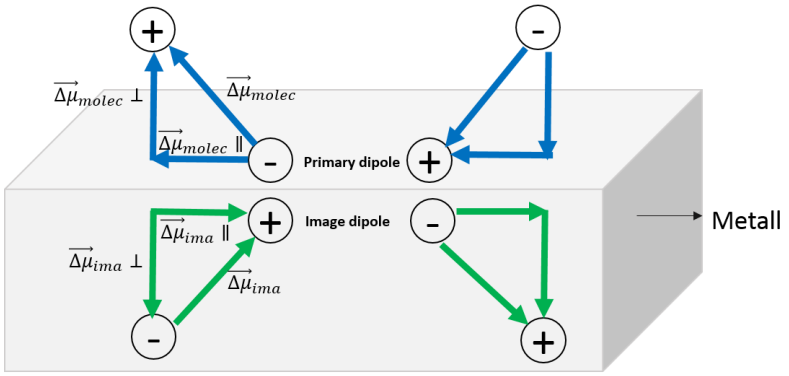


Figure 5.10. Model of the transition dipole moment of a vibrating molecule adsorbed on a metal surface (film or thin layer). A dynamic situation is illustrated [170].

5.3.2.2. Description of the adsorption experiments

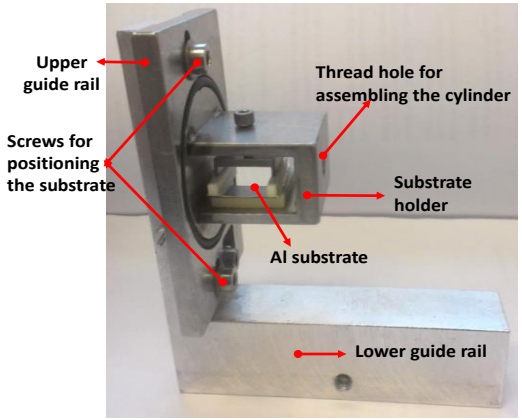
Materials

The aluminum substrate and the SSMC used for the experiments have been described in section 5.3 and 4.4, respectively. The solvent used for preparing the diluted solutions and cleaning the substrate was tetrahydrofuran (THF) (Carlo Erba Reagents, France), GC analytical grade (99.9% purity) with 200-400 mg/kg of BHT31 stabilizer and water content ≤ 10 mg/kg. The selection of this solvent was based on previous works [8,52,53] which demonstrated that THF does not adsorb onto aluminum. Hence, competitive adsorption between the solvent and the solute towards aluminum is negligible. Additionally, the vapor pressure of THF (200 mbar at 20 °C) ensures its evaporation during the drying process at RT after deposition. This implies that only spectra ascribed to thin layers of SSMC are attained. Although no adsorption of THF on aluminum occurs, changes to the surface composition take place when the substrate is rinsed with pure THF, as contaminants are removed. For PDMS polymers THF has

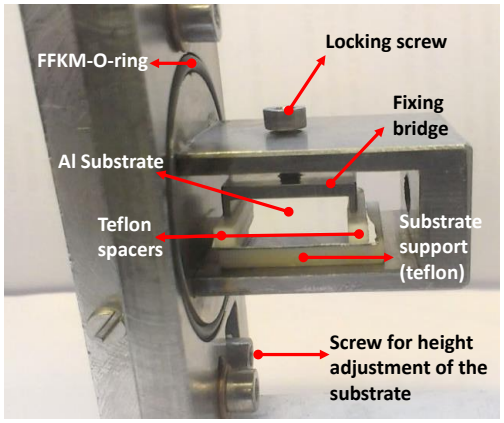
been categorized as a good solvent [355]; thus, possible competitive interactions between the SSMC with aluminum and with the solvent could exist.

Adsorption device

The substrate holder was originally designed for the work of Wehlack and Nies [43,52] with specific dimensions that allowed it to fit inside the IR measurement compartment. It contained a removable hood (cylinder) which allowed the execution of rinsing steps inside the IR measurement camera, ensuring good sealability and preventing the leaking of solvent into the spectrometer, avoiding damage. The holder and its accessories were corrosion and solvent resistant. Lastly, the device enabled the optimization of the IR light path by adjusting the height of the substrate holder. The adsorption device or substrate holder was made of stainless steel and consisted of two main parts: a lower part acting as a guide rail for positioning the cell inside the IR measuring chamber, and a second upper part (rear) serving as a guide rail for the substrate holder (Figure 5.11a). By means of three freely movable screws, two for positioning (Figure 5.11a) and one lever for height adjustment (Figure 5.11b), the substrate could be optimally positioned for detecting a maximum reflecting signal of the IR light beam. Furthermore, the cylinder contained four exterior tubes for carrying out the rinsing steps (Figure 5.11c). The two vertical tubes, labelled 3 and 4, were used for the input and drainage of liquid, and the two laterals (1 and 2) were utilized for purging the substrate with dry air. The volume of the cylinder was ~ 30 ml. In addition, an internal tube with three holes was located inside the cylinder at the position of the external tube 1 (Figure 5.11d). The internal tube was situated at the same height of the substrate, which allowed a good circulation of air over the aluminum surface.



(a)



(b)

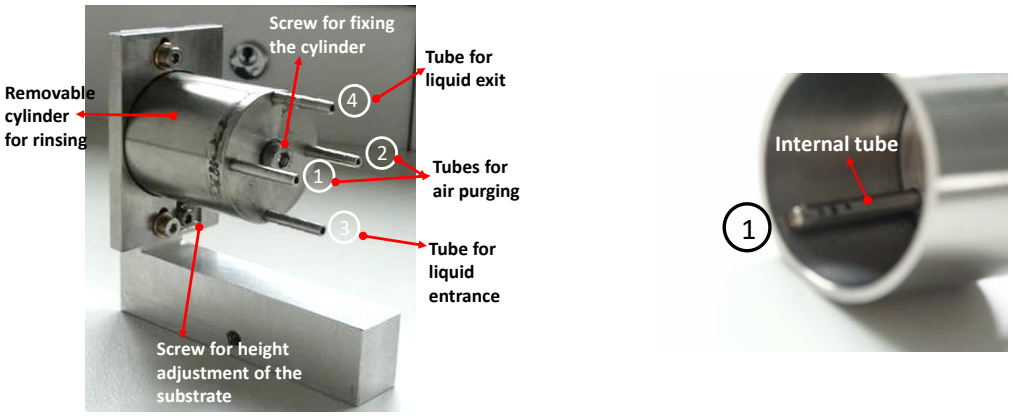


Figure 5.11. Sample holder for in-situ FTIR-ERA (a) lateral view, (**b**) enhancement of the substrate holder, (c) cylinder (hood) for liquid rinsing and (d) interior of the cylinder containing an internal tube with 3 holes for air circulation to the substrate during solvent drying [52,53,335].

FTIR-ERAS Measurements

Infrared spectra were measured in a Bruker IFS 66v/s FTIR spectrometer (Bruker AG, Karlsruhe, Germany) equipped with a MCT detector (Appendix A). Specifications of the spectrometer are given in Appendix A. p-Polarized mid-IR light (4000-400 cm^{-1}) at an incidence angle of 80° was used for irradiating the samples. The IR beam passed through an aperture of 2 mm. A total of 1000 scans at 4 cm^{-1} resolution were averaged, resulting in spectral peak-to-peak noise levels of approximately 3 x 10^{-4} between 1800 and 1900 cm^{-1} (Appendix C). The measurement temperature was kept at 297 ± 1 K and the IR measurement compartment was continuously purged with dry air (T_{dp} ~ -65 °C).

Experimental procedure

During the execution of the experiments, all elements including glassware, accessories, sample holder, and the aluminum substrate were handled carefully in order to avoid possible contamination of the metal surface that could lead to misinterpretation of the spectra. The procedure of the adsorption experiments consisted of three main stages shown in Figure 5.12 and described below in detail.

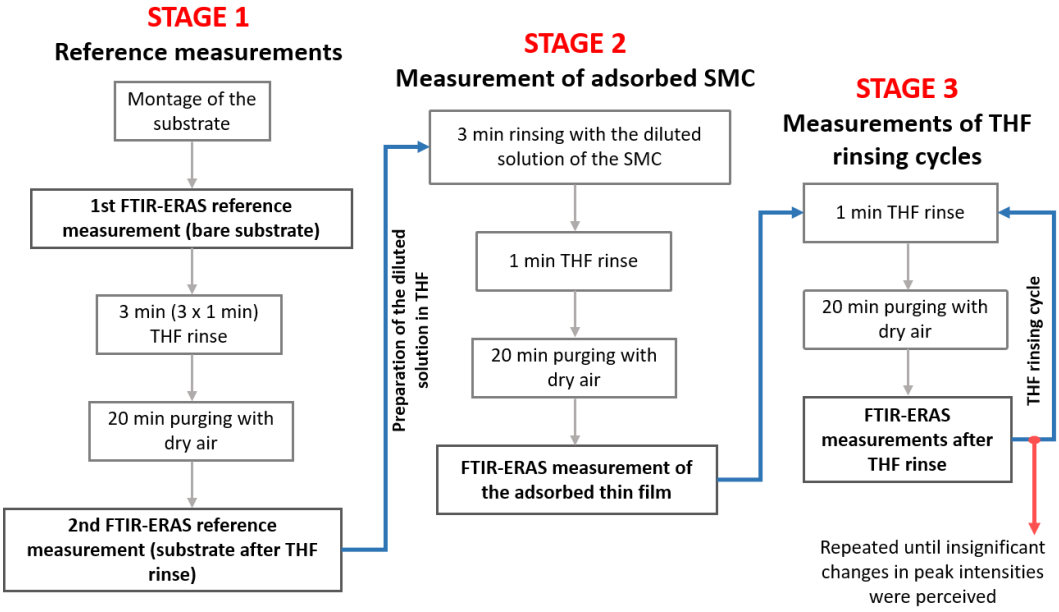


Figure 5.12. Diagram describing the procedure of the in-situ adsorption experiments

STAGE 1. Reference measurements

- **1st reference measurement:**

The aluminum substrate was mounted on the substrate holder as shown in Figure 5.11b, and fixed tightly into the IR spectrometer (Figure 5.13) to ensure analysis of the same area throughout the whole experiment. Subsequently, the detected IR signal was optimized manually by modifying the position of the substrate with help of the two positioning screws (Figure 5.11a) and the screw for height regulation (Figure 5.11b). The signal was then maximized by the "automatic adjustment" option of the interferometer. Subsequently, after waiting 10 min for atmospheric stabilization in the measurement compartment, three spectra of the bare aluminum surface were recorded

- **2nd reference measurement:**

The removable cylinder with four Tygon® Se-200 hoses attached (PVC hoses coated with FEP (fluorinated ethylene propylene), Saint Gobain), was attached to the sample holder for rinsing the substrate with pure THF. The lower vertical hose (3) was connected to the syringe containing the THF, whereas the upper vertical hose (4) was coupled to an empty syringe for liquid draining (Figure 5.13). The two lateral hoses (1 and 2) were sealed with Teflon® stoppers for preventing leakage of solvent during rinsing. The total time of solvent rinsing was 3 min. Next, the solvent was evacuated and the substrate was dried with dry air (T_{dp} ~-65 °C) for 20 min in order to eliminate

THF molecules. Approximately six or seven FTIR-ERA spectra were collected after 10 minutes of atmospheric stabilization. The single-channel (SC) spectrum of the substrate after being rinsed with THF (2nd reference measurement) was taken as reference for obtaining the spectra of adsorbed thin layers from Equation 5-26.

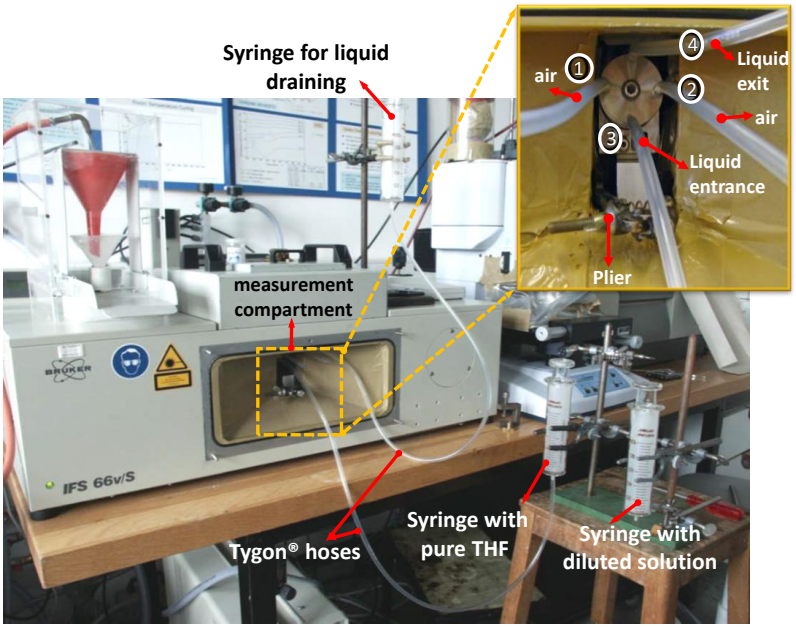


Figure 5.13. FTIR spectrometer with the sample holder inside. The connections of the cylinder are: 1 and 2 for dried air flushing, 3 and 4 for input and output of the solvent or diluted solution. The syringe at the top serving as overflow [52,53,335].

The effect of the THF rinsing on the bare aluminum surface was evaluated by dividing the single channel spectrum of reference 2 over the single channel spectrum of reference 1. The cleanliness effect of the surface after THF rinsing was found to be satisfactory Additionally, it was consistently observed that THF did not adsorb onto aluminum.

STAGE 2. Measurements of adsorbed thin layers of the SSMC

- **Preparation of the diluted solution:**

Solutions of the SSMC in THF were prepared at a 1:100 ratio (SSMC/THF, v/v). This value was selected based on the work of Nies [52], who observed that deposited layers of PU monomers on different metals were imperceptible to the eye when such volume ratio was employed. This was also perceived in the case of adsorbed layers of the SSMC.

In a typical procedure, the amount of each SSMC (Table 5.3) was measured gravimetrically in a Glovebox filled with dry air (T_{dp} ~ -65 °C). Then 60 ± 0,5 ml of THF were added and the solution flask was immediately covered with aluminum foil to prevent mass loss. Subsequently, the solution was stirred in a magnetic stirrer for 30 seconds. Meanwhile, 60 ± 0,5 ml of THF were poured into a different beaker also covered with aluminum foil. Ultimately, the two protected beakers, containing the THF solvent and the diluted solution, were quickly transported to the IR room, where the adsorption experiments took place.

Table 5.3. Experimental concentration of the diluted solution of the SSMC in THF

SSMC	Volume (ml)	Density (g/ml)	Measured mass (g)	Experimental concentration [M]
Bifunctional Vinyl PDMS	0,6	0,968	0,5808 ± 0,0004	$7,2 \times 10^{-3}$
Bifunctional Hydride PDMS	0,6	0,928	0,5569 ± 0,0006	$1,14 \times 10^{-2}$
Tetrakis (dimethylsiloxy)silane	0,6	0,888	0,5329 ± 0,0008	$2,7 \times 10^{-2}$
Allyltrimethoxysilane	0,6	0,958	0,5748 ± 0,0005	$5,6 \times 10^{-2}$
Karstedt Catalyst	0,6	0,97	0,5868 ± 0,0006	$2,94 \times 10^{-2}$

- **Rinsing of the substrate with the SSMC diluted solution (3 min):**

The syringe assigned to the diluted solution (Figure 5.13) was filled up and the liquid was injected into the cylinder. The solution was in contact with the substrate during 3 min and afterwards it was evacuated.

- **Rinsing step with THF (1 min):**

Immediately after contact with the diluted solution, the substrate was rinsed with pure THF for 1 min to eliminate excess of weakly adsorbed molecules on the surface. Thereafter, the THF was sucked off and the two stoppers of the lateral hoses were detached to purge the substrate with dry air (T_{dp} = -65 °C) for 20 min.

- **FTIR-ERAS measurement of the adsorbate:**

Six to eight FTIR-ERAS spectra were recorded once the atmosphere of the IR camera was stabilized for 10 min. The resulting single channel spectra of the adsorbate were divided over the single channel spectrum of reference 2, according to Equation 5-26.

STAGE 3. Consecutive THF rinsing cycles

Various solvent rinsing steps, of 1 min duration each, were repeated consecutively in order to remove further weakly adsorbed molecules and to attain a stable adsorbed thin layer. Additionally, through the sequential rinsing steps with THF, the adsorption-desorption equilibrium between the adsorbate and the metal surface could be inspected. The successive rinsing followed the same procedure described for the rinsing steps mentioned previously.

The consecutive solvent rinsing cycles were repeated until no significant changes in the intensity of the spectra were detected. Normally, up to four or five THF rinsing cycles were applied in each experiment. The number of rinsing steps was limited by the fact that the detector must be cooled every 8 h.

During the experimental procedure, different factors could have affected the quality of the spectra, such as the cooling of the MET-detector, water and CO_2 content inside the IR measurement compartment, and the variation of the baseline due to the approach to a monolayer analysis [52].

5.4. Spectra evaluation-Methodology

In order to extract analytical information from the ERA spectra that permits the elucidation of adhesion mechanisms, the measured spectra must be compared to "model" spectra in which intermolecular interactions at the interface and molecular orientation effects are nonexistent; i.e. spectra with bulk properties.

Experimentally, infrared spectra of the SSMC in bulk were obtained via ATR-FTIR. However, direct comparison between measured ATR and ERA spectra is inappropriate since the two methods differ in their optical configuration (angle of incidence and optical function of the participating media). To overcome this problem, a reliable procedure that enables proper comparison between measured spectra of the adsorbate and in bulk was implemented based on previous works [8,52]. The approach consisted of simulating a spectrum of an adsorbed film with bulk properties but in ERAS configuration. The simulated spectrum was a function of the optical parameters (complex refractive index, $\hat{n}$) of the substrate and the adsorbate (SSMC), film thickness, substrate thickness, angle of incidence (80°) and p-polarized light. The simulated spectrum is referred, in this work, to a "calculated bulk-like spectrum".

The optical function or complex refractive index, $\hat{n}$ (Equation 5-10) was the key parameter used for simulating the spectra, because it is distinctive for every material

and it is independent of the IR optical configuration applied. Typically, the optical function $(\hat{n})$ of the sample of interest is extracted by the so-called "inversion calculation" from the measured ATR spectrum of the sample [8,52,356]. Direct calculation of the optical function of the thin adsorbed layer from the FTIR-ERA spectrum is unsuitable, because properties needed for this purpose such as the refractive index in visible light of the thin layer and film thickness cannot be feasibly measured. Additionally, the low intensity of the ERA spectra and the undefined homogeneity of the adsorbate restrains this possibility.

The procedure applied for obtaining simulated bulk-like spectra is described as follows:

1. **"Inverse calculation" of the optical function $\hat{n}$:**

The optical function describes both the optical and dielectric properties of a homogeneous, isotropic, semi-infinite material since $\hat{n}$ is correlated to the dielectric function $\hat{\varepsilon}$ by Equation 5-28. Accordingly, the dielectric function describes the interaction of light with a dielectric medium and its real and imaginary parts are given by Equation 5-29.

$$\hat{\varepsilon} = \varepsilon' + i\varepsilon'' = \hat{n}^2 = (n + ik)^2 = n^2 - k^2 + i2nk \qquad (5\text{-}28)$$

$$\varepsilon' = n^2 - k^2 \; ; \; \varepsilon'' = 2nk \qquad (5\text{-}29)$$

The dielectric function of a medium depends on its electric susceptibility χ by the relation: $\hat{\varepsilon} = \varepsilon_0(1 + \chi)$, and χ is related to the polarizability P by the electric field (E) as: $P = \varepsilon_0 \chi E$; where ε_0 is the permittivity of vacuum. Since a linear and casual correlation between the polarizability and the electric field exists, according to the so-called linear response function and causality principle; the real and imaginary parts of the dielectric function $(\hat{\varepsilon})$ or the optical function $(\hat{n})$, are not independent but comply with the Kramers-Kronig (KK) relations [356]. In practical terms, the KK relations enable one to find the real part of the answer in a linear passive system if the imaginary part of the response is known at all frequencies, and viceversa.

In this work, the software tool FSOS [357] was used for calculating $\hat{n}(\nu)$. The program employs the Knight-Peterson transform (equivalent to the Kramers-Kronig (KK) transform) for the calculation of $\hat{n}(\nu)$ from the measured ATR spectra of the SSMC in bulk. Moreover, the real refractive indexes (n) of the SSMC in the visible spectral range were required. The refractive indexes were measured three times for each

SSMC by means of a refractometer and by using the program ABBEEMAT-PC. The average values obtained are listed in Table 5.4.

Table 5.4. Measured refractive index (n) of the SSMC

SSMC	refractive index, n
Prepolymer 1 (Hydride-PDMS)	1.4051 ± 0.0003
Prepolymer 2 (Vinyl-PDMS)	1.3997 ± 0.0001
Crosslinker (TDMS)	1.3813 ± 0.005
Adhesion promoter (ATMS)	1.4031 ± 0.0001
Karstedt catalyst	1.4158 ± 0.0004

Through the KK relation, a reflectance spectrum is mathematically decomposed to two separate spectra: one corresponding to the extinction coefficient (k) (imaginary part of $\hat{n}$) and the other to the refractive index spectrum (n) (real part of $\hat{n}$). Figure 5.14 illustrates the individual spectra n and k of the optical function calculated for the prepolymer 1 (bifunctional hydride terminated PDMS).

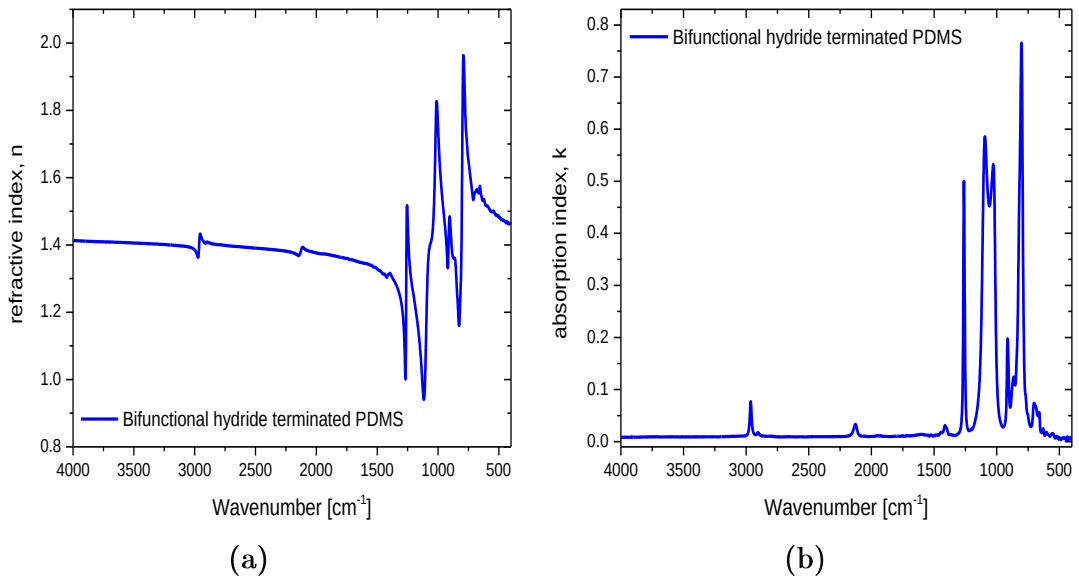


Figure 5.14. Optical function of bifunctional hydride terminated PDMS determined from a FTIR-ATR measurement at an angle of incidence of 60°, p-polarized light and using a ZnSe crystal as the IRE. (a) refractive index spectrum and (b) absorption index spectrum.

2. Simulation of the "bulk-like" spectra:

Once the real and imaginary parts of the optical function were obtained, the bulk-like spectra were then simulated in the specialized software SCOUT® [358]. A multilayer model with parallel phase boundaries consisting of an isotropic, semi-infinite incidence medium (air), an isotropic adsorbate film of thickness d (5-10 nm), and an isotropic, semi-infinite aluminum substrate of 100 nm thickness with an oxide layer of 3 nm on top was used in this work. The software offers the possibility to simulate spectra, varying the optical properties of the substrate and the layer thicknesses. The simulated spectra obtained included the optical properties of the bulk material and the optical experimental configuration of an ERAS measurement.

Finally, the analysis of the measured ERA spectra is based on a qualitative contrast and comparison with the simulated spectra, in order to identify different features that evidence the influence of the surface on the vibrating state of the SSMC.

5.5. Results and interpretation

Prior to analysis, the quality of all measured spectra was improved by removing atmospheric effects as H_2O an CO_2 bands. The procedure employed for their elimination was the well-known spectra subtraction method and it included the use of absorption spectra of gaseous CO_2 and H_2O in ERAS configuration. The software OPUS® was used for that purpose. It was also important to examine the state of the aluminum surface before proceeding with the analysis of the adsorbate spectra of the SSMC in order to discern the correct chemical state of the adsorbate. The assignment of the bands on the ERA spectra was based on the FTIR-ATR spectra of the SSMC described in Section 4.4 (Table 4.18) and on published work related FTIR-ERAS of siloxanes [44,136,359].

For ease of interpretation, the obtained spectra are in all cases illustrated in four separate regions: I) from 4000 to 3100 cm^{-1}, II) from 3100 to 2800 cm^{-1}, III) from 2250 to 2200 cm^{-1}, and IV) from 1800 to 500 cm^{-1}. Additionally, analysis of the adsorption dynamics of the two prepolymers 1 and 2 during 24 h is also included. Three principal characteristics of the spectra were investigated as potential evidence of structural differences for the adsorbed states of the SSMC: shifting in peak position (wavenumber, cm-1), change of peak shape and overall variation of the spectral intensities.

5.5.1. Prepolymer 1 - bifunctional hydride terminated PDMS

Two scenarios were considered for the analysis of the adsorption behavior of bifunctional hydride terminated PDMS on aluminum. They consisted in varying the storage time in dried air after rinsing the substrate with the diluted solution (Stage 2, Figure 5.12). The objective was to study the dynamics of adsorption, or the time evolution of the adsorbed layer, towards a more equilibrated state. In polymers, attainment of this stable state may require long times since polymer chain mobility is restrained by the adherence to the surface and by entanglement with neighbor chains [325]. The two cases of study are denoted here as short (1 h) and long (24 h) storage times, as in that period of time, the adsorbed polymer is in the process of relaxing towards a conformation of lower energy.

5.5.1.1. Case 1: short storage time (1 h)

First, the spectrum of the aluminum surface prior to adsorption of prepolymer 1 is analyzed (Figure 5.15). At first glance, it seems that THF was effective in removing organic impurities from the surface as peaks related to stretching of C-H bonds are imperceptible. However, closer inspection reveals that traces of carbonaceous impurities were present on the surface, shown as two weak peaks in the ν-C-H region. Such contaminants might have been readsorbed from the environment after THF rinsing. A peak associated with the vibration mode of aluminum oxide (α-Al_2O_3) is also recognized at ~1004 cm^{-1} [360]. These aspects along with a slightly inclined baseline, affirm that besides of cleaning, THF causes some changes to the structure of the aluminum oxide layer, but does not adsorb.

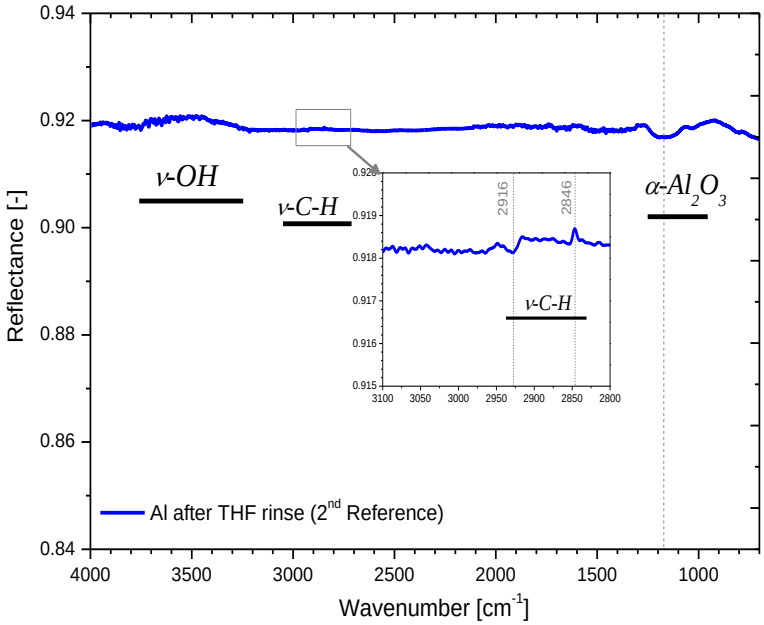
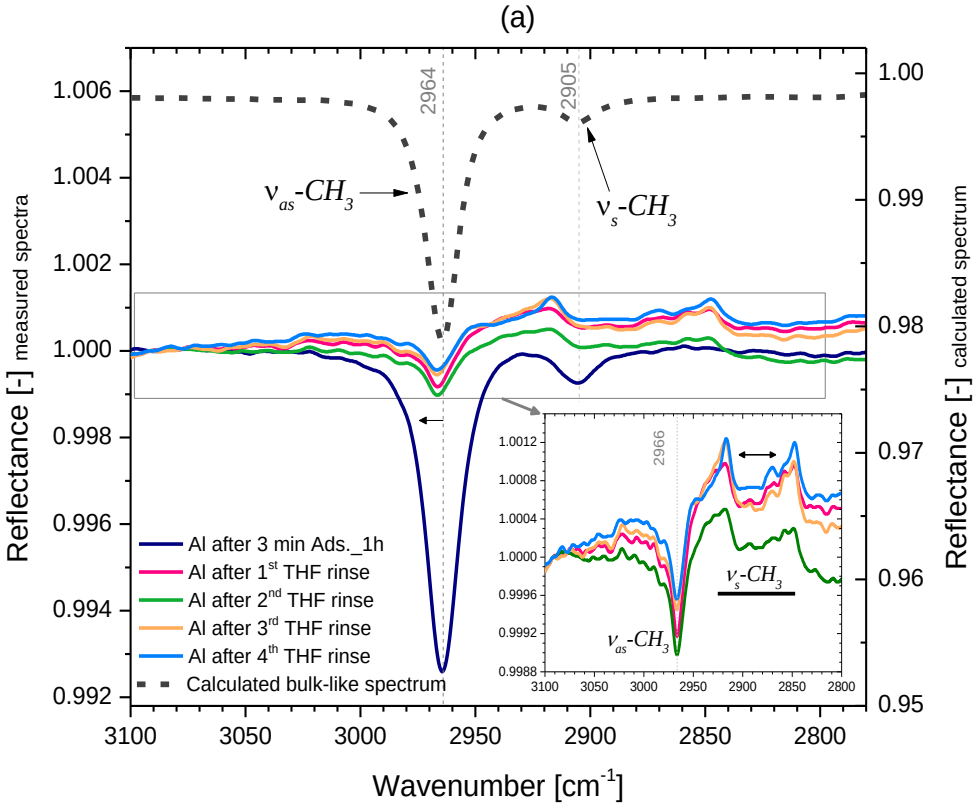
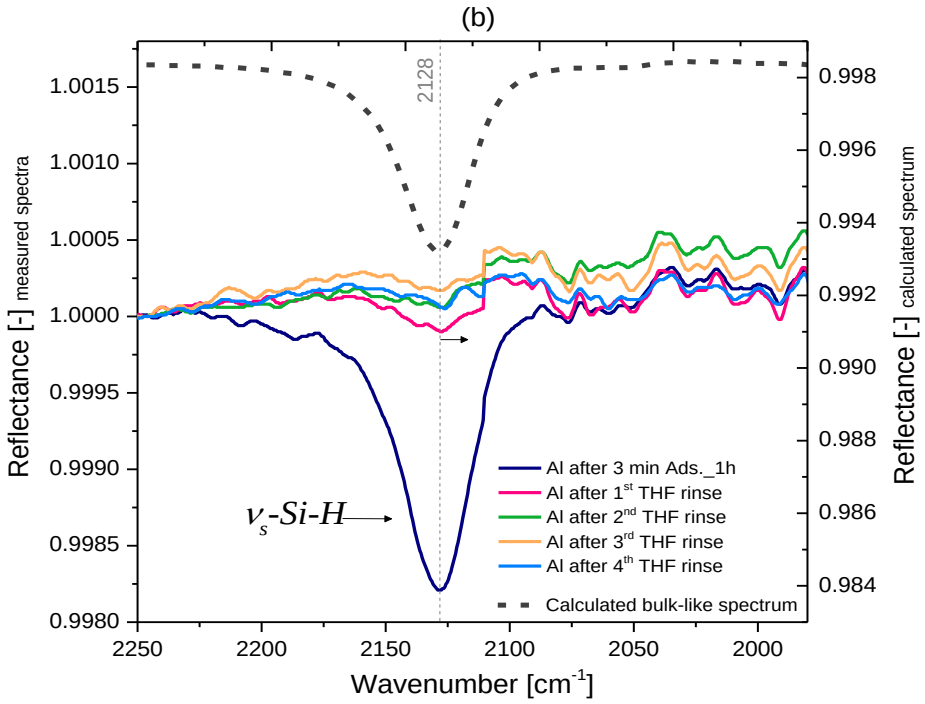


Figure 5.15. Spectrum of the aluminum surface after being rinsed with THF for 3 min (2nd reference spectrum). Weak peaks in the ν-C-H region can be associated with carbonaceous contaminants.

The chemical state of the adsorbed prepolymer 1 on the native aluminum (Al) surface after sequential THF rinsing steps is presented in Figure 5.16a-c. The calculated spectrum is included as reference. Interestingly, the measured spectrum after 3-min adsorption replicates the simulated spectrum very well. This suggests that at that experimental stage, the adsorbate is many layers thick and thus displaying bulk properties. It is seen that even for these relatively low molar mass prepolymer, a considerable high amount of molecules were adsorbed from the dilute solution. The remarkable decrease in band intensities observed after the 1st THF rinse, due to the removal of weakly adsorbed molecules on the Al surface, gives a qualitative support to a dense coverage after the 3-min adsorption step. The peak intensities between THF rinses varied only slightly, pointing out to the approach of a stable adsorbed ultra-thin layer or monolayer coverage which is able to resist up to four THF rinsing cycles.


(a)
2964
2905
ν_{as}-CH_3
ν_s-CH_3
Al after 3 min Ads._1h
Al after 1st THF rinse
Al after 2nd THF rinse
Al after 3rd THF rinse
Al after 4th THF rinse
Calculated bulk-like spectrum
2966
Reflectance [-] measured spectra
Reflectance [-] calculated spectrum
Wavenumber [cm-1]


(b)
2128
ν_s-Si-H
Al after 3 min Ads._1h
Al after 1st THF rinse
Al after 2nd THF rinse
Al after 3rd THF rinse
Al after 4th THF rinse
Calculated bulk-like spectrum
Reflectance [-] measured spectra
Reflectance [-] calculated spectrum
Wavenumber [cm-1]

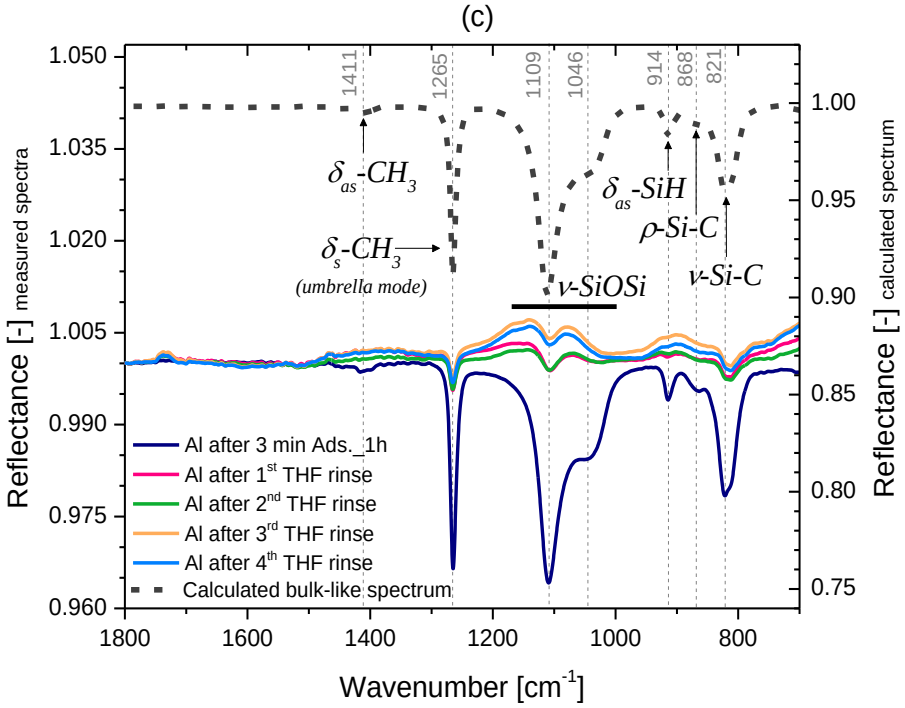


Figure 5.16. ERA spectra of adsorbed prepolymer 1 (di-hydride terminated PDMS) on native Al after 1 h of storage time and four consecutive THF rinses. Spectral regions: (a) from 3100 to 2800 cm^{-1}, (b) 2250-2000 cm^{-1} and (c) fingerprint region from 1800 to 700 cm^{-1}. The peak positions [cm^{-1}] indicated at the top correspond to the spectrum after the 3-min adsorption step.

In the stretching vibration region of C-H bonds (Figure 5.16a), the peaks associated with asymmetric (ν_{as}–CH) and symmetric (ν_s–CH) stretching vibration of methyl groups are identified at 2964 and 2905 cm^{-1}, respectively. The zoomed region in Figure 5.16a reveals different features after THF rinsing steps. First, the ν_{as}–CH band is slightly shifted to a higher wavenumber (~2966 cm^{-1}), although this displacement is within the spectra resolution (4 cm^{-1}). This upper shift could also be due to a significant contribution of the refractive index to the reflectivity of the adsorbed sample with rapid changes in the refractive index [361]. In addition, the peak ν_{as}–CH is broadened and distorted into an asymmetric line shape with a noticeable tail on the lower frequency side. Such low-frequency absorption tail is distinctive of vibrational coupling of randomly distributed molecules [362]. The ν_s–CH bands show asymmetric broadening on the low-frequency side as well. The observed changes in the spectra upon solvent rinsing can be attributed to intermolecular interactions and to changes in the mobility of adsorbed PDMS oligomers as the system approaches monolayer coverage.

Analysis of line broadening could help to understand metal-molecule interactions [362]. The broadening of IR bands has been categorized into inhomogeneous and homogenous modes [362,363], the first mode is related to an inhomogeneous distribution of the individual vibrational frequencies of molecules adsorbed at different sites, and to an irregular distribution of the intermolecular distances between molecules [362,363], whereas the homogeneous mode arises from the damping of vibration as a result of short-range interactions of the vibrating adsorbate with the metal surface [362,363]. The observed peak broadening could be attributed to the inhomogeneous type, which is then associated with an order-disorder transition of the layer, indicating physical adsorption interactions of the CH_3 groups [102,362,363]. Also, according to Painter [364], this kind of broadening is common in systems where there are strong dipole-dipole interactions. Despite that methyl groups are believed to interact weakly [102], the peak broadening observed for the methyl bands could suggest the opposite.

Possible contribution to the peak intensities and peak broadening from carbonaceous contaminants adsorbed on the surface might exist, as all C-H bonds present in the system are featured in this region. In effect, the slight displacement of the baseline can be considered an indication of plausible readsorption of contaminants on aluminum. These aforementioned factors limited the possibility to define bands ascribed to methyl groups as the internal standard for spectra normalization and quantitative analysis. Although peak area and height had been calculated for $\nu_{as,s}$-C-H peaks, these values might be influenced by possible organic contaminations.

The representative symmetric stretch vibration of Si-H groups (ν_s-Si-H) is presented in Figure 5.16b. For both calculated and experimental spectra after 3-min adsorption, the band is located at 2128 cm^{-1}. In contrast to the other bands, the ν_s-Si-H peak intensity is considerably decreased even after the 1st THF rinse. This evidences not only that the prepolymer molecules have been washed away from the Al surface, but also demonstrates the dependency of the peak intensity on the concentration of the vibrating oscillator (Equation 5-27). From the characterization in bulk (Section 4.5) an average degree of polymerization n ~14 was estimated for this prepolymer. For every 14 -Si(CH_3)-O- units there are 2 -Si-H units. Hence, the removal of weakly adsorbed molecules through consecutive THF rinses, dramatically decreases the concentration of Si-H groups, which causes the weak detection of ν_s-Si-H in the ERA spectra upon successive THF rinsing cycles.

The consumption of Si-H bonds in a chemical reaction with the surface could have also contributed to the decrease in intensity of the ν_s-Si-H peak. Thus, involvement of the Si-H groups in chemisorption could be speculated either by formation of -Si-OH groups via hydrolysis and subsequent condensation towards Si-O-Al bonding (Figure

5.17), or by direct reaction with the -OH groups of the aluminum surface, as proposed by Cosgrove et al. [33]. However, chemisorption is only possible when segments are in a suitable location and orientation with respect to the surface groups [33]. In this case, due to the gradual removal of weakly interacting molecules, the chains could have reoriented or rearranged on the Al surface in a way that may have favored chemisorption. Additionally, those possible changes in orientation could have also influenced the peak intensity of the ν_s-Si-H band due to the so-called "surface selection rule" in metals (Section 5.3.2.1).

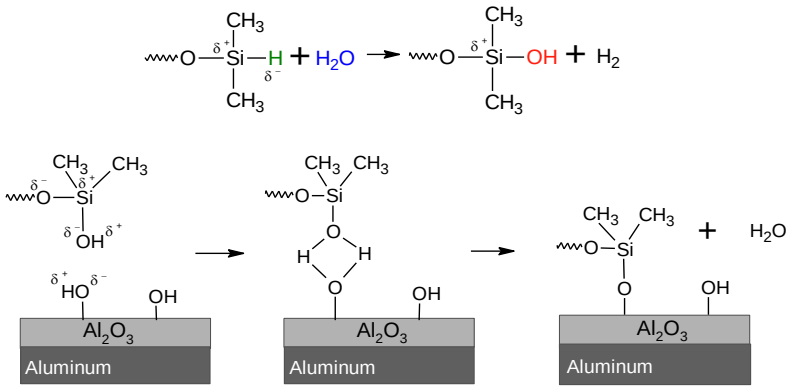


Figure 5.17. Possible chemisorption involving Si-H groups of prepolymer 1 towards final formation of Si-O-Al bonds [32,47].

However, the incidence of chemisorption via -Si-H groups seems unlikely in this experimental approach. First because the measurement compartment was continuously purge with dry air, minimizing the water content. Second, bands corresponding to ν-Si-OH groups are not perceived in the spectra at any experimental stage (Figure 5.18), suggesting that production of Si-OH was negligible or in traces levels. Nevertheless, newly formed -OH traces could have been rapidly consumed by condensation with the -OH groups of the aluminum surface. Thus, chemisorption is not ruled out.

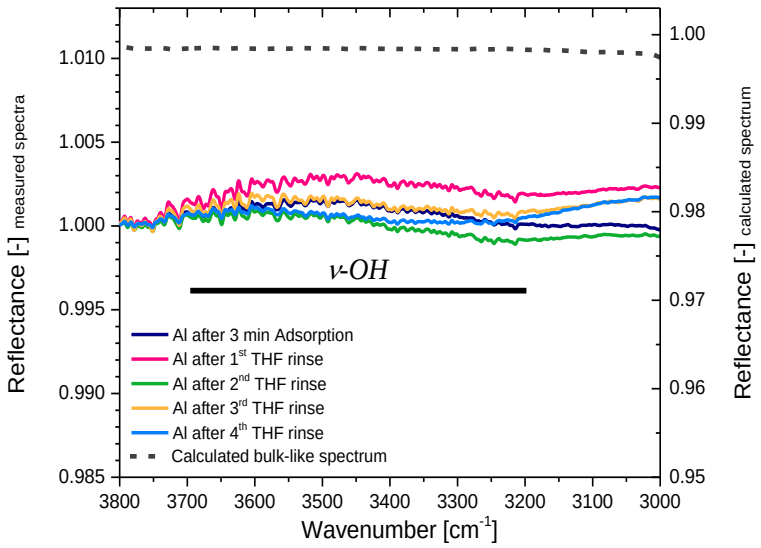


Figure 5.18. O-H stretching vibration mode. Lack of bands suggests no occurrence of hydrolysis of PDMS towards Si-OH formation.

Likewise, a remarkable reduction in peak intensities after the 1st THF rinse in the fingerprint region from 1800 to 700 cm^{-1} (Figure 5.16c) due to the removal of weakly attached molecules is displayed. In contrast, the band intensities are only insignificantly altered from the 1st to the 4th THF rinsing cycles. New spectral features emerged in this region, interpreted as indicating kind of strong interactions between hydride PDMS and Al that allows it to resist up to four rinses with THF.

The spectrum after 3-min adsorption is dominated by features centered at ~ 1414 and 1265 cm^{-1} in the C-H bending region. These are, respectively, the asymmetric and symmetric bending frequencies of the methyl groups. The spectrum also displays two predominant bands between 1000 and 1100 cm^{-1} which originated from the stretching vibrations of Si-O-Si groups. Based on the works of Tsao [124,365], these two bands can be resolved to symmetric (higher frequency) and to asymmetric (lower frequency) stretching modes of Si-O bonds. The respective positions of these two peaks are: 1110 cm^{-1} for ν_s-Si-O-Si and 1046 cm^{-1} for ν_{as}-Si-O-Si. In addition, the distinct absorption band due to asymmetric bending of Si-H is recognized at 914 cm^{-1}. Finally, bands associated with rocking and stretching vibration modes of Si-C bonds are identified at 868 and 821 cm^{-1}, respectively.

The spectra of PDMS adsorbed onto Al (from the 1st to the 4th THF rinsing steps) are magnified for the fingerprint region in Figure 5.19. The interaction of the prepolymer 1 with the native aluminum surface appears to have a pronounced effect on the vibration modes of different absorption bands. First, the range of δ_{as}-CH_3 bands

after solvent rinsing are displayed negatively (reverse direction). In contrast, the symmetric bending (δ_s-CH_3) is perceived always at the same position of the bulk-like calculated spectrum. This indicates that the vibration frequency remains practically unchanged on adsorption and unaffected by the conformation of the adsorbate onto aluminum. Although the symmetry of the peak is disturbed, it might be due to the contiguous bands and baseline effects.

Furthermore, the Si-O-Si stretching bands also undergo important changes upon solvent rinsing which demonstrates that adsorption of PDMS has a strong impact on this vibration mode. Firstly, the two separate components: ν_s-Si-O-Si and ν_{as}-Si-O-Si are more clearly resolved. Secondly, the two bands experience peak shifting towards lower frequencies, especially, the asymmetric mode. The ν_s-Si-O-Si band is shifted by 4 cm^{-1} while the ν_{as}-Si-O-Si bands by more than 20 cm^{-1}. The shift to lower wavenumbers can be interpreted as the weakening of the vibrating frequencies due to a slowing down of the vibrational and rotational movement of the oligomer chains, or to an immobilization of the siloxane group on adsorption to aluminum [102]. Thirdly, the absorption band ν_{as}-Si-O-Si at 1027 cm^{-1} is increased, broaden, and overlapped with a new emerging band at 990-930 cm^{-1}; thus, a final broad band is seen in the entire range from 1070 to 920 cm^{-1}.

As the whole spectral region from 1150 to 920 cm^{-1} is quite complex and displays the most remarkable features; a simple peak fitting procedure was performed on the spectra using a Voigt profile [366], and the software tool OriginPro® 8.6 was employed for this purpose. The aim was to examine the spectra more closely and to provide a tentative peak position for the new emerging band.

Figure 5.20 presents the peak fitting obtained. The plots show that both the calculated and the 3-min adsorption spectra are resolved into two peaks corresponding to the asymmetric and symmetric vibration modes of Si-O-Si. The spectra from the 1st to the 4th THF rinsing steps however, were resolved into three peaks with the new band centered near 970 cm^{-1}. This new band is broadened and shifted to lower frequencies upon THF rinsing. As previously mentioned, the ν_{as}-Si-O-Si band is also shifted to lower frequencies ($\Delta\nu \sim 26$ cm^{-1}), and peak broadening is observed for the two bands located at lower frequencies.

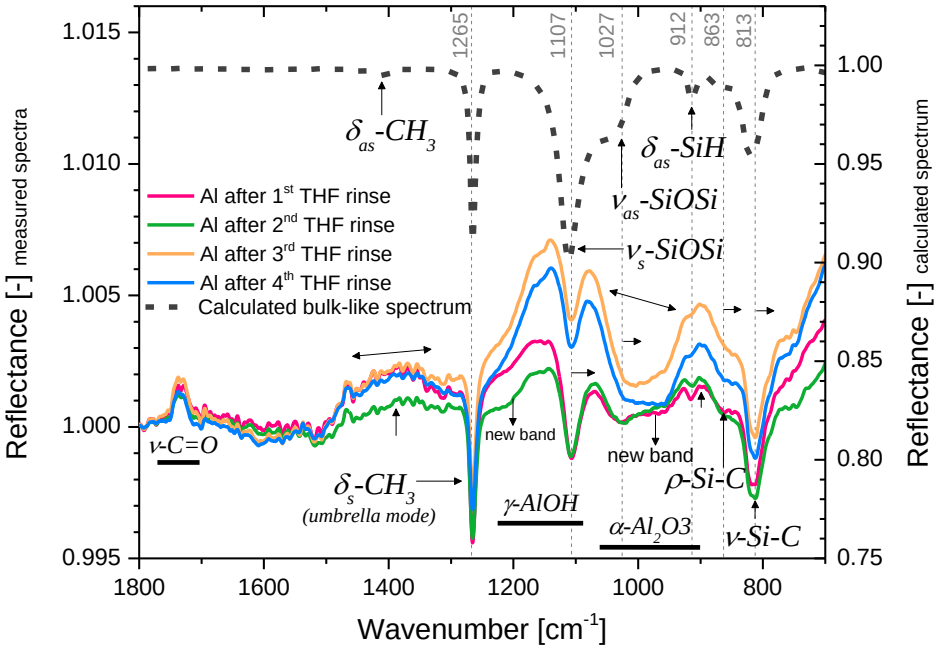
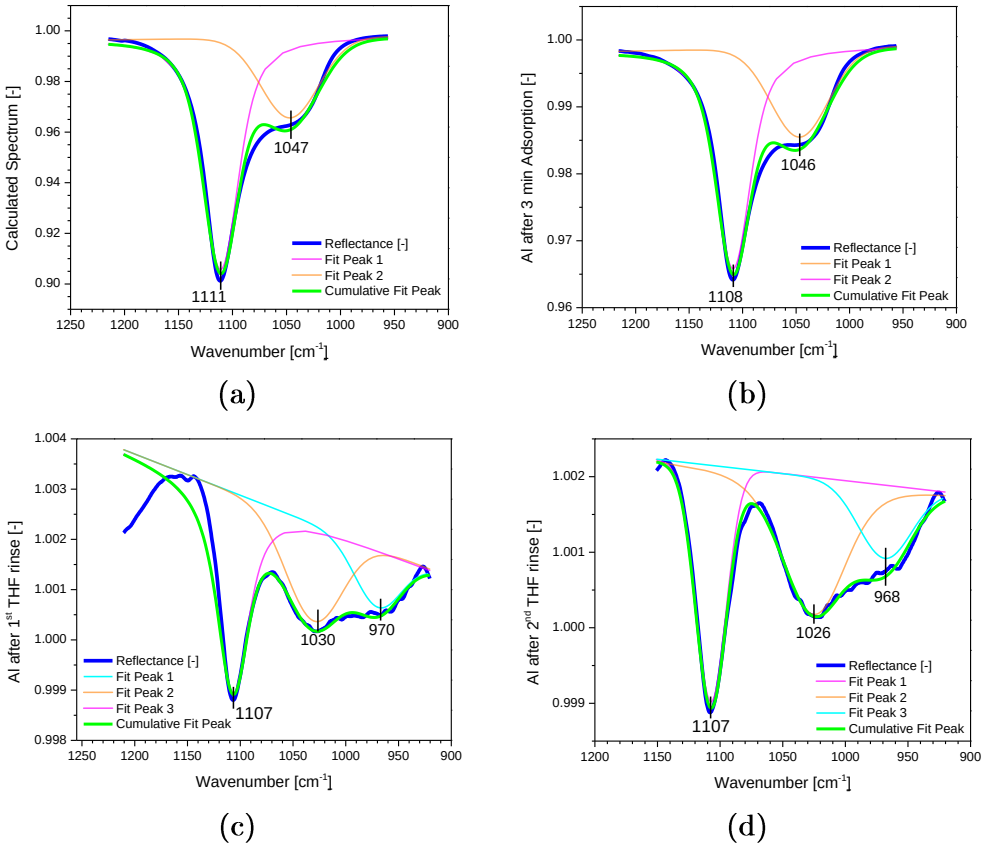


Figure 5.19. Magnified ERA spectra of the adsorbed prepolymer 1 (di-hydride PDMS) on native Al in the fingerprint from 1800 to 700 cm^{-1}.



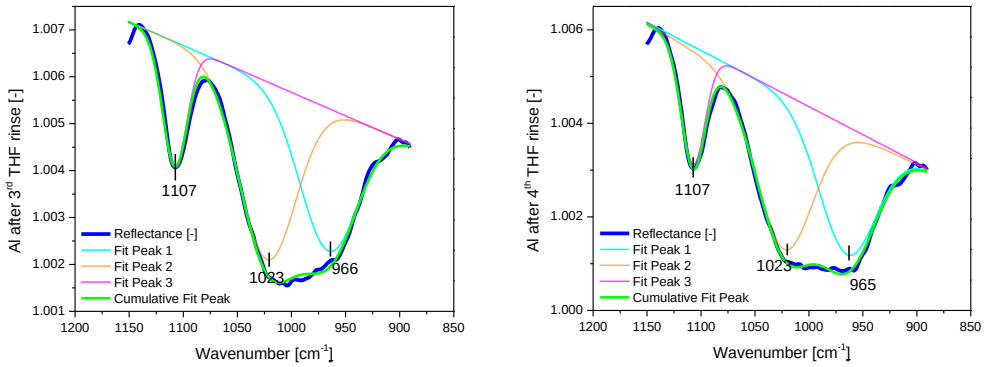


Figure 5.20. Spectral fitting of the FTIR-ERA bands from 1250 to 900 cm^{-1} using a Voigt profile. The calculated bulk-like spectrum (a) and the spectrum after 3-min adsorption (b) were fitted in two peaks corresponding to symmetric and asymmetric stretching of Si-O-Si. The spectra after 1st THF (c), 2nd THF (d), 3rd THF (e) and 4th THF (f) rinsing steps were resolved in three peaks, two associated with stretching modes of Si-O-Si and the new one centered near 970 cm^{-1}.

The appearance of a new band near 970 cm^{-1} is marked evidence of strong interactions existing at the PDMS-Aluminum interface. This spectral feature was also observed by Soga [325] for an IR spectrum of adsorbed PDMS on oxidized germanium (Ge). According to the author, such a band arose from bound siloxane segments to the surface via hydrogen-bonding (H-bonding) with OH groups on the surface [325]. Moreover, Underhill et al. [154], tentatively assigned a new broad band near 1000 cm^{-1} to Si-O-Al bonds formed by the deposition of glycidoxypropyltrimethoxysilane on aluminum. In addition, Jemmet [30], found that siloxanes at the interface with metals cause a peak shifting towards lower frequencies and modification of the peak shape of the -Si-O-Si stretching vibration mode. Therefore, the siloxane bond (Si-O-Si) can be tentatively defined as the adhesion partner for prepolymer 1. The ability of the siloxane bond in establishing strong interactions can be attributed to the polar nature and highly ionic character of the Si-O bond [73,367].

Yet, despite the inherent strong ionic nature of the Si-O bond, the formation of hydrogen bonds involving siloxane groups is actually not a common characteristic of the such bond, as explained by Grabowsky et al. [368,369]. First, due to the helical molecular configuration of PDMS, where the highly polar Si-O bonds are shielded with non-polar alkyl substituents projected towards the outer surface. Second and more importantly, to the low basicity of the Si-O-Si bonds at angles in which siloxane linkages naturally occur (130-180°) [369]. However, it has been established that such low basicity can be significantly increased when the siloxane angle is reduced to values

around the tetrahedral angle [369]. These factors suggest that in order for PDMS molecules to bind with Al-OH groups through H-bonding, a change in the molecular configuration should occur in the vicinity of the surface. The results obtained here could indicate that molecular rearrangement occurred and the methyl groups should have unshielded the Si-O-Si segments allowing them to be oriented towards the Al surface. This assumption was also suggested by Perkel and Ullman [32], who claimed that a considerable distortion of the methyl-silicon linkages must occur near an Si-O group to allow adsorption. Also, the bond angles might have been positively affected in the sense of increasing basicity of the Si-O bonds that favors the formation of hydrogen bonds. Accordingly, such inability of Si-O-Si bonds in creating hydrogen bonds could support the statement of Barthel and Nikitina [102], who have claimed that in terms of interaction energies, classical H-bonding shows a minor contribution in the interactions at the interface between PDMS and fumed silica, and instead, van der Waals forces governed the system, with the Si-O dipole interactions playing the dominant role. In this direction, in the adsorption of prepolymer 1 onto aluminum, most likely, van der Waals forces (dipole-dipole interactions) might have also played a leading role at the interface.

The progressive increase in peak intensity of the new band at 1070-930 cm^{-1} upon solvent rinsing may be attributed to an strengthening in the interactions by an increment in the number of bound segments via H-bonding of the remaining molecules adsorbed on the surface. This suggests that, paradoxically, despite of interacting strongly with the surface, the oligomer chains have sufficient mobility to rearrange towards the enhancement of molecular interactions, i.e. by increasing the amount of bound Si-O-Si segments. Therefore, orientation effects also play an important role as the adsorbate approaches monolayer coverage.

All these features observed for the Si-O-Si stretching vibration are explained by changes in molecular orientation, chain conformation and molecular environment of the siloxane group. These aspects indicate the formation of some sort of surface complex due to strong interactions between the siloxane group and the substrate. Besides the aforementioned hydrogen-bonding, van der Waals forces such as electrostatic interactions and dipole-dipole interactions, donor acceptor interactions and inductive interactions may also be playing an important role as well [102,370]. In summary, all these forces and effects were sufficiently marked to prevent total desorption of prepolymer 1 upon sequential THF rinsing.

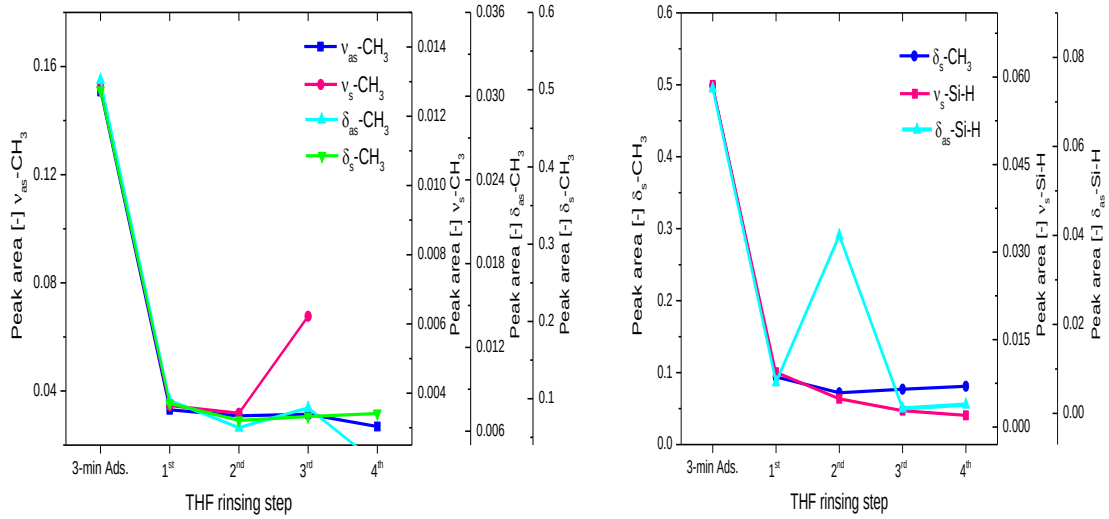
Further analysis in the fingerprint region (Figure 5.19), reveals that the band assigned to δ_{as}-Si-H is only shifted by 3 cm^{-1} and even though its intensity is continuously

decreased, it can be perceived after four consecutive THF rinses. Consequently, the involvement of Si-H in chemisorption was not the case or occurred insignificantly.

Additionally, the variations of the bands related to rocking and stretching of Si-C bonds include peak broadening and a noticeable peak shifting to lower frequencies of 5 cm^{-1} and 8 cm^{-1} for ρ-Si-C and ν-Si-C, respectively. This displacement reflects the impact that the Si-O-Si interactions with the surface have on the Si-C bond.

Ultimately, a new shoulder at ~ 1200 cm^{-1} featuring band broadening after THF rinsing is also identified in the fingerprint region. Its exact assignment is undefined yet but it presumably results from a change in the structure of the aluminum surface due to THF rinses.

The variation of peak intensities upon rinsing steps was quantified by the peak areas estimated employing the software OriginPro® 8.6 and using a Voigt function. This function was selected because for FTIR spectra, it has been found that the Voigt profile is more suitable than either the Lorentzian or Gaussian profiles, as it leads to more accurate and descriptive spectral peak parameters [88,90]. Appendix D contains the individual fitting obtained for the bands associated with the stretching vibration modes of Si-O-Si in prepolymer 1, as an example. The peak areas against the number of rinsing steps have been plotted in different graphs, grouped according to the functionalities which constitute the prepolymer 1 (Figure 5.21a-d). The band ascribed to δ_s-CH_3 is included as a "reference" in the four graphs for comparison purposes.



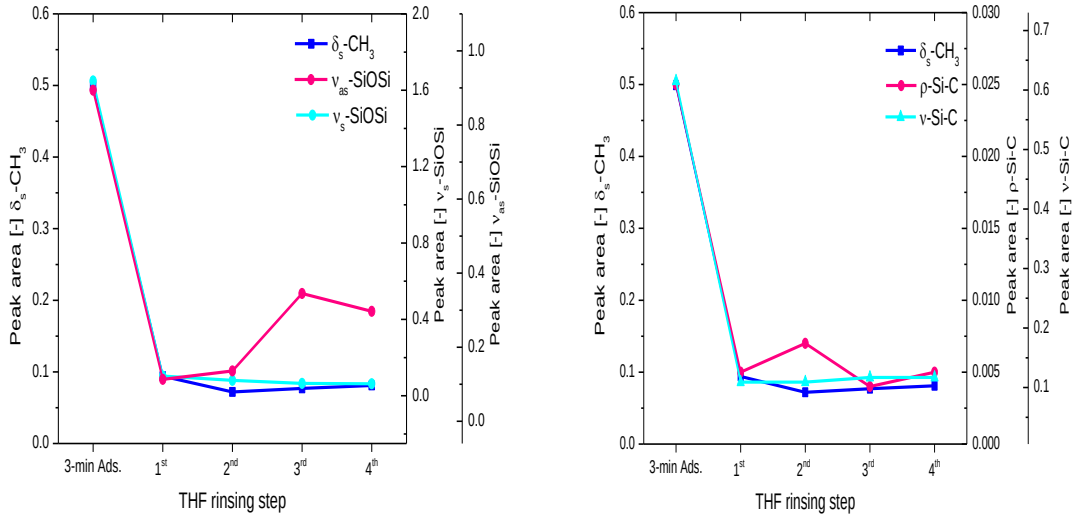


Figure 5.21. Variation of peak areas within rinsing cycles of the IR bands of adsorbed hydride terminated PDMS on Al. (a) bands ascribed to CH_3 groups (CH_3), (b) bands ascribed to Si-H groups, (c) bands ascribed to Si-O-Si groups and (d) bands ascribed to Si-C bonds. Peak ascribed to δ_s-CH_3 is included in all plots as reference.

As mentioned previously, a dramatic reduction in peak areas are seen for all bands after the 1st THF rinse. The reduction follows a consistent trend as superposition of the lines for all bands coincides well within them in that initial stage. This behavior indicates that all groups were desorbed at the same velocity. Thus, the reduction of all peak areas after 1st THF rinse are merely due to the removal of weakly interacting molecules by THF. Upon further THF rinses the areas remain almost invariable, and the fluctuations observed can be attributed to molecular orientation effects. The driving force for molecular reorientation is the minimization of the Gibbs energy of the system defined by Equation 5-30.

$$\Delta G = \Delta H - T\Delta S \qquad \textbf{5-30}$$

With ΔG: change in Gibbs energy between two different states or molecular rearrangements, ΔH: change in enthalpy, ΔS: change in entropy and T: temperature of the system [K].

The minimization of ΔG is achieved by a competition between the reduction of internal energy or enthalpy due to intermolecular-intramolecular interactions, chemical bonding or interphase boundary, with the enhancement of entropy derived from self-entanglement and reorientation of the prepolymer chains [8].

In summary, the adsorption of bifunctional hydride terminated PDMS resulted in the formation of a stable ultra-thin layer interacting strongly with the aluminum surface via H-bonding and Van der Waals forces, presumably with Si-O dipole interactions playing a key role. The molecules are believed to rearrange in a more favorable conformation in which the Si-O-Si bonds are oriented towards the surface in order to establish interactions.

5.5.1.2. Case 2: long storage time (24 h).

Examination of the chemical state of the aluminum surface prior to adsorption, i.e., after being rinsed with THF reveals the presence of surface-adsorbed hydrocarbon contaminants (Figure 5.22). The spectrum displays notable peaks in the region characteristic of stretching vibration of C-H bonds from 3100 to 2800 cm^{-1}, and bands associated with bending of C-H bonds from 1500 to 1200 cm^{-1}. The distinctive vibration of aluminum oxide is recognized at 900-1050 cm^{-1}. Based on the work of Gilbert [371], who studied potential sources of contaminations on native aluminum surface during the adsorption experiments, the bands detected in the ν-C-H region can be attributed to impurities arising from the purging air after the surface has been rinsed once with THF, and to possible traces of Scotch tape dissolved in THF. Experimentally, the scotch tape was used for joining the Tygon® hoses with a Pasteur pipette for solvent and solution extraction. The presence of these bands exhibits the well-known ability of aluminum to easily accumulate surface contaminants. The presence of such contaminants on the Al surface used here, can provide valuable information regarding the behavior of PDMS in contaminated surfaces, as it is a usual situation in real applications.

The adsorbed state of hydride terminated PDMS after 3-min adsorption step, and 24 h storage time is represented in the ERA spectra of Figure 5.23a-c. Similarly, to the previous case, the spectra after 3-min adsorption resembles the bulk-like calculated spectrum, suggesting multilayer coverage with bulk properties. Expectedly, the peak intensities fluctuate over time as result of molecular rearrangement and orientation effects.

The two peaks corresponding to symmetric and asymmetric stretching vibration of methyl groups are presented in Figure 5.23a. Compared with the bulk-like spectrum, the two bands remain unchanged in their peak position but not in their peak shape. Both peaks have broadened remarkably in the low frequency range towards an asymmetric form, which is consistent with the trend observed in the previous case-

study. This modification of peak shape evidences a different chemical environment of the methyl groups when the prepolymer is adsorbed, affecting their vibrational and rotational behavior.

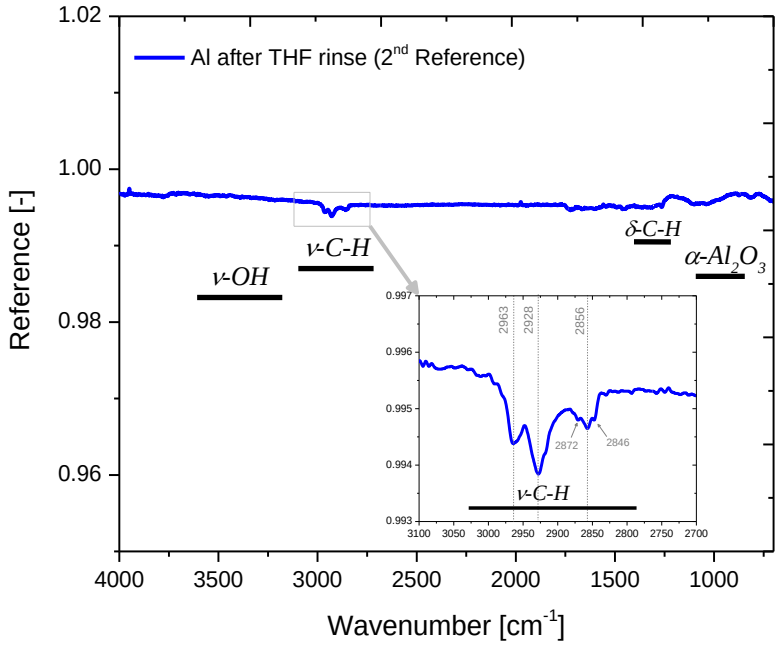


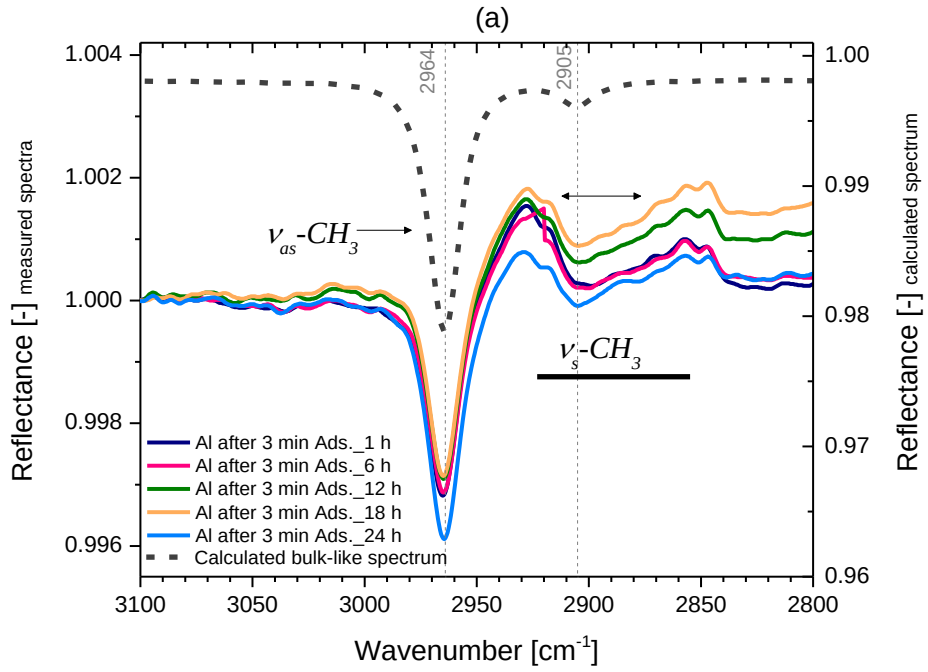
Figure 5.22. Chemical state of the Al surface after THF rinsing. Presence of bands in the ν −C-H region reveal the presence of hydrocarbon contaminants on the surface prior to adsorption.

The asymmetric or inhomogeneous broadening observed, has been associated with weak interactions of the methyl groups with the substrate [102]. Additionally, the corresponding bands $\nu_{s,as}$-CH_3 of the prepolymer 1 are always dominant in the spectra, while peaks related to contaminants are weak. Hence, it can be suggested that adsorption of PDMS is almost unaffected by the presence of organic impurities on the aluminum surface and indicates that PDMS has the ability to displace contaminants, as documented by Abel [48].

The occurrence of chemisorption involving the silyl group -Si-H (Figure 5.17) seems insignificant as bands ascribed to symmetric stretch, ν_s-Si-H (Figure 5.23b) and asymmetric bending δ_{as}-Si-H (Figure 5.23c) are recognized over time. Also, the absence of bands in the spectral region from 3700 to 3200 cm^{-1} demonstrate that the concentration of -Si-OH bonds was essentially unaltered during storage time (Figure

5.24). Nevertheless, silanol traces might be present in the adsorbate as they were detected in the bulk material.

The features in the fingerprint region from 1800 to 700 cm^{-1}, Figure 5.23c, duplicate those in the bulk-like spectrum. Nevertheless, as a result of adsorption, the appearance of a band located near 960 cm^{-1} is revealed. This new feature is consistent with the one observed for 1 h storage time. The new band evolves with time, suggesting that the interactions were strengthened and can even be created for thicker PDMS adsorbed layers if sufficient time is given. Further evidence of interactions at the interface is inferred from the displacement of the bands associated with ν_s-Si-O-Si and ν_{as}-Si-O-Si to lower frequencies. This peak shifting is ascribed to the strained environment of the siloxane moieties as a result of adsorption on the native aluminum surface [33].



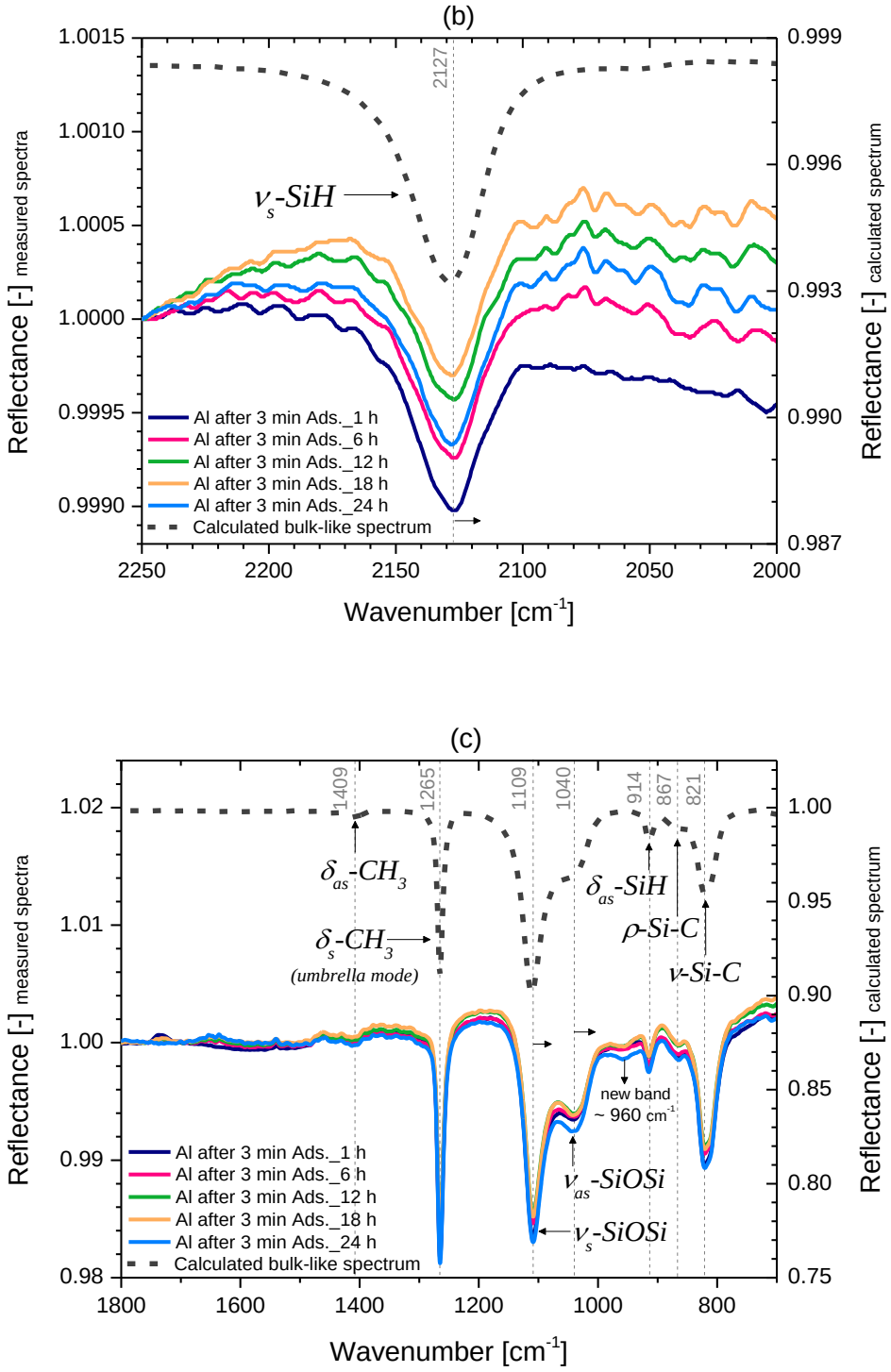


Figure 5.23. ERA spectra of adsorbed bifunctional hydride terminated PDMS on native Al after 24 h of storage time at different spectral regions: (a) from 3100 to 2800 cm^{-1}, (b) 2250-2000 cm^{-1} and (c) fingerprint region from 1800 to 700 cm^{-1}.

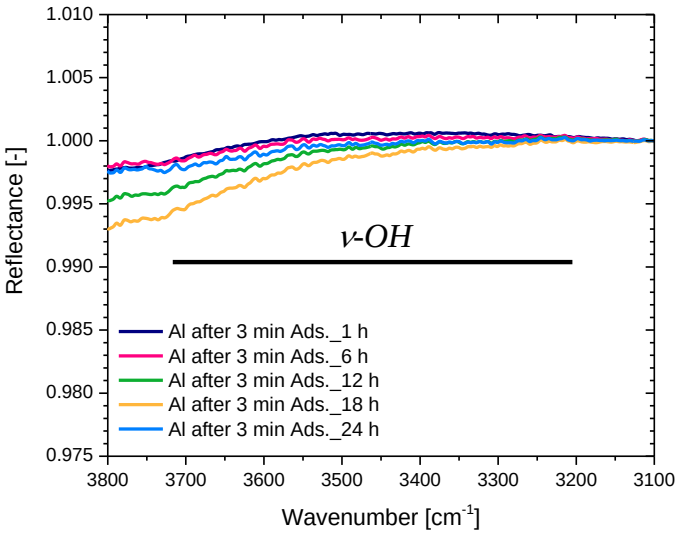


Figure 5.24. ERA spectra of the stretching of OH groups in bifunctional hydride terminated PDMS.

Following the same peak fitting process, mentioned previously, the peak areas of the bands during the storage time (24 h) were estimated. They were plotted against time in Figure 5.25a-d. Regular variation of the peak areas over time is rather observed. This evidences molecular reorientation of the prepolymer chains on the metal surface towards a more stable state, and reveals high mobility of the adsorbed molecules. However, during the first 12 h there is a tendency of the intensities to decrease but then to increase in the last 6 h, with the exception of the bands δ_{as}-CH_3 and the new band at 960 cm^{-1} which increase progressively over time (Figure 5.25b,c, respectively). The continuous increment in intensity of the new band at 960 cm^{-1}, whose assignation is undefined but is associate with Si-O · · Al vibration [189,190], points out that molecular reorientation occurs towards the enhancement of increasing interacting sites of the Si-O-Si groups with the aluminum substrate. Lastly, based on the "surface selection rule", the increase in peak intensities observed in the last 6 h can be attributed to polymer chains with transition dipole moment vector more oriented perpendicular to the surface which enhances their intensity in the ERA spectra.

The continuous change in peak areas even after 24 h, demonstrates that the adsorption of prepolymer 1 on Al proceeded toward a more equilibrated state. However, the attainment of such state takes a long time because polymer chain mobility is in some extent restricted by attachment to the surface as well as by the entanglement with neighbor chains [325].

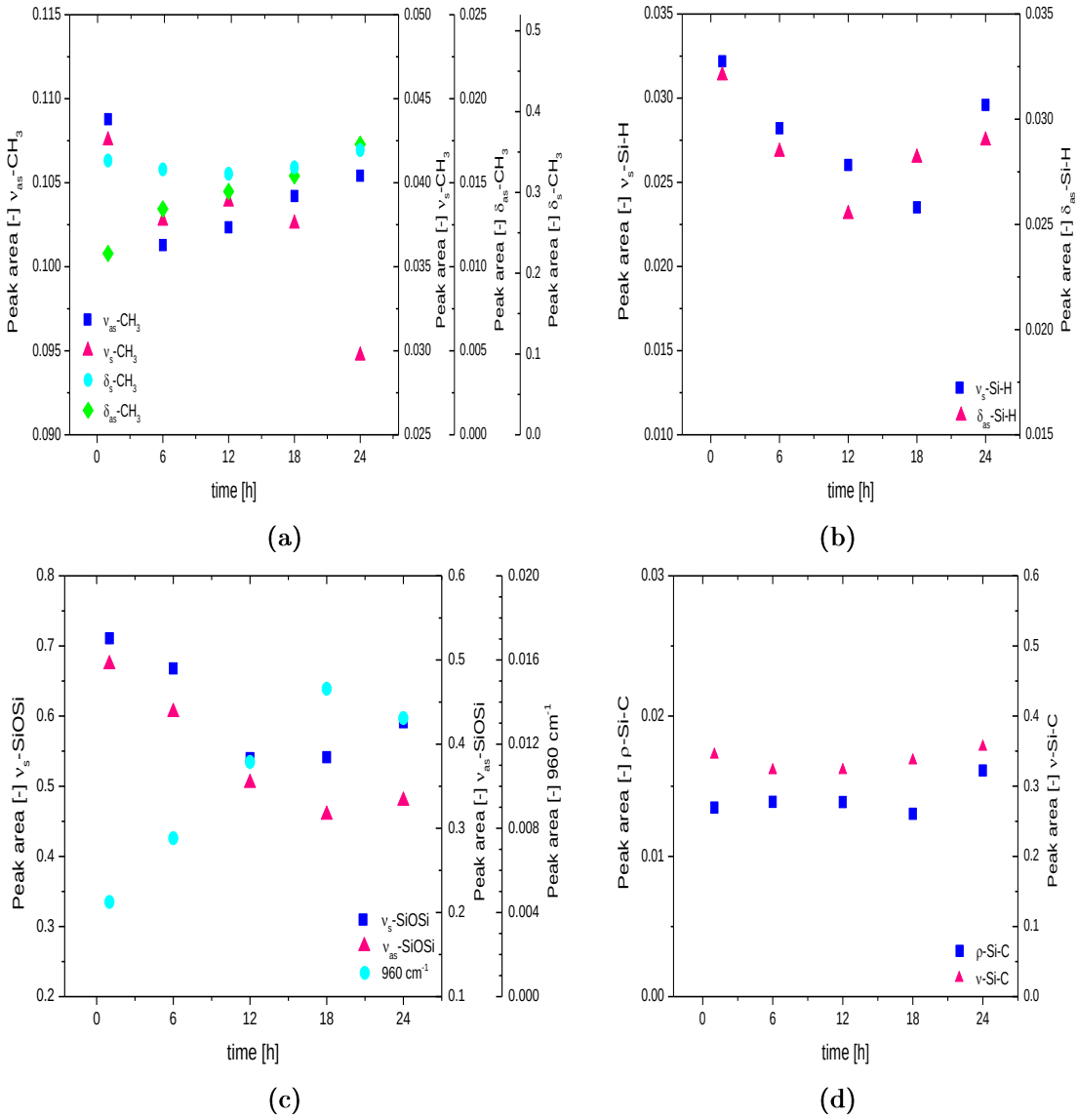


Figure 5.25. Variation of peak areas over storage time for adsorbed hydride terminated PDMS on Al (a) bands related to CH_3 groups, (b) bands related to Si-H groups, (c) bands related to Si-O-Si groups and (d) bands related to Si-C bonds.

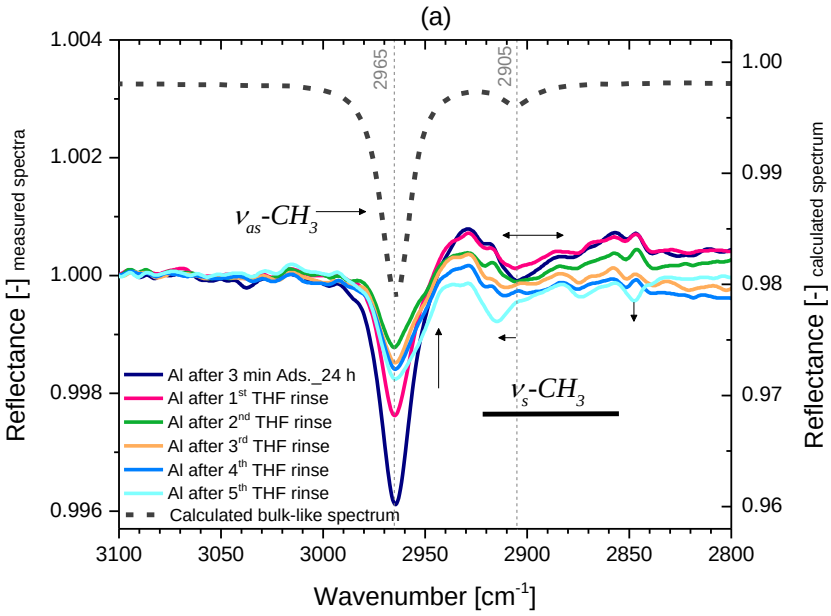
After 24 h of storage time, THF rinsing steps were carried out. Upon consecutive solvent rinses, the spectra do not exactly replicate the calculated bulk-like spectrum anymore and special features are observed (Figure 5.26a-c).

As expected, the peak intensities decrease successively up to the 3rd THF rinse, as weakly bonded adsorbed molecules were sequentially washed off by the solvent. However, after the 1st THF rinse the reduction was not as dramatic as the one observed for a shorter storage time. Thus, the influence of longer storage times in the attainment of more stable adsorbates is exhibited. Moreover, the baseline seems to tilt slightly by

progressive THF rinsing steps, which indicates that the aluminum surface has experienced changes in its structure upon THF rinses [42]. This modification could be principally attributed to some adsorption-desorption events of carbonaceous contaminants [42]. Ultimately, the stability of the adsorbate was proven by its resistance to up to five THF rinsings steps.

Analysis of the stretching mode of C-H bonds from 3100 to 2800 (Figure 5.26a) reveals peak broadening accompanied with change in peak shape for $\nu_{as,s}$-CH_3, indicating that the vibration modes of these two peaks have been affected by the interactions of prepolymer 1 with Al. The presence of small peaks not corresponding to prepolymer 1 suggests possible readsorption of contaminants on the surface at ultra-thin coverage.

Unlike the ν-CH_3 bands, the peak shape of ν_s-Si-H has been only slightly altered (Figure 5.26b), but its intensity decreases remarkably until its almost complete disappearance. By the consecutive removal of weakly adsorbed molecules, concentration of -Si-H decreases drastically in a ratio of Si-H:-Si-O-Si- = 2:14 which causes poor detection in the ERA spectra. Additionally, participation of Si-H towards formation of silanol (-Si-OH) could have contributed to its disappearance. Examination of the -OH stretching region from 3700 to 3200 cm^{-1} (Figure 5.27), reveals negligible -OH formation. Possibly, -OH content was at trace levels being undetected by the FTIR-ERAS technique.



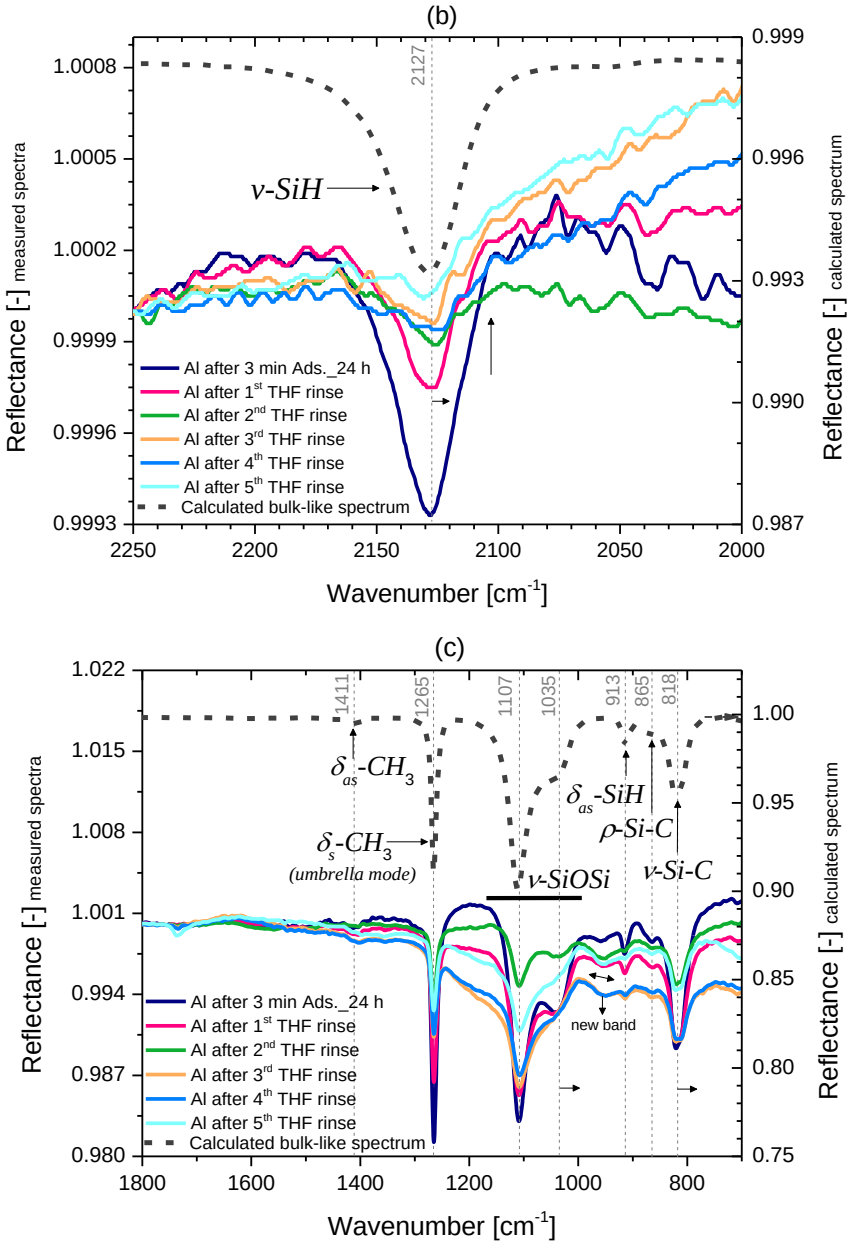


Figure 5.26. ERA spectra of adsorbed bifunctional hydride terminated PDMS on native Al after five consecutive THF rinses at different spectral regions: (a) from 3100 to 2800 cm^{-1}, (b) 2250-2000 cm^{-1} and (c) fingerprint region at 1800-700 cm^{-1}. The dotted line represents the calculated "bulk-like" spectrum.

Furthermore, in the fingerprint region (Figure 5.26c), the successive THF rinses caused frequency shifting of ν_{as}-Si-O-Si from 1043 to 1035 cm^{-1} with a trend of this peak to disappear after three solvent rinsings. These features clearly show interactions of the siloxane bond with the aluminum substrate and orientation effects. In contrast, the

peak at 1107 cm^{-1} (ν_s-Si-O-Si) remains invariable in position but shows increment in peak intensity after the 3rd THF rinse, most likely due to orientation effects. The new peak observed in figure 5.26c also becomes more intense and slightly broader upon THF rinsing, which is consistent with the spectral features observed for 1 h storage time. It is also observed that δ_s-CH_3 peak at 1265 cm^{-1} is practically unaffected in position and shape.

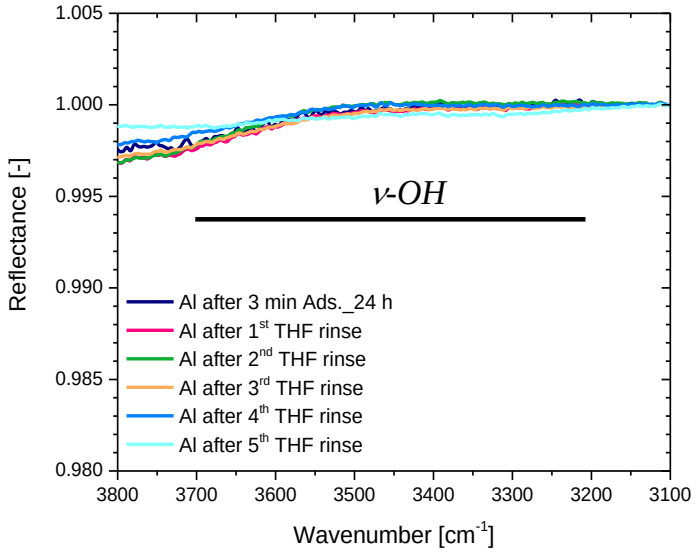


Figure 5.27. ERA spectra of stretching of OH groups in bifunctional hydride terminated PDMS after sequential THF rinses.

For evaluating the change in peak intensities upon THF rinsing, the peak areas of the absorption bands were plotted against the THF rinsing steps (Figure 5.28a-d). The peak areas were estimated using a Voigt function and employing the software tool OriginPro® 8.6. It can be observed that after up to two THF rinses the peak intensities tend to decrease for most IR bands, with the exception of the new band at 960 cm^{-1}. However, after the 3rd THF rinse the peak areas slightly increase, suggesting that by removing weakly adsorbed chains, additional space at the surface to which additional polymer molecules could diffuse was freed. Also, the stronger attached molecules within the adsorbate layer vary their orientation in such a way that the transition dipole moment vector component perpendicular to the surface is enhanced. Upon further rinsings, the peak areas fluctuate slightly, indicating that the molecules have the opportunity for reorientation. The bands related to ν-Si-O-Si display the most

noticeable alteration in peak areas, which demonstrates their key role in interactions at the interface and the effect of orientational adjustments.

As the adsorption from the solution was fast (3 min), one can hypothesize that the adsorbate is not in equilibrium; the chains possess sufficient mobility for improving interactions, orientation and packing density over the storage time given (24 h). After THF rinsing steps, the exhibited spectral features can be attributed to some preferential orientation of the strongly adsorbed prepolymer molecules on the surface. Such orientation might be achieved, in the case of prepolymer 1, by the Si-O-Si segments pointing towards the aluminum surface for enhancing interactions, as deduced from the remarkable changes in their vibrating modes.

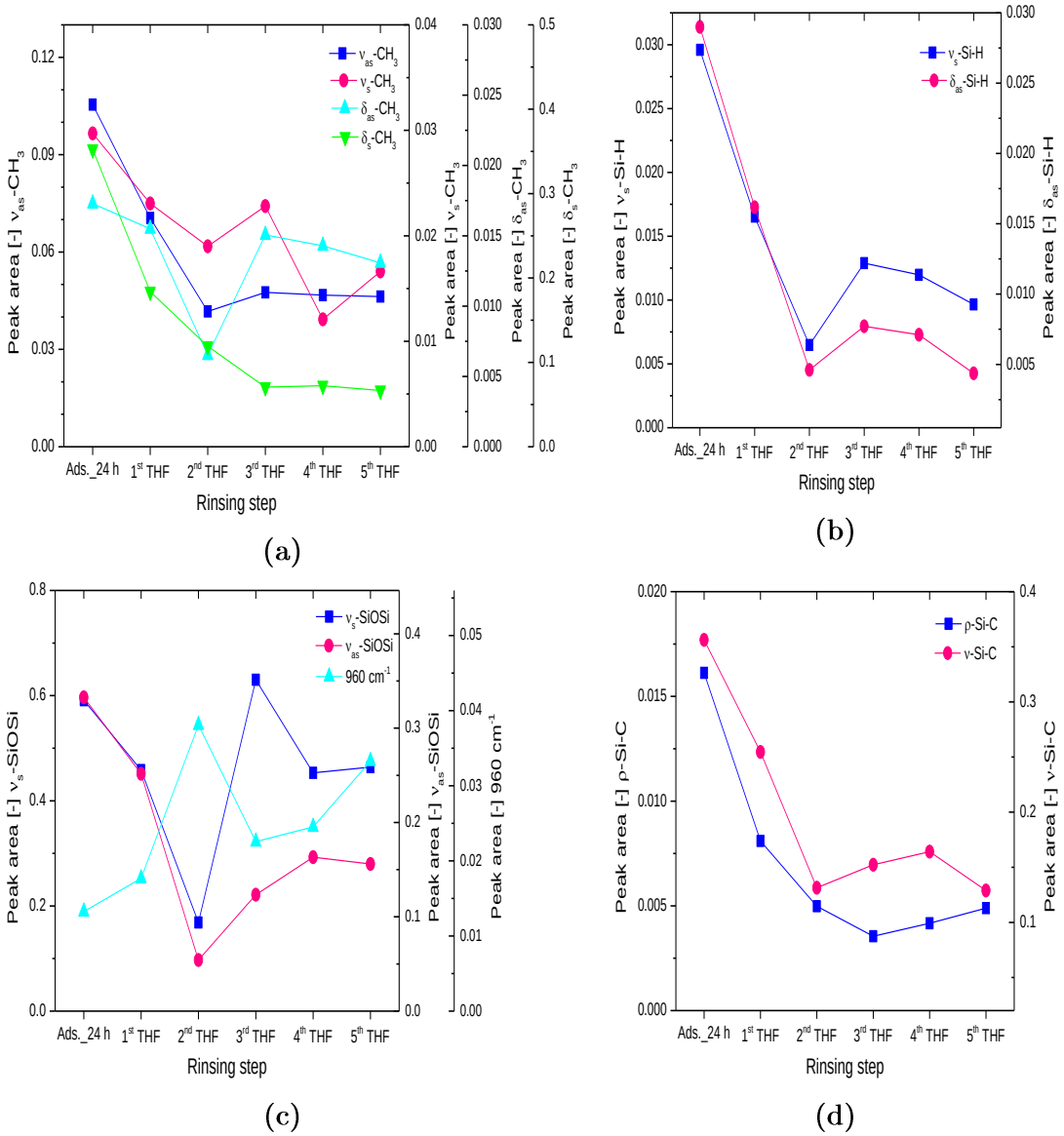


Figure 5.28. Variation of peak areas upon THF rinsing for prepolymer 1 on Al, for bands related to: (a) CH_3 groups, (b) Si-H groups, (c) Si-O-Si groups and (d) Si-C bonds.

5.5.2. Prepolymer 2 - bifunctional vinyl terminated PDMS

5.5.2.1. Case 1: short storage time (1 h).

First, the chemical state of the Al surface prior to adsorption of prepolymer 2 is examined (Figure 5.29). The presence of hydrocarbon contaminants on the surface before adsorption is confirmed by three weak peaks in the ν-C-H region. According to the work of Gilbert [371], they could correspond to contaminants from the purging air after rinsing the substrate once with THF. The presence of -OH groups is undetectable in the ERA spectrum of the Al surface, possibly due to low concentration. A positive band, characteristic of aluminum oxide, is recognized at ~ 975 cm^{-1} [360], indicating growth of the oxide layer upon THF washing.

Figure 5.30a,b illustrates the change in the chemical state of adsorbed bifunctional vinyl terminated PDMS on a native aluminum surface after four THF rinses. The ERA spectrum after 3-min adsorption step replicates the bulk-like spectrum without displaying new peaks, which is consistent with the results seen for di-hydride terminated PDMS (1 h). This suggests that at the first experimental stage, the adsorbate is many layers thick and their vibration states are unaffected by the substrate. So far, no indication of strong interactions with the metal surface can be inferred [42,43].

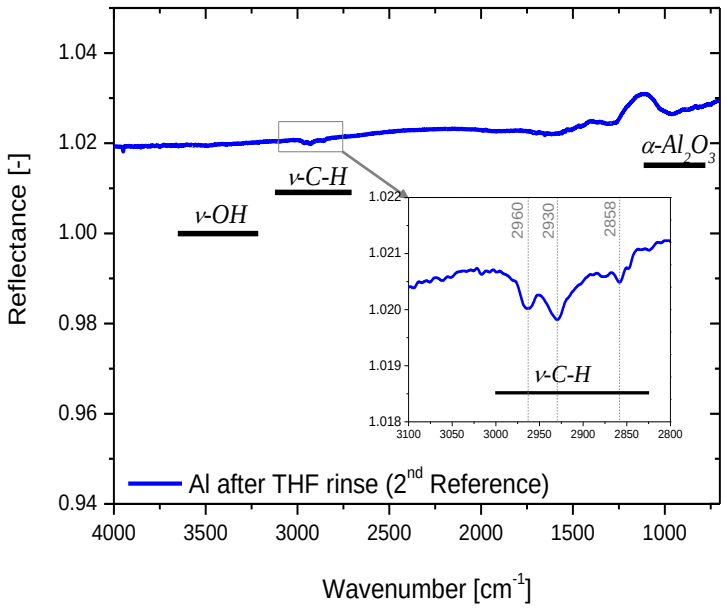


Figure 5.29. State of the aluminum surface after one THF rinsing and prior to adsorption of prepolymer 2 (1 h storage time).

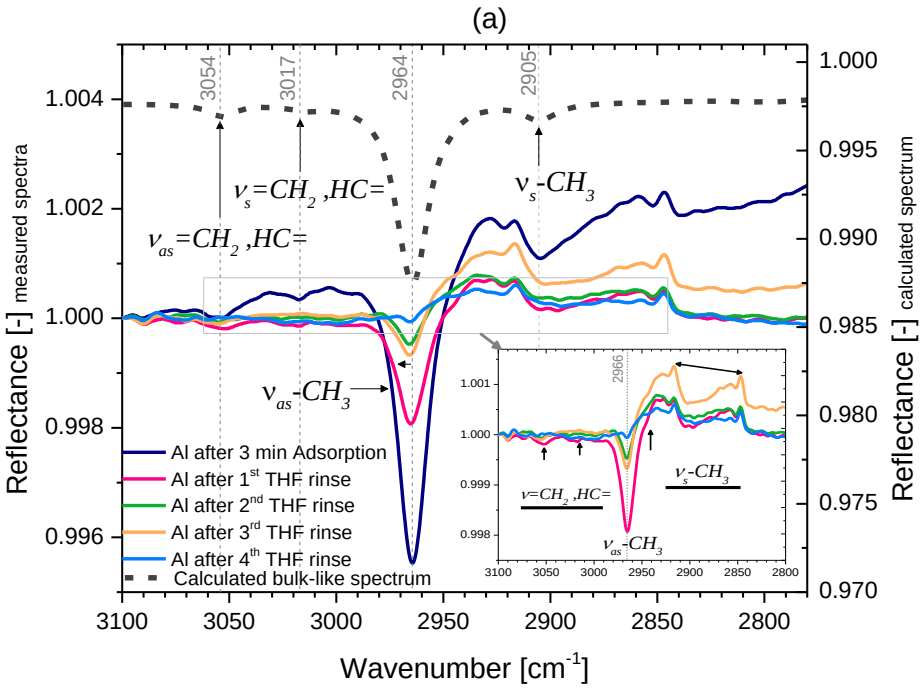
However, significant changes upon solvent rinsing are perceived, in particular the abrupt decrease in intensity after the 1st THF rinse, indicating that a considerable amount of weakly adsorbed molecules were washed away from the surface. The intensities decrease further upon sequential rinsing, advocating that desorption was a progressive process. However, total desorption did not occur and the residual molecules adhered strongly on the native oxide layer, resisting up to four THF washing cycles. This behavior is in agreement with that observed for prepolymer 1, and implies that adsorbed molecules did not reach an equilibrium state at early stages of the experiment. The equilibrium structure of an adsorbate is the result of balancing factors such as temperature, relative humidity and adsorption, which is very complex to predict [372]. Interestingly, a different trend is perceived after the 3rd THF rinse, which could be due to an artefact or to a transition state of the adsorbate.

The 3100-2800 cm^{-1} spectral region (Figure 5.30a) covers the C-H stretching vibrations in vinyl and methyl groups. The four absorption bands perceived in this range are: ν_{as}=CH_2,-CH= at 3053 cm^{-1}, ν_{s}=CH_2,-CH= at 3017 cm^{-1}, ν_{as}–CH_3 at 2965 cm^{-1} and ν_{s}–CH_3 at 2905 cm^{-1}. Essentially, the ERA spectra "see" all of the interactions between a molecule and its neighbors [364]. Thus, peak broadening of the two bands related to methyl groups ($\nu_{as,s}$-CH_3) evokes a variation in the chemical neighborhood of methyl groups when prepolymer 2 is adsorbed onto Al. Peak broadening occurs due to overlapping of frequency shifts (from the unperturbed stretching mode) from all possible relative orientations of the adsorbed molecules, as describe by Painter et al. [364]. In effect, the bands are broadened asymmetrically on the low-frequency side, which is a typical feature in systems where strong dipole-dipole interactions occur and inhomogeneities within the layer exists [362,364]. This same feature was also observed for prepolymer 1, which suggests that independently of the terminal groups, the stretching modes of CH_3 groups in PDMS are substantially affected upon its adsorption on Al. Moreover, these two bands are slightly shifted in peak position, evidencing intermolecular interactions between the adsorbate and the substrate. Two short peaks at 2920 and 2852 cm^{-1}, associated with ν–CH of aliphatic alkanes, reveal possible readsorption of carbonaceous contaminants during the measurement. Deposition of contaminants onto the metal surface was difficult to avoid, despite precautions taken during the execution of the experiments. They could come from the purging air, the prepolymer itself, the solvent, or the accessories employed.

The two bands associated with stretching of vinyl groups are seen to be invariable in shape and peak position, indicating that they are not greatly affected by the adsorption of prepolymer 2 on Al. However, they tend to vanish upon solvent rinsing, most likely due to concentration effects rather than orientation effects. For prepolymer

2, even a slight removal of weakly adsorbed molecules causes a considerable decrease in vinyl content in the system since the molar ratio of vinyl/siloxane groups is 2:10 (–Si-CH=CH_2:Si(CH_3)$_2$O-). Simultaneously, molecular orientation effects towards a more stable conformation, after successive THF rinses, may have contributed to poor visibility of vinyl bands on the ERA spectra.

Furthermore, modifications observed in peak shape, symmetry and position of different bands in the fingerprint region (Figure 5.30b) confirm the existence of physico-chemical interactions between the adsorbate and the substrate. The most remarkable features are perceived for the symmetric and asymmetric stretch vibration mode of Si-O-Si at 1108 and 1049 cm^{-1}, respectively. The enhanced spectra (Figure 5.31) reveal that these two bands are shifted to lower wavenumbers after THF rinsing, indicating a different chemical environment of the siloxane groups in their adsorbate state than in the bulk state. Such different chemical neighborhood causes a weakening of the siloxane bond vibration (reduction of frequency) due to coupling of PDMS with the Al substrate [370].



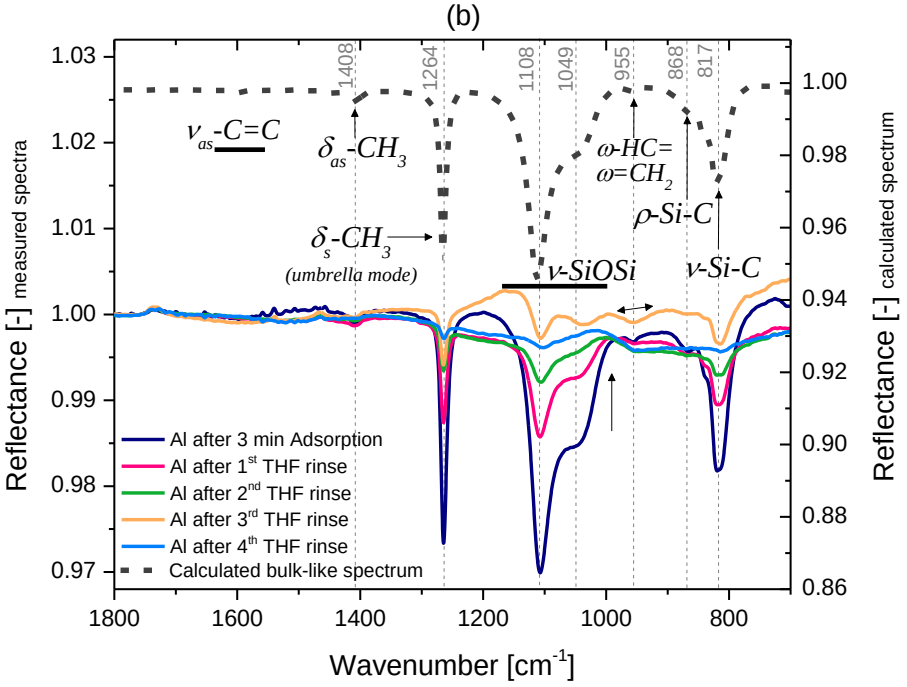


Figure 5.30. ERA spectra of adsorbed prepolymer 2 (di-vinyl terminated PDMS) on native aluminum oxide in the spectral range (a) from 3100 to 2800 cm^{-1} and (b) fingerprint region from 1800 to 700 cm^{-1}.

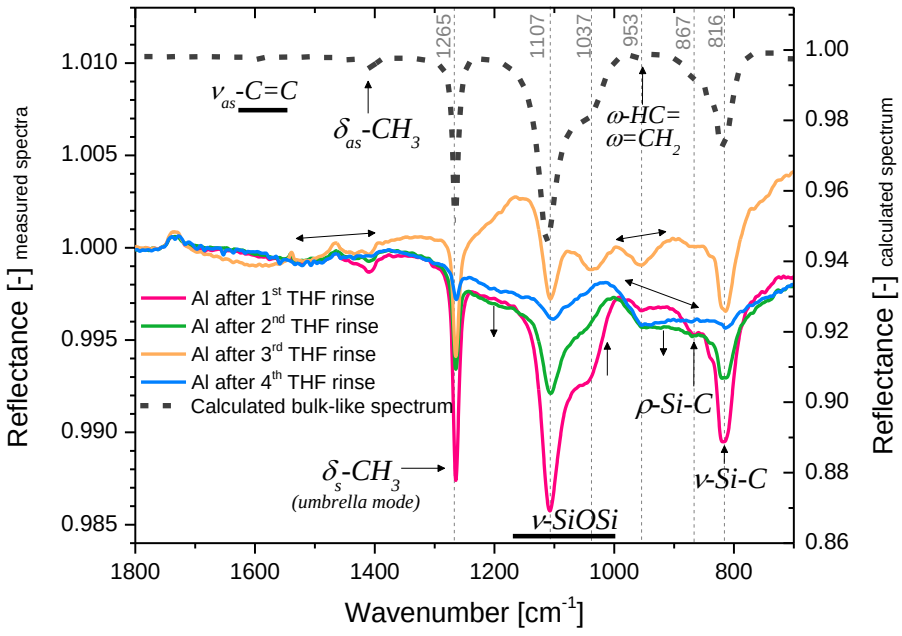
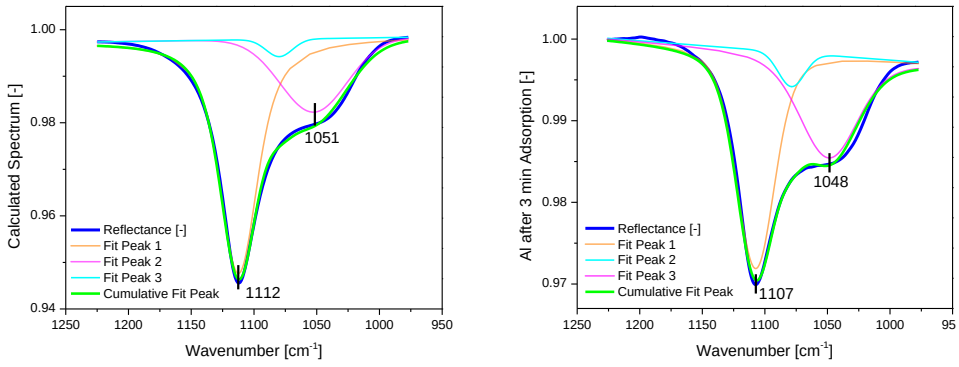


Figure 5.31. Magnified fingerprint region from 1800 to 700 cm^{-1} of the ERA spectra of adsorbed prepolymer 2 on native Al after THF rinses.

The weak band at 955 cm^{-1} corresponding to ω-CH=CH_2 is broadened upon THF rinsing, possibly due to overlapping with a new emerging band at ~970-960 cm^{-1} associated with bound Si-O-Si segments with Al [36,154,325]. These features described before are in close agreement with those observed for hydride terminated PDMS. The two bands related to rocking and stretching of Si-C are also slightly shifted to lower frequencies as a consequence of intermolecular interactions involving the polymer backbone and, therefore, -Si-CH_3 groups. Interestingly, as with prepolymer 1, the umbrella mode of CH_3 groups remains unmodified in peak position, although its peak shape is slightly distorted in the low-frequency side, most likely due to adjacent bands and baseline effects.

Examination by peak fitting of the broad band at 1200 to 980 cm^{-1} yields the molecular state of the Si-O-Si groups adsorbed on Al. The intense band can be resolved into two components centered at ~ 1107 ascribed to ν_s-Si-O-Si and at 1050 cm^{-1} assigned to ν_{as}-Si-O-Si (Figure 5.32a-f).

Comparing the bands in the bulk-like spectrum (Figure 5.32a) with those in the measured spectra (Figure 5.32b-f), the ν_s-Si-O-Si is shifted a total of ~9 cm^{-1} towards lower frequency, while the ν_{as}-Si-O-Si is shifted by ~13 cm^{-1} after the 3rd THF rinse but disappears after the 4th wash. This peak shifting of the Si-O-Si stretch modes in prepolymer 2 is consistent with that observed in prepolymer 1.



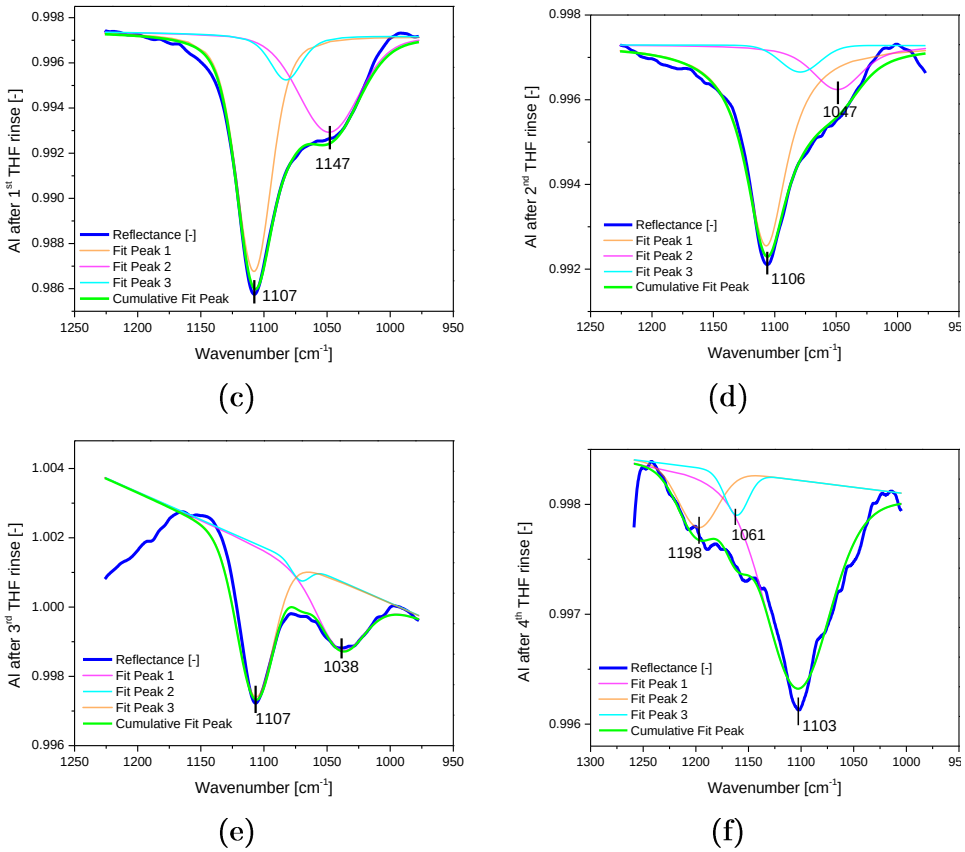


Figure 5.32. Fitted Si-O-Si stretching mode bands of prepolymer 2 in the spectra: (a) calculated bulk-like spectrum (b) after 3-min adsorption (c) after 1st THF (d) (d) after 2nd THF, (e) after 3rd THF, and (f) after 4th THF.

A tendency of the doublet to merge into a single band centered at ~ 1103 cm^{-1} is observed after four THF rinses. The disappearance of the ν_{as}-Si-O-Si band can be attributed to molecular orientation effects within the adsorbed layer that causes the dipole vector of this vibration mode to lie virtually parallel to the metal surface, and therefore, to be unnoticed in the spectra. Consequently, the concomitant behavior of these two bands can be related to local variations in molecular packing around the oscillating dipoles or to an increase in the number of highly oriented molecules [359]. These features of the siloxane stretching modes indicate the mobility of the molecules within the adsorbed permitted reorientation of the Si-O-Si groups after exposure to THF. Furthermore, it is believed that the well-known high flexibility of PDMS favors rearrangement towards strengthening the interactions with the substrate and improving packing density. In addition, a new band at ~1198 cm^{-1} is perceived after two and four THF rinses, which is in agreement with the previous results of prepolymer 1.

The spectral changes of the Si-O-Si absorption bands can be interpreted as resulting from adsorption interactions of siloxane groups with the native aluminum oxide, most likely from H-bonding between the oxygen of Si-O-Si segments and the proton of hydroxyl groups on the surface [32,34,325], and dipole-dipole interactions [32,102]. Accordingly, surface organization and reorientation may be enlarged by the formation of H-bonds with the surface OH groups, or restricted by the size and shape of the functional Si-O-Si group [372]. Moreover, the incidence of chemical reactions such as hydrolysis of Si-O-Si bonds leading to formation of Si-OH groups is excluded, as the spectral region from 3700 to 3200 cm^{-1} (Figure 5.33), characteristic of O-H stretching mode, lacks absorption bands.

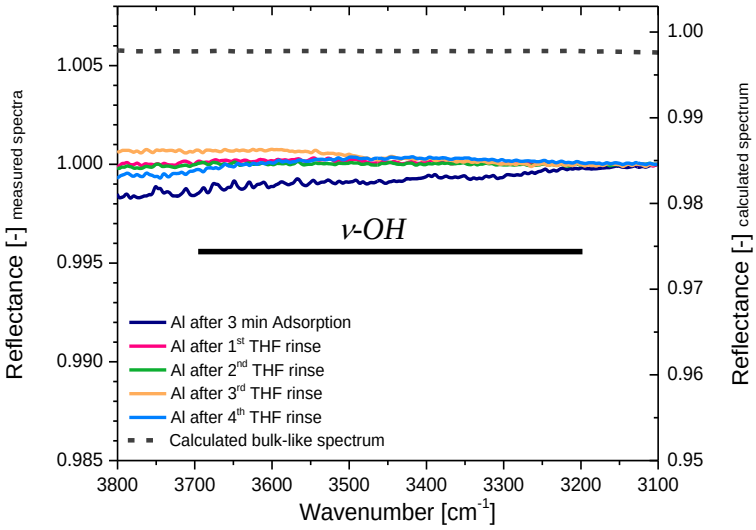


Figure 5.33. O-H stretching mode of prepolymer 2 on Al.

The effect of molecular orientation was evaluated by the variation of the peak areas upon THF rinsing (Figure 5.34a-d). The areas were estimated using a Voigt profile in the software tool OriginPro® 8.6. After the 1st THF rinse all peak areas decreased at the same velocity (parallel lines) due to the same event: removal of weakly interacting molecules. After the 3rd THF rinse, there is a marked increase either due to a baseline artefact or to an important change in molecular orientation.

The variation between peak areas for the different bands is rather regular, following a similar trend, except for the ω-CH=CH_2 band at ~956 (Figure 5.34a), which increases continuously in intensity due to the appearance of a new band at ~970-960 cm^{-1} related to bound Si-O-Si segments via H-bonding [325].

The slight relative variation observed in peak areas suggest molecular mobility that allowed the di-vinyl terminated PDMS molecules to possibly adopt a preferential orientation close to the Al surface [42,43]. The molecular orientation in adsorbed prepolymer 2 was a dynamic process affected by successive solvent rinsing, proving that a thermodynamically stable adsorbate layer was not attained up to three THF rinses.

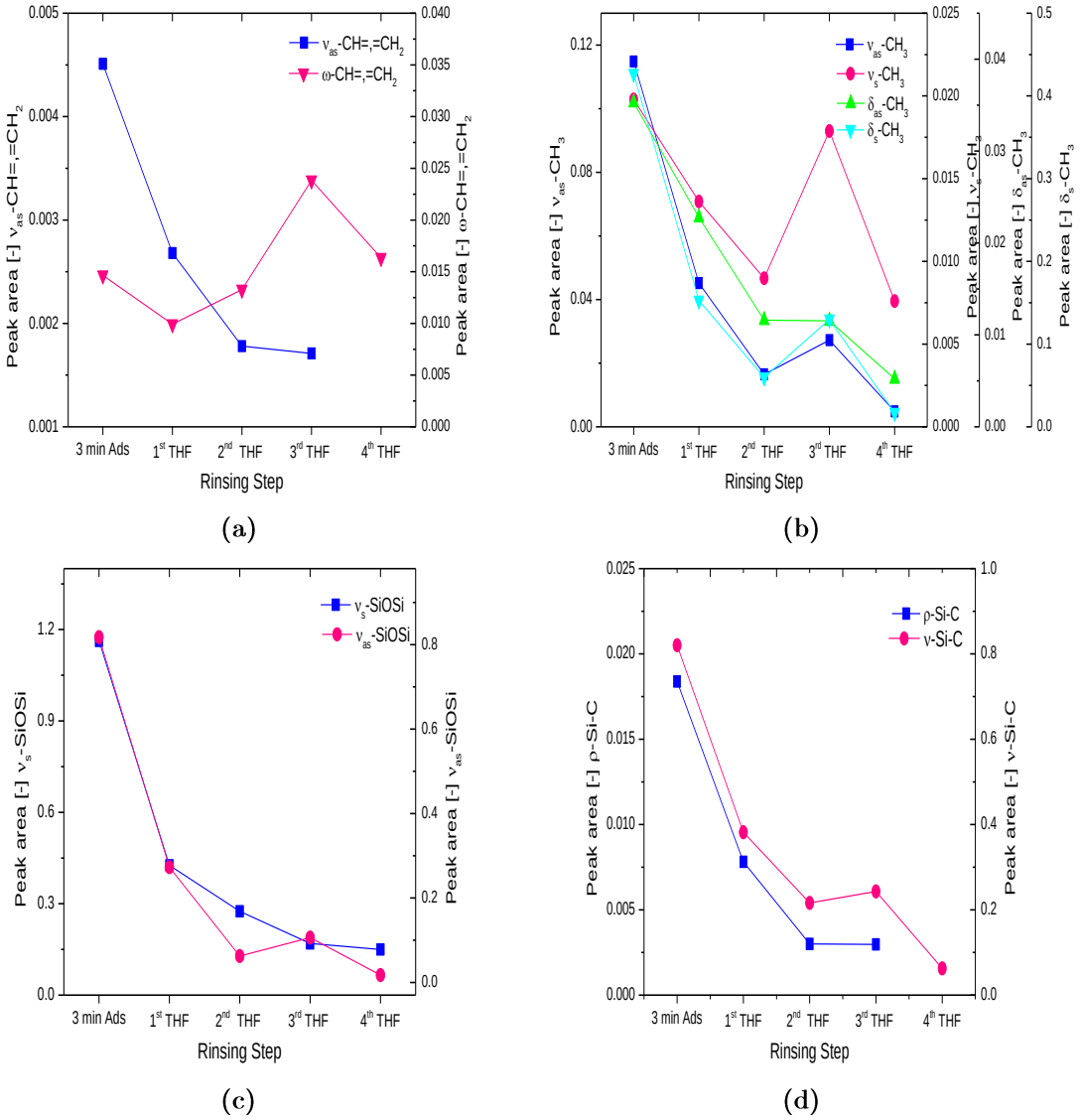


Figure 5.34. Variation of peak areas upon THF rinsing for adsorbed di-vinyl terminated PDMS on Al for: (a) bands related to $CH{=}CH_2$ groups, (b) bands related to CH_3 groups, (c) bands related to Si-O-Si groups and (d) bands related to Si-C bonds.

Summarizing, the adsorption of di-vinyl terminated PDMS at a short storage time was governed by strong interactions of the siloxane bonds with the substrate, causing peak broadening and significant peak shifting of the Si-O-Si stretching modes toward lower frequencies. Prominent broadening of the peak at 956 cm^{-1}, most likely due to the emerging of a new band at ~ 970-960 cm^{-1}, ascribed to siloxane segments attached to the surface, was also recognized. Changes observed in the vibration modes can be related to chemical bonds, intermolecular interactions and molecular rearrangement, which allows the elucidation of adhesion mechanisms. There is sufficient evidence to tentatively assign the siloxane group as the adhesion partner of prepolymer 2 on Al. Considering that prepolymer 2 contains an average of 10 -Si-O-Si- units capable of creating interactions, it can be postulated that prepolymer 2 molecules oriented with the highest number of Si-O-Si groups horizontally to the surface. However, from a thermodynamic point of view, the entropy of the system decreases as the polymer chains are completely stretched out; thus, restrictions upon chain flattening suggests that the conformation of adsorbed prepolymer 2 may consist of short loops and trains of adsorbed sets of Si-O-Si segments. In addition, readsorption of impurities on the surface during the experiment was inferred from the presence of small peaks in the C-H stretching region and from drifting of the baseline, which also evoked alterations of the Al surface structure upon solvent washing, as mentioned Fug et al. [42].

5.5.2.2. Case 2: long storage time (24 h).

As usual, the chemical state of the aluminum surface prior to adsorption (after being rinsed once with pure THF) was evaluated first. The spectrum reveals that carbonaceous contaminants were present on the surface (Figure 5.35). Impurities could arise from the purging air and/or traces of Scotch tape dissolved in THF [371]. Preventing readsorption of impurities from the atmosphere was difficult during the experimental procedure. The lack of peaks in the O-H stretching mode indicate that the concentration of hydroxyl groups was unchanged by the solvent. Ultimately, the positive band associated with vibration of aluminum oxide at 1095 cm^{-1} [360], suggests oxide growth after THF rinsing. These results are consistent with those evaluated previously, advocating reproducible states of the Al surface prior to adsorption.

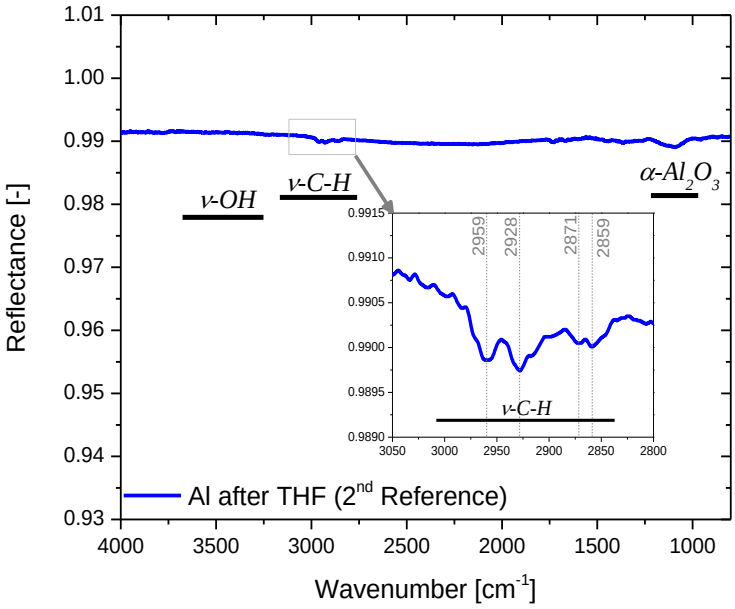


Figure 5.35. Chemical State of the aluminum surface after THF rinsing and prior to adsorption of prepolymer 2 for 24 h storage time.

The chemical state of adsorbed vinyl terminated PDMS on Al over time is illustrated in Figure 5.36a-b. The measured spectra replicate the calculated spectrum very well at all times, implying that the effect of aluminum surface on the chemical structure of adsorbed prepolymer 2 is unnoticeable after the 3-min adsorption step. Accordingly, the spectra display bulk properties due to multilayer coverage in which physico-chemical interactions of PDMS with the substrate are virtually unnoticed. This consistent behavior noticed for prepolymer 1 and 2 prior to THF rinsing cycles shows to be independent of the storage time and end-group termination. As claimed by O'Shaughnessy and Vavylonis [373], surfaces in contact with even extremely dilute polymer solutions can readily develop very dense polymer layers.

Four distinctive bands of C-H stretching modes are exhibited in the spectral region from 3100 to 2800 cm^{-1} (Figure 5.36a), they are: ν_{as}=CH_2, HC= at 3053 cm^{-1}, ν_{s}=CH_2, HC= at 3017 cm^{-1}, ν_{as}-CH_3 2965 cm^{-1}, and ν_{s}-CH_3 at 2905 cm^{-1}. Unlike hydride PDMS after a long storage time, the CH_3 stretching modes in di-vinyl terminated PDMS feature less remarkable changes in peak shape and line broadening when compared to the bulk-like spectrum. Importantly, bands assigned to vinyl groups are perceived in all spectra, indicating that they were not involved in any important chemical process over time. In addition, for the spectrum at 1 h, two small peaks located at 2917 and 2848 cm^{-1} are shown, implying the presence of organic impurities on the metal surface.

However, their intensities are reduced over time, advocating dislocation by adsorbed PDMS molecules.

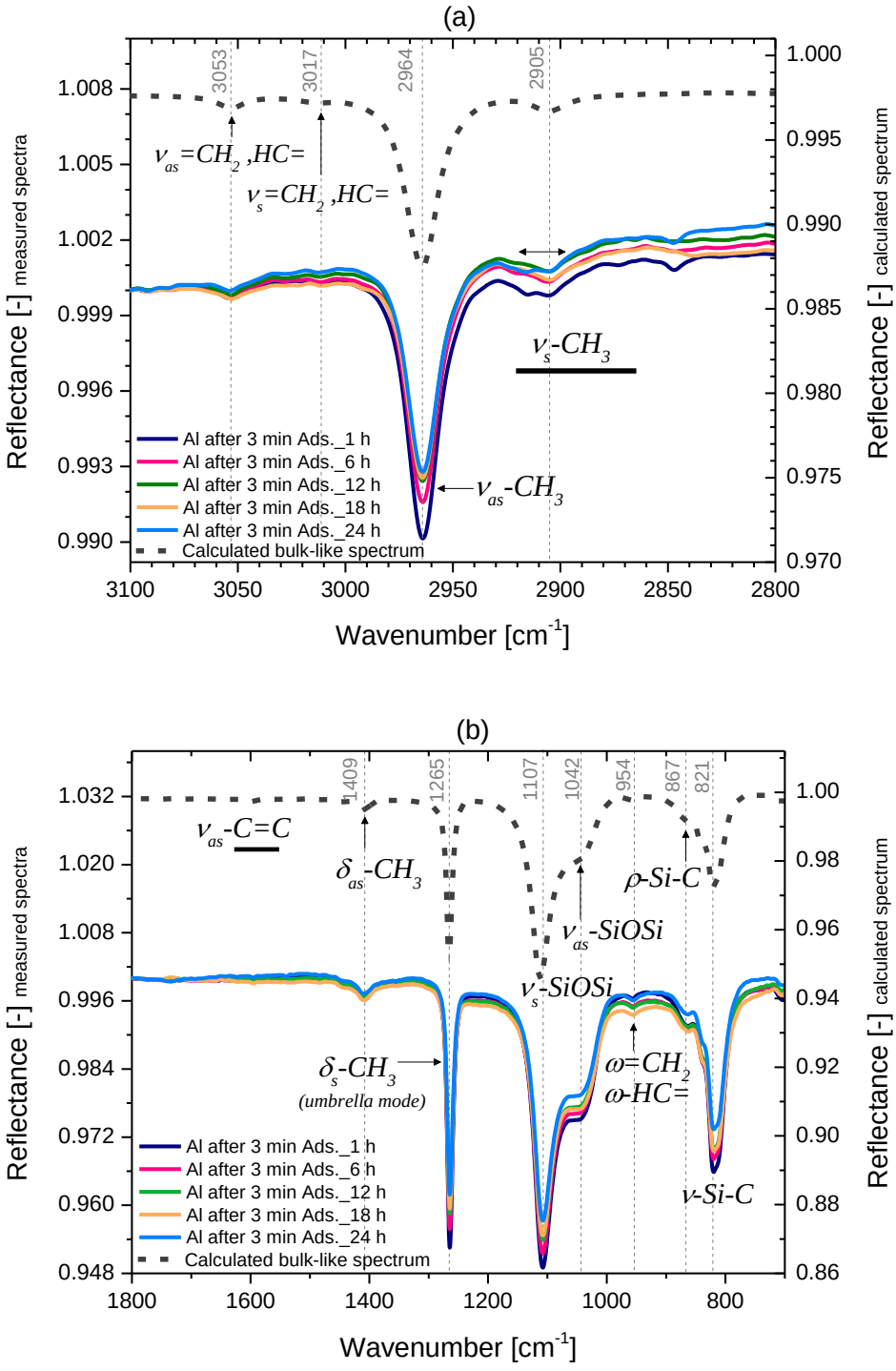


Figure 5.36. ERA spectra of adsorbed di-vinyl terminated PDMS on native aluminum oxide during 24 h at two different regions: (a) from 3100 to 2800 cm^{-1} and (b) fingerprint region at 1800-700 cm^{-1}. The wavenumbers on the top correspond to the spectrum at 1 h of storage time.

In the fingerprint region (Figure 5.36b), the distinctive Si-O-Si stretching modes are shifted to lower frequencies in comparison to the bulk-like spectrum; the ν_{as}-Si-O-Si is shifted from 1112 to 1107 cm^{-1} and ν_{s}-Si-O-Si from 1046 to 1042 cm^{-1}. They result from the weakening of the Si-O-Si bonds due to interactions. The band centered at 955 cm^{-1} also discloses disparities with the bulk-like spectrum, particularly peak broadening over time on the low-frequency side. Such line broadening was also observed for the new emerging band at ~970-950 cm^{-1} in adsorbed di-hydride PDMS. Hence, interactions of prepolymer 2 with the surface also lead to the appearance of a new band, which in this case overlaps with the wagging vibration mode of vinyl groups. On the other hand, additional bands displayed in this range do not feature important changes compared with the bulk-like spectrum.

The viability of chemical reactions leading to the formation of Si-OH groups was assessed by the evolution of the O-H stretching mode in Figure 5.37. Contrasting with previous cases, a weak broad band is observed for prepolymer 2 at 3700-3200 cm^{-1} after 12 h, addressing increase of -OH moieties over time. A plausible explanation for this particular behavior is the considerably high content of shorter lineal oligomers in prepolymer 2, demonstrated by GPC and NMR measurements (Section 4.5.2). Most likely, such oligomers were more prone to undergo siloxane bond cleavage towards formation of Si-OH moieties with time. However, investigations about the incidence of hydrolysis of PDMS suggest that it usually does not take place at room temperature [374], and even in the presence of a catalyst, water reacted slowly with PDMS at 150°C, where an equilibrium was reached after 3 months [375]. However, PDMS oligomers in their adsorbate state could have endorsed the occurrence of hydrolysis. Other possibilities supporting the increase of OH groups with time include readsorption of contaminants with -C-OH groups and physisorption of water molecules.

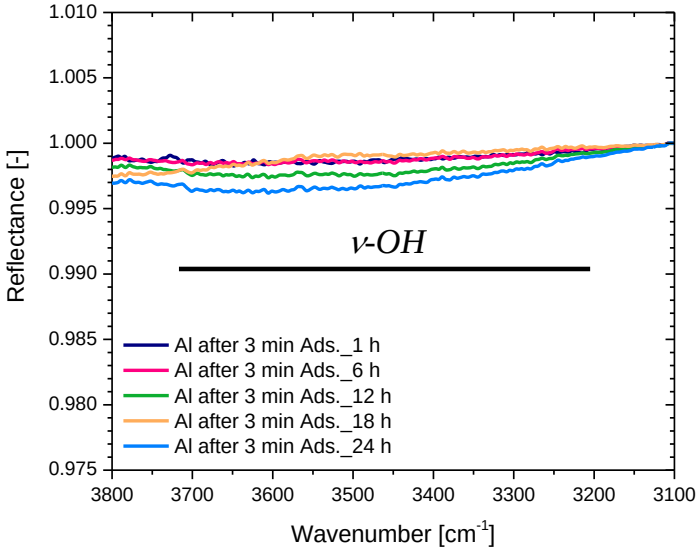


Figure 5.37. Evolution of the O-H stretching vibration mode of prepolymer 2 over time.

Longer storage times of adsorbed polymers cause variation of peak intensities with time. This effect was evaluated by plotting the peak areas against time in Figure 5.38a-d. The peak areas were estimated using a Voigt function in OriginPro® 8.6. The relative variations of the areas evoke molecular orientation effects over time. However, the simultaneous decrease in intensity for the two Si-O-Si stretching bands, accompanied with the increment in peak area for the band at 950-960 cm^{-1}, could supports the supposition of siloxane bond breakage towards the formation of Si-OH moieties. The continuous change in peak areas during the evaluated time implies that the adsorbed molecules did not attain equilibrium in 24 h. Dynamics of adsorbed polymer layers have been described as typically very slow for macromolecules, because a single chain possesses many surface anchoring sites and interacts with numerous other chains, impeding its motion. Consequently, irreversibility and non-equilibrium effects are common in adsorption of polymers [373]. The ability of adsorbed vinyl PDMS molecules to rearrange and orientate in a preferential conformation over time indicates that the adsorbed molecules were fairly movable. Time allows successive transitions from a less organized assembly to a more organized one by decreasing the molecular area and improving the packing of molecules [45]. After 24 h the conformation of the adsorbate is, therefore, expected to be more stable than that acquired after just 1 h.

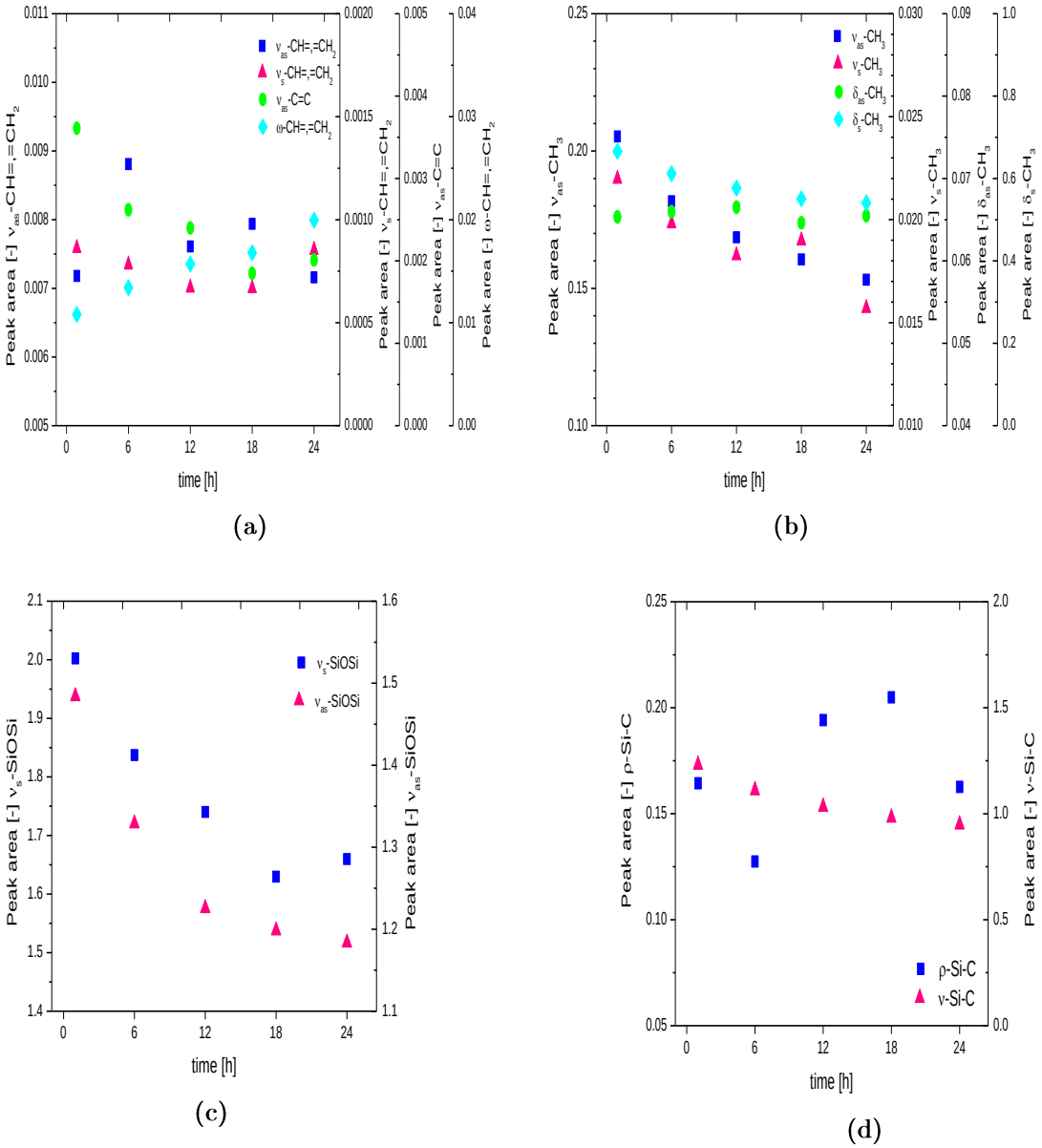
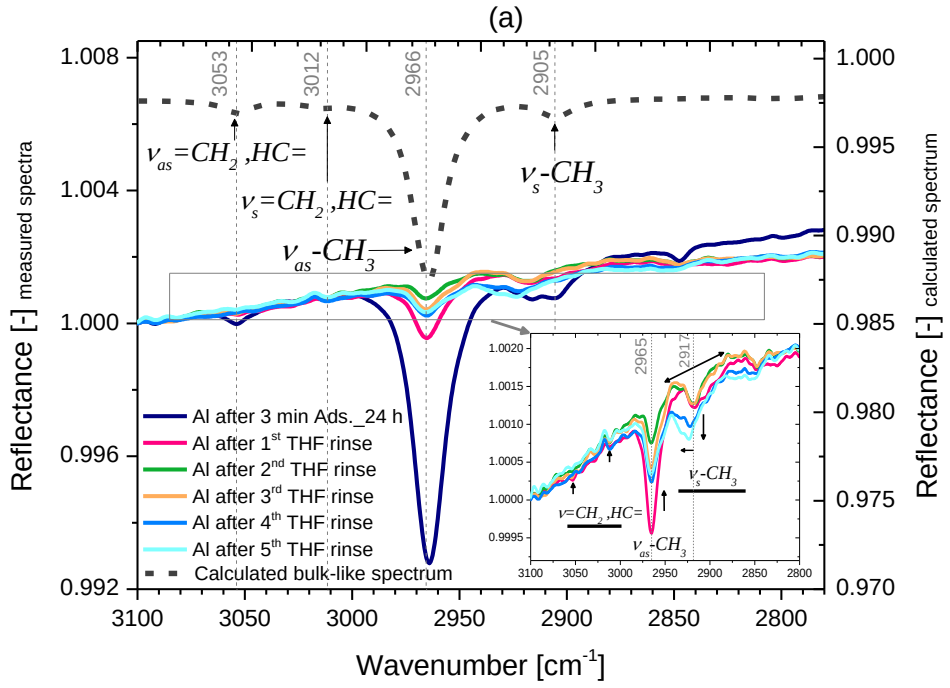


Figure 5.38. Variation of peak areas over time (24 h storage time) for adsorbed bifunctional vinyl terminated PDMS on Al (a) bands related to CH=CH_2 groups, (b) bands related to CH_3 groups, (c) bands related to Si-O-Si groups and (d) bands related to Si-C bonds.

After 24 h of storage time, the aluminum surface was exposed to five consecutive rinses with pure THF. The spectra after each rinsing step are presented in Figure 5.39a-b. Unlike the spectra over time, the spectra after THF rinses do not replicate the calculated spectrum, thus, changes due to interacting forces, and orientation effects at the interface become obvious. The absorption bands of the adsorbed PDMS layers after THF rinsing are broader than those observed for the calculated bulk-like spectrum. This observation is consistent with the previous cases analyzed.

A remarkable decrease in intensity after the first THF rinsing is perceived, indicating the desorption of weakly attached molecules. However, not all peaks decrease consistently upon solvent washing; in particular, the bands ascribed to Si-O-Si stretch modes markedly increase in intensity after the 2nd and 3rd THF rinse cycles, but decrease again after the 4th rinse, remaining almost invariable afterwards. The invariability of intensity, advocates the attainment of a stable adsorbed layer after four THF rinses and irreversible adsorption of PDMS on aluminum. As claimed by O'Shaughnessy et al. [373], for long chains irreversible effects are, in practice, the rule rather than the exception, whether physical or chemical bonding is involved.



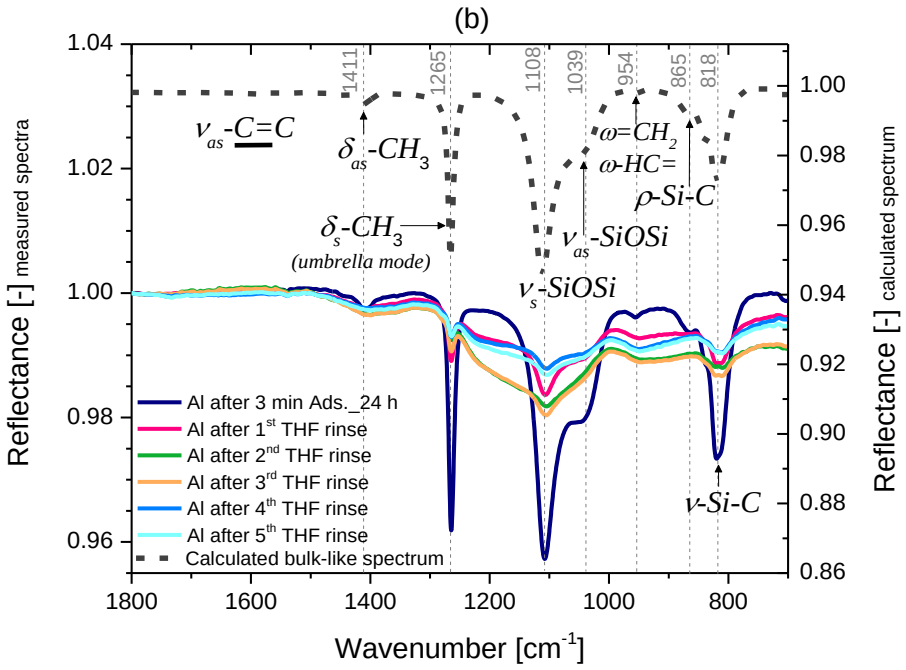


Figure 5.39. ERA spectra of adsorbed prepolymer 2 (di-vinyl PDMS) on native Al after 24 h of storage and successive THF rinsing cycles. (a) Spectral range from 3100 to 2800 cm^{-1} and (b) fingerprint region from 1800 to 700 cm^{-1}.

For the bands ascribed to ν_{as}-CH_3 and ν_s-CH_3 at 2966 and 2905 cm^{-1} (Figure 5.39a), peak broadening and change in peak shape are identified. Also, the peak at 2905 cm^{-1} displays a remarkable peak shifting to higher frequencies (~18 cm^{-1}) after the 4th THF rinse. Due to possible contribution from contaminants to these spectral features, exclusive attribution to adsorption effects is imprecise. Bands related to C-H stretching of vinyl groups are not present due to the removal of weakly attached molecules, which substantially decreased the vinyl concentration. In addition, vinyl groups are usually weakly displayed in FTIR [189], which affects their poor detection in the spectra after THF rinsing cycles. Moreover, inclination of the baseline occurs as a possible consequence of structural changes of the aluminum oxide layer caused by the pure solvent or by a dynamic adsorption/desorption process of contaminants [42].

For the sake of clarity, the fingerprint region has been magnified after THF rinses in Figure 5.40. The spectral features displayed are consistent with those previously observed for hydride PDMS and vinyl PDMS (1 h), specially the increase in band intensity of the Si-O-Si stretching mode. Because methyl groups are attached to Si atoms, interactions of the siloxane segments with the aluminum surface significantly affects this vibration mode of methyl substituents. Additionally, possible physical forces

such as dipole-dipole interactions, arising from the difference in electronegativity of Si and C atoms, could possibly exist between -Si-CH_3 segments and the substrate.

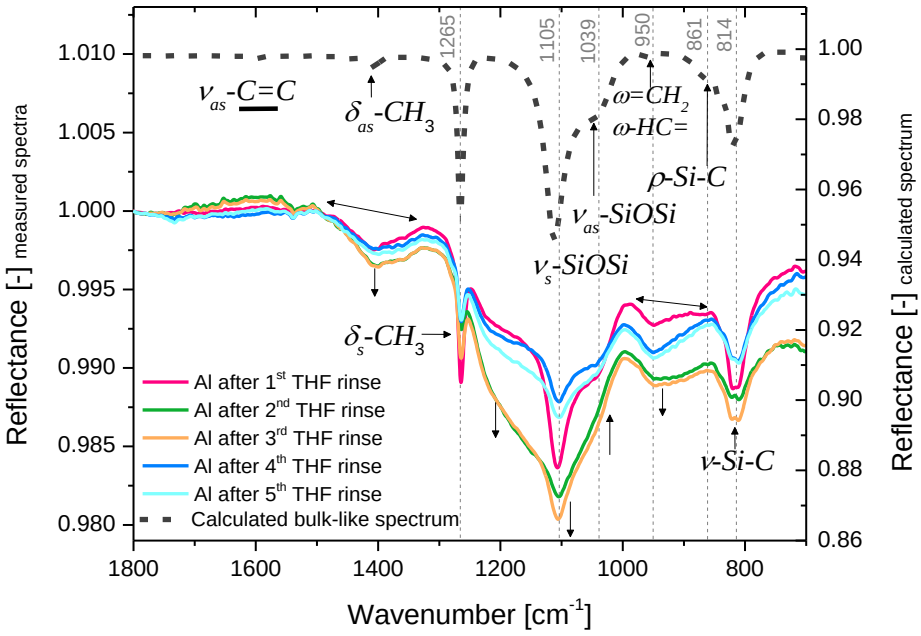


Figure 5.40. Enlarged ERA spectra of adsorbed prepolymer 2 on Al after THF rinses in the fingerprint region from 1800-700 cm^{-1}.

(ii) Peak shifting to lower frequencies and strong shape distortion of the Si-O-Si stretching vibrations. Referred to the bulk-like spectrum, the ν_s-Si-O-Si peak is shifted by 8 cm^{-1} and the ν_{as}-Si-O-Si band by 2 cm^{-1}. Shape distortion and peak broadening on the high-frequency side of the ν_s-Si-O-Si band due to the emerging of a new shoulder at 1220-1180 cm^{-1} is also discernable. The assignment of this shoulder is still undefined, but it is related to changes in the structure of the aluminum surface upon contact with THF [371] .These features of the siloxane groups are considered as strong evidence of interactions at the interface with aluminum. In addition, the asymmetric mode (ν_{as}-Si-O-Si) seems to be masked by the broad band after the 2nd and 3rd THF rinses, but after the 4th and 5th rinses the band is discernible again. Such fluctuations advocate molecular orientation from an ordering process in which the perpendicular component of the transition dipole moment of this ν_{as}-Si-O-Si vibration mode tends to become weak.

Fitting of the Si-O-Si bands of the measured spectra (Figure 5.41a-f) reveals bands at ~1200 and ~1150-1160 cm^{-1}. Apparently, the ν_{as}-Si-O-Si does not shift to lower frequencies, whereas the peak ν_s-Si-O-Si is shifted from 1108 to 1104 cm^{-1}.

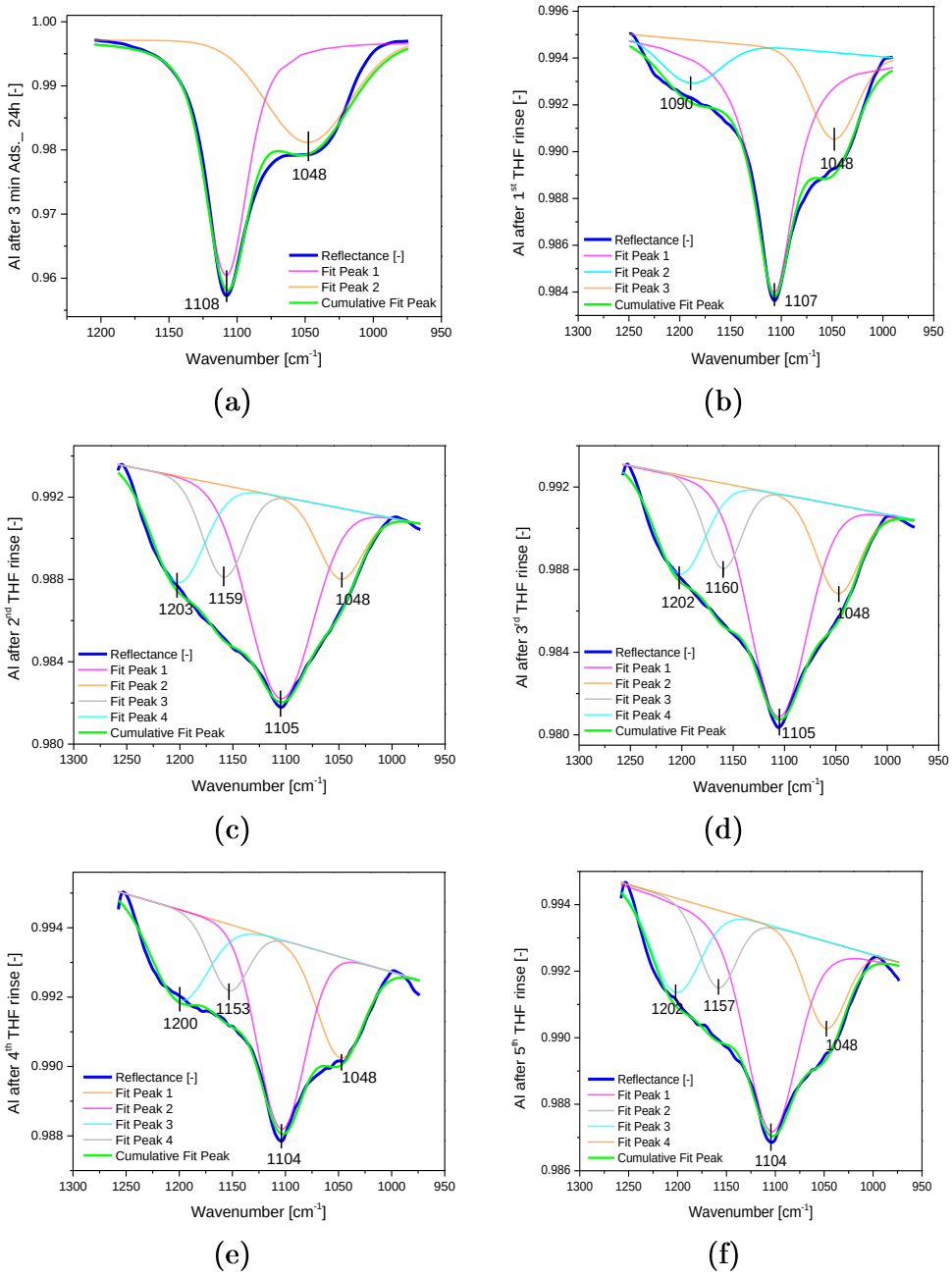


Figure 5.41. Fitted Si-O-Si stretching mode bands of prepolymer 2 in the spectra: (a) 3-min adsorption_24 h storage (c) after 1st THF (d) after 2nd THF and (d) after 3rd THF, (e) after 4th THF and (f) after 5th THF rinse.

(iii) Peak shifting of the ω-CH=CH_2 band at 957 cm^{-1} (bulk-like) to ~ 950 cm^{-1} accompanied by peak broadening. The broad band is found at 987-851 cm^{-1} where also stretching of Si-OH groups are typically displayed, and presumably, a new band is arising at 970-960 cm^{-1} associated with bounded siloxane segments to Al. It was shown that concentration of -OH groups increased over time (Figure 5.37) and traces of Si-

OH were found in the characterization of the prepolymer in bulk. The presence of -OH groups on the system was examined in the spectral region from 3700 to 3200 cm^{-1} (Figure 5.42). Interestingly, a decrease in the intensity of the band upon solvent rinsing is observed, which could be due to two main reasons: consumption of Si-OH groups in chemical bonding with the surface, forming Si-O-Al bonds, and to removal of physisorbed water and organic impurities containing -COH groups by THF.

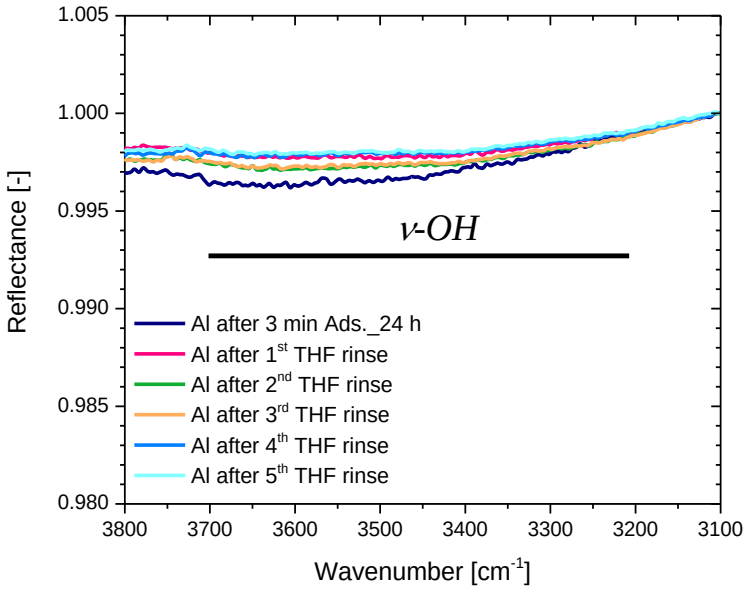


Figure 5.42. O-H stretching mode of prepolymer 2 (24 h storage time) upon THF rinsing.

Variation in molecular orientation towards a more stable adsorbed layer is represented by relative changes in peak areas of the characteristic bands of prepolymer 2 (Figure 5.43a-c). A sequential decreasing between THF rinses is not shown; instead, slight fluctuations are observed. The intensity fluctuations imply that some orientational adjustments occurred. The concomitant behavior between the δ_{as}-CH_3 and ν_s-Si-O-Si bands is verified by the similar trend displayed in the variation of the peak areas upon THF washing (Figure 5.43a,b).

In summary, by giving longer storage times, PDMS molecules were able to change their orientation and conformation on the surface, suggesting that mobility of the polymer chains was not significantly restricted by interactions but rather favored by removal of weakly adsorbed molecules. During 24 h of storage time, the adsorbed layer did not reach equilibrium conditions, although, the adherence of the prepolymer on the metal

was strong enough to resist up to 5 THF rinsing cycles. The Si-O-Si bond is tentatively assigned as the adhesion partner for prepolymer 2 on aluminum; however, existence of Si-OH groups should have also been responsible for strong adsorption.

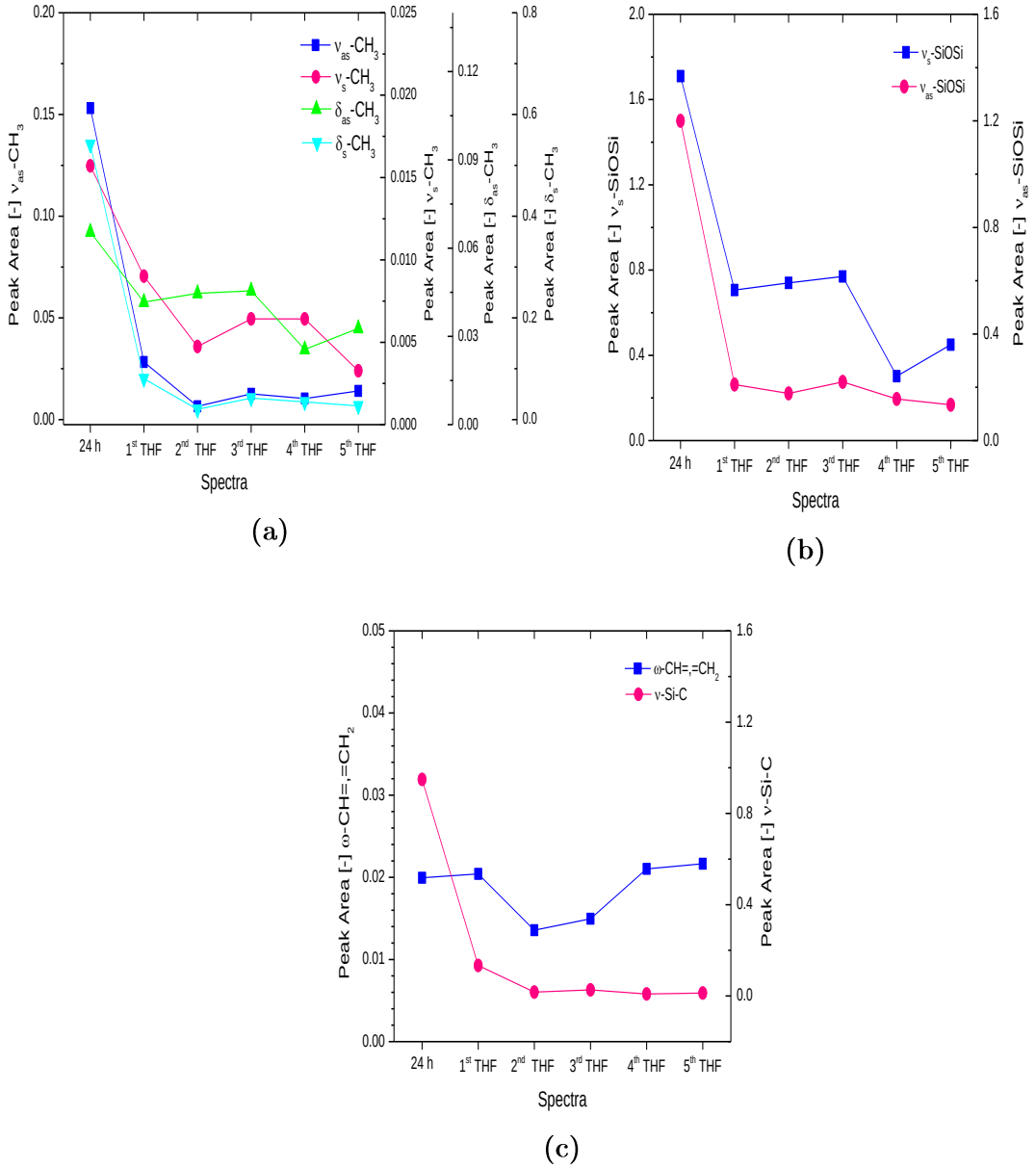


Figure 5.43. Variation of peak areas upon THF rinsing adsorption after 24 h of storage time for adsorbed di-vinyl terminated PDMS on Al, (a) bands related to CH_3 groups, (b) bands related to Si-O-Si groups and (d) bands related to $CH{=}CH_2$ an Si-C bonds.

5.5.3. Crosslinker – Tetrakis(dimethylsiloxy)silane (TDMS)

Unlike the two previous components, the adsorption behavior of TDMS on Al was only analyzed for 1 h storage time. TDMS possesses the same building units of di-hydride terminated PDMS; therefore, the adsorption of this component can give hints about effects of molecular size and structure in the adsorption of siloxane compounds.
First, the chemical state of the substrate prior to adsorption is evaluated by the ERA spectrum after it was rinsed once with THF (Figure 5.44). The spectrum reveals small negative absorbance bands (reverse spectrum) in the aliphatic C-H vibration region from 3000 to 2800 cm^{-1}, indicating removal of anchored contaminants. The positive band ascribed to the vibration mode of aluminum oxide (α-Al_2O_3) is found at ~975 cm^{-1} [360,376], suggesting oxide growth after THF rinse. Thus, besides cleaning the surface, THF induces structural changes to the aluminum oxide/hydroxide layer, which is consistent with previous observations.

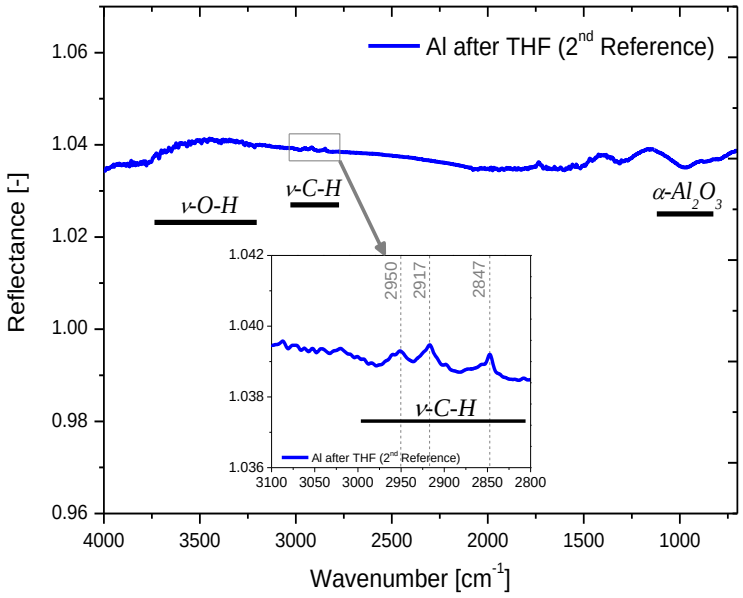


Figure 5.44. ERA spectrum of the Al surface after being rinsed once with THF and prior to adsorption of TDMS.

On the other hand, the spectra presented in Figure 5.45 yield information about the C-H stretching vibration modes of adsorbed TDMS on Al. Unlike prepolymer 1 and 2, the experimental spectra of TDMS do not replicate the calculated spectrum right after the 3-min adsorption, exposing the attainment of a thin adsorbed layer far from

bulk properties. Neither of the peak intensities decreased remarkably after the 1st THF rinse, as with the adsorption of PDMS.

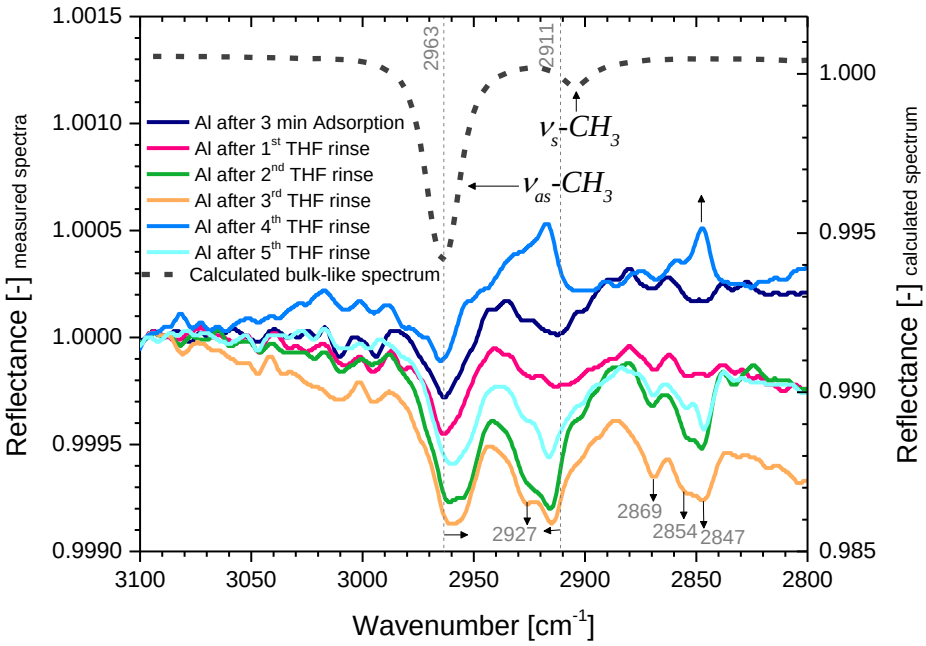


Figure 5.45. ERA spectra, recorded for p-polarization at θ=80° of TDMS on Al in the spectral range from 3100 to 2800 cm^{-1} related to C-H stretching vibration modes. The wavenumbers on the top correspond to the 3-min adsorption spectrum.

The interactions of the surface environment with adsorbed TDMS are a complex result of many different effects, and hence, such interactions are responsible for the most notable differences identified between the measured spectra and the bulk-like spectrum. The main features observed are:

- **Peak shifting of ν_{as}-CH_3.** The band shift from 2964 cm^{-1} (bulk-like and 3-min adsorption) to ~2959 cm^{-1} (after 5th THF rinses), advocating a variation in the chemical environment of CH_3 groups due to surface-induced changes in the structure of adsorbed TDMS. As explained by Piwowar [136], peak shifting in energy position towards lower frequencies clearly indicates modification of the chemical environment by either strengthening or weakening of the adsorption energy.
- **Progressive peak shifting of the ν_s-CH_3 band.** This peak is shifted to higher frequencies from 2905 cm^{-1} (bulk-like) to 2911 cm^{-1} after 3-min adsorption, and to 2916 cm^{-1} after five THF rinses. This consecutive peak shifting indicates continuous changes in the neighborhood of the methyl groups coming from different molecular

arrangements of TDMS within the adsorbed layer. As previously mentioned, FTIR position shift is sensitive to chemical and electronic environmental changes affected by a reaction, conformational changes, H-bonding, and strong intermolecular forces.

- **Peak shape distortions including peak broadening for ν_{as}-CH_3 and ν_s-CH_3.** These band shape distortions could have resulted, in part, from the anomalous dispersion of the refractive index of TDMS in the adsorbate state [351], and partly from intermolecular interactions and orientation effects.
- **Appearance of small bands at 2869, 2854, 2827 and 2847 cm^{-1}.** Most probably, they are associated with deposition of carbonaceous contaminants. This demonstrates that organic impurities can be readsorbed by the aluminum surface even after adsorption of TDMS, and competitive adsorption between traces of impurities and TDMS molecules could have taken place. This shows that the size of siloxane-containing species significantly affects the displacement and the adsorption of impurities. The presence of such contaminants was not as remarkable in PDMS as it seems to be for TDMS.
- **Dissimilar behavior of the spectrum after the 4th THF rinse.** This spectrum has not followed the expected trend, principally because the ν_s-CH_3 and the peaks at 2847 and 2854 cm^{-1} are no longer present. This behavior was either due to molecular orientation effects or to a measurement artefact. Vanishing due to chemical bonding involving methyl groups is discarded since the band related to ν_{as}-CH_3 is displayed in the same spectrum, and also after the 5th washing, the two bands are again recognized.

The variation in peak areas upon solvent rinsing of the ν_{as}-CH_3 and ν_s-CH_3 bands is illustrated in Figure 5.46. The peak areas were determined by fitting the peaks using Voigt profiles in the software tool OriginPro® 8.6. The peak areas of the bands change uniformly after successive contact with THF, confirming that they followed the same path upon solvent washing. The fluctuations observed within rinsing steps are attributed to orientation, interaction effects and readsorption of contaminants rather than removal of weakly adsorbed molecules. The variability of the peak areas exposes the inherent higher mobility of smaller molecules and the influence of adsorbed impurities.

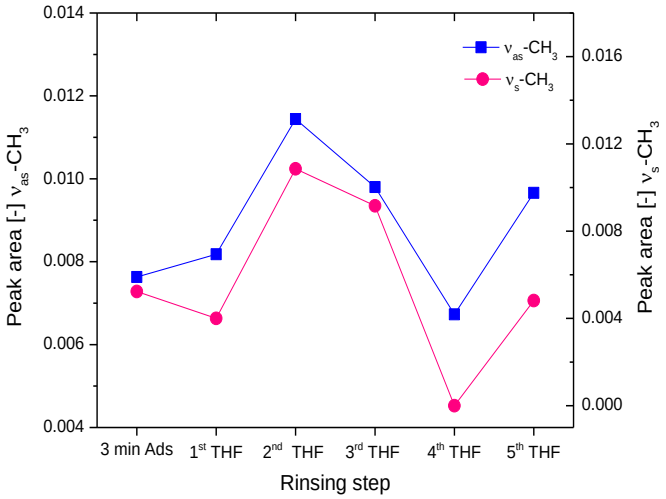


Figure 5.46. Variation of peak area upon rinsing step for the asymmetric and symmetric stretching modes of $-CH_3$ in TDMS.

Another important feature of adsorbed TDMS on Al, is peak shifting of the symmetric stretching mode of Si-H bonds (Figure 5.47). In effect, this band shifts irregularly towards both lower and higher wavenumbers with THF rinsing. This again suggests conformational changes of adsorbed molecules upon contact with fresh solvent, causing variations in the strength and specificity of the interactions involving Si-H bonds [377]. In addition, peak shifting is seen to be accompanied with distortion in peak shape and decrease in band intensity. These features indicate a distribution of different chemical states of Si-H segments within the adsorbed layer, arising from orientation effects and from attractive forces at the interface. The band did not vanish after five consecutive solvent rinses. Thus, the remaining Si-H peak comes either from unreacted segments of TDMS that are attached to the surface or from molecules unattached that were not washed off during THF rinses.

The change in intensity after THF washes was quantified by the peak area presented in Figure 5.48. The variation of the peak areas of ν-Si-H differs to the trend perceived for the stretching modes of methyl in Figure 5.46, which clearly indicates molecular conformational and orientational effects after each solvent rinsing. This confirms high mobility of the adsorbed molecules that leads to a dynamic process towards equilibrium, and demonstrates that a stable state was not attained at any stage of the experiment.

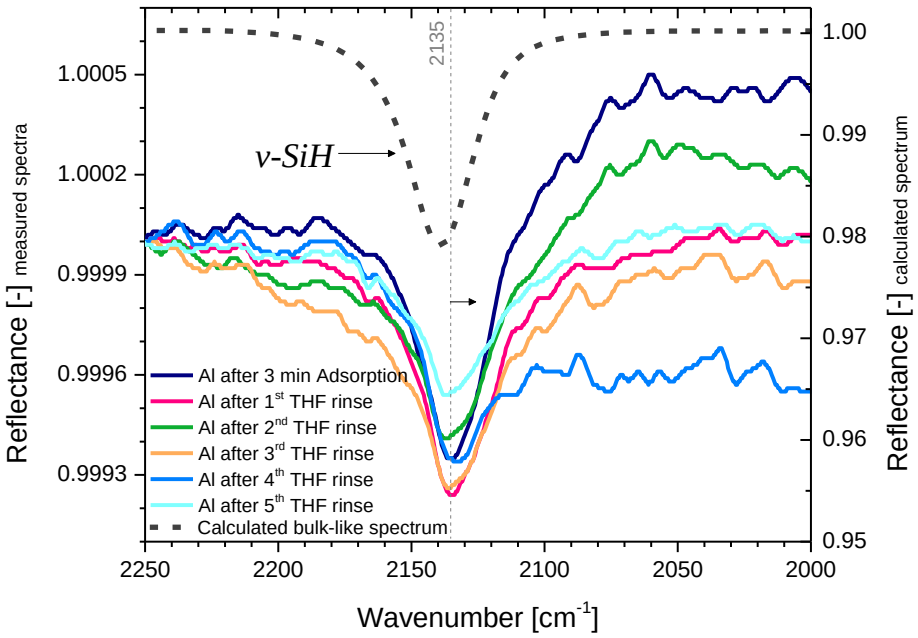


Figure 5.47. ERA spectra recorded for p-polarization at θ=80° of TDMS on Al in the spectral range from 2250 to 2000 cm^{-1} related to Si-H stretching mode. The wavenumber on the top correspond to the 3-min adsorption spectrum.

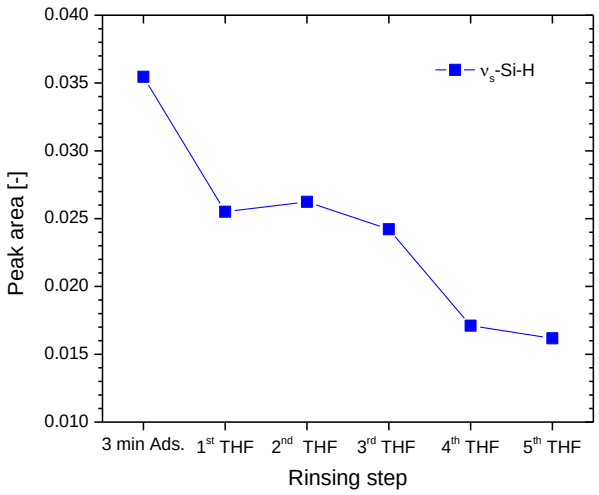


Figure 5.48. Peak area vs. rinsing step of ν_s-Si-H in TDMS.

On the other hand, reduction in peak intensity could be attributed to participation of silyl groups in a chemical reaction, e.g. towards formation of silanol groups (Figure 5.17). Simultaneously, -Si-OH groups could have either reacted with –OH groups on the metal surface, creating Si-O-Al covalent bonds, or with other SiOH groups forming Si-O-Si segments. The spectral range from 3900 to 3100 cm^{-1} corresponding to O-H

stretching mode is inspected for verifying the occurrence of any reaction yielding Si-OH (Figure 5.49). The ERA spectra lack bands in the ν-OH region, indicating that if -Si-H reacted to form -Si-OH groups, the latter were either rapidly chemisorbed on the surface or condensated towards -Si-O-Si- formation.

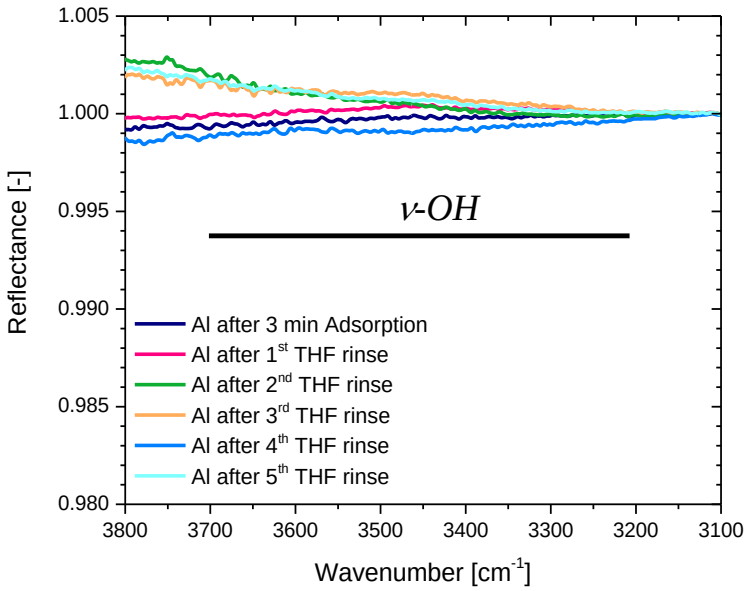


Figure 5.49. ERA spectra from 3800 to 3100 of O-H stretching mode in adsorbed TDMS.

In Figure 5.50, the ERA spectra in the fingerprint region show rich spectral features that evidently differ from the bulk state of TDMS. In contrast to the adsorption of PDMS, neither the spectrum after 3-min adsorption nor the spectra after THF rinses replicate the calculated bulk-like spectrum. Moreover, the peak intensities do not strictly decrease upon solvent rinsing, instead, there is a fluctuating behavior associated with variations in the transition dipole moment of the system, proving once again molecular orientation effects. The bands are recognized after rinsing the sample extensively with THF, which proves that TDMS was strongly attached to the aluminum surface.

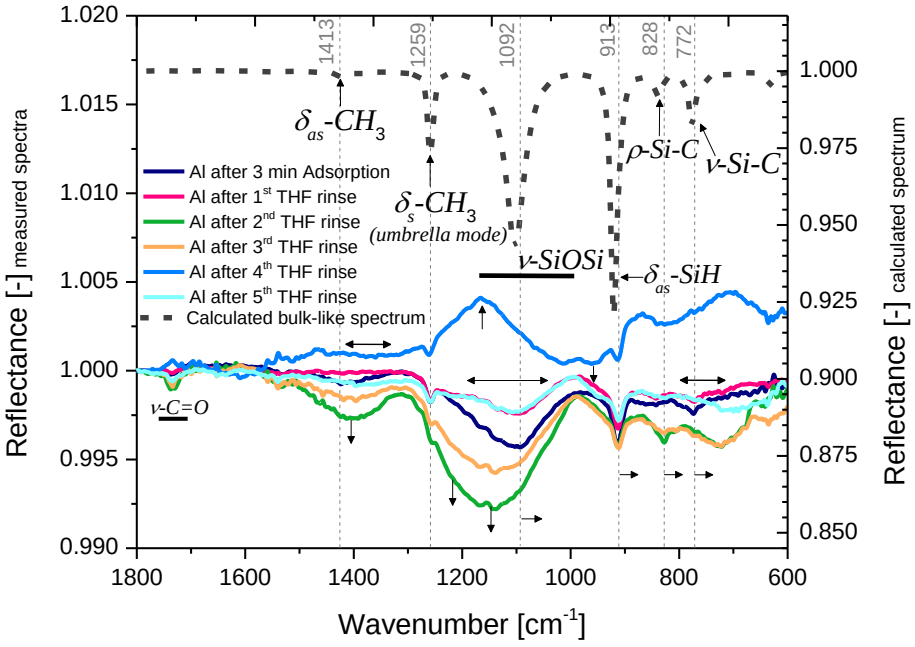


Figure 5.50. Fingerprint region of the adsorbed TDMS on aluminum after 3-min adsorption step and five THF rinsing cycles. The dotted spectrum corresponds to the calculated bulk-like one. The wavenumbers given on top correspond to the spectrum after 3-min adsorption, except for the band at 828 cm^{-1} which corresponds to the spectrum after the 2nd THF rinse.

Closer inspection of the spectral region from 1500 to 1320 cm^{-1} reveals shifting of the δ_{as}-CH_3 band from 1429 cm^{-1} to lower frequencies ~1403 cm^{-1}, accompanied by outstanding peak broadening. This feature was also identified in the adsorption of the two prepolymers, indicating that when siloxane-containing molecules are adsorbed onto Al, peak broadening of δ_{as}-CH_3 will occur. However, this effect seems more noticeable for TDMS than for PDMS, probably because deposition of organic impurities on the surface was favored in the adsorption of TDMS. Contaminants could have come from different sources including: dissolved Scotch tape in THF, PVC tubes dissolved in THF and the purging air after rinsing with THF [371]. Consequently, the influence of contaminants on the vibration modes of methyl groups is confirmed. The shifting in peak position towards lower frequencies upon solvent rinsing reveals weakening of the bond energy due to a change in the chemical environment of the methyl groups in the adsorbate state [136,370]. Additionally, a concomitant behavior is observed between this absorption band and the one ascribed to stretching vibrations of Si-O-Si, which is consistent with previous observations in the adsorption of PDMS.

Comparison of the spectra between rinsing steps in the region ascribed to stretching mode of Si-O-Si at 1250 to 950 cm^{-1} exhibits marked peak shape distortion, peak

broadening and arbitrary changes in intensity. Peak broadening in the high-frequency side is possibly due to peak overlapping, with new bands emerging at 1200-1150 cm^{-1}, whereas broadening on the low-frequency side can be attributed to siloxane segments attached to the surface by H-bonding. Application of the so-called "surface selection rule" to these ERA spectra allows us to propose that the observed intensification of the bands after some solvent rinses was due to an orientation effect, in which the perpendicular component (in respect to the surface) of the transition dipole moments for the vibrational modes was enhanced. Thus, throughout THF rinses, the molecules changed their configurational distribution and packing density arbitrarily. In addition, the ν_{as}-Si-O-Si band undergoes peak shifting from 1102 cm^{-1} (calculated spectrum) to 1094 cm^{-1} (measured spectra) evidencing strong interactions such as H-bonding involving hydroxyl protons of the surface and the siloxane oxygen atoms of TDMS (Al-OH · · · OSi-). All these outstanding features allow us to define siloxane segments as the adhesion partners of TDMS on aluminum, which is consistent with previous suppositions done for the two prepolymers.

More detailed analysis of the Si-O-Si stretching band was achieved by peak fitting of the broad bands using a Voigt function. The fitted bands are presented in Figure 5.51a-e and the data of the peaks are given in. In all cases, the broad band is dominated by a peak centered at 1094-1096 cm^{-1} assigned to Si-O-Si asymmetric stretching mode. Three peaks at 1171, 1136, and 1040 cm^{-1} are also distinguished for all five spectra, along with an additional peak at ~1220 cm^{-1} only for the spectra after the 2nd and 3rd THF rinses. Exact assignment of these additional peaks is still undefined; however, previous adsorption experiments of prepolymers showed that upon solvent rinsing, bands or shoulders at 1240-1130 cm^{-1} emerged, and a broad weak band between 930 and 1050 cm^{-1} appeared. The shoulder was tentatively related to changes on the aluminum surface induced by successive contact of the substrate with pure THF solvent. In effect, peaks around 1200, 1130 and 1038 cm^{-1} were recognized by Gilbert [371] when the substrate was rinsed once and several times with THF. Moreover, the band at 930-1050 cm^{-1} has been associated with bounded -Si-O-Si- segments to aluminum either through H-bonding [325], or with -Si-O-Al covalent bonds [36,154].

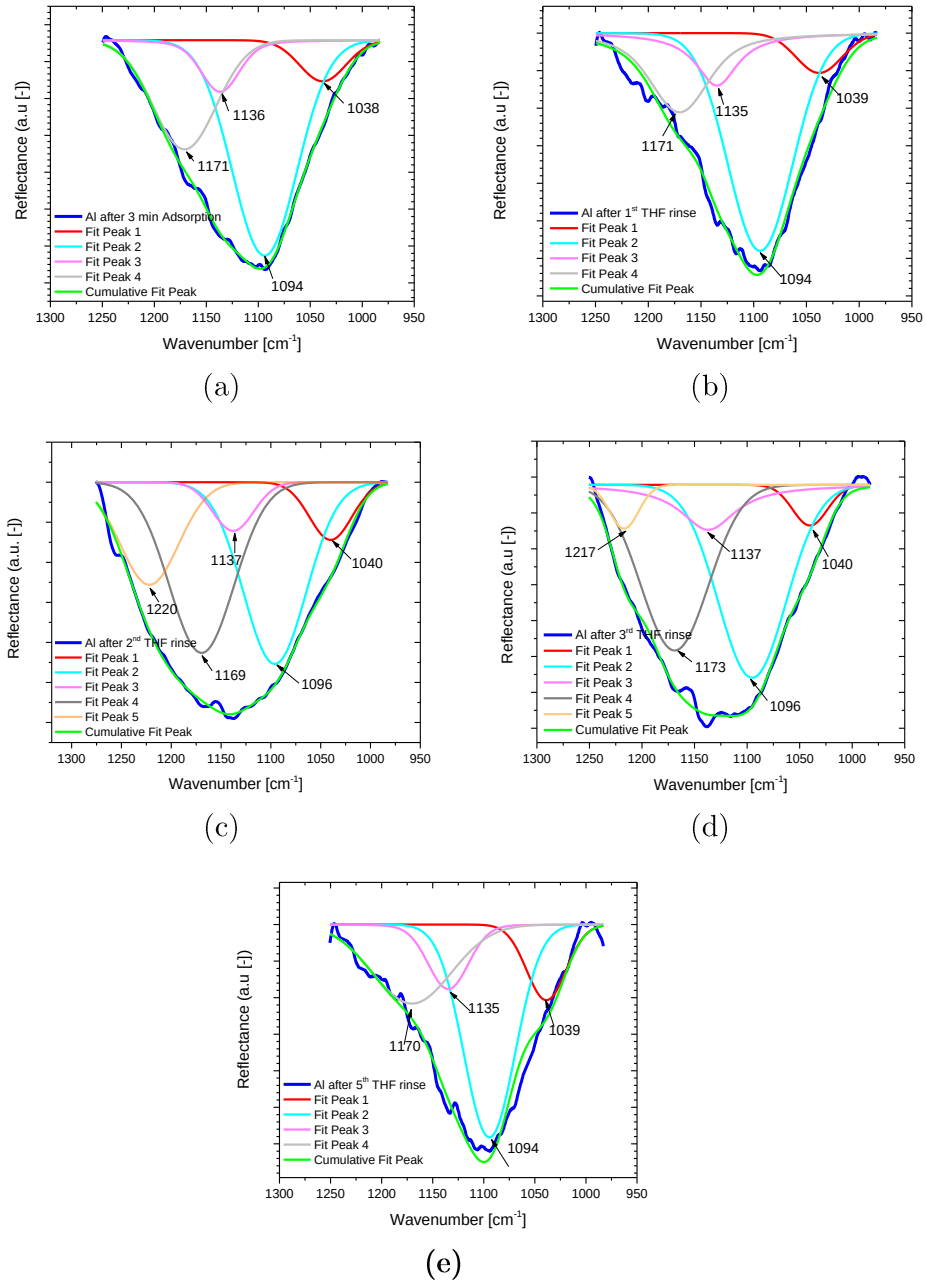


Figure 5.51. Fitting of the asymmetric stretch vibration of Si-O-Si in TDMS for the measured spectra: (a) Al after 3 min adsorption, (b) Al after 1st THF rise, (c) Al after 2nd THF rinse, (d) Al after 3rd THF rise and (e) Al after 5th THF rinse.

Additional spectral changes identified in the fingerprint region of the measured spectra of adsorbed TDMS are: **(i)** peak shifting of the Si-H asymmetric bending (δ_{as}-Si-H) from 921 cm^{-1} (bulk-like spectrum) to 913 cm^{-1} (measured spectra), attributed to intermolecular interactions. The peak is noticeable even after five THF rinsings, confirming that if Si-H species were involved in any chemical process, they were not

totally consumed; **(ii)** peak shifting and tendency of vanishing for ρ-Si-C at 828 cm^{-1} and ν-Si-C at 772 cm^{-1}. The shift in position evidences the effect of intermolecular interactions of the Si-O-Si segments on the Si-C bonds, whereas vanishing reveals strong orientation and conformation effects, **(iii)** transformation of the baseline upon exposure to pure THF into a more buckled type. This advocates alterations in the structure of the aluminum surface partly attributed to adsorption/desorption events of carbon-containing species, and to changes in absorption of the surrounding atmosphere of the sample [352]; **(iv)** absence of the broad bands at 1500-1320 cm^{-1} and at 1250-930 cm^{-1} points to remarkable orientation and conformation effects but not to desorption, since bands at 1259 and 913 cm^{-1} associated with δ_s-CH_3 and δ_{as}-Si-H, respectively, are perceived. This behavior might have also resulted from an unknown artefact; (v) positive peak at 1735 cm^{-1} (ν-C=O). This peak is perceived in the reference spectrum (Figure 5.44) as a negative signal, but it is exhibited as a positive band upon solvent rinsing (Figure 5.50). This supports the readsorption of contaminants during the execution of the experiments [371]; **(v)** Stability of the δ_s-CH_3 band centered at 1259 cm^{-1}. As it was observed in the adsorption of the two prepolymers, this band remains unaffected in position upon solvent washing.

Molecular orientation effects are evidenced by relative fluctuations in the peak areas of the bands in the fingerprint region (Figure 5.52a-c). These variations consistently suggest that the adsorbate did not reach its most stable thermodynamic state during the whole experiment. Molecular arrangements at the interface were governed by an interchange between energetics of surface-specific interactions and the entropic factors associated with molecular conformations and improvement of packing density [378]. This conformational effect seems to be more remarkable in TDMS than in PDMS due to the noticeable differences in molecular size and structure. It could be assumed that TDMS molecules orientated on the substrate with siloxane and silyl bonds parallel to the surface in order to enhance intermolecular interactions with the surface. Based on its molecular structure (Table 4.15), TDMS possesses four Si-O-Si and four Si-H segments available for interactions; however, due to steric hindrance it is impossible to have all such groups simultaneously oriented near the metal surface. Consequently, fluctuation in peak areas can be attributed to the numerous possible orientations that TDMS molecules could adopt with different siloxane and silyl groups pointing randomly to the surface.

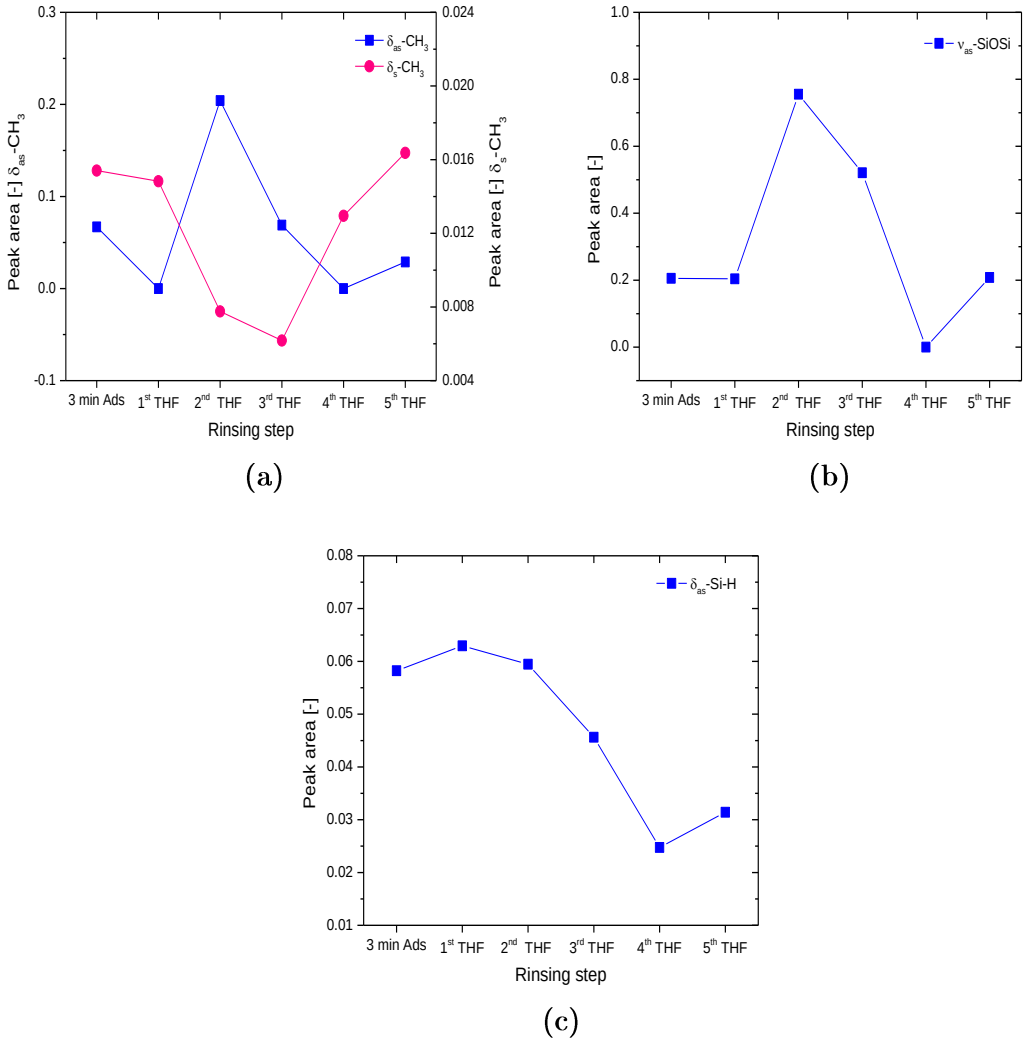


Figure 5.52. Change in peak areas upon rinsing steps of the main bands in the fingerprint region of adsorbed TDMS: (a) $\delta_{as,s}$-CH_3, (b) ν_{as}-Si-O-Si, and (c) δ_{as}-Si-H. Peak areas of the bands ascribed to ρ-Si-C and ν-Si-C were not included due to ambiguities.

In summary, the adsorption behavior of TDMS seems to be more sensitive to readsorption of contaminants when compared with the adsorption of PDMS prepolymers. Hence, the molecular size and packing density of siloxane-containing species play an important role in the ability of displacing or inhibiting physisorption of impurities, but not in the strength of adhesion. TDMS shows strong adherence to the substrate, as it was not desorbed after five consecutive THF rinsing cycles.

5.5.4. Karstedt catalyst: Pt(0)-divinyltetramethyldisiloxane complex in monovinyl terminated PDMS.

First, the state of the aluminum substrate prior to is illustrated in Figure 5.53. The spectrum reveals a negative band at ~2982 cm^{-1} together with two positive weak peaks at 2933 and 2857 cm^{-1} assigned to stretching modes of C-H bonds in alkanes. The negative peak confirms partial elimination of contaminants by the solvent, while the positive peaks indicate readsorption of impurities, but only to a small extent. The positive band displayed at 1015 cm^{-1} is assigned to vibrations of the aluminum oxide layer [189,360,371] and suggests a growth of the oxide layer after contact with pure THF. Features at 1400-900 cm^{-1} accompanied with drifting of the baseline, suggests that THF induces certain structural changes to the aluminum oxide layer, as previously claimed.

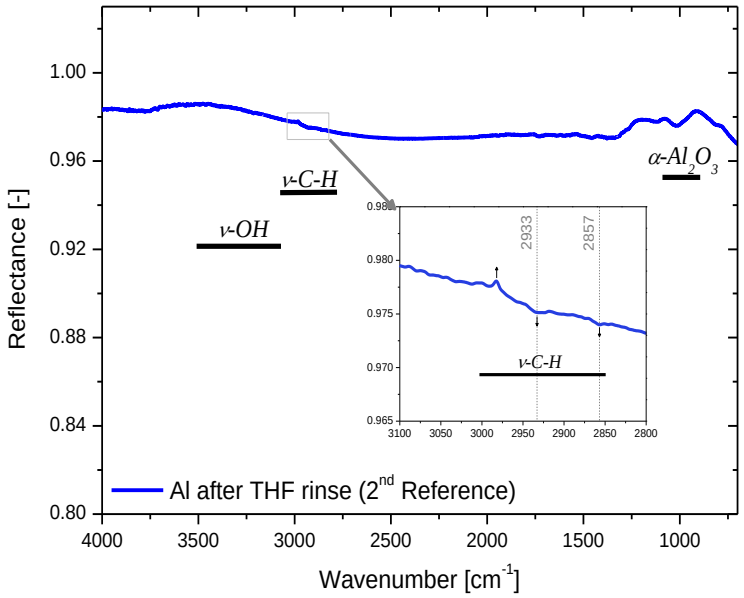
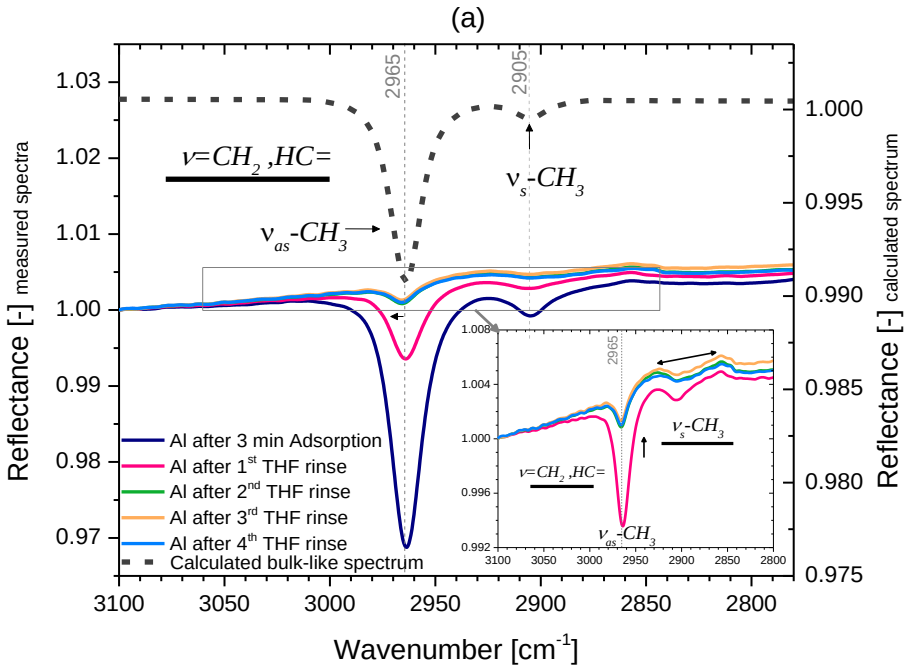


Figure 5.53. ERA spectrum of the aluminum surface prior to adsorption of the Karstedt catalyst (after one THF rinse)

The measured spectra of the adsorbate state of the Karstedt catalyst on Al upon THF rinsing (Figure 5.54a-b) shows that after the 3-min adsorption step, the sample has a bulk environment, i.e., the adsorbate is many layers thick, presenting bulk characteristics. This indicates that the vibration modes of the catalyst are initially

unaffected by the substrate; thus, insignificant changes in peak positions and peak shape are perceived, and neither new peaks nor disappearance of absorption bands are noticed at this experimental stage. This behavior is consistent with previous observations in adsorbed di-vinyl and di-hydride PDMS, which also replicated the calculated spectrum right after adsorption. Based on the results attained so far, it can be stated as a general rule that independently of the molar mass and end-functionality, adsorbed PDMS from diluted solution in THF will reproduce a bulk-like spectrum under the experimental conditions used here (3 min adsorption at RT on native aluminum oxide surface).

Comparison of the spectra before and after the 1st THF washing shows a prominent reduction in peak intensities as a consequence of significant desorption of bulk catalyst after solvent contact. Upon further consecutive rinses, the peak intensities are seen to be almost invariable, advocating the attainment of a stable state. Consequently, for obtaining a thermodynamically stable adsorbed layer of Karstedt catalyst only two THF rinses were required; by contrast, three or four THF rinsing cycles were usually needed for the two prepolymers 1 and 2. In addition, the FTIR baseline seems to drift during the experimental procedure, addressing possible structural changes of the surface [42,371], small changes in the environmental conditions of the system [352], and scattering of light on the thin layer [42,52].



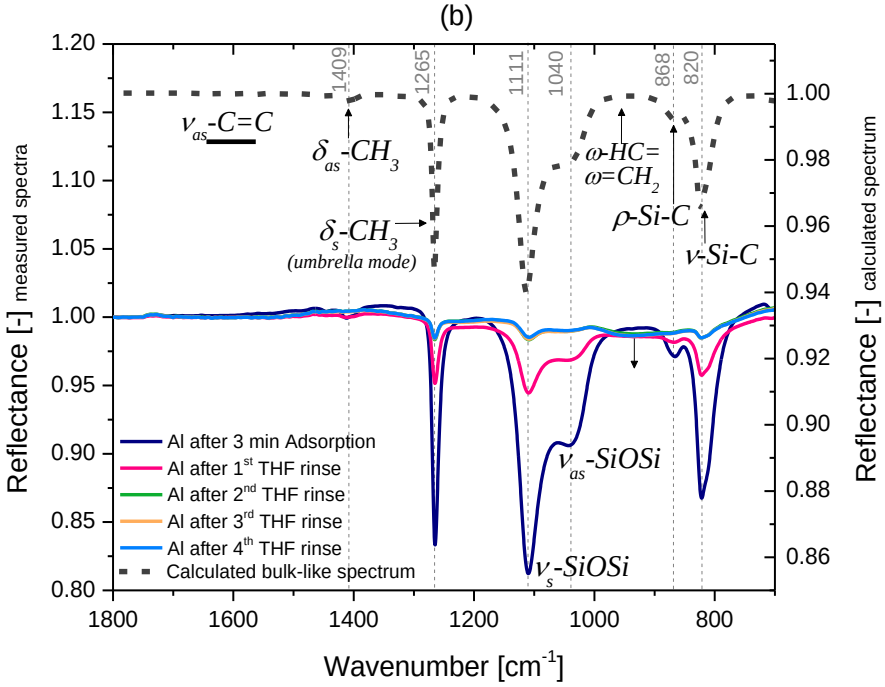


Figure 5.54. Calculated bulk-like spectrum and measured ERA spectra of adsorbed Karstedt catalyst on Al after THF rinsing steps (a) from 3100 to 2800 cm^{-1} and (b) fingerprint region from 1800 to 600 cm^{-1}.

The IR bands of C-H asymmetric and symmetric stretching modes of methyl groups at 2965 cm^{-1} (ν_{as}–CH_3) and at 2095 cm^{-1} (ν_s–CH_3), respectively, are presented in Figure 5.54a. Interestingly, despite the Karstedt catalyst being dissolved in mono-vinyl terminated PDMS, the respective asymmetric and symmetric vibrations of C-H bonds in vinyl groups at 3100-3000 cm^{-1} are imperceptible in the measured spectra. In fact, these bands were also weakly displayed in the bulk ATR spectrum; thus, it is not surprising that they are indistinguishable here.

Moreover, following the consistent trend observed in the adsorption of the two prepolymers, the ν_s–CH_3 band of the catalyst is broadened irregularly and the ν_s–CH_3 peak is distorted in the low-frequency side. This broadening is believed to be caused both by attraction forces at the interface affecting the stretching vibration modes of methyl groups, and by inhomogeneities within the adsorbed layer [362]. Such features involving methyl groups lead to the assumption that independently of the molar mass and chemical nature of the end-groups, -CH_3 stretching modes in PDMS will display line broadening as a consequence of intermolecular interactions and possible dispersion effects of the refractive index of the adsorbate [351]. Electronic structure studies of PDMS interacting with silica, executed by Evmenenko and coworkers [378], have

determined that the dominant adhesive interaction is created between the H atoms on PDMS methyl groups and the O atoms in the surface hydroxyl groups (-$OSiCH_3 \cdot \cdot \cdot$ OH-Si), whereas the interaction between the Si-O groups of PDMS molecules and silica surface was defined to be very weakly adhesive via van der Waals bonds[378]. In effect, Barthel and Nikitina [102] who also studied a PDMS-silica system, have also declared that interactions involving siloxane bonds were weak in nature. Contrary to those studies, the results obtained in this work indicate that the dominant interactions between PDMS and aluminum involve the siloxane bond, most likely via H-bonding between the oxygen of siloxane units in PDMS and protons of the hydroxyl groups of the surface (-SiO $\cdot \cdot \cdot$ HO-Al), and via dipole-dipole interactions. However, interactions involving methyl groups must also play a relevant role in the adsorption of PDMS on Al. In order for methyl groups to interact, PDMS molecules might be oriented with some methyl groups near the aluminum surface.

It is interesting to observe that no peaks related to contaminants are perceived in this region, indicating that initial physisorbed carbon-containing species were reversibly adsorbed and can be replaced by catalyst molecules from solution. Furthermore, the readsorption of aliphatic contaminants is seen to be inhibited throughout the experiment, exposing again the ability of PDMS molecules to displace contaminants. This indicates that long siloxane-containing molecules dislocate physisorbed contaminants more effectively than their smaller counterparts.

Analysis of the magnified measured spectra in the fingerprint region from the 1st to the 4th THF rinsing steps (Figure 5.55) allows for the discussion of important spectral features of the detected absorption bands, as follows:

- **Negative peak at 1743 cm^{-1} (ν–C=O).** This peak indicates that concentration of the carbonyl group on the surface decreased in comparison to the reference spectrum (Figure 5.53). Thus, carbonyl groups from impurities were removed during the 3-min adsorption step and upon pure THF rinsing; they were not readsorbed again on the surface.
- **Broadening and blending of the peak at 1409 cm^{-1} (δ_{as}-CH_3).** This feature is consistent with previous observations upon adsorption of PDMS and TDMS. Line broadening possibly reveals environmental changes in the vicinity of the methyl groups, affecting their electronic structure and hence, the force constants of the molecule. However according to Gilbert [371], perturbations in the baseline are present between 1500 and 1380 cm^{-1} when metal surfaces, including aluminum, are rinsed by THF.

- **Steadiness of the umbrella mode at 1265 cm^{-1} (δ_s-CH_3).** This peak remains invariable in position, sharpness and symmetry within the measured spectra. Slight alterations observed can be attributed to buckling of the baseline. This behavior of δ_s-CH_3 was also perceived in the three SSMC analyzed before; consequently, it can be claimed that δ_s-CH_3 is unaffected by interactions created upon adsorption of silicones on aluminum.

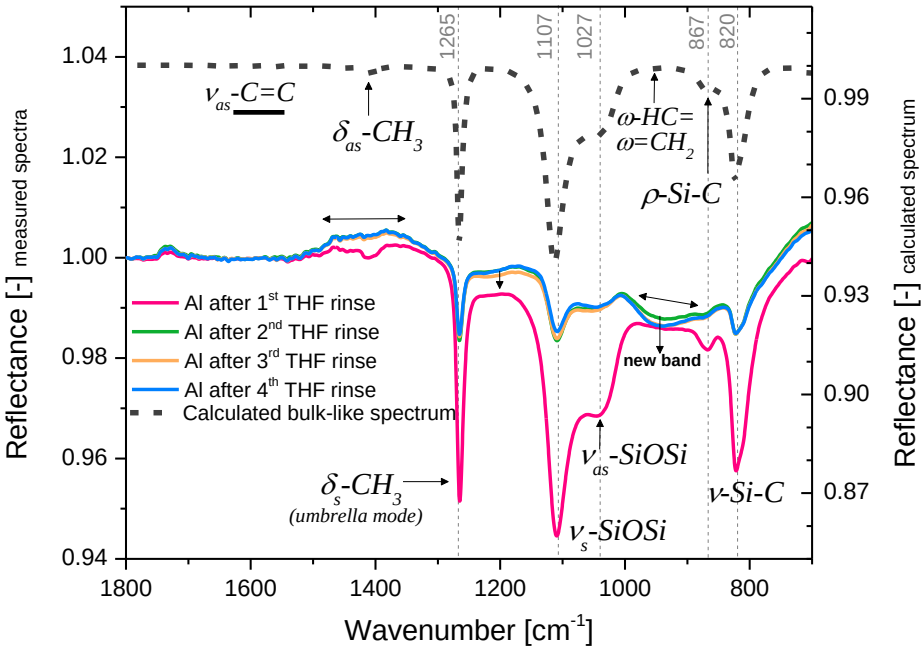


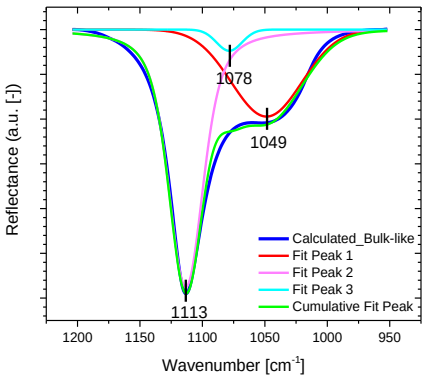
Figure 5.55. Magnified ERA spectra of Al after THF rinsing steps in the fingerprint region from 1800 to 700 cm^{-1}.

- **New emerging shoulder at 1240-1180 cm^{-1}:** The precise assignment of this new band is undefined. Its appearance could have four possible causes: first, adsorption of impurities; second, involvement of catalyst in a chemical reaction, third, modification in the chemical structure of the aluminum (hydro)oxide layer, and fourth, to vibrations related to methylene groups from n-butyl terminal functionalities. The first possibility is very unlikely to have occurred, since bands related to contaminants were hardly visible in the measured spectra. Also, IR absorption bands associated with common contaminants in the experiments are not usually displayed in this region [371]. Participation of the Karstedt catalyst in a chemical reaction is uncertain since bands ascribed to vinyl groups are imperceptible in all measured spectra, thus, it is not possible to follow the evolution of vinyl groups

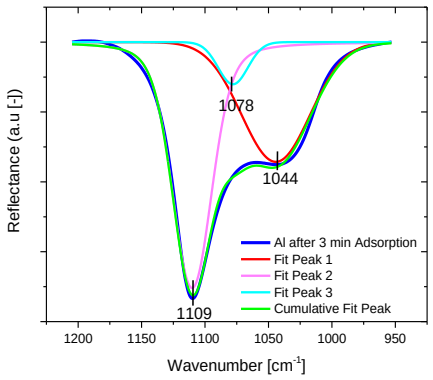
upon THF rinsing. This new shoulder was consistently perceived in the adsorption of the two prepolymers and TDMS, indicating that it is not an exclusive feature of Karstedt catalyst. Contribution from vibrating modes of Si-CH_2 groups is very likely, as the catalyst is dissolved in n-butyl terminated PDMS. Contribution due to structural modifications of the aluminum surface after rinsing with THF also seems very probable. As previously mentioned, the spectral range from 1400 to 900 cm^{-1} of the aluminum substrate is normally sensitive to changes upon contact with THF.

- **Peak shifting of the ν-Si-O-Si bands at 1200-950 cm^{-1}:** To examine carefully the shifting of the doublet at 1200-950 cm^{-1}, peak fitting was performed in OriginPro® 8.6 using a Voigt function (Figure 5.56a-e). The ν_s-Si-O-Si and ν_{as}-Si-O-Si are both displaced by 4 cm^{-1} in the measured spectra. As with the two PDMS prepolymers and TDMS, such peak shifting is an outstanding sign of intermolecular interactions existing at the interface [362]. Moreover, the consistent trend of the peak at the lower frequency to decrease upon exposure to THF is also shown here. Table 5.8 shows that the additional peak at 1078 cm^{-1} broadens progressively in order to compensate for the decrease in intensity of the ν_{as}-Si-O-Si band. In contrast, the two IR absorption bands narrow successively until the 2nd THF rinse, when a stable adsorbed layer is attained.

This behavior of the siloxane bond was previously elucidated in the work of Jemmett [122,123], who observed that the silicon-oxygen absorption peak moved slightly to a lower wavenumber and had altered in shape as a result of the interactions between the metal surface and the oxygen in the siloxane molecule.



(a)



(b)

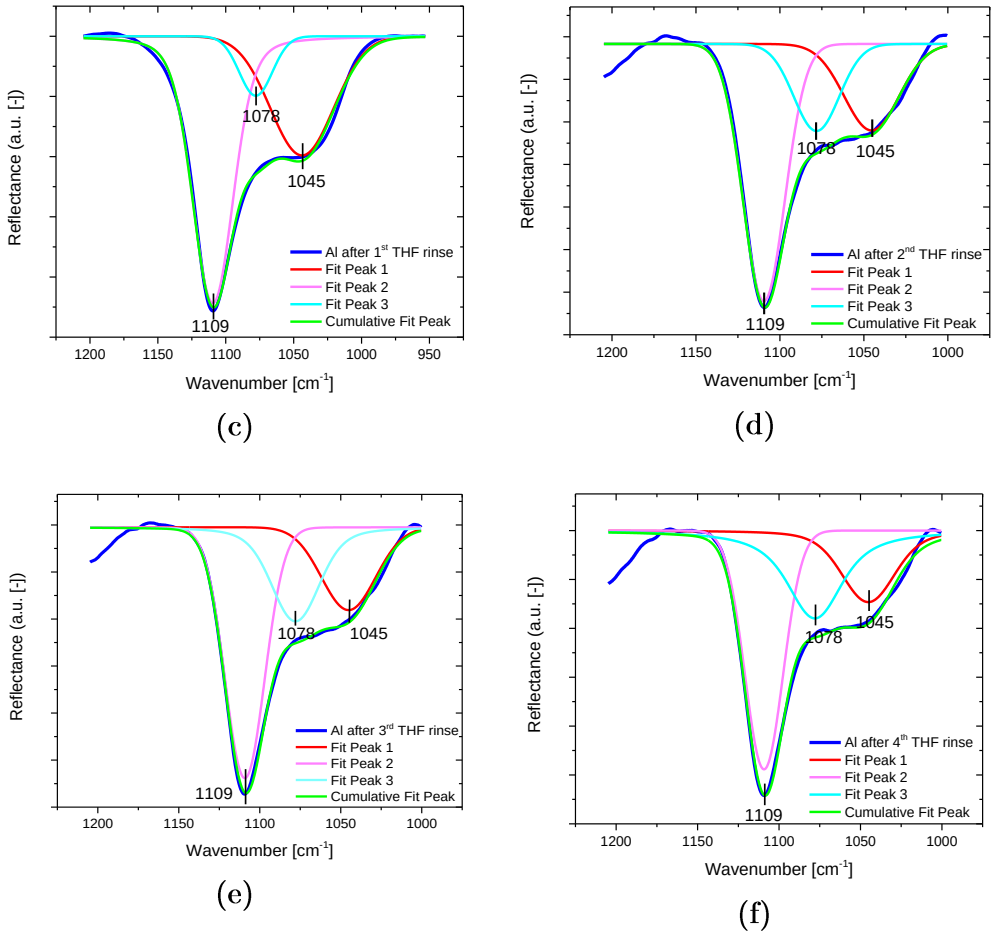


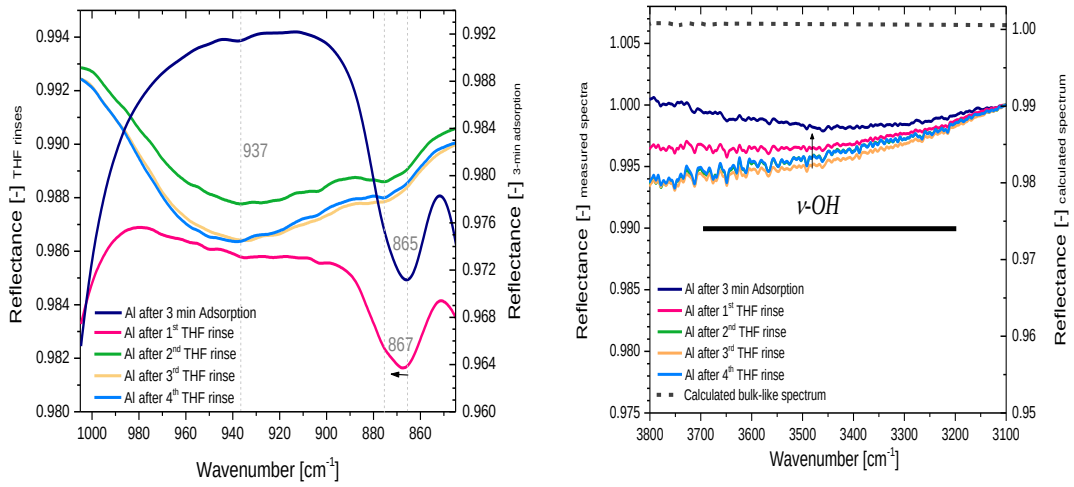
Figure 5.56. Peak fitting of the Si-O-Si stretch vibration mode of adsorbed Karstedt catalyst on Al. (a) Calculated bulk-like spectrum, (b) Al after 3 min adsorption, (c) Al after 1st THF rise, (d) Al after 2nd THF rinse, (e) Al after 3rd THF rise and (f) Al after 4th THF rinse

- **New band at 1000-850 cm^{-1}:** This feature is in agreement with previous results obtained in the adsorption of the two prepolymers and the crosslinker. Therefore, as a general assumption, adsorption from diluted solution of siloxane-containing species on aluminum will display a new band at 1000-850 cm^{-1}. Principally, this band has been assigned to siloxane segments bound to aluminum. The appearance of this new feature centered at ~940 cm^{-1} (Figure 5.57a) supports that adsorption of silicones on aluminum is governed by strong interactions at the interface involving the siloxane bond. The homogeneous peak broadening observed in this band could suggest preferential short-range interactions at the interface.

Nevertheless, different overlapping vibrations modes in this range could presumably have contributed to the intensity and broadening of this band, such as: **(i)** vibration mode of the aluminum oxide layer (α-Al_2O_3) is typically displayed at 1080-860 cm^{-1}

[360], thus, possible uncovered aluminum regions could be detected in the analyzed area; **(ii)** stretching vibration mode of Si-OH groups from traces of hydroxyl terminated PDMS or from newly formed silanol groups from siloxane bond cleavage (Figure 4.7). Analysis of the O-H stretching mode in the ERA spectra (Figure 5.57b) does not reveal plausible formation of OH groups upon THF washing; consequently, contribution of OH groups to peak broadening upon solvent rinsing can be considered insignificant; **(iii)** vibration of Si-O-Al bonds [36,189,190,379]. The relatively rapid attainment of a stable adsorbed layer, just after two THF rinses, could support the occurrence of chemisorption. Possibly, Si-O-Al bonds were created by the reaction between Si-OH groups (from traces) and Al-OH on the surface. In order for this reaction to occur, initial traces of molecules containing Si-OH groups must have been adsorbed onto the aluminum oxide simultaneously with PDMS and Pt-complex molecules. In competitive adsorption, polymers of different adsorption energies will experience surface selectivity [380]; thus, more polar polymers would be preferentially adsorbed first [381]. In addition, shorter chains are first adsorbed but displaced by longer molecules due to entropic effects [382]. Hence, due to the high polarity, the good proton-donor-acceptor properties of -OH groups [383], and the shorter size of -OH terminated PDMS, shorter chains with OH were likely to be adsorbed first, creating strong interactions with Al-OH. The role of the Pt catalyst in stabilizing or favoring the formation of -Si-OH groups, Si-O-Al bonds or creating a kind of siloxane-aluminum complex is still undefined; but an effect exists, as thermodynamic equilibrium was attained more rapidly than its equivalent di-vinyl PDMS prepolymer. So far as the author is aware, there is no available literature discussing this issue. However, secondary reactions during hydrosilylation in Figure 4.7, suggest that condensation between silanols and hydride siloxane occur in the presence of Pt catalysts. It could be supposed that the Pt(0) complex plays a similar role between Si-OH and OH-Al groups.

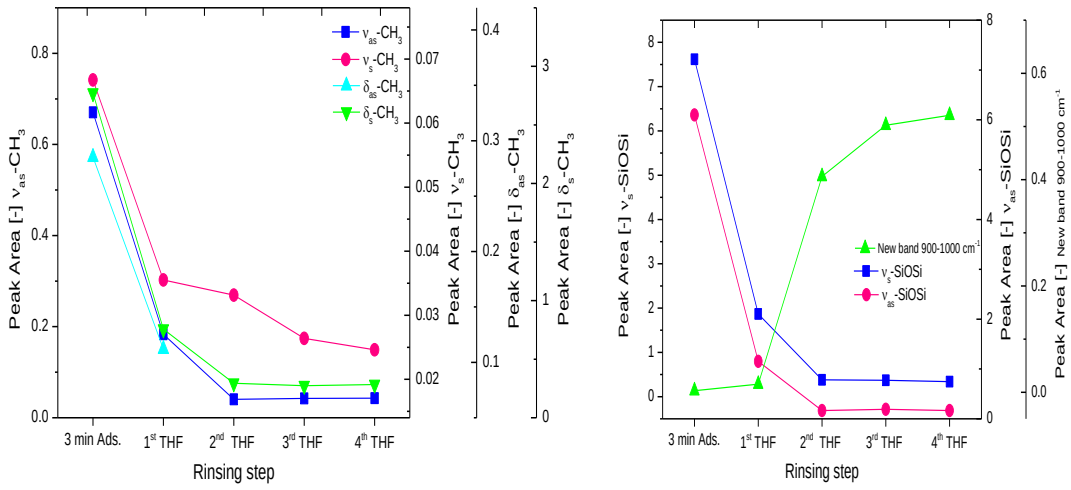
- **Peak shifting of the ρ-Si-C and ν-Si-C bands**. These two bands are slightly shifted to lower frequencies in the measured spectra when compared to the bulk-like spectrum, indicating weakening of the Si-CH_3 units due to interactions of PDMS with the surface.



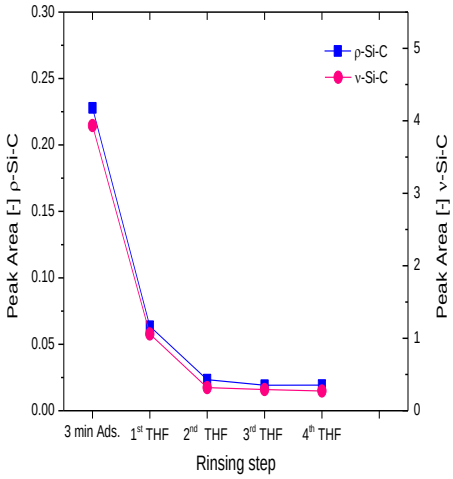
(a) (b)

Figure 5.57. Evolution upon rinsing of: (a) new spectral band at 1004-844 cm^{-1} and (b) O-H stretching vibration mode at 3700-3200 cm^{-1} of adsorbed Karstedt catalyst on Al.

Finally, molecular orientation effects are examined by plotting the integrated peak areas as a function of the rinsing step (Figure 5.58a-c). The plots exhibit a clear uniform trend in the variation of peak intensities to decrease up to the 2nd THF rinse and remain unchanged with further solvent rinses. However, the new band at ~ 938 cm^{-1} increases upon THF washing, suggesting strengthening of the interaction at the interface. Interactions created after the 2nd THF rinse are strong enough to suppress the molecular orientation effects, advocating short-range interactions or chemisorption.



(a) (b)



(c)

Figure 5.58. Variation of peak areas of the absorption bands of Karstedt catalyst upon rinsing steps of (a) methyl groups, (b) siloxane groups, and (c) Si-CH_3.groups

In summary, adsorbed catalyst displayed infrared absorption bands typical of vinyl PDMS polymers, since it was dissolved in monovinyl terminated PDMS. As expected, the spectrum right after adsorption duplicated the calculated bulk-like spectrum, and upon further solvent washing, the spectra exhibited features that indicated the formation of intermolecular interactions between the catalyst and the Al surface. As it was defined for the other SSMC, the siloxane bond is tentatively claimed as the adhesion partner in the adhesion of the Karstedt catalyst on Al. The appearance of a broad band with the center at ~938 cm^{-1}, after the 2^{nd} THF rinsing, attributed to bounded Si-O-Si segments may also imply that adhesion mechanisms of the catalyst on Al were also dominated by covalent Si-O-Al bonds. Such covalent interaction was probably favored by the Pt-complex through Si-OH groups. The Si-OH groups could have been either produced during the experimental trial or already contained in the bulk catalyst sample. The role of the Pt(0) complex in the adsorption of PDMS is still unclear, but based on the results obtained in this study, it shall favor -Si-OH or Si-O-Al formation promoting covalent bonding with the substrate. The rapid attainment of a stable adsorbate layer, just after two THF rinses, supports the hypothesis of possible chemisorption. From previous adsorption experiments of the two PDMS prepolymers, four or even more THF rinsings were necessary to reach a thermodynamically stable adsorbed layer. The results also suggest that interactions involve CH_3 groups of dimethylsiloxane segments. Finally, the ability of PDMS in displacing contaminants from the aluminum surface was suggested during the adsorption of the catalyst, since dislocation behavior did not occur in the adsorption of TDMS.

5.5.5. Adsorption of Allyltrimethoxysilane (ATMS)

Prior to the adsorption of ATMS, the chemical state of the substrate is analyzed from Figure 5.59. The negative broad band (reverse direction) between 3700-3200 cm^{-1} region is attributed to a reduction in concentration of hydroxyl groups (-OH) coming from: -COH impurities, Al-OH and adsorbed H_2O on the surface. The main elimination can be associated with contaminants and physisorbed water, corroborated by a very weak negative band perceived at 1650-1600 cm^{-1}. The removal of organic contaminants anchored on the bare metal surface is corroborated by the absence of peaks in the ν-C-H region at 3100-2800 cm^{-1} (magnified region on the left), the negative peaks centered at 1736 cm^{-1}, corresponding to stretching of carbonyl groups (ν-C=O), and the lack of band at 1410 cm^{-1}, assigned to deformation of -C-H bonds. On the other hand, the band associated to the vibration mode of aluminum oxide $\alpha(Al_2O_3)$ is perceived at 973 cm^{-1} [360,384], and evidences a growth of the oxide layer after THF rinse. A side effect of rinsing the surface with THF is the changes caused in the hydroxylated aluminum (γ(AlOOH)), inferred from the apparent negative bump observed at ~ 1150 cm^{-1} [360,371,384]. As declared previously, THF not only acts as a cleaning but it seems to induce changes in the chemical structure of the native aluminum oxide layer.

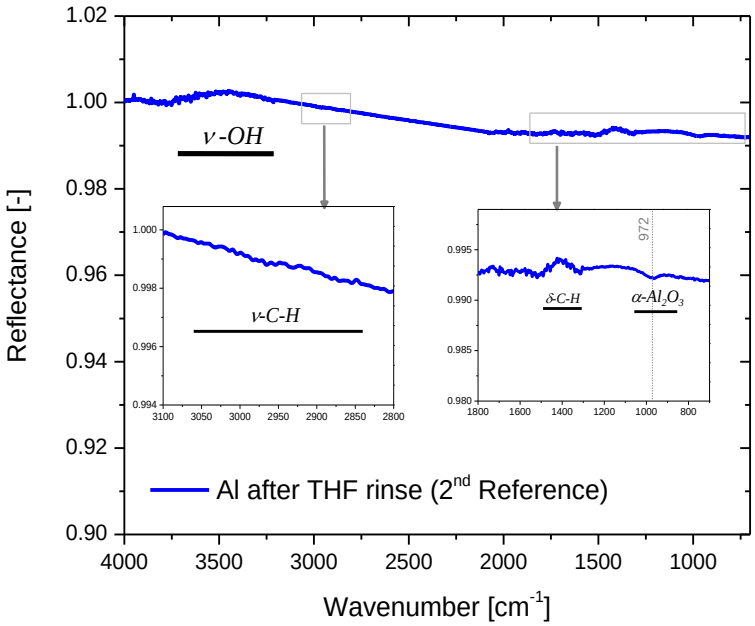
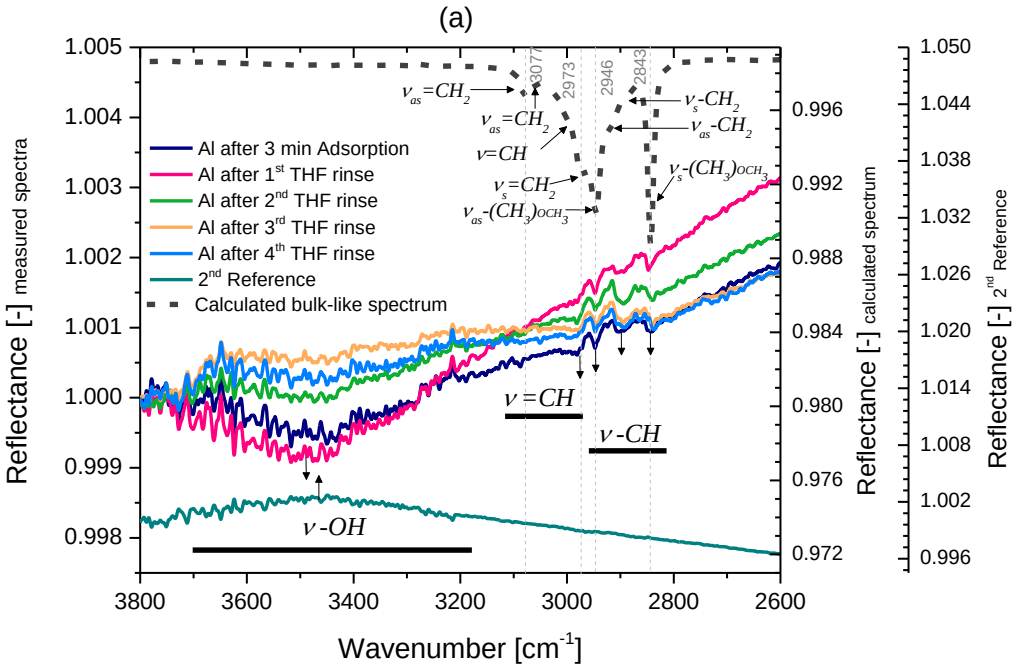


Figure 5.59. ERA spectrum of the Al surface after one THF rinse, and prior to adsorption of ATMS. Zoomed regions at 3100-2800 cm^{-1} and at 1800-700 cm^{-1}. Contaminants are not recognized.

Figure 5.60.a,b exhibits the adsorption behavior of ATMS on Al. Essentially, the measured spectra lack well-defined positive bands, and instead notable negative bands are recognized straight away. Also, a consistent behavior within the measured spectra is observed, revealing slight effects of THF washing cycles on the chemical state of the surface after adsorption of ATMS. These qualitative aspects suggest two possible scenarios: first, under the conditions used here, ATMS did not adsorb or adsorbed very weakly onto Al; second, ATMS did adsorb onto Al and the spectral features disclosed are attributed to interactions and orientation effects.



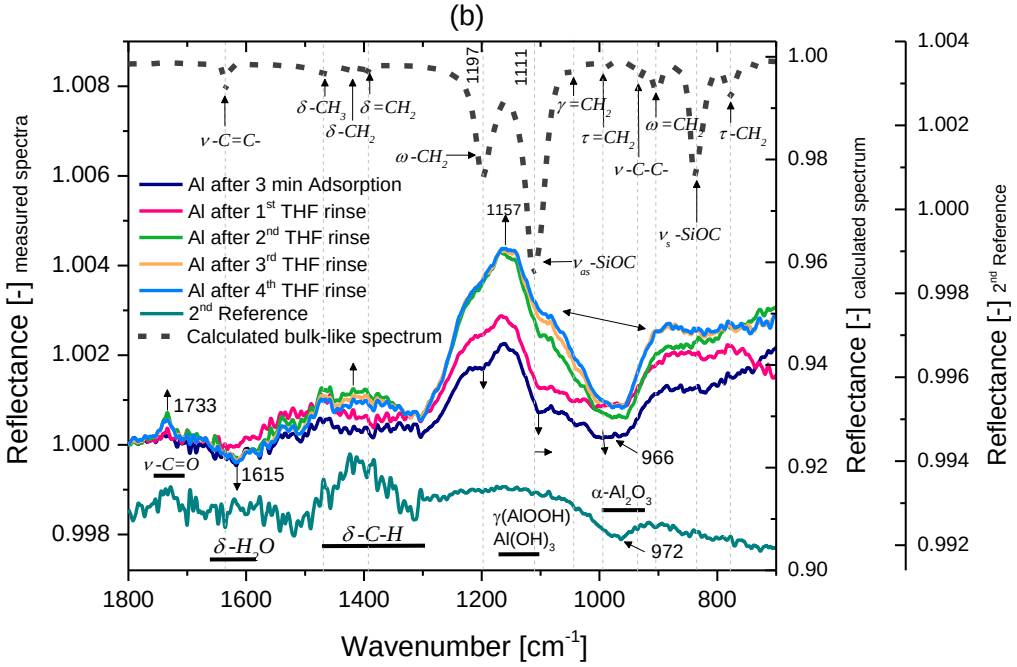


Figure 5.60. Measured ERA spectra of adsorbed ATMS on Al (a) from 3800 -2600 cm^{-1} and (b) fingerprint region from 1800 – 700 cm^{-1}. The 2nd reference spectrum (Al after one THF rinse) is included for analysis. The wavenumbers provided on the top correspond to the calculated bulk-like spectrum [160].

For the sake of clarity and ease of interpretation, the measured spectrum of the substrate prior to adsorption is also included in Figure 5.60a,b. The measured spectra display close similarities to the 2nd reference spectrum in the fingerprint region (Figure 5.60b), supporting the argument for insignificant, or a total lack of, adsorption of ATMS on Al. In order to draw decisive conclusions regarding the adsorption of the adhesion promoter on Al, the principal features of the spectra are analyzed in more detail:

- **Band at 3700-3200 cm^{-1}:** The measured spectra reveal initial presence of -O-H groups in the adsorption of ATMS, but decreasing progressively upon solvent rinsing (Figure 5.60a). The content of hydroxyl groups on the surface could be affected by different events such as: **(i)** physisorption of water molecules, which is also supported by a weak band at 1660-1580 cm^{-1} related to δ-H_2O (Figure 5.59b). The intensity of this weak band remains almost invariable upon THF rinsing, whereas the ν-O-H band intensity decreases. This indicates that the band at 1660-1580 cm^{-1} may have contributions from other vibrating modes such as: -CH=CH_2 from ATMS and possibly $-COO^-$ from contaminants [360]; **(ii)** Increase in concentration of Al-OH groups. In case

water was physisorbed, it could have reacted with aluminum oxide, increasing the concentration of Al-OH moieties. However, the reduction in intensity observed after THF contact for the ν-O-H band could be associated with changes in the hydroxide layer; **(iii)** Readsorption of organic contaminants containing –COH species. The presence of organic contaminants containing -COH species can be supported by examination of the measured spectra at 1200-1000 and 900-750 cm^{-1} (characteristic IR absorption ranges for alcohols); however, their recognition is challenging due to noise background; **(iv)** Presence of -Si-OH groups from existing traces or formed either from hydrolysis of methoxy groups, as suggested in literature [160,209]. Analysis in the range at 955-830 cm^{-1} related to ν-SiOH, neither confirm nor refute the presence of Si-OH groups. Also, due to its high reactivity, traces of Si-OH could have been rapidly consumed in condensation reactions either with -Si-OH groups or Al-OH groups on the surface.

- **Weak bands at 2970-2800 cm^{-1}:** This spectral region is characterized by C-H stretching vibrations; hence, C-H bonds from ATMS and carbonaceous contaminants are displayed in this range (Figure 5.60a). Four distinct peaks with similar intensity can be recognized in this region for all the measured spectra. However, there is ambiguity in the assignment of these peaks either to adsorbed ATMS or to contaminants. The ability of contaminants to be favorably readsorbed upon adsorption of a monomer was observed in the adsorption of TDMS.
- **Negative band at 1732 cm^{-1}:** This peak corresponds to stretching vibration of carbonyl group (ν-C=O), the negative band (Figure 5.60b), also observed in the Al surface prior to adsorption, indicates that carbonyl groups were not present during the adsorption of ATMS.
- **Negative broad band at 1485-1405 cm^{-1}:** This spectral region is characteristic of deformation vibration modes of C-H bonds. The calculated bulk-like spectrum displays three characteristic peaks in that region: δ-CH_3, δ-CH_2 and δ=CH_2, which are imperceptible in the measured spectra (Figure 5.60b). Alternatively, the negative broad bump is recognized for all measured spectra including the 2nd reference spectrum, suggesting that this band results from further structural changes of the aluminum surface upon THF rinsing rather than from adsorption of ATMS, advocating lack of adsorption and being in agreement with the findings of Gilbert [371].
- **Negative broad bump centered at 1157 cm^{-1}:** This feature can be associated with vibrations of the oxide/hydroxy layer of aluminum [360,384], and it is recognized in all measured spectra including the one previous to adsorption (Figure 5.60b). This proves the insignificant adsorption of ATMS on Al, as the vibration mode of the substrate can be perceived. Moreover, it is seen that the intensity of this negative bump

increases progressively up to the 2nd THF rinse, but stabilizes afterwards. This confirms that upon successive THF contact, the aluminum surface undergoes structural changes.

- **Bands associated with adsorbed ATMS in the fingerprint region**: Despite the evidence found so far indicating lack of adsorption of ATMS on Al under the experimental conditions used in this work, different bands were perceived in the fingerprint region associated with traces of ATMS. These bands are: **(1)** weak shoulder centered at 1198 cm^{-1} related to wagging vibration of methylene (ω-CH_2) which vanishes after the 1st THF rinse, indicating desorption. **(2)** a weak peak ascribed to the asymmetric stretching of Si-O-C bonds (ν_{as}-Si-O-C). In the calculated spectrum, this peak is intense, sharp and symmetric, whereas in the measured spectra it is asymmetric, broad and exceedingly weak. Peak shifting, broadening and change in shape may have resulted from effects arising from the adjacent intense negative bump or from dispersion of the refractive index due to poor adsorption of ATMS. Effects from interactions of the Si-O-C polar bond with the aluminum substrate might be insignificant. The intensity of this peak decreases successively with THF rinsing cycles, indicating desorption. **(3)** Broad band from 1080 to 905 cm^{-1}, the features in this region resemble the bare substrate prior to adsorption, suggesting that the principal contribution to this band arises from the vibration mode of the aluminum oxide layer (α-Al_2O_3). Changes upon solvent rinsing such as peak broadening and the increase of intensity evoke changes in the chemical structure of the Al surface. **(4)** The weak band at 1044 cm^{-1} is ascribed to γ=CH_2 of allyl groups. The band has vanished after the 2nd THF rinse, demonstrating the ease of adsorbed ATMS to desorb upon solvent washing.

In summary, adsorption of ATMS under the experimental conditions applied in this work was exceedingly weak or insignificant, suggesting that the affinity between THF and ATMS is greater than that between ATMS and Aluminum. After two THF rinses, the small amount adsorbed is believed to be desorbed from the surface. Therefore, the four main peaks detected in the region of C-H stretching modes (Figure 5.60a) can be mainly attributed to contaminants rather than to ATMS, although overlapping with ATMS bands may exist in the initial stages of the experiment. Besides the weak adsorption of ATMS, the surface underwent structural alterations. Because no pre-hydrolysis step of the silane was carried out, the well-known mechanism of adhesion for silanes containing trimethoxy groups did not occur. This indicates that natural hydrolysis of methoxy groups was restricted at ambient conditions, as suggested by Osterholtz and Pohl [385]. Consequently, the results here emphasize that specific conditions are required in the adhesion of organosilanes. The hydrolysis of methoxy groups towards creation of -SiOH bonds that allow further covalent bonding with a

hydroxylated surface seems to be crucial. It can be stated that traces of ATMS were principally adsorbed.

5.6. Conclusive Discussion

The adsorption of the SSMC was effectively evaluated through in-situ FTIR-ERAS measurements. The studies revealed significant changes in the vibrational states of the adsorbed SSMC on native aluminum oxide when compared to their respective calculated bulk-like spectra. Therefore, important aspects which could have influenced the adsorption of the SSMC from diluted solution on Al are to be discussed.

5.6.1. Effect of end-group on the adsorption of PDMS

Two types of end-groups in PDMS were analyzed in this work: vinyl (-Si-CH=CH_2) and hydride or silyl (-Si-H). Affinity of the terminal groups with the surface, i.e. their ability for establishing adhesive interactions, will influence different aspects such as: (a) nature of adsorption (physisorption or chemisorption), (b) molecular conformation of PDMS molecules on the surface, (c) amount of adsorbed PDMS molecules, (d) strength or reversibility of adsorption (proven in this work by sequential THF rinsing cycles), and (e) dynamics of adsorption.

a. Nature and type of adsorption:
For di-hydride terminated PDMS, chemisorption was suggested via hydrolysis of Si-H bonds, forming -Si-OH groups that react covalently with -OH groups of the aluminum surface (Figure 5.17). However, the results revealed that hydrolysis of Si-H under the experimental conditions applied here (dry air atmosphere) was very unlikely to occur. Hence, different mechanisms involving Si-H bonds should have prevailed in the adsorption of prepolymer 1. One possibility is that Si-H moieties undergo a condensation reaction with hydroxyl groups associated with the surface, by the elimination of molecular hydrogen and becoming chemically bound to the surface as proposed by Cosgrove and coworkers [33]. The authors found that chemisorption was preceded by physisorption (H-bonding), and its extent was dependent on time, initial solution concentration, polymer type (cyclic, linear, position of Si-H), orientation of Si-H on the surface, and chemical environment (T, pH, contact to active sites of the surface). The mechanism proposed for chemical bonding between Si-H and Al-OH on

the surface, based on the model of Cosgrove et al., is depicted in Figure 5.61. Experimental evidence that supports significant consumption of Si-H groups in a chemical reaction was not found in the ERA spectra neither for short nor for long storage times; thus, if chemisorption of prepolymer 1 took place via Si-H bonds (Figure 5.61), it occurred to a very low extent. Conversely, peak shifting of the Si-H vibration modes to lower frequencies in the measured spectra suggested that the bond was weakened by intermolecular interactions, e.g. H-bonding or van der Waals forces.

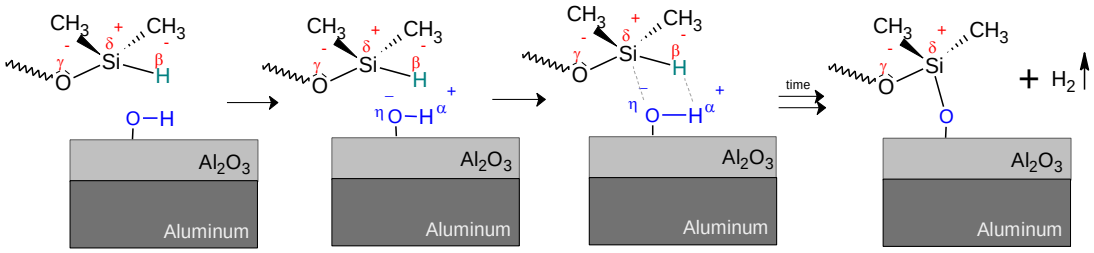


Figure 5.61. Representation of possible chemical bonding of Si-H to native aluminum oxide [33]

Consequently, it can be suggested that under the experimental conditions applied in this work, prepolymer 1 did not chemisorb via Si-H bonds. Most likely, H-bonding and van der Waals forces involving Si-H moieties dominated in the adsorption of prepolymer 1. Possibly, the prepolymer was in a pre-stage for chemisorption. Conceivably, at longer contact times of prepolymer 1 with aluminum, chemisorption involving Si-H moieties could occur. Other plausible interactions leading to the physisorption of Si-H groups of prepolymer 1 on Al are illustrated in Figure 5.62. Due to the lower electronegativity of Si compared to H, the bond has a dipole moment.

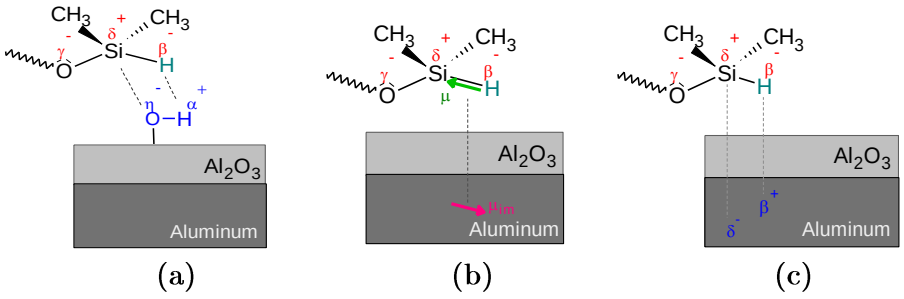


Figure 5.62. Representation of possible interactions involving terminal Si-H bonds of di-hydride terminated PDMS with the aluminum surface: (a) hydrogen bonding [33] (b) permanent dipole-induced dipole interactions (c) electrostatic interactions.

On the other hand, for bifunctional vinyl terminated PDMS, there was insufficient spectral evidence regarding interactions between -Si-CH=CH_2 terminal groups and the surface. Principally, restrictions arose from the limitation of the FTIR spectroscopy method in displaying weak bands related to double bonds in the spectra. The experimental results revealed that after the 1st THF rinse, bands corresponding to vinyl groups were no longer clearly discernible. However, it is not possible to conclude whether disappearance of the bands was due to molecular orientation, interactions or technique restrictions. In theory, π electrons of the double bonds in vinyl groups could interact with the 3d empty orbitals of aluminum that are available on the outer oxide layer by non-covalent bonds, since vinyl groups are considered weak nucleophiles or bases [174,386]. However, basicity of vinyl derivatives of silicon element is much lower than in carbon analogues due to the so-called $(p\text{-}d)_\pi$ interaction [73,387]. The interactions of electrons from the vinyl group with Al is thus restricted by the $(d\text{-}p)_\pi$ interaction between the electrons of the double bond and the 3d empty orbitals of Si. It can be suggested, that vinyl groups interact weakly with the aluminum surface, probably only by van der Waals interactions.

b. Molecular conformation of PDMS molecules:

Due to the low molar mass of the two prepolymers ($<M_w>\leq 2000$ g/mol), the influence of the terminal functionalities on the adsorption behavior of PDMS is believed to be greater than for polymers with higher molar mass [34,35]. Four molecular conformations can be proposed for di-functional terminated polymers adsorbed on a surface (Figure 5.63a-d) [34,388]. The first is the loop type, which occurs when only the two end-groups interact with the surface. The second is the brush or tail type adopted when only one end-group interacts. The third is the train type, occurring when end-groups do not interact but segments of the backbone do. Finally, the fourth is a mixed type where end-groups and chain segments simultaneously interact with the surface.

The results suggested that the adsorption behavior of the two prepolymers and the catalyst was governed by interactions involving siloxane bonds independently of the nature of the end-group. Consequently, configurations (a) and (b) in Figure 5.63, with exclusively terminal groups interacting with the surface, are discarded.

For di-hydride terminated PDMS, not only the siloxane (Si-O) bonds possess affinity to the surface but also the Si-H terminal groups. Therefore, the molecular arrangement of di-hydride terminated PDMS on Al could be proposed to be of type (d) with Si-H end-groups near the surface for enhancing interactions. However, different factors such as entanglement and degree of coiling could have affected the position of Si-H groups in respect to the surface.

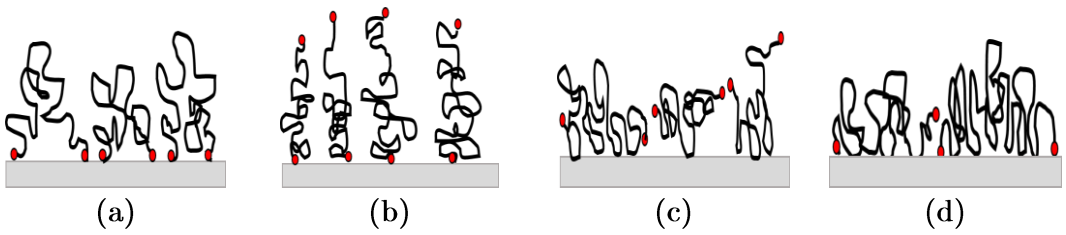


Figure 5.63. Configuration of PDMS molecules depending on the noncovalent interactions of the terminal groups with the aluminum surface (a) loop type, (b) tail or brush type, (c) train type and (d) mixed type [34].

For di-vinyl terminated PDMS and the catalyst, most likely, configuration (c) was the predominant type; however, interactions involving terminal Si atom and π electrons can be established; therefore, conformation of type (d) may also exist.

c. Amount of adsorbed PDMS molecules:

Conclusions regarding the dependency of the terminal functionalities on the amount of adsorbed molecules cannot be specified from the results obtained by FTIR-ERAS technique. In traditional FTIR spectroscopy (ATR or transmission) intensity of the IR absorption peaks in the spectra can be directly related to the amount of the sample evaluated, according to Beer law [167]. However, for FTIR-ERAS method, intensity of the peaks depends on both the concentration of the oscillator (chemical group) and the orientation of the molecules (Equation 5-27). Therefore, direct correlation of ERA intensity with the amount of adsorbed molecules is inappropriate.

Based on the results obtained by Patel et al. [34], who studied different end-functionalized PDMS on silica and alumina, it would then be expected that prepolymer 1 adsorbed to a greater extent than prepolymer 2.

The intensity of the measured ERA spectra of the two prepolymers was found to be in the same range after the 3-min adsorption step, even regardless of the molar mass difference ($M_n|_{prepolmyer1} > M_n|_{prepolymer2}$). This result can be attributed to the dominant role of siloxane segments in the adsorption of PDMS. Thus, despite the different affinity of the end-groups to the native aluminum surface, if they do not chemisorb, they seem to play an insignificant role concerning the amount of adsorbed PDMS on Al. In addition, the spectra right after adsorption duplicated the bulk-like spectrum for both prepolymers, suggesting a thick polymer layer with bulk properties. Thus, it is concluded that in the deposition step both prepolymers adsorbed thickly on Al regardless of molar mass and end-functionalities.

d. Strength, stability and reversibility of adsorption (evaluated throughout sequential THF rinsing cycles):

For the two end-functionalized PDMS, total desorption did not occur when they were rinsed consecutively with pure THF, considered a good solvent for PDMS [355]. Both oligomeric PDMS species displayed strong adsorption, resisting up to four or five THF rinsing cycles and attaining a stable adsorbed layer at the end. Hence, irreversible adsorption of PDMS on Al is suggested independently of the end-groups. This confirms first, the inherent irreversibility and non-equilibrium nature associated with the adsorption of polymers even on mildly attractive surfaces, as explained by O'Shaughnessy and Vavylonis [332]; and second, the principal role of Si-O-Si units in the adsorption of PDMS, as previously claimed.

Consecutive pure THF rinsing cycles proved to be very effective for examining the strength, stability and reversibility in the adsorption of PDMS on native aluminum oxide. Experimentally, THF was capable of removing weakly adsorbed molecules and left only those interacting strongly with the surface. This suggests that oligomers which were adsorbed from solution, desorbed when exposed to pure solvent due to a distribution of adsorption states (from strong to weak adsorbed) existing at the interface [325]. As suggested by Soga and Granick [325], partial desorption may have resulted from simultaneous effects: first, concentration effects, where weakly adsorbed molecules that were in an equilibrium state may have desorbed in pure solvent to reach a new equilibrium state; and second, from different conformational arrangements of polymer molecules within the adsorbed layer, i.e. some polymer chains spread on the surface occupying more sites, thus, repelling neighborhood molecules by steric repulsion and creating poorly interacting molecules that are desorbed by the solvent. For instance, longer chains tend to displace shorter ones from the surface due to entropic effects and favoring the removal of the latter by the solvent. Execution of experiments including smaller siloxane molecules with the same end functionalities are proposed in order to study in detail the influence of end-groups on the irreversibility and stability in the adsorption of PDMS on aluminum. Previous work has demonstrated that adsorption stability did depend on the chain length for different end-functionalities in PDMS [34].

d. Dynamics in the adsorbed state:

From the ERA spectra of the two prepolymers after 24 h storage time, it was observed that the intensities of all bands fluctuated over time and the absorption bands of Si-H and Si-vinyl were unchanged in position and shape. This observation indicates that

mobility and orientation of the molecules within the adsorbed layer were almost unaffected by the nature of the end-groups and by the possible interactions of such end groups with the surface. As explained by Levresse et al.[35], if interactions of the end-groups with the surface are dominant, the adsorption process is accelerated and stability is attained faster because once a chain end is attached to the surface, the number of additional bonds needed to be anchored is lowered. Therefore, the slow dynamics observed for the two prepolymers evidences that interactions involving the end-groups were not dominant. By contrast, they are thought to have been governed by the Si-O-Si bonds.

5.6.2. Influence of storage time on the adsorption of PDMS

Dynamics of polymer adsorbed layers is a complex process [388]. The time needed to relax to an equilibrium state upon polymer adsorption depends on different factors such as: molar mass of the polymer, head group size, distance between surface sites, surface pressure, chain branching, intermolecular adsorbent–adsorbate interactions and temperature [389,390]. Effects of storage time on (a) molecular orientation of PDMS, (b) occurrence of chemical reactions, and (c) stability of the adsorbate, are discussed hereafter.

a. Molecular orientation of PDMS.

The measured ERA spectra of the two prepolymers reveal relative variation in peak intensities over time, addressing orientational changes. The continuous variations suggest that a steady state was not attained during the 24 h of evaluation time. Preferential orientation of PDMS on different surfaces has been widely studied [124,136,325,365,391]. The variation of the intensity ratios involving three vibration modes: ν_s-Si-O-Si, ν_{as}-Si-O-Si and δ_s-CH_3 are of interest because the directions of the local transition dipole moments of such modes are either parallel or perpendicular to the chain axis as illustrated in Figure 5.64 [125].

Three different intensity ratios, calculated from the peak areas (A), were used for evaluating the effect of storage time on molecular orientation. They are defined as follows:

- $r_1 = A_{\nu_{as}-SiOSi}/A_{\nu_s-SiOSi}$
- $r_2 = A_{\delta_s-CH_3}/A_{\nu_s-SiOSi}$
- $r_3 = A_{\nu_{as}-SiOSi}/A_{\delta_s-CH_3}$.

The intensity ratios over time for the two prepolymers are presented in Figure 5.65.

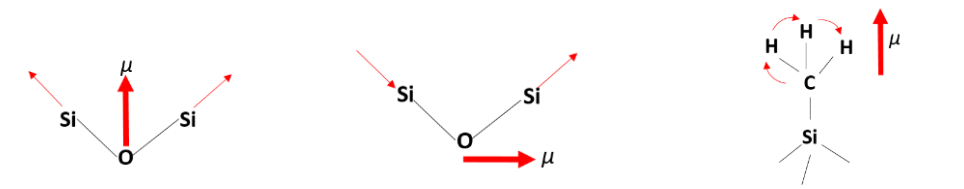


Figure 5.64. Representation of the local transition dipole moment of (a) ν_s-Si-O-Si, (b) ν_{as}-Si-O-Si and (c) δ_s-CH_3 (umbrella mode) vibration modes [125].

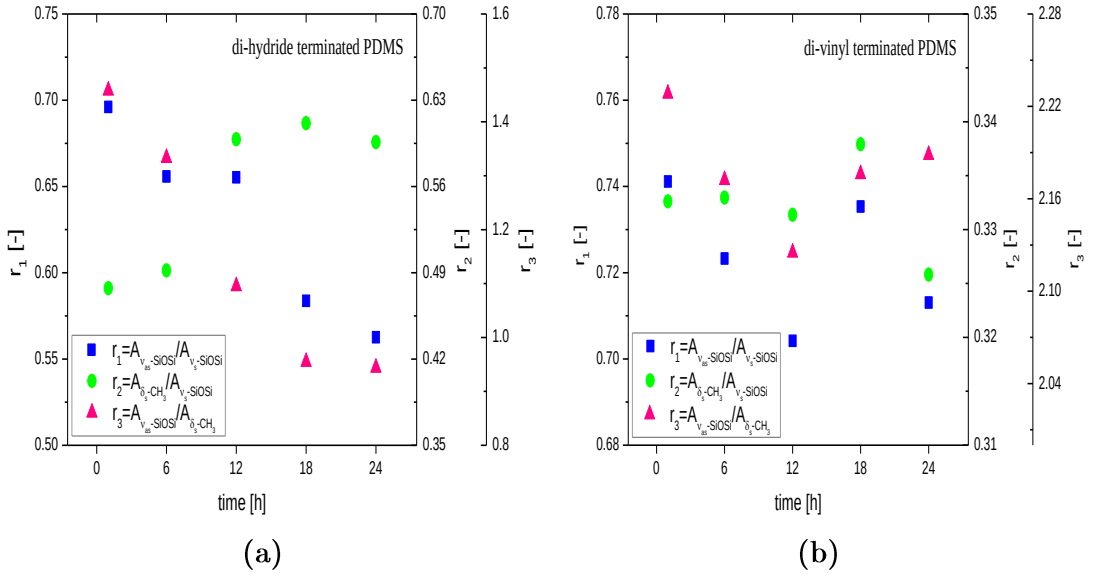


Figure 5.65. Variation of the peak area ratios with storage time in (a) di-hydride terminated PDMS and (b) di-vinyl terminated PDMS.

Changes in r_1 for di-hydride and di-vinyl PDMS suggest either a decrease in the intensity of the asymmetric Si-O-Si stretch (ν_{as}-Si-O-Si) or an increase in intensity of the Si-O-Si symmetric stretch (ν_s-Si-O-Si) in the polymer backbone. Each case supports the idea that the polymer backbone is adopting a preferential orientation that is considerably horizontal or parallel with respect to the substrate surface. This orientation is also accompanied by an increment of CH_3 groups oriented perpendicular to the chain axis, as inferred from the trend of the r_2 ratio to increase with time. However, this preferential orientation seems to be discontinued for di-vinyl terminated

PDMS after 12 h, due to the increase of r_3 advocating a deviation from this flattened orientation by prepolymer 2 molecules. This suggests that for some prepolymer 2 molecules, the backbone lifts and methyl groups are no longer strictly perpendicular to the surface [136]. Thus, after a certain time, di-vinyl PDMS may have adopted a more extended helical or caterpillar coil structure [51,136].

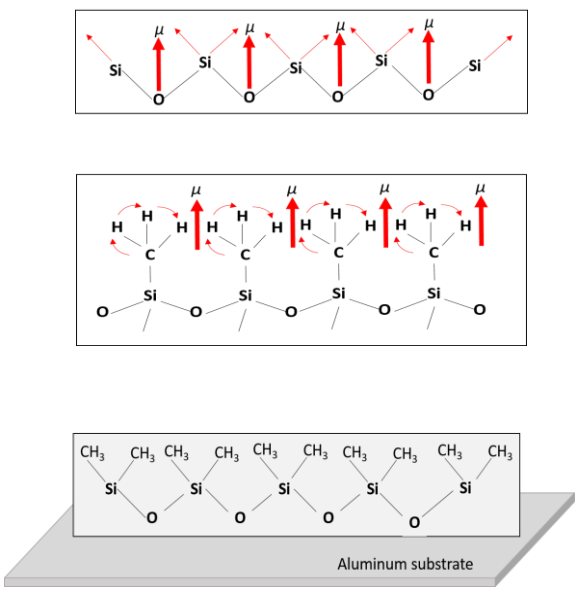
It can be assumed that adsorbed di-hydride PDMS changed its orientation over time towards a fully extended configuration, whereas di-vinyl PDMS initially followed the same flattening trend but after a certain time (t>12h) it adopted a more coiled conformation. The feasibility of Si-H terminal groups to interact with the surface and the higher average molar mass in prepolymer 1 seems to favor progressive chain flattening of PDMS over time, whereas the poor interaction of vinyl groups, accompanied with the high content of short oligomers in di-vinyl PDMS, limited or distorted the chain extension process. Normally, the fraction of segments attached to the surface and the configuration of the molecules on the surface will differ depending on the molecular size [377]. In the adsorption of polymers, the larger the fraction of the attached segments per chain, the flatter the configuration will be [377]. Thus, the lower average molar mass of di-vinyl PDMS may have contributed to its less flattened conformation. In addition, increment of -OH concentration upon adsorption of di-vinyl PDMS favoring chemisorption of end-groups could have favored a loop conformation, therefore altering the flattening process of this prepolymer. The process proposed for the di-hydride PDMS and for di-vinyl PDMS (during the first 12 h) molecules is represented in Figure 5.66. It can be suggested that most of the chain segments after 24 h of contact consisted of trains and short loops on the oxide surface [392].



Figure 5.66. Proposed flattening process of PDMS adsorbed molecules over storage time.

This tendency of adsorbed PDMS to acquire an extended configuration is in agreement with previous studies of PDMS samples adsorbed on gold, alumina and silica surfaces [49,104,117,125,325,391–393]. The flattening conformation is even acquired in thick polymer films, most likely due to enhancement of dipole-dipole interactions between molecules in the adsorbate. From a thermodynamic point of view, the flattened configuration allows more chains to be in contact with the surface, reducing the total

energy of the system and enhancing the interactions at the interface; thus, strengthening the adhesion [125]. In an ideal, fully extended PDMS configuration, the Si-O-Si plane is in the same direction as the substrate normal (Figure 5.67), deduced from the orientation of the local transition dipole moment of the symmetric stretching mode (ν_s-Si-O-Si) (Figure 5.64). The orientation of the methyl groups would be preferably non-parallel to the surface in order to clear up the siloxane groups in the backbone to allow them to interaction with the metal surface.



Backbone plane with local transition dipole moments of the ν_s-Si-O-Si band parallel to the siloxane plane

(a)

Si-O-Si plane containing Si-CH_3 groups with the local dipole vector of δ_s -CH_3 lying parallel to the siloxane plane

(b)

Ideal fully extended PDMS with Si-O-Si bonds parallel to the surface (plane of the backbone perpendicular to the surface) and methyl groups far from the surface.

(c)

Figure 5.67. Representation of the local transition dipole moments of (a) ν_s-Si-O-Si with respect to the Si-O-Si plane, (b) δ_s-CH_3 with respect to the backbone plane, and (c) illustration of an ideal preferential flattened configuration of adsorbed PDMS chains on Al, with the backbone plane perpendicular to the surface [124,125].

When a polymer chain spreads on a surface, it occupies more sites and repels neighbor molecules by steric repulsion, leading to weaklier interacting molecules. This fact generates a distribution of molecular configurations at the interface, ranging from fully extended to more coiled. Due to such distribution, different situations can occur simultaneously over storage time. First: flattening of the polymer chains, second: possible diffusion of shorter chains towards the surface, and third: changes in conformation of the weakly interacting molecules for enhancing interactions with the surface. Interestingly, despite the prepolymers displaying bulk properties due to relatively high surface coverage right after the 3-min adsorption step, it is remarkable

that PDMS backbone still showed tendency of net horizontal orientation. This indicates that chain flattening was not occurring only for isolated adsorbed polymers but also for polymers within the adsorbed layer. This observation is consistent with the work of Soga and Granick [325].

b. Occurrence of chemical reactions

Longer storage times could have promoted the incidence of chemical reactions strengthening adhesion of PDMS on Al. Peak shifting, peak broadening and appearance of a new band were indistinct evidence that physical and chemical processes were occurring at the interface. Specifically, the emerging and continuous broadening of a band at ~ 960-970 cm^{-1} suggested Si-O-Si segments bound via H-bonding [325], and also possible formation of Si-O-Al covalent bonds [154,189,190]. Terminal groups as Si-H and Si-OH could have preceded the formation of such bonds. Hydroxyl terminated PDMS molecules were present at trace levels in the bulk samples but they could have also been created by hydrolysis of Si-H or Si-O-Si bonds. However, according to Fox et al. [394], the rate of hydrolysis of Si-O-Si bonds in polysiloxane chains adsorbed as a monolayer at 20 °C was found to be insignificant. In the measured spectra of hydride terminated PDMS, direct indication of hydrolysis was not found, whereas for di-vinyl PDMS the O-H stretching mode increased over time, indicating increment of -OH groups. Probably, the shorter oligomers present in prepolymer 2 were more prone to undergo hydrolysis.

c. Stability and strength of adsorption

The stability and strength of adsorbed PDMS was effectively evaluated throughout sequential THF rinsing steps after 24 h storage time for both prepolymers. It was found that the decrease in intensity was smoother for longer storage times than for shorter ones, i.e. the decrease in peak intensities after the first solvent washing was not as dramatic as it was for shorter times. Although direct correlation of peak intensity with the amount or concentration is incorrect, the final peak intensities after the 5^{th} THF rinse (24 h) compared to those after 4^{th} THF rinse (1 h) suggest that more weakly adsorbed molecules existed in the adsorbate state at shorter storage times. This is reasonable, because longer times could imply the enhancement of interactions.

It can be claimed that longer storage times positively affected the stability of adsorption of PDMS on aluminum, Although, under the conditions applied in this work, it was found that equilibrium was not attained in 24 h of observation.

5.6.3. Effect of molecular size in the adsorption of siloxanes on Al

The main feature that makes polymer adsorption different from small molecule adsorption is the chain inherent nature of the molecules. A polymer molecule can occupy more than one site on the surface, and yet all its segments do not need to be attached [377]. The fraction of segments attached to the surface and the configuration of the molecules on the surface will differ depending on the molecular size [377]. However, the adhesion mechanisms that lead to adsorption (i.e. chemical bonds, hydrogen bonds, dispersive forces, etc.) are the same for small molecules and macromolecules of the same chemical nature [377].

In this work, the effect of molecular size on the adhesion of siloxane-containing species on aluminum, is analyzed from the adsorption behavior of prepolymer 1 and TDMS, since both components are chemically equivalent; i.e. they contain the same building units: terminal Si-H bonds, Si-O-Si and -O-Si-$(CH_3)_2$ bonds. Prepolymer 1 is a lineal oligomer with 2 terminal Si-H groups and 14 repeating units in average, while TDMS is a tetrafunctional star-like monomer with 4 Si-H end-groups and 4 Si-O-Si units. Based on the experimental results obtained, the following aspects have been found to be affected by the molecular size:

- **Molecular orientation.** Contrary to PDMS, TDMS did not adopt a specific or preferential orientation. The prominent peak broadening perceived for the Si-O-Si stretching mode at 1120-950 cm^{-1} indicated inhomogeneous broadening of collective oscillations arising from an inhomogeneous distribution of molecular orientations, intermolecular distances and interactions [362]. Thus, TDMS changed its orientation and packing density randomly throughout sequential THF washings. This behavior justifies the fluctuations observed in the peak width and intensity of the ν-Si-O-Si band. Although the driving force for molecular orientation in both components is the maximization of the attractive interactions between Si-O-Si bonds and the surface, greater feasibility of interactions via Si-H bonds, steric effects and low molecular packing density may have influenced the arbitrary orientation of TDMS molecules on Al. Possible molecular orientations adopted by TDMS on Al are suggested in Figure 5.68. Due to significant steric effects, a considerable amount of methyl groups should be oriented near the aluminum surface, which supports changes in their vibrational modes.

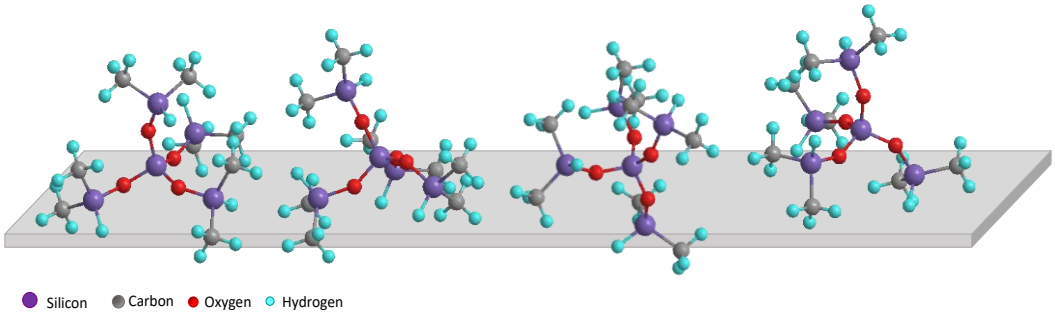


Figure 5.68. Possible orientations of TDMS molecules on Al. Due to steric hindrance, parallel orientation of all Si-O-Si segments is highly restricted. Interactions involving methyl groups seem to be significant in adsorption of TDMS.

- **Displacement of contaminants.** Unlike TDMS, PDMS molecules of prepolymer 1 were able to dislocate physisorbed contaminants on the surface and prevent further deposition of impurities. This behavior could be attributed to the ability of PDMS molecules to spread over the surface in a flattening configuration. By contrast, due to steric hindrance and probable low packing density of adsorbed TDMS, some uncovered regions in the surface could have given opportunity for re-contamination.
- **Thickness of the adsorbed layer.** From the intensities of the ERA spectra of prepolymer 1 and TDMS, it can be inferred that higher surface coverage was attained by prepolymer 1 just after the 3-min adsorption step. The marked decrease in peak intensities after the 1st THF rinse for prepolymer 1 indicated considerable removal of bulk or weakly interacting molecules. In contrast, for adsorbed TDMS intensities did not decrease remarkably; instead they fluctuated from the beginning, suggesting the attainment of a thin layer with high mobility since the initial stage of the experiment.
- **Strength of interactions.** The results obtained for both prepolymer 1 and TDMS confirmed that the energy of adsorption was not restricted by the molecular size. The two components adhered strongly and irreversibly to Al, resisting up to five THF rinses. In both cases, Si-O-Si bond was tentatively defined as the adhesion partner.
- **Involvement of methyl groups in intermolecular interactions.** Due to steric effects of TDMS, a considerable amount of CH_3 groups are believed to be located near the surface, and thus involved in interactions. The spectra of TDMS displayed remarkable features in the vibrating modes related to methyl groups, supporting this scenario. For PDMS it was also inferred that CH_3 groups were involved in interactions, but this situation seems to be more significant in the adsorption of TDMS.

5.6.4. Adsorption of alkoxysilanes vs. siloxanes

Despite the well-known mechanism of adhesion of alkoxysilanes on metal substrates in which Si-O-Al bonds are formed (Figure 3.8), neither chemisorption nor physisorption was observed for allyltrimethoxysilane (ATMS) under the experimental conditions applied in this work. Contrarily, the other four SSMC, whose contain siloxane linkages featured positive adhesion on Al. The poor adsorption displayed in this work by the ATMS could have been due to different aspects such as:

- **Lack of pre-hydrolysis step.** As described in Section 3.3.2, the adhesion mechanism of silanes involves hydrolysis of alkoxy groups yielding -Si-OH species that can further bond covalently to the substrate via condensation with -OH groups on the surface. Thus, not implementing such hydrolysis step could have impeded the adsorption of ATMS on aluminum. In contrast, effective adsorption of hydrolyzed ATMS on Al has been found by Li et al. [160].

Previous investigation by Underhill et al. [154] has exposed the importance of hydrolysis on the strength of adsorption of silanes. The authors shown that the extent of hydrolysis has little effect on the amount of silane adsorbed, but it has a significant influence on the adherence stability of the deposited film. In their work, unhydrolyzed GPS (3-glycidoxypropyltrimethoxysilane) featured weak adherence even upon adsorption at 60 °C.

The lack of adsorption of pristine ATMS also suggests that spontaneous hydrolysis of Si-O-CH_3 groups did not occur under the experimental conditions applied here. This is most likely due to low content of water present in the measurement atmosphere, since it was continuously purged with dry air (T_{dp}=-65 °C), and due to the removal of physisorbed water on the substrate by THF washes. As stated by Osterholtz and Pohl [385], a considerable amount of water molecules is required for the spontaneous hydrolysis of silanes to occur. Thus, the presence of water is in effect, a key factor during hydrolysis and condensation of Si-OH groups, and subsequently, in the adhesion of real silicone systems. It has been described that the hydrolysis of silanes is a complex, intractable process subjected to different variables including chemical composition of the silane, the availability of water, catalyst, and the type of solvent [157]. Accordingly, in real and practical applications, the hydrolysis of silanes must be controlled adequately to achieve the desired results of the final product. Many potential applications of silanes have either been considered as failures or have been completely overlooked, partially due to a misunderstanding on the importance of controlling hydrolysis before, during and after product manufacturing processes, as explained [153].

- **Poor interactions of Si-O-C bonds with the substrate.** The lack of adsorption of pristine ATMS suggests that the Si-O-C bonds were not able to interact strongly with the surface. The oxygen atom in Si-O-C has greater basicity than in Si-O-Si bonds [395,396], exhibiting electron-donor properties that allows it for H-bonding with surface hydroxyl groups [397]. On the other hand, the silicon atom bound to the alkoxy group exhibits electron-acceptor properties, which enables it to perform coordination with electron-donor molecules [397]. However, the number of alkoxy groups attached to the central silicon atom debilitates the electron-donor properties of the alkoxy groups, because steric effects restrict the accessibility of oxygen atoms and cause a decrease in the polarity of the Si-O-C bond [397]. Possibly, steric effects have prevented any possible electron-donor interactions of the silane with aluminum, since a reduction in basicity from monofunctional to tetrafunctional alkoxysilanes has been observed for the Si-O bond [398].
- **Inadequate solvent and temperature.** The deficient adsorption of ATMS from diluted solution in THF suggests that ATMS had higher affinity with the solvent (THF) than with the surface. Thus, the free energy of the system was lower for ATMS-THF than ATMS-Al, inhibiting adsorption. It was demonstrated that THF was an adequate solvent in the adsorption of the other SSMC, whose contain siloxane bonds, while for ATMS it seems to be inappropriate. Usually alcohols and aqueous solutions are preferred for deposition of silanes. Therefore, a more adequate solvent for the adsorption of ATMS at room temperature can be selected. Additionally, adsorption experiments at higher temperatures for unhydrolyzed ATMS could improve its adhesion to the substrate.
- **Nature of the alkyl substituent**. Adsorption of silanes can be also accomplished by the alkyl substituent attached to the silicon atom. For instance, aminosilanes (APS) have displayed good adsorption even when they have not been hydrolyzed [399]. The results obtained suggest that allyl group was insignificantly interacting with the surface.

Concluding, the siloxane species evaluated in this work presented higher affinity to the surface than unhydrolyzed ATMS, under the same conditions of solvent and temperature. Possible use of polysiloxanes as coupling agents or adhesion promoters is suggested. The viability of low molar mass functional polysiloxanes employed as adhesion promoters for improving adhesion at the interface of glass fibers with a polymeric matrix have been studied by Britcher et al. [220,400], Bennet et al. [118] and Kazakevich [112]. They have demonstrated that such polysiloxanes adhered to a glass fiber more effectively than typical silane coupling agents used in the glass-fiber/polymer composites industry. Compared to silanes, siloxanes could offer numerous advantages

during industrial processes such as better surface coverage, no requirement of hydrolysis step (which prevents the use of solvents), possibility to add functionalities at the end and in the backbone, and effective displacement of carbonaceous contaminants on the surface. Studies considering the role of polysiloxanes as adhesion promoters can be proposed. Availability of current research studies regarding this issue is limited.

5.6.5. Role of -Si-OH traces in the adsorption of PDMS

The presence of Si-OH species plays a very important role in adsorption, especially because they can bond covalently to the surface, imparting stability to the adsorbed layer. Silanols are known for being of ambident character, i.e. showing acidic and basic character, which allows them to act as proton donors or acceptors forming relatively strong acid-base interactions as hydrogen bonds and nucleophilic substitution [196].

From the characterization in bulk of the two prepolymers, -SiOH groups were detected in the bulk samples at traces levels, which is a common aspect in commercial PDMS or silicones due to the nature of their industrial preparation process [49]. The effect of -SiOH groups on the adhesion of silicones has been discussed for approximately 60 years by numerous authors. The opinions are divided, some have claimed that chemisorption via Si-OH bonds only occur at high temperatures [50], whereas others have demonstrated that chemisorption is viable at room temperature [117]. In all cases, it has been agreed that adsorption stability is favored by the presence of Si-OH groups.

As previously discussed, the new band observed in the spectra of adsorbed PDMS samples at 1050-900 cm^{-1} can be partly associated with interactions of adsorbed traces of silanol molecules. Hypothetically, traces of -OH terminated PDMS were adsorbed faster than PDMS molecules from the dilute solution due to its higher affinity to aluminum and lower molar mass. It could be suggested that Si-OH traces contributed to the stability of the adsorbed layer on aluminum, as they resisted desorption by THF. The mechanisms of adhesion proposed for O-H terminated PDMS onto aluminum involves double H-boning with -OH groups of the aluminum surface (Figure 5.69). It is considered that H-bonds between -Si-OH groups and -OH on the aluminum surface are stronger than the single hydrogen bonds involving polymeric siloxane (Si-O-Si) groups.

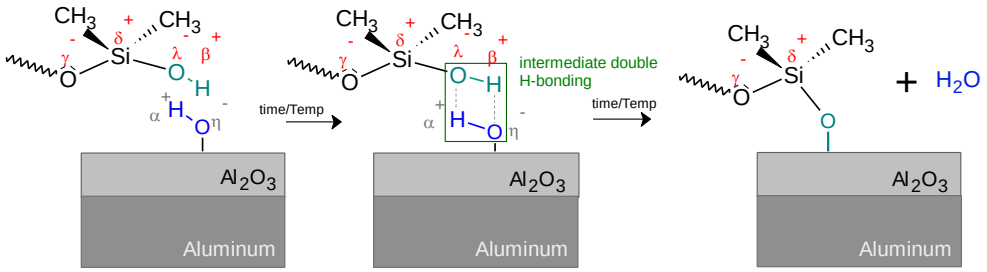


Figure 5.69. Mechanism of adhesion proposed for O-H terminated PDMS, creating with hydroxyl groups of the aluminum surface. First, double H-bonding is created, subsequently, possible covalent bonding to the substrate could occur [19,117].

5.6.6. Influence of the Pt complex (Karstedt catalyst)

It was shown that the Karstedt catalyst, dissolved in mono-vinyl terminated PDMS, displayed typical adsorption spectra features of PDMS polymers. However, the bands related to vinyl terminated moieties were almost imperceptible in the spectra due to their low concentration. A noticeable difference observed upon adsorption of the Karstedt catalyst solution in PDMS and the two PDMS prepolymers was the rapid attainment of a stable adsorbed layer for the catalyst after 2 THF rinses. Therefore, besides its well-known role in catalyzing hydrosilylation reactions of addition-curing silicone adhesives, the Karstedt catalyst contributes to the stability of the adsorbed layer. Hypothetically, the Pt complex catalyzes chemical bonding of PDMS with the surface. The exact adhesion mechanism of vinyl terminated PDMS under the influence of the Karstedt catalyst is undefined. However, possible reactions yielding -OH groups and subsequent Si-O-Al formation could have been Pt catalyzed.

5.6.7. Adsorption/desorption of organic contaminants

Prior to adsorption, the adventitious carbon contamination layer on the aluminum surface was desorbed by rinsing the substrate with pure THF. However, it was consistently observed that traces of contaminants were very likely to be readsorbed by the bare substrate after cleaning. The principal sources of potential contaminants present during the execution of the experiments include the SSMC, the solvent (THF), PVC tubes, Tesa tape, purging air, and glassware [371]. However, as already discussed, it was found that such traces of impurities were reversibly adsorbed and replaced by PDMS and TDMS molecules from the dilute solution. In conclusion, the adsorption of the single components was not significantly affected by the presence of traces of carbon-

species. In particular, the ability of PDMS molecules in their adsorbate state to dislocate impurities was exposed in this work.

The more buckled baseline perceived upon THF rinsing, suggests that the surface underwent some structural changes. Possibly, a dynamic process of adsorption/desorption of contaminants took place, as less adsorbed molecules remained on the surface [42]. As claimed by Gilbert [371], rinsing with pure THF must have modified the chemical potential of the surface of the metallic substrate and consequently increased the kinetic of adsorption of contaminants. The lesser effect in readsorption of contaminants displayed by PDMS is believed to be beneficially influenced by chain flattening. Such configuration maximizes the surface coverage and enhances intermolecular interactions with the surface, restricting deposition of impurities. This special feature of PDMS represents a great advantage in industrial applications, e.g. as a protective barrier for different surfaces. It can be concluded that despite the ease of re-contamination on aluminum, the adsorption of PDMS and TDMS was not significantly distorted by the presence of traces of physisorbed contaminants.

5.6.8. Effect of the solvent (THF)

In adsorption from dilute solution, the nature of the solvent is key in order to obtain desirable results. During the execution of the adsorption experiments, THF played different roles that are discussed as follows:

- **Effect on the bare Al surface**. The results obtained were consistent with surface cleaning with THF. The chemical state of the bare aluminum surface after a single THF rinse was reproducible: partial removal of contaminants and physisorbed water, growth of the oxide layer, and slight changes in the hydroxide layer. Variations observed between different batches can be attributed to the extent of re-contamination of the surface. It can be concluded that THF was an effective cleaning agent, but it also imparted some chemical and structural changes to the aluminum oxide layer that were beneficial to adsorption. THF was not adsorbed on aluminum; hence, interactions solvent-surface were insignificant, favoring the adsorption of the SSMC on aluminum.
- **Effect on adsorption.** It has been claimed that in bad solvents (low solubility) strong adsorption can be expected because solute-surface interaction forces are higher than the solute-solvent ones; contrarily, in good solvents (high solubility) poor adsorption occurs [34,401,402]. However, the opposite behavior, in which good solvents lead to good adsorption, has also been documented [402,403]. The discrepancies perceived in the effect of solvents on the adsorption of polymers have been attributed to conformational changes in the polymer coils [403], and to extra affinity of end-groups

with the surface [34]. THF has been classified as a high-solubility (good) solvent for PDMS at room temperature [355,404]. The results showed that the two prepolymers, the catalyst and TDMS adsorbed strongly on the aluminum surface. This indicates that in those cases, the solute-surface interactions were higher than the solute-solvent attractive forces. Thus, despite the fact that THF is a good solvent for PDMS, it allowed its adsorption on aluminum. On the other hand, ATMS exhibited poor adsorption, advocating that interactions ATMS-THF were stronger than ATMS-Aluminum. Moreover, flattening of adsorbed PDMS on aluminum may have been favored by THF, since the polymer was already extended in the dilute solution. Mu et al. [133], also found strong adsorption of PDMS from good solvent and the polymer chains also adopted the flattening configuration.

- **Effect on desorption - stability of the adsorbed layer.** THF solvent was efficient for evaluating desorption and stability of the adsorbed layer. Throughout sequential rinsing steps, it was observed that THF was able to remove weakly interacting PDMS and TDMS molecules, implying that only those which were interacting strongly remained on the surface. Additionally, upon solvent washing, THF also imparted mobility to the molecules and permitted them to rearrange on the surface, enlarging their anchoring sites. Importantly, the interactions created at the interface led to the formation of stable "bound" PDMS or TDMS adsorbed layer, which consisted (by definition) of molecules resisting extraction by a good solvent at room temperature. In all cases, the adsorbed layer resisted up to five consecutive rinses by THF.

In conclusion, strong adsorption of PDMS from dilute solution using a good solvent was demonstrated. Therefore, THF can be defined as a suitable solvent for evaluating adsorption of silicone components containing siloxane bonds, and also as an effective solvent for studying the stability of the adsorbed layer. On the other hand, the lack of adsorption of unhydrolyzed ATMS suggests that most suitable solvents should be selected.

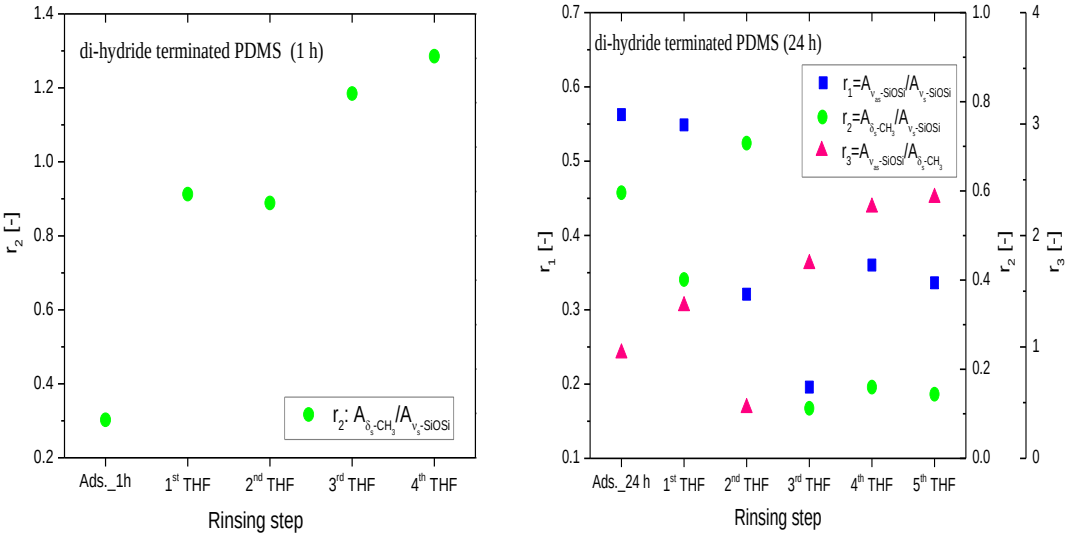
5.6.9. Chemical state of the aluminum surface

The analysis by FTIR-ERAS of the chemical state of the surface prior to adsorption revealed that reproducible qualitative chemical states of the aluminum surface were attained after rinsing it with pure THF. Slight variations perceived can be attributed to re-contamination of the surface or to small changes in air humidity and temperature that could have affected the composition of the upper hydro/oxide layer. Consequently, the lack of adsorption of ATMS is not attributed to an inadequate chemical state of

the surface. In conclusion, the substrate preparation method employed here and the implementation of a cleaning step with pure THF were effective, and allowed the adsorption of silicone components (siloxanes)

5.6.10. Molecular orientation of adsorbed PDMS on Al

The results have suggested that PDMS chains tend to adopt a flat configuration with the siloxane segments parallel or horizontally oriented with respect to the surface. The flattening behavior of adsorbed PDMS is favored by the high flexible backbone, high mobility of polymer molecules (room temperature>>$T_{g|PDMS}$) and the Si-O ionic character. In order to examine the changes in molecular orientation of PDMS molecules in the near surface region, the intensity ratios r_1,r_2 and r_3, defined in Section 5.6.2, are estimated for the two prepolymers (di-vinyl and di-hydride terminated PDMS) and the catalyst upon THF rinsing (Figure 5.70a-e). The ratios of the two prepolymers include long and short storage times



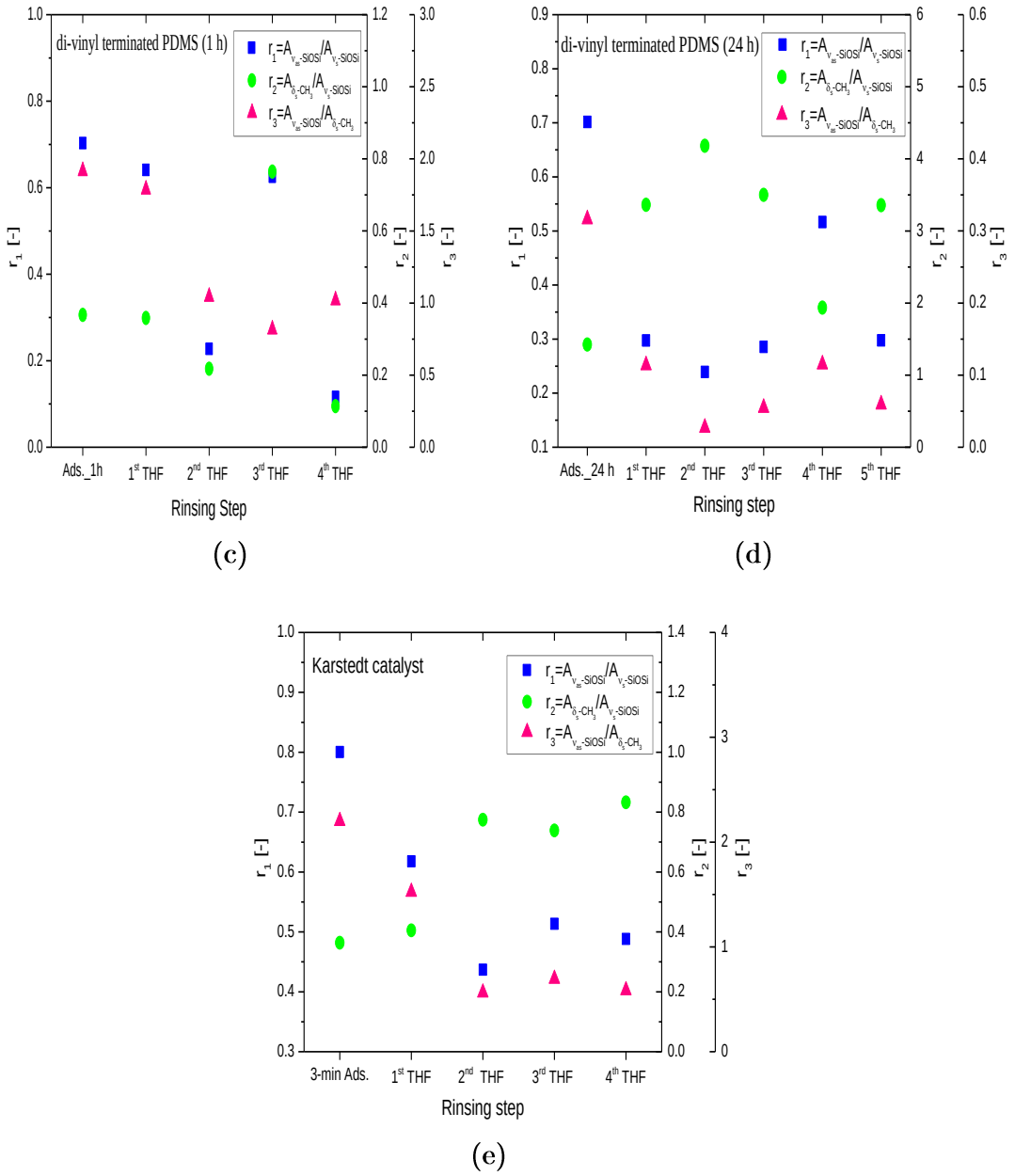


Figure 5.70. Intensity ratios r_1,r_2 an r_3 upon THF rinsing for di-hydride terminated PDMS at (a) 1 h and (b) 24 h of storage time, for di-vinyl terminated PDMS at (c) 1 h and (d) 24 h of storage time, and (e) for Karstedt catalyst (1 h).

A tendency of r_1 and r_3 to decrease, and r_2 to increase is observed, indicating chain flattening of PDMS in the near surface region as well. Thus, Si-O-Si segments tended to be horizontally oriented to the surface. Analysis of the variation of the intensity ratio for each PDMS sample is given as follows:

- **di-hydride terminated PDMS.** In the spectra for short storage time (Figure 5.19), it was detected that ν_{as}-Si-O-Si overlaps with a new emerging band. Thus, in

order to avoid misinterpretation, the ratios involving the peak area of ν_s-Si-OSi, r_1 and r_3, are not estimated and only r_2 is plotted (Figure 5.70a). The plot shows that r_2 increases upon solvent rinsing, suggesting that some methyl groups were vertically oriented with respect to the chain axis. For longer storage time (Figure 5.70b), chain flattening is also inferred as r_1 decreases up to the 3rd THF. However, after the 3rd THF r_1 increases again. This suggests that the flattening process was restricted at a certain point. The fluctuation of r_2 suggests that methyl groups were changing their orientation both horizontally and vertically to the chain axis after contact with pure THF. These trends of r_1 and r_2, accompanied with the tendency of r_3 to increase, suggests that more loops or backbone segments were lifting from the surface after the 3rd THF rinse.

- **di-vinyl terminated PDMS**. For short storage time (Figure 5.70c), there is a trend of r_1 and r_2 to decrease up to the 2nd THF rinse, but it increases after the 3rd THF rinse, suggesting a change in orientation or a measurement artefact. The tendency of r_1 and r_3 to decrease suggests horizontal orientation of the backbone, and the reduction of r_2 indicates that methyl groups were not necessarily vertically oriented with respect to the chain axis. In the case of longer storage times (Figure 5.70d), the trend observed for r_1 and r_3 again supports the chain flattening configuration. The disruption observed after the 4th THF rinse could be due to an artefact or a restriction experienced by the polymer chains. The behavior of r_2 is seen to be rather ambiguous, suggesting again no preferential orientation of methyl groups at the interface.
- **Karstedt catalyst**. Chain flattening upon solvent rinsing is also suggested by the decrease in r_1 (Figure 5.70e). The increase in r_2 indicates that methyl groups might be oriented rather vertically to the backbone axis

It can be assumed that the continuous removal of weakly interacting molecules with the substrate surface favored the chain flattening process of PDMS, as more surface sites could be occupied by a single molecule. However, some restrictions appeared in the system after certain THF rinses, which apparently changed the degree of freedom of PDMS molecules. These restrictions could have been chemisorbed segments and the presence of other loosely adsorbed PDMS molecules with fewer adsorbed segments. Consequently, the adjustment of the remaining PDMS molecules in the system possibly caused an increase in the size and number of the polymer loops. It can be hypothesized that the adsorbed layer was comprised of two distinct types of conformations, one was flattened and tightly bound to the surface, and the other loosely adsorbed with fewer adsorbed segments. The results also suggest that the chain flattening process was more effective in PDMS of higher molar mass, as less restrictions

were inferred for the intensity ratios in the Karstedt catalyst when compared with those of the two prepolymers.

Concerning the methyl groups, it is seen that they can adopt different orientations, either horizontal or vertical with respect to the surface. Despite that there is a tendency of methyl groups to be oriented vertically to the surface, the possibility of methyl groups to be in contact with the surface (horizontally oriented) imparts conformational stability to the extended chain. Such configuration causes the backbone plane to be oriented at a certain tilt angle θ with respect to the substrate normal (Figure 5.71a), and the Si-O-Si segment at certain angle φ with respect to the surface plane (Figure 5.71b). The maximum inclination they can attain occurs when two hydrogen atoms in CH_3 are in contact with the surface.

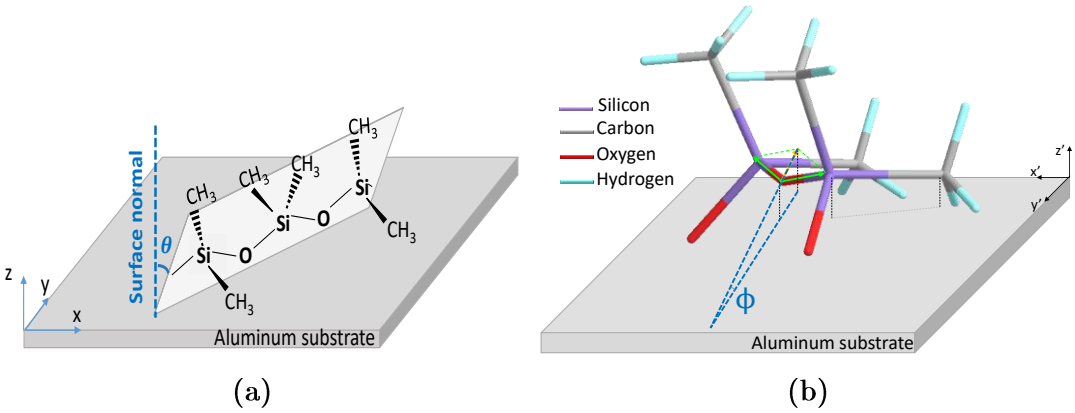


Figure 5.71. Proposed model of oriented PDMS chains on the aluminum surface. (a) θ: tilt angle of the backbone plane with respect to the substrate normal and (b) ϕ: angle of the Si-O-Si bond with respect to the surface when a chain fragment with two methyl groups are in contact with the surface by two hydrogen atoms.

Possible chain conformations are proposed in the model of Figure 5.72, in which the number of CH_3 groups oriented towards the surface changes. If one methyl group is oriented horizontally to the surface, this implies a higher degree of orthogonality of the other methyl group attached to the same Si atom. In fact, this situation supports the increase of the intensity ratio, r_2. Representations of the three-dimensional (3-D) views of a single possible conformation of the adsorbed chains are given in Figure 5.73. In reality, extended caterpillar or extended helix configurations can possibly be adopted by the PDMS chains [51]. In this proposed model, the inclination of the backbone with methyl groups in direct contact with the surface, causes the oxygen atom to be lifted at certain height from the surface.

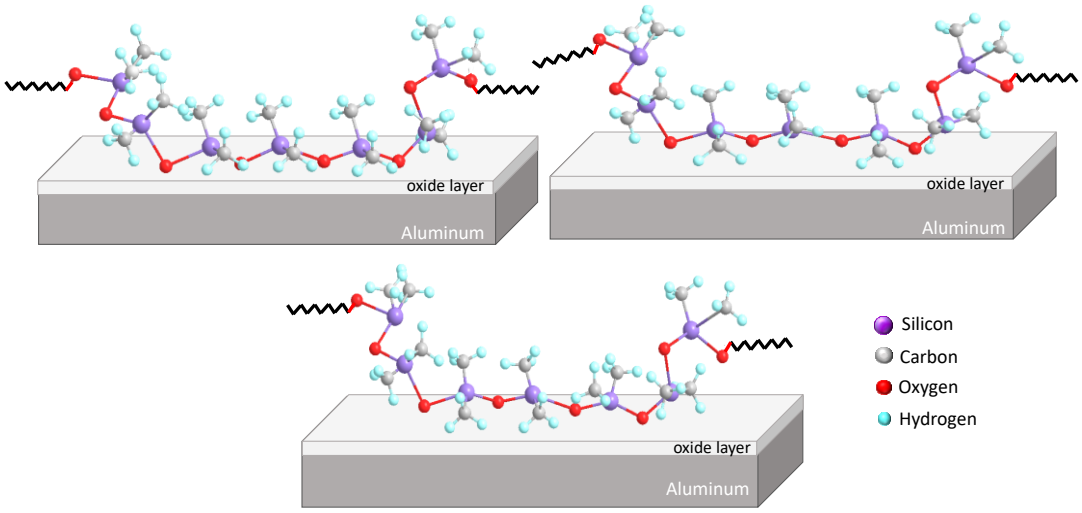


Figure 5.72. Possible conformations proposed for a single PDMS chain adsorbed on aluminum, depending on the number of methyl groups in direct contact with the surface

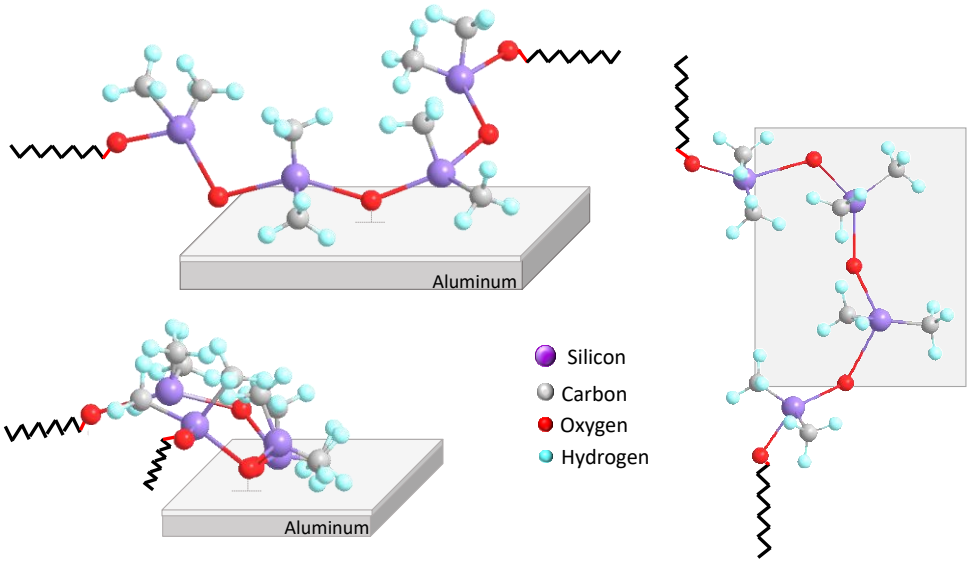


Figure 5.73. 3-D representation of the front, side and top views of an adsorbed PDMS segment in the orientation proposed having methyl groups in direct contact with the surface. In this conformation, the oxygen atom is lifted from the surface.

Interestingly, the molecular orientation proposed in this work, with PDMS having one methyl group pointing to the surface and the other pointing outwards, has been also postulated by Kim and coworkers [393] for PDMS at the water/air interface. They have inferred two possible PDMS conformations to account for the results. In the first, the

methyl groups are totally random-oriented, and in the other they are plane-symmetric to the interface, i.e. one methyl group points out into the air and the other points into the water. In their case, as methyl groups are hydrophobic, the first option was more likely to occur.

In conclusion, the model proposed in this work of PDMS oriented at certain tilt angle respect to the surface and one methyl group pointing to the surface, could justify some of the spectral features observed, such as broadening of Si-O-Si and CH_3 absorption bands, and could support the maximization of attractive forces such as permanent-induce dipole-dipole interactions of Si-O-Si bonds and CH_3 groups with the aluminum surface.

5.6.11. Adhesion mechanisms of silicones on Al

The consistent features observed in the measured spectra at 1110-900 cm^{-1}, related to Si-O-Si stretching modes, have enabled the assignment of the Si-O-Si bond as the adhesion partner of silicones. This assignment is in good agreement with previous investigations about the adsorption of PDMS on different substrates described in Section 3.3.1. However, significant contribution to adhesion could be due to Si-OH end-groups and, to a lesser extent, to Si-H terminal groups.

Different types of forces involved in the interfacial region are believed to have contributed to the overall adhesion of PDMS on aluminum. These interactions include covalent bonding and secondary bonding forces such as hydrogen bond (or, in a more general sense, the acid-base interaction), permanent-induced dipole interactions, electrostatic forces and other donor-acceptor interactions. Moreover, dispersive forces can arise from instantaneous dipoles originating from the presence of the delocalized electrons in the metallic surface. It has been claimed that the secondary forces play a key role in the adhesion of most adhesives [405].

Defining a specific dominant mechanism is not straight forward and the studies should be complemented by quantum mechanical calculations, to draw final conclusions. As mentioned in Section 3.3.1, many attempts have been made in the past in order to understand the nature of such interactions between siloxanes and solid surfaces, which have led to opposite conclusions.

In this thesis, based on the experimental results, the deduction of the siloxane bond as the adhesion partner, and the preferential orientation of adsorbed PDMS with methyl groups pointing to the surface, a set of different adhesion mechanisms involving Si-O-Si bonds are proposed. They are presented schematically below.

- **Mechanism I: Covalent bonding**

The mechanisms of possible covalent bonding via Si-H and Si-OH bonds have already been illustrated in Figure 5.61 and 5.69.

- **Mechanism II: Hydrogen bonding**

In a broader sense, H-bonding is considered an acid-base interaction [126,406,407], thus, the protons in the OH groups of the surface are considered proton donors (Lewis acids), while the lone pair electrons of the oxygen in Si-O groups are defined as proton acceptors (Lewis bases). However, the Si-O bond has been classified as a very weak base due to the high ionic nature of the bond, and hyperconjugation effects [69,76], and the ability of Si-O bonds towards hydrogen bonding formation has been questioned [368]. Therefore, despite that H-bonding has been frequently proposed as a key mechanism of adhesion of silicones, it is not an obvious situation.

From the results obtained in this work, a new band located near 960 cm^{-1} suggested the existence of Si-O-Si segments bound to the surface by hydrogen bonds. Hence, the strong adsorption performed by PDMS indicates that the conditions for forming H-bonding were favorable. More likely, the orientation and chain conformation of PDMS on the surface and proposed in this work, allowed the creation of hydrogen bond interactions.

The mechanism of adhesion via hydrogen bonds between Si-O-Si and OH groups on the surface of an adsorbed PDMS chain segment is illustrated in Figure 5.74. This mechanism is assumed to be also valid for TDMS, or siloxane compounds, on native aluminum oxide. Hydrogen bonding has been prior proposed by different researches [34,49].

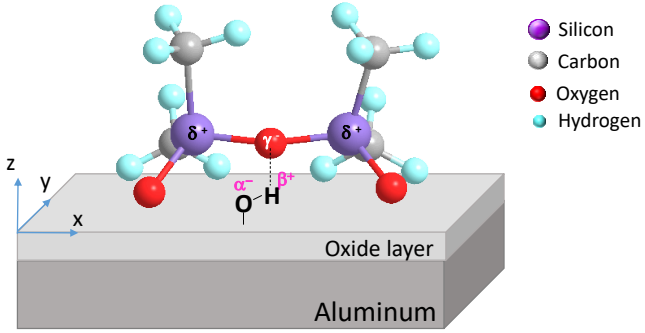


Figure 5.74. Mechanism of adhesion due to H-bonding between the oxygen atom in Si-O-Si and hydrogen of –OH groups on aluminum. Illustration for an adsorbed PDMS segment oriented with methyl groups pointing to the surface.

Another plausible mechanism involving hydrogen bonds is between Si-O-Si groups and physisorbed water molecules on the surface (Figure 5.75). Nevertheless, the strong adsorption displayed by PDMS and TDMS suggests that this type of H-bonding was weaker than the one suggested before.

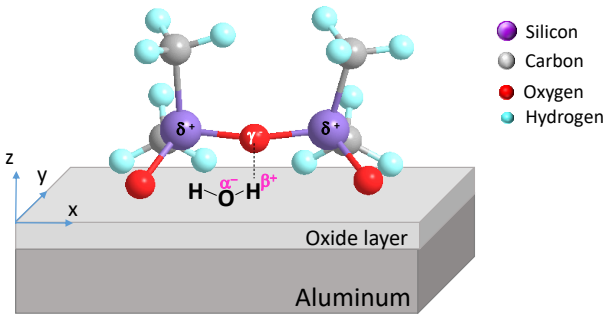


Figure 5.75. Mechanism of adhesion due to H-bonding between Si-O-Si and physisorbed water molecules on the surface. Representation for an adsorbed PDMS segment oriented with methyl groups in contact with aluminum.

- **Mechanism III: Permanent-induced dipole-dipole interactions**

Due to the difference in electro negativities between silicon and oxygen, the disiloxane bond possesses a permanent dipole moment, μ~ 0.63 D [408], which above the metal surface induces a charge redistribution in the substrate that can be classically described as an interaction of a dipole with its self-induced image dipole [409]. This permanent-induced dipole interaction is attractive and is maximized when adsorbed PDMS is oriented with methyl groups pointing to the surface (Figure 5.76a). Thus, the tilted permanent dipole vector with respect to the surface enhances the interaction with its image dipole vector in the substrate (Figure 5.76b). Additionally, for Si-H terminal groups dipole-dipole interactions were also proposed and illustrated in Figure 5.62b.

An additional adhesion mechanism could be proposed in which the permanent dipole existing between Si and C atoms, due to the difference in electronegativities, interacts with the substrate by a permanent-induced dipole-dipole interaction.

Considering the proposed model of oriented PDMS on Al with methyl groups in direct contact with the surface, in such orientation, the interaction between the Si-C bond dipole with an induced dipole is maximized.

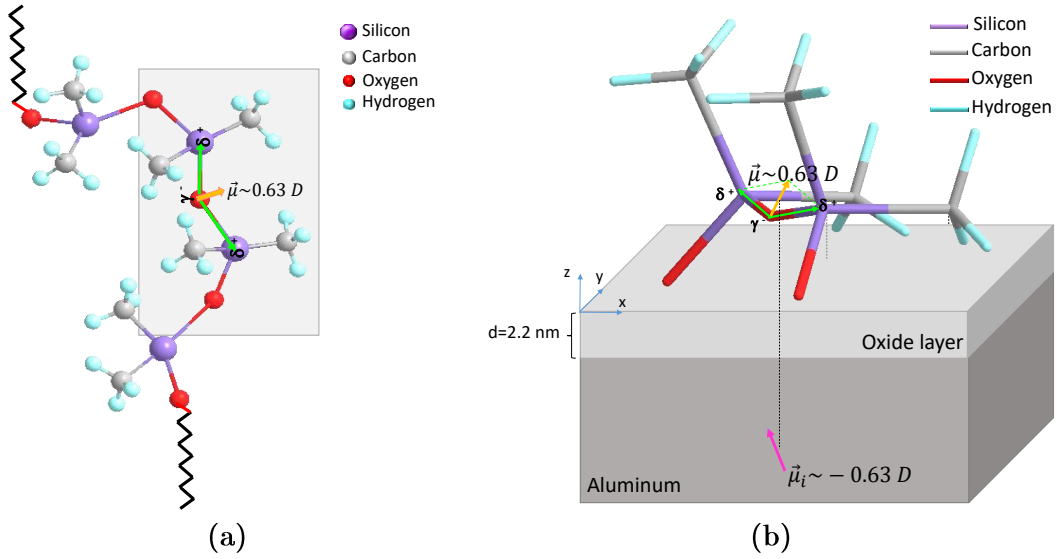


Figure 5.76. (a) Top view of the Si-O-Si permanent dipole moment of an adsorbed PDMS chain with methyl groups horizontally oriented to the surface, (b) Mechanism of adhesion due to permanent-induced dipole interaction of the Si-O-Si bond. Representation of a Si-O-Si segment adsorbed on Al with two methyl groups pointing into the surface.

In this specific orientation of PDMS, the energy for an individual permanent-induced dipole interaction can be calculated from the Keesom energy equation (Equation 5-31) [410], for two dipoles A and B if the distance R and the angle 2ϕ between the two dipoles $\vec{\mu} = \vec{p}_A$ and $\vec{\mu}_i = \vec{p}_B$ is known (Figure 5.77).

$$E_{AB}^{dipol} = \frac{1}{4\pi\varepsilon_o R^3}\left[-\vec{p}_A \cdot \vec{p}_B + 3\frac{(\vec{p}_A \cdot \vec{R})(\vec{p}_B \cdot \vec{R})}{R^2}\right] \qquad \textbf{(5-31)}$$

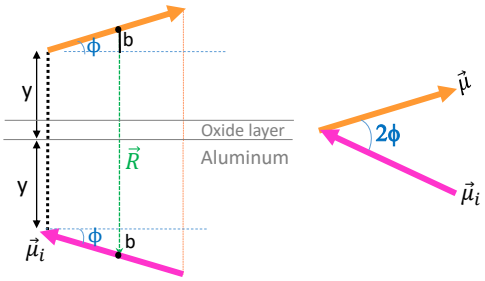


Figure 5.77. Geometrical considerations between the Si-O-Si permanent and the induced dipole moments, $\vec{\mu}$ and $\vec{\mu}_i$, respectively.

- **Mechanism IV: Electrostatic forces**.

Physisorption of PDMS also occurs due to electrostatic attraction between its partial atomic charges and the aluminum substrate. Because aluminum consists of positive ions and free electrons, upon adsorption, the partial atomic charges of PDMS cause the redistribution of charges with opposite sign on the substrate [411]. Therefore, electrostatic attractive forces are established. The proposed adhesion mechanism is illustrated in Figure 5.78.

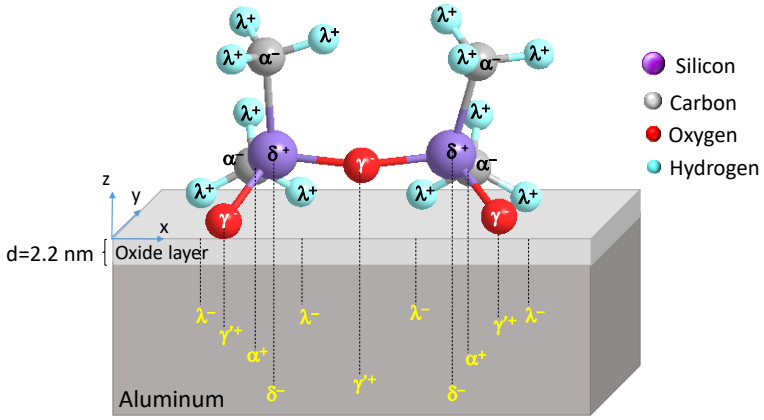


Figure 5.78. Mechanism of adhesion due to electrostatic attraction between partial atomic charges in PDMS and the aluminum substrate. Illustration for an adsorbed PDMS segment with methyl groups parallel to the surface.

In general, the electrostatic force on charge point q_i due to electrostatic interactions with point q_j at a distance r_{ij}, can be calculated based on the Coulomb interaction law (Equation 5-32) [412,413], as follows:

$$F_i = \frac{1}{4\pi\varepsilon_o}\frac{|q_i q_j|}{{r_{ij}}^2} = k_e\frac{|q_i q_j|}{{r_{ij}}^2} = 8.988\times 10^9\frac{N\,m^2}{C^2}\frac{|q_i q_j|}{{r_{ij}}^2} \qquad \textbf{(5-32)}$$

Thus, from the illustrated model in Figure 5.78, local electrostatic interaction forces for each of the atoms in contact with the surface (two oxygen and two hydrogen atoms) can be calculated from Equation 5-33. The partial atomic charges for PDMS are extracted from quantum chemistry calculations given in the work of Smith et al. [113].

$$F_O = 8.988 \times 10^9 \frac{N\,m^2}{C^2} \frac{|\gamma^+\gamma^-|}{(2d + 2r_O)^2}$$
$$F_H = 8.988 \times 10^9 \frac{N\,m^2}{C^2} \frac{|\lambda^+\lambda^-|}{(2d + 2r_H)^2} \quad \textbf{(5-33)}$$

Where d is the thickness of the oxide layer, r_O and r_H are the atomic radii of oxygen and hydrogen, respectively; and the partial atomic charges for oxygen and hydrogen are: $\gamma = -7.402 \times 10^{-20}$ C, and $\lambda = 2.195 \times 10^{-20}$ C, respectively [113]. Thus, the electrostatic force estimated for the two oxygen and hydrogen atoms are:

$$F_O = 4.87 \times 10^{-12}\ N$$
$$F_H = 4.28 \times 10^{-13}\ N$$

Accordingly, the same can be done for the partial atomic charges of carbon (α), silicon (δ) and the other hydrogen atoms in PDMS if the distances between the partial charges and the surface are known. However, this is not the case. The total electrostatic interaction energy is then the sum of each of the individual forces.

- **Mechanism V: Donor-acceptor interactions.**

Due to a difference in electronegativities between Si and O atoms, a significant amount of the σ Si-O-Si bonds electron density is concentrated around the oxygen atom [76,383], and therefore available for donation [76]. Thus, a mechanism of adhesion could be proposed in which the lone pairs of electrons of oxygen in the Si-O-Si bond can interact with empty d orbitals of the Al in the oxide layer, and the lone pairs of electrons of oxygen in the oxide layer can interact with d orbitals of silicon atom of PDMS.

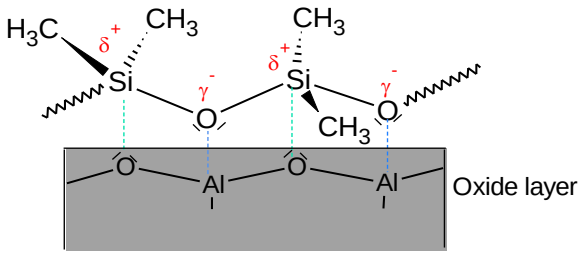


Figure 5.79. Mechanism of adhesion due to interactions between lone pairs of electrons of oxygen and empty d orbitals of Al and Si.

6 Co-Adsorption of the SSMC on Aluminum

6.1. Aim of coadsorption experiments

Formation of the interface is a complex process when structural adhesives are employed due to the multicomponent character of such materials and the requirement of polymer network formation for practical applications[8]. Adhesives, in their original state, consist of a fluid mixture of at least two components or reactive partners, either as monomers or prepolymers [8,17]. When applied to a surface, adhesives must spread and wet the surface first and then continue with the formation of the network by crosslinking [2,8]. Hence, adsorption proceeds in competition with crosslinking under the influence of possible molecular immobilization due to strong adhesion, presence of unreacted material and evolving of the polymer network[8]. Therefore, a distribution of properties such as molecular mobility, interactions, concentration of components, Complexity at the interface also arises from the newly bonds created upon crosslinking that can be capable of specific adhesion interactions with the substrate surface, and from the substrate itself which can have either a catalytic or inhibition effect on crosslinking [8]. Consequently, the formation and stability of the interface involving reactive systems is still not well understood. The superposition of events such as adsorption mechanisms and chemical reactions under the influence of the substrate surface makes the situation rather complex.

In order to contribute to the understanding of the formation of the interface between an aluminum surface and a reactive silicone system, co-adsorption experiments with the reactive mixture employed in the formulation of a model silicone adhesive, FMSA, were executed. In co-adsorption experiments, the reactive partners are exposed

to the surface simultaneously, a process which closely resembles typical application procedures of adhesives on a substrate. Since three SSMC (di-vinyl PDMS, TDMS and Karstedt catalyst) with differences in their chemical structure and molecular size, constitute the reactive mixture, concurrent adsorption between the three SSMC is expected to exist as well.

The aim of performing co-adsorption experiments is to gain knowledge of how the adsorption and crosslinking of silicones proceed competitively onto aluminum. The purpose is firstly to obtain insights in how all these competitive phenomena occur at the interface, and to examine their effect on the adhesion mechanisms proposed for the SSMC from individual adsorption experiments. Additionally, it is intended to determine if the aluminum surface has any catalytic effect on crosslinking.

From the results obtained in the previous chapter, the three SSMC contained in the reactive mixture, individually exhibited high affinity with the substrate. Consequently, they are expected to co-adsorb on aluminum, which also suggests that crosslinking at the interface is likely to occur.

6.2. Experimental methodology

The experimental process employed in the co-adsorption experiments followed the same steps of the individual adsorption experiments of the SSMC, already described in Section 5.3.2.2. In this case, however, the viability of implementing co-adsorption experiments was verified first. For this purpose, the course of the crosslinking reaction in THF solution, via Karstedt-catalyzed hydrosilylation, was monitored by ATR-FTIR. After the feasibility of performing co-adsorption was validated, the process continued with the execution of the in-situ co-adsorption experiments via FTIR-ERAS. Concurrent events of competitive adsorption and crosslinking reaction at the interface were investigated, both with and without the Karstedt catalyst. The analysis of the results was focused on understanding the differences between the measured ERA spectra and the corresponding bulk-like calculated spectra of the SSMC that were included in the reactive system.

6.2.1. Materials

The substrate employed was the same Al-PVD used for the individual adsorption experiments of the SSMC. Its preparation method and characterization can be found

in Section 5.3.1. The system evaluated consisted of bifunctional vinyl terminated PDMS (prepolymer 2), TDMS (crosslinker), and the Karstedt catalyst. The reader is directed to Section 4.4. for further details regarding the properties of these components in bulk. The solvent used for preparing the dilute solution and for the successive washing cycles was THF, whose specifications are provided in Section 5.3.2. The measurement cell device employed for the co-adsorption experiments was the same as that which was utilized for the adsorption experiments of the SSMC and its details can be found in Section 5.3.2.

6.2.2. Viability of co-adsorption experiments

The viability of executing in-situ co-adsorption experiments with the SSMC was first examined. The purpose was to determine if the Karstedt-catalyzed reaction takes place in dilute solution in THF. Preferably, the reaction should not occur during the first 5 min from the solution preparation, as this was the time usually needed between preparation and rinsing with the dilute solution. The question arose from the fact that the Karstedt-catalyzed crosslinking of FMSA in bulk occurred very rapidly, after only 8 min (Section 4.5.3). The reactive mixture, consisting of prepolymer 2, TDMS and Karstedt catalyst, dissolved in THF was monitored by ATR-FTIR for a total time of 7 min. On the other hand, no concerns were raised about the incidence of crosslinking in solution without catalyst. It was found that crosslinking reaction in bulk did not take place at room temperature during 65 h of observation when the catalyst was not included (Section 4.5.3).

Preparation of the solution

The crosslinking reaction of the reactive mixture (FMSA) in THF was examined from a more concentrated solution than the one used for executing adsorption experiments. The reason lies in the difficulty of identifying the characteristic Si-H stretching mode in the ATR-FTIR spectrum when the dilute solution was used. By diluting a reactive mixture, the dilution effect causes a slowing down of the reaction; therefore, if the crosslinking of the FMSA in solution does not occur at the higher concentration used here, it ensures that it does not take place in the dilute solution either.

The volume ratio of FMSA in THF used was 1:10 (instead of 1:100 used for adsorption experiments). For the solution preparation, in a glovebox purged with dry air (T_{dp}=-65 °C), the precise amount of prepolymer 2 (0.4421 g) was weighed inside a glass flask. Then, the respective amount of TDMS (0.158 g) was added. The molar ratio of Si-

H/Si-Vi was always kept at 1.5/1.0. Separately, 0.5 ml of pure Karstedt catalyst was poured into another glass flask for later use. The two flasks, one containing the multicomponent mixture, and the other the catalyst, were hermetically closed and carefully transported to the FTIR room. There, 6 ml of THF was added to the reactive mixture (prepolymer 2+TDMS), and the solution was stirred for approximately 1 min. Subsequently, 0.3 µl of Karstedt catalyst (equivalent to 20 ppm Pt(0) relative to vinyl-PDMS) were added to the solution and stirred once again during approximately 30 s. Immediately after, the ATR measurement cell (Figure 4.5) was filled with the solution and the spectra were collected at 1 min intervals for a total time of 7 min.

Results

The band of interest at 2130 cm^{-1} in the spectra (Figure 6.1), corresponding to the Si-H symmetric stretching mode, has been magnified inside the spectra. The peak intensity of the ν_s-Si-H band over time is seen to be invariable, indicating that crosslinking reaction of the reactive system dissolved in THF did not occur for 7 min. In this regard, the crosslinking was, in this case, stopped by the dilution and did not proceed during the time of interest (5 min). Consequently, the viability of executing co-adsorption experiments of the reactive system or the FMSA is validated.

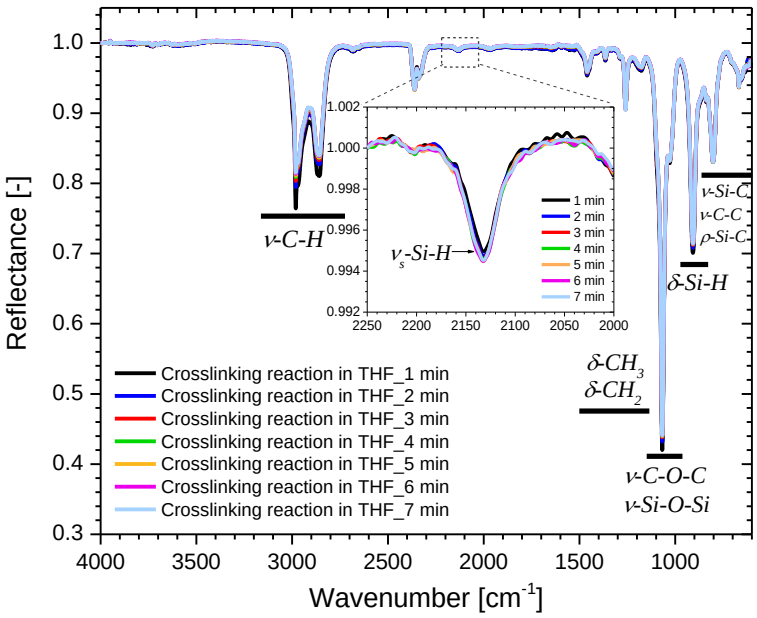


Figure 6.1. ATR-FTIR spectra of the reactive mixture dissolved in THF. No variation in peak intensity of ν_s-Si-H at 2130 cm^{-1} indicates that crosslinking reaction via hydrosilylation did not occur in THF.

6.2.3. In-situ co-adsorption experiments

The procedure applied for the in-situ co-adsorption experiments is the same as that implemented in the adsorption of the SSMC on aluminum, which is described in more detail in Section 5.3.2.2 (Figure 5.12). The main difference was the preparation of the dilute solution, since a multicomponent reactive system is used here. Also, the storage time applied after the 3-min co-adsorption step (before consecutive THF rinses) was extended to 50 h in order to analyze both the dynamics of the adsorbate and the incidence of the crosslinking reaction at the interface. Co-adsorption was first evaluated without the Karstedt catalyst with the aim of elucidating any possible catalytic effect of the aluminum surface on the crosslinking at the interface. Then, co-adsorption including the Karstedt catalyst was examined with the purpose to inspect simultaneous events at the surface, such as competitive adsorption and Karstedt-catalyzed hydrosilylation. Once the 50 h were completed, the substrate was consecutively rinsed with pure THF until no significant changes in peak intensities were observed. In total, four to five solvent rinsing cycles were applied.

Preparation of the dilute solution

The volume ratio of the FMSA in THF was always kept at 1/100. This ratio was the same employed in the individual adsorption of the SSMC on Al. The contribution of the catalyst to the total mass of the mixture is neglected, since it was added at very low concentration (20 ppm $Pt^{(0)}$, relative to prepolymer 2). Additionally, the crosslinker (TDMS) was added in a molar ratio in respect to vinyl DPMS of Si-H/Si-Vi = 1.5/1.0. The concentration of each component in the dilute solution is presented in Table 6.1.

Table 6.1. Concentration of the TDMS and Prepolymer 2 in the dilute solution for co-adsorption experiments.

Component	Mass [g]	Concentration (g/ml_{THF})	Concentration [M]
Bifunctional vinyl terminated PDMS -Prepolymer 2	0.4421 ± 0,0004	0.00737	$2.137x10^{-05}$
Tetrakis (dimethylsiloxy) silane (TDMS)-Crosslinker	0.158 ± 0.0003	0.00263	$3.167x10^{-05}$
Karstedt Catalyst (Pt complex solution)	$3x10^{-4}$ g ~ 0.28 µl	$5x10^{-6}$	-

The standard procedure for the preparation of the dilute solution was the same as that described for evaluating the reaction in THF. The only difference is that 60 ml of THF

were added to the reactive mixture. The concentrations of TDMS and prepolymer 2 were kept constant in all experiments.

Spectra evaluation-methodology

The interpretation of the co-adsorption results is based on a qualitative comparison between a bulk-like calculated spectra and the measured ERA spectra of the adsorbate. Because in this case a multicomponent reactive system is employed, the comparative analysis should include a bulk-like calculated spectrum of such a reactive mixture. However, the analysis using a single bulk-like spectrum of the reactive system (FMSA) is inappropriate for two reasons. First, the state of the reactive system changes over time due to crosslinking. This implies that several bulk-like spectra must be calculated for a correct interpretation. Secondly, simultaneous events, such as competitive adsorption, preferential adsorption and crosslinking, would be difficult to discern. Alternatively, the measured ERA spectra of the adsorbate are compared with the individual calculated bulk-like spectra of each component included in the reactive mixture, i.e. prepolymer 2, the TDMS and the Karstedt catalyst.

6.3. Results and interpretation

Two different scenarios were investigated. Firstly, the Karstedt catalyst was not added to the reactive system, thus a possible catalytic effect of the aluminum surface on crosslinking can be elucidated. Secondly, the Karstedt catalyst was included in the reactive mixture, hence the possible occurrence of the Pt catalyzed hydrosilylation reaction at the interface can be inspected.

6.3.1. Co-Adsorption – without the Karstedt catalyst

First, the chemical state of the Al substrate after being rinsed with THF and before co-adsorption was examined (Figure 6.2). The positive band observed at ~990 cm^{-1} is assigned to the aluminum oxide [360]. Its appearance after the THF rinse indicates a growth of the native oxide layer. Small peaks in the -C-H region are also observed in the magnified spectrum, suggesting recontamination of the surface after solvent rinse. These observations are in good agreement with those previously observed for the SSMC, confirming that a reproducible chemical state of the aluminum surface was obtained in

this work after solvent cleaning. Reactive aluminum oxide surfaces, able to feature good bonding capacity towards the adsorbate layer, were consistently obtained.

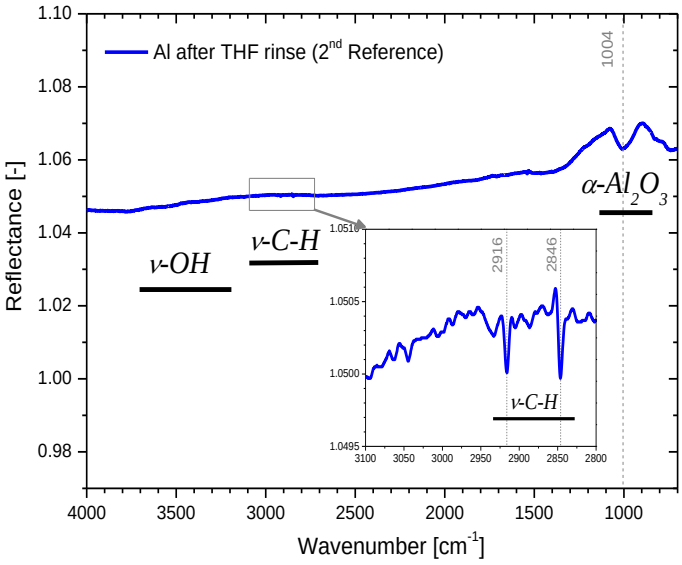


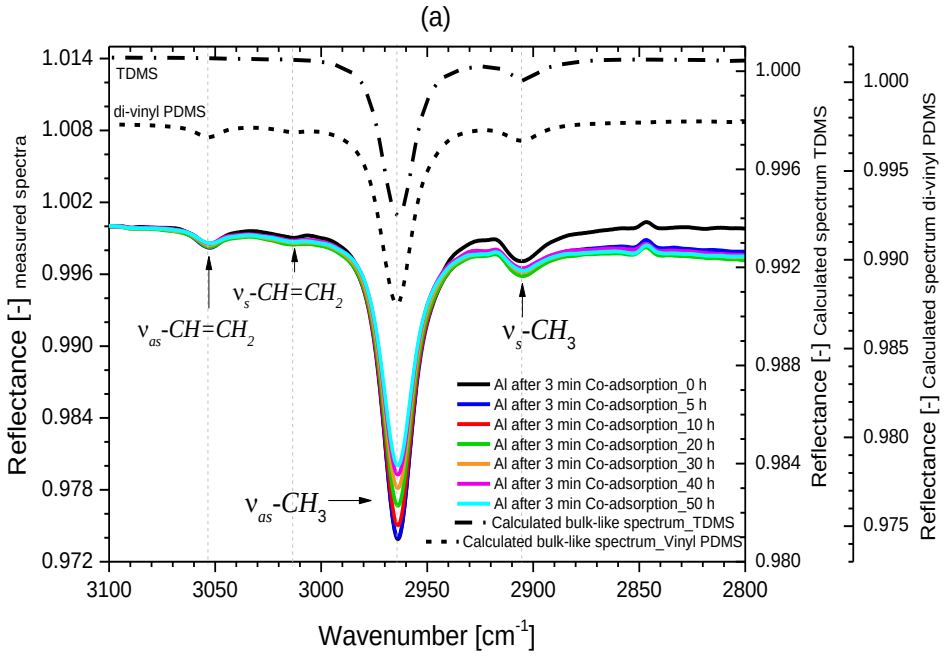
Figure 6.2. Chemical state of the aluminum surface after being rinsed with pure THF and before the co-adsorption experiments.

The spectra of the adsorbate over time is displayed in Figure 6.3a-c. The calculated bulk-like spectra of the single components TDMS and prepolymer 2 are included for ease of comparison. The principal absorption bands identified in the spectra are listed in Table 6.2 with their respective assignments based on previous results in Chapter 4 and 5. The measured spectra of the adsorbate replicate, at all times, the spectral features of the bulk-like spectrum of di-vinyl PDMS. This fact indicates that immediately after the 3-min co-adsorption step, the adsorbate was predominantly a dense layer of vinyl terminated PDMS with bulk properties, which also suggests preferential adsorption of vinyl PDMS over TDMS. Plausible preferential adsorption of PDMS evidences the dominant role of Si-O-Si bonds in the adsorption of siloxane-containing species. From the individual adsorption results, the Si-O-Si bond was defined as the adhesion partner; therefore, as the number of Si-O-Si bonds is higher in prepolymer 2, it would be preferentially adsorbed. In this way, more surface sites can be occupied by a single PDMS chain in comparison with a TDMS molecule.

At first sight, the lack of the distinctive band associated with Si-H groups at ~2138 cm^{-1} (Figure 6.3b) suggests that TDMS was not adsorbed. However, the absence of the ν_s-Si-H band can also be associated with two possible situations. First, that TDMS was

only weakly adsorbed on aluminum, and is masked by the considerably high amount of PDMS molecules in the adsorbate layer. Secondly, that Si-H groups were consumed in a chemical reaction either with the substrate or with vinyl PDMS (crosslinking). The participation of Si-H groups in hydrosilylation implies simultaneous consumption of -Si-CH=CH_2 groups over time, which can be inferred either by the vanishing or by the decrease in intensity of the vinyl absorption bands in the spectra. However, peaks of vinyl functionalities are detected during the whole experimental time, ruling out a possible crosslinking process via hydrosilylation. In fact, the lack of bands at 1150-1220 cm^{-1}, related to Si-CH_2-CH_2-Si groups formed from hydrosilylation, also suggests that crosslinking did not take place without the Karstedt catalyst in a lapse of 50 h.

In order to support this assumption, the representative bands: $\nu_{as,s}$-CH=CH_2, at 3053-3000 cm^{-1} and δ_{as}-Si-H, at 913 cm^{-1} are inspected in more detail in Figure 6.4. Interestingly, the δ_{as}-Si-H band is observed in all the spectra, indicating the presence of TDMS in the adsorbate layer but to a lesser extent than prepolymer 2. This band is slightly shifted by 3 cm^{-1} to lower frequencies over time, evoking a change in the chemical environment of the Si-H groups in the adsorbate state. The bands ascribed to vinyl groups are also perceived in the spectra, indicating that neither vinyl nor Si-H groups were involved in crosslinking over time. It can be suggested that the aluminum surface does not have any catalytic effect on hydrosilylation.



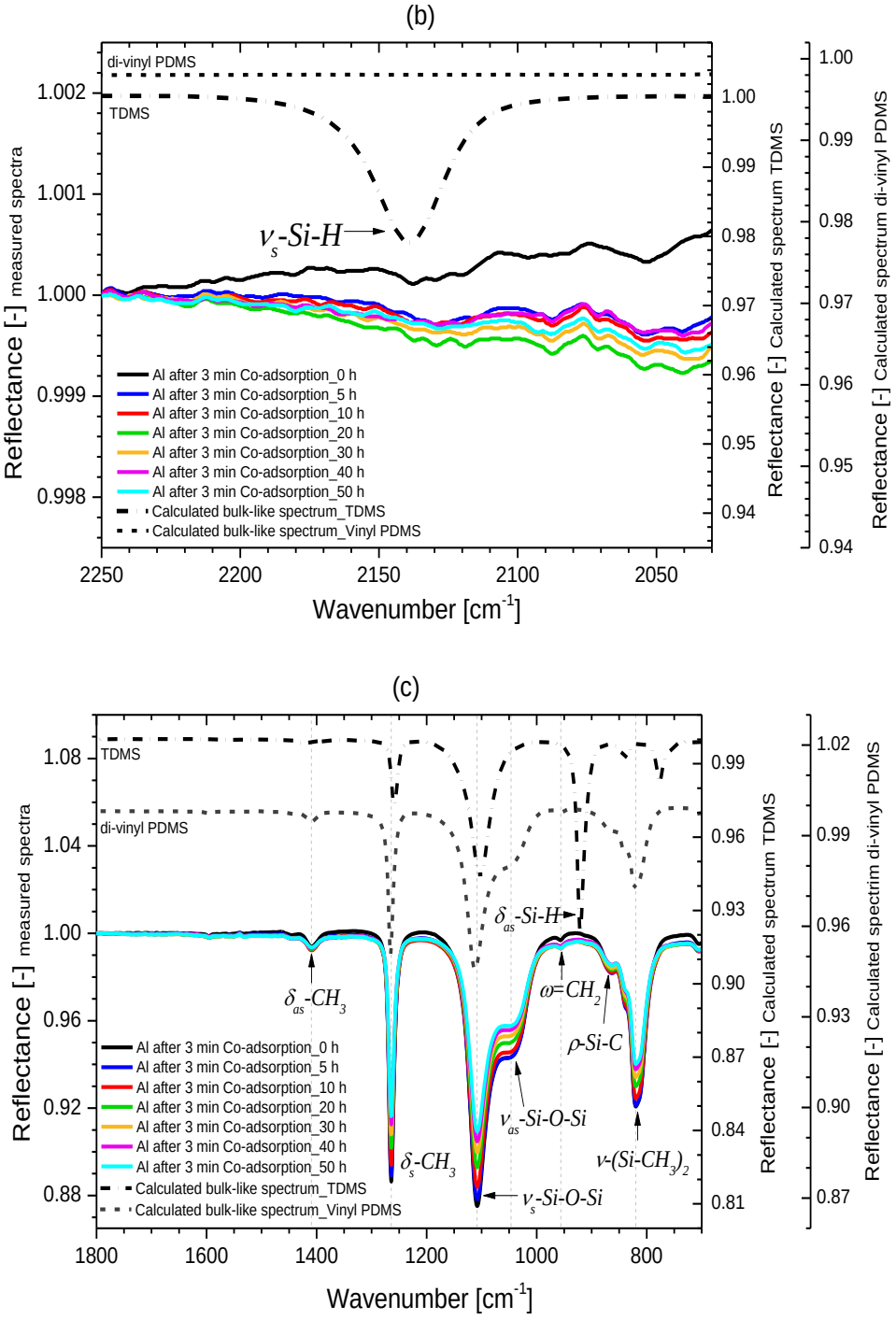


Figure 6.3. FTIR-ERA spectra over storage time of co-adsorbed TDMS and di-vinyl PDMS (no catalyst). The bulk-like calculated spectra are included. The spectra are displayed in three separate regions: (a) at 3100-2800 cm^{-1}, (b) at 2250-2000 cm^{-1} and (c) at 1800-700 cm^{-1}.

Table 6.2. Characteristic IR bands of the adsorbate obtained after the 3-min co-adsorption step of TDMS and Prepolymer 2.

Peak	Wavenumber [cm^{-1}]	Assignment
1	3053	ν_{as}=CH$_2$, CH=
2	3012	ν_{s}=CH$_2$, CH=
3	2964	ν_{as}-CH$_3$
4	2904	ν_{s}-CH$_3$
5	1409	δ_{as}-CH$_3$
6	1265	δ_{s}-CH$_3$
7	1107	ν_{s}-Si-O-Si
8	1050	ν_{as}-Si-O-Si
9	957	ω=CH$_2$
10	864	ρ-Si-C
11	816	ν-Si-C

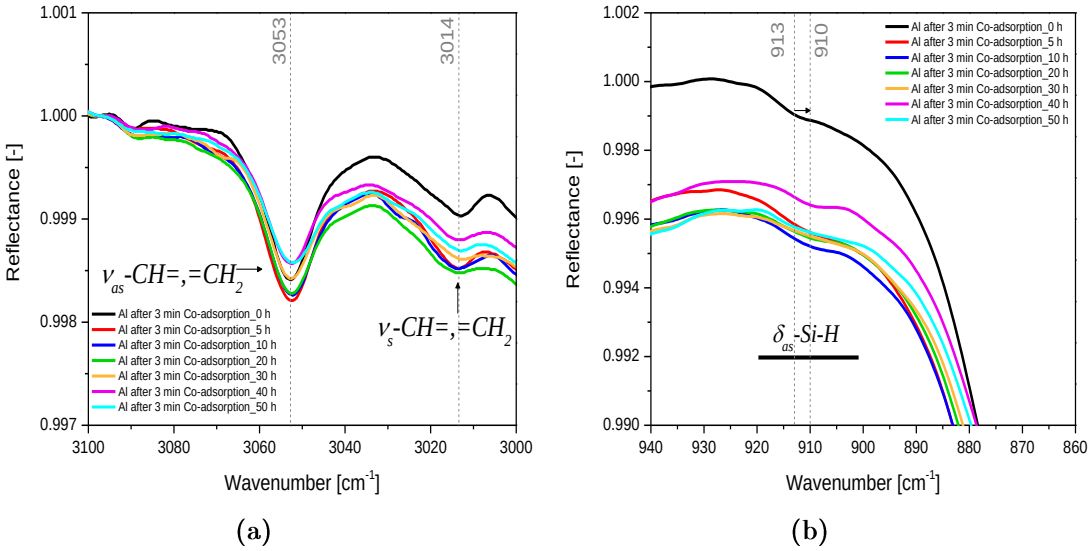


Figure 6.4. Magnified spectra after the 3-min co-adsorption step of the bands associated with: (a) vinyl groups at 3100-3000 cm^{-1} and (b) Si-H groups at 913 cm^{-1}, in the absence of the Karstedt catalyst.

Individual peak fitting of the IR absorption bands was used for supporting the interpretation of the spectra. In this case, the absorption bands listed in Table 6.2 were fitted to a Voigt function in the software OriginPro® 8.6. The calculated peak areas against time are shown in Figure 6.5. A parallel decrease in peak areas over time is observed between absorption bands, which indicates that the functional groups in PDMS were all desorbing at the same velocity. Most likely, PDMS molecules that were

weakly interacting, or were not in direct contact with the surface, desorbed progressively with time. Those poorly interacting molecules plausibly consisted of short lineal oligomers, since they are considered highly volatile at room temperature, as claimed by Yan et al. [414], Lenk et al. [51], Noll et al. [19] and Liu et al. [415]. Volatility of low molar mass PDMS molecules was also suggested by TGA analysis of FMSA. This desorption behavior was not observed in the individual adsorption of prepolymer 2, which indicates that the presence of adsorbed TDMS molecules influences this behavior. Steric effects could have favored successive desorption of low molar mass molecules. A distribution of adsorbed states (from strongly to weakly) existed for the molecules within the adsorbate.

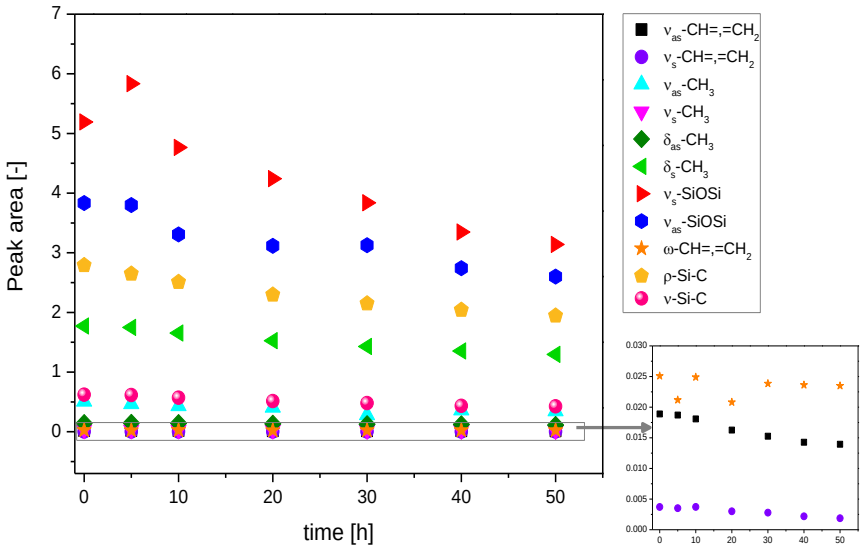


Figure 6.5. Variation of the peak areas over time of the absorption bands in the spectra after the 3-min co-adsorption step without the Karstedt catalyst.

For a more precise analysis of orientational changes over time, the intensity ratios r_1, r_2 and r_3, previously defined in Section 5.6.3, are estimated and plotted in Figure 6.6. The trends observed for the intensity ratios indicate that desorption and orientational adjustments occurred simultaneously over time. The increase of r_1 suggests some deviation away from the flattened orientation, indicating that the backbone chain lifts and possibly, loops are formed. This supports the idea that the polymer is adopting an orientation with certain degree of orthogonality with respect to the substrate surface [136]. In the individual adsorption of di-vinyl PDMS (prepolymer 2), the chain flattening process was also seen to be interrupted after a certain time. Possibly, the

weak interactions of the terminal vinyl groups with the surface contribute to the deviation from chain flattening of PDMS, as suggested by Patel et al. [34]. The flattening process of PDMS could also be influenced by the presence of adsorbed TDMS molecules, which could have induced PDMS to adopt a more coiled conformation. Therefore, PDMS molecules with a variable fraction of segments oriented parallel to the surface were more likely obtained.

On the other hand, the slight trend observed for r_2 to increase over time suggests that methyl groups tend to be vertically oriented with respect to the chain axis. The invariability observed for r_3 over time suggests that coiling of the backbone and vertical orientation of methyl groups compensates. In summary, these conformational changes evidence that the adsorbate was not in equilibrium and that the adsorbed molecules possess the sufficient mobility for enhancing interactions and improving orientation and packing density with time.

Ultimately, the region of the O-H stretching vibration mode at 3700-3200 cm^{-1} (Figure 6.7) was inspected to examine if hydrolysis of Si-O-Si or Si-H bonds took place during the 50 h of storage time and led to the formation of Si-OH groups. The spectra do not reveal bands associated with hydroxyl groups, which suggests the incidence of hydrolysis over time. However, the presence of Si-OH groups cannot be discarded, as they could be masked by the bulk PDMS molecules or could be chemisorbed forming Si-O-Al covalent bonds.

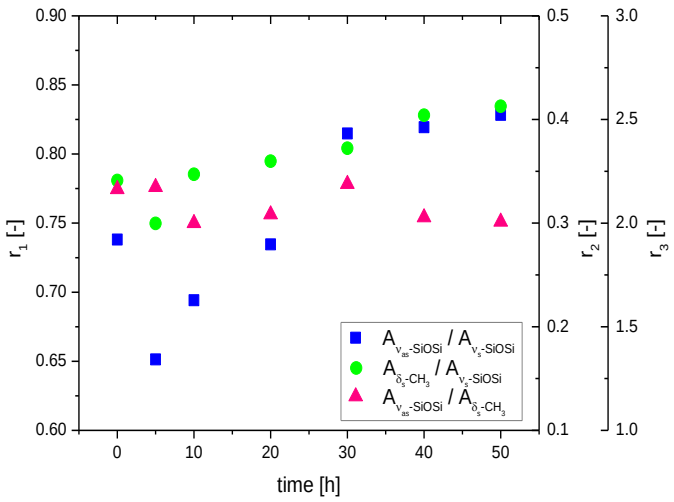


Figure 6.6. Variation of the peak intensity ratios r_1, r_2 and r_3 over time after the 3-min co-adsorption step without the Karstedt catalyst.

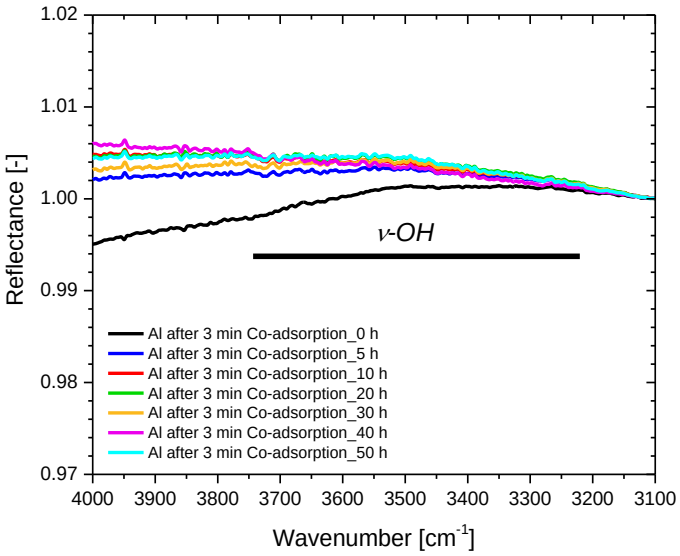
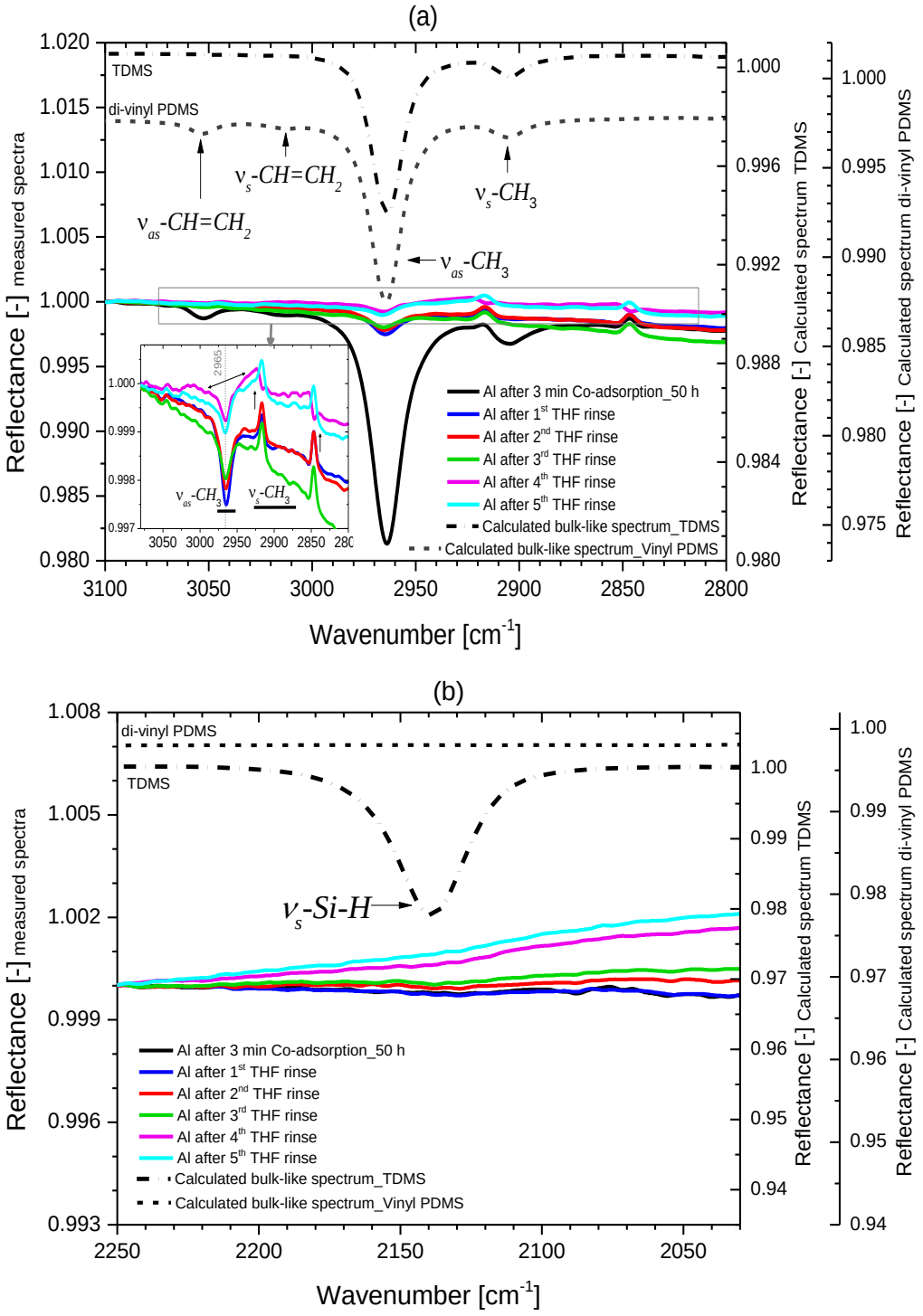


Figure 6.7. Evolution of the O-H stretching mode over time after the 3-min co-adsorption step without the Karstedt catalyst.

After the 50 h of storage time were completed, five sequential THF rinsing cycles were carried out. The spectra after those rinses are shown in Figure 6.8a-c. The peak intensities after the 1st THF rinse decrease remarkably, pointing to the removal of bulk polymer or weakly interacting molecules. Desorption of loosely adsorbed molecules is driven by the attainment of a new equilibrium and more stable state in solution with THF than with the surface [325]. Slight drift of the baseline into a buckled type is observed, indicating that structural modifications to the aluminum surface occurred upon solvent washing. Comparison of the measured spectra with the bulk-like calculated spectra reveal different features which evidence strong interactions at the interface.

In the spectral region from 3100 to 2800 cm^{-1} (Figure 6.8a), the ν_{as}-CH_3 band displays a peak shape alteration, and a slight peak shift towards higher frequencies after four solvent rinses. On the other hand, the bands ascribed to stretching modes of vinyl groups are imperceptible in the spectra, most likely due to the usual weak intensity of bands related to vinyl groups in FTIR, and to the progressive removal of material. The ν_{s}-CH_3 peak is indistinct due to the presence of the two negative peaks related to desorption of carbon-contaminants during solvent washing.


(a)
TDMS
di-vinyl PDMS
ν_s-CH=CH$_2$
ν_{as}-CH=CH$_2$
ν_s-CH$_3$
ν_{as}-CH$_3$
Al after 3 min Co-adsorption_50 h
Al after 1st THF rinse
Al after 2nd THF rinse
Al after 3rd THF rinse
Al after 4th THF rinse
Al after 5th THF rinse
Calculated bulk-like spectrum_TDMS
Calculated bulk-like spectrum_Vinyl PDMS
Reflectance [-] measured spectra
Reflectance [-] Calculated spectrum TDMS
Reflectance [-] Calculated spectrum di-vinyl PDMS
Wavenumber [cm^{-1}]
(b)
di-vinyl PDMS
TDMS
ν_s-Si-H
Al after 3 min Co-adsorption_50 h
Al after 1st THF rinse
Al after 2nd THF rinse
Al after 3rd THF rinse
Al after 4th THF rinse
Al after 5th THF rinse
Calculated bulk-like spectrum_TDMS
Calculated bulk-like spectrum_Vinyl PDMS
Reflectance [-] measured spectra
Reflectance [-] Calculated spectrum TDMS
Reflectance [-] Calculated spectrum di-vinyl PDMS
Wavenumber [cm^{-1}]

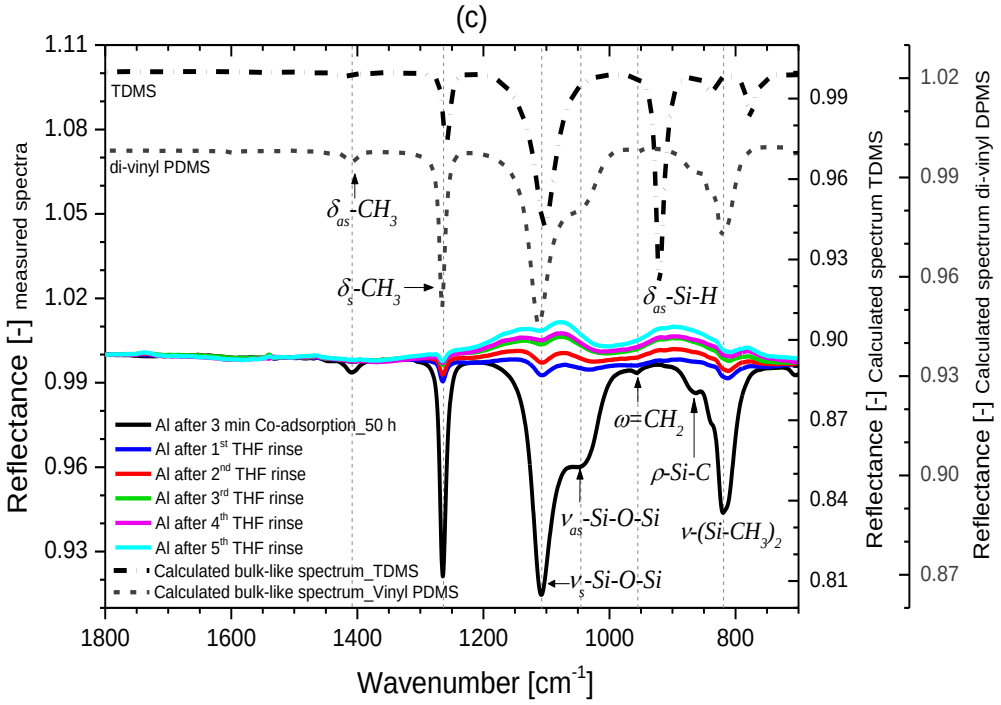


Figure 6.8. FTIR-ERA spectra upon solvent rinsing of co-adsorbed TDMS and di-vinyl PDMS at different spectral regions: (a) from 3100 to 2800 cm^{-1}, (b) from 2250 to 2030 cm^{-1}, and (c) fingerprint region from 1800 to 700 cm^{-1}.

As observed prior to THF rinses, the spectral region at 2250-2050 cm^{-1} (Figure 6.8b) lacks the characteristic ν_s-Si-H peak; therefore, closer inspection of the δ_{as}-Si-H band in the fingerprint region is suggested. For this purpose, the fingerprint region has been magnified in Figure 6.9. The spectra show a progressive decrease in peak intensities due to the removal of further weakly adsorbed material, up to the 3rd THF rinse which evokes the attainment of a stable adsorbed layer. Additional features in the fingerprint region, which are consistent with those previously observed for the individual adsorption of SSMC, are described next.

- **Broadening and intensification of the band centered at ~1600 cm^{-1}.** Usually, the C=C stretching mode is displayed at 1595 cm^{-1}. However, due to the inherent low intensity of bands ascribed to vinyl groups in FTIR, this broad and magnified band can rather be assigned to baseline effects or to changes in the aluminum structure due to THF rinsing [371], than to interactions of vinyl groups with the surface.
- **Recognition of the δ_s-CH_3 and ν_s-Si-O-Si bands after every THF rinse.** These bands are slightly affected in peak position upon solvent washing and are always recognized in the spectra. From the direction of the local transition dipole moments of

these vibration modes (Figure 5.64), it can be assumed that adsorbed Si-O-Si segments of PDMS are preferentially oriented horizontally to the surface. Although it was observed that the adsorbate over storage time adopted a less extended conformation, it is hypothesized that upon solvent rinsing, as fewer molecules are present, the segments in direct contact to the surface and those in the loops orientate with the backbone parallel to the surface. In this way, interactions between the strongly adsorbed segments and the surface, and between loosely (in loops) and strongly adsorbed segments, are maximized.

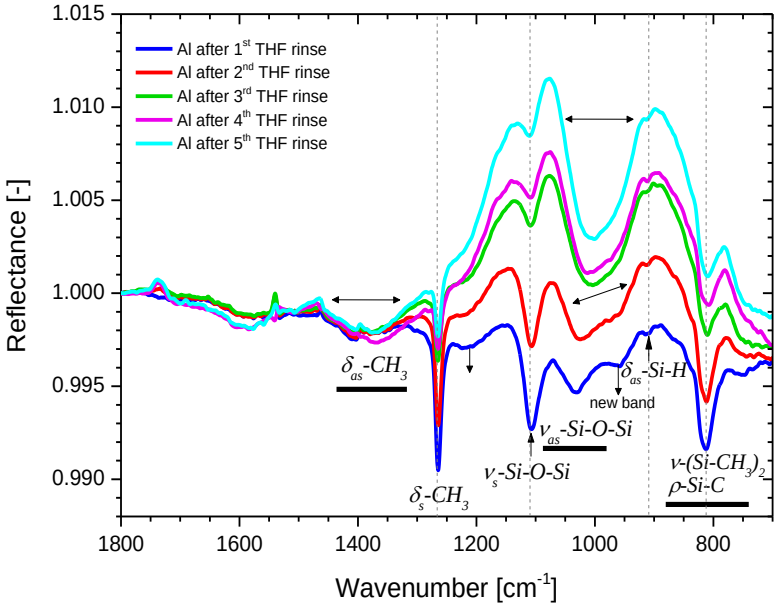


Figure 6.9. Magnified fingerprint region from 1800 to 700 cm^{-1} of the measured ERA spectra of co-adsorption, without the Karstedt catalyst, of TMDS and prepolymer 2 upon THF washing.

- **Peak broadening and appearance of a new band at 1080-900 cm^{-1}.** This outstanding feature advocates strong interactions between the adsorbate and the surface. The involvement and key role of Si-O-Si bonds in such interactions are therefore confirmed. After the 1st THF rinse, the two bands characteristic of Si-O-Si stretching modes can be clearly distinguished, and a new band of medium intensity close to 956 cm^{-1} is recognized. The appearance of this new feature is consistent with earlier results. The band has been associated with siloxane segments bound to the surface via H-bonding, strong dipole interactions and possible covalent Si-O-Al bonds formed from chemisorption of Si-OH traces [154,325]. Yet, after the 2nd THF rinse the

ν_{as}-Si-O-Si band and the new band at 956 cm^{-1} are resolved into a single broad peak centered at 1030 cm^{-1}. This broad peak is further broadened and magnified upon additional solvent washing. These features evidence that the adsorbed molecules are interacting strongly with the aluminum surface. Moreover, the ω=CH_2 peak usually displayed at 957 cm^{-1} may also contribute to the total intensity of the broad band.

- **New shoulder centered at ~1216 cm^{-1}.** This shoulder has been consistently perceived in all results. It has been attributed to an unidentified change in the oxide structure upon THF washing.
- **Small peak at 912 cm^{-1}.** This peak is ascribed to Si-H asymmetric bending mode. The assignment of this peak is based on the results obtained for the individual adsorption of hydride terminated PDMS and TDMS where this band was also detected at 913 cm^{-1}. Hence, it can be confirmed that TDMS was adsorbed in the near surface region, but to a lesser extent than di-vinyl PDMS. The peak shifts from 921 cm^{-1} in the bulk-like state to 912 cm^{-1} in the adsorbate state, indicating that Si-H linkages in TDMS were involved in interactions with the surface. Despite the adsorption of TDMS, there is no indication that crosslinking occurred at the interface. Specifically, the δ_{as}-Si-H band is identified in all spectra, suggesting that Si-H bonds were not consumed in a chemical reaction. Moreover, the lack of peak at 1180-1120 cm^{-1}, ascribed to -Si-CH_2-CH_2-Si- groups formed in hydrosilylation, confirms that crosslinking did not take place near the surface. Consequently, it is again corroborated that the aluminum surface does not have any catalytic effect in the crosslinking of silicones via hydrosilylation.
- **Peak shifting of bands related to Si-C bonds (ρ-Si-C and ν-Si-C).** These two bands, detected in all experimental spectra, are shifted progressively to lower frequencies upon THF washing. A shift in the position indicates a change in the chemical environment of the Si-C bonds by either a strengthening or a weakening of the chemical bond energy. Thus, interactions at the interface are also affecting the Si-C vibration modes.

Finally, possible formation of Si-OH at the interface was also examined in the spectral region at 4000-3100 cm^{-1} (Figure 6.10). The spectrum does not display any peak that can be associated to OH groups either from traces or produced from hydrolysis.

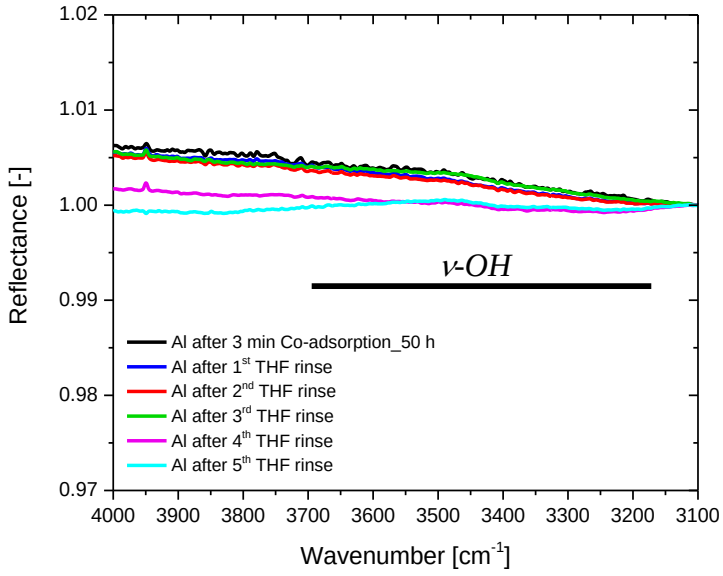


Figure 6.10. O-H stretching mode of the co-adsorbed TDMS and prepolymer 2 on Al upon THF rinsing.

In summary, co-adsorption of TDMS and di-vinyl PDMS without the Karstedt catalyst resulted in simultaneous adsorption of both components on aluminum, confirming their good affinity to the substrate. Possibly, due to the inherent nature of vinyl PDMS polymer with more Si-O-Si units, this component was adsorbed to a larger extent than TDMS. From the remarkable spectral features involving the Si-O-Si bonds, the mechanisms of adhesion proposed in section 5.6.11 are also valid at the interface between co-adsorbed TDMS/prepolymer 2 and aluminum. It was revealed that simultaneous adsorption of TDMS and PDMS causes deviation to the flattening process of adsorbed PDMS over time. Finally, it can be stated that crosslinking does not occur at the interface if Karstedt catalyst is not included in the system, and the aluminum surface does not play any catalytic role in the crosslinking of silicones via hydrosilylation reaction.

6.3.2. Co-Adsorption – with Karstedt catalyst

The chemical state of the aluminum surface prior to the co-adsorption experiments is first examined (Figure 6.11). As expected, the solvent rinsing eliminated carbonaceous contaminants that were anchored to the surface. This fact is evidenced by the two negative peaks (reverse spectrum) in the -C-H region at 3100-2800 cm^{-1} (magnified spectrum). A negative, broad band is identified in the region of the O-H stretching

mode, suggesting the removal of physisorbed water and a possible modification to the hydroxide layer. The positive peak at 900-1000 cm^{-1} indicates growth of the aluminum oxide layer after solvent exposure. These observations are in agreement with the previous chemical states of aluminum surface studies.

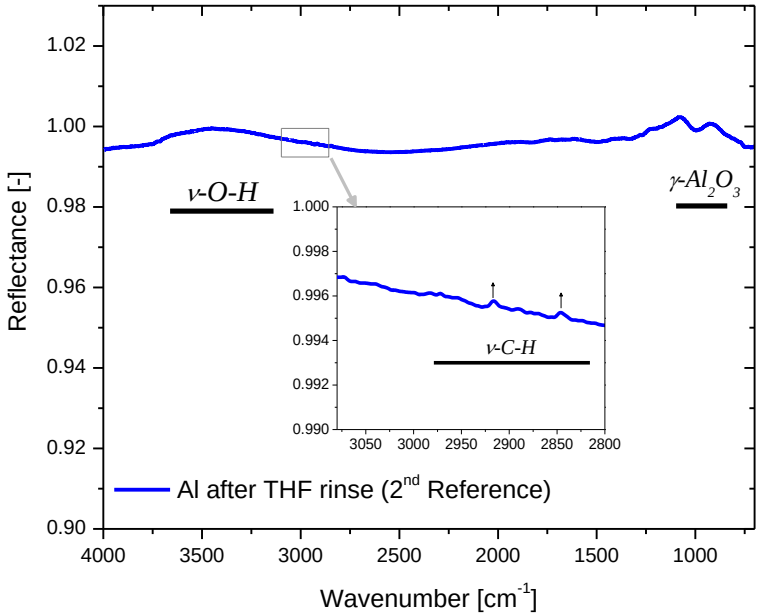
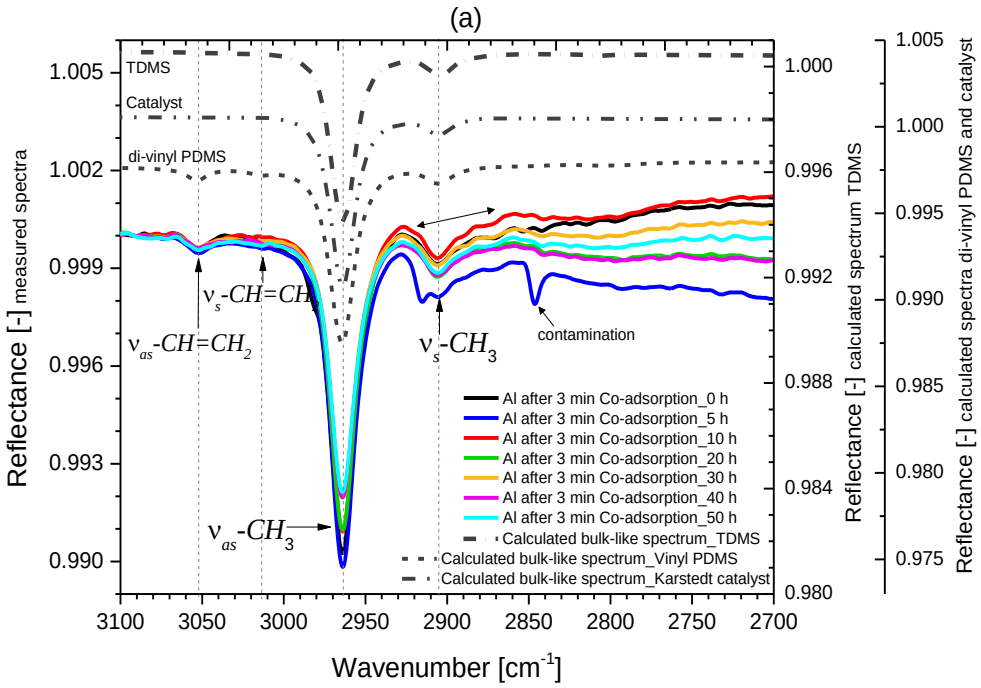


Figure 6.11. Chemical state of the aluminum surface after one THF rinse and prior to the co-adsorption experiments with the Karstedt catalyst.

Figure 6.12 illustrates the measured ERA spectra obtained after the 3-min co-adsorption step. The principal IR bands identified in the spectra over time are listed in Table 6.3. At all times, the experimental spectra replicate the bulk-like spectrum of di-vinyl PDMS, which is consistent with the results obtained without the Karstedt catalyst. This observation suggests that at the initial stage of co-adsorption, the vibration states of the adsorbed layers are almost unaffected by the substrate. So far, the formation of strong interactions at the interface cannot be inferred. On the other hand, the spectral region at 2250-2000 cm^{-1} (Figure 6.12b) does not display the distinctive Si-H stretching mode of TDMS, pointing out to a lack of adsorption of TDMS. However, closer examination of the spectral region from 960 to 900 cm^{-1} corresponding to δ_{as}-Si-H (Figure 6.13a), reveals a weak band at 908 cm^{-1} in the spectrum at 0 h, which confirms that TDMS was also adsorbed. Most likely, the adsorbed molecules of TDMS were masked by the dense layer of vinyl PDMS, as with

the previous analyzed case without the catalyst. Interestingly, the δ_{as}-Si-H peak is no longer perceived after 5 h, indicating involvement of Si-H groups in a chemical process such as crosslinking or hydrolysis. The occurrence of crosslinking is verified from the examination of the bands associated with vinyl groups at 3100-3000 cm^{-1} (Figure 6.13b). The disappearance of the ν_s-CH=,=CH_2 band at 3013 cm^{-1} and the reduction in intensity of the ν_{as}-CH=,=CH_2 band at 3053 cm^{-1}, suggest that some degree of crosslinking occurred, which implicitly indicates that the Karstedt catalyst was adsorbed as well. On the other hand, hydrolysis of the Si-H groups leading to the formation of Si-OH is unlikely, since the spectral region at 3700-3200 cm^{-1} (Figure 6.14), characteristic of the O-H stretching mode, does not exhibit an absorption band. Moreover, the two bands perceived at 2915 and 2846 cm^{-1} in the measured spectrum at 5 h (Figure 6.12a), advocates recontamination of the surface over time. However, the peaks disappear in the next spectrum, evidencing the ability of PDMS molecules to displace carbon-contaminants.



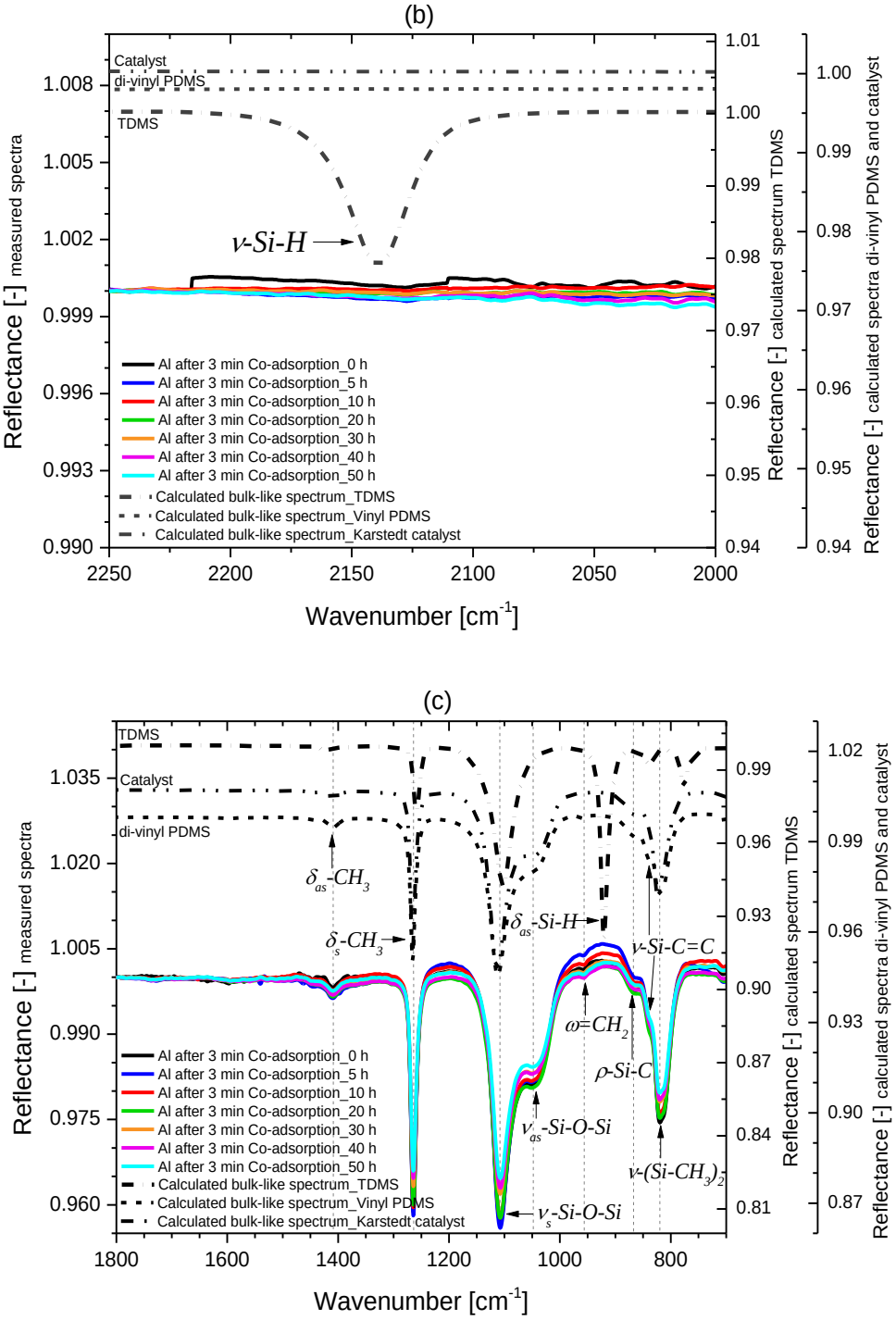


Figure 6.12. FTIR-ERA spectra of the co-adsorbed TDMS, Karstedt catalyst and di-vinyl terminated PDMS. The spectra are sectioned in three regions: (a) at 3100-2800 cm^{-1} (b) at 2250-2000 cm^{-1} and (c) fingerprint region from 1800 to 700 cm^{-1}.

Table 6.3. Characteristic IR bands resulted from co-adsorption of di-vinyl PDMS, TDMS and Karstedt catalyst after the 3-min co-adsorption step

Peak	Wavenumber [cm^{-1}]	Assignment
1	3052	ν_{as}=CH$_2$, CH=
2	3013	ν_{s}=CH$_2$, CH=
3	2964	ν_{as}-CH$_3$
4	2905	ν_{s}-CH$_3$
5	1407	δ_{as}-CH$_3$
6	1264	δ_{s}-CH$_3$
7	1108	ν_{s}-Si-O-Si
8	1047	ν_{as}-Si-O-Si
9	955	ω=CH$_2$
10	866	ρ-Si-C
11	818	ν-Si-C

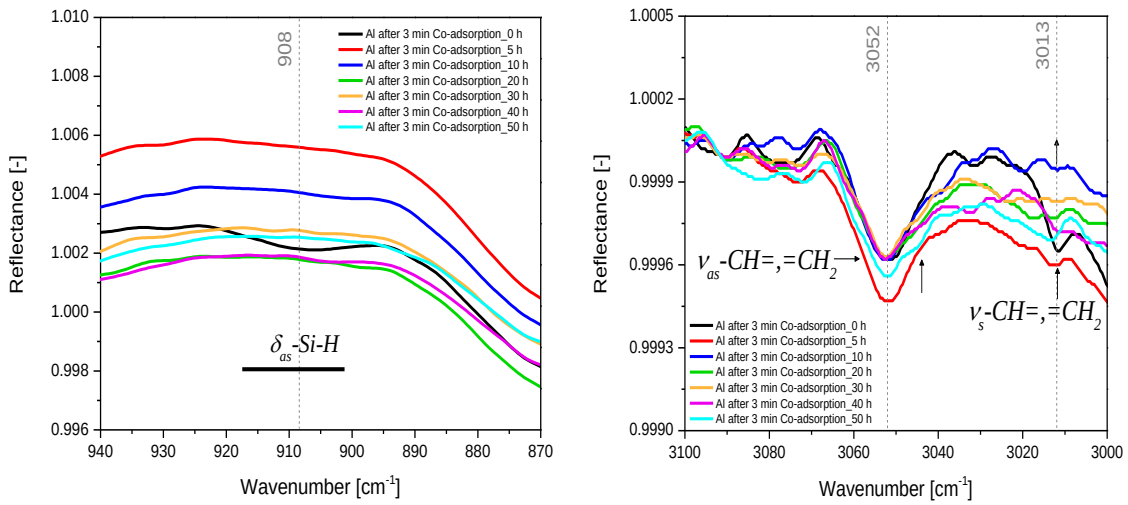


Figure 6.13. Absorption bands associated with (a) Si-H groups at 908 cm^{-1}, and (b) vinyl groups at 3100-3000 cm^{-1} over storage time in co-adsorption with the Karstedt catalyst.

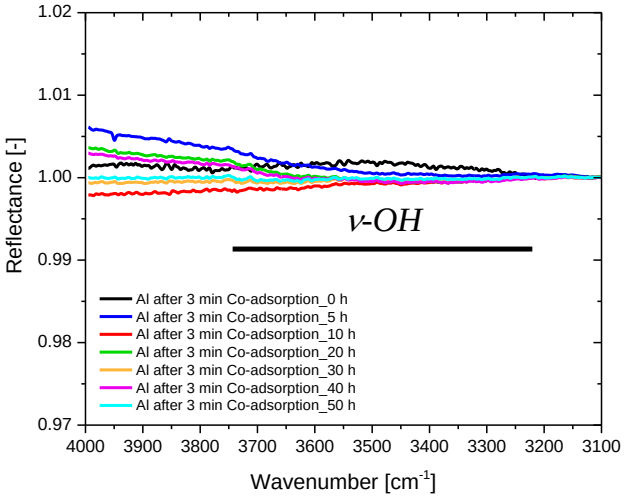


Figure 6.14. Evolution of the O-H stretching mode over time in the co-adsorption including Karstedt catalyst

The spectra are further analyzed by the variation of the peak intensities over time (Figure 6.15). The areas of the absorption bands in Table 6.3 were estimated from peak fitting using a Voigt function in the software OriginPro® 8.6. The trend followed by the peak areas over time, when the catalyst is present, differs slightly from the behavior observed when the catalyst was not included. Principally, there is not a marked progressive decrease in peak areas with time, and the areas do not change significantly within absorption bands. However, the variation behavior between different peaks appears to also be parallel. Based on the results obtained in the previous case, two principal reasons are associated with changes in peak intensities: first, desorption of weakly adsorbed low molar mass oligomers, and second, molecular orientation effects within the adsorbate. The pattern observed here suggests that neither desorption nor molecular orientation occurred significantly.

Moreover, the change in peak area for the ν_{as}-CH=CH$_2$ band (enlarged image in Figure 6.15) decreases over time, confirming that vinyl groups were more likely partially consumed in the crosslinking reaction. In contrast, the ω-CH=CH$_2$ peak increases progressively, due to the strengthening of the interactions at the interface. It has been consistently observed that a new band at ~960 cm^{-1} appears as a consequence of the strong interactions between Si-O-Si bonds and the surface.

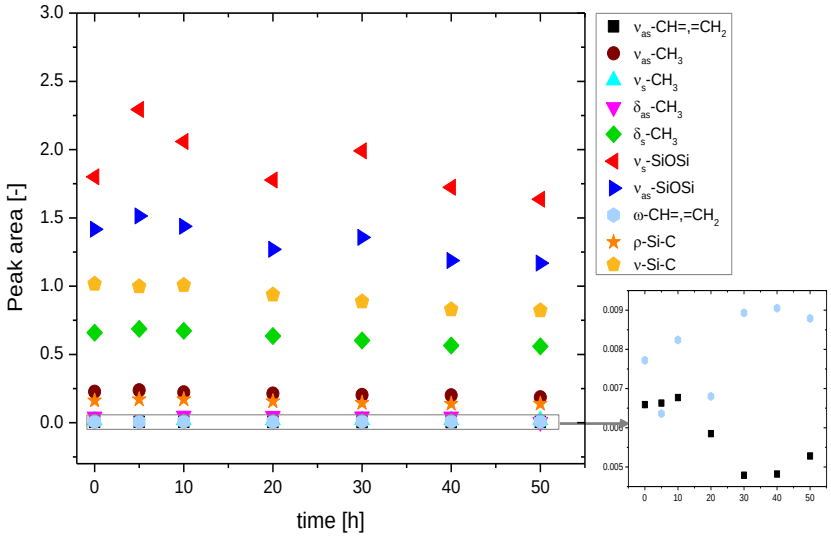


Figure 6.15. Variation of the peak areas over time for the principal bands identified in the co-adsorption with the Karstedt catalyst.

To investigate the orientational adjustments in more detail, the intensity ratios r_1, r_2 and r_3 were estimated and plotted over time in Figure 6.16. The three intensity ratios remain almost invariable over time, suggesting that when the catalyst was present molecular orientation was restricted, most likely due to partial crosslinking. Therefore, the slight decrease in peak intensities observed in Figure 6.15 can be principally attributed to a desorption process. Since the crosslinking seems to suppress orientational effects, it can be suggested that the crosslinking reaction was faster than molecular orientation. From the characterization of the crosslinking in bulk, it was determined that in the presence of the Karstedt catalyst the reaction occurred very rapidly; hence, this condition seems to be valid in the adsorbate state thus, the crosslinking was plausible faster than the molecular orientation. As the mobility of both the crosslinked segments and the unreacted chains was restricted, it seems reasonable that the desorption process when the catalyst was present was not as remarkable as the mass loss when the catalyst was not included.

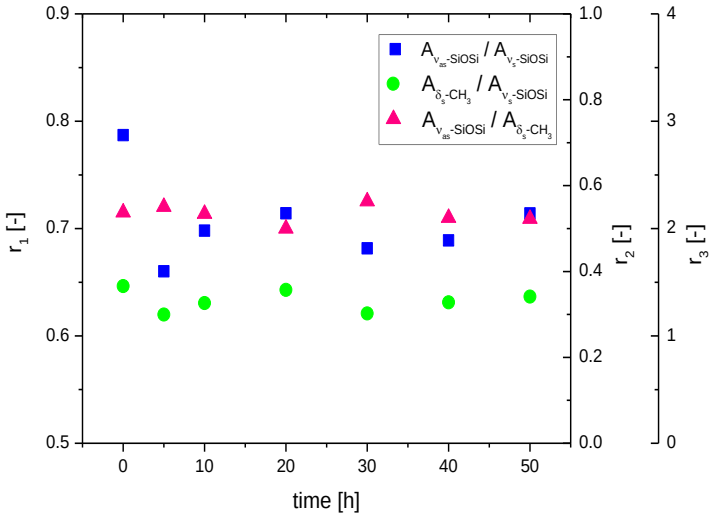
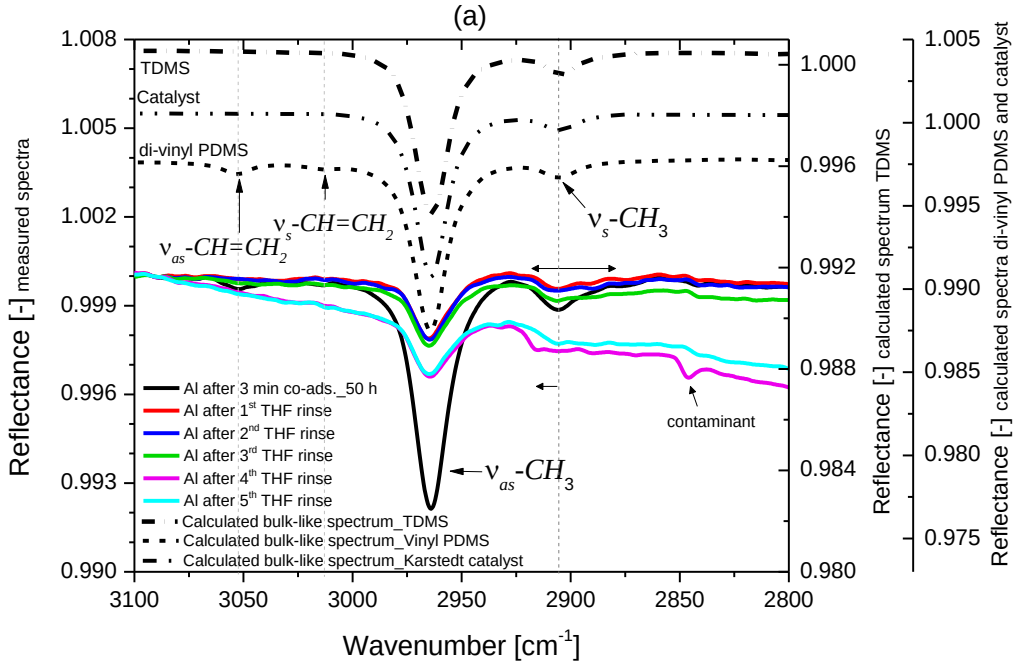
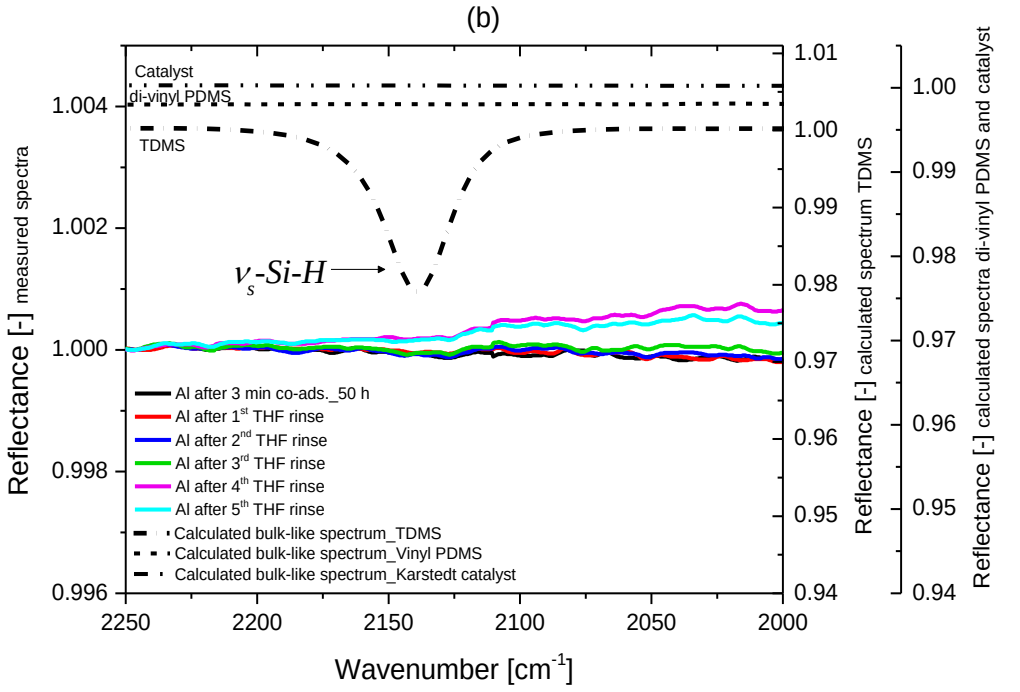


Figure 6.16. Variation of the intensity ratios r_1, r_2 and r_3 over time, for co-adsorption when the Karstedt catalyst is present.

After the 50 h of storage time were finished, the substrate was rinsed consecutively with pure THF. The measured ERA spectra upon solvent rinsing (Figure 6.17.a-c) exhibit a remarkable decrease in intensity after the 1st rinse, due to substantial removal of weakly adsorbed molecules. However, the peak intensities remain almost invariable after further additional rinses, which indicates that a stable adsorbed layer was attained rapidly, just after the first solvent rinse. This fact implies that besides crosslinking, chemisorption also possibly occurred; therefore, molecular orientation effects and further solvent rinses have an insignificant impact in the behavior of the peak intensities upon solvent washing. The effect of the Karstedt catalyst on the stability of the adsorbate due to plausible chemisorption was also observed in the individual adsorption of the catalyst. The observations here seem to support the hypothesis that the Karstedt catalyst favors chemisorption with the surface.


(a)
TDMS
Catalyst
di-vinyl PDMS
ν_{as}-$CH{=}CH_2$
ν_s-$CH{=}CH_2$
ν_s-CH_3
ν_{as}-CH_3
contaminant
Al after 3 min co-ads._50 h
Al after 1st THF rinse
Al after 2nd THF rinse
Al after 3rd THF rinse
Al after 4th THF rinse
Al after 5th THF rinse
Calculated bulk-like spectrum_TDMS
Calculated bulk-like spectrum_Vinyl PDMS
Calculated bulk-like spectrum_Karstedt catalyst
Reflectance [-] measured spectra
Reflectance [-] calculated spectrum TDMS
Reflectance [-] calculated spectra di-vinyl PDMS and catalyst
Wavenumber [cm-1]


(b)
Catalyst
di-vinyl PDMS
TDMS
ν_s-Si-H
Al after 3 min co-ads._50 h
Al after 1st THF rinse
Al after 2nd THF rinse
Al after 3rd THF rinse
Al after 4th THF rinse
Al after 5th THF rinse
Calculated bulk-like spectrum_TDMS
Calculated bulk-like spectrum_Vinyl PDMS
Calculated bulk-like spectrum_Karstedt catalyst
Reflectance [-] measured spectra
Reflectance [-] calculated spectrum TDMS
Reflectance [-] calculated spectra di-vinyl PDMS and catalyst
Wavenumber [cm-1]

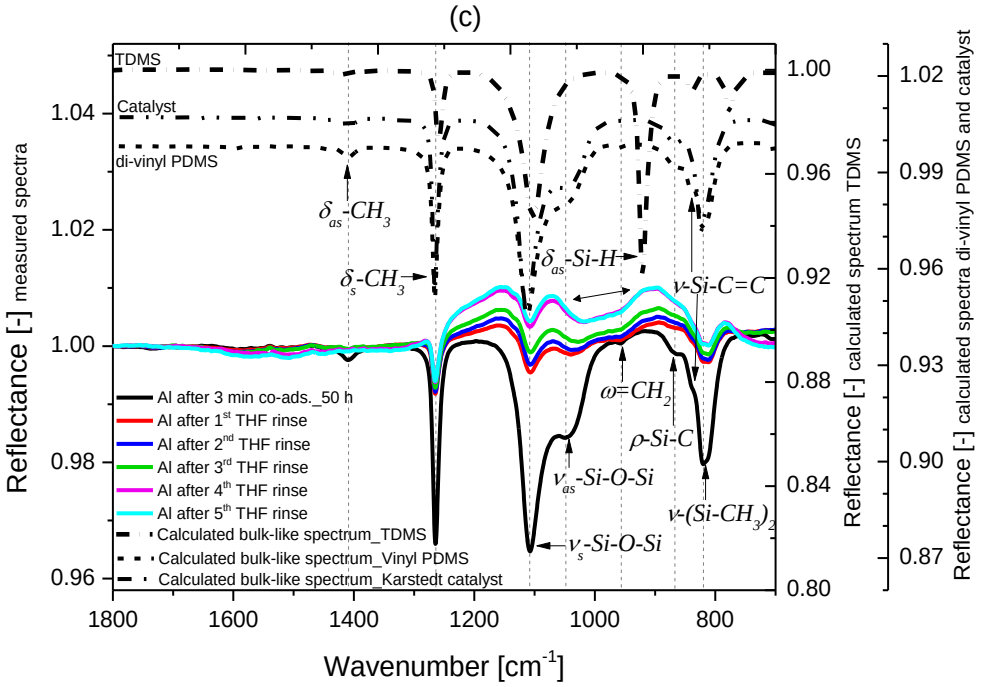


Figure 6.17. FTIR-ERA spectra upon THF rinsing obtained from the co-adsorption of TDMS, di-vinyl PDMS and Karstedt catalyst onto aluminum at different spectral regions: (a) from 3100 to 2800 cm^{-1}, (b) from 2250 to 2030 cm^{-1} and (c) fingerprint region from 1800-700 cm^{-1}.

In the region associated with stretching vibrations of C-H bonds (Figure 6.17a), the bands ascribed to unreacted vinyl groups are no longer visible upon solvent washing. The vanishing of the bands can be attributed to three different reasons. First, to the consumption of vinyl groups in further crosslinking, second, to a decrease in concentration due to the removal of weakly adsorbed molecules, and third, to molecular orientation effects. On the other hand, the bands associated with methyl groups are perceived in all spectra. The ν_s-CH_3 mode exhibits the typical peak broadening on the low-frequency side due to inhomogeneities and interactions at the interface. Two weak peaks at 2916 and 2846 cm^{-1} are distinguished after the 4th THF rinse, indicating re-contamination of the surface; however, they are desorbed again after the next THF rinse. This adsorption/desorption process is believed to be responsible for the marked drift of the baseline observed in the last two spectra [42,371]. The bands related to the newly formed CH_2 bonds at ~2875 cm^{-1} are unnoticed in this C-H stretching region, most likely due to the technique's limitations in displaying signals of groups at very low concentrations.

The distinct ν_s-Si-H peak in the spectral region at 2250-2050 cm^{-1} (Figure 6.17b) is unnoticed upon solvent rinsing. This band was also not displayed in the spectra before THF rinses, advocating low concentration of Si-H groups.

The fingerprint region (Figure 6.17c) exhibits significant features that are consistent with previous results. The fingerprint region has been enlarged in Figure 6.18. The principal features observed are described below.

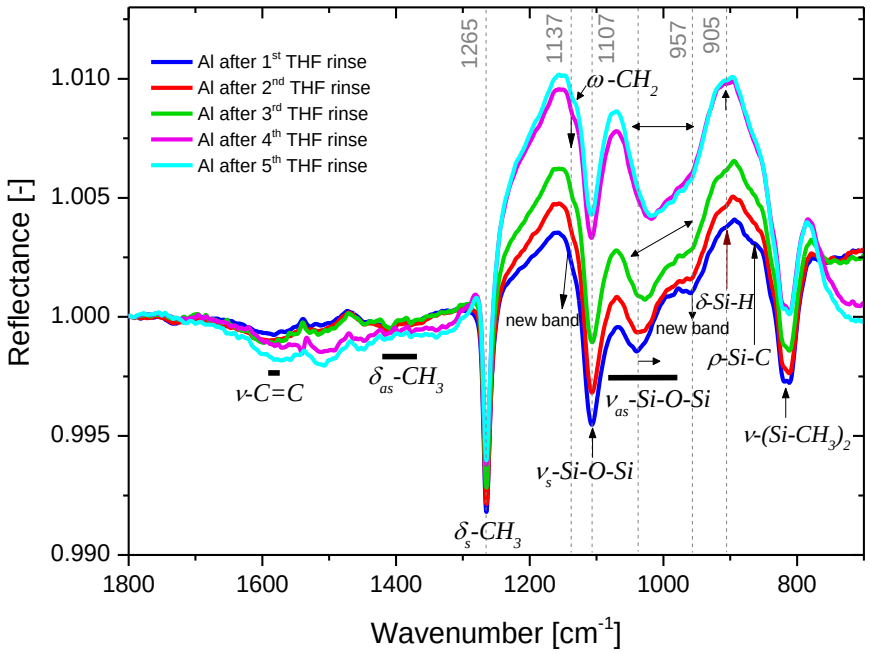


Figure 6.18. Enlarged FTIR-ERA spectra of co-adsorbed di-vinyl PDMS, TDMS and the Karstedt catalyst in the fingerprint region from 1800 to 700 cm^{-1} upon THF rinsing.

- **New shoulder centered at 1265 cm^{-1}.** This feature was constantly observed in the adsorption of the SSMC and in the co-adsorption without the Karstedt catalyst. It has been assigned to undefined structural changes of the aluminum surface upon solvent washing.
- **Changes of the Si-O-Si band from 1100-1000 cm^{-1}.** The asymmetric stretching band (ν_{as}-Si-O-Si) is shifted from 1038 to 1029 cm^{-1} upon solvent rinsing, which evidences the direct participation of the siloxane bonds in the interactions with the aluminum surface. Moreover, this ν_{as}-Si-O-Si peak and a new peak located at ~957 cm^{-1} merge progressively into one single broad band. This broad peak has been attributed to siloxane segments bound to the surface via H-bonding and van der Waals interactions [30,325]. This new broad peak features further line broadening upon solvent

rinsing, evoking strengthening of the interactions at the interface. On the other hand, the Si-O-Si symmetric stretching mode (ν_s-Si-O-Si) and the δ_s-CH_3 band at 1265 cm^{-1} remain almost invariable, both in peak position and intensity. This indicates that no significant orientational changes took place upon solvent washing. However, the relatively high intensity of these peaks suggests that, most likely, the adsorbed segments of PDMS molecules are oriented with the Si-O-Si groups parallel to the surface. All these observations are in agreement with previous results obtained from the individual adsorption and co-adsorption without the catalyst.

- **Further crosslinking in the near surface region.** In order for crosslinking to occur in the near surface region, unreacted Si-H and vinyl groups must exist close to the surface. The presence of Si-H groups of TDMS near the aluminum surface is evidenced by the weak peak at ~905 cm^{-1} assigned to δ_{as}-Si-H. This band is displayed in the bulk-like spectrum at ~912 cm^{-1}; but it has been shifted to lower frequencies in the adsorbate state. The intensity of this band decreases upon THF rinsing, pointing to consumption in further crosslinking. The crosslinking in the near surface region is corroborated by the emergence of a weak shoulder at ~1137 cm^{-1}, ascribed to newly formed methylene bridges (-CH_2-CH_2-) based on the characterization of the FMSA in bulk (Section 4.5.3). This result also demonstrates that despite the catalyst being included at very low concentration, it was strongly adsorbed, promoted crosslinking within the adsorbed layer and near the surface, and possibly favored chemisorption. These findings also indicate that the interactions of the end-groups Si-H and Si-vinyl with the surface were neither covalent nor dominant in the co-adsorption process. The end-groups prefer to participate in crosslinking when the Karstedt catalyst is present, rather than in interactions with the surface. Plausibly, further crosslinking at the near surface region restricts the mobility of the adsorbed molecules; therefore, the orientation effects were also insignificant upon THF washes. This supports the hypothesis that crosslinking is faster than molecular orientation.

In summary, the results of co-adsorption including the Karstedt catalyst exhibited the high affinity of the three components to the surface, as they were all simultaneously adsorbed. However, di-vinyl PDMS was seen to be adsorbed to a larger extent than TDMS, pointing to some preferential adsorption. Based on the outstanding spectral features observed in the Si-O-Si stretching region, the siloxane bond is also assigned as the adhesion partner in the co-adsorption of the multicomponent reactive system including the catalyst. The interactions established at the interface are strong enough to make the adsorbate resistant to up to five THF rinses. In contrast with previous observations, the chain flattening process was restricted before and after solvent rinsing,

most likely due to the incidence of crosslinking which is believed to occur faster than molecular reorientation, and possible chemisorption with the surface. Finally, it can be presumed that the crosslinking reaction prevails over end-group interactions with the surface.

6.4. Conclusive discussion

6.4.1. Crosslinking of silicones at the interface

The results obtained indicate that the aluminum surface does not play any catalytic role in the crosslinking of silicones via hydrosilylation. Without the catalyst, the crosslinking reaction of the model silicon system FMSA did not occur. In contrast, when the Karstedt catalyst was added, crosslinking occurred even in a dense adsorbed layer and also near the surface. The results in the adsorbate state are in good agreement with those attained in the bulk state. In conclusion, crosslinking of the FMSA via hydrosilylation reaction at room temperature occurs when the Karstedt catalyst is present, either in bulk or in the adsorbate state. Furthermore, in both states the Karstedt-catalyzed crosslinking reaction occurs very rapidly. Therefore, the presence of the Karstedt catalyst plays the key role in the incidence of crosslinking of silicones at the interface via hydrosilylation reaction at room temperature. Moreover, the role of the Karstedt catalyst seems to be not limited only to crosslinking, since possible covalent bonding of PDMS with the surface is believed to occur under the influence of the Karstedt catalyst. This last effect was also observed in the individual adsorption results. Plausible chemisorption due to the presence of the Karstedt catalyst imparts greater stability to the interface.

The spectra also suggest that crosslinking proceeded non-uniformly within the adsorbate. First partial crosslinking took place in the dense layer and subsequently, by removal of weakly adsorbed molecules, it proceeded further in the near surface region. Also, the rapid crosslinking prevented orientational changes of the adsorbed PDMS molecules. These observations advocate that across the interface, there was a distribution of properties such as: adsorbed strength (from strongly to weakly), concentration of unreacted components, network density, molecular mobility and orientation. Since crosslinking occurs favorably near the surface, a gradient of concentration of unreacted TDMS, catalyst and di-vinyl PDMS is presumed to exist from the surface in direction to the adsorbate layer.

Importantly, the incidence of crosslinking at the interface suggests that the interactions of the Si-H and Si-vinyl end-groups with the surface were non-covalent, as they did not prevent their participation in the hydrosilylation reaction.

6.4.2. Preferential adsorption

Usually, the prediction of which chemical specie in a mixture will attach to a surface is not straightforward due to equilibrium and non-equilibrium effects that must be contended with [416]. In general terms, entropic and enthalpic aspects are considered for preferential adsorption [417]:

- **Entropic aspects:** preferential adsorption with respect to molecular weight or size. At equilibrium, larger chains adsorb preferentially over smaller ones [417,418]. It has been found conclusively that at the initial stage of simultaneous adsorption, shorter chains are preferentially adsorbed due to rapid diffusion onto the interface; however, they are gradually displaced by longer chains [417]. The driving force for such exchange is the net gain in entropy when a higher amount of smaller molecules are returned to solution and larger molecules are adsorbed to equal the surface coverage by fewer number of molecules [418].
- **Enthalpic effects:** Chemically different molecules have different affinity for the surface, which leads to preferential adsorption [417]. Thus, the molecules with the highest adsorption energy, or segmental adsorption energy in the case of polymers, will be preferentially adsorbed. Even a small mismatch in chemical nature such as the presence of a single polar functionality or polar chain ends can result in strong selective adsorption.

In simultaneous adsorption, the difference in segmental adsorption energy (enthalpic effects) prevails over the chain-length difference (entropic effects) [418]. A long polymer is easily displaced by a shorter molecule if the latter has a higher adsorption energy [418]. Other factors influencing preferential adsorption include: intrinsic stiffness [419,420], intramolecular geometry and molecular flexibility.

Experimentally, the results of co-adsorption with and without the Karstedt catalyst confirmed the high affinity of the components with the surface as they were simultaneously adsorbed. Nevertheless, it was found that di-vinyl PDMS was adsorbed in a larger extent than TDMS, suggesting preferential adsorption of prepolymer 2 over TDMS. The three components are of similar chemical nature. All of them containing Si-O-Si groups but differing in end-groups: Si-H for TDMS and Si-vinyl for prepolymer 2 and the catalyst. Moreover, the Si-O-Si bond was assigned as the adhesion partner

for the three components, which denotes that the local segmental adsorption energy for the components is similar. On the other hand, contrarily to terminal vinyl groups, the Si-H of TDMS can also interact with the surface. Therefore, the adsorption energy of TDMS is presumably enlarged by the contribution of the end-group. Due to such enlargement, TDMS could be preferentially adsorbed; nevertheless, this was not observed. This suggests that enthalpic effects were not dominant in the co-adsorption of the three SSMC. Consequently, entropic effects were governing in the co-adsorption with and without the Karstedt catalyst. Prepolymer 2 was preferentially adsorbed over TDMS due to its higher molar mass, larger number of Si-O-Si segments per molecule, and higher flexibility. Additionally, due to steric hindrance and inherent stiffness of the TDMS molecules, it was not possible that all 4 Si-O-Si segments in TDMS were simultaneously adsorbed on the surface, decreasing its adsorption energy. It can be hypothesized that during the 3-min contact of the multicomponent solution with aluminum, TDMS and shorter PDMS oligomers were first adsorbed on the surface and exchange of shorter chains by longer ones took place.

Even though the results indicate that the Si-O-Si played the key role in competitive adsorption, the presence of Si-H groups have allowed TDMS molecules to compete effectively in the co-adsorption with PDMS molecules and to be strongly adsorbed in the near surface region despite steric effects and higher molecular stiffness.

6.4.3. Effect of time

The main effect of storage time on crosslinking reaction, molecular orientation and desorption are discussed as follows:

- **Incidence of crosslinking:** In the absence of the Karstedt catalyst, the reaction did not take place at the interface in 50 h; whereas when Karstedt catalyst was added to the multicomponent system, the reaction at the interface did take place. Thus, time influences insignificantly crosslinking, while the inclusion of the Karstedt catalyst is the key factor.
- **Molecular orientation:** the well-known flattening process of PDMS chains was constrained in co-adsorption. When the catalyst was not present in the system, chain extension was restricted by the presence of adsorbed TDMS molecules within the adsorbed layer. Most likely, due to steric effects and the fact that some surface sites were already occupied by adsorbed TDMS molecules, thus a fewer number of sites at the surface were available for chain extension of PDMS. Consequently, adsorbed PDMS molecules adopted an orientation with a higher degree of orthogonality with respect to the substrate surface. This suggests that some polymer backbone segments were lifting

from the surface. Figure 6.19 illustrates one possible situation of co-adsorbed TDMS and PDMS on the Al surface.

On the other hand, when catalyst was included in the system, the adsorbed TDMS molecules and the occurrence of crosslinking reaction highly limited the molecular mobility of PDMS chains at the interface. Therefore, no significant orientational adjustments were perceived over time. It can be postulated that the simultaneous adsorption of TDMS and PDMS molecules on aluminum restricts the chain flattening process of PDMS over time. It is supposed that when crosslinking of silicones, via hydrosilylation, occurs at the interface, the rate of the reaction will determine the extent of molecular orientation.

- **Desorption:** spontaneous desorption of molecules took place over the storage time in the absence and presence of the catalyst, suggesting that the system was not in equilibrium at any time. This behavior was more remarkable in the absence of the Karstedt catalyst. Plausibly, an exchange process between long and short chains near the surface region took place over time, causing the shorter oligomers to interact weakly with the surface and to escape to the atmosphere. The desorption process was seen to be slowed down when the Pt catalyzed crosslinking reaction occurred at the interface. This suggests that desorption depends on both the simultaneous adsorption and on the rate of crosslinking, rather than on time. This hypothesis is supported by the fact that in the individual adsorption of prepolymer 2, desorption was not significantly perceived.

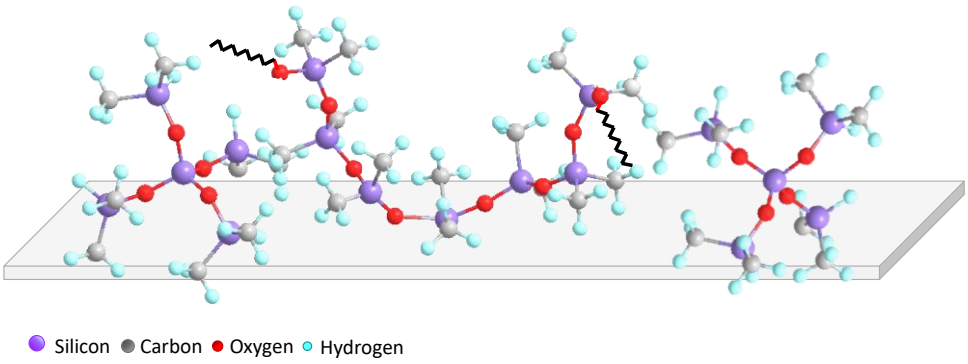


Figure 6.19. Possible molecular arrangement at the interface of adsorbed TDMS and PDMS on Al. Steric effects restricted the chain flattening of PDMS molecules.

7 Outlook: CSA on technical Aluminum

7.1. Introduction and aim of the study

The possibility to join two materials together offers the industry the opportunity to produce complex pieces from relatively simple parts. However, despite the rapid applicability of polymer-metal joints and the numerous available literature related to its analysis [421–424], there are still important issues to be solved for specific adhesive-metal systems. The formation of a stable interface between the adhesive and the substrates which ensures the required joint strength, durability and joint performance is one of the biggest concerns. The main requirement for lasting durability and high strength of an adhesive joint, is to guarantee suitable properties in the polymer and metal surface that allow the creation of strong interactions. This is usually achieved by applying adequate surface pretreatment methods to the metal and by selecting a correct joint configuration. Surface pretreatment constitutes an important prerequisite of polymer metal joining and one of the critical challenges in different industries such as aircraft, rail, automotive and marine, where adhesive bonding of aluminum structures is widely employed [425–427].

The general purpose of applying surface pretreatments to aluminum is to enhance the surface cleanliness and homogenize the surface properties for adhesive bonding such as macro-or micro-roughness, surface chemistry and surface free energy [9,428]. An initial cleaning via solvent degreasing may be sufficient, since it contributes to the total or partial removal of certain contaminants; however, for achieving long-term stable joints, more elaborate pretreatments such as mechanical, chemical or electrochemical treatments are necessary [9,428]. Each of these pretreatments can remove the

mechanically weak thin layer of native surface oxides and replace it with a new uniform oxide layer with constant thickness, roughness, topography and chemical stability. Usually, aluminum surfaces exhibit more favorable adhesion when they are chemically or electro-chemically pretreated, but there are disadvantages associated with the disposal of the chemicals employed, long pretreatment times and high operational costs [429]. In addition, the new legislation of the European Union (EU) which regulates the Registration, Evaluation and Authorization of Chemicals (REACH) has significantly restricted the use of wet methods for surface treatment of aluminum [430]. On the other hand, mechanical pretreatments do not always offer satisfactory adhesion and long-term stability [428]. Consequently, alternative techniques such as plasma, arc-discharge and laser pretreatments are now becoming more common, since they are environmentally friendly, economically attractive and easily automatized [429].

The main aim of this chapter is to study the effectiveness of three different pretreatment methods for improving the initial bonding adhesion between a technical aluminum substrate and the commercial silicone adhesive (CSA) used as reference in this work. The three surface pretreatment methods were suggested by Robert Bosch GmbH based on their internal applicability. They are solvent (acetone) degreasing, chemical etching (P2 etch) and air atmospheric pressure plasma. The specific purposes of the analysis are to identify the changes in surface chemistry and topography induced by those pretreatments and to assess their influence on bond strength by comparing single lap-shear tests of non-aged aluminum adhesive joints.

7.2. Preparation of the aluminum surface

In this study, three different surface pretreatments were selected to modify the surface of a technical aluminum substrate (AlMg3 alloy). Description of the technical aluminum substrate and the pretreatments employed in this work are given as follows.

7.2.1. Technical aluminum substrate

The aluminum substrate used in this work was an alloy of wide applicability in the automotive industry, the AlMg3 alloy (EN AW-5754). The specimens were supplied by Rocholl GmbH (Aglasterhausen, Germany) with the composition tabulated in Table 7.1, which was provided by the supplier [431]. They were provided as two

samples with different geometries, one with a disc shape ($\varphi \times t$) 30 mm × 1.2 mm for surface characterization, and the other with a rectangular prism form with dimensions of ($w \times h \times t$) 100 mm for bonding analysis. The two substrate samples are illustrated in Figure 7.1.

Table 7.1. Chemical composition by weight of EN AW 5754 aluminum provided by the manufacturer [431].

Element content by weight [%]											
Si	Fe	Cu	Mn	Mg	Cr	Ni	Zn	Ti	Ga	V	Al
0,2	0,15	0,016	0,12	2,75	0,006	0,004	0,004	0,016	0,08	0,013	96.64

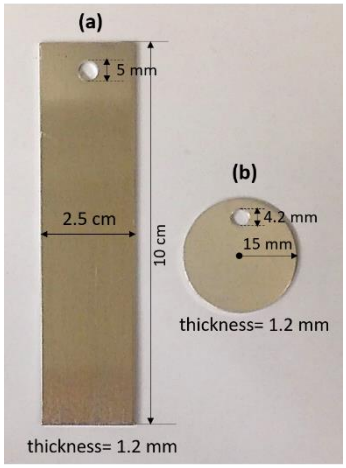


Figure 7.1. Technical Al substrate samples of two different geometries (a) sheets for lap-shear tests (bonding analysis) and (b) discs for surface characterization.

7.2.2. Surface pretreatments

7.2.2.1. Acetone degreasing

Technical aluminum surfaces are, due to the forming process, covered with lubricating and protective oils, which must be removed before use [346]. Degreasing is the simplest method of achieving relatively clean surfaces; it ranges from simple immersion or wiping techniques to vapor degreasing or ultrasonic cleaning [9].

In this work, the surface contaminants, residues of the manufacturing process and airborne contamination of the aluminum surface were removed by ultrasonic solvent degreasing with acetone (Merck, Darmstadt, Germany) (analytical grade, 97%). Ten aluminum disc samples were immersed in 200 ml of acetone for 10 min at room temperature (~24 °C) in an ultrasonic bath (Figure 7.2). In the case of the aluminum sheets for lap shear tests, ten specimens were immersed in 400 ml of acetone. After the ultrasonic acetone cleaning, the specimens were dried under ambient conditions (~24 °C and 50 %RH) until residual solvent was evaporated. Finally, the samples were stored in a desiccator for approximately 24 h prior to surface characterization and for fabrication of the single-lap shear joints.

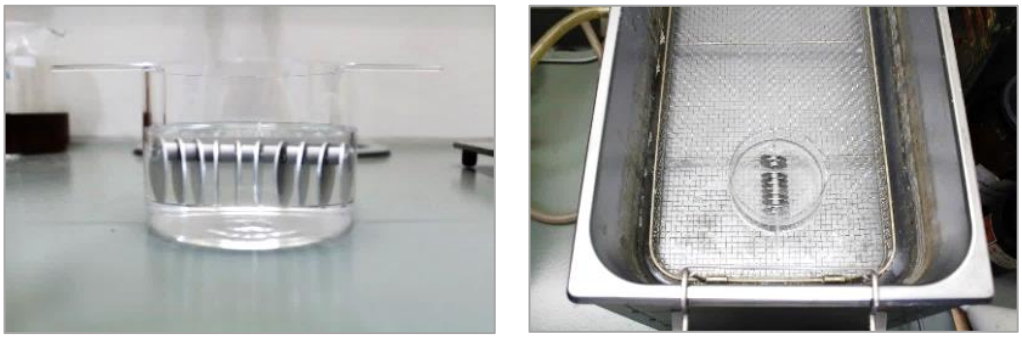


Figure 7.2. Experimental set-up of acetone degreasing in an ultrasonic bath applied to the aluminum disc samples.

7.2.2.2. P2 Etching

P2 etching is a patented environmentally friendly aluminum treatment developed as an alternative to the more traditional FPL (Forest Products Laboratory) etching process [432,433]. The FPL process has been prohibited due to the presence of hexavalent chromium, which is considered carcinogenic and toxic to the respiratory system. Typical P2 etching processes are accomplished by immersion of a pre-treated aluminum sample in a recipient of hot etchant solution, consisting of an aqueous acidic solution (sulfuric acid) with Fe (III) [432–434]. Ferric salts are corrosive to Al, causing pitting of the alloy surface. Additionally, Mg is also attacked by ferric salts, which act as oxidizing agents and cause selective etching of Mg and probably other components in the alloy [435]. P2 etching allows the formation of an oxide layer with enhanced porosity and roughness due to the creation of numerous pits on the alloy surface [434,436].

In this study, the chemical etching was carried out by immersion of the aluminum samples in the P2 etchant solution. The process consisted of two consecutive steps: solvent cleaning and etching. The specimens were first cleaned with acetone, following the process described previously (Section 7.2.2.1). For the etching step, ten aluminum disc samples were immersed in 200 ml of the aqueous etching solution consisting of 3.85 M (370 g/l) of sulfuric acid (Merck, analytical grade 97%) and 0.375 M (150 g/l) of ferric(III) sulfate (anhydrous, Riedel de Haen). The etching was performed at 65 °C for 12 min. For the aluminum sheets, ten specimens were immersed in 400 ml of the etching solution. The experimental set-up of the etching method by immersion employed in this work is illustrated in Figure 7.3. After etching, the substrates were rinsed in cold running tap water for 3 min and then rinsed with deionized water for 2 min. Afterwards, the specimens were placed in an air circulating oven at 50 °C for 1 h for drying. Finally, the samples were stored in a desiccator for approximately 24 h previous to their characterization and the preparation of the adhesive joints.

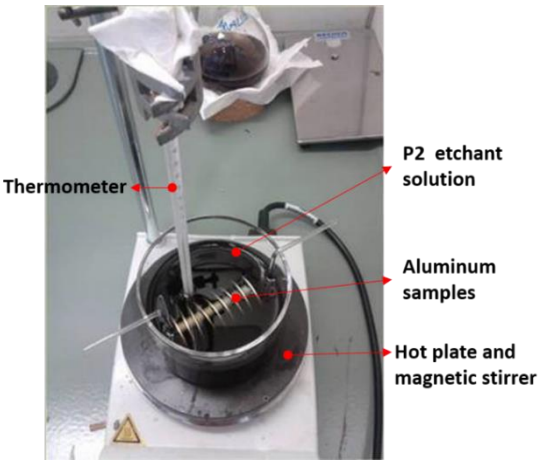


Figure 7.3. Experimental set-up for the P2 etching

7.2.2.3. Atmospheric pressure air plasma

The use of plasma treatment is of great interest because it is a dry process that avoids the disposal of damage wastes, and therefore represents an effective alternative to wet chemical methods or labor-intensive sanding/grit blasting [437]. Plasma is defined as an electrically neutral ionized gas, often considered as a “fourth” state of matter [437]. Plasma allows the generation of reactive gases with chemistries that are advantageous for the surface cleaning and the surface activation of an extensive variety of materials.

This surface treatment induces the formation of functional groups rich in oxygen, such as hydroxyl groups (-OH), which are beneficial for adhesion [4]. However, the effect of plasma treatment is not permanent, hence, it is highly recommended to use the treated surface for bonding as soon the treatment is finished [438]. Through plasma the surface is exposed to heat fluxes which can produce "erosions", ablation and material melting, modifying the surface texture and roughness [439].

The atmospheric pressure air plasma process used in this work also included a preliminary degreasing step with acetone, as the one described previously. The plasma treatment was performed using an Openair® Plasmatreat system from Plasma Technology (Plasmatreat GmbH, Steinhagen, Germany). A 3-axis robot controlled RD 1004 rotary nozzle was used for irradiating the plasma on the substrate surface. The robot-controlled nozzle irradiated the area of interest for adhesive bonding while the specimens were kept stationary (Figure 7.4, left). The plasma generator was an FG 3001 system (Plasmatreat GmbH, Germany), which consists of an impulse discharged loading of double resonance operating at 50/60 Hz, 230 V and 16 A. The system worked with compressed air at a pressure between 4-8 bar. The gap distance between the nozzle and the aluminum specimen's surface was set to approximately 20 mm. Each specimen was treated over a 35 mm high band, as illustrated in Figure 7.4 (right). A stainless-steel support was used for positioning the test pieces. In the case of the aluminum discs, two samples were treated in one single plasma application, whereas for the aluminum sheets, four specimens were treated simultaneously. The irradiation of plasma lasted from 2 to 4 min depending on the type of aluminum samples used.

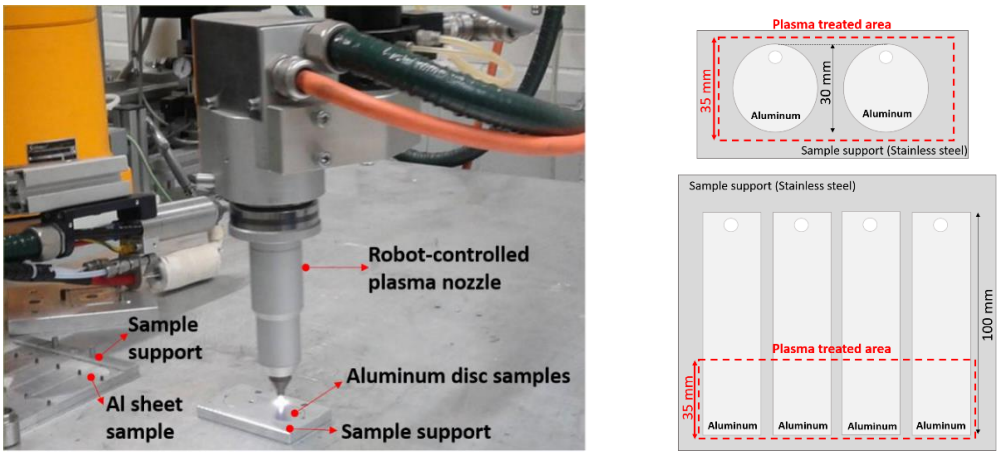


Figure 7.4. (left) Openair® plasma during the treatment of the aluminum disc samples with the robot-controlled nozzle. (right) Area treated with plasma for the two types of aluminum samples.

7.3. Characterization of the pretreated surfaces

The external appearance of the aluminum samples after each pretreatment is shown in Figure 7.5. To the naked eye, the surface texture of the treated aluminum sheets are different, indicating different levels of alteration of the surfaces. In particular, the specimens that underwent chemical etching and atmospheric plasma exhibit the most significant difference in their appearance. In order to analyze the topographic changes in the submicroscopic range, the surface topography of the substrates was qualitatively analyzed by scanning electron microscopy (SEM) and scanning force microscopy (SFM). The chemical state of the surfaces was primarily evaluated by X-ray photoelectron spectroscopy (XPS) and Energy-Dispersive-X-ray spectroscopy (EDX). A schematic representation of the surface methods used in this work for characterization was illustrated by Bockenheimer [440] and presented in Figure 7.6.

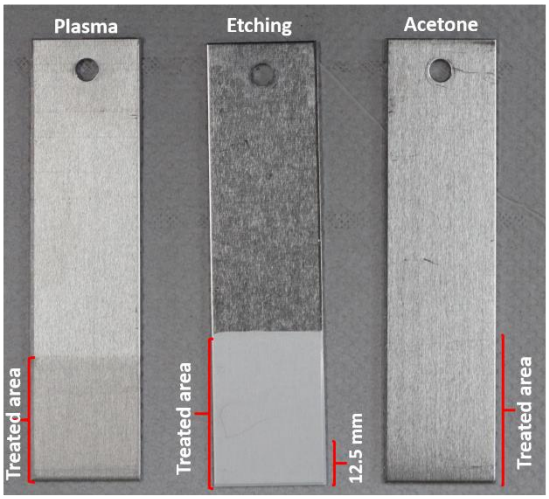


Figure 7.5. External appearance of the aluminum surfaces after different surface pretreatment methods applied in this work.

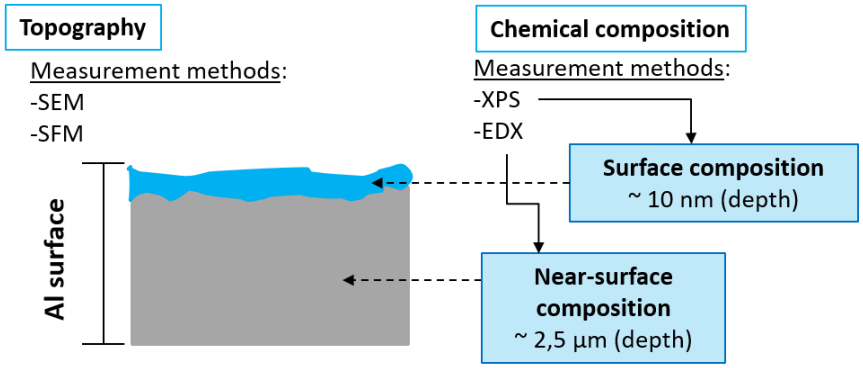


Figure 7.6. Methodology representation for surface analysis of the pretreated aluminum alloy surfaces [440].

7.3.1. Topography

7.3.1.1. Scanning Electron Microscopy (SEM)

SEM is a high-resolution imaging method of surfaces (a few nanometers of spatial resolution). It is a technique in which electron scattering is used to image the topography of a sample surface, providing a three-dimensional visual representation, which makes the qualitative analysis relatively straight forward [4]. To create a SEM image, the beam of incident electrons is swept over a conductive sample surface, or rendered so by gold coating [441]. The beam of incident electrons is generated in a column above the sample chamber by a thermal emission source, such as a heated tungsten-filament, or by a field emission cathode [264,441]. Scanning coils near the end of the column direct and position the focused beam onto the sample surface. The beam interacts with a thin surface layer of the specimen (a few micrometers or less in thickness), causing the emission of electrons from the sample due to elastic and inelastic scattering events [441]. High-energy electrons ejected by elastic collisions of incident electrons are referred to as backscattered electrons, and their energy is comparable to that of the incident electrons. Lower-energy electrons, referred to as secondary electrons, are also emitted due to inelastic scattering [441]. All emitted electrons are detected for each position in the scanned area by an electron detector. The resulting electron vacancies, due to emission of electrons, are filled by electrons from a higher state, and X-ray is emitted to balance the energy difference between the two electron states. The X-ray energy is characteristic of the element from which it was emitted.

Therefore, chemical composition can be evaluated via SEM by the method Energy Dispersive X-ray Spectroscopy (EDX) [441].

Experimental

The SEM analyses of the different pretreated AlMg3 substrates used in this work were performed by Mr. Christian Hoffmann of the CR/ANA department at Robert Bosch GmbH (Renningen, Germany). The apparatus employed was a field emission FE-SEM Supra® 55VP instrument (Carl Zeiss AG, Germany) with an acceleration voltage from 0.02 to 30 kV and a resolution of 0.8 nm at 15 kV. It was equipped with a thermal field emission type emitter, a 2 EDS (VP mode), and a charge-coupled device camera (CCD-camera) with IR illumination. The penetration of the beam at 15 kV is approximately 2 µm. The instrument was equipped with the following detectors: inLens (SE), Everhart-Thornley Secondary Electron Detector and VPSE detector (VP mode). The range of magnification of the images was from 12 to 1,000,000 X and the software for processing the images was SmartSEM® (Carl Zeiss AG, Germany). Element mapping was obtained from a rectangular surface area of 235 × 170 μm^2.

Results

SEM images of the pretreated surfaces are displayed in Figure 7.7a-c. Examination of the images reveals, as expected, that the microstructural states of the pretreated surfaces are different. In all cases, darker and brighter regions are discernible, indicating that the surfaces are neither completely flat nor smooth. For the three samples, a common undulating background topography can be recognized. Such rippled topography (accompanied with ridges and grooves), is typically displayed by technical aluminum substrates as a result of the rolling manufacturing process employed [426] This undulated profile is more remarkable for the surface cleaned with acetone (Figure 7.7a), hence, the pretreated surface with acetone can be considered, as far as the topography is concerned, as the aluminum alloy ‘‘as received’’ and retains the initial characteristics of the bare aluminum surface topography.

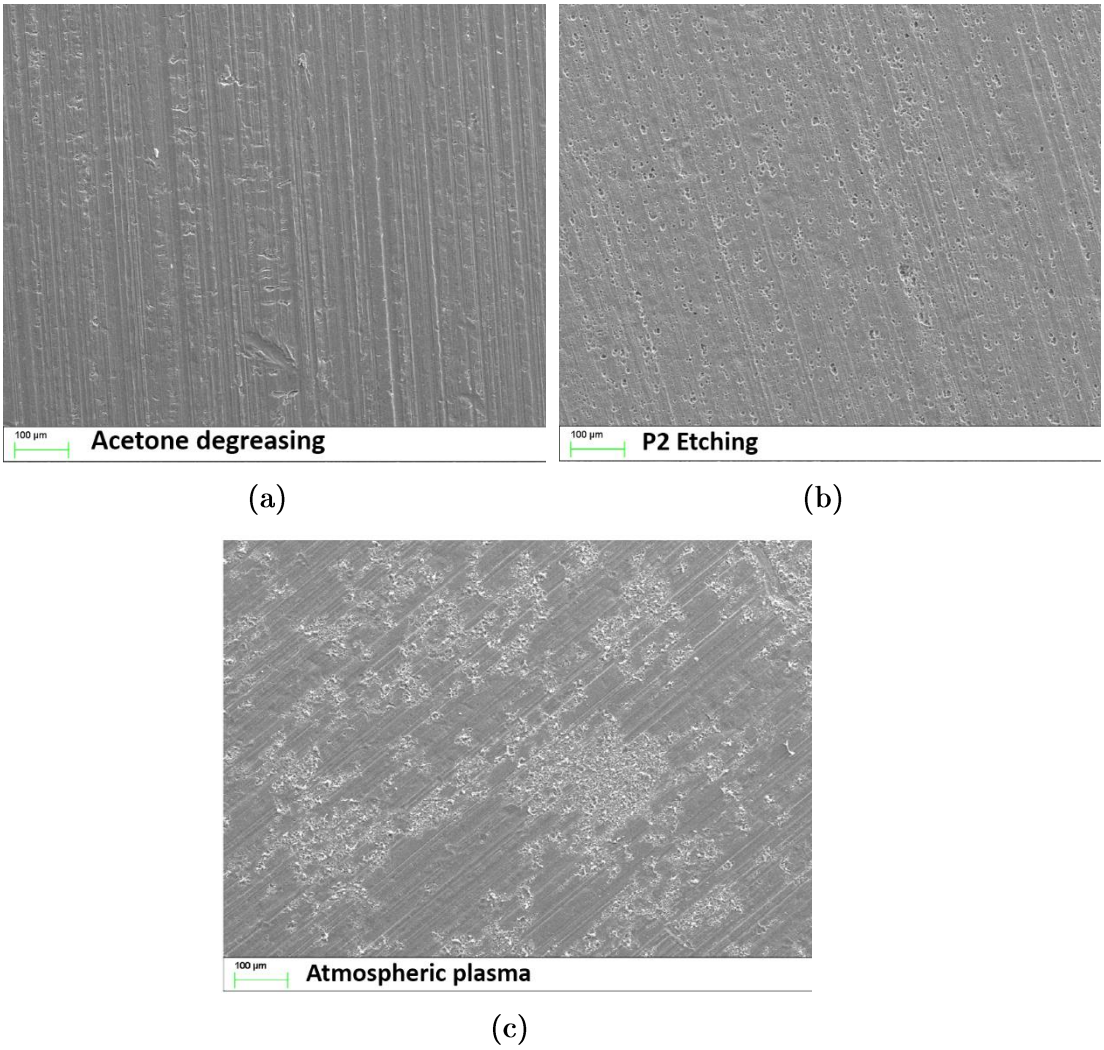


Figure 7.7. SEM images of EN AW 5754 aluminum alloy after surface pretreatment: (a) acetone degreasing (b) P2 etching and (c) air plasma treatment.

For the P2 etched surface (Figure 7.7b) the undulated background topography is recognized, and well-distributed micropores or pits are observed all over the surface. Therefore, pit nucleation was favored and pit growth occurred. During P2 etching, the sulfuric acid attacks the entire aluminum surface and would, if not for the presence of ferric ions, simply dissolve the aluminum. Thus, the ferric sulfate assists the formation of the ideal oxide layer by concentrating its attack on the magnesium (or other components such as Cu and Si) to form pits and, simultaneously, to slow down the effect that the sulfuric acid would have on the entire aluminum surface [434]. The surface texture created after P2 etching is consistent with reported SEM images of different aluminum alloys treated by this etching process [435,436]. It is also observed that the pits generated on the surface are not all of the same size and shape.

Finally, the topography of the surface after atmospheric air plasma treatment is presented in Figure 7.7c. The surface presents the mentioned rippled background texture, but shows evidence of ablated and melted material that has been redeposited [442]. This is recognized by the much brighter domains in the SEM image, associated with molten material at the surface. When aluminum is irradiated with plasma the significant amount of heat that evolves in the near surface can eventually produce very rapid melting of a thin layer [443,444]. Typically, only a few hundred nanoseconds are required for the metal liquid to solidify. The ablation process is believed to take place in regions close to the irradiated spot, whereas melting would occur in the vicinity of such irradiated edges [443]. The micrograph displays irregular arrangements of such brighter domains which do not cover the entire surface, which evidences a lack of homogeneity attained through the plasma method applied here.

Analysis carried out at higher magnification (Figure 7.8a-c) shows that the acetone degreased surface exhibits microcracks, microvoids and scratches (Figure 7.8a) due to the stresses caused by the aluminum manufacturing process. Furthermore, such topographical characteristics followed a preferential direction and suggest a microscopically rough surface. The etched surface (Figure 7.8b) features a less pronounced rolling texture and the circular pits can be recognized all over the surface. Many pits were merged together and created clusters, evidencing a tendency of pits to form in bunches. Clustering probably occurred as a consequence of a reduced rate of pit nucleation over time on Mg sites. Albeit, it can also suggest that pits were also formed at surface discontinuities. Ultimately, the micrograph of plasma treated AlMg3 (Figure 7.8c), illustrates a marked change in the aluminum surface morphology due to melting and cooling events caused by the discharges. The ablation caused by plasma produced a more dramatic change in the morphology on the surface when compared to the other two pretreatments. According to Khan et al. [442], the plasma treatment leads to the ejection of molten material onto the top surface in the form of a crater-like volcano top, and the molten material solidifies to form various polymorphs. This volcano-type feature is in fact observed for the plasma treated surface. Closer inspection (expanded area in red) reveals that microcavities were also created on the surface. In summary, plasma discharges created non-uniformly distributed defects like surface roughness, microvoids, microcavities, and volcano-like features.

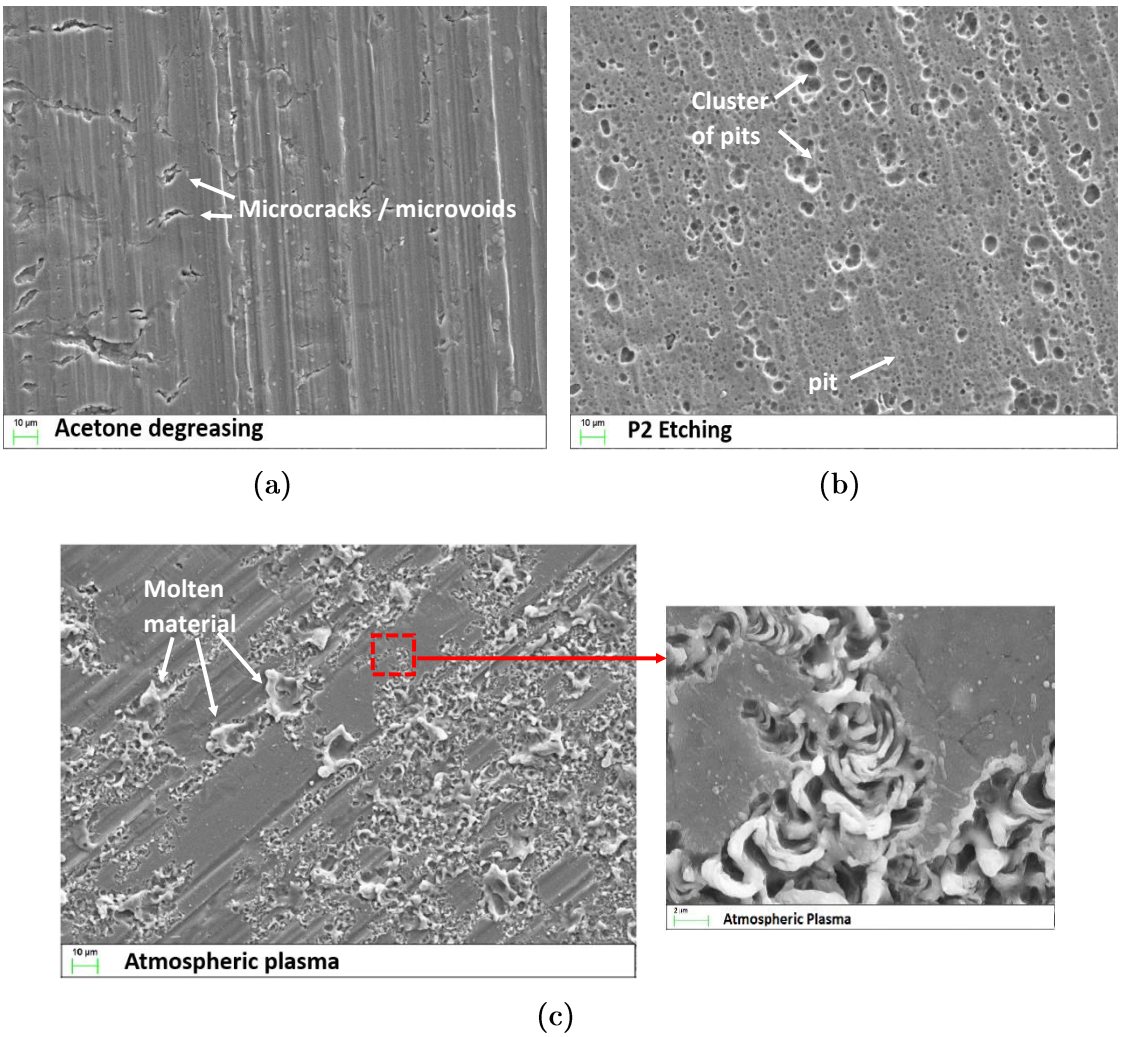


Figure 7.8. Microstructure of AlMg3 alloy (EN AW 5754) after different surface pretreatments (a) acetone degreasing, (b) P2 etching and (c) atmospheric pressure air plasma.

7.3.1.2. Scanning Force Microscopy (SFM)

Scanning force microscopy (SFM), also known as atomic force microscopy (AFM), is a widely used technique to generate topographic maps of surfaces, offering versatile possibilities. SFM has progressed significantly, and surfaces can be analyzed with respect to topography, hardness, roughness, adhesion, friction, and charge or magnetism [441]. The method is also very adaptable to different environments including vacuum, air, inert atmosphere and even liquids [441]. SFM uses a mechanical flexible cantilever with a very fine tip (radius of ~ 10-30 nm) attached at one of its ends [445]. The tip, which lies perpendicular to the longest axis of the cantilever, is swept over the sample surface. The deflections of the cantilever, arising from interactions and forces

between the tip and the surface atoms, are detected by a laser beam which is bounced off the rear of the cantilever (optical lever principle) and thus, recorded as a function of raster position [441,445]. Normally, the sample is supported on a piezoelectric xyz translator, which is moved up and down via a servo controlled mechanism. In such a way, the vertical displacements of the sample can be displayed as a function of x- and y- position to provide a three-dimensional morphological image of the sample [441,445]. In contact mode, the tip is constantly in contact with the sample, and as it moves over the surface, the cantilever deflects and the z piezo moves the sample up or down to maintain a constant deflection set point [446]. By means of SFM, the surface roughness can be expressed quantitatively using a roughness factor (R_a or R_{rms}) usually expressed in nanometers.

Experimental

The samples were imaged in an SFM TopoMetrix (TopoMetrix Corporation, C.A., U.S.A) apparatus consisting of a PR 1000 decoder and a 1000 modulation unit. The microscope was operated through a software SPM V.3.0x (TopoMetrix Corporation, C.A., U.S.A). The SFM equipment was mounted on a damping table to prevent any vibration influencing the measurements. The device was used in contact mode using SNL-10 sharpened silicon tips (Bruker, AXS S.A.S., Marne La Vallee Cedex 2, France) with Silicon Nitride cantilevers of 0.06-0.35 N/m and reflective gold coating. The cantilevers have a thickness of 4.0 ± 0.5 µm, a height of 2.5-8.0 µm, length of 125 ± 5 µm and width of 30 ± 5 µm. The tips have a resonance frequency between 18 and 65 kHz and a tip radius below 10 nm. The cantilever mounter was a 1560-00 Bruker. The surface was scanned in areas of 150x150 μm^2 and 50x50 μm^2. Five different areas were scanned for each sample and the velocity of scanning was set at 300 µm/s. Micro-roughness (R_a and R_{rms}) was automatically assessed by the software (SPM V3.0x Software) and mean image roughness was calculated. Each image was considered as a statistical unit. All measurements were carried out in a conditioned laboratory environment (23 °C and 50% RH).

Results

The SFM images (Figures 7.9-7.11) provide insight into the surface structure of the pretreated substrates by means of top views as well as 3-D pictures at two different magnifications. Upon inspection of all AFM images, the pretreated surfaces exhibit the previously observed, rippled profile. As previously discussed, such undulations are the result of the aluminum alloy manufacturing process. The topographical alterations deduced from SEM analyses for each pretreatment were confirmed by SFM. The three-

dimensional (3-D) SFM images of the surfaces show similar surface roughness after the pretreatments.

The SFM images of aluminum alloy surface after acetone cleaning show evidence of the presence of native microstructural defects such as undulations, dislocations, particle boundaries, microcracks and microvoids (Figure 7.9). The darker areas correspond to discontinuities or cavities.

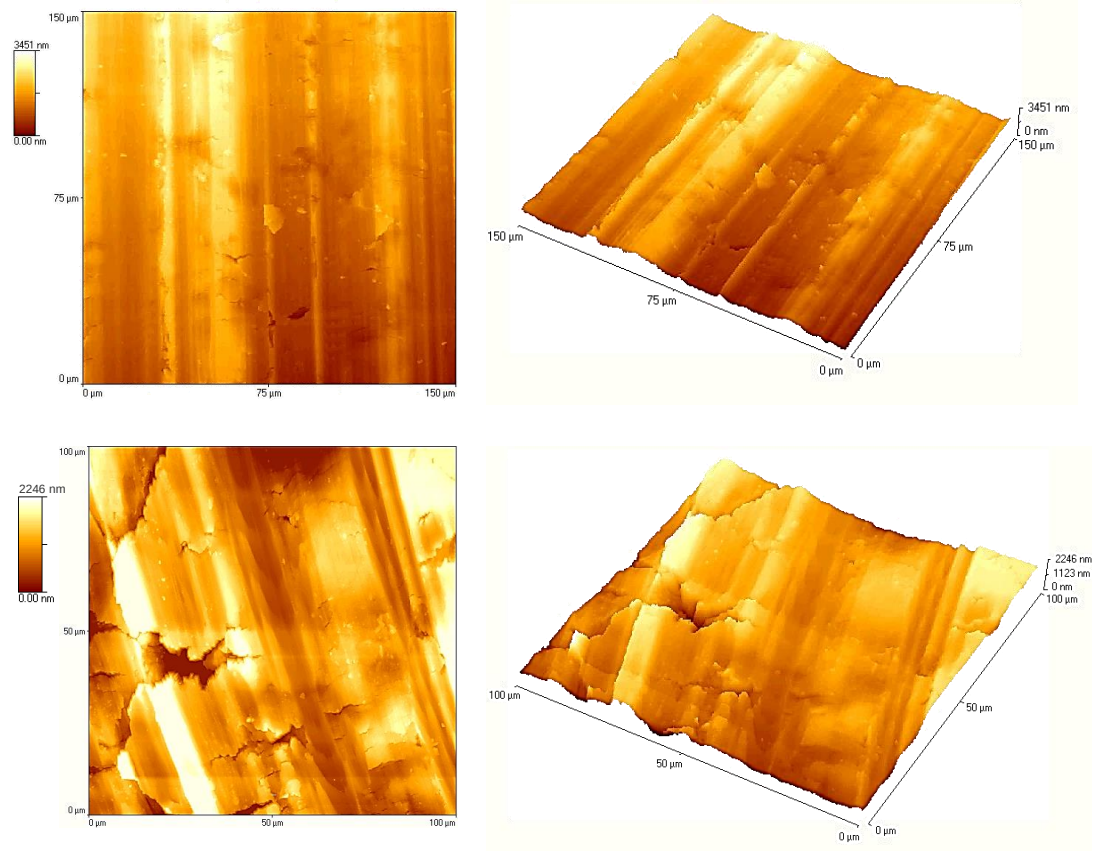


Figure 7.9. SFM images of the aluminum alloy (EN AW 5754) surface cleaned with acetone at two different scanning areas: (top) 150 x 150 µm² and (bottom) 100 x 100 µm²

For the P2 etching process, the surface topographies are shown in Figure 7.10. The microstructures of the surfaces show the characteristic pits or pores formed during the etching process. The image on the top exhibits numerous clusters of pits which are of irregular shapes (flake shape) and can be identified as darker spots. The image at greater magnification (bottom) displays singular pits which have a preferential circular form. The SFM images also evidence a homogeneous distribution of pits.

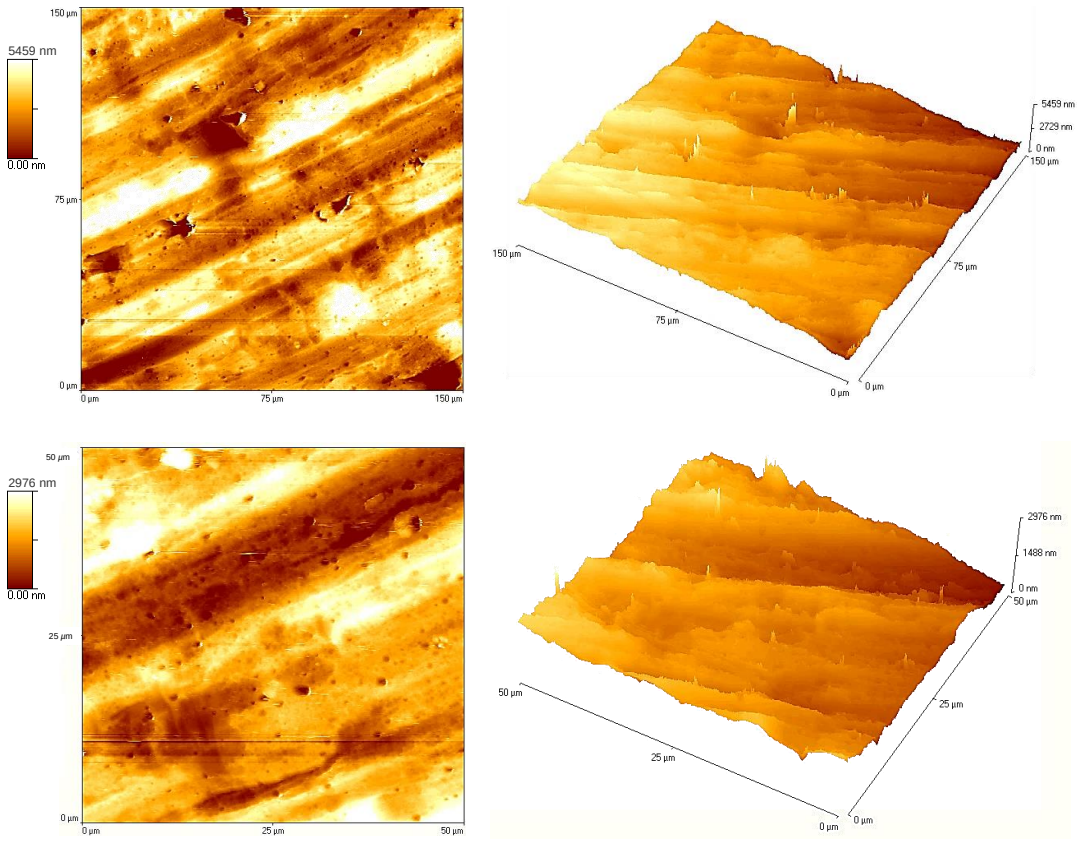


Figure 7.10. SFM topographic images of P2 etched aluminum alloy surfaces (EN AW 5754) at two different magnifications: (top) 150 x 150 µm^2 and (bottom) 50 x 50 µm^2.

The SFM micrographs of the aluminum after plasma treatment (Figure 7.11) evidence the tracks of the plasma scan by regions changing in appearance from an undulating profile to one with small peaks and hollows. As discussed previously, the morphology change is due to melting and re-solidification events occurring at the surface due to plasma shower. In fact, molten material at the surface following the irradiation path can be identified. The SFM images also reveal that the irradiated surface experienced a non-controlled melting, since cavities or surface asperities are observed only at certain areas of the treated surface. The SFM images evidence the poor homogeneity associated with the applied plasma pretreatment, since the topography is not uniform across the evaluated area.

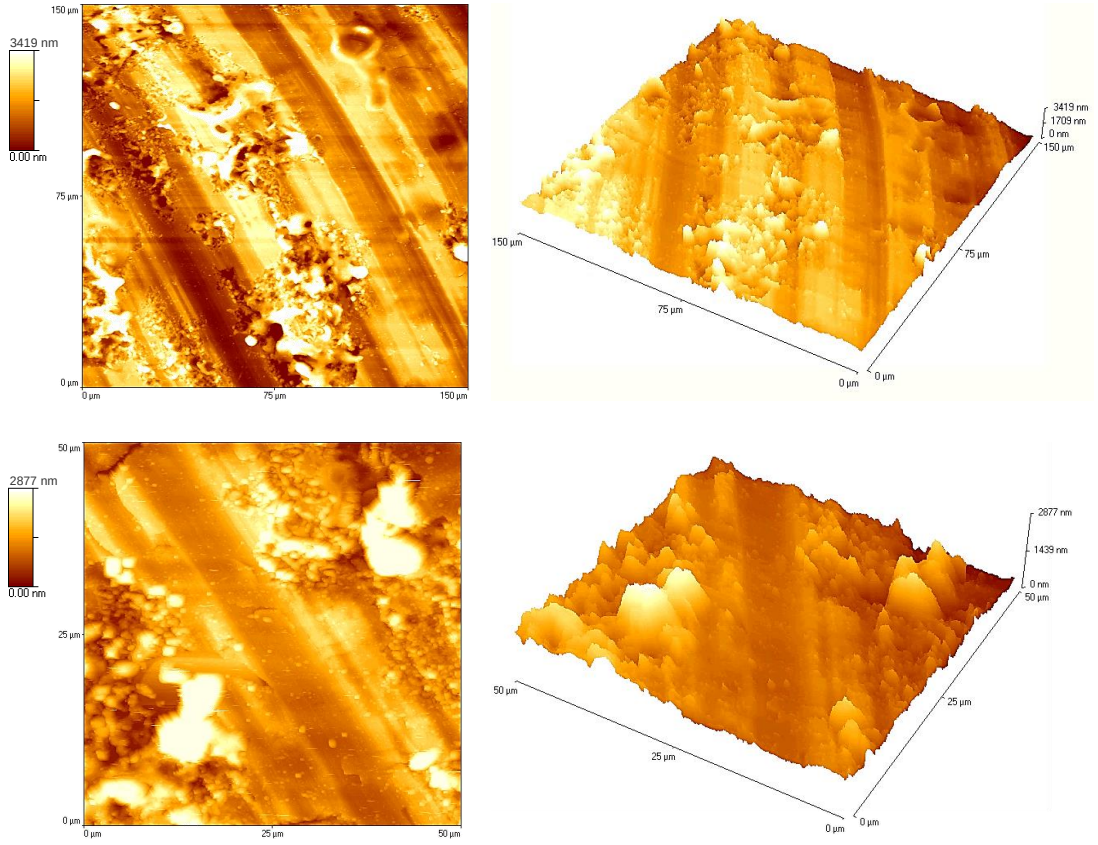


Figure 7.11. Contact mode topographic SFM images of air plasma pretreated AlMg3 surfaces at two different magnifications: (top) 150 x 150 µm^2 and (bottom) 50 x 50 µm^2.

Table 7.2 contains the values of surface roughness obtained for the three different pretreated surfaces. The root-mean-square roughness (R_{rms}), arithmetic roughness (R_a) were obtained for each pretreatment in a surface area of 150 x 150 µm^2.

Table 7.2. Surface roughness of the different pretreated aluminum alloy surfaces.

Surface pretreatment	Average R_{rms} [nm]	Average R_a [nm]
Acetone degreasing	563.2 ± 25.1	462.2 ± 12.3
P2 Etch	336.8 ± 17.8	268.6 ± 28.6
Atmospheric air plasma	442.9 ± 30.25	355.7± 31.9

The estimated values suggest insignificant changes in surface roughness at the nanometer scale. Despite the pretreatments had effects on the topography of the aluminum alloy surfaces, the average roughness is unaffected.

7.3.2. Chemical composition

7.3.2.1. X-Ray Photoelectron Spectroscopy (XPS)

Brief introduction to XPS technique can be found in Section 5.3.1.

Experimental

In this work, the chemical characterization of the pretreated aluminum surfaces via XPS were performed externally on behalf of Robert Bosch GmbH by Dr. Zumin Wang at the Max Planck Institute for Intelligent Systems (Stuttgart, Germany). The samples were analyzed as received in a Thermo VG Thetaprobe system (operating pressure of $1x10^{-9}$ mbar) employing a monochromatic Al-K as an X-ray radiation source (h =1486.68 eV; beam spot size 400 µm), while operating in the so-called 'standard' lens mode by simultaneously collecting all photoelectrons over the detection angle range between 23° and 83° (with respect to the surface's normal; i.e. the central detection angle equals 53°). The XPS survey spectra were recorded with a step size of 0.05 eV at constant pass energy of 50 eV covering a binding energy (BE) range of 0 eV to 1200 eV. The assignment, fitting (Gaussian function), and deconvolution of the signals were carried out with the WVASE32 software package (version 3.449). After initial survey spectra were completed, high resolution spectra were recorded for the detected elements.

Results

<u>Overall composition</u>

The survey spectra in Figure 7.12 display the XPS surface atomic composition and reveal the presence on all surfaces of carbon (C 1s), oxygen (O 1s, 2s), aluminum (Al 2s,2p) and magnesium (Mg 1s, 2s). Further elements were identified on the surfaces, evidencing inorganic contamination. The assignments of the peaks are based on XPS characterization of aluminum substrates [336,340,447]. The ability of aluminum to readsorb carbonaceous contaminants from the atmosphere was confirmed by the relatively high intensity of the C 1s peaks displayed for the pretreated surfaces. However, a reduction in intensity of the C 1s peak is perceived after P2 etching and

plasma treatment when compared to the acetone treatment. The presence of peaks related to oxygen confirm the existence of an oxide layer, as expected. Hence, the multilayer model illustrated for the aluminum substrate used in the adsorption experiments is also valid for technical aluminum.

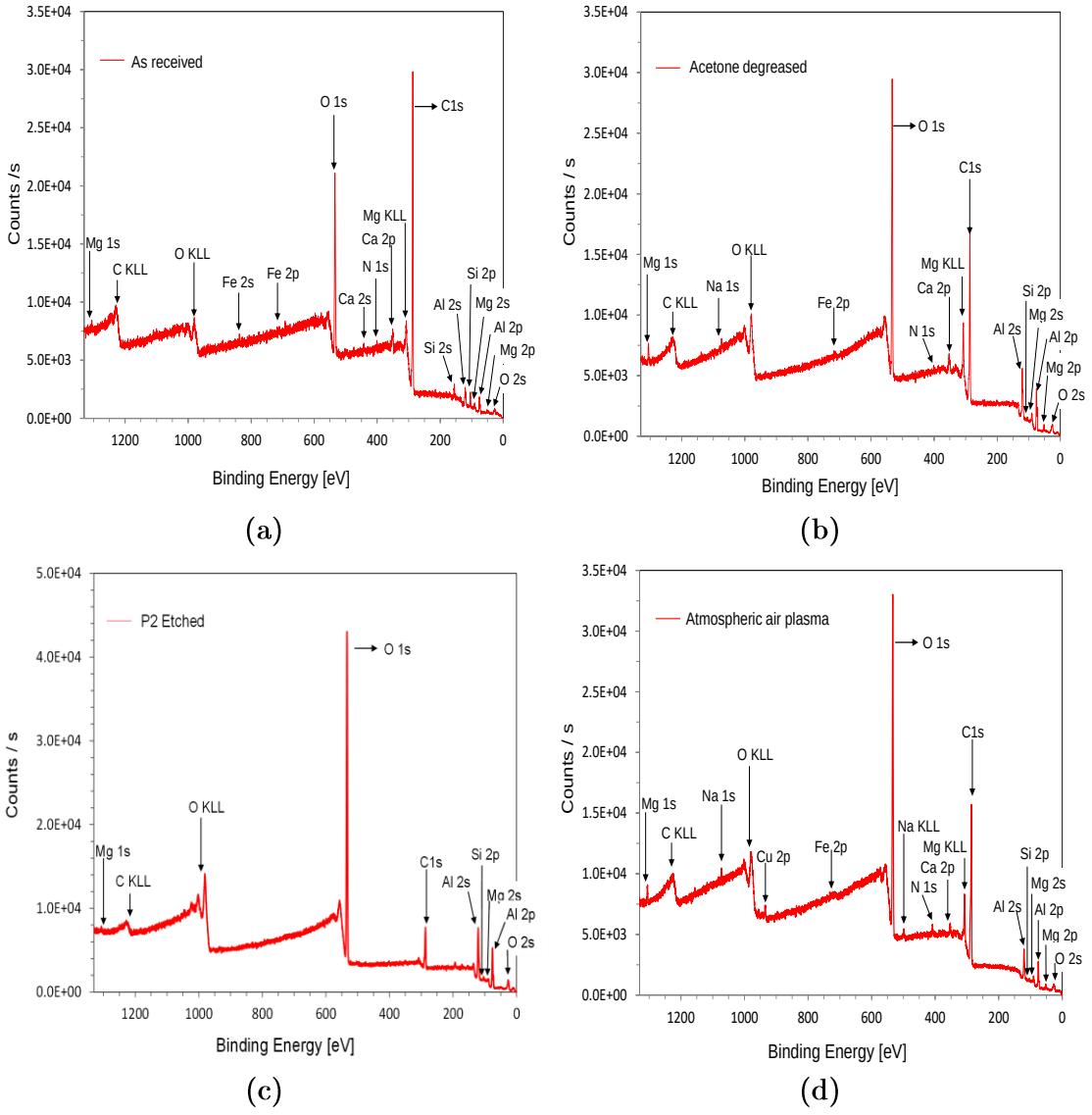


Figure 7.12. XPS survey spectra of (a) as received, (b) acetone degreased, (c) P2 etched and (d) plasma treated aluminum alloy surfaces.

The XPS spectrum of the "as received" surface (Figure 7.12a) besides of aluminum, magnesium, oxygen and carbon, it also exhibits the presence of calcium (Ca 2p,2s), nitrogen (N 1s) and iron traces (Fe 2p). The C 1s is the most prominent photopeak,

indicating that the aluminum oxide in its delivery state is highly contaminated. Silicon is present at the surface (Si 2p and Si 2s peaks) in relatively high concentration, which indicates that silicone oils were employed during the forming process. In conclusion, the as received aluminum substrates were highly contaminated and therefore, their use in adhesive bonding was inappropriate.

After applying the acetone degrease procedure (Figure 7.12b), slight changes on the chemical state of the surface are noticeable in comparison with the initial state. Signals of contaminant elements such as C, Na, N, Ca can still be identified, suggesting that acetone cleaning has limitations in removing all contaminants. Degreasing the surface with acetone resulted in a slight growth of the oxide layer.

Comparing the elemental composition of the P2 etched surface (Figure 7.12c) with that prior to the pretreatment (i.e. acetone degreased surface), it is observed that carbonaceous contaminants were more effectively removed. This surface exhibits the lowest hydrocarbon contamination level. Growth of the oxide layer is evidenced by the increase of the O 1s peak and the slight reduction of the Al 2p,2s peaks. Additionally, the Mg 2p peak is no longer observed, a fact that supports the hypothesis of the involvement of Mg in pit formation. However, identification of Mg 1s and Mg 2s peaks suggests that magnesium is still present on the surface but at very low concentrations. Additional elements such as N, Na, Ca, Fe and residues of the etching solution, represented by Fe and S signals, were not detected on the surface, indicating that the water washing procedure was appropriate.

The elemental composition of the surface after plasma pretreatment is given in Figure 7.12d. This spectrum differs from that of the acetone pretreatment in the enhancement of the O 1s peak and in the loss of intensity of the aluminum related peaks. In addition, a slight increase of the nitrogen peak is observed. However, it is still a very contaminated surface. From the SEM and SFM analysis, it was evidenced that the plasma treatment was not homogeneous, and therefore, the XPS spectrum exhibits the composition of both treated and non-treated regions. This fact can explain the similarities with the spectrum after acetone cleaning.

The relative intensities of both Al 2p and O 1s peaks for the surfaces after pretreatment are compared, in order to determine quantitatively the main changes of the chemical state of the surfaces.

Al 2p peak

Figure 7.13a-c illustrates the deconvoluted Al 2p peak of the alloy surface after the three pretreatments. For all pretreatments, the Al 2p peak is resolved into two peaks, one at lower photoelectron binding energy associated with metallic aluminum, and the

other at higher photoelectron binding energy related to oxidized aluminum [340]. This second peak includes the aluminum atoms in the oxide, as well as those bound to OH-groups. The energy difference ΔBE between the two peaks offers information about the increase of OH groups at the surface [336,448]. The binding energies of the two components are listed in Table 7.3 together with the determined XPS compositions (quoted as atomic percentages), the ΔBE and the thickness of the oxide layer, *d*, calculated according to Equation 5-4. The values of ΔBE disclose that there is a difference in the electronic structure of the oxide layer after etching when compared to those after plasma and acetone pretreatments. The values of ΔBE could suggest that, after P2 etching, the surfaces possess a higher amount of hydroxyl groups bound to the surface. In contrast, for acetone and plasma treatments, the concentration of O-H groups does not differ considerably. The thickness *d* of the oxide layer is also similar for all three kinds of pretreatment. The differences can be considered insignificant in the nanometer scale.

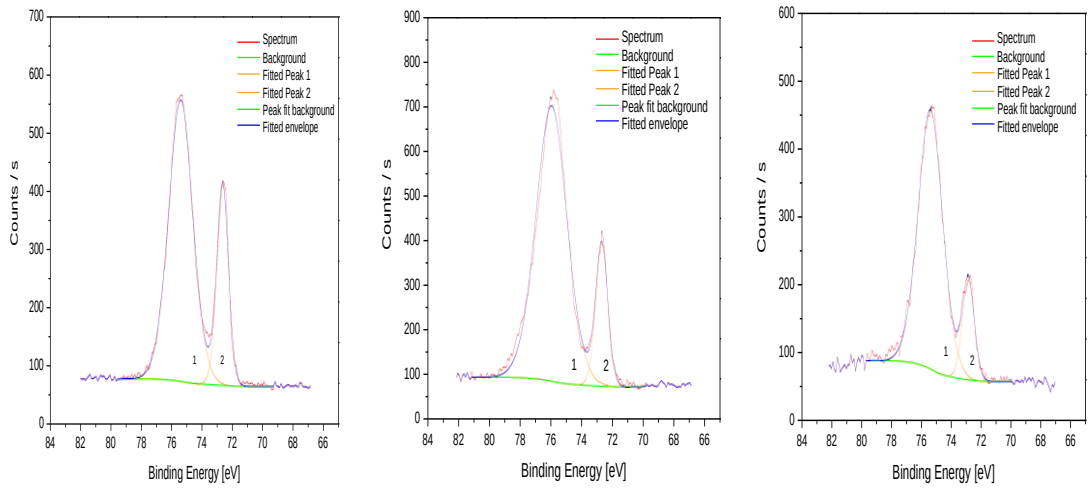


Figure 7.13. Al 2p spectrum resolved into a metallic and oxidic component for pretreated aluminum alloy surfaces by (a) acetone degreasing, (b) P2 etching and (c) air plasma.

When comparing the results in this chapter with those obtained for a model aluminum substrate described in Section 5.3.1 (Figure 7.14), the two peaks were identified and the thickness of the oxide layer lies in the same nanometer scale. Therefore, the Al-PVD substrate used in adsorption experiments is an appropriate model Al surface. Albeit, the metallic and oxide aluminum peak binding energies in the case of the model Al-PVD (native aluminum oxide layer) are slightly lower than those

of the technical surface, suggesting variation in the chemical electronic structure of the oxide layer due to discrepancies in the preparation methods applied. THe

Table 7.3. Binding energies of the resolved Al 2p spectrum into a metal and oxide component with their respective atomic percentage for each pretreated surface.

Pretreatment	Al 2p					
	Metal		Oxide		ΔBE [eV]	*d* [nm]
	Peak [eV]	Atomic composition [%]	Peak [eV]	Atomic composition [%]		
Acetone	72.78	25.35	75.49	74.64	2.71	4.37
P2 etch	72.79	16.86	75.99	83.14	3.2	5.57
Plasma	72.82	15.66	75.33	84.34	2.51	5.76

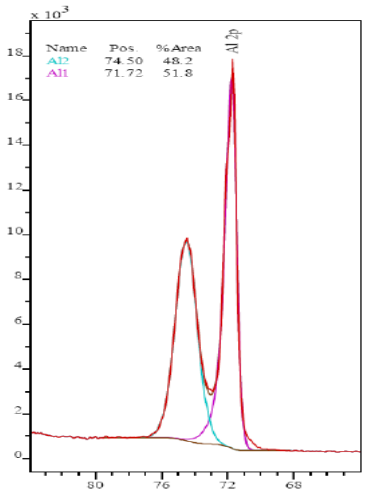


Figure 7.14. Al 2p peak of the model Al-PVD aluminum surface employed for adsorption and co-adsorption experiments.

O 1s peak

After etching, the peak associated with oxygen (Figure 7.15) is slightly broadener than the peak for plasma and acetone treated surfaces, suggesting slight increment of hydroxyl groups after etching. On the other hand, the O 1s peaks for acetone cleaned and plasma treated surfaces are similar, suggesting no significant differences in the chemical state of their oxide layers.

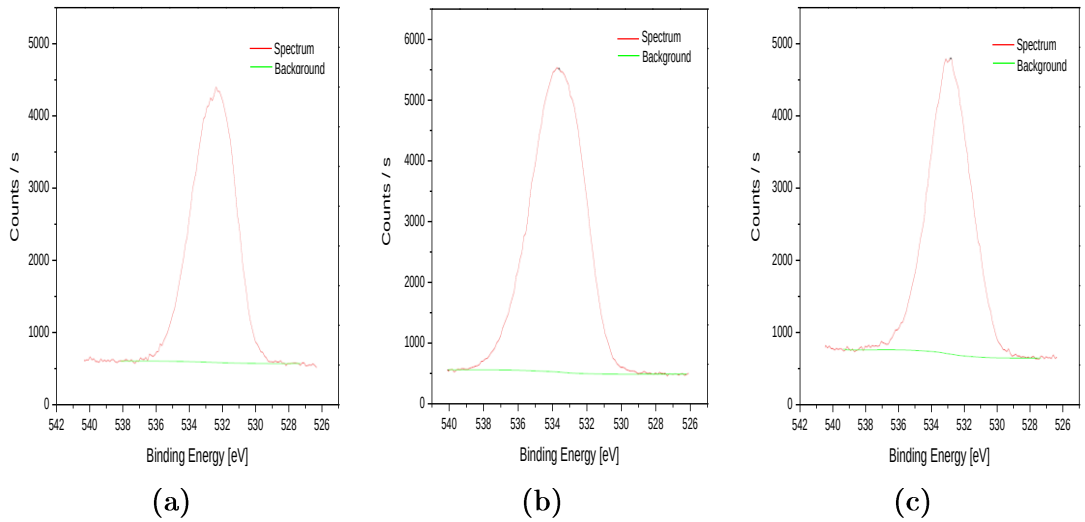


Figure 7.15. High resolution spectrum of the O 1s peak of the surfaces treated with (a) acetone, (b) P2 etchant and (c) atmospheric pressure air plasma.

Mg 2p peak

The features displayed by the peak related to magnesium (Mg 2p) (Figure 7.16) suggest that a high amount of magnesium was involved in pit nucleation during P2 etching, and therefore, the respective XPS peak is vanished. In contrast, for the acetone and plasma treated surfaces, the magnesium is still recognizable after the pretreatments.

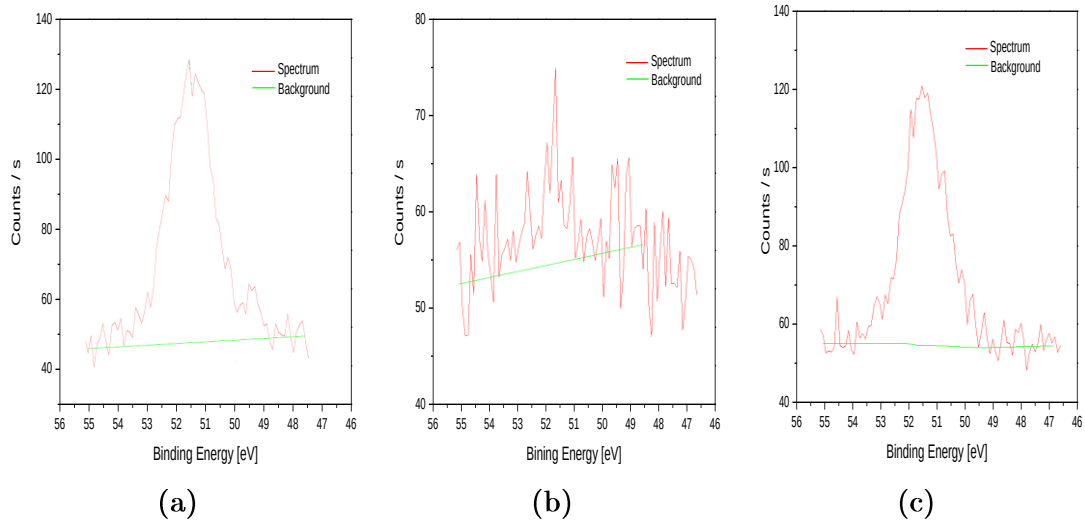


Figure 7.16. Mg 2p photoelectron peak for aluminum alloy pretreated with (a) acetone, (b) P2 etchant and (c) atmospheric pressure air plasma.

C 1s peak

The recognition of peaks related to C 1s confirms the presence of adventitious carbon contaminants. The etched surface exhibited the lowest content of these contaminants as inferred from the intensities of the carbon peaks in the different spectra. Although in principle the pretreatments partially removed the surface impurities, re-contamination could happen. For each treated surface, the C 1s signal is resolved in three peaks which are represented in Figures 7.17a-c. The binding energies and atomic percentage of each deconvoluted peak are also listed in Table 7.4. Carbon atoms can be distinguished according to the number of bonds to neighbor oxygen atoms with associated emissions at different binding energies. The peak 3 at ~286 eV is, for example, associated with the binding energy of C atoms in hydrocarbon chains (C–C/C–H bonds) [340]. The peak 2 at ~288 eV is attributed to the binding energy of C-O groups, and finally, the peak 1 at ~ 290-291 eV is associated with carboxyl groups -C=O [340]. The atomic compositions [%] of the peaks varied according to the type of pretreatment applied, as observed in Table 7.4. The peak 1 related to -C=O at ~290 eV displays the most noticeable variations; for example, after air plasma the peak increased significantly in comparison to the other pretreatments.

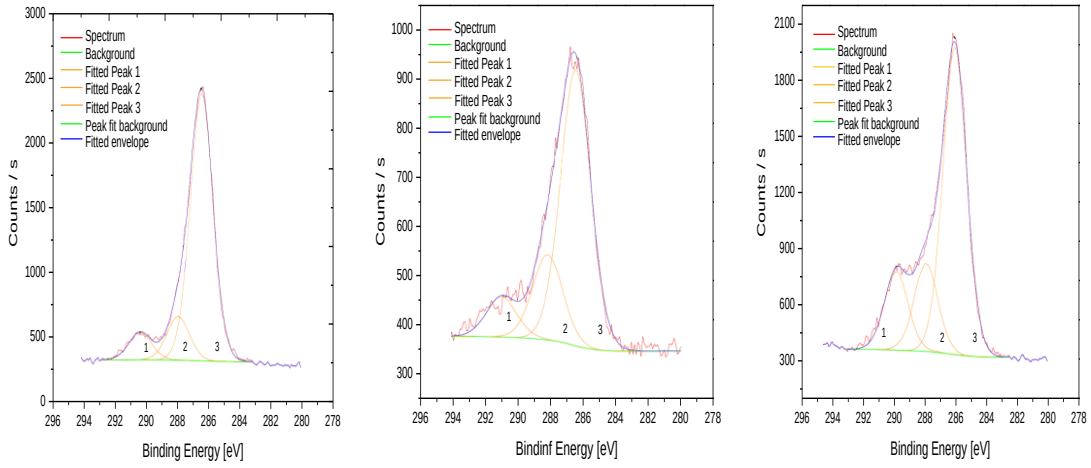


Figure 7.17. C 1s peak for the aluminum alloy surfaces after (a) acetone degreasing, (b) P2 etching and (c) air plasma treatment. The peak is deconvoluted in three signals for each case.

Table 7.4. XPS C 1s spectra and the corresponding deconvoluted peaks of the pretreated aluminum alloy surfaces

Pretreatment	Binding Energy (BE) [eV]			Atomic composition [%]		
	Peak 1 (C–C/C–H)	Peak 2 (C–O)	Peak 3 (C=O)	Peak 1 (C–C/C–H)	Peak 2 (C-O)	Peak 3 (C=O)
Acetone	290.3	287.9	286.4	8.2	12.85	78.9
P2 Etch	291.0	288.2	286.5	10.1	21.2	68.7
Plasma	289.8	287.9	286.0	16.6	18.5	64.9

In summary, the XPS results show that the surface composition of the pretreated technical aluminum alloy surface is consistent with that presented in Figure 7.14 for a model pure aluminum surface. An aluminum oxide layer containing an outer layer of carbonaceous contaminants was identified. The effectiveness of the pretreatments in the removal of such organic impurities is not as effective as expected. XPS analyses allow one to track the effect of the pretreatments on the growth of the oxide layer and chemical composition of the top carbon layer.

7.3.2.2. Energy-Dispersive X-ray Spectroscopy (EDX) - mapping

The local distribution of elements at the near-surface (2 µm depth) was investigated by SEM-EDX element mapping following the experimental specifications described previously for SEM analysis (section 7.3.1.2). The SEM images are shown together with the EDX maps of Al, Mg, O and C elements in Figures 7.18a-c for the three pretreated surfaces. The EDX element mapping shows that the detected elements are distributed differently in the scanned area and, in all cases, carbon is detected, showing again that the surfaces are very likely to be recontaminated with carbon-based substances. In particular, the chemical composition of the near-surface region of the P2 etched aluminum substrates (Figure 7.19b) seems to be more homogeneous than those for acetone cleaned (Figure 7.18a) and plasma treated (Figure 7.1c) surfaces, although, it shows an organic contaminant. The scanned plasma treated surface exhibits some Mg accumulations, which possibly result from the ablation process during the treatment. In addition, the plasma treated surface exhibits the highest Mg content. In contrast, the Mg content for the etched substrate is the lowest, confirming the hypothesis of its consumption during pit creation. This also suggests that the etching process took place in the µm in region. The images associated with oxygen indicate that its content in the near-surface was enriched after plasma, albeit, it was not regularly distributed.

Moreover, the distribution of carbon for the plasma near-surface compared to the other two surfaces suggests a higher amount of carbonaceous impurities on the surface. These aspects show the inconveniences of the plasma treatment applied in this study for attaining an aluminum alloy surface with homogeneous properties.

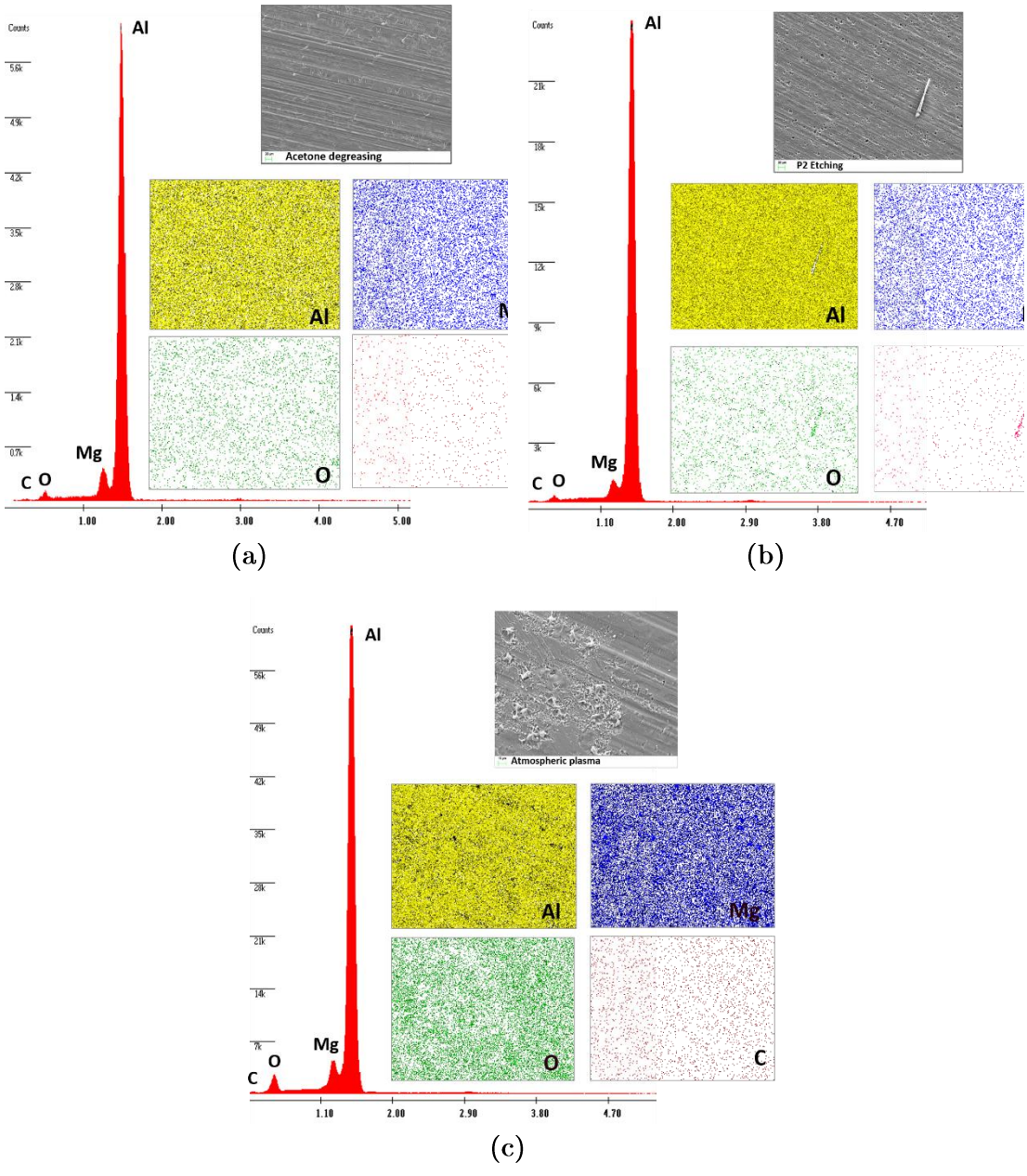


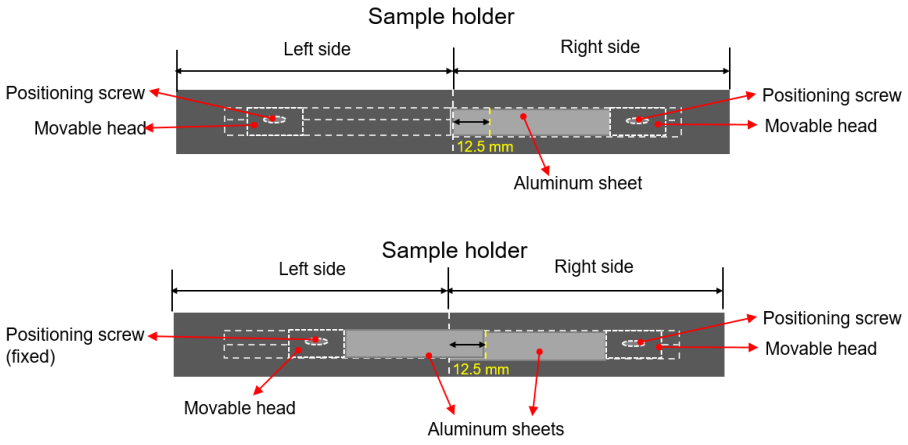
Figure 7.18. SEM images of aluminum substrates with EDX element maps of Al, Mg, O and C, after three different surface pretreatments (a) acetone degreasing, (b) P2 etch and (c) atmospheric pressure plasma.

7.4. Bonding analysis

Mechanical tests such as tensile shear tests are one of the most commonly used methods for evaluating joint strength. These tests are useful for quality control, however they are destructive, and cannot always predict failure for in-service components [427]. Among the standard tests used in the industry to understand mechanisms of failure and predict joint strength, the single-lap shear test is one of the most convenient and simple for testing quality of adhesive joints [423,449]. In this work, the effectiveness of the surface pre-treatments applied to the technical aluminum surface was evaluated by single lap shear tests, following the DIN EN 1465 standard.

7.4.1. Fabrication of the single lap adhesive joints

For each pretreated substrate, the single lap joints were assembled following a standard procedure. The method allows the attainment of reliable sample geometries. In the first step, the position of the aluminum specimen holder was calibrated. In this calibration procedure, two non-pretreated aluminum sheets were used. In one of them, a visible line was marked at 12.5 mm from one border with the help of a digital caliper. Subsequently, the marked aluminum sheet was located on the right side of the specimen holder (Figure 7.19a). Afterwards, the second sheet was placed on the left side and the positioning screw of the specimen holder was fixed at the required overlapping distance (Figure 7.19b-c). Once the left positioning screw was also fixed, both aluminum sheets were removed and the specimen holder was ready to be used for the fabrication of the single lap shear joints (SLSJ) specimens with the pretreated substrates.



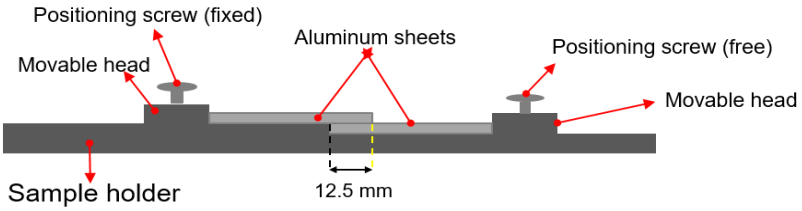


Figure 7.19. Set-up of the specimen holder for assembling the single-lap shear joints of constant geometry: (a) Positioning of the aluminum sheet with the visible marked line at 12.5 mm (yellow dashed line), and (b) positioning of the second aluminum sheet at the marked overlapping distance. (c) Front view of the sample holder set-up at the required overlapping distance for the SLSJ.

Once the technical substrates were treated and available for preparing the SLSJ, the commercial silicone adhesive, CSA, was applied at one edge of the two substrates. Two spacers of stainless steel were disposed equidistant within the CSA. Then, the second aluminum sheet was placed on the left side of the holder, and the two metal sheets were brought into contact and compressed with a hook, ensuring that the adhesive thickness between the two substrates equaled the diameter of the spacers (0.15 mm). The joints were then taken apart from the sample holder and the excess of adhesive was cleaned. For each surface pretreatment method, ten single lap shear joints were fabricated. Each series of ten SLSJ samples were immediately placed in an air circulating oven at 130 °C for 1 h for curing the silicone adhesive, CSA. After the curing process, the compression hooks were removed and the SLSJ samples were conditioned at 23 °C and 50 %RH for 24 h, previous to the single-lap shear tests. The detailed configuration and dimensions of the SLSJ are shown in Figure 7.20.

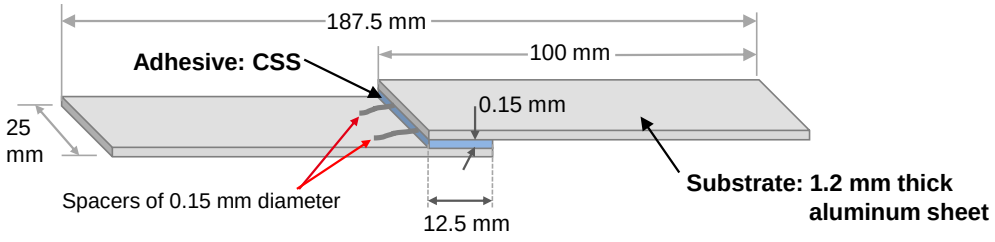


Figure 7.20. Configuration and dimensions of the adhesively bonded joint (SLSJ) samples used for the single-lap shear tests.

7.4.2. Single-lap shear testing

The single-lap shear tests were conducted at 23 °C and 50 %RH in a Zwick Roell Z020 universal testing machine (Ulm, Germany) with a load cell of 20 kN and setting a cross-head speed of 10 mm/min. The specimens were centered in the clamps using an alignment tab. The initial set-up before the single-lap shear tests can be observed in Figure 7.21. At least 10 SLSJ samples with the same surface pretreatment were tested for performing the statistical analysis of the single-lap shear tests.

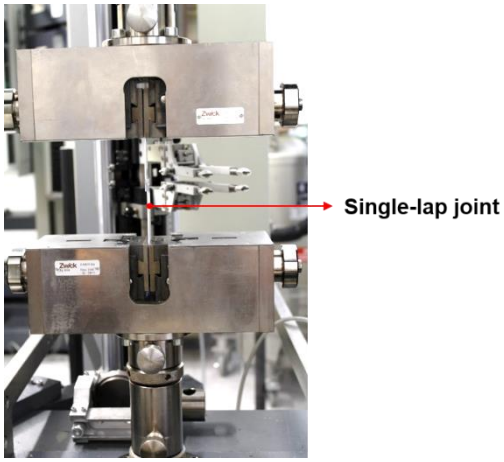


Figure 7.21. Initial setup of the single lap-shear tests on the universal testing machine

The results of the single-lap shear tests for the unaged SLSJ samples are presented in Figure 7.22. The single-lap shear curves for each pretreatment can be found in the Appendix E. The results show that the pretreatments applied to the surfaces have no effect on the lap-shear strength. Thus, the etching and plasma pretreatments applied in this work did not cause a significant increase in the lap shear strength of the unaged SLSJ samples. From the surface characterization of the pretreated substrates, it was found that surface roughness and thickness of the oxide layer were almost unaltered by the pretreatments, which could explain the similar shear strength results. Possibly, a similar mechanical interlocking effect, due to the identified surface grooves and the same surface roughness in the three surfaces, could also explain the similarity in the lap shear strength [450].

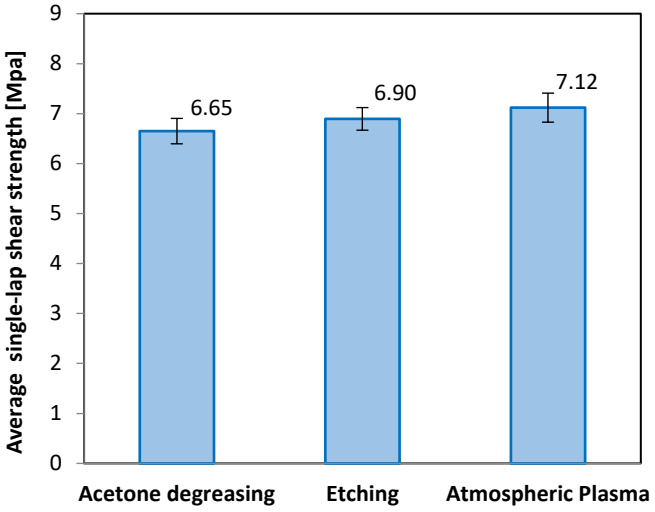


Figure 7.22. Influence of the surface pretreatments on the single-lap shear strength measured for aluminum-CSA joints. Error bars correspond to a 95% confidence interval.

7.4.3. Classification of interfacial failure

The fractured surfaces of the single lap-shear tests were photographed (Figure 7.23) and investigated by optical microscopy (Figure 7.24) in order to identify the type of interfacial failure. In general, the interfacial failure is classified into three different modes: (1) cohesive failure, (2) adhesive failure and (3) mixed failure. In the cohesive failure, the fracture occurs within the adhesive, leaving residues on both substrate surfaces. This type of fracture suggests that the interfacial strength was higher than the strength of the bulk adhesive. In an adhesive failure, the fracture occurs between the adhesive and the substrate surface. Finally, a mixed failure refers to a fracture that happens cohesively and adhesively.

To the naked eye, the fracture surfaces feature a mixed failure (Figure 7.23). However, macroscopic examination of the fractured surfaces (Figure 7.24a-c) indicate that a cohesive failure took place for all SLSJ samples regardless of the pretreatment applied to the aluminum substrates. The lap shear tests display the same shear strength and also the same cohesive failure mode, implying that the commercial silicone system (CSA) was able to create a stable and strongly interacting interface independent of the pretreatments applied to the aluminum substrates.

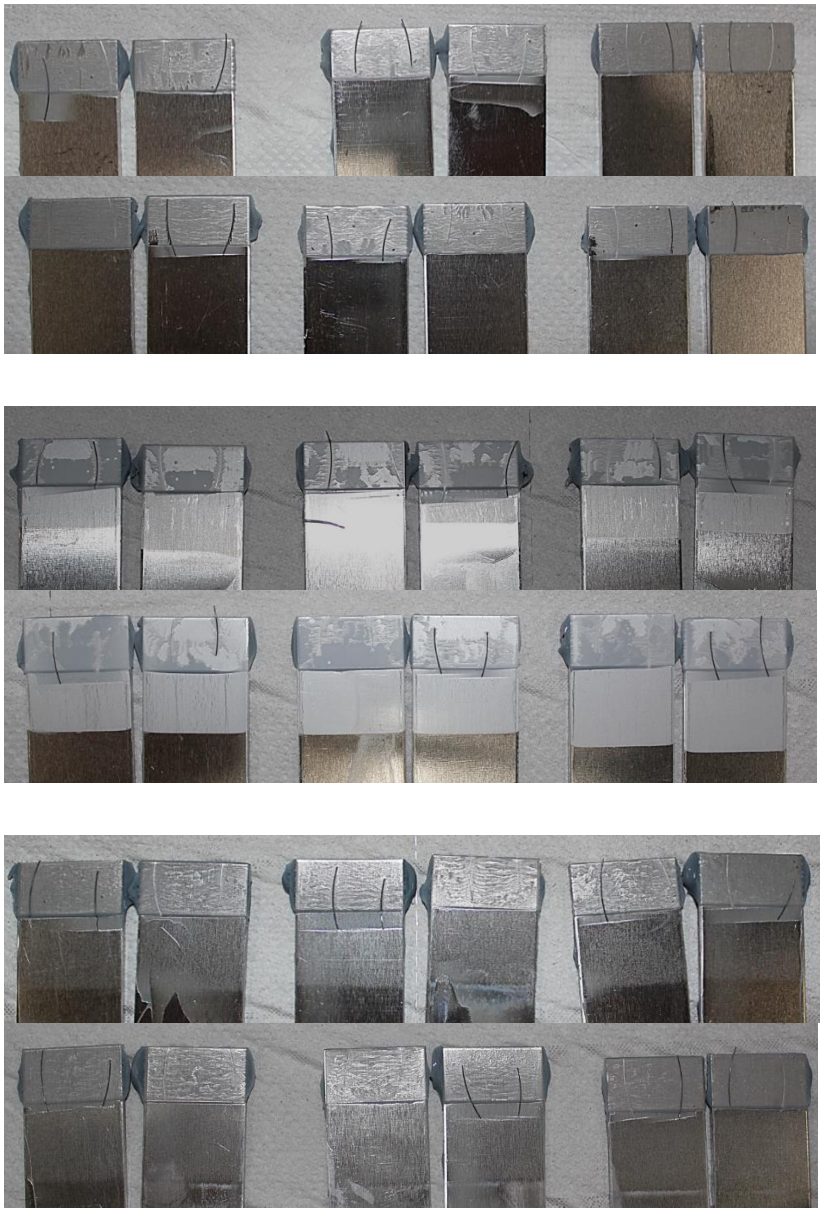


Figure 7.23. Photos of the fractured surfaces after single-lap shear testing of the SLSJ samples in which the aluminum sheets were pretreated by (a) acetone degreasing, (b) P2 etching and (c) atmospheric pressure air plasma.

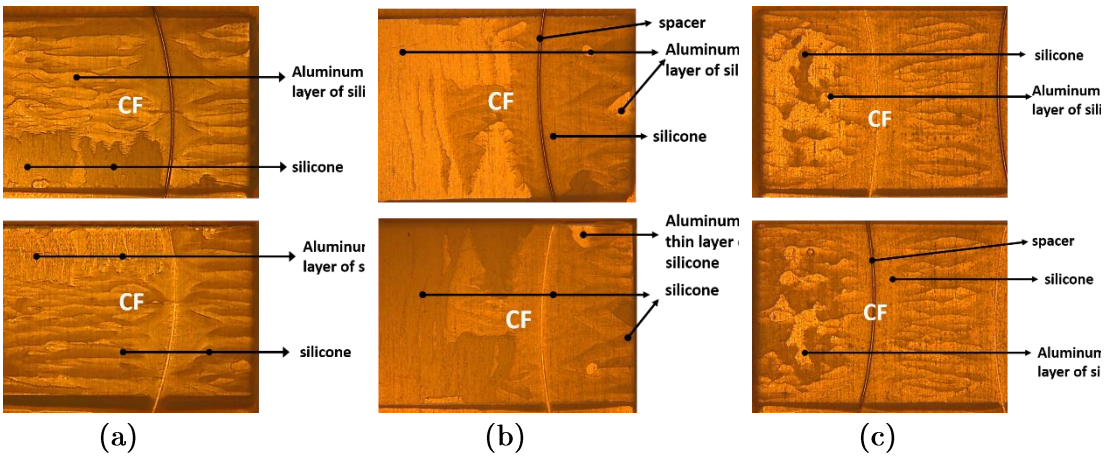


Figure 7.24. Optical micrographs of the fractured aluminum surfaces for each pretreatment applied (a) acetone degreasing, (b) P2 etch and (c) atmospheric pressure air plasma. A cohesive failure (CF) is identified independently on the pretreatment applied.

7.5. Summary

- Three different surface treatments were performed on the EN AW 5754 alloy with the purpose of improving the adhesion strength of bonded joints with the commercial silicone adhesive, CSA. The pretreatments were acetone degreasing, P2 etching and atmospheric pressure air plasma. Topography analysis by SFM and SEM, in conjunction with chemical analysis by XPS and EDX, proved to be effective for characterizing the different pretreated aluminum surfaces.
- The topography characterization by SFM findings was in strong agreement with that made by SEM. The acetone degreased surface displayed the topography of an "as received" surface with a typical undulated profile, whereas the P2 etched surface featured the most homogeneous topography and displayed the characteristic pits of an etched aluminum surface. On the contrary, the plasma treated surface evidenced the lowest level of homogeneity in terms of topography. In terms of roughness, the different treated aluminum surfaces cannot be distinguished.
- The chemical analysis of the surfaces by XPS and EDX techniques confirmed the formation of aluminum oxide on the surface and evidenced the ability of the pretreated surfaces to readsorb contaminants. However, the P2 etched surface was the less contaminated one. The thickness of the oxide layer, determined from the deconvoluted Al 2p peak of the XPS spectra, was similar in all pretreatment cases.

- The effectiveness of the pretreatments applied were discerned using single-lap shear tests of unaged adhesively bonded joints. Samples made with acetone-cleaned aluminum were taken as reference for the other two pretreatments (P2 etch and plasma). The results showed that P2 etch and plasma treatment did not affect the shear strength of the joints. A cohesive failure mode was identified in all cases, suggesting that, independently of surface roughness and thickness of the oxide layer, the CSA adhesive and the treated alloy surface can form strong interactions.
- Future investigations should be directed in order to identify alternative treatment techniques that favor the enhancement of the joint strength. In particular, additional conditions of the atmospheric pressure plasma method applied should be evaluated in order to attain a more homogeneous surface.

8 Conclusions and Perspectives

Final conclusions

Commercial silicones bearing Si-H or Si-vinyl groups were effectively characterized in bulk by comprehensive techniques, such as ATR-FTIR, 1-D and 2-D NMR, GPC, DSC and TGA, which are recommended to be used by those interested in verifying the structures and compositions of silicone adhesives or silicone materials in general. The characterization in bulk of a commercial silicone system (CSA) allowed the selection of suitable single silicone model components (SSMC) for formulating a model silicone (FMSA) and for studying adsorption onto aluminum. The methods used enabled the identification of different organosilanes, traces of cyclic siloxanes and presence of OH terminated silicones in the CSA. They also helped to determine the nature of the substituents at the silicon atom, to estimate the molar Si-H/Si-vinyl ratio and to infer chain linearity or the location of Si–H and Si-vinyl groups in the polymer chain. Distinctive properties of silicones, such as good thermal and thermo-oxidative stability, as well as high flexibility, were evidenced by onset degradation temperatures of the CSA above 350 °C, both in air and nitrogen, and by the low T_g (-120 °C). The stability of the commercial system was improved by the inclusion of phenyl substituents and silica filler, since the onset degradation temperature for pure PDMS, evaluated by FMSA, was found to be lower. In fact, a double T_g was identified for the CSA which suggests the existence of two domains with different molecular mobility. Hypothetically, the higher T_g (-112 °C) was associated with PDMS bound to the filler, and the lower T_g (-119 °C) was related to non-bound PDMS polymer. From the examination of the isothermal curing process of the CSA at 130 °C, a reduction of the curing time can be

proposed, as the Pt catalyzed crosslinking reaction was found to occur very rapidly, even at room temperature. Shortening of the curing time would represent lower operational costs, which would be of great benefit in industrial applications. The key role of the Pt catalyst on the crosslinking or curing reaction was demonstrated from the characterization in bulk of the FMSA.

The individual adsorption of the five SSMC on a native aluminum surface resulted in positive adsorption of the SSMC containing siloxane bonds (di-vinyl PDMS, di-hydride PDMS, Karstedt catalyst and TDMS) but in the lack of adsorption of the silane ATMS (adhesion promoter) under the experimental conditions applied in this work. It is not immediately obvious why the silane did not adsorb onto aluminum. Most likely a sum of different factors, such as unsuitable solvent, inappropriate temperature, lack of pre-hydrolysis step and slow spontaneous hydrolysis, contributed to its inefficient adsorption. Therefore, the mechanism of adhesion based on silanes forming covalent bonds to hydroxylated surfaces was not evidenced in this work.
Consistently, the in situ FTIR-ERA spectroscopy study showed that independently of the termination, PDMS displayed bulk properties after immediate contact with the surface but exhibited noticeable changes on their vibrational state upon THF rinsing. A significant part of PDMS could be rinsed away by the 1st THF rinse, but in all cases, there remained a more firmly adhered polymer, indicating that weakly interacting molecules, not in direct contact with the surface, were more prone to be desorbed upon contact with pure THF. Indeed, the resistance against solvent washing and new IR features support the hypothesis that remaining PDMS molecules were adsorbed stably and firmly to the surface.
The dynamics of the PDMS layer reveal that the adsorbed molecules were significantly movable at the interface, being able to reorient towards a more stable state. The results suggest chain flattening and preferential orientation of PDMS with Si-O-Si segments lying parallel to the surface. Flattening is assumed to occur in all molecules of the adsorbate, including those not in direct contact with the surface. The enhancement of permanent-permanent dipole interactions between PDMS molecules in the adsorbate layer can be proposed as one of the driving forces behind chain flattening in molecules not in direct contact with aluminum. A proposed scheme of PDMS chains oriented at the interface was given in this work. The model includes adsorbed Si-O-Si segments parallel to the surface with one methyl substituent pointing to the surface and the other pointing outwards. Such orientation causes the backbone to incline at a certain tilt angle with respect to the surface normal. The proposed model differs from that commonly described in literature for PDMS, which usually suggests that both methyl

substituents are vertically oriented to the chain axis but not in contact with the surface, i.e. methyl groups pointing into the air. In the hypothesized orientation given here, such inclination of the adsorbed backbone allows for the maximization of permanent-induce dipole interactions and electrostatic forces. Furthermore, it imparts geometrical stability to the adsorbed segments.

The remarkable alterations observed in the ERA spectra at 1150-1000 cm^{-1}, accompanied with the appearance of a new band at 1000-900 cm^{-1}, allowed for the assignment of the Si-O-Si bond as the adhesion partner in silicones (except for -OH terminated PDMS). It is reasonable to relate the strong adhesion to interactions involving the siloxane bond, but contribution of silanol (Si-OH) traces to chemisorption may exist as well. Consequently, four main adhesion mechanisms of silicones on aluminum, involving the siloxane bond, were proposed. They included: hydrogen bonding, permanent-induced dipole interactions, electrostatic forces and donor-acceptor interactions. Assignment of a dominant mechanism at the interface is not straightforward. In terms of energy, hydrogen bonding has been classified between physical and chemical interactions, thus, it could be thought of as the governing interaction. However, some studies have demonstrated that the contribution of hydrogen bonding to strong adhesion of PDMS is not as significant as dipole-dipole interactions. However, based on the results obtained in this work, a final conclusion in this direction cannot be drawn. It can be assumed that the strong adsorption displayed by PDMS and TDMS arose from the simultaneous interactions proposed in this work, and others involving the methyl groups, such as dipoles interactions.

The co-adsorption experiments demonstrated that the three siloxane components required for crosslinking were simultaneously adsorbed at the interface. However, preferential adsorption of vinyl PDMS over TDMS was observed. This behavior evidences that entropic considerations are dominant in concurrent adsorption of molecules with similar chemical nature but differing in molecular size. Molecular orientation was found to be greatly affected by such a concurrent adsorption and crosslinking reaction. In the absence of catalyst (no crosslinking) the presence of TDMS molecules distorted the chain flattening process of PDMS molecules and at the same time endorsed desorption of shorter oligomeric PDMS. However, in the presence of catalyst, crosslinking occurs very rapidly, restricting molecular orientation effects and lessening the desorption of shorter oligomeric species. Upon removal of weakly interacting molecules by THF, crosslinking continued in the near surface region. It can be conjectured that different domains or distribution of properties existed at the interface varying in the concentration of adsorbed components, presence of unreacted

segments, crosslinking degree, molecular mobility and orientation. Despite the inhomogeneities at the interface, the ERA spectra of co-adsorption, with and without the catalyst, exhibited the distinctive features at 1150-900 cm^{-1} which confirms the key role of Si-O-Si bonds in the adhesion of silicones. Thus, the mechanisms of adhesion postulated from the individual adsorption of the SSMC are also valid for silicone networks and co-adsorbed siloxane-species. Possibly, in the presence of Karstedt catalyst, chemical reactions between the adsorbate and the surface were competing with crosslinking in the near-surface region, since the stability of the adsorbed layer was significantly improved, advocating chemisorption. Co-adsorption results support the previous claims of strong adsorption of silicones on aluminum and showed that PDMS networks also adhered firmly on the surface. Lastly, no catalytic activity of aluminum on crosslinking via hydrosilylation was observed.

Analysis of adhesively bonded joints fabricated with three different pretreated technical aluminum (AlMg3) substrates and the commercial silicone (CSA), resulted in similar single-lap shear strengths, indicating that the pretreatment methods have an insignificant effect on the adhesion strength. Analysis of the fractured surfaces evoked cohesive failure, suggesting that interfacial interactions between silicone and aluminum were stronger than the cohesive forces of the bulk material. These findings correlate well with the previous claims of strong adhesion of silicones on aluminum. Consequently, the adhesion mechanisms proposed from adsorption and co-adsorption of model components seems to justify the strong adhesion at the interface between a commercial silicone and technical aluminum substrate.

It can be concluded that the good and stable adsorption found for the two PDMS prepolymers, catalyst and TDMS at the interface, strongly indicate that silicones stick firmly on aluminum and could be competitively used as adhesives in many applications where significant interfacial strength is required. The proposed adhesion mechanisms are compatible within the results from individual adsorption and co-adsorption. They support the strong adhesion of silicones either as single components or as a polymer network. The exhibited strong adsorption opposes some conventional beliefs that claim adhesion of silicones is weak due to the lack of covalent bonding with a substrate. The results obtained in this study endorse the fact that in real applications, the strength of an adhesively bonded joint is the sum of many factors, including the interactions at the interface between the adhesive network and the surface, bulk properties of the adhesive and the substrate, and surface properties of the polymer network and the substrate.

Perspectives

To obtain an optimum understanding of the adhesion of silicones on aluminum, research could be extended in many directions. With regard to the characterization of the commercial silicone system, CSA, it would be interesting to investigate the curing process in more detail in order to optimize the curing conditions. This could be achieved by implementing further DSC and ATR-FTIR measurements. It was shown that isothermal curing of the CSA at 130 °C was completed in less than 5 min, which is a much shorter time than the 1 h suggested by the manufacturer. Thus, the curing time at 130 °C could be potentially reduced. Such time reduction could represent lower operational costs, which would be beneficial in industrial processes. Furthermore, both temperature and time can be adjusted to more convenient values depending on the desired application of the CSA. Moreover, the surface properties of the CSA can be evaluated in an attempt to correlate such properties with the strength of adhesive joints. For surface analysis of the silicone, various methods can be applied, such as contact angle measurements, SEM, XPS and TOF-SIMS. In this direction, an alternative method to the single-lap shear test for analyzing the adhesion strength in adhesively bonded joints could be employed for a better analysis of the effect of surface pretreatments on the adhesion of the CSA. It is also recommended to optimize the conditions of the plasma treatment applied in this study in order to improve the homogeneity of the surface properties.

Promising work to be performed in the future, concerning the adsorption and co-adsorption of silicones on aluminum, could comprise:

- Supplementary analysis and characterization of the interface by XPS and ToF-SIMS methods in order to support and complement the results obtained by FTIR-ERAS. In this way, the chemical state of the adsorbate can be further examined, for instance, prior to and after THF rinsing cycles. Application of these methods could provide more evidence that help answer the question: were covalent bonds formed at the silicone-aluminum interface?
- Examination of the adsorption behavior of hydroxyl terminated PDMS in order to verify the claimed feasibility of these molecules in undergoing condensation with OH groups on the surface and leading to the formation of covalent Si-O-Al bonds. Competitive self-condensation reaction forming Si-O-Si bonds can be evaluated as well from OH terminated PDMS.
- Adsorption experiments including rinsing cycles with corrosive or aggressive substances. Silicones used in the automotive industry are usually exposed to

corrosive and aggressive chemicals during service, which is detrimental to adhesion. Silicones are well-known as water repellent and chemical resistant materials; therefore, it would be interesting to conduct adsorption experiments that, as well as THF rinses, include washes with typical aggressive chemicals in automotive applications such as water, methanol and ethanol. The ERA spectra could indicate how the chemical state and adhesion of PDMS is affected upon contact with these substances.

- Execution of adsorption experiments using a typical crosslinker added to commercial systems, e.g. PDMS with middle Si-H groups. These trials could help to clarify if covalent bonding between Si-H groups and OH groups on the surface occur, and to confirm the role of Si-O-Si bonds as the adhesion partner.
- Performing co-adsorption experiments between vinyl PDMS and hydride terminated PDMS in order to understand the role of the end-groups in the adhesion of silicones, more specifically to evaluate possible preferential adsorption for PDMS polymers differing in end-groups. Another proposal is to conduct co-adsorption experiments with the Karstedt catalyst, vinyl PDMS and a different crosslinker (hydride PDMS). In addition, it would be interesting to analyze the effect of the concentration of the dilute solution on the crosslinking reaction at the interface.
- Adsorption experiments with corresponding single model components for different silicone systems could be carried out following the methodology implemented in this study. Hence, the validity of the mechanisms of adhesion proposed in this work for an addition-curing silicone system could be verified for the condensation-curing and radical-curing silicone systems as well. In the same direction, co-adsorption of the single model components selected for those systems could be performed in order to study competitive adsorption and crosslinking reaction at the interface.
- Quantum mechanical modeling is categorically proposed for future work, in order to support the molecular orientation model presented in this study, as well as the mechanisms of adhesion postulated.

9 Bibliography

[1] Materials, A.S. for T. and. (1982). ASTM 6354-1982. Definitions of terms relating to adhesives.

[2] Hon, D. (2003). 14. Analysis of adhesives. Handbook of Adhesive Technology. New York, U.S.A.: Taylor & Francis Group, LLC. pp. 293–324.

[3] Grundmeier, G. and Stratmann, M. (2005). Adhesion and De-Adhesion Mechanism At Polymer/Metal Interfaces: Mechanistic Understanding Based on In Situ Studies of Buried Interfaces. *Annual Review of Materials Research*, 35, pp. 571–615. DOI:10.1146/annurev.matsci.34.012703.105111.

[4] Awaja, F., Gilbert, M., Kelly, G., Fox, B., and Pigram, P.J. (2009). Adhesion of Polymers. *Progress in Polymer Science*, 34, pp. 948–968. DOI:10.1016/j.progpolymsci.2009.04.007.

[5] Baldan, A. (2012). Adhesion phenomena in bonded joints. *International Journal of Adhesion and Adhesives*, 38, pp. 95–116.

[6] Kneafsey, A.R. and Sabongi, G.J. (1986). Structural adhesives. Chemistry and Technology. Hartshorn SR, editor New York and London: Plenum Press. 505-508 p. DOI:10.1002/0470014229.ch17.

[7] Batal, J. (2011). Charakterisierung der Mechanischen Grenzschicht in Polymer-Metall-Klebungen University of Saarland.

[8] Wehlack, C. (2008). Chemische Struktur und ihre Entstehung in dünnen Epoxid- und Polyurethanschichten auf Metallen Dissertation University of Saarland.

[9] Critchlow, G. (2011). General Introduction to Surface Treatments. *Handbook of Adhesion Technology*, pp. 120–150.

[10] Budzik, M. (2010). Fracture in Asymmetric Bonded Joints Bordeaux University and Gdansk University of technology.

[11] (FEICA), A. of E.A.S.M. (2015). Our Industry. Accessed 19 March 2015.

[12] He, X. (2011). A review of finite element analysis of adhesively bonded joints. *International Journal of Adhesion and Adhesives*, 31(*4*), pp. 248–264.

[13] De Buyl, F. (2001). Silicone Sealants and Structural Adhesives. *International Journal of Adhesion and Adhesives*, 21, pp. 411–422. DOI:10.1016/S0143-7496(01)00018-5.

[14] Erdman, D., Battiste, R., Boeman, R., and Klett, L. (2000). Characterization of a Structural Adhesive in Automotive Environments. *SAE Technical Paper Series*,(*2000-01–1559*), pp. 1–17. DOI:10.4271/2000-01-1559.

[15] Adams, R.D. and Wake, W.C. (1986). Adhesive Joints in Engineering. 2nd Edtion. London and New Yoirk: Elsevier Applied Science Publishers. 309 p. DOI:10.1007/978-94-009-5616-2.

[16] Lunder, O., Olsen, B., and Nisancioglu, K. (2002). Pre-treatment of AA6060 aluminium alloy for adhesive bonding. *International Journal of Adhesion and Adhesives*, 22, pp. 143–150. DOI:10.1016/S0143-7496(01)00049-5.

[17] Lower, L.D. and Klosowski, J.M. (2003). Silicone Adhesives and Sealants. In: Pizzi A, Mittal KL, editors. Handbook of Adhesive Technology, Second Edition, Revised and Expanded. USA: Taylor & Francis Group, LLC.

[18] Clarson, S.J. (2004). Silicones and Silicone-Modified Materials: A Concise Overview. *ChemInform*, 35, pp. 1–10.

[19] Noll, W. (1968). Chemistry and Technology of Silicones. Leverkusen, Germany: Academic Press. 1-708 p.

[20] Abe, Y. and Gunji, T. (2004). Oligo- and polysiloxanes. *Progress in Polymer Science (Oxford)*, 29(*3*), pp. 149–182. DOI:10.1016/j.progpolymsci.2003.08.003.

[21] Voronkov, M.G., Yuzhelevskii, Y., and Mileshkevich, V.P. (1975). The Siloxane Bond and its Influence on the Structure and Physical Properties of Organosilicon Compounds. *Russian Chemical Reviews*, 44(*4*), pp. 355–372. DOI:10.1070/RC1975v044n04ABEH002273.

[22] Andriot, M., Degroot, J. V., Meeks, R., et al. (2007). Silicones in Industrial Applications. *Dow Corning*, pp. 61–161.

[23] Kuo, a C.M. (1999). Poly (dimethylsiloxane). Polymer Data Handbook. p. 411.

[24] Wacker Chemie AG. (2014). Technical Data Sheet of the Commercial Silicone System (CSA). *Technical Data Sheet*, pp. 1–2.

[25] Custo Dio, J. (2015). Structural adhesives. 717-771 p. DOI:10.1007/978-3-319-08236-3_16.

[26] Jones, R.G., Ando, W., and Chojnowski, J. (2000). Silicon-Containing Polymers. The Science and Technology of Their Synthesis and Applications. Springer Science+ Business Media B.V. 1-766 p. DOI:10.1007/978-94-011-3939-7.

[27] Picard, L., Phalip, P., Fleury, E., and Ganachaud, F. (2015). Bonding of Silicone Rubbers on Metal: (1) Chemistry of Adhesion. *Progress in Organic Coatings*, 87, pp. 250–257. DOI:10.1016/j.porgcoat.2015.02.022.

[28] Picard, L., Phalip, P., Fleury, E., and Ganachaud, F. (2015). Bonding of Silicone Rubbers on Metal (2) Physical Chemistry of Adhesion. *Progress in Organic Coatings*, 87, pp. 258–266. DOI:10.1016/j.porgcoat.2015.03.020.

[29] Picard, L., Phalip, P., and Fleury, E. (2015). Chemical adhesion of silicone elastomers on primed metal surfaces: A comprehensive survey of open and patent literatures. *Progress in Organic Coatings*, 80, pp. 120–141. DOI:10.1016/j.porgcoat.2014.11.022.

[30] Jemmett, A.E. (1968). Chemical Behaviour of Siloxanes at Metal Interfaces. *Tribology*, pp. 173–177.

[31] Jemmett, A.E. (1968). Chemical Behaviour of Siloxanes at Metal Interfaces -2. *Tribology*, 1, pp. 237–239.

[32] Perkel, R. and Ullman, R. (1961). The Adsorption of Polydimethylsiloxanes from Solution. *Journal of Polymer Science*, 54, pp. 127–148.

[33] Cosgrove, T., Prestidge, C.A., and Vincent, B. (1990). Chemisorption of Linear and Cyclic Polymethylsiloxanes on Alumina Studied by Fourier-transform Infrared Spectroscopy. *Journal of the Chemical Society, Faraday Transactions*, 86(*9*), pp. 1377–1382.

[34] Patel, A., Cosgrove, T., Semlyen, J.A., Webster, J.R.P., and Scheutjens, J.M.H.M. (1994). Adsorption Studies of Different End-Functionalised Poly(dimethylsiloxane). *Colloids and Surfaces A: Physicochemical and Engineering Aspects*, 87, pp. 15–24.

[35] Levresse, P., Feke, D.L., and Zloczower, I.M. (1998). Analysis of the Formation of Bound Poly(dimethylsiloxane) on Silica. *Polymer*, 39(*17*), pp. 3919–3924.

[36] Vast, L., Delhalle, J., and Mekhalif, Z. (2009). 7-Octenyltrimethoxysilane, a Model Coupling Molecule to Study the Adhesion Promotion of a Silicone Elastomer on an Al 2024 Alloy. *International Journal of Adhesion and Adhesives*, 29, pp. 286–293. DOI:10.1016/j.ijadhadh.2007.07.002.

[37] Allen, K.W., Hansrani, A.K., and Wake, W.C. (1981). The Structure and Properties of Films of

Siloxane Coupling Agents. *Journal Of Adhesion*, 12(*3*), pp. 199–219. DOI:10.1080/00218468108071201.

[**38**] Li, Y. and Vecchio, N.E. (2007). Studies of Thiol Additions of Silane Coupling Agents by Vibrational Spectroscopy. *Spectrochimica Acta - Part A: Molecular and Biomolecular Spectroscopy*, 67, pp. 1321–1325. DOI:10.1016/j.saa.2006.09.043.

[**39**] Quinton, J., Thomsen, L., and Dastoor, P. (1997). Adsorption of Organosilanes on Iron and Aluminium Oxide Surfaces. *Surface and Interface Analysis*, 25, pp. 931–936.

[**40**] Comyn, J., Day, J., and Shaw, S.J. (1997). Durability of aluminium-sealant joints in jet-fuel, water and antifreeze. *International Journal of Adhesion and Adhesives*, 17(*3*), pp. 213–221. DOI:10.1016/S0143-7496(97)00006-7.

[**41**] Petersson, L., Meier, P., Kornmann, X., and Hillborg, H. (2010). Effect of surface cleanliness of aluminium substrates on silicone rubber adhesion. *Journal of Physics D: Applied Physics*, 44, pp. 34011. DOI:10.1088/0022-3727/44/3/034011.

[**42**] Fug, F., Nies, C., and Possart, W. (2014). in situ FTIR study of adhesive interactions of 4,4′-methylene diphenyl diisocyanate and native metals. *International Journal of Adhesion and Adhesives*, 52, pp. 66–76.

[**43**] Nies, C., Wehlack, C., Ehbing, H., Dijkstra, D.J., and Possart, W. (2012). Adhesive Interactions of Polyurethane Monomers with Native Metal Surfaces. *The Journal of Adhesion*, 88(*8*), pp. 665–683. DOI:10.1080/00218464.2012.682865.

[**44**] Kycia, A.H., Koczkur, K., Leitch, J.J., Lipkowski, J., Zamlynny, V., and Petryk, M.W.P. (2013). Application of PM-IRRAS to study thin films on industrial and environmental samples. *Analytical and Bioanalytical Chemistry*, 405, pp. 1537–1546. DOI:10.1007/s00216-012-6469-6.

[**45**] Tolstoy, V.P., Chernyshova, I. V., and Skryshevsky, V. a. (2003). Handbook of Infrared Spectroscopy of Ultrathin Films. New Jersey, U.S.A.: John Wiley & Sons, Inc. 732 p.

[**46**] Greenler, R.G. (1966). Infrared Study of Adsorbed Molecules on Metal Surfaces by Reflection Techniques. *The Journal of Chemical Physics*, 44(*1*), pp. 310–315.

[**47**] Witucki, G.L. (1993). A Silane Primer: Chemistry and Applications of Alkoxy Silanes. *Journal of Coatings Technology*, 65(*822*), pp. 57–60.

[**48**] Abel, M.-L. (2011). Organosilanes: Adhesion Promoters and Primers. In: da Silva LFM, Öchsner A, Adams RD, editors. Handbook of Adhesion Technology. pp. 238–257. DOI:10.1007/978-3-642-01169-6.

[**49**] Ashmead, B. V. and Owen, M.J. (1971). Adsorption of Polydimethylsiloxanes from Solution on Glass. *Journal of Polymer Science: Part A-2*, 9, pp. 331–343.

[**50**] Cosgrove, T., Patel, A., Semlyen, J.A., Webster, P., and Zarbakhsh, A. (1993). Study of Chemisorption of Poly(hydrogen methylsiloxane) Using Neutron Reflectometry and Small-Angle Neutron Scattering. *Langmuir*, 9(*9*), pp. 2326–2329.

[**51**] Lenk, T.J., Lee, D.H.T., and Koberstein, J.T. (1994). End Group Effects on Monolayers of Functionally-Terminated Poly (dimethylsiloxanes) at the Air-Water Interface. *Langmuir*, 10(*6*), pp. 1857–1864.

[**52**] Nies, C. (2010). Chemische Adhäsionswechselwirkungen zwischen Polyurethan-Monomeren und Metallsubstraten University of Saarland, Germany.

[**53**] Erlangung, Z. and Fug, F. (2011). Chemische Adhäsionswechselwirkungen zwischen Isocyanaten und Metallsubstraten University of Saarland, Germany.

[**54**] Carle, D. and Blount, G. (1999). The suitability of aluminium as an alternative material for car bodies. *Materials and Design*, 20, pp. 267–272.

[**55**] Miller, W.S., Zhuang, L., Bottema, J., Wittebrood, A.J., De Smet, P., Haszler, A., and Vieregge, A. (2000). Recent development in aluminium alloys for the automotive industry. *Materials Science and Engineering. Reports: A Review Journal*, 280, pp. 37–49.

[**56**] Grundmeier, G. and Stratmann, M. (2005). Adhesion and De-Adhesion Mechanisms at Polymer/Metal Interfaces: Mechanistic Understanding Based on In Situ Studies of Buried Interfaces. *Annual Review of Materials Research*, 35(*1*), pp. 571–615.

[**57**] Eaborn, C. (1960). Organosilicon Compounds. London: Butterworths Scientific Publications. 1-

530 p.

[58] Auner, N. and Weis, J. (2008). Organosilicon Chemistry I - From Molecules to Materials. First Edit. WILEY-VCH Verlag GmbH & Co. KGaA. 1-371 p. DOI:10.1002/9783527620777.

[59] Rochow, E.G. (1947). An Introduction to the Chemistry of Silicones. Second Ed. USA: John Wiley & Sons, Inc. 1-159 p.

[60] Koerner, G. (1991). Silicones: Chemistry and Technology. 0th Editio. CRC Press. 1-125 p.

[61] Ziegler, J.M. and Gordon Fearon, F.W. (1989). Silicon-Based Polymer Science. A Comprehensive Resource. American Chemical Society. 801 p. DOI:10.1021/ba-1990-0224.

[62] Voronkov, M.G., Mileshkevich, V.P., and Yuzhelevskii, Y.A. (1978). The siloxane bond. Physical properties and physical transformations. First Ed. New York, U.S.A.: Consultants Bureau. 1-493 p.

[63] Marciniec, B., Maciejewski, H., Pietraszuk, C., and Pawluc, P. (2009). Hydrosilylation: A Comprehensive Review on Recent Advances. Matisons JG, Marciniec B, editors Poland: Springer Science+ Business Media B.V. 159-190 p. DOI:10.1007/978-1-4020-8172-9.

[64] Abe, Y. and Gunji, T. (2004). Oligo- and polysiloxanes. *Progress in Polymer Science*, 29(*3*), pp. 149–182. DOI:10.1016/j.progpolymsci.2003.08.003.

[65] 7 Polysilanes and Other Silicon-Containing Polymers 7.1(n.d.). *Most*,.

[66] Clarson, S.J. (2010). Advanced Materials Containing the Siloxane Bond. Advances in Silicones and Silicone-Modified Materials. pp. 3–10.

[67] Rücker, C. and Kümmerer, K. (2015). Environmental Chemistry of Organosiloxanes. *Chemical Reviews*, 115, pp. 466–524. DOI:10.1021/cr500319v.

[68] Wacker Chemie AG. (2011). Silicones - Compounds and Properties, pp. 1–32. Accessed 23 April 2012.

[69] Weinhold, F. and West, R. (2011). The Nature of the Silicon-Oxygen Bond. *Organometallics*, 30, pp. 5815–5824.

[70] Bürger, H. (1973). Anomalies in the Structural Chemistry of Silicon. *Angewandte Chemie. International Edition*, 12(*6*), pp. 474–486.

[71] Voronkov, M.G. and Ya., D.A. (1964). The Donor-Acceptor Properties of the Siloxane Bond. *Zhurnal Strukturnoi Khimii*, 5(*3*), pp. 482–489.

[72] Mecham, J. (1997). Synthesis and Characterization of Cycloaliphatic and Aromatic Polester/Poly(dimethylsiloxane) Segmented Copolymers Virginia Polytechnic Institute and State University.

[73] Voronkov, M.G., Yuzhelevskii, Y., and Mileshkevich, V.P. (1975). The Siloxane Bond and Its Influence on the Structure and Physical Properties of Organosilicon Compounds. *Russian Chemical Reviews*, 44(*4*), pp. 355–372. DOI:10.1070/RC1975v044n04ABEH002273.

[74] Wilk, I.J. (1957). Comparative Organic Chemistry: Carbon and Silicon. Proceedings of the Pacific SouthWest Association of Chemistry Teachers. Vol. 34. pp. 463–465.

[75] Weinhold, F. and West, R. (2013). Hyperconjugative Interactions in Permethylated Siloxanes and Ethers: The Nature of the SiO Bond. *Journal of the American Chemical Society*, 135, pp. 5762–5767. DOI:10.1021/ja312222k.

[76] Passmore, J. and Rautiainen, J.M. (2012). On The Lower Lewis Basicity of Siloxanes Compared to Ethers. *European Journal of Inorganic Chemistry*, pp. 6002–6010. DOI:10.1002/ejic.201200881.

[77] Nakajima, Y. and Shimada, S. (2015). Hydrosilylation Reaction of Olefins: Recent Advances and Perspective. *RSC Adv.*, 5(*26*), pp. 20603–20616.

[78] Chakraborty, R. (2008). Development of Novel Cycloaliphatic Siloxanes for Thermal and UV-Curable Applications University of Akron.

[79] Marciniec, B. (1992). Comprenhensive Handbook on Hydrosilylation. 1-754 p.

[80] Meister, T.K., Riener, K., Gigler, P., Stohrer, J., Herrmann, W.A., and K??hn, F.E. (2016). Platinum Catalysis Revisited-Unraveling Principles of Catalytic Olefin Hydrosilylation. *ACS Catalysis*, 6(*2*), pp. 1274–1284. DOI:10.1021/acscatal.5b02624.

[81] Lewis, B.L.N., Stein, J., Gao, Y., and Colborn, R.E. (1997). Platinum Catalysts Used in the

Silicones Industry. *Platinum Metals Rev.*, 41(*2*), pp. 66–75.

[**82**] Faglioni, F., Blanco, M., Goddard, W.A., and Saunders, D. (2002). Heterogeneous inhibition of homogeneous reactions: Karstedt catalyzed hydrosilylation. *Journal of Physical Chemistry B*, 106(*7*), pp. 1714–1721. DOI:10.1021/jp0128933.

[**83**] Stein, J., Lewis, L.N., Smith, K.A., and Lettko, K.X. (1991). Mechanistic Studies of Platinum-Catalyzed Hydrosilylation. *Journal of Inorganic and Organometallic Polymers*, 1(*3*), pp. 325–334.

[**84**] Stein, J., Lewis, L.N., Gao, Y., and Scott, R.A. (1999). In situ determination of the active catalyst in hydrosilylation reactions using highly reactive Pt(0) catalyst precursors. *Journal of the American Chemical Society*, 121(*15*), pp. 3693–3703. DOI:Doi 10.1021/Ja9825377.

[**85**] Lewis, L.N. and Lewis, N. (1986). Platinum-Catalyzed Hydrosilylation-Colloid Formation as the Essential Step. *Journal of the American Chemical Society*, 108(*9*), pp. 7228–7231. DOI:10.1021/ja00283a016.

[**86**] Parker, S.E. (2015). 1 , 2-Selective Hydrosilylation of Conjugated Dienes Harvard University.

[**87**] Chalk, A.J. and Harrod, J.F. (1965). Homogeneous Catalysis. II. The Mechanism of the Hydrosilation of Olefins Catalyzed by Group VIII Metal Complexes 1. *Journal of the American Chemical Society*, 87(*1*), pp. 16–21.

[**88**] Nyczyk, A., Paluszkiewicz, C., Hasik, M., Cypryk, M., and Pospiech, P. (2012). Cross-linking of Linear Vinylpolysiloxanes by Hydrosilylation - FTIR Spectroscopic Studies. *Vibrational Spectroscopy*, 59, pp. 1–8.

[**89**] Roy, A.K. and Taylor, R.B. (2002). The first alkene-platinum-silyl complexes: Lifting the hydrosilation mechanism shroud with long-lived precatalytic intermediates and true Pt catalysts. *Journal of the American Chemical Society*, 124(*32*), pp. 9510–9524. DOI:10.1021/ja0127335.

[**90**] Kinloch, A.J. (1987). Adhesion and Adhesives. London, UK: Springer Science+ Business Media B.V. 451 p.

[**91**] Kinloch, A.J. (1980). Review. The science of Adhesion. *Journal of Materials Science*, 15, pp. 2141–2166.

[**92**] Zhang, C., Hankett, J., and Chen, Z. (2012). Molecular Level Understanding of Adhesion Mechanisms at the Epoxy/Polymer Interfaces. *Applied Materials & Interfaces*, 4, pp. 3730–3737.

[**93**] Hunter, M.J., Gordon, M.S., Barry, A.J., Hyde, J.F., and Heidenreich, R.D. (1947). Properties of Polyorganosiloxane Surfaces on Glass. *Industrial and Engineering Chemistry*, 39(*11*), pp. 1389–1395.

[**94**] Fox, H.W., Taylor, P.W., and Zisman, W. (1947). Polyorganosiloxanes. Surface Active Properties. *Industrial & Engineering Chemistry*, 39(*11*), pp. 1401–1409.

[**95**] Sato, T., Tanaka, T., and Yoshida, T. (1967). The Adsorption of Poly(dimethylsiloxane) at a Liquid-Solid Interface. *Polymer Letters*, 5, pp. 947–953.

[**96**] Eltekov, Y.A. and Kiselev, A. V. (1977). Adsorption of Macromolecules on the Solid Adsorbents Surfaces. *Journal of Polymer Science Part C-Polymer Symposium*, 437(*61*), pp. 431–437.

[**97**] Eltekov, Y.A. (1967). Adsorption of Polystyrene, Poly(dimethyl Siloxane), and Poly(methyl Methacrylate) from Diluted Solution. *Journal of Polymer Science: Part C,*(*16*), pp. 1931–1936.

[**98**] Berrod, G., Vidal, A., Papirer, E., and Donnet, J.B. (1981). Reinforcement of siloxane elastomers by silica. Chemical interactions between an oligomer of poly(dimethylsiloxane) and a fumed silica. *Journal of Applied Polymer Science*, 26(*3*), pp. 833–845. DOI:10.1002/app.1981.070260309.

[**99**] Cosgrove, T., Prestidge, C.A., King, S.M., and Vincent, B. (1992). Fourier Transform Infrared Spectroscopy and Monte Carlo Studies on the Dynamics of Physisorbing and Chemisorbing Polymers. *Langmuir*, 8(*9*), pp. 2206–2209.

[**100**] Cosgrove, T., Turner, M.J., and Thomas, D.R. (1997). The Adsorption of Polydimethylsiloxane onto Silica from the Melt. *Polymer*, 38(*15*), pp. 3885–3892.

[**101**] Nikitina, E., Khavryutchenko, V., Sheka, E., Barthel, H., and Weis, J. (1999). Intermolecular interactions of polydimethylsiloxane oligomers with hydroxylated and silylated fumed silica. *Composite Interfaces*, 6(*1*), pp. 3–17. DOI:10.1163/156855499X00242.

[**102**] Barthel, H. and Nikitina, E. (2002). INS and IR study of intermolecular interactions at the fumed silica-polydimethylsiloxane interphase. *Silicon Chemistry*, 1, pp. 261–279.

[**103**] Nikitina, E., Khavryutchenko, V., Sheka, E., Barthel, H., and Weis, J. (2008). Intermolecular Interactions of Polydimethylsiloxane Oligomers with Hydroxylated and Silylated Fumed Silica: Quantum Chemical Modeling. *Organosilicon Chemistry I: From Molecules to Materials*,(*December 2014*), pp. 745–762. DOI:10.1002/9783527620777.ch118c.

[**104**] Litvinov, V.M., Barthel, H., and Weis, J. (2002). Structure of a PDMS Layer Grafted onto a Silica Surface Studied by Means of DSC and Solid-State NMR. *Macromolecules*, 35(*11*), pp. 4356–4364. DOI:10.1021/ma0119124.

[**105**] Sheka, E., Natkaniec, I., Khavryutchenko, V., Nikitina, E., Barthel, H., and Weis, J. (2000). INS study of intermolecular interaction at the silicone-fumed silica interface. *Physica B: Condensed Matter*, 276–278, pp. 244–246. DOI:10.1016/S0921-4526(99)01473-8.

[**106**] Li, J., Turunen, M., Niiranen, S., Chen, H., and Paulasto-Kröckel, M. (2012). A reliability study of adhesion mechanism between liquid crystal polymer and silicone adhesive. *Microelectronics Reliability*, 52(*12*), pp. 2962–2969.

[**107**] Roberts, C., Cosgrove, T., Schmidt, R.G., and Gordon, G. V. (2001). Diffusion of Poly(dimethylsiloxane) Mixtures with Silicate Nanoparticles. *Macromolecules*, 34(*3*), pp. 538–543.

[**108**] Klonos, P., Kyritsis, A., and Pissis, P. (2015). Interfacial Dynamics of Polydimethylsiloxane Adsorbed on Fumed Metal Oxide Particles of a Wide Range of Specific Surface Area. *Polymer*, 77, pp. 10–13.

[**109**] Leger, L. and Creton, C. (2008). Adhesion mechanisms at soft polymer interfaces. *Philosophical Transactions of The Royal Society. A*, 366, pp. 1425–1442. DOI:10.1098/rsta.2007.2166.

[**110**] Prause, S., Spange, S., and Barthel, H. (2005). Surface Polarity of Dimethylsiloxane-Grafted Silica Particles. *Macromolecular Chemistry and Physics*, 206, pp. 364–371. DOI:10.1002/macp.200400399.

[**111**] Fadeev, A.Y. and Kazakevich, Y. V. (2002). Covalently Attached Monolayers of Oligo (dimethylsiloxane)s on Silica: A Siloxane Chemistry Approach for Surface Modification. *Langmuir*, 18(*7*), pp. 2665–2672.

[**112**] Kazakevich, Y. V. and Fadeev, A.Y. (2002). Adsorption Characterization of Oligo(dimethylsiloxane)-Modified Silicas: An Example of Highly Hydrophobic Surfaces with Non-Aliphatic Architecture. *Langmuir*, 18(*8*), pp. 3117–3122.

[**113**] Smith, J.S., Borodin, O., Smith, G.D., and Kober, E.M. (2007). A Molecular Dynamics Simulation and Quantum Chemistry Study of Poly(dimethylsiloxane)- Silica Nanoparticle Interactions. *Journal of Polymer Science Part B: Polymer Physics*, 45, pp. 1599–1615. DOI:10.1002/polb.

[**114**] Cosgrove, T., Prestidge, C.A., and Vincent, B. (1990). Chemisorption of Linear and Cyclic Polymethylsiloxanes on Alumina Studied by Fourier-Transform Infrared Spectroscopy. *Journal of Chemical Society. Faraday Transactions*, 86(*9*), pp. 1377–1382.

[**115**] Gupta, S., Ramamurthy, P.C., and Madras, G. (2011). Covalent Grafting of Polydimethylsiloxane over Surface-Modified Alumina Nanoparticles. *Industrial & Engineering Chemistry Research*, 50, pp. 6585–6593.

[**116**] Petrunin, M.A., Nazarov, A.P., and Mikhailovski, Y.N. (1996). Formation Mechanism and Anticorrosive Properties of Thin Siloxane Films on Metal Surfaces. *Journal of Electrochemical Society*, 143(*1*), pp. 251–257.

[**117**] Marinova, K.G., Christova, D., Tcholakova, S., Efremov, E., and Denkov, N.D. (2005). Hydrophobization of Glass Surface by Adsorption of Poly(dimethylsiloxane). *Langmuir*, 21(*19*), pp. 11729–11737.

[**118**] Bennett, D.R., Matisons, J.G., Netting, A.K., Smart, R.S.C., and Swincer, A.G. (1992). Silicones on Glass Surfaces. *Polymer International*, 27(*2*), pp. 147–156.

[**119**] Bhattacharya, S. (2003). Plasma Bonding of Poly(dimethyl) Siloxane and Glass Surfaces and Its Application to Microfluidics Texas Tech University, U.S.A.

[**120**] Botter, W., Soares -Ferreira, R., and Galembeck, F. (1992). Interfacial Reactions and self-Adhesion of Polydimethylsiloxanes. *Journal of Adhesion Science and Technology*, 6(*7*), pp. 791–805. DOI:10.1163/156856192X00449.

[**121**] Theodorakis, M.C., Kutris, A.M.-., and Renitakis, N.K. (1980). A Study on Particulate Formation of Silicone-Coated Glass Surfaces. *International Journal of Pharmaceutics*, 6, pp. 333–337.

[**122**] Vallat, M.F., Nebesarova, I., Schultz, J., and Pouchelon, A. (1998). Energy of Adhesion of Polydimethylsiloxane Networks/Glass and Polycarbonate Assemblies. *Journal of Adhesion Science and Technology*, 12(*4*), pp. 433–443. DOI:10.1163/156856198X00137.

[**123**] Zha, J., Lu, X., and Xin, Z. (2015). Hydrogen Bonding Effect on Wettability of Polysiloxane Coatings. *The Journal of Physical Chemistry C*, 119, pp. 420–425. DOI:10.1021/jp510010d.

[**124**] Tsao, M., Pfeifer, K., Rabolt, J.F., Castner, D.G., and Ringsdorf, H. (1997). Formation and Characterization of Self-Assembled Films of Thiol-Derivatized Poly(dimethylsiloxane) on Gold. *Macromolecules*, 30(*19*), pp. 5913–5919.

[**125**] Elzein, T., Galliano, A., and Bistac, S. (2003). Chains Anisotropy in PDMS Networks Due to Friction on Gold Surfaces. *Journal of Polymer Science Part B: Polymer Physics*, 42, pp. 2348–2353. DOI:10.1002/polb.20054.

[**126**] Choi, G.Y., Kang, J.F., Ulman, A., Zurawsky, W., and Fleischer, C. (1999). Acid-Base Interaction in the Adhesion between Two Solid Surfaces. *Langmuir*, 15(*8*), pp. 8783–8786.

[**127**] Koh, K., Chin, J., Chia, J., and Chiang, C. (2012). Quantitative Studies on PDMS-PDMS Interface Bonding with Piranha Solution and its Swelling Effect. *Micromachines*, 3, pp. 427–441. DOI:10.3390/mi3020427.

[**128**] Oláh, A. and Vancso, G.J. (2005). Characterization of Adhesion at Solid Surfaces: Development of an Adhesion-Testing Device. *European Polymer Journal*, 41, pp. 2803–2823. DOI:10.1016/j.eurpolymj.2005.06.008.

[**129**] Hansal, W.E.G., Hansal, S., Pölzler, M., Kornherr, A., Zifferer, G., and Nauer, G.E. (2006). Investigation of Polysiloxane Coatings as Corrosion Inhibitors of Zinc Surfaces. *Surfaces and Coatings Technology*, 200, pp. 3056–3063. DOI:10.1016/j.surfcoat.2005.01.049.

[**130**] Lee, K.S. and Ram, R.J. (2009). Plastic – PDMS Bonding for High Pressure Hydrolytically Stable Active Microfluidics. *Lab on a Chip*, 9, pp. 1618–1624. DOI:10.1039/b820924c.

[**131**] Petrunin, M. a., Maksaeva, L.B., Yurasova, T. a., Terekhova, E. V., Kotenev, V. a., Kablov, E.N., and Tsivadze, a. Y. (2012). The directional formation and protective effect of self-assembling vinyl siloxane nanolayers on copper surface. *Protection of Metals and Physical Chemistry of Surfaces*, 48(*6*), pp. 656–664.

[**132**] Ismail, A.E., Grest, G.S., Heine, D.R., and Stevens, M.J. (2009). Interfacial Structure and Dynamics of Siloxane Systems: PDMS-Vapor and PDMS-Water. *Macromolecules*, 42(*8*), pp. 3186–3194.

[**133**] Mu, D. and Li, J. (2012). A Study of the Adsorption and Diffusion Behavior of a Single Polydimethylsiloxane Chain on a Silicon Surface by Molecular Dynamics Simulation. In: Wang L, editor. Molecular Dynamics – Theoretical Developments and Applications in Nanotechnology and Energy. Shangai, China: InTech. pp. 327–338.

[**134**] Chae, S.S., Oh, J.Y., Park, J.H., Choi, W.J., Han, J.H., Lee, J., Baik, H.K., and Lee, T. Il. (2015). Strong Hydrophobizer: Laterally Chemisorbed low-molecular-weight polydimethylsiloxane. *Chemical Communications*, 51, pp. 5844–5847.

[**135**] Tsige, M., Soddemann, T., Rempe, S.B., et al. (2003). Interactions and Structure of Poly (dimethylsiloxane) at Silicon Dioxide Surfaces: Electronic Structure and Molecular Dynamics Studies. *The Journal of Chemical Physics*, 118(*11*), pp. 5132–5142. DOI:10.1063/1.1545091.

[**136**] Piwowar, A.M. and Gardella, J.A. (2008). Reflection – Absorption Fourier Transform Infrared Spectroscopic Study of Transferred Films of Poly (dimethylsiloxane) Using the Langmuir – Blodgett Technique. *Macromolecules*, 41(*7*), pp. 2616–2619.

[**137**] Piwowar, A.M. and Gardella, J.A. (2007). Time-of-Flight Secondary Ion Mass Spectrometric Analysis of Polymer Tertiary Structure in Langmuir Monolayer Films of Poly

(dimethylsiloxane). *Analytical Chemistry*, 79(*11*), pp. 4126–4134.

[**138**] Ding, Y., Garland, S., Howland, M., Revzin, A., and Pan, T. (2011). Universal Nanopatternable Interfacial Bonding, pp. 5551–5556. DOI:10.1002/adma.201102827.

[**139**] Iguchi, N., Cady, C., Snoeberger III, R.C., et al. (2008). Characterization of Siloxane Adsorbates Covalently Attached to TiO2. *Physical Chemistry of Interfaces and Nanomaterials Vii*, 7034(*70340C–2*), pp. 1–8. DOI:10.1117/12.798938.

[**140**] Smith, J.S., Borodin, O., and Smith, G.D. (2004). A quantum chemistry based force field for poly(dimethylsiloxane). *Journal of Physical Chemistry B*, 108(*52*), pp. 20340–20350. DOI:10.1021/jp047434r.

[**141**] Shaw, S.J. (2006). Editorial. Silanes. *International Journal of Adhesion & Adhesives*, 26, pp. 2006. DOI:10.1016/j.ijadhadh.2005.03.010.

[**142**] Huser, J., Bistac, S., Brogly, M., Delaite, C., Lasuye, T., and Stasik, B. (2013). Investigation on the Adsorption of Alkoxysilanes on Stainless Steel. *Applied Spectroscopy*, 67(*11*), pp. 1308–1314. DOI:10.1366/13-07073.

[**143**] Ishida, H. (1993). Controlled Interphases in Glass Fiber and Particulate Reinforced Polymers: Structure of Silane Coupling Agents in Solutions and on Substrates. Cleveland, Ohio. U.S.A. 169-199 p.

[**144**] Tesoro, G. and Wu, Y. (1991). Silane Coupling Agents: the Role of the Organofunctional Group. *Journal of Adhesion Science and Technology*, 5(*10*), pp. 771–784. DOI:10.1163/156856191X00206.

[**145**] Plueddemann, E.P. (1970). Adhesion Through Silane Coupling Agents. *Journal Of Adhesion*, 2(*3*), pp. 184–201. DOI:10.1080/0021846708544592.

[**146**] Johansson, U., Holmgren, A., Forsling, W., and Frost, R.L. (1999). Adsorption of Silane Coupling Agents onto Kaolinite Surfaces. *Clay Minerals*, 34, pp. 239–246.

[**147**] Pantoja, M., Díaz-Benito, B., Velasco, F., Abenojar, J., and del Real, J.C. (2009). Analysis of Hydrolysis Process of γ-Methacryloxypropyltrimethoxysilane and its Influence on the Formation of Silane Coatings on 6063 Aluminum Alloy. *Applied Surface Science*, 255, pp. 6386–6390. DOI:10.1016/j.apsusc.2009.02.022.

[**148**] Altmann, S. and Pfeiffer, J. (2003). The Hydrolysis/Condensation Behaviour of Methacryloyloxyalkylfunctional Alkoxysilanes: Structure-Reactivity Relations. *Monatshefte für Chemie*, 134, pp. 1081–1092. DOI:10.1007/s00706-003-0615-y.

[**149**] Brochier Salon, M., Bayle, P.-A., Abdelmouleh, M., Boufi, S., and Belgacem, M.N. (2008). Kinetics of Hydrolysis and Self Condensation Reactions of Silanes by NMR Spectroscopy. *Colloids and Surfaces A : Physicochemical and Engineering Aspects*, 312, pp. 83–91. DOI:10.1016/j.colsurfa.2007.06.028.

[**150**] Brochier Salon, M. and Belgacem, M.N. (2011). Hydrolysis-Condensation Kinetics of Different Silane Coupling Agents. *Phosphorus, Sulfur, and Silicon and the Related Elements*, 186(*2*), pp. 240–254. DOI:10.1080/10426507.2010.494644.

[**151**] Osterholtz, F.D. and Pohl, E.R. (1992). Kinetics of the Hydrolysis and Condensation of Organofunctional Alkoxysilanes: A Review. *Journal of Adhesion Science and Technology*, 6(*1*), pp. 127–129. DOI:10.1163/156856192X00106.

[**152**] Macan, J. and Ivankovi, H. (2006). Influence of Hydrolysis Conditions on Curing and Properties of an Epoxy-Silane based Hybrid Material. 11. Conference on Materials, Processes, Friction and Wear MATRIB'06. Vela Luka: MATRIB. pp. 99–104.

[**153**] Parker, A.A. (2002). The Effect of Silane Hydrolysis on Aluminum Oxide Dispersion Stability in Ceramics Processing. *Journal of Adhesion Science and Technology*, 16(*6*), pp. 679–701. DOI:10.1163/156856102760099889.

[**154**] Underhill, P.R., Goring, G., and DuQuesnay, D.L. (1998). A Study of the Deposition of 3-Glycidoxypropyltrimethoxysilane on Aluminum. *International Journal of Adhesion and Adhesives*, 18(*5*), pp. 307–311. DOI:10.1016/S0143-7496(97)00045-6.

[**155**] Underhill, P.R., Goring, G., and Duquesnay, D.L. (2000). Effect of Humidity on the Curing of 3-Glycidoxypropyltrimethoxy Silane. *International Journal of Adhesion and Adhesives*, 20, pp.

195–199. DOI:10.1016/S0143-7496(99)00041-X.

[**156**] Underhill, P.R., Goring, G., and DuQuesnay, D.L. (1998). A Study of the Curing of 3-Glycidoxypropyltrimethoxy Silane Films on Aluminum. *International Journal of Adhesion and Adhesives*, 18(*5*), pp. 313–317. DOI:10.1016/S0143-7496(97)00046-8.

[**157**] Bascom, W.D. (1972). Structure of Silane Adhesion Promoter Films on Glass and Metal Surfaces. *Macromolecules*, 5(*6*), pp. 792–798.

[**158**] Franquet, a., Van Schaftinghen, T., De Graeve, I., Laha, P., Le Pen, C., Terryn, H., and Vereecken, J. (2004). Silane Coating of Metal Substrates, pp. 1–4.

[**159**] Franquet, a., Terryn, H., Bertrand, P., and Vereecken, J. (2002). Use of optical methods to characterize thin silane films coated on aluminium. *Surface and Interface Analysis*, 34, pp. 25–29. DOI:10.1002/sia.1245.

[**160**] Li, Y., Vecchio, N.E., Wang, Y., and Mcnutt, C. (2007). Vibrational Spectra of Metals Treated with Allyltrimethoxysilane Sol-Gel and Self-Assembled Monolayer of Allytrichlorosilane. *Spectrochimica Acta - Part A: Molecular and Biomolecular Spectroscopy*, 67, pp. 598–603. DOI:10.1016/j.saa.2006.07.043.

[**161**] Boeiro, F.J. (1981). Structure and Properties of Polymers and Organosilanes Adsorbed onto Oxidized Aluminum and Titanium. Cincinnati, Ohio. U.S.A. 1-36 p.

[**162**] Jenkins, M.L., Dauskardt, R.H., and Bravman, J.C. (2004). Important Factors for Silane Adhesion Promoter Efficacy: Surface Coverage, Functionality and Chain Length. *Journal of Adhesion Science and Technology*, 18(*13*), pp. 1497–1516.

[**163**] Najari, A., Lang, P., Lacaze, P.C., and Mauer, D. (2012). Adsorption of g-Mercaptopropyltrimethoxysilane on Zinc: A Study of the Competition between Thiol and Silanol Functions Related to the Age of the Siloxane Solution, its pH and the Oxidation State of the Surface. *Surface Science*, 606(*3–4*), pp. 137–145.

[**164**] Gelest. (2006). Silane Coupling Agents: Connecting Across Boundaries. *Gelest*, pp. 1–9.

[**165**] Maxwell, R.S., Lewicki, J.P., Mayer, B.P., Maiti, A., and Harley, S.J. (2013). The Development and Application of NMR Methodologies for the Study of Degradation in Complex Silicones. Livermore, CA.- U.S.A. 1-62 p.

[**166**] Smith, B.C. (1998). Infrared Spectral Interpretation. A systematic Approach. U.S.A: CRC Press LLC. 1-288 p.

[**167**] Stuart, B. (n.d.). Infrared Spectroscopy: Fundamentals and Applications. Wiley.

[**168**] Escobar Barrios, V., Rangel Méndez, J.R., Pérez Aguilar, N. V., Andrade Espinosa, G., and Dávila Rodríguez, J.L. (2012). FTIR – An Essential Characterization Technique for Polymeric Materials. *Infrared Spectroscopy - Materials Science, Engineering and Technology*, pp. 195–212.

[**169**] Chew, M.Y., Zhou, X., and Tay, Y.M. (2000). Application of ATR in Characterizing Aging Conditions of Polyurethane Sealants. *Polymer Testing*, 20, pp. 87–92. DOI:10.1016/S0142-9418(00)00005-2.

[**170**] Possart, W. (2012). Dünne Organische Schichten - Herstellung und Charakterisierung, pp. 1–257.

[**171**] Ekgasit, S. (2000). ATR spectral intensity: what is the upper limit of weak absorption? *Applied Spectroscopy*, 54, pp. 756–758. DOI:10.1366/0003702001950058.

[**172**] Mirabella, F.M. (1998). Attenuated Total Reflection Spectroscopy. In: Mirabella FM, editor. Modern Techniques in Applied Molecular Spectroscopy. Techniques in Analytical Chemistry Series. John Wiley & Sons, Inc. pp. 127–185.

[**173**] Smith, L. and McHard, J.A. (1959). Spectroscopic Techniques for Identification of Organosilicon Compounds. *Analytical Chemistry*, 31(*7*), pp. 1174–1179.

[**174**] Carey, F.A. (2000). Organic Chemistry. Fourth Edi. U.S.A: Mc Graw Hill. 1275 p.

[**175**] Harris, R.K. and Kimber, B.J. (1975). 29Si NMR as a Tool for Studying Silicones. *Applied Spectroscopy Reviews*, 10(*1*), pp. 117–137.

[**176**] Dixon, A.M. and Larive, C.K. (1999). NMR Spectroscopy with Spectral Editing for the Analysis of Complex Mixtures. *Applied Spectroscopy*, 53(*11*), pp. 426A–440A.

[**177**] Birkenfeld, A.B., Bertermann, R., Eckert, H., and Pfleiderer, B. (2003). Liquid- and Solid-State High-Resolution NMR Methods for the Investigation of Aging Processes of Silicone Breast

Implants. *Biomaterials*, 24, pp. 35–46.

[**178**] Kuzmany, H. (2009). Solid-State Spectroscopy. Second Edi. Wien, Austria: Springer-Verlag Berlin Heidelberg. 550 p.

[**179**] Chary, K.V.R. and Govil, G. (2008). NMR in Biological Systems. From Molecules to Humans. Kaptein R, editor Dordrecht - Netherlands: Springer Science+ Business Media B.V. 550 p.

[**180**] Blümich, B. (2005). Essential NMR. Aachen, Germany: Springer-Verlag Berlin Heidelberg. 246 p.

[**181**] Slichter, C.P. (1990). Principles of Magnetic Resonance. Third Edit. New York, USA: Springer-Verlag Berlin Heidelberg. 662 p.

[**182**] Günther, H. (2013). NMR Spectroscopy. Basic Principles, Concepts and Applications in Chemistry. Third Edit. Weinheim, Germany: Wiley-VCH Verlag GmbH &Co. KGaA. 1-736 p.

[**183**] Ionin, B.I. and Ershov, B.A. (1970). NMR Spectroscopy in Organic Chemistry. New York, USA: Plenum Press. 1-395 p.

[**184**] Claridge, T.D.W. (2009). High-Resolution NMR Techniques in Organic Chemistry. Second Edi. Bäckvall JE, Baldwin JE, Williams RM, editors Amsterdam, The Netherlands: Elsevier Ltd. 1-399 p.

[**185**] Delak, K.M., Farrar, T.C., and Sahai, N. (2005). 29Si NMR Sensitivity Enhancement Methods for the Quantitative Study of Organosilicate Hydrolysis and Condensation. *Journal of Non-Crystalline Solids*, 351, pp. 2244–2250. DOI:10.1016/j.jnoncrysol.2005.05.013.

[**186**] Schulze-Sünninghausen, D., Becker, J., and Luy, B. (2014). Rapid Heteronuclear Single Quantum Correlation NMR Spectra at Natural Abundance. *Journal of the American Chemical Society*, 136, pp. 1242–1245. DOI:10.1021/ja411588d.

[**187**] Mckenzie, J.S., Charlton, A.J., and Wilson, J.C. (2010). Peak fitting in 2D 1 H–13 C HSQC NMR Spectra for Metabolomic Studies. *Metabolomics*, 6, pp. 574–582. DOI:10.1007/s11306-010-0226-7.

[**188**] Lenick, A.J.O. (1999). Basic Silicone Chemistry - A Review. *Silicone Spectator*, pp. 1–23.

[**189**] Socrates. (2004). Infrared and Raman Characteristic Group Frequencies Contents. Third Ed. New York, U.S.A.: John Wiley & Sons, Inc. 1-347 p.

[**190**] Launer, P.J. (1987). Infrared Analysis Of Organosilicon Compounds: Spectra-Structure Correlations. *Silicone Compounds Register and Review*, pp. 100–103.

[**191**] Smith, L.A. (1960). Infrared Spectra-Structure Correlations for Organosilicon Compounds. *Spectrochimica Acta*, 16, pp. 87–105.

[**192**] Smith, A.L. and Angelotti, N.C. (1959). Correlation of the SiH stretching frequency with molecular structure. *Spectrochimica Acta*, pp. 412–420.

[**193**] Richards, R.E. and Thompson, H.W. (1949). Infrared Spectra of Compound of High Molecular WEight. Part IV. Silicones and Related Compounds, pp. 124–132.

[**194**] Cai, D., Neyer, A., Kuckuk, R., and Heise, H.M. (2010). Raman, Mid-Infrared, Near-Infrared and Ultraviolet-Visible Spectroscopy of PDMS Silicone Rubber for Characterization of Polymer Optical Waveguide Materials. *Journal of Molecular Structure*, 976, pp. 274–281.

[**195**] Lipp, E.D. (1991). Measurement of Trace Silanol in Siloxanes by IR Spectroscopy. *Applied Spectroscopy*, 45(*3*), pp. 477–483.

[**196**] Cypryk, M. (1997). Ab Initio Study of the Basicity and Propensity of Siloxanols Towards Hydrogen Bond Formation. *Journal of Organometallic Chemistry*, 545–546(*97*), pp. 483–493.

[**197**] Aragão, B.J.G. and Messaddeq, Y. (2008). Peak Separation by Derivative Spectroscopy Applied to FTIR Analysis of Hydrolized Silica. *Journal Brazilian Chemical Society*, 19(*8*), pp. 1582–1594.

[**198**] Vučković, M. V. and Govedarica, M.N. (2006). Determination of Silanol End Groups in Polysiloxanes Obtained from Dimethyldichlorosilane Hydrolysate (DDSH). *Journal of the Serbian Chemical Society*, 71(*3*), pp. 257–261. DOI:10.2298/JSC0603257D.

[**199**] Al-Oweini, R. and El-Rassy, H. (2009). Synthesis and Characterization by FTIR Spectroscopy of Silica Aerogels Prepared Using Several Si(OR)4 and R''Si(OR')3 Precursos. *Journal of Molecular Structure*, 919(*1–3*), pp. 140–145.

[**200**] Oostendorp, D.J., Bertrand, G.L., and Stoffer, J.O. (1992). Kinetics and Mechanism of the

Hydrolysis and Alcoholysis of Alkoxysilanes. *Journal of Adhesion Science and Technology*, 6(*1*), pp. 171–191. DOI:10.1163/156856192X00124.

[**201**] Hamilton, R. (n.d.). Hydrolysis of Silicone Polymers in Aqueous Systems University of Ontario.

[**202**] Esteves, a. C.C., Brokken-Zijp, J., Lavèn, J., Huinink, H.P., Reuvers, N.J.W., Van, M.P., and de With, G. (2010). Garnet particles effect on the cross-linking of PDMS and the network structures formed. *Polymer*, 51, pp. 136–145. DOI:10.1016/j.polymer.2009.11.021.

[**203**] Loch, C.L., Ahn, D., and Chen, Z. (2006). Sum Frequency Generation Vibrational Spectroscopic Studies on a Silane Adhesion-Promoting Mixture at a Polymer Interface. *Journal of Physical Chemistry. B*, 110(*2*), pp. 914–918.

[**204**] Deshpande, G. and Rezac, M.E. (2001). The effect of Phenyl Content on the Degradation of Poly(dimethyl diphenyl) Siloxane Copolymers. *Polymer Degradation and Stability*, 74, pp. 363–370. DOI:10.1016/S0141-3910(01)00186-0.

[**205**] Deshpande, G. and Rezac, M.E. (2002). Kinetic Aspects of the Thermal Degradation of Poly(dimethyl siloxane) and Poly(dimethyl diphenyl siloxane). *Polymer Degradation and Stability*, 76, pp. 17–24. DOI:10.1016/S0141-3910(01)00261-0.

[**206**] Pape, P.G. and Plueddemann, E.P. (1991). Methods for Improving the Performance of Silane Coupling Agents. *Journal of Adhesion Science and Technology*, 5(*10*), pp. 831–842. DOI:10.1163/156856191X00242.

[**207**] Villegas, J.A., Olayo, R., and Cervantes, J. (2003). Effect of Side Groups on the Conformation of a Series of Polysiloxanes in Solution. *Journal of Inorganic and Organometallic Polymers*, 13(*4*), pp. 205–222.

[**208**] Balazs, B. and Maxwell, R.S. (2002). Thermal and Chemical Analyses of Silicone Polymers for Component Engineering Lifetime Assessments. 3rd Heat Flow Clorimetry Symposium. French Lick, IN. - U.S.A. pp. 1–8.

[**209**] Cassidy, P.E. and Yager, B.J. (1975). Coupling Agents as Adhesion Promoters. *Journal of Macromolecular Science, Part D - Reviews in Polymer Processing*, 1(*1*), pp. 1–49. DOI:10.1080/03602557108545009.

[**210**] Jandke, M. and Brennenstuhl, W. (2010). Pt-Catalyzed, Addition-Crosslinking Silicone Compositions Self-Adhesive at Room Temperature. (*US 2010/0256300 A1*), pp. 1–8. DOI:US 20100322867A1.

[**211**] Karlsson, A. (2003). New Analytical Methods For Silicone Elastomers Used in Drug Delivery Systems Royal Insitute of Technology. Stockholm, Sweden.

[**212**] Pop, C. (2006). Herstellung von monodispersen Polydimethylsiloxan-Netzwerken und Charakterisierung der Mikrostruktur und der Permeationseigenschaften Bayerischen Julius-Maximilians-Universität Würzburg, Germany.

[**213**] Wong, C.P. (1990). Electrical performance and reaction kinetics of silicone gels. *Journal of Materials Research*, 5(*4*), pp. 795–800. DOI:10.1557/JMR.1990.0795.

[**214**] Jackson, K.D.O. (1997). A Guide to Identifying Common Inorganic Fillers. *Journal of Natural Rubber Research*, 12(*1*), pp. 102–111.

[**215**] Leadley, S., O'Hare, L.A., and McMillan, C. (2012). Surface Analysis of Silicones. In: Owen MJ, Dvornic PR, editors. Silicone Surface Science. Midland, USA: Springer Science+Business Media. pp. 319–334.

[**216**] Wright, N. and Hunter, M.J. (1947). Organosilicon Polymers. III. Infrared Spectra of Methylpolysiloxanes. *Journal American Chemical Society*, 69, pp. 803–809.

[**217**] Fulmer, G.R., Miller, A.J.M., Sherden, N.H., Gottlieb, H.E., Nudelman, A., Stoltz, B.M., Bercaw, J.E., and Goldberg, K.I. (2010). NMR Chemical Shifts of Trace Impurities: Common Laboratory Solvents, Organics , and Gases in Deuterated Solvents Relevant to the Organometallic Chemist. *Organometallics*, 29, pp. 2176–2179. DOI:10.1021/om100106e.

[**218**] Nishiyama, N. and Horie, K. (1987). Hydrolysis and Condensation Mechanisms of a Silane Coupling Agent Studied by 13C and 29N M R. *Journal of Applied Polymer Science*, 34, pp. 1619–1630.

[**219**] Duplock, S.K., Matisons, J.G., Swincer, A.G., and Warren, R.F.O. (1991). Synthesis of Siloxanes

Containing Reactive Side Chains. *Journal of Inorganic Organometallic Polymers*, 1(*3*), pp. 361–375.

[**220**] Britcher, L.G., Kehoe, D.C., Matisons, J.G., and Swincer, A.G. (1995). Siloxane Coupling Agents. *Macromolecules*, 28(*9*), pp. 3110–3118.

[**221**] Findeisen, M. and Roth, H. (1992). 1H and 13C High Resolution NMR Analysis of a Siloxane Polymer with Phenyl Benzoate Side-Chains. *Magnetic Resonance in Chemistry*, 30(*1*), pp. 87–88. DOI:10.1002/mrc.1260300118.

[**222**] Birkefeld, A.B., Bertermann, R., Eckert, H., and Pfleiderer, B. (2003). Liquid- and Solid-State High-Resolution NMR Methods for the Investigation of Aging Processes of Silicone Breast Implants. *Biomaterials*, 24, pp. 35–46. DOI:10.1016/S0142-9612(02)00241-7.

[**223**] Bovey, F.A. and Mirau, P.A. (1996). NMR of Polymers. San Diego, U.S.A.: Academic Press. 1-459 p.

[**224**] Delmulle, L. and van der Kelen, G.P. (1980). NMR Study (1H, 13C AND 29Si) of the Methylallylsilanes. *Jounral of Molecular Structure*, 66, pp. 315–318.

[**225**] Engelhardt, G., Jancke, H., Mägi, M., Pehk, T., and Lippmaa, E. (1971). Über die 1H-, 13C- und 29Si-NMR Chemischen Verschiebungen einiger Linearer, Verzweigter und Cyclischer Methyl-Siloxan-Verbindungen. *Journal of Organometallic Chemistry*, 28, pp. 293–300.

[**226**] Engelhardt, G. (1968). 1H-NMR-Spektroskopische Untersuchungen zum Substituenten- und Kettenlängeneinfluss auf die SiOSi-Bindungsstruktur in a,w-Disubstituierten Polydimethylsiloxanen. *Journal of Organometallic Chemistry*, 11, pp. 243–252.

[**227**] Tomlins, P.J., Woodcock, M.G.L., Spencer, N., and Kirkby, G.R. (2007). Nuclear Magnetic Resonance Analysis of Emulsified Silicone Oil RMN-3 (Oxane HD). *Br Journal Ophthalmolo*, 91, pp. 1379–1380. DOI:10.1136/bjo.2006.110346.

[**228**] Schraml, J., Chvalovsky, V., Mägi, M., and Lippmaa, E. (1977). 29Si and 13C-NMR Spectra of Vinyl- and Allylsilanes. *Collection Czechslovak Chemical Communications*, 42, pp. 306–317.

[**229**] Hampton, J.F., Lacefield, C.W., and Hyde, J. (1965). Identification of Organosilanols by Nuclear Magnetic Resonance Spectroscopy. *Inorganic Chemistry*, 4(*11*), pp. 1659–1670.

[**230**] Alam, T.M. (2002). Quantitative Analysis of Microstructure in Polysiloxanes Using High Resolution Si NMR Spectroscopy : Investigation of Lot Variability in the LVM97 and HVM97 PDMS / PDPS Copolymers. Livermore, CA.- U.S.A. 1-22 p.

[**231**] Schraml, J., Nguyen, D.-C., Chvalovsky, V., Mägi, M., and Lippmaa, E. (1975). NMR Study of Organosilicon Compounds. III. Silixon-29, Nitrogen-14, Carbon-13 and Proton NMr Spectra of Silylalkylamines. *Organic Magnetic Resonance*, 7, pp. 379–385.

[**232**] Gualandris, V., Babonneau, F., Janicke, M.T., and Chmelka, B.F. (1998). NMR Studies on Hydrolysis and Condensation Reactions of Alkoxysilanes Containing Si-H Bonds. *Journal of Sol-Gel Science and Technology*, 12, pp. 75–80.

[**233**] Ebsworth, E. a. V. and Turner, J.J. (1962). Nuclear Magnetic Resonance Spectra of Silicon Hydrides and Derivatives. I. Coupling Constants Involving Hydrogen. *The Journal of Chemical Physics*, 36(*10*), pp. 2628–2634.

[**234**] Ebsworth, E.A. V. and Turner, J.J. (1963). N.M.R. Spectra of Silicon Hydride Derivatives: II. Chemical Shifts in Some Simple Derivatives. *Journal of Physical Chemistry*, 67, pp. 805–807.

[**235**] Ebsworth, E.A. V. and Turner, J.J. (1963). The N.M.R. Spectra of Silicon Hydrides and Derivatives. Part 4. -Disilane and Trisilane. *Transactions Faraday Society*, 59, pp. 256–263.

[**236**] Yactine, B., Boutevin, B., and Ganachaud, F. (2009). Do-it-yourself functionalized silicones part 1: Basic methods for characterization of commercial products. *Polymers for Advanced Technologies*, 20(*1*), pp. 66–75. DOI:10.1002/pat.1281.

[**237**] Gudat, D. (2013). NMR Characterization of Silicone Samples. Stuttgart, Germany. 1-9 p.

[**238**] Naghash, H.J., Mohammadidehcheshmeh, I., and Mehrnia, M. (2012). Synthesis and Characterization of a Novel Hydroxy Terminated Polydimethylsiloxane and its Application in the Waterborne Polysiloxane-Urethane Dispersion for Potential Marine Coatings. *Polymer Advanced Technologies*, 24, pp. 307–317. DOI:10.1002/pat.3084.

[**239**] Plett, K.L. (2008). Development and Characterization of Polysiloxane Polymer Films for Use in

Optical Sensor Technology Queen's University. Canada.

[**240**] Huang, J., Jiang, Y., Du, X., and Bi, J. (2010). A New Siloxane Polymer for Chemical Vapor Sensor. *Sensors and Actuators, B: Chemical*, 146(*1*), pp. 388–394.

[**241**] Brus, J. and Dybal, J. (2002). Hydrogen-Bond Interactions in Organically-Modified Polysiloxane Networks Studied by 1D and 2D CRAMPS and Double-Quantum 1H MAS NMR. *Macromolecules*, 35(*27*), pp. 10038–10047.

[**242**] Buyl, F. De. and Kretschmer, A. (2008). Understanding Hydrolysis and Condensation Kinetics of γ-Glycidoxypropyltrimethoxysilane. *The Journal of Adhesion*, 84(*2*), pp. 125–142.

[**243**] Jancke, H. (1992). Analysis of silicone resins by methods of 29Si NMR spectroscopy. *Fresenius' Journal of Analytical Chemistry*, 342, pp. 846–849. DOI:10.1007/BF00322146.

[**244**] Pereira, A.G.B., Muniz, E.C., and Hsieh, Y. (2015). 1H NMR and 1H-13C HSQC Surface Characterization of Chitosan-Chitin Sheath-Core Nanowhiskers. *Carbohydrate Polymers*, 123, pp. 46–52.

[**245**] Frydman, L., Lupulescu, A., and Scherf, T. (2003). Principles and Features of Single-Scan Two-Dimensional NMR Spectroscopy. *Journal of the American Chemical Society*, 125, pp. 9204–9217.

[**246**] Paudel, L., Adams, R.W., Kiryly, P., et al. (2013). Simultaneously Enhancing Spectral Resolution and Sensitivity in Heteronuclear Correlation NMR Spectroscopy. *Angewandte Chemie. International Edition*, 52, pp. 11616–11619. DOI:10.1002/anie.201305709.

[**247**] Kupce, E. and Wrackmeyer, B. (2010). Multiple Receiver Experiments for NMR Spectroscopy of Organosilicon Compounds. *Applied Organometallic Chemistry*, 24, pp. 837–841. DOI:10.1002/aoc.1692.

[**248**] Geyer, A. (2005). NMR-Spektroskopie : Struktur und Dynamik organischer Moleküle. Marburg, Germany. 1-39 p.

[**249**] Torry, S.A., Campbell, A., Cunliffe, A. V., and Tod, D.A. (2006). Kinetic Analysis of Organosilane Hydrolysis and Condensation. *International Journal of Adhesion & Adhesives*, 26, pp. 40–49. DOI:10.1016/j.ijadhadh.2005.03.008.

[**250**] Hoebbel, D., Nacken, M., and Schmidt, H. (n.d.). A NMR Study on the Hydrolysis , Condensation and Epoxide Ring-Opening Reaction in Sols and Gels of the System Glycidoxypropyltrimethoxysilane-Water-Titaniumtetraethoxide pp. 169–179.

[**251**] Connell, L.S., Romer, F., Valliant, E.M., Zhang, Z., Peter, D., Smith, M.E., Hanna, J. V., and Jones, J.R. (2013). Electronic supplementary information for : Chemical characterisation and fabrication of Chitosan-Silica hybrid scaffolds with 3-glycidoxypropyl trimethoxysilane, pp. 53–56.

[**252**] Maxwell, R.S., Lewicki, J.P., Mayer, B.P., Maiti, A., and Harley, S.J. (2013). The Development and Application of NMR Methodologies for the Study of Degradation in Complex Silicones. Concise Encyclopedia of High Performance Silicones.

[**253**] Harris, R.K., Kimber, B.J., Wood, M.D., and Holt, A. (1976). 29Si NMR Studies of Oligo-and Poly-meric Siloxanes. III. Cyclic Siloxanes of General Formula [MeRSiO]n. *Journal of Organometallic Chemistry*, 116, pp. 291–298.

[**254**] Uhlig, F. and Marsmann, H.C. (2000). 29Si NMR Some Practical Aspects. *Gelest, Inc.*, 2, pp. 208–222.

[**255**] Yactine, B., Ratsimihety, A., and Ganachaud, F. (2010). Do-it-yourself Functionalized Silicones Part 2: Synthesis by Ring Opening Polymerization of Commercial Cyclosiloxanes. *Polymers Advanced Technologies*, 21, pp. 139–149. DOI:10.1002/pat.1509.

[**256**] Engelhardt, G., Mägi, M., and Lippmaa, E. (1973). 29Si-NMR-Spektroskopische Untersuchungen an Methyl- und Methyl-Phenyl-Siloxanen und Ihre Anwendung in der Silikonanalytik. *Journal of Organometallic Chemistry*, 54, pp. 115–122.

[**257**] Schraml, J. and Bellama, J.M. (1976). 29Si Nuclear Magnetic. In: Nachod FC, Zuckerman JJ, Randall EW, editors. Determination of Organic Structures by Physical Methods. New York and London: Academic Press, Inc. pp. 203–269.

[**258**] Kintzinger, J.-P. and Marsmann, H. (1981). Vol. 17. Oxygen-17 and Silicon-29. In: Diehl P, Fluck E, Kosfeld R, editors. NMR Basic Principles and Progress. Springer-Verlag Berlin

Heidelberg. pp. 31–49. DOI:10.1007/978-3-642-87762-9.

[**259**] Tsantes, G., Auner, N., Müller, T., Chemie, A., Wolfgang, J., and Frankfurt, G. (2008). Chapter 56. Si NMR Chemical Shifts of Siloxanes: Ab Initio and Density Functional Study. In: Auner N, Weis J, editors. Organosilocon Chemistry Set: From Molecules to Materials. Weinheim, Germany: Wiley-VCH Verlag GmbH &Co. KGaA. pp. 334–338. DOI:10.1002/9783527620777.ch56d.

[**260**] Hoebbel, D., Reinert, T., and Schmidt, H. (1996). 29Si NMR Investigation of Condensation Reactions of Diphenylsilanediol in Presence of Ti-, Zr-, Al-, Sn- and Si-Alkoxides. *Journal of Sol-Gel Science and Technology*, 7, pp. 217–224.

[**261**] Remarks, G. and Si, M. (2008). Chemical Shifts and Coupling Constants for Silicon-29. 45278 p.

[**262**] Blechta, V., Sykora, J., Hetflejs, J., Sabata, S., and Schraml, J. (2006). 29Si NMR in LC–NMR analysis of silicones. *Magnetic Resonance in Chemistry*, 44, pp. 7–10. DOI:10.1002/mrc.1715.

[**263**] Gray, G.W., Hawthorne, W.D., Lacey, D., White, M.S., and Semlyen, J.A. (1989). 29Si N.M.R. investigations of polysiloxanes. *Liquid Crystals*, 6(*5*), pp. 503–513.

[**264**] Sperling, L.H. (2006). Introduction to Physical Polymer Science. Fourth Edi. U.S.A: John Wiley & Sons, Inc. 845 p.

[**265**] Determann, H. (1969). Gel Chromatography Gel Filtration · Gel Permeation · Molecular Sieves. 204 p.

[**266**] Berek, D. (2010). Size Exclusion Chromatography – A Blessingand a Curse of Science and Technology of Synthetic Polymers. *Journal of Separation Science*, 33, pp. 315–335. DOI:10.1002/jssc.200900709.

[**267**] García-Lopera, R., Codoñer, A., Bañó, M.C., Abad, C., and Campos, A. (2005). Size-Exclusion Chromatographic Determination of Polymer Molar Mass Averages Using a Fractal Calibration. *Journal of Chromatographic Science*, 43.

[**268**] Hunt, B.J. and Holding, S.R. (1989). Size Exclusion Chromatography. Second Edi. Hunt BJ, Holding SR, editors Springer Science+ Business Media B.V. 1-292 p. DOI:10.1007/978-1-4615-7861-1.

[**269**] Rodriguez, F., Kulakowski, R.A., and Clark, O.K. (1966). Characterization of Silicones by Gel Permeation Chromatography. *I&EC Product Research and Development*, 5(*2*), pp. 121–125.

[**270**] Kendrick, T.C. (1969). Gel-Permeation Chromatography of Polydimethylsiloxanes. *Journal of Polymer Science: Part A-2*, 7, pp. 297–307.

[**271**] Saunders, G. and MacCreath, B. (2011). Analysis of Elastomers by GPC/SEC. Application Compendium. UK. 1-16 p.

[**272**] Saunders, G. and Maccreath, B. (n.d.). Polysiloxane Analysis on Agilent PLgel 5 µm MIXED-D using Gel.

[**273**] Shah, G.B. (2008). Characterisation of Silicone Prepolymers and Disparity in Results. *eXPRESS Polymer Letters*, 2(*11*), pp. 829–834. DOI:10.3144/expresspolymlett.2008.96.

[**274**] Gores, F. (2012). GPC-Analyse von 6 Probe-Mustern zur Bestimmung der mittleren Molmasse und der Molmassenverteilung. Mainz, Germany. 1-12 p.

[**275**] Cai, G. and Weber, W.P. (2002). Synthesis and Chemical Modification of Poly(divinylsiloxane). *Polymer*, 43, pp. 1753–1759.

[**276**] AG, W.C. (2008). Silicones in Automotive Engineering. Always a step Ahead, pp. 1–18. Accessed 4 March 2012.

[**277**] Vallés, E., Sarmoria, C., Villar, M., Lazzari, M., and Chiantore, O. (2000). Model Polydimethylsiloxanes Subjected to Thermal Weathering: Effect on Molecular Weight Distributions. *Polymer Degradation and Stability*, 69, pp. 67–71. DOI:10.1016/S0141-3910(00)00041-0.

[**278**] Lavery, M. (2002). Sealants in the automotive industry. *International Journal of Adhesion and Adhesives*, 22(*July*), pp. 443–445. DOI:10.1016/S0143-7496(02)00026-X.

[**279**] Menczel, J.D., Judovits, L., Prime, R.B., Bair, H.E., Reading, M., and Swier, S. (2009). Thermal Analysis of Polymers. Fundamentals and Applications. Menczel JD, Primer RB, editors U.S.A.: John Wiley & Sons, Inc. 1-688 p.

[**280**] Hoyt-Lalli, J.K. (2002). Synthesis of Functionalized Polysiloxanes and Investigation of Highly Filled Thermally Conductive Microcomposites Virginia Polytechnic Institute and State University.

[**281**] Jovanovic, J.D., Govedarica, M.N., Dvornic, P.R., and Popovic, I.G. (1998). The Thermogravimetric Analysis of Some Polysiloxanes. *Polymer Degradation and Stability*, 61, pp. 87–93. DOI:10.1016/S0141-3910(97)00135-3.

[**282**] Cai, G. and Weber, W.P. (2004). Synthesis of terminal Si-H irregular tetra-branched star polysiloxanes. Pt-catalyzed hydrosilylation with unsaturated epoxides. Polysiloxane films by photo-acid catalyzed crosslinking. *Polymer*, 45, pp. 2941–2948. DOI:10.1016/j.polymer.2004.02.057.

[**283**] Chen, D., Yi, S., Fang, P., Zhong, Y., Huang, C., and Wu, X. (2010). Synthesis and characterization of novel room temperature vulcanized (RTV) silicone rubbers using Vinyl-POSS derivatives as cross linking agents. *Polymer*, 51, pp. 3867–3878.

[**284**] Zhang, Y., Li, Y., Zheng, J., Guo, H., Guan, X., Lu, M., Wu, K., and Liang, L. (2015). Synthesis and Characterization of Vinyl-Polyhedral Oligomeric Silsesquioxanes-Reinforced Silicone Resin with Three-Dimensional Cross-Linking Structure. *Journal of Applied Polymer Science*,(*42187*), pp. 1–8. DOI:10.1002/app.42187.

[**285**] Bowens, A.D. (1999). Synthesis and Characterization of Poly(Siloxane Imide) Block Copolymers and End-Functional Polyimides for Interphase Applications Virginia Polytechnic Institute and State University.

[**286**] Camino, C., Lomakin, S.M., and Lazzari, M. (2001). Polydimethylsiloxane Thermal Degradation Part 1. Kinetic Aspects. *Polymer*, 42, pp. 2395–2402. DOI:10.1016/S0032-3861(00)00652-2.

[**287**] Chen, D., Nie, J., Yi, S., Wu, W., Zhong, Y., Liao, J., and Huang, C. (2010). Thermal Behaviour and Mechanical Properties of Novel RTV Silicone Rubbers Using Divinyl-hexa[(trimethoxysilyl)ethyl]-POSS as Cross-Linker. *Polymer Degradation and Stability*, 95(*4*), pp. 618–626.

[**288**] Ghanbari-Siahkali, A., Mitra, S., Kingshott, P., Almdal, K., Bloch, C., and Rehmeier, H.K. (2005). Investigation of the hydrothermal stability of cross-linked liquid silicone rubber (LSR). *Polymer Degradation and Stability*, 90, pp. 471–480. DOI:10.1016/j.polymdegradstab.2005.04.016.

[**289**] Camino, G., Lomakin, S.M., and Lageard, M. (2002). Thermal polydimethylsiloxane degradation. Part 2. The degradation mechanisms. *Polymer*, 43(*2002*), pp. 2011–2015. DOI:10.1016/S0032-3861(01)00785-6.

[**290**] Tomer, N.S., Delor-Jestin, F., Frezet, L., and Lacoste, J. (2012). Oxidation , Chain Scission and Cross-Linking Studies of Polysiloxanes upon Ageings. *Open Journal of Organic Polymer Materials*, 2, pp. 13–22.

[**291**] Vera-Graziano, R., Hernandez-Sanchez, F., and Cauich-Rodriguez, J. V. (1995). Study of crosslinking density in polydimethylsiloxane networks by DSC. *Journal of Applied Polymer Science*, 55(*4*), pp. 1317–1327.

[**292**] Thomas, T.H. and Kendrick, T.C. (1969). Thermal Analysis of Polydimethylsiloxanes. I. Thermal Degradation in Controlled Atmospheres. *Journal of Polymer Science: Part A-2*, 7, pp. 537–549.

[**293**] Ramirez, I., Cherney, E.A., Jayaraml, S., and Gauthier, M. (2008). Thermogravimetric and Spectroscopy Analyses of Silicone Nanocomposites. *2008 Annual Report Conference on Electrical Insulation Dielectric Phenomena*, pp. 249–252.

[**294**] Mutlur, S. (n.d.). Thermal Analysis of Composites Using DSC. Advanced Topics in Characterization of Composites. pp. 11–33.

[**295**] Dollase, T., Spiess, H.W., and Gottlieb, M. (2002). Crystallization of PDMS : The effect of physical and chemical crosslinks. *Europhysics Letters*, 60(*3*), pp. 390–396.

[**296**] Gupta, S., Ramamurthy, P.C., and Madras, G. (2011). Mechanistic overview of the curing behavior of hydride terminated polydimethylsiloxane with allyl functionalized alumina by calorimetry and rheometry. *Thermochimica Acta*, 524(*1–2*), pp. 74–79.

[**297**] Gupta, S., Ramamurthy, P.C., and Madras, G. (2011). Synthesis and characterization of silicone polymer/functionalized mesostructured silica composites. *Polymer Chemistry*, 2, pp. 2643. DOI:10.1039/c1py00316j.

[**298**] Esteves, a. C.C., Brokken-Zijp, J., Laven, J., Huinink, H.P., Reuvers, N.J.W., Van, M.P., and de With, G. (2009). Influence of cross-linker concentration on the cross-linking of PDMS and the network structures formed. *Polymer*, 50(*16*), pp. 3955–3966.

[**299**] Kownacki, I., Marciniec, B., Steinberger, H., et al. (2009). Effect of triorganophosphites on platinum catalyzed curing of silicon rubber. *Applied Catalysis A: General*, 362, pp. 106–114. DOI:10.1016/j.apcata.2009.04.027.

[**300**] Lin, S., Tsay, W., Chen, Y., and Lee, C. (1994). Application of a new micro FT-IR/DSC technique to the study of the curing kinetics of silicone elastomer. *Journal of Controlled Release*, 31, pp. 277–282.

[**301**] Bogner, R.H., Liu, J.-C., and Chien, Y.W. (1990). Kinetics of curing and physicomechanical behavior of silicone membrane. *Journal of Controlled Release*, 14, pp. 11–19.

[**302**] Andersson, L.H.U. and Hjertberg, T. (2003). Silicone Elastomers for Electronic Applications . I . Analyses of the Noncrosslinked Fractions. *Journal of Applied Polymer Science*, 88, pp. 2073–2081.

[**303**] Farahmandghavi, F., Imani, M., Mirzadeh, H., and Jolly, C. (2012). Curing behavior of silicone elastomer in the presence of two corticosteroid drugs. *Journal of Biomedical Materials Research B: Applied Biomaterials*, 100B(*6*), pp. 1636/1644. DOI:10.1002/jbm.b.32732.

[**304**] Boyer, R.F. (1973). An apparent double glass transition in semicrystalline polymers. *Journal of Macromolecular Science, Part B*, 3–4, pp. 503–537. DOI:10.1080/00222347308201635.

[**305**] Clarson, S.J., Dodgson, K., and Semlyen, J.A. (1985). Studies of Cyclic and Linear Poly(dimethylsiloxanes): 19. Glass Transition Temperatures and Crystallization Behaviour. *Polymer*, 26, pp. 930–934.

[**306**] Birkefeld, A.B., Eckert, H., and Pfleiderer, B. (2004). A Study of the Aging of Silicone Breast Implants Using 29Si, 1H Relaxation and DSC Measurements. *Biomaterials*, 25, pp. 4405–4413. DOI:10.1016/j.biomaterials.2003.10.093.

[**307**] Dollase, T., Wilhelm, M., and Spiess, H.W. (2003). Effect of Interfaces on the Crystallization Behavior of PDMS. *Interface Science*, 11, pp. 199–209.

[**308**] Maus, A. and Saalwa, K. (2007). Crystallization Kinetics of Poly(dimethylsiloxane) Molecular-Weight Blends — Correlation with Local Chain Order in the Melt? *Macromolecular Chemistry and Physics*, 298, pp. 2066–2075. DOI:10.1002/macp.200700051.

[**309**] Chojnowski, J., Cypryk, M., Fortuniak, W., Rózga-Wijas, K., and Cibiorek, M. (2002). Controlled synthesis of vinylmethylsiloxane-dimethylsiloxane gradient, block and alternate copolymers by anionic ROP of cyclotrisiloxanes. *Polymer*, 43, pp. 1993–2001. DOI:10.1016/S0032-3861(01)00793-5.

[**310**] Soucek, J., Engelhardt, G., Stransky, K., and Schraml, J. (1976). 29Si and 13C-NMR Spectra of Non-Geminal Divinylhexamethylcyclotetrasiloxanes. *Collection of Czechoslovak Chemical Communications*, 41, pp. 234–238.

[**311**] Saunders, G. and MacCreath, B. (2012). Low Molecular Weight Resins - Analysis of Low Molecular Weight Resins and Prepolymers by GPC/SEC. Application Compendium. UK. 1-20 p.

[**312**] Yoshikawa, M., Wakabayashi, R., Tamai, M., and Kuroda, K. (2014). Synthesis of a multifunctional alkoxysiloxane oligomer. *New Journal of Chemistry*, 38, pp. 5362–5368.

[**313**] Abel, M., Joannic, R., Fayos, M., Lafontaine, E., Shaw, S.J., and Watts, J.F. (2006). Effect of solvent nature on the interaction of g -glycidoxy propyl trimethoxy silane on oxidised aluminium surface : A study by solution chemistry and surface analysis. *International Journal of Adhesion & Adhesives*, 26, pp. 16–27. DOI:10.1016/j.ijadhadh.2002.10.001.

[**314**] Stein, J. and David, M.W. (1995). Room Temperature Addition-Curable Silicone Adhesive Compositions and N-Heterocyclic Silane Adhesion Promoters, pp. 1–6.

[**315**] Gelest. (2013). Reactive silicone, pp. 64.

[**316**] Fustin, C.A., Sclavons, M., Pantoustier, N., Bebelman, S., and Bailly, C. (2005). Reactivity of

Si-H and Si-Vinyl End Functionalized Siloxanes Toward PBT: A Model System Study. *Polymer Engineering and Science*, pp. 1067–1072. DOI:10.1002/pen.20375.

[**317**] Chaudhry, a. N. and Billingham, N.C. (2001). Characterisation and oxidative degradation of a room-temperature vulcanised poly(dimethylsiloxane) rubber. *Polymer Degradation and Stability*, 73, pp. 505–510. DOI:10.1016/S0141-3910(01)00139-2.

[**318**] Bosq, N., Guigo, N., Persello, J., and Sbirrazzuoli, N. (2014). Melt and glass crystallization of PDMS and PDMS silica nanocomposites. *Physical Chemistry Chemical Physics*, 16, pp. 7830–7840. DOI:10.1039/c4cp00164h.

[**319**] Drumright, R.E., Gruber, P.R., and Henton, D.E. (2000). Polylactic Acid Technology. *Advanced Materials*, 12(*23*), pp. 1841–1846.

[**320**] Hutchinson, J.M. and Kriesten, U. (1994). Physical Aging and Enthalpy Relaxation in Polypropylene. *Journal of Non-Crystalline Solids*, 172, pp. 592–596. DOI:Doi 10.1016/0022-3093(94)90493-6.

[**321**] Hay, J.N. and Jenkins, M.J. (1999). Enthalpic relaxation and the glass transition in polymer blends. *Macromolecular Symposia*, 143(*1*), pp. 121–148.

[**322**] Cernosek, Z., Holubova, J., Cernoskova, E., and Liska, M. (2002). Enthalpic Relaxation and the Glass Transition. *Journal of Optoelectronics and Advanced Materials*, 4(*3*), pp. 489–503. DOI:10.1002/masy.19991430112.

[**323**] Maksimova, O.G., Maksimov, A. V., and Moiseeva, A.I. (2016). Influence of interface on the formation process of polymer coatings on metal. *Journal of Advanced Dielectrics*, 6(*1*), pp. 1–5. DOI:10.1142/S2010135X16500041.

[**324**] Hoffmann, H., Mayer, U., and Krischanitz, A. (1996). Structure of Alkylsiloxane Monolayers on Silicon Surfaces Investigated by External Reflection Infrared Spectroscopy. *Langmuir*, 11(*4*), pp. 1304–1312.

[**325**] Soga, I. and Granick, S. (1998). Infrared Dichroism and Surface Conformational Dynamics of Adsorbed Poly (dimethylsiloxane). *Macromolecules*, 31(*16*), pp. 5450–5455.

[**326**] Dabrowski, A. (2001). Adsorption--from theory to practice. *Advances in colloid and interface science*, 93, pp. 135–224. DOI:10.1016/S0001-8686(00)00082-8.

[**327**] Klein, J. (1986). Surface Interactions with Adsorbed Macromolecules. *Journal of Colloid and Interface Science*, 111(*2*), pp. 305–313. DOI:10.1016/0021-9797(86)90037-8.

[**328**] McMillan, W.G. (1954). Forces and Adsorption at Solid Surfaces. *Clays and Clay Minerals*, 3, pp. 473–481. DOI:10.1346/CCMN.1954.0030138.

[**329**] Lyubchik, S., Lyubchik, A., Lygina, O., Lyubchik, S., and Fonseca, I. (2011). Comparison of the Thermodynamic Parameters Estimation for the Adsorption Process of the Metals from Liquid Phase on Activated Carbons. In: Moreno-Pirajan JC, editor. Thermodynamics - Interaction Studies - Solids, Liquids and Gases. InTech. p. 930. DOI:10.5772/19514.

[**330**] Reed, A.E., Curtiss, L.A., and Weinhold, F. (1988). Intermolecular Interactions from a Natural Bond Orbital , Donor-Acceptor Viewpoint. *Chemical Reviews*, 88, pp. 899–926.

[**331**] Koral, J., Ullman, R., and Eirich, F.R. (1958). The Adsorption of Polyvinyl Acetate. *Journal of Physical and Chemical Reference Data*, 62(*5*), pp. 541–550. DOI:10.1021/j150563a007.

[**332**] O'Shaughnessy, B. and Vavylonis, D. (2003). Irreversible Adsorption from Dilute Polymer Solutions. *The European Physical Journal E*, 11, pp. 213–230. DOI:10.1140/epje/i2003-10015-9.

[**333**] Nies, C., Fug, F., Otto, C., and Possart, W. (2014). Adhesion of polyurethanes on native metal surfaces – stability and the role of urea-like species. *International Journal of Adhesion and Adhesives*, 52, pp. 19–25.

[**334**] Ohring, M. (2001). Materials Science of Thin Films. Deposition and Structure. Second Edi. Academic Press. 794 p.

[**335**] Summa, J. (2014). Co-Adsorption von Polyurethanmonomeren auf Nativem Aluminium University of Saarland, Germany.

[**336**] Olefjord, I. and Nylund, A. (1994). Surface Analysis of Oxidized Aluminium. 2. Oxidation of Aluminium in Dry and Humid Atmosphere Studied by ESCA, SEM, SAM and EDX. *Surface and Interface Analysis*, 21(*5*), pp. 290–297. DOI:10.1002/sia.740210505.

[**337**] Watts. and Wolstenholme. (2003). An Introduction to Surface Analysis by XPS and AES. England: John Wiley & Sons, Inc. 225 p.

[**338**] King, D.E. and Swart, W.E. (1987). Variable-Angle X-ray Photoelectron Spectroscopic Determination of the Thickness of the Oxide layer on Aluminum Metal. *Journal of Chemical Education*, 64(*11*), pp. 981–983.

[**339**] Oswald, S., Zier, M., Reiche, R., and Wetzig, K. (2006). Angle-resolved XPS: a critical evaluation for various applications. *Surface and Interface Analysis*, 38, pp. 590–594. DOI:10.1002/sia.

[**340**] McCafferty, E. and Wightman, J.P. (1998). Determination of the concentration of surface hydroxyl groups on metal oxide films by a quantitative XPS method. *Surface And Interface Analysis*, 26(*March*), pp. 549–564.

[**341**] Petrie, E.M. (2007). Adhesion and Bonding. Adhesive bonding of Aluminum Alloys. *Metal Finishing*, pp. 49–56. DOI:10.1016/S0026-0576(09)80033-0.

[**342**] Goldberg, S., Davis, J.A., and Hem, J.D. (1996). The Surface Chemistry of Aluminum Oxides and Hydroxides. In: Sposito G, editor. The Environmental Chemistry of Aluminum. U.S.A.: Lewis Publishers. pp. 272–318.

[**343**] Deimel, M. and Feld, H. (2014). Kurz Bericht. Charakterisierung der Chemischen Zusammensetzung einer Al-Schicht auf einem Si-Wafer. Münster, Germany. 1-10 p.

[**344**] Alexander, M.R., Thompson, G.E., and Beamson, G. (2000). Characterization of the oxide/hydroxide surface of aluminum using X-ray photoelectron spectroscopy: A procedure for curve fitting the O 1s core level. *Surface and Interface Analysis*, 29(*November 1999*), pp. 468–477. DOI:10.1002/1096-9918(200007)29:7<468::AID-SIA890>3.0.CO;2-V.

[**345**] Vinodh, M.S. (2006). On the Initial Oxidation of MgAl Alloys Max Planck Institute and University of Stuttgart, Germany.

[**346**] Li, H., Belkind, a., Jansen, F., and Orban, Z. (1997). An in situ XPS study of oxygen plasma cleaning of aluminum surfaces. *Surface and Coatings Technology*, 92, pp. 171–177. DOI:10.1016/S0257-8972(97)00079-0.

[**347**] Strohmeier, B.R. (1990). An ESCA Method for Determining the Oxide Thickness on Aluminum Alloys. *Surface And Interface Analysis*, 15, pp. 51–56.

[**348**] Lide, D.R. (2005). Handbook of Chemistry and Physics, Internet Version 2005. 85th Editi. Boca Raton, Fl, USA: CRC Press. 2661 p.

[**349**] Mielczarski, J. a. (1993). External Reflection Infrared-Spectroscopy At Metallic, Semiconductor, and Nonmetallic Substrates .1. Monolayer Films. *Journal of Physical Chemistry*, 97(*11*), pp. 2649–2663. DOI:10.1021/j100113a029.

[**350**] Gericke, A., Michailov, a V., and Huhnerfuss, H. (1993). Polarized External Infrared Reflection Absorption Spectrometry at the Air-Water-Interface - Comparison of Experimental and Theoretical Results for Different Angles of Incidence. *Vibrational Spectroscopy*, 4(*1993*), pp. 335–348. DOI:Doi 10.1016/0924-2031(93)80007-3.

[**351**] Porter, M.D. (1988). IR External Reflection Spectroscopy: A Probe for Chemically Modified Surfaces. *Analytical Chemistry*, 60(*20*), pp. 0.

[**352**] Buffeteau, T., Desbat, B., and Turlet, J.M. (1991). Polarization Modulation FT-IR Spectroscopy of Surfaces and Ultra-thin Films: Experimental Procedure and Quantitative Analysis. *Applied Spectroscopy*, 45(*3*), pp. 380–389. DOI:10.1366/0003702914337308.

[**353**] Handke, M., Milosevic, M., and Harrick, N.J. (1991). External Reflection Fourier-Transform Infrared-Spectroscopy - Theory and Experimental Problems. *Vibrational Spectroscopy*, 1, pp. 251–262. DOI:10.1016/0924-2031(91)85002-5.

[**354**] Lvovsky, A.I. (2013). Fresnel Equations. Encyclopedia of Optical Engineering. Taylor & Francis Group, LLC. pp. 1–6. DOI:10.1081/E-EOE-120047133.

[**355**] Lee, J.N., Park, C., and Whitesides, G.M. (2003). Solvent Compatibility of Poly(dimethylsiloxane)-Based Microfluidic Devices. *Analytical Chemistry*, 75(*23*), pp. 6544–6554. DOI:10.1021/ac0346712.

[**356**] Kuzmenko, a. B. (2005). Kramers-Kronig constrained variational analysis of optical spectra. 1,

pp. 10.

[**357**] Hopfe, V., Klobes, P., and Grählert, W. (1996). FSOS Software Package for IR-Vis-UV Spectroscopy of Solids, Interfaces and Layered Systems.

[**358**] Theiss, W. (2004). SCOUT 2 - Spectrum Interpretation by Simulation.

[**359**] Blaudez, D., Bonnier, M., Desbat, B., and Rondelez, F. (2002). Two-Dimensional Polymerization in Langmuir Films: A PM-IRRAS Study of Octadecyltrimethoxysilane Monolayers. *Langmuir*, 18(*24*), pp. 9158–9163.

[**360**] Giner, I., Maxisch, M., Kunze, C., and Grundmeier, G. (2013). Combined In Situ PM-IRRAS/QCM Studies of Water Adsorption on Plasma Modified Aluminum Oxide/Aluminum Substrates. *Applied Surface Science*, 283, pp. 145–153.

[**361**] Kim, D.H. and Jo, W.H. (2000). Studies on Polymer - Metal Interfaces. 2. Competitive Adsorption between Oxygen- and Nitrogen-Containing Functionality in Model Copolymers onto Metal Surfaces. *Macromolecules*, 33(*8*), pp. 3050–3058.

[**362**] Hoffmann, F. (1983). Infrared reflection-absorption spectroscopy of adsorbed molecules. *Surface Science Reports*, 3(*2–3*), pp. 107.

[**363**] Suetaka, W. and Yates, J.T. (1995). Surface Infrared and Raman Spectroscopy: Methods and Applications. Springer Science+Business Media, LLC. 270 p.

[**364**] Painter, P.C., Pehlert, G.J., Hu, Y., and Coleman, M.M. (1999). Infrared Band Broadening and Interactions in Polar Systems. *Macromolecules*, 32(*6*), pp. 2055–2057.

[**365**] Tsao, M.W., Pfeifer, K.H., Rabolt, J.F., Holt, D.B., Farmer, B.L., Interrante, L. V., and Shen, Q.H. (1996). Studies of the solid-state conformation of polysilaethylene: An organic/inorganic hybrid polymer with an alternating C/Si backbone. *Macromolecules*, 29(*22*), pp. 7130–7135.

[**366**] Reilly, J.T., Walsh, J.M., Greenfield, M.L., and Donohue, M.D. (1992). Analysis of FT-IR spectroscopic data: the Voigt profile. *Spectrochimica Acta*, 48A(*10*), pp. 1459–1479.

[**367**] Abraham, R.J. and Grant, G.H. (1988). A theoretical study of the Si-O bond in disiloxane and related molecules. *Journal of Computer-Aided Molecular Design*, 2, pp. 267–280.

[**368**] Grabowsky, S., Beckmann, J., and Luger, P. (2012). The Nature of Hydrogen Bonding Involving the Siloxane Group. *Australian Journal of Chemistry*, 65, pp. 785–795.

[**369**] Grabowsky, S., Hesse, M.F., Paulmann, C., Luger, P., and Beckmann, J. (2009). How to Make the Ionic Si-O Bond More Covalent and the Si-O-Si Linkage a Better Acceptor for Hydrogen Bonding. *Inorganic Chemistry*, 48(*10*), pp. 4384–4393.

[**370**] Yilgör, E., Burgaz, E., Yurtsever, E., and Yilgör, I. (2000). Comparison of hydrogen bonding in polydimethylsiloxane and polyether based urethane and urea copolymers. *Polymer*, 41, pp. 849–857. DOI:10.1016/S0032-3861(99)00245-1.

[**371**] Gilbert, B. (2015). Project Report. Contaminations on Native Metal Surfaces. Saarbrücken, Germany. 113 p.

[**372**] Ulman, A. (1996). Formation and Structure of Self-Assembled Monolayers. *Chemical Reviews*, 96, pp. 1533–1554. DOI:10.1021/cr9502357.

[**373**] O'Shaughnessy, B. and Vavylonis, D. (2005). Non-equilibrium in adsorbed polymer layers. *Journal of Physics: Condensed Matter*, 17, pp. R63–R99.

[**374**] West, J.K. (1997). Theoretical analysis of hydrolysis of polydimethylsiloxane (PDMS). *Journal of Biomedical Materials Research*, 35, pp. 505–511. DOI:10.1002/(SICI)1097-4636(19970615)35:4<505::AID-JBM10>3.0.CO;2-A.

[**375**] Cypryk, M. and Apeloig, Y. (2002). Mechanism of the acid-catalyzed Si-O bond cleavage in siloxanes and siloxanols. A theoretical study. *Organometallics*, 21(*6*), pp. 2165–2175. DOI:10.1021/om011055s.

[**376**] Sheibley, D.W. and Fowler, M.H. (1966). Infrared Spectra of Various Metal Oxides in the Region of 2 to 26 microns. Washington, D. C., U.S.A. 1-63 p.

[**377**] Konstadinidis, K., Thakkar, B., Chakraborty, A., Potts, L.W., Tannenbaum, R., Tirrell, M., and Evans, J.F. (1992). Segment Level Chemistry and Chain Conformation in the Reactive Adsorption of Poly(methylmethacrylate) on Aluminum Oxide Surfaces. *Langmuir*, 8(*5*), pp. 1307–1317. DOI:10.1021/la00041a012.

[**378**] Evmenenko, G., Mo, H., Kewalramani, S., and Dutta, P. (n.d.). Conformational Rearrangements in Thin Films of Polydimethylsiloxane Melt. Evanston, Illinois, U.S.A. 19 p.

[**379**] Underhill, P.., Goring, G., and DuQuesnay, D.. (1998). The Drying of 3-Glycidoxypropyltrimethoxy Silane. *Applied Surface Science*, 134, pp. 247–253. DOI:10.1016/S0169-4332(98)00254-2.

[**380**] Fu, Z. and Santore, M.M. (1998). Competitive Adsorption of Poly(ethylene oxide) Chains with and without Charged End Groups. *Langmuir*, 14(*Copyright (C) 2010 American Chemical Society (ACS). All Rights Reserved.*), pp. 4300–4307. DOI:10.1021/la971382y.

[**381**] Kawaguchi, M., Itoh, K., Yamagiwa, S., and Takahashi, A. (1989). Random Copolymer Adsorption. 2. Competitive and Displacement Adsorption. *Macromolecules*, 22(*5*), pp. 2204–2207.

[**382**] David, K., Dan, N., and Tannenbaum, R. (2007). Competitive adsorption of polymers on metal nanoparticles. *Surface Science*, 601, pp. 1781–1788. DOI:10.1016/j.susc.2007.01.054.

[**383**] Csakvari, B., Csakvari, E., Gomory, P., and Vertes, A. (1975). Mössbauer Study of the Donor Character of Oxygen in Si-O Bonds. *Journal of Radioanalytical Chemistry*, 25, pp. 275–282.

[**384**] Ohwaki, T. (2004). Characterization of native oxide on aluminum by infrared spectroscopy. *Journal of Japan Institute of Light Metals*, 54(*1*), pp. 31–36.

[**385**] Osterholtz, F.D. and Pohl, E.R. (1992). Kinetics of the Hydrolysis and Condensation of Organofunctional Alkoxysilanes: A Review. *Journal of Adhesion Science and Technology*, 6(*1*), pp. 127–149. DOI:10.1163/156856192X00106.

[**386**] Quinonero, D., Garau, C., Rotger, C., Frontera, A., Ballester, P., Costa, A., and Dey, P.M. (2002). Anion-p Interactions: Do They Exist? *Angewandte Chemie. International Edition*, 41(*18*), pp. 3389–3392.

[**387**] Egorochkin, A.N., Vyazankin, N.S., and Khorshev, S.Y. (1972). Effect of dp-pp Interaction in Organic Compounds of Group IVB Elements. *Russian Chemical Reviews*, 41(*5*), pp. 425–438.

[**388**] Santore, M.M. (2005). Dynamics in Adsorbed Homopolymer Layers: Understanding Complexity from Simple Starting Points. *Current Opinion in Colloid and Interface Science*, 10, pp. 176–183. DOI:10.1016/j.cocis.2005.05.005.

[**389**] Källrot, N. and Linse, P. (2007). Dynamic Study of Single-Chain Adsorption and Desorption. *Macromolecules*, 40(*13*), pp. 4669–4679.

[**390**] Panja, D., Barkema, G.T., and Kolomeisky, A.B. (2009). Non-equilibrium dynamics of single polymer adsorption to solid surfaces. *Journal of physics. Condensed matter : an Institute of Physics journal*, 21(*24*), pp. 242101.

[**391**] Besbes, S., Cermelli, I., Bokobza, L., Monnerie, L., Bahar, I., Erman, B., and Herz, J. (1992). Segmental Orientation in Model Networks of Poly(dimethylsiloxane): Fourier Transform Infrared Dichroism Measurements and Theoretical Interpretation. *Macromolecules*, 25(*7*), pp. 1949–1954.

[**392**] van Alsten, J. (1991). Experimental Measurements of Local Mobility in Adsorbed Poly(dimethylsiloxane) Layers. *Macromolecules*, 24(*19*), pp. 5320–5323.

[**393**] Kim, C., Gurau, M.C., Cremer, P.S., and Yu, H. (2008). Chain Conformation of Poly(dimethyl siloxane) at the Air/Water Interface by Sum Frequency Generation. *Langmuir*, 24(*18*), pp. 10155–10160.

[**394**] Fox, H.W., Solomon, E.M., and Zisman, W.A. (1950). Reaction of Polyorganosiloxane monolayers with Aqueous Substrates. *Journal of Physical Chemistry*, 54(*5*), pp. 723–731.

[**395**] West, R., Wilson, L.S., and Powell, D.L. (1979). Basicity of siloxanes, alkoxysilanes and ethers toward hydrogen bonding. *Journal of Organometallic Chemistry*, 178(*1*), pp. 5–9. DOI:10.1016/S0022-328X(00)87856-0.

[**396**] West, R., Whatley, L.S., and Lake, K.J. (1961). Hydrogen Bonding Studies. V. The relative Basicity of Ethers, Alkoxysilanes and Siloxanes and the Nature of the Silicon-Oxygen Bond. *Journal of the American Chemical Society*, 83(*4*), pp. 761–764.

[**397**] Voronkov, M.G. and Deich, A.Y. (1964). The donor-acceptor properties of the siloxane bond. *Zhurnal Strukturnoi Khimii*, 5(*3*), pp. 482–489.

[**398**] Huang, N., Xu, J., Zhang, H., and Xu, Z. (2015). The origin of the decreasing basicity from

monofunctional alkoxysilane to tetrafunctional alkoxysilane: A combined IR and theoretical study. *Journal of Molecular Structure*, 1089, pp. 216–221.

[**399**] Plueddemann, E.P. (1991). Reminiscing on Silane Coupling Agents. *Journal of Adhesion Science and Technology*, 5(*4*), pp. 261–277. DOI:10.1163/156856191X00350.

[**400**] Britcher, L.G., Kehoe, D.C., Matisons, J.G., Smart, R.S.C., and Swincer, A.G. (1993). Silicones on Glass Surfaces. 2. Coupling Agent Analogs. *Langmuir*, 9(*7*), pp. 1609–1613.

[**401**] Mizuhara, K., Hara, K., and Imoto, T. (1967). Adsorption of Polymers at the Solution-Solid Interface. *Kolloid-Zeitschrift und Zeitschrift für Polymere*, 229(*1*), pp. 17–21.

[**402**] Bellmann, C. (2008). Surface Modification by Adsorption of Polymers and Surfactants. In: Stamm M, editor. Polymer Surfaces and Interfaces. Characterization, Modification and Applications. Dresden, Germany: Springer-Verlag Berlin Heidelberg. p. 324.

[**403**] Pekel, N. and Güven, O. (2002). Solvent, Temperature and Concentration Effects on the Adsorption of Poly (n-Butyl Methacrylate) on Alumina from Solutions. *Turkisch Journal of Chemistry*, 26, pp. 221–227.

[**404**] MedArray. (2011). Silicone (PDMS) Chemical Compatibility. *Permselect*, pp. 1–7. Accessed 3 December 2013.

[**405**] Lunder, O. (2003). Chromate-free pre-treatment of aluminum for adhesive bonding Norwegian University of Science and Technology.

[**406**] Fowkes, F.M. and Mostafa, M.A. (1978). Acid-Base Interactions in Polymer Adsorption. *Industrial and Engineering Chemistry Product Research and Development*, 17(*1*), pp. 3–7. DOI:10.1021/i360065a002.

[**407**] van den Brand, J. (2004). On the Adhesion between Aluminium and Polymers Technical University Delft. Netherlands.

[**408**] Mark, J.E. (1968). Dipole Moments of Dimethylsiloxane Chains. *The Journal of Chemical Physics*, 49(*3*), pp. 1398.

[**409**] Kokalj, A. (2011). Electrostatic model for treating long-range lateral interactions between polar molecules adsorbed on metal surfaces. *Physical Review B - Condensed Matter and Materials Physics*, 84(*4*). DOI:10.1103/PhysRevB.84.045418.

[**410**] Possart, W. (2012). Lecture: “Polymer – Festkörper Interphasen.” Saarbrücken, Germany. 308 p.

[**411**] Schmidt, W.G., Seino, K., Preuss, M., Hermann, A., Ortmann, F., and Bechstedt, F. (2006). Organic molecule adsorption on solid surfaces: Chemical bonding, mutual polarisation and dispersion interaction. *Applied Physics A: Materials Science and Processing*, 85(*4*), pp. 387–397. DOI:10.1007/s00339-006-3691-0.

[**412**] Schravendijk, W.J. (2007). Computational Modeling of Surface Interactions Johannes Gutenberg-University of Mainz.

[**413**] Zhao, L., Liu, L., and Sun, H. (2007). Semi-ionic model for metal oxides and their interfaces with organic molecules. *Journal of Physical Chemistry C*, 111(*28*), pp. 10610–10617. DOI:10.1021/jp071775y.

[**414**] Yan, W., Ammon, Jr, D., Gardella, Jr, J., Maziarz, III, E., Hawkridge, A., Grobe, III, G., and Wood, T. (1998). Quantitative mass spectrometry of technical polymers: a comparison of several ionization methods. *European Journal of Mass Spectrometry*, 4(*1*), pp. 467. DOI:10.1255/ejms.272.

[**415**] Liu, X.M., Maziarz, E.P., Heiler, D.J., and Grobe, G.L. (2003). Comparative Studies of Poly(Dimethyl Siloxanes) Using Automated GPC-MALDI- TOF MS and On-Line GPC-ESI-TOF MS. *Journal of American Society for Mass Spectrometry*, 14, pp. 195–202. DOI:10.1016/S1044-0305(02)00908-X.

[**416**] Frantz, P., Leonhardt, D.C., and Granick, S. (1991). Enthalpic Effects in Competitive Polymer Adsorption: Adsorption Isotope Effect and Chain End Effect. *Macromolecules*, 24(*8*), pp. 1868–1875.

[**417**] Csempesz, F., Csaki, K., Kovacs, P., and Nagy, M. (1995). Simultaneous competitive adsorption of polymers from ternary solutions at solid/liquid interfaces. *Colloids and Surfaces A : Physicochemical and Engineering Aspects*, 101, pp. 113–121.

[**418**] Dijit, J.C., Cohen Stuart, M.A., and Fleer, G.J. (1994). Competitive Adsorption Kinetics of Polymers Differing in Length. *Macromolecules*, 27(*12*), pp. 3219–3228.

[**419**] Källrot, N. and Linse, P. (2010). Dynamics of Competitive Polymer Adsorption onto Planar Surfaces in Good Solvent. *Journal of Physical Chemistry*, 114(*11*), pp. 3741–3753.

[**420**] Sintes, T., Sumithra, K., and Straube, E. (2001). Adsorption of Semiflexible Polymers on Flat, Homogeneous Surfaces. *Macromolecules*, 34(*5*), pp. 1352–1357.

[**421**] Amancio-Filho, S.. and dos Santos, J.F. (2009). Joining of Polymers and Polymer – Metal Hybrid Structures : Recent Developments and Trends. *Polymer Engineering and Science*, pp. 1461–1476. DOI:10.1002/pen.21424.

[**422**] da Silva, L.F.M. (2011). Technology of Mixed Adhesive Joints. *Advanced Structural Materials*, 6, pp. 283–309. DOI:10.1007/8611.

[**423**] da Silva, L.F.M., das Neves, P.J.C., Adams, R.D., and Spelt, J.K. (2009). Analytical models of adhesively bonded joints-Part I: Literature survey. *International Journal of Adhesion and Adhesives*, 29, pp. 319–330. DOI:10.1016/j.ijadhadh.2008.06.005.

[**424**] Baldan, A. (2004). Review. Adhesively-Bonded Joints in Metallic Alloys, Polymers and Composite Materials: Mechanical and Environmental Durability Performance. *Journal of Materials Research*, 39, pp. 4729–4797.

[**425**] Phung, L.H., Kleinert, H., Jansen, I., Häßler, R., and Jähne, E. (2004). Improvement in strength of the aluminium/epoxy bonding joint by modification of the interphase. *Macromolecular Symposia*, 210, pp. 349–358. DOI:10.1002/masy.200450639.

[**426**] Dunlop, H. and Benmalek, M. (1997). Role and Characterization of Surfaces in the Aluminium Industry. *Journal de Physique IV*, 7(*C6*), pp. 163–174. DOI:10.1051/jp4:1997614.

[**427**] Hohman, A. and Standard, C. (1992). Durability of Adhesively Bonded Structure. Update on Engineering and Structural Adhesives. pp. 137–154.

[**428**] Critchlow, G.W. and Brewis, D.M. (1996). Review of surface pretreatments for aluminium alloys. *International Journal of Adhesion and Adhesives*, 16(*4*), pp. 255–274. DOI:10.1016/S0143-7496(96)00014-0.

[**429**] Anagreh, N. and Robaidi, A. Al. (2010). Improvement in Adhesion Behavior of Aluminum Due to Surfaces Treatment with Arc Discharge. *Jordan Journal of Mechanical and Industrial Engineering*, 4(*2*), pp. 330–339.

[**430**] Registration, Evaluation and Authorization of Chemicals (REACH)(n.d.). Accessed 2 October 2016.

[**431**] GmbH, R. (2012). Chemical composition AlMg3 (EN AW 5754).

[**432**] Grohs, J.W. (2007). Comparing In Situ and Bulk Constitutive Properties of a Structural Adhesive.

[**433**] Rusell, W. and Garnis, E. (1978). Chromate-Free Method of Preparing Aluminum Surfaces for Adhesive Bonding. Dover, USA. 1-29 p.

[**434**] Gross, D. and Sutton, C. (2016). Investigation of Outlife Time on the Environmental Durability of P2-Etched , Adhesively-Bonded Aluminum Alloys Using the ASTM Wedge Test. 1-26 p.

[**435**] Barkhimer, J., Erich, M., and Nair, G. (2015). Effect of Time Delay Between Etching and Adhesive Bonding ("Outlife" Time) on Lap-Shear Strength of Aluminum Alloys Using Environmentally-Friendly P2 Etch. 1-35 p.

[**436**] Digby, R.P. and Packham, D.E. (1995). Pretreatment of aluminium: topography, surface chemistry and adhesive bond durability. *International Journal of Adhesion and Adhesives*, 15(*2*), pp. 61–71. DOI:10.1016/0143-7496(95)98739-9.

[**437**] Williams, T.S. (2013). Surface Modification by Atmospheric Pressure Plasma for Improved Bonding University of California.

[**438**] Prysiazhnyi, V., Zajickova, L., Slavicek, P., and Zahoran, M. (2009). Aluminium Surface Activation Using Atmospheric-pressure Plasma, pp. 182–187.

[**439**] Diab, F., El-Aragi, M., El-Kashef, G.M., and Saudy, A.H. (2013). Aluminum Surface Analysis after Exposed to Dense Electro thermal Launcher Plasma. *Arab Journal of Nuclear Science and Applications*, 46(*2*), pp. 204–214.

[**440**] Bockenheimer, C. (2003). Epoxid und Aluminium im Kleberverbund nach mechanischer Vorbehandlung und Alterung University of Saarland.

[**441**] Materials Evaluation and Engineering Inc. (2001). Handbook of Analytical Methods for Materials. Plymouth. U.S.A.: Materials Evaluation and Engineering, Inc. 1-50 p.

[**442**] Khan, R.H.U., Yerokhin, A., Li, X., Dong, H., and Matthews, A. (2010). Surface characterisation of DC plasma electrolytic oxidation treated 6082 aluminium alloy: Effect of current density and electrolyte concentration. *Surface and Coating Technology*, 205, pp. 1679–1688. DOI:10.1016/j.surfcoat.2010.04.052.

[**443**] Yilbas, B.S., Matthews, A., Karatas, C., Leylamd, A., Khaled, M., Abu-Dheir, N., Al-Aqeeli, N., and Nie, X. (2014). Laser Texturing of Plasma Electrolytically Oxidized Aluminum 6061 Surfaces for Improved Hydrophobicity. *Journal of Manufacturing Science and Engineering*, 136(*54501*), pp. 1–8. DOI:10.1115/1.4027977.

[**444**] Langer, M., Rechner, R., Thieme, M., Jansen, I., and Beyer, E. (2012). Surface analytical characterisation of Nd:YAG-laser pre-treated AlMg3 as a preparation for bonding. *Solid State Sciences*, 14(*7*), pp. 926–935.

[**445**] Feldman, K., Fritz, M., Hähner, G., Marti, A., and Spencer, N.D. (1998). Surface forces, surface chemistry and tribology. *Tribology International*, 31(*98*), pp. 99–105. DOI:10.1016/S0301-679X(98)00012-7.

[**446**] Dechene, J.M. (2010). Surface Modifications of Poly(dimethylsiloxane) for Biological Application of Microfluidic Devices The University of Western Ontario.

[**447**] Bland, D.J., Kinloch, A.J., Stolojan, V., and Watts, J.F. (2008). Failure Mechanisms in Adhesively Bonded Aluminium: An XPS and PEELS Study. *Surface and Interface Analysis*, 40, pp. 128–131. DOI:10.1002/sia.2651.

[**448**] Possart, W. and Dieckhoff, S. (1999). Adhesion mechanisms in a cyanurate prepolymer on silicon and on aluminum. *International Journal of Adhesion and Adhesives*, 19, pp. 425–434. DOI:10.1016/S0143-7496(99)00005-6.

[**449**] da Silva, L.F.M., das Neves, P.J.C., Adams, R.D., Wang, a., and Spelt, J.K. (2009). Analytical models of adhesively bonded joints-Part II: Comparative study. *International Journal of Adhesion and Adhesives*, 29, pp. 331–341. DOI:10.1016/j.ijadhadh.2008.06.007.

[**450**] Zhang, J., Zhao, X., Zuo, Y., Xiong, J., and Zhang, X. (2008). Effect of Surface Pretreatment on Adhesive Properties of Aluminum Alloys. *Journal of Materials Science and Technology*, 24(*2*), pp. 236–240.

10 Appendices

10.1. Appendix A

Operational parameters of the Bruker IFS 66v/s FTIR spectrometer (Bruker, Karlsruhe, Germany) employed in ATR-FTIR and FTIR-ERAS measurements.

Description	Parameters
Polarization of light	*s,p*-polarized light
Angle of incidence	60°-80°
Beam splitter	Ge multilayer coating on KBr
Detector	MET-Detector (cool with N2)
Polarizator	KRS-5
Number of scans	500-1000
Mirror velocity	40 kHz
Aperture	2 mm
Resolution	4 cm-1
Wavenumber range	MIR: 4000 - 400 cm^{-1}
Zero filling factor	8
Apodization function	Blackman Harris 3-Term
Atmosphere of the IR sample compartment	dry air
Temperature in the IR sample compartment	24 °C
Operating vacuum	< 3 mbar inside the optics bench

10.2. Appendix B

Number-average molar mass (M_n) determination by ^{1}H-NMR

Prepolymer 1: di-hydride terminated PDMS

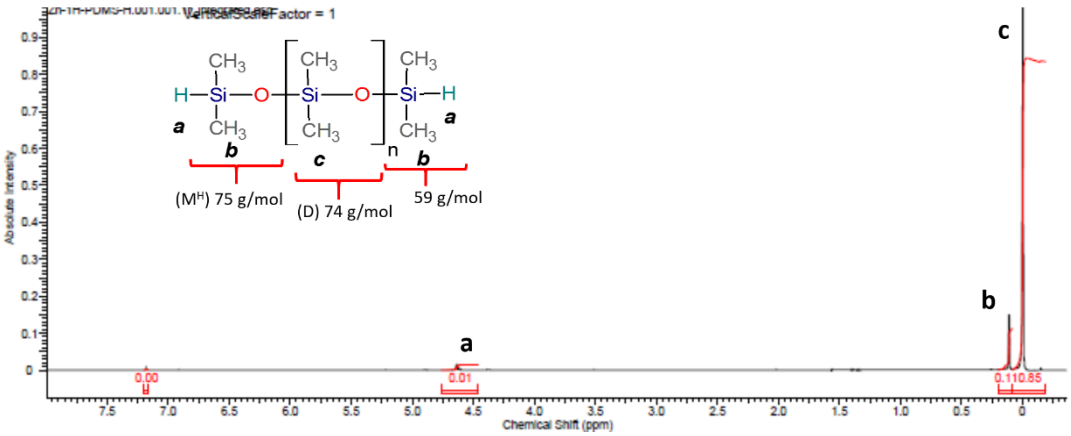


Figure 10.1. Integrated 1H-NMR spectrum of di-hydride terminated PDMS (Prepolymer 1)

Determination of the integral ratio of the ^{1}H NMR signals of methyl protons from middle (Integral of b, I_b) and end groups (Integral of c, I_c) of:

$$\frac{I_b}{I_c} = \frac{0.85}{0.11} \sim \frac{7.7}{1}$$

Thus, for the bifunctional prepolymer 1, the relative integrals are approximately 15.4:2, which allows to assess an average chain length of approximately 15 repetition units (n~15). Thus, from the molar mass of the building units show in the spectrum of Figure 10.1, the number-average molar mass for prepolymer 1 is:

$$M_n\ [g\ mol^{-1}] = 75 + (15 \times 74) + 59$$

$$M_n|_{prepolymer\ 1} \sim 1244\ [g\ mol^{-1}]$$

Prepolymer 2: di-vinyl terminated PDMS

Following the same procedure of prepolymer 1, the integral ratio of the ^{1}H NMR signals of methyl protons from middle (I_e) and end groups (Integral of d, I_d) from Figure 10.2, is:

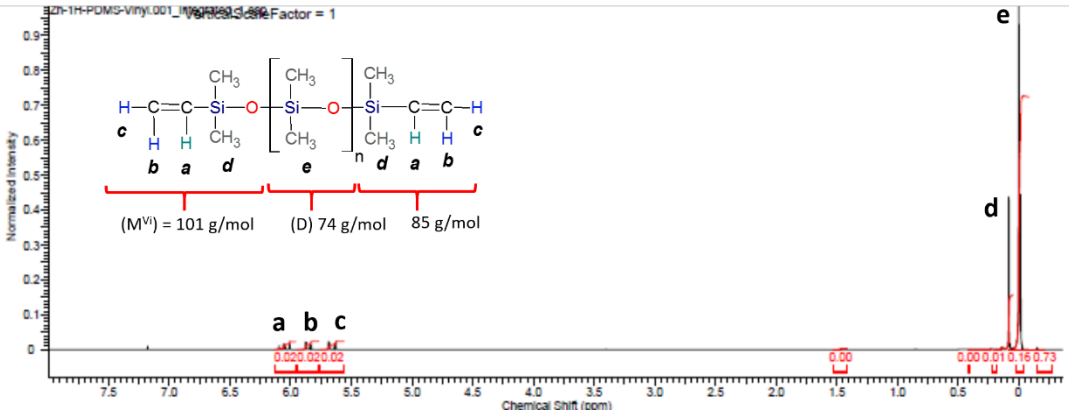


Figure 10.2. Integrated 1H-NMR spectrum of di-vinyl terminated PDMS (Prepolymer 2)

$$\frac{I_e}{I_d} = \frac{0.73}{0.16} \sim \frac{4.5}{1}$$

Thus, for the bifunctional prepolymer 1, the relative integrals are approximately 9:2, which allows to assess an average chain length of approximately 9 repetition units (n~9). Thus, from the molar mass of the building units show in the spectrum of Figure 10.2, the number-average molar mass for prepolymer 2 is:

$$M_n\ [g\ mol^{-1}] = 101 + (9 \times 74) + 85$$

$$M_n|_{prepolymer\ 2} \sim 852\ [g\ mol^{-1}]$$

10.3. Appendix C

Peak-to-peak noise

The peak to peak noise levels were estimated from a spectral region where the prepolymers and TDMS do not display any absorption band. The spectral region selected in all cases was from 1800 to 1900 cm^{-1}. As example the peak-to-peak levels of prepolymer 1 and 2 and TDMS are shown. It is seen that the peak-to-peak level is kept at the order of ~10^{-4}.

Prepolymer 1: di-hydride terminated PDMS

	ERA Spectra				
	3 min Adsorption	1st THF	2nd THF	3rd THF	4th THF
Max. intensity	1,00047	1,00171	1,00075	1,00199	1,00205
Min. intensity	1,00030	1,00128	1,00046	1,00155	1,00181
Peak-to-peak noise	0,00017	0,00043	0,00029	0,00044	0,00024

Prepolymer 2: di-vinyl terminated PDMS

	ERA Spectra				
	3 min Adsorption	1st THF	2nd THF	3rd THF	4th THF
Max. intensity	1,00175	0,99944	0,99899	0,99955	0,99960
Min. intensity	1,00151	0,99935	0,99889	0,99909	0,99946
Peak-to-peak noise	0,00024	0,00009	0,0001	0,00046	0,00014

Tetrakis(dimethylsiloxysilane) - TDMS

	ERA Spectra					
	3 min Adsorption	1st THF	2nd THF	3rd THF	4th THF	5th THF
Max. intensity	1,00145	0,99908	0,99857	0,99721	0,99992	0,99898
Min.intensity	1,00129	0,99897	0,99839	0,99693	0,99976	0,99882
Peak-to-peak noise	0,00016	0,00011	0,00018	0,00028	0,00016	0,00016

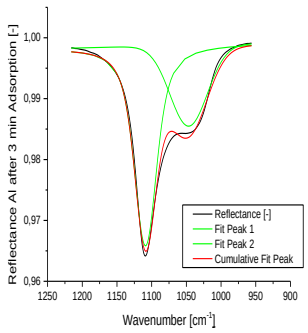
10.4. Appendix D

Peak fitting of the IR absorption bands

The Fitting of all peaks in this work were carried out in the software OriginPro®8.6 using the Peak and Analysis option. All peaks were fitted to a Voigt function which is included in the software for calculating area, peak height and for determining the peak position. The results of peak fitting for the $\nu_{s,as}$-Si-O-Si bands in the spectra for 1h storage time are shown here as a representation.

Si-O-Si stretching vibration modes in prepolymer 1

3 min adsorption



Parameters

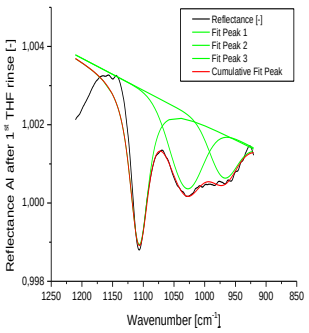
		Value	Shared	Standard Error
Peak1(Voigt)	y0	0	0	0
	xc	1046,6773	0	0
	A	-0,89464	0	0,00933
	wG	63,22149	0	0,67047
	wL	1,69867E-19	0	4,5047E7
	FWHM	63,22149		2,40821E7
Peak2(Voigt)	y0	0	0	0
	xc	1108,86841	0	0
	A	-1,75903	0	0,01488
	wG	23,39381	0	0,84529
	wL	24,62752	0	0,80919
	FWHM	39,21662		0,29127

Reduced Chi-sqr = 6,94423039961E-7
COD(R^2) = 0,99272890271544
Iterations Performed = 3
Total Iterations in Session = 54
Fit converged - Chi-sqr no longer changed.
Some parameter values were fixed.
FWHM are derived parameter(s).

Statistics

	Reflectance
Number of Points	540
Degrees of Freedom	534
Reduced Chi-Sqr	6,94423E-7
Residual Sum of Squares	3,70822E-4
Adj. R-Square	0,99266
Fit Status	Succeeded(101)

1st THF rinse



Parameters

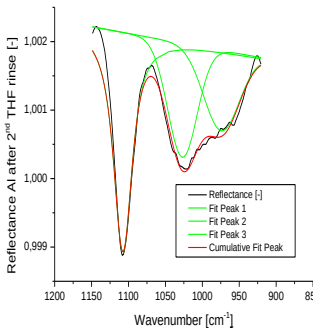
		Value	Shared	Standard Error
Peak1(Voigt)	y0	0	0	0
	xc	969,81183	0	3,64086
	A	-0,06378	0	0,01127
	wG	51,52917	0	5,51347
	wL	2,88503E-16	0	--
	FWHM	51,52917		-1,#IND
Peak2(Voigt)	y0	0	0	0
	xc	1030,28339	0	2,63512
	A	-0,12841	0	0,01145
	wG	62,41886	0	5,24939
	wL	4,16041E-17	0	--
	FWHM	62,41886		5,24939
Peak3(Voigt)	y0	0	0	0
	xc	1106,93994	0	0
	A	-0,21548	0	0
	wG	15,97	0	0
	wL	29,547	0	0
	FWHM	36,87041		0

Reduced Chi-sqr = 1,83965153E-7
COD(R^2) = 0,79969775206778
Iterations Performed = 7
Total Iterations in Session = 24
Fit converged. Chi-Sqr tolerance value of 1E-6 was reached.
Some parameter values were fixed.
FWHM are derived parameter(s).

Statistics

	Reflectance
Number of Points	603
Degrees of Freedom	595
Reduced Chi-Sqr	1,83965E-7
Residual Sum of Squares	1,09459E-4
Adj. R-Square	0,79734
Fit Status	Succeeded(100)

2nd THF rinse



Parameters

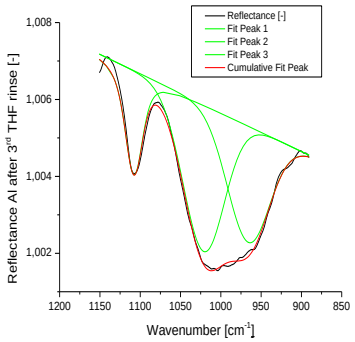
		Value	Shared	Standard Error
Peak1(Voigt)	y0	0	0	0
	xc	974,25612	0	0
	A	-0,07064	0	0,00204
	wG	56,58825	0	1,72517
	wL	7,24021E-62	0	5,30336E7
	FWHM	56,58825		2,83517E7
Peak2(Voigt)	y0	0	0	0
	xc	1026,96599	0	0,41815
	A	-0,08278	0	0,00166
	wG	46,76835	0	0,97221
	wL	2,78001E-17	0	--
	FWHM	46,76835		0,97221
Peak3(Voigt)	y0	0	0	0
	xc	1107,61868	0	0
	A	-0,1476	0	0
	wG	10,329	0	0
	wL	26,89	0	0
	FWHM	30,60209		0

Reduced Chi-sqr = 3,15667095337E-8
COD(R^2) = 0,94808478587317
Iterations Performed = 7
Total Iterations in Session = 70
Fit converged. Chi-Sqr tolerance value of 1E-6 was reached.
Some parameter values were fixed.
FWHM are derived parameter(s).

Statistics

	Reflectance
Number of Points	475
Degrees of Freedom	468
Reduced Chi-Sqr	3,15667E-8
Residual Sum of Squares	1,47732E-5
Adj. R-Square	0,94742
Fit Status	Succeeded(100)

3rd THF rinse



Parameters

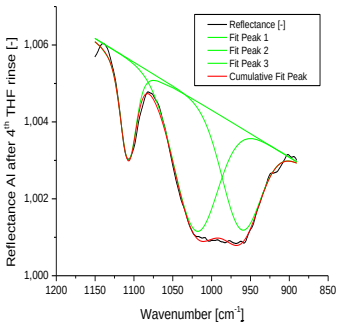
		Value	Shared	Standard Error
Peak1(Voigt)	y0	0	0	0
	xc	985,96872	0	0,92592
	A	-0,19736	0	0,00712
	wG	61,19794	0	1,02213
	wL	7,98127E-26	0	2,41397E8
	FWHM	61,19794		1,29051E8
Peak2(Voigt)	y0	0	0	0
	xc	1021,34512	0	0,71388
	A	-0,24429	0	0,00711
	wG	59,9892	0	1,0709
	wL	4,1806E-17	0	--
	FWHM	59,9892		1,0709
Peak3(Voigt)	y0	0	0	0
	xc	1107,90417	0	0
	A	-0,0966	0	0
	wG	16,63	0	0
	wL	15,59	0	0
	FWHM	26,47831		0

Reduced Chi-Sqr = 1,57729147051E-8
COD(R^2) = 0,99251438147948
Iterations Performed = 48
Total Iterations in Session = 48
Fit converged. Chi-Sqr tolerance value of 1E-6 was reached.
Some parameter values were fixed.
FWHM are derived parameter(s).

Statistics

	Reflectance
Number of Points	541
Degrees of Freedom	533
Reduced Chi-Sqr	1,57729E-8
Residual Sum of Squares	8,40696E-6
Adj. R-Square	0,99242
Fit Status	Succeeded(100)

4th THF rinse



Parameters

		Value	Shared	Standard Error
Peak1(Voigt)	y0	0	0	0
	xc	982,0381	0	0,58618
	A	-0,16075	0	0,00426
	wG	57,06027	0	0,69833
	wL	3,11789E-20	0	--
	FWHM	57,06027		-1.#IND
Peak2(Voigt)	y0	0	0	0
	xc	1020,57285	0	0,54004
	A	-0,23593	0	0,0043
	wG	65,19587	0	0,90745
	wL	1,32388E-15	0	--
	FWHM	65,19587		0,90745
Peak3(Voigt)	y0	0	0	0
	xc	1107,42206	0	0
	A	-0,0831	0	0
	wG	18,29	0	0
	wL	10,94	0	0
	FWHM	24,83398		0

Reduced Chi-Sqr = 9,7912310964E-9
COD(R^2) = 0,99367051382232
Iterations Performed = 19
Total Iterations in Session = 68
Fit converged. Chi-Sqr tolerance value of 1E-6 was reached.
Some parameter values were fixed.
FWHM are derived parameter(s).

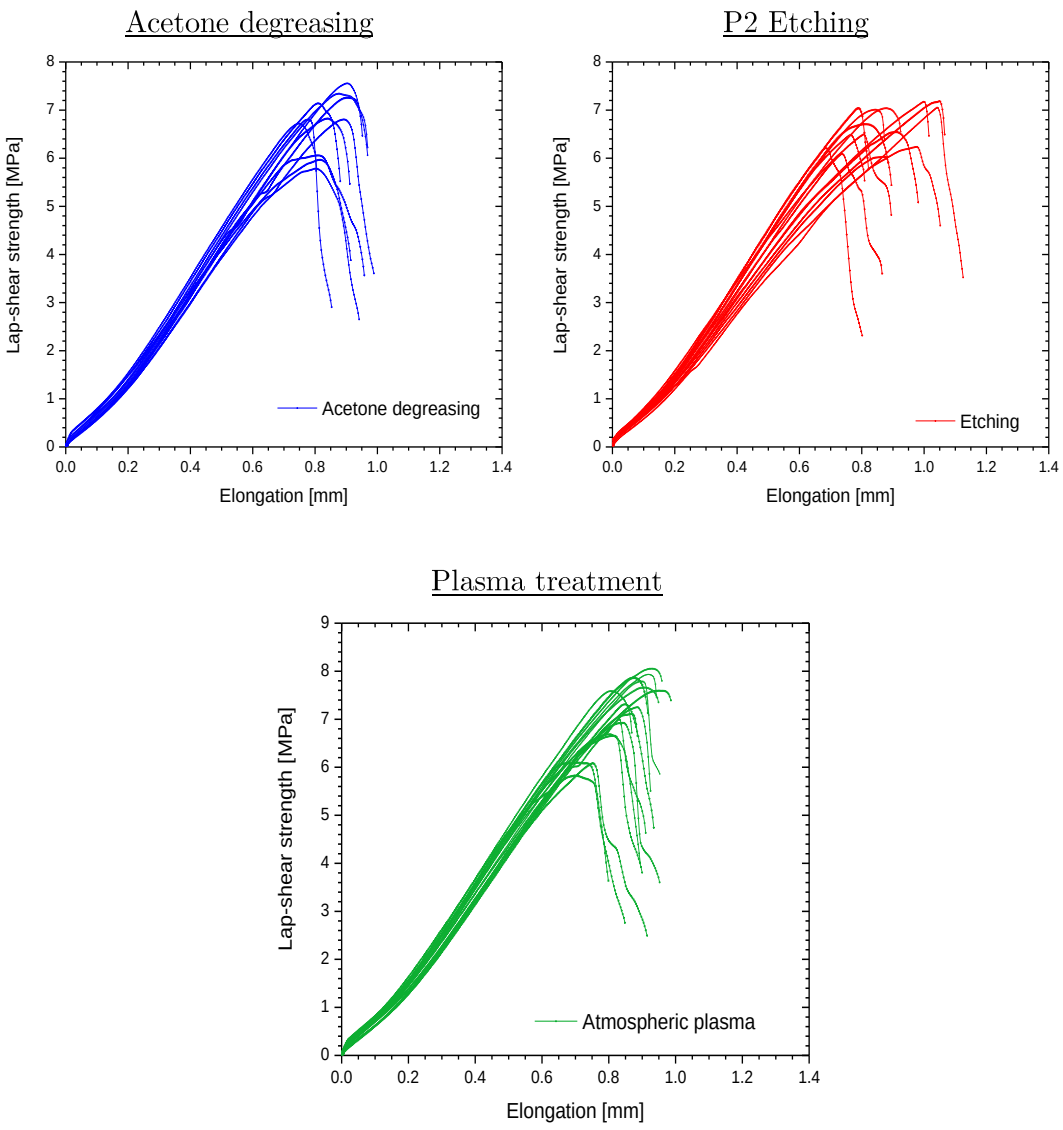
Statistics

	Reflectance
Number of Points	540
Degrees of Freedom	532
Reduced Chi-Sqr	9,79123E-9
Residual Sum of Squares	5,20893E-6
Adj. R-Square	0,99359
Fit Status	Succeeded(100)

10.5. Appendix E

Single-lap shear tests

Results of the single-lap shear tests executed to the specimens prepared with the pretreated aluminum substrates by acetone, P2 etching and air plasma (Chapter 7).

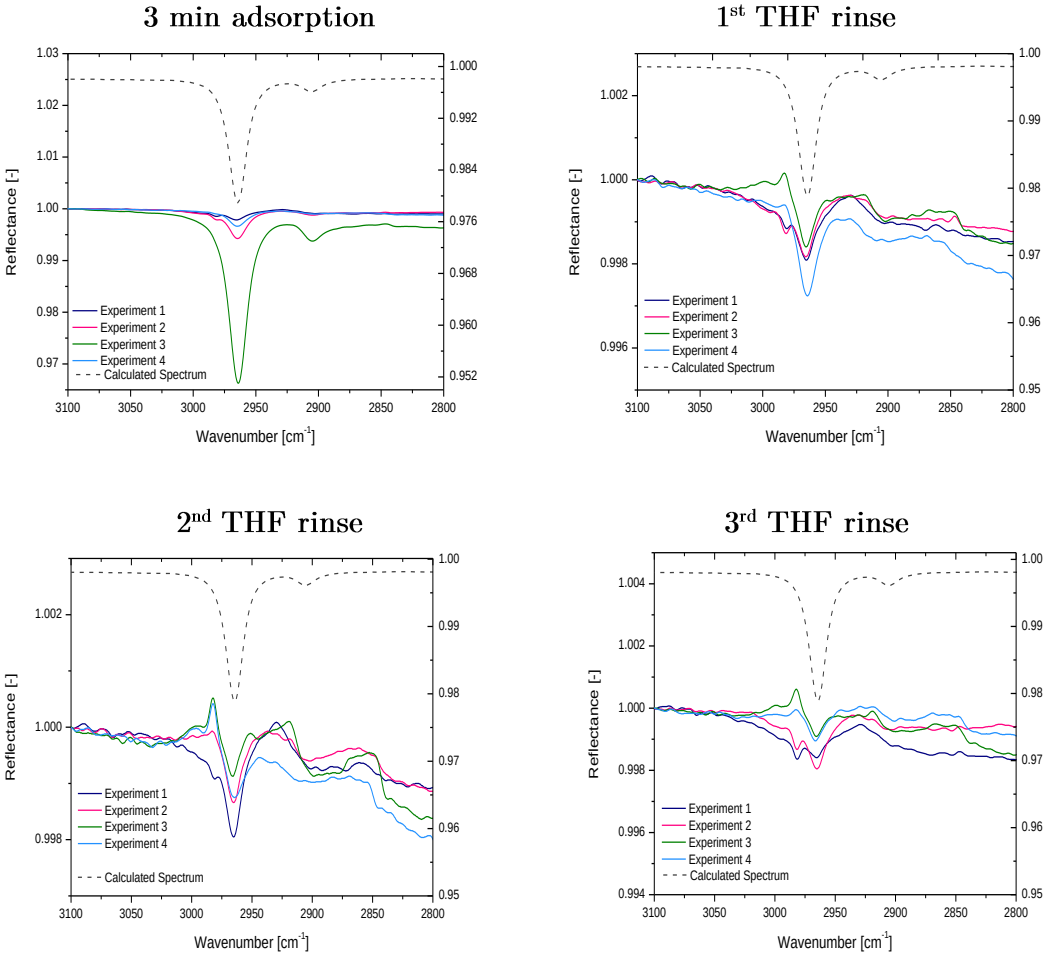


10.6. Appendix F

FTIR-ERA spectra of additional adsorption experiments are included as representation of reproducibility

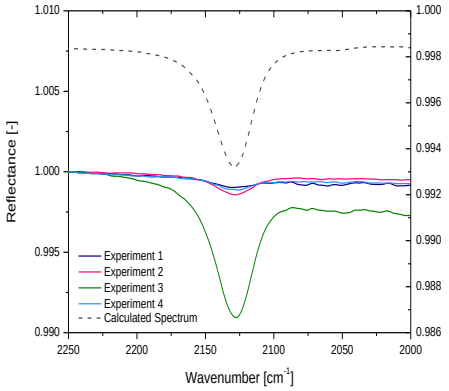
Prepolymer 1: di-hydride terminated PDMS

Region 1

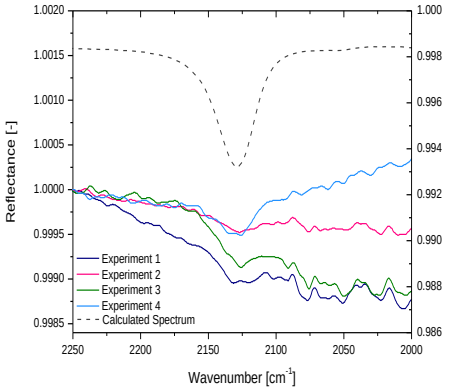


Region 2

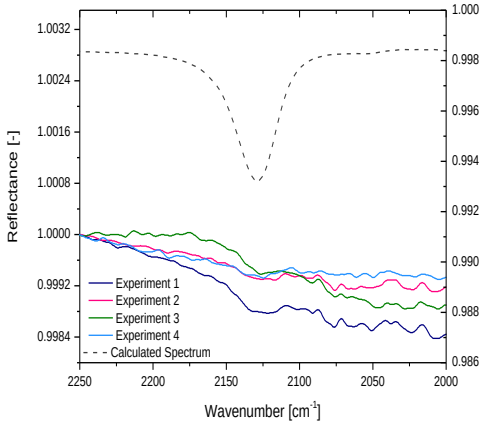
3 min adsorption



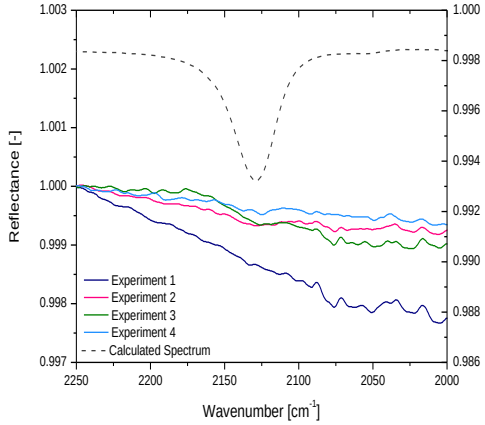
1st THF rinse



2nd THF rinse

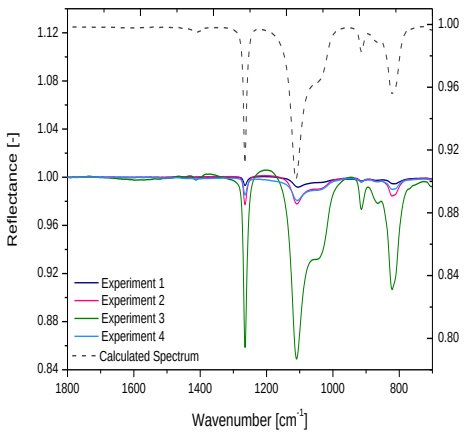


3rd THF rinse

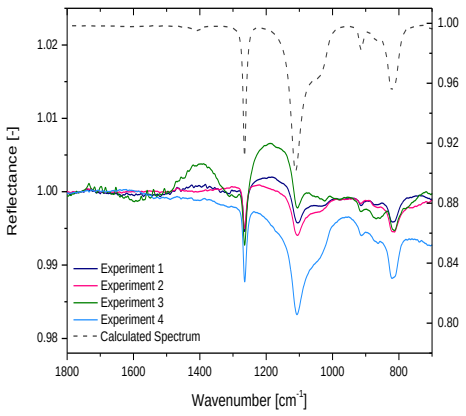


Region 3

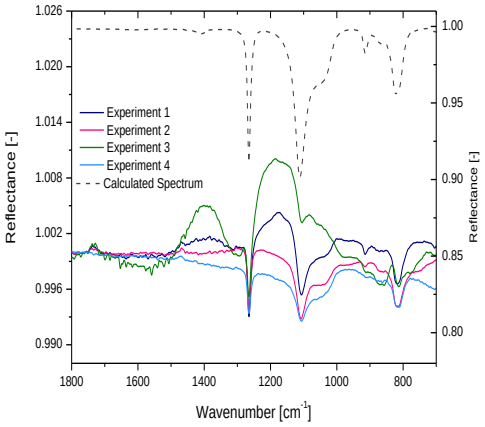
3 min adsorption



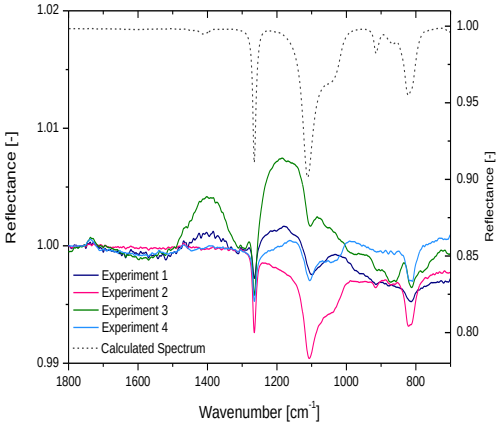
1st THF rinse



2nd THF rinse



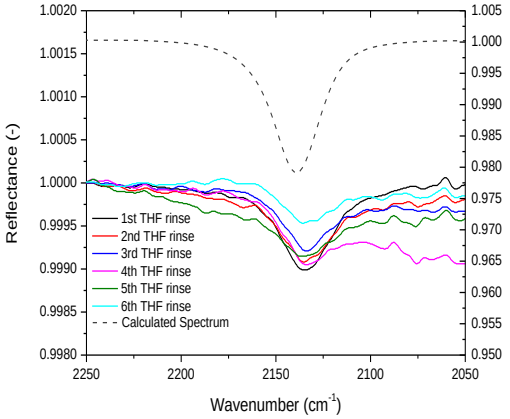
3rd THF rinse



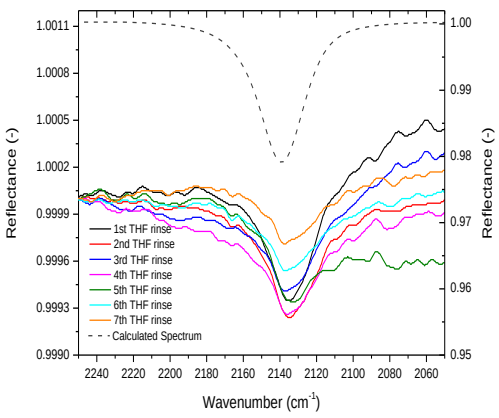
Tetrakis(dimethylsiloxysilane) – TDMS

Region 1

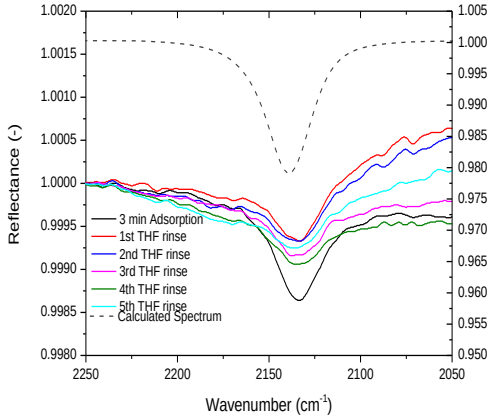
Experiment 1



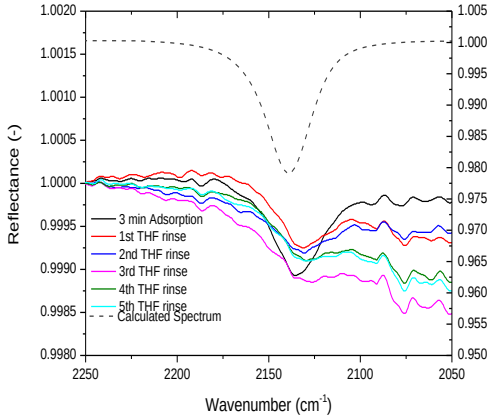
Experiment 2



Experiment 3

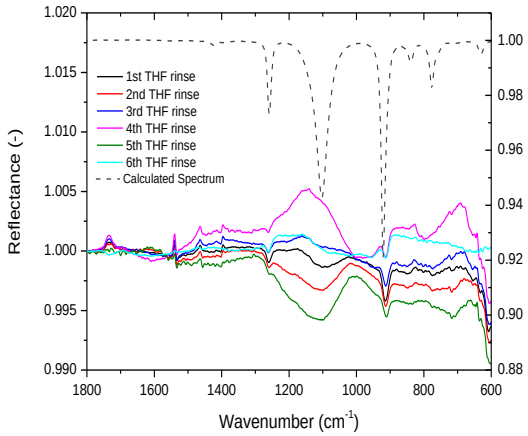


Experiment 4

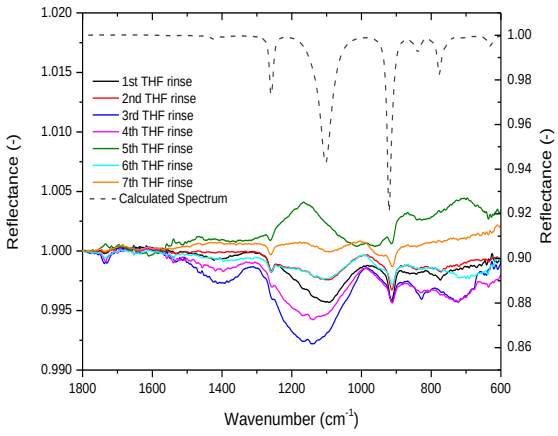


Region 2

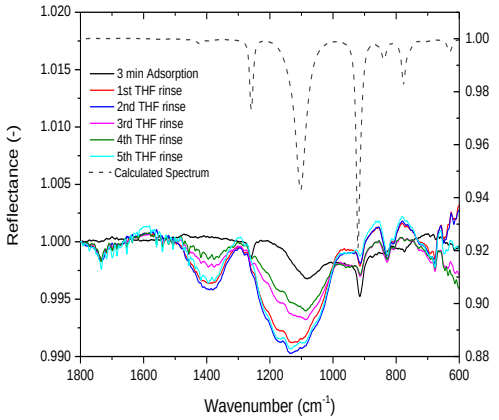
Experiment 1



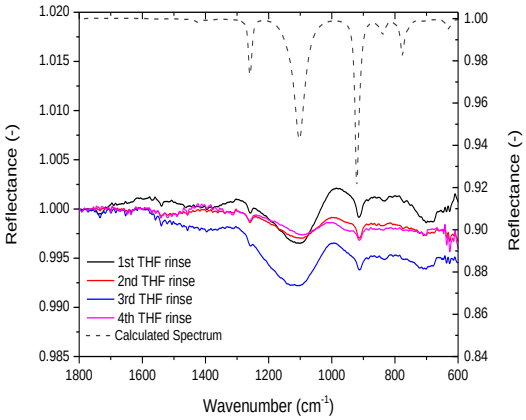
Experiment 2



Experiment 3



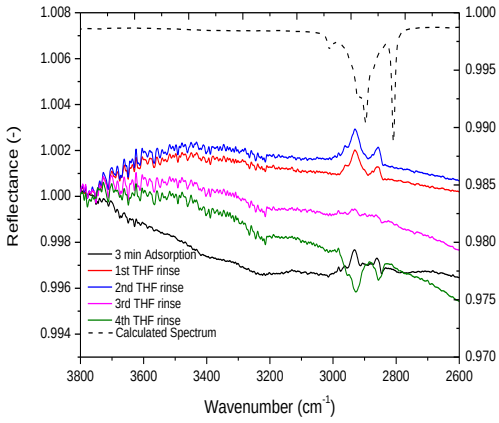
Experiment 4



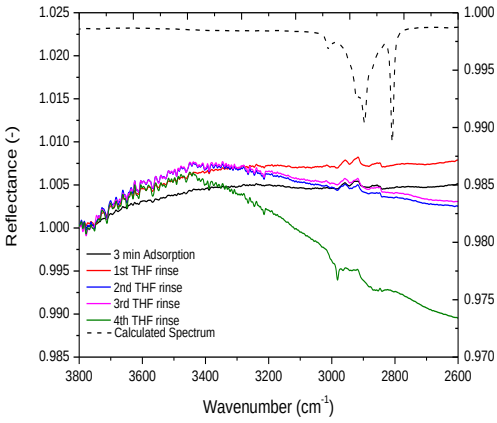
Allyltrimethoxysilane (ATMS)

Region 1

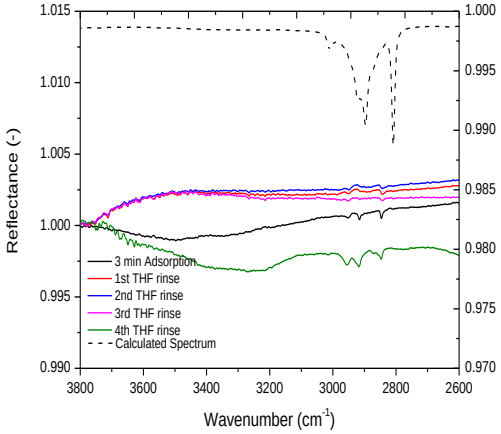
Experiment 1



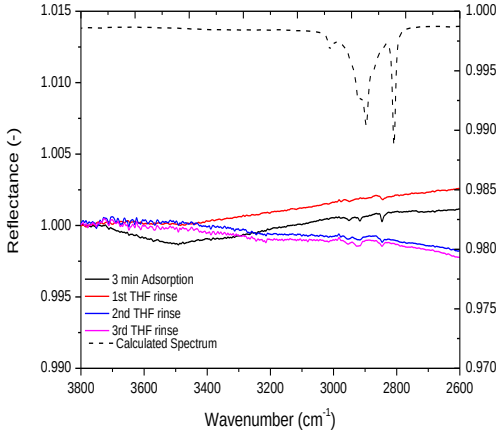
Experiment 2



Experiment 3

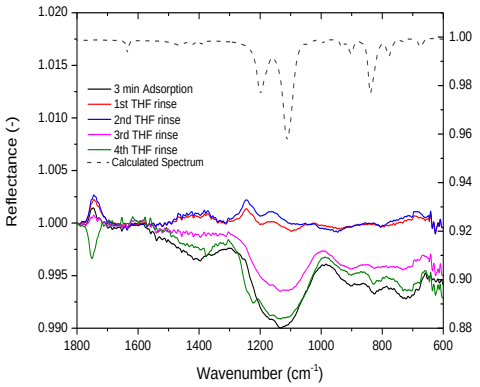


Experiment 4

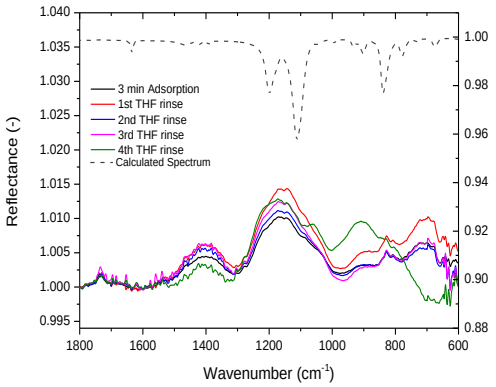


Region 2

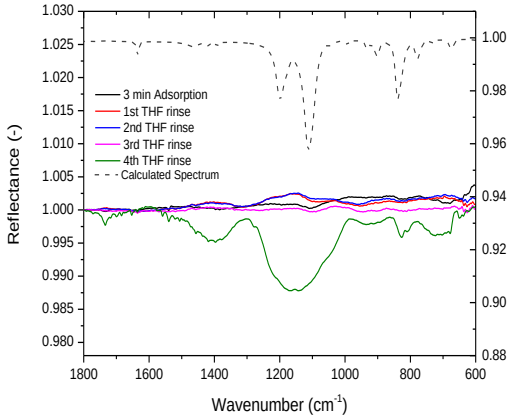
Experiment 1



Experiment 2



Experiment 3



Experiment 4

